



**HAL**  
open science

# Study of elastic and electronic interaction effects in low-dimensional field theories

Simon Metayer

► **To cite this version:**

Simon Metayer. Study of elastic and electronic interaction effects in low-dimensional field theories. General Physics [physics.gen-ph]. Sorbonne Université, 2023. English. NNT : 2023SORUS245 . tel-04638980

**HAL Id: tel-04638980**

**<https://theses.hal.science/tel-04638980>**

Submitted on 8 Jul 2024

**HAL** is a multi-disciplinary open access archive for the deposit and dissemination of scientific research documents, whether they are published or not. The documents may come from teaching and research institutions in France or abroad, or from public or private research centers.

L'archive ouverte pluridisciplinaire **HAL**, est destinée au dépôt et à la diffusion de documents scientifiques de niveau recherche, publiés ou non, émanant des établissements d'enseignement et de recherche français ou étrangers, des laboratoires publics ou privés.

**THÈSE DE DOCTORAT  
DE SORBONNE UNIVERSITÉ**

**Spécialité : Physique Théorique**

**École doctorale n°564: Physique en Île-de-France**

réalisée

au Laboratoire de Physique Théorique et Hautes Energies

sous la direction de Sofian TEBER

présentée par

**Simon METAYER**

pour obtenir le grade de :

**DOCTEUR DE SORBONNE UNIVERSITÉ**

Sujet de la thèse :

**Étude de l'effet des interactions élastiques et électroniques dans  
les théories de champs en basse dimension**

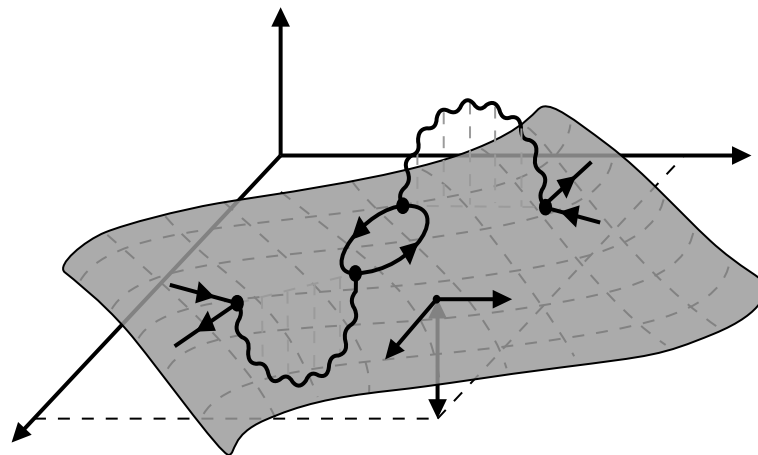
soutenue le 7 Juillet 2023

devant le jury composé de :

M.	Francesco BENINI	Membre invité
M.	Sergio BENVENUTI	Rapporteur
M.	Andrey FEDORENKO	Examineur
M.	Valery GUSYNIN	Membre invité
M <sup>me</sup>	Delphine HARDIN	Présidente
M.	Michael SCHERER	Rapporteur
M.	Sofian TEBER	Directeur de thèse
M.	Kay WIESE	Examineur



# STUDY OF ELASTIC AND ELECTRONIC INTERACTION EFFECTS IN LOW-DIMENSIONAL FIELD THEORIES



PhD thesis by **Simon METAYER**  
Under the supervision of Sofian TEBER  
Laboratory of Theoretical and High Energy Physics (LPTHE)  
Sorbonne University / CNRS / Doctoral school 564 Physique Île-de-France  
Paris – 7<sup>th</sup> July 2023  
(CURRENT VERSION: Saturday 7<sup>th</sup> October, 2023)



# Acknowledgments

First and foremost, I am deeply grateful to my PhD advisor and scientific father, Sofian Teber, to whom I owe the entirety of this work. Since more than 5 years, including two internships and this PhD, he offered me his guidance, shared with me his expertise and taught me so many, scientifically, professionally and sometimes personally. Sofian gave me the opportunity to collaborate with him on elucidating some of the deepest questions in field theory. He allowed me to take part in many events and let me explore my own projects with his constant support. For your kindness, your patience, your brightness and your fascinating ability to explain the most difficult ideas in the simplest terms, thank you.

I would like to thank all my colleagues from the Laboratory of Theoretical and High Energy Physics (LPTHE) at Sorbonne University (SU). In particular, Michela Petrini, as the head of the lab as well as the members of my advisory committee, Kalliopi Petraki and Piotr Tourkine, both former members of LPTHE. They have proved to be great advisors in tense situations. A special thank goes to Françoise Got for her constant kind administrative support, and to whom I wish the best retirement. I am thankful to the professors I met for my teaching mission at SU, in particular Delphine Hardin and Julien Bolmont for giving me the opportunity to teach in multiple flavors, including math lectures and tutorials for second year students as well as nuclear lab work for master students. I would like to thank the SACADO service team from the MESU supercomputer at SU, especially Nicolas Benoit, for his constant kind technical support on very heavy computations.

I am grateful to the referees of this manuscript; Sergio Benvenuti and Michael Scherer, for kindly accepting to examine my work, as well as the other members of the jury; Francesco Benini, Andrey Fedorenko, Valery Gusynin, Delphine Hardin and Kay Wiese. Their encouragements and their inspiring questions, comments, and suggestions to improve the manuscript were highly appreciated. A special thanks also goes to John Gracey who should have been part of this jury, but also for our exchanges resulting in crucial suggestions. I also kindly thank Leo Radzihovsky for our brief but insightful discussions. I am grateful to Dominique Mouhanna, for our many fruitful collaborations, for his kindness and for having been an inexhaustible source of interesting projects, for our rich discussions and for sharing his deep knowledge of membrane physics.

I am thankful to all the students with whom I shared space and time during these three years, Andrei, Andriani, Anthony, Francesco C., Francesco M., Maxl, Vincent, Wenqi, Yann, and especially my former and new office mates, Grégoire, Carlo, Pierre, Yehudi, Jordan, Greivin, who all contributed to install and keep a healthy and pleasant atmosphere in our office. Special thanks should be given; To Yehudi, for his absolute kindness and his administrative omnipotence; To Francesco M. for the awesome parties he is able to organize; To Pierre, for his endless epic stories and the excellent mountain hike we did together. It was my pleasure to organize with you those social events like the student talks or the lab tea.

Je souhaiterais enfin remercier mes plus proches amis, Maxime et Valentin, ainsi que toute ma famille et plus particulièrement mes sœurs, Lilou et Chloë, et mes parents, Céline et Maï, pour leur soutien inconditionnel dans tous mes projets, sans oublier ma Laura, ma femme, à qui je dois tout.



# Introduction

In theoretical physics, *Quantum Field Theory* (QFT) is historically the theoretical framework describing the behavior of subatomic particles and their interactions. It is based on the principles of quantum mechanics, special relativity and classical field theory. QFT assumes that particles are not discrete objects with a finite number of degrees of freedom (position, velocity, ...), but rather excitations of underlying quantum fields, with an infinite number of degrees of freedom. These fields interact with each other and with themselves, and the study of their interplay allows physicists to make predictions about the behavior of interacting particles. It is considered one of the most successful physical frameworks to date, as it provides accurate predictions of various phenomena, from the behavior of elementary particles to the properties of condensed matter physics systems.

The development of QFT can be traced back to the early 20th century, with the pioneering work of physicists such as, *e.g.*, Max Planck, Albert Einstein, Niels Bohr and Paul Dirac. The first significant developments emerged later in the 40s and 50s, with the works of, *e.g.*, Richard Feynman, Julian Schwinger, Sin-Itiro Tomonaga and Freeman Dyson. This period witnessed the emergence of essential techniques like *Feynman diagrams* and *renormalization*. QFT reached its maturity in the 70s with the work of t'Hooft, who proved the renormalizability of non-abelian gauge field theories and introduced the technique of *dimensional regularization*. At the same time, Ken Wilson introduced the modern understanding of the *renormalization group* (RG) and helped to provide a new approach to complex systems, *i.e.*, composed of numerous interacting particles and subject to emergent phenomena such as phase transitions.

In high energy physics, QFT is naturally designed to describe systems with a variable number of particles, via creation and annihilation processes. Indeed, an interacting relativistic quantum theory automatically implies a non-conserved particle number. For particle physics, the fundamental QFT model is quantum electrodynamics (QED), the abelian gauge theory of light and matter. From it, several generalizations are possible. A prominent example is Quantum Chromodynamics (QCD), the non-abelian gauge theory of quarks and gluons which are the components of the atom's nucleus. Another example is the electroweak theory, the unified description of QED and weak nuclear forces. All together, with the Higgs boson, they form the extremely successful standard model of particle physics. It is, still to this day, the model that has the greatest predictive power. It has allowed innumerable experimental verifications in collision experiments, with a precision of tens of digits for certain quantities.

The fundamental developments that led to the development of QFT in high-energy physics have had profound impact on other areas of theoretical physics. In condensed matter physics, QFT is used as a tool to construct models of interacting quasi-particles, the collective excitations allowing, *e.g.*, the description of metals, insulators, and other remarkable phases of matter such as superconductors. Moreover, QFT had a significant impact on the development of *statistical field theory* (SFT). The latter focuses on the study of critical phenomena in many-particle systems subject to thermal fluctuations. SFT provides tools to study systems in the vicinity of critical points, where the correlation length diverges and the system exhibits scale-invariant behavior. It is particularly successful in the description of phase transitions. In SFT, the fundamental model is the so-called  $\phi^4$  theory, *i.e.*, the continuous version of the Ising model, a spin lattice toy-model for ferromagnetism. There are countless modern applications for SFT, but an original motivation came from soft matter systems such as polymers and, later, membranes.



A profound aspect of modern theoretical physics is that quantum and statistical field theories can be considered as equivalent. Indeed, they are related via Wick rotation from Minkowski to Euclidean space, *i.e.*, replacing (imaginary) time with temperature, so that a quantum system in  $d$  spacial dimensions is equivalent to a  $(d+1)$ -dimensional statistical mechanics one. Put simply, quantum fluctuations in  $d$  dimensions are equivalent to thermal ones in  $d+1$  dimensions. Therefore, the techniques associated with QFT and SFT are usually encompassed in a single unifying term, *field theory*.

For a given model subject either to thermal or quantum fluctuations, the field theory framework provides tools for the systematic computation of correlation functions, or equivalently Green's functions. These key objects are directly related to various physical observables of the system, such as scattering amplitudes or scaling anomalies. For usual systems of interest, these functions are extremely challenging to compute and one usually relies on perturbation theory to systematically take into account of interaction effects. Each order in perturbation theory is conventionally represented in terms of Feynman diagrams, *i.e.*, a pictorial representation of the integral (and associated coefficients) describing a given process at a given order, like a scattering or a self-interaction. Precision calculations often require going to large orders in perturbation theory. However, both the number of diagrams and their complexity grows drastically with the order. Moreover, these increasingly challenging diagrams may be divergent and, in the first place, need to be regularized by introducing, *e.g.*, a cut-off. In this work, we will use dimensional regularization, which is the most convenient approach for practical calculations. Once the theory is regularized, a second step consists in absorbing the (non-physical) regulator in a redefinition of the couplings and fields of the model. This step is the renormalization process.

Renormalizing a model implies several features. First, it promotes the bare parameters of the theory to renormalized ones that “run” with the energy-scale, or equivalently, the length scale. This is, *e.g.*, the origin of running couplings in QFT, whose dependence on the (renormalization) scale is encoded in the beta-function. This important RG function allows distinguishing between theories where the coupling increases with the energy (such as QED and  $\phi^4$ ), those where the coupling decreases (the origin of asymptotic freedom in QCD) and the scale (possibly conformal) invariant theories for which the beta function vanishes, *i.e.*, has a fixed point. Second, the correlation functions may have their asymptotic behavior modified once renormalized. In the long-range or equivalently in the infra-red (IR), their scaling is affected by interactions through anomalous dimensions. Near a phase transition, *i.e.*, in the vicinity of a fixed point, these anomalies are also called critical exponents. The latter are measurable experimentally, and they control the scaling of physical observables near phase transitions. These exponents fall into various universality classes, *i.e.*, categories of systems sharing the same macroscopic properties, independently of their microscopical details. The determination of the critical exponents is achieved by a careful study of the divergent structures at play in the renormalization process.

In some cases, interactions may have such drastic effects that they profoundly affect the ground state of the system with respect to the non-interacting case. Perturbation theory is then not able to account for these so-called non-perturbative effects. A prominent example is the dynamical breaking of a symmetry like chirality. As a matter of fact, during the last decades, extensive studies have been carried out on dynamical chiral symmetry breaking (D $\chi$ SB) in QED (and QCD). It implies, in high energy physics terms, the radiative generation of an electron (or quark) mass and, in low energy physics terms, the dynamical opening of a gap in the single-particle electron spectrum. In principle, for a given model, going beyond perturbation theory requires solving the infinite tower of coupled Schwinger-Dyson integral equations, *i.e.*, the non-linear equations of motions of the correlation functions. For the majority of models, such a task is of fantastic complexity. One usually relies on truncation and clever ansatz, while hoping to capture the essential non-perturbative physics of the system.

Within this general background, this thesis focuses on the study of perturbative and non-perturbative interaction effects in quantum or statistical field theories, with a special focus on low dimensional models. The manuscript is divided in two independent parts, with field theory as a thread. The first part

focuses on the elastic properties of two-dimensional membranes subject to thermal fluctuations. The second part focuses on the electronic properties of fermionic planar systems subject to quantum fluctuations. In both parts, for all models, our main goal will be to obtain high precision estimates of the critical exponents and possibly other related physical observables. Part of the success achieved in the high order computations comes from recent advances witnessed during the last decade in automated computations specifically for this task. We now provide an introductory outline of the manuscript.

## PART I – ELASTIC PROPERTIES OF MEMBRANES

This part addresses a first line of research, carried out with my PhD advisor S. Teber and in collaboration with D. Mouhanna. It is devoted to the study of multiple variants of highly derivative massless field theories associated with models of tethered elastic membranes subject to thermal fluctuations. These models are ubiquitous in physics, from the mechanical properties of lipid bilayers in cells, to polymerized planar condensed matter systems such as graphene and graphene-like systems and, possibly, even to the dynamics of (mem-)branes in string theory. Common to these systems are the intriguing universal mechanical properties induced by long-range correlations, such as an anomalous stiffness or a negative Poisson's ratio. Our study focuses on the field theory describing (phantom) polymerized membranes in a flat phase. This model, built from the two-dimensional elasticity stress tensor, includes in-plane (elastic/phonons) and transverse (capillary/flexural) modes. In the loop expansion, going beyond the leading order in this model has remained a technical challenge for over 30 years due to its intricate derivative structure.

**Chapter 1 – Critical elastic properties of flat membranes.** In this chapter, we first provide a basic introduction to the elastic properties of classical planar systems and motivate the study of the critical properties of (pure and phantom) polymerized membranes in a flat phase. We present a two-field model based on longitudinal and transverse mechanical degrees of freedom, where elastic moduli act as couplings, as well as an effective model with longitudinal modes integrated out. In both models, we perform the complete calculation, at one, two and three loops, of all relevant RG functions. The flow diagram is analyzed and the structure of the perturbative series is discussed. A particular focus is set on the precise determination of the critical exponent governing the anomalous stiffness of the system at long scales,  $\eta$ . This exponent, alone, is enough to determine all the other power-law scaling behaviors of the theory in the IR regime. This study significantly increased the accuracy of the previously calculated universal critical exponents and resulted in the Letter [1] (*Phys. Rev. E Letter* 105(1):L012603), as well as the conference proceedings (ACAT 2021) [2] (*J. Phys. Conf. Ser.* 2438 (2023) 1, 012141).

Since the computations performed in [1] are exact order by order in perturbation theory, we use them to benchmark other less controlled computational methods such as the non-perturbative renormalization group (NPRG) and the self-consistent screening approximation (SCSA). We observe unprecedented agreement between our work and these techniques on multiple universal physical quantities. We believe that such agreement originates from the perturbative series behaving (surprisingly) well for these models. Indeed, a striking feature of our results (which is extremely rare in field theory) is that the asymptotic series appears to be in a convergent regime, *i.e.*, the first coefficients of the  $\varepsilon$ -series are small and decreasing, thus providing reliable results as early as low orders and without the need for resummations.

**Chapter 2 – Critical elastic properties of disordered flat membranes.** In this chapter, we pursue our study of elastic planar systems with a generalization to the case of polymerized membranes subject to quenched disorder, such as partial polymerization or dilution. This model provides opportunities for direct experimental measurements on realistic material samples, such as graphene or graphene-like materials, which inherently exhibit defects and disorder. In the replica formalism,

we perform the complete RG calculation, from one to three loops. This work was performed in an independent collaboration with D. Mouhanna and led to the publication [3] (*Phys. Rev. E* 106, 064114).

Following the results of [3], we present the subtle analysis of the flow diagram of this model and confirm the existence of a new non-trivial IR critical fixed point ( $P_c$ ), seen for the first time in recent NPRG calculations, controlling a finite disorder and finite temperature wrinkling transition. Our study confirms the existence of a glassy phase at low temperature in flat membranes. In such a state, experimentally accessible and interesting effects occur, such as the modulus of elasticity being paradoxically increased by the density of defects.

## PART II – ELECTRONIC PROPERTIES OF MEMBRANES

This part addresses a second line of research, carried out with my PhD advisor, S. Teber. It is devoted to the study of multiple abelian gauge theories, with a particular interest for strongly correlated planar fermionic systems. The latter are particularly well described, deep in the IR, by some variants of QED. The main model of interest in this part is the so called reduced (or mixed dimensional) QED model, where photons live in a (possibly) bigger space-time than electrons. Then, varying the dimensions for gauge and matter fields allows this general model to encompass several interesting variants of QED. First, considering electrons and photons both in 3+1 dimension leads to QED<sub>4</sub>, the electrodynamics theory from particle physics that we experience every day. Second, considering both fields restricted to 2+1 dimensions leads to QED<sub>3</sub>. This model was first introduced as a toy model for high temperature QCD, with which it shares key features such as confinement and asymptotic freedom. QED<sub>3</sub> is nowadays a celebrated model for various planar condensed matter systems with relativistic-like gapless quasiparticle excitations at low-energies such as high- $T_c$  superconductors, planar antiferromagnets and possibly surface states of topological insulators as well as half-filled fractional quantum Hall systems. Third, considering different dimensions for the light and matter fields, *e.g.*, fermions trapped on a 2+1 dimensional plane, while photons are in a 3+1 dimensional bulk, leads to QED<sub>4,3</sub>. This model shares many features of QED<sub>3</sub> and is a direct description, in the IR, of the electronic properties of graphene and graphene-like materials.

**Chapter 3 – Critical properties of QED and reduced QED.** We first motivate the study of the general reduced QED model and introduce the basics needed for its study. In this framework, encompassing all the above-mentioned QED variants, we compute the electron self-energy and the photon polarization up to two loops in a small-coupling expansion, in an arbitrary covariant gauge, and obtain all the anomalous dimensions. Our results are then applied to graphene in its ultra-relativistic limit, for which we compute the optical conductivity. We also revisit the well known case of QED<sub>4</sub>, that allows for a minimal check of our general formulation. We then proceed in studying the critical properties of reduced QED and study thoroughly the eventuality of a phase transition from a metallic to an insulating phase in these models. This work led to the publication [4] (*JHEP*09(2021)107).

One of the main achievements of our study is to provide a new way to address  $D\chi SB$ . Indeed, a primary challenge in gauge theories is to solve the old problem of the existence of a dynamical fermion mass. The historical approach to obtain the gap equation that describes such a phenomenon is to solve the Schwinger-Dyson equations self-consistently. However, this task is of tremendous complexity and usually results in, among other things, gauge dependency problems. To overcome this issue, we showed, in [4], that such a gap equation can be semi-phenomenologically constructed directly from the gauge-invariant mass anomalous dimension of the electron. This allows for a simplified calculation of the gauge invariant critical coupling constant  $\alpha_c$  (and the corresponding critical number of fermionic flavors  $N_c$ ) above which a dynamic mass may be radiatively generated for the electron, inducing an interaction-driven (semi-)metal to (excitonic) insulator transition. This process is of crucial importance in planar systems such as graphene, as it would eventually allow for graphene-based transistors. In QED<sub>4</sub>, according to initial motivations, such a non-trivial ultraviolet (UV) fixed point would save the

model from triviality by avoiding the Landau pole. In [4], we predicted analytically a wide range of new improved values for  $\alpha_c$  and  $N_c$ , for all the above-mentioned QED models. Our conclusions are twofold. On the one hand, at very large coupling, our results for  $N_c$  indicates that in graphene, the dynamical opening of a gap in the fermion spectrum, due to pairing, is possible. A similar result is found for QED<sub>4</sub> where D $\chi$ SB may take place in such large coupling regime. On the other hand, for arbitrary  $N_f$ , our results for  $\alpha_c$  indicates that both graphene and QED<sub>4</sub> remains in a conformal phase at observable energy scales.

**Chapter 4 – Critical properties of QEDs in three dimensions.** In this last chapter, we study several abelian gauge theories in the large- $N_f$  expansion, the prototype of which is QED<sub>3</sub>. One of our main goals will be the study of the minimal ( $\mathcal{N} = 1$ ) supersymmetric (SUSY) extension of QED<sub>3</sub>. Such supersymmetric theories have recently attracted considerable interest. For example, in the context of a possible emergence of SUSY in some condensed matter physics systems, our results could find direct applications to the properties of an eventual super-graphene material. It is also a rich laboratory where to study infra-red dualities that may provide non-perturbative insights on the structure of these models. Since SUSY models result from the introduction of bosonic particles for each fermionic particle, and vice versa, we will also be interested in the subcase of (pure) bosonic (or scalar) QED<sub>3</sub>. In order to study all of these models at once, we introduce a general action encompassing the fermionic, bosonic and minimally supersymmetric QED<sub>3</sub>. In this general framework, we compute all the corresponding self-energies and polarizations, up to next-to-leading order in a large- $N_f$  expansion and compute exactly all the anomalous dimensions at that order. Our results are also mapped to a model of super-graphene, for which we compute the optical conductivity. From the study of their critical properties, following the previous chapter, we discuss the phase structure of these gauge theories. This work resulted in the review [5] ([Symmetry 15091806](#)), the letter [6] ([Phys. Lett. B.2023.137729](#)), and the publication [7] ([arXiv:2102.02722](#)).

Our main results apply to the optical conductivity of super-graphene and to the semi-phenomenological determination of the critical number of flavors  $N_c$  below which a mass for the electron and its superpartner can be dynamically generated. We show that SUSY produces interesting interaction effects with respect to the non-SUSY case. On the one hand, the optical conductivity is enhanced by SUSY. On the other hand, it decreases the critical exponents associated with the masses of the matter fields. We are also able to obtain strong evidence that, while a dynamical (parity-even) mass is indeed generated radiatively for a small number of electron flavors in non-SUSY QED<sub>3</sub>, the addition of superpartners creates the opposite effect, so that no mass is ever dynamically generated in  $\mathcal{N} = 1$  SUSY QED<sub>3</sub>, and by extension, in super-graphene.

## Technicalities

In closing this introduction, let us underline some technical achievements related to this thesis. Perturbative computations beyond the leading order often involve extremely tedious algebraic manipulations. This is especially the case in the models studied through this manuscript.

In the first part of this thesis, dedicated to the elastic properties of membranes up to three loops, the highly derivative structures present in the actions, once Fourier transformed, will lead to Feynman integrals involving a very large number of numerators. Furthermore, for the disordered extension, the use of the replica trick will introduce new couplings and non-trivial tensorial structures, increasing drastically the length of the computations. In the second part of this manuscript, dedicated to planar gauge theories, the computations will be very challenging as early as two loops, due to the introduction of non-local photons, inducing branch cuts in the Feynman integrals, making the master integrals highly non-trivial to compute. The fermion traces over a large number of Dirac gamma matrices will also induce a large number of scalar products in Feynman integrals numerators. Finally, in the supersymmetric extension in chapter four, SUSY will more than double the number of fields,

inherently increasing the number of diagrams to compute. In short, calculations in this thesis are extremely tedious. Each of the above-mentioned project requires the (fully analytical) calculation of several tens of Feynman diagrams, each containing thousands of Feynman integrals, so that computer based algebraic tools are mandatory.

A big part of the work carried out for this thesis was focused on the automation, optimization, and parallelization of the latest perturbative analytical computation techniques, based on the state-of-the-art computer algebra tools currently available. Carrying out the computations for these projects required the development of a complete multi-loop computational set-up. My codes implement efficiently all aspects of analytical multi-loop computations in a fully automated manner: generation of Feynman diagrams and corresponding expressions (in a small-coupling or large- $N_f$  expansions), multidimensional tensorial algebra, dimensional regularization, reduction of the integrals (including integrals with half-integers or arbitrary power indices) to a smaller set of master integrals, analytical evaluation of these masters, numerical checks, complete renormalization of the model (without the need for explicit counter-terms), and finally, the evaluation of all the renormalized amplitudes and anomalous dimensions/critical exponents, with eventual resummations. Depending on the complexity of the model, these automated calculations are performed up to two to three loops. For this manuscript, the choice has been made to focus as much as possible on the physics for the main text, rather than on the technicalities related to multi-loop integral computations. To this end, we provide in Appendix A, an overview of the integral results needed in this thesis, as well as a glimpse of the automation procedures for integrals reduction and computation.

# Contents

<b>I</b>	<b>ELASTIC PROPERTIES OF MEMBRANES</b>	<b>15</b>
<b>1</b>	<b>Critical elastic properties of flat membranes</b>	<b>17</b>
1.1	Introduction and motivations . . . . .	18
1.2	Flat membranes model(s) . . . . .	23
1.2.1	The two-field model . . . . .	23
1.2.2	Effective flexural theory (EFT) . . . . .	25
1.3	Setup and conventions in the EFT . . . . .	26
1.3.1	Feynman rules . . . . .	26
1.3.2	Fate of infra-red divergences . . . . .	27
1.3.3	Dyson equations . . . . .	28
1.3.4	Renormalization conventions . . . . .	29
1.4	Perturbative calculations up to three loops in the EFT . . . . .	32
1.4.1	One-loop analysis . . . . .	32
1.4.2	Two-loop analysis . . . . .	35
1.4.3	Three-loop analysis . . . . .	40
1.5	Renormalization group and fixed points . . . . .	47
1.5.1	Gaussian fixed point $P_1$ . . . . .	47
1.5.2	Shearless fixed point $P'_2$ . . . . .	48
1.5.3	Infinitely compressible fixed point $P_3$ . . . . .	49
1.5.4	Non-trivial fixed point $P_4$ . . . . .	50
1.5.5	Phase diagram . . . . .	52
1.6	Comparisons with other approaches . . . . .	52
1.6.1	Benchmarking the NPRG approach . . . . .	53
1.6.2	Benchmarking the SCSA approach . . . . .	54
1.6.3	Comparison with large- $d_c$ approaches . . . . .	55
1.6.4	Comparison of $\eta(P_4)$ with the literature . . . . .	57
1.7	Conclusion . . . . .	58
<b>2</b>	<b>Critical elastic properties of disordered flat membranes</b>	<b>61</b>
2.1	Introduction and motivation . . . . .	62
2.2	Disordered flat membranes model . . . . .	64
2.2.1	Disordered model . . . . .	64
2.2.2	Scalings and exponents in the IR . . . . .	66
2.2.3	Replica algebra . . . . .	67
2.2.4	Feynman rules . . . . .	67
2.2.5	Dyson equations for the flexuron and phonon fields . . . . .	69
2.2.6	Renormalization conventions . . . . .	70
2.3	Perturbative calculations up to three loops . . . . .	72
2.3.1	One-loop analysis . . . . .	72
2.3.2	Two-loop analysis . . . . .	74
2.3.3	Three-loop analysis . . . . .	77
2.4	Renormalization group . . . . .	80

2.4.1	Renormalization constant derivation . . . . .	80
2.4.2	Renormalization group functions . . . . .	81
2.5	Fixed points and results . . . . .	83
2.5.1	Purely non-disordered fixed points . . . . .	83
2.5.2	How to find the disordered fixed points . . . . .	87
2.5.3	Disordered fixed points and results up to three loops . . . . .	91
2.5.4	Phase diagram . . . . .	94
2.6	Comparison with other approaches . . . . .	96
2.6.1	Benchmarking the NPRG approach . . . . .	96
2.6.2	Benchmarking the SCSA approach . . . . .	97
2.6.3	Comparison with large- $d_c$ approaches . . . . .	97
2.6.4	Non-perturbative comparison summary . . . . .	98
2.7	Conclusion . . . . .	99
 <b>II ELECTRONIC PROPERTIES OF MEMBRANES</b>		<b>101</b>
<b>3</b>	<b>Critical properties of QED and reduced QED</b>	<b>103</b>
3.1	Introduction . . . . .	104
3.1.1	Basics of QED in four dimensions (QED <sub>4</sub> ) . . . . .	104
3.1.2	Motivations for reduced QED . . . . .	107
3.2	The QED <sub><math>d_\gamma, d_e</math></sub> model, conventions, and renormalization setup . . . . .	111
3.2.1	Model . . . . .	111
3.2.2	Perturbative setup . . . . .	112
3.2.3	Renormalization setup . . . . .	115
3.3	General perturbative calculations up to two loops in QED <sub><math>4, d_e</math></sub> . . . . .	117
3.3.1	One-loop calculations . . . . .	118
3.3.2	Two-loop calculations . . . . .	121
3.3.3	Electron field and mass anomalous dimensions . . . . .	126
3.4	Results for the different models of interest . . . . .	128
3.4.1	Results for QED <sub>4</sub> . . . . .	128
3.4.2	Results for reduced QED <sub><math>4,3</math></sub> (Graphene) . . . . .	128
3.4.3	Results for QED <sub>3</sub> (Large- $N_f$ ) . . . . .	131
3.4.4	Case of parity-odd mass term in QED <sub><math>4,3</math></sub> . . . . .	131
3.5	Critical properties . . . . .	136
3.5.1	Leading-order solution of SD equations for QED <sub><math>4, d_e</math></sub> . . . . .	136
3.5.2	Gap equation and criterion for dynamical mass generation . . . . .	137
3.5.3	Application to quenched QED <sub><math>4, d_e</math></sub> . . . . .	139
3.5.4	Application to unquenched QED <sub><math>4, d_e</math></sub> . . . . .	142
3.6	Conclusion . . . . .	150
3.A	QED <sub>4</sub> at three loops . . . . .	151
<b>4</b>	<b>Critical properties of many flavor QEDs in three dimensions</b>	<b>157</b>
4.1	Motivations for QED <sub>3</sub> and its supersymmetric extension. . . . .	158
4.2	Models of three-dimensional QEDs in large- $N_f$ . . . . .	161
4.2.1	Three-dimensional (fermionic) Quantum Electrodynamics (QED <sub>3</sub> ) . . . . .	161
4.2.2	Bosonic Quantum Electrodynamics (bQED <sub>3</sub> ) . . . . .	165
4.2.3	Minimally supersymmetric Quantum Electrodynamics ( $\mathcal{N} = 1$ SQED <sub>3</sub> ) . . . . .	165
4.2.4	Super-graphene model (SQED <sub><math>4,3</math></sub> ) . . . . .	167
4.3	Presentation of the general gQED <sub>3</sub> model . . . . .	168
4.4	Perturbative calculations at NLO in gQED <sub>3</sub> . . . . .	177
4.4.1	Gauge-multiplet polarizations at LO . . . . .	177

4.4.2	Matter-multiplet self-energies at LO . . . . .	181
4.4.3	Vanishing contributions and generalized Furry theorem . . . . .	184
4.4.4	Gauge-multiplet polarizations at NLO . . . . .	187
4.4.5	Matter-multiplet self-energies at NLO . . . . .	191
4.4.6	Renormalized self-energies . . . . .	196
4.5	Results summary and discussion . . . . .	197
4.5.1	Results for QED <sub>3</sub> . . . . .	197
4.5.2	Results for $\mathcal{N} = 1$ SQED <sub>3</sub> . . . . .	198
4.5.3	Results for bosonic bQED <sub>3</sub> . . . . .	199
4.5.4	Results for reduced QED <sub>4,3</sub> (Graphene) . . . . .	199
4.5.5	Results for reduced $\mathcal{N} = 1$ SQED <sub>4,3</sub> (Super-Graphene) . . . . .	200
4.5.6	Discussion of the stability of the fixed point . . . . .	202
4.6	Critical $N_f$ for dynamical electron mass generation . . . . .	202
4.6.1	Schwinger Dyson equations at LO . . . . .	203
4.6.2	Semi-phenomenological gap equation . . . . .	204
4.7	Conclusion . . . . .	210
<b>A</b>	<b>Multi-loop massless techniques</b> . . . . .	<b>213</b>
A.1	One loop . . . . .	214
A.2	Introduction to IBP reduction . . . . .	215
A.3	Two loops . . . . .	217
A.4	Three loops . . . . .	220
A.5	Arbitrary and half-integer indices . . . . .	222
A.5.1	One loop . . . . .	222
A.5.2	Two loops . . . . .	223





## Part I

# ELASTIC PROPERTIES OF MEMBRANES



# Chapter 1

## Critical elastic properties of flat membranes

This chapter is partly based on the publications

[1] S. Metayer, D. Mouhanna and S. Teber, *Phys. Rev. E Letter* 105(1):L012603, “Three-loop order approach to flat polymerized membranes”,

[2] S. Metayer, D. Mouhanna and S. Teber, *J. Phys. Conf. Ser.* 2438 (2023) 1, 012141, “Flat polymerized membranes at three-loop order”.

We introduce the basics of elastic planar systems and motivate the study of the critical properties of pure phantom membranes in a flat phase. We present a two-field model based on longitudinal and transverse mechanical fluctuations, where elastic moduli act as couplings, as well as an effective model with longitudinal fluctuations integrated out. In both models, we perform the complete computation of the renormalization-group functions up to three loops and derive all the critical exponents. The flow diagram is analyzed and the structure of the perturbative series is discussed. In particular, the latter appear to be surprisingly convergent, which allows us to precisely estimate physical quantities such as the anomalous stiffness induced in the flat phase, as well as benchmarking other approaches relying on less controlled approximations.

### Contents

---

1.1	Introduction and motivations . . . . .	<b>18</b>
1.2	Flat membranes model(s) . . . . .	<b>23</b>
1.2.1	The two-field model . . . . .	23
1.2.2	Effective flexural theory (EFT) . . . . .	25
1.3	Setup and conventions in the EFT . . . . .	<b>26</b>
1.3.1	Feynman rules . . . . .	26
1.3.2	Fate of infra-red divergences . . . . .	27
1.3.3	Dyson equations . . . . .	28
1.3.4	Renormalization conventions . . . . .	29
1.4	Perturbative calculations up to three loops in the EFT . . . . .	<b>32</b>
1.4.1	One-loop analysis . . . . .	32
1.4.2	Two-loop analysis . . . . .	35
1.4.3	Three-loop analysis . . . . .	40
1.5	Renormalization group and fixed points . . . . .	<b>47</b>
1.5.1	Gaussian fixed point $P_1$ . . . . .	47
1.5.2	Shearless fixed point $P'_2$ . . . . .	48
1.5.3	Infinitely compressible fixed point $P_3$ . . . . .	49
1.5.4	Non-trivial fixed point $P_4$ . . . . .	50
1.5.5	Phase diagram . . . . .	52
1.6	Comparisons with other approaches . . . . .	<b>52</b>
1.6.1	Benchmarking the NPRG approach . . . . .	53
1.6.2	Benchmarking the SCSA approach . . . . .	54
1.6.3	Comparison with large- $d_c$ approaches . . . . .	55
1.6.4	Comparison of $\eta(P_4)$ with the literature . . . . .	57
1.7	Conclusion . . . . .	<b>58</b>

---

## 1.1 Introduction and motivations

Linear elasticity theory probably dates back to Robert Hooke, who first stated his famous law in 1676, first as a latin anagram; “*ceiinossttu*” and two years later, gave the solution; “*Ut tensio, sic vis*”, “As the extension, so the force” [8]. Since we cannot go through three hundred years of history here, we will jump directly to the 60s, at the end of Lev Landau’s era, and take as a base reference the textbook “Theory of elasticity” by Landau and Lifshitz (Vol. 7) [9].

The elasticity of a material is quantified by quantities called elastic moduli, such as the Young modulus ( $Y$ ), the bulk modulus ( $B$ ) or the shear modulus ( $\mu$ ), which measure the amount of stress needed to achieve a unit of strain. A higher modulus indicates that the material is harder to deform. These properties can be defined for materials in arbitrary dimensions. The most obvious case is probably that of three-dimensional materials, ubiquitous in mechanical engineering. Another case, simpler for theoretical studies, is that of one-dimensional materials, a prominent example being polymers, see, *e.g.*, the seminal work of de Gennes [10]. Finally, in between these two cases, lie the two-dimensional structures (embedded in three-dimensional space). These can have many forms: planar materials, interfaces or surfaces, in one word, we call them *membranes*. In this thesis, we focus our interest on these planar systems and, more specifically in this chapter, on their elastic properties. For the next few paragraphs, we follow in essence the review by Bowick and Travesset [11], see also [12–14].

Membrane physics originally appeared as an extension of polymer physics and as a part of the broader field of soft condensed matter systems. Membranes, unlike polymers, exhibit distinct types of microscopic realizations with, *e.g.*, fluid, hexatic and crystalline order, which appear in multiple forms, such as flat, tubular or crumpled phases, see figure 1.1. All these variants lead to distinct large scale behaviors and consequently to a rich physics.

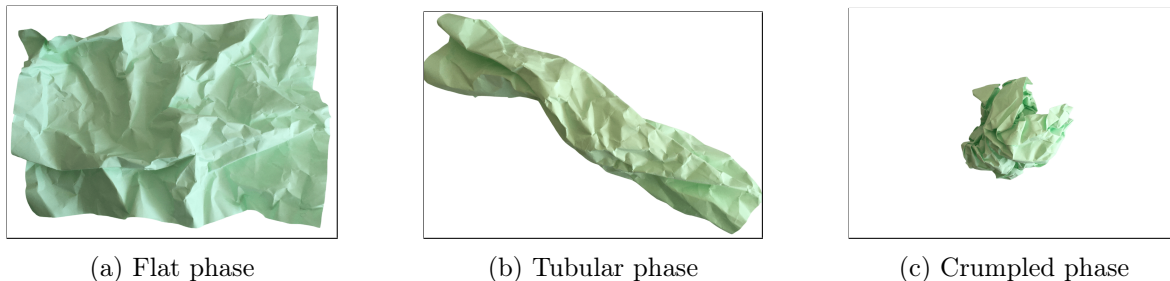


Figure 1.1: Transition from a wrinkled to completely crumpled membrane, through an intermediate tubular phase.

Membranes are ubiquitous in physics and there are many concrete realizations of them in nature, which greatly enhances the significance of their study. A natural occurrence of a polymerized membrane is the cytoskeleton of cell surfaces, essential to the cell stability and functionality, as well as determining its shape. A prominent example is the spectrin skeleton of mammal erythrocytes, *i.e.*, the red blood cells. Their surface is made of a fishnet-like network of triangular plaquettes formed primarily by the proteins called spectrin and actin, and provide a beautiful experimental realization for tethered membranes, see, *e.g.*, [15] as well as [16] for an experimental evidence of a flat phase in red-blood cells membranes and its role in their peculiar biconcave disc shape. Other realizations, more artificial, are inorganic crystalline membranes. There are well-known examples, such as graphene (see, *e.g.*, [17] and the review [18]) and graphene-like materials, whose mechanical properties in a crumpled phase or close to a crumpling transition have been studied by suspension in liquids, see the early works [19–21] on graphite oxide. There are numerous other membrane realizations, such as amphiphilic bilayer membranes, or water/oil interfaces in surfactant microemulsions, see, *e.g.*, [22]. On a more abstract level, one can meet membranes within the context of high-energy physics, see, *e.g.*, [23, 24], initially through high temperature expansions of lattice gauge theories, then in the large- $N$  limit of gauge

theories, in two-dimensional quantum gravity, in string theory as the world-sheet of a string and, finally, in (mem-)brane theory.

A natural way to study membranes theoretically is the renormalization group that allows one to access the critical properties of such systems. Indeed, in the long wavelength (infra-red) limit, the properties of membranes are independent of their chemical or mechanical nature and fall into universality classes. The microscopic details are erased in the thermodynamic limit and allow the computation of the critical exponents of the system. This is why systems with very different microscopic realizations exhibit similar macroscopic features (This, in essence, is why we can illustrate the properties of tethered membranes such as graphene or cell membranes with a simple sheet of paper!). Theoretically, the most general (isotropic) elastic membrane model one could define would certainly contain at least the following parameters:

- $\kappa$ , the bending rigidity; the coupling to the extrinsic curvature (the square of the Gaussian mean curvature). For large and positive bending rigidity, flatter surfaces are favored.
- $t, u, v$ , the elastic constants; these parameters encode the microscopic elastic properties of the membrane.
- $s$ , the excluded volume or self-avoiding coupling; this is the coupling that imposes an energy penalty for the membrane to self-intersect.
- $\Delta_\kappa, \Delta_u, \Delta_v, \dots$ ; additional parameters controlling the disorder variance.

In this chapter, we restrict ourselves to

*pure phantom crystalline membranes in a wrinkled isotropic flat phase,*

that we may simply call flat membranes. Let us break down what it means. First, we consider “crystalline”, or equivalently polymerized or tethered, membranes. These are planar structures made of individual monomers that are rigidly bound together. They possess an in-plane elastic moduli as well as a bending rigidity. A prominent example of such a material is graphene, which is a one atom thick carbon honeycomb lattice. Second, we focus on planar membranes subject to small wrinkling deformations, *i.e.*, in a “flat phase”, see figure 1.1a. In this case, for a  $d$ -dimensional membrane, the elastic constants  $t, u, v$  may be related to the two Lamé parameters of Landau elastic theory,  $\lambda$  and  $\mu$ , so that they reduce to

$$u = \mu, \quad v = \lambda/2 \quad t = -4(\mu + d\lambda/2) < 0, \quad (1.1)$$

where we specify in (1.1) that  $t < 0$ , in order to stay in the flat phase, because  $t > 0$  would lead to a transition towards a crumpled phase, see figure 1.1c. In other words, we impose  $d\lambda + 2\mu > 0$  as a mechanical stability condition together with positive shear modulus,  $\mu > 0$ . Third, we will consider “phantom” membranes, which mean that we allow self-crossing. This amounts to set  $s = 0$ , *i.e.*, no self-avoidance, which is a reasonable assumption for membranes in a flat phase, where self-crossing should be negligible (not the case for a crumpled phase!). Fourth and finally, we consider “pure” (or equivalently “clean”) membranes, *i.e.*, we neglect disorder such as topological defects that may induce transitions to hexatic and fluid universality classes (the disordered model will be considered in the next chapter). Note that a simple sheet of paper, slightly wrinkled, fits this whole description remarkably well and provides a good image to keep in mind, helping us to illustrate some properties of such membranes.

Before going into technical details, let us illustrate some interesting features of flat crystalline membranes. As a first interesting property, these systems exhibit a surprising negative Poisson ratio induced by wrinkling deformations, see *e.g.*, [25]. We recall that the Poisson effect is the deformation (expansion or contraction) of a material in directions perpendicular to the specific direction of the applied force. Intuitively, for a three-dimensional elastic material, compressing it along the  $x$  axis by an amount  $dx$  should lead to an expansion in the  $(y, z)$  plane and gives a positive Poisson ratio since

it is defined as  $\nu = -dy/dx = -dz/dx > 0$ . In striking contrast, for flat wrinkled membranes, a simple tabletop experiment with a sheet of paper shows, see figure 1.2, that expanding the membrane along one axis causes it to expand also in the transverse direction, so that  $\nu = -dx/dy < 0$ , *i.e.*, a negative Poisson ratio. Materials exhibiting such feature are called “auxetics”. This also means that compressing the membrane in one direction causes it to shrink in the transverse direction. In other words, applying pressure to this material increases its hardness, making it extremely resistant to pressure and impact.

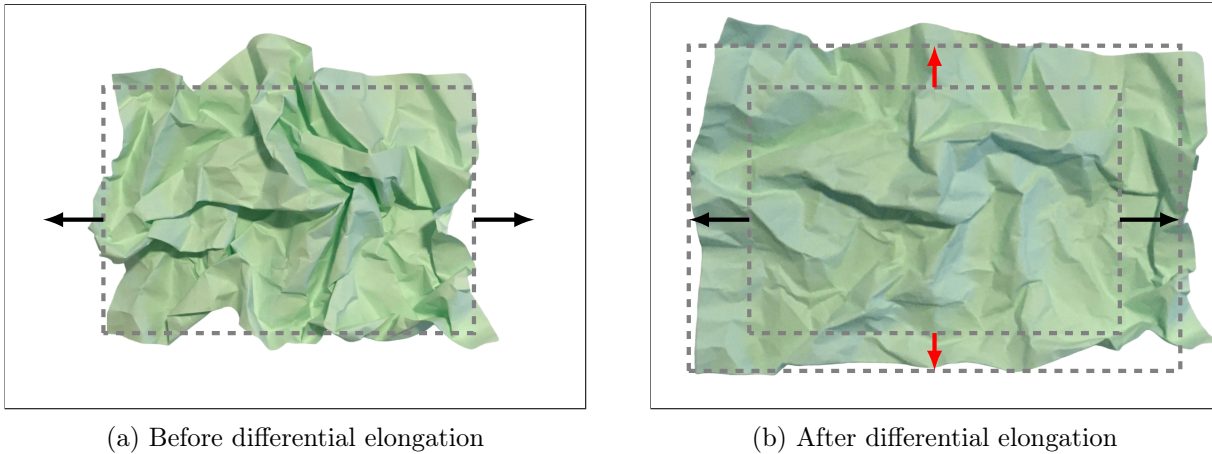


Figure 1.2: Simple tabletop experiment with a sheet of paper to illustrate the auxetic properties of a wrinkled membrane. Applying a strain (horizontal black arrows) result in a transverse elongation of the same sign (vertical red arrows), yielding a negative Poisson ratio ( $\nu < 0$ ).

Another striking effect of crystalline flat membranes, which will be our main interest in the rest of this chapter, is the anomalous stiffness induced by the wrinkling deformations. Indeed, adding wrinkle to a membrane considerably increases its stiffness, as illustrated in figure 1.3 on a simple sheet of paper standing by itself thanks to wrinkling. This effect is quantified by the so-called anomalous stiffness exponent ( $\eta$ ) that we will define in the next lines.

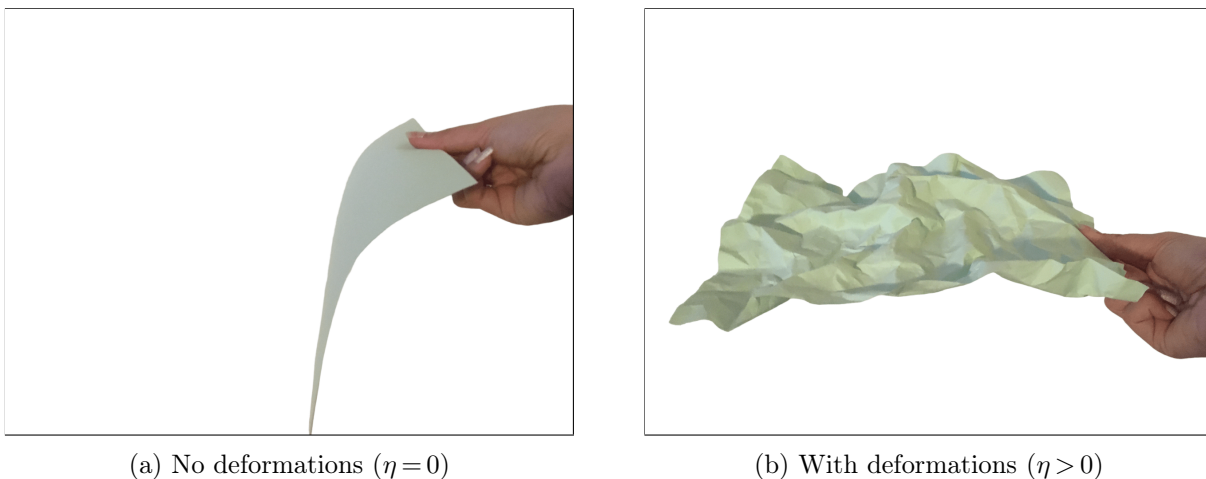


Figure 1.3: Simple tabletop experiment with a sheet of paper to illustrate the anomalous stiffness (or rigidity),  $\eta$ , induced by elastic deformations. Without deformations, the membrane exhibits low stiffness, while with small elastic deformations, an anomalous stiffness induced by long-range correlations appears, such that the paper sheet remains rigidly flat.

The flat phase of polymerized membranes has recently been the subject of intense theoretical investigations mainly motivated by the fact that it seems to encode satisfyingly the elastic degrees of freedom of nowadays trendy materials such as graphene [26, 27] and, more generally, graphene-like systems (see, *e.g.*, the textbook [17]). Early, mean field [28] and perturbative [29] computations have revealed the stability of such a phase, ensured by a mechanism of coupling of the out-of-plane (flexural),  $\vec{h}$ , modes to the in-plane (phonons),  $\vec{u}$ , modes (and allowing to circumvent the Mermin-Wagner theorem; see, *e.g.*, [30] for an explanation). This flat phase is controlled by a fully stable infrared fixed point, characterized by power-law behaviors for the phonon-phonon and flexural-flexural correlation functions [29, 31–33]

$$\langle u(p)u(-p) \rangle \sim p^{-(2+\eta_u)} \quad \text{and} \quad \langle h(p)h(-p) \rangle \sim p^{-(4-\eta)}, \quad (1.2)$$

where the elasticity softening exponent  $\eta_u$  and the anomalous stiffness exponent  $\eta$  are two nontrivial anomalous dimensions related by the Ward identity [29, 31–33]

$$\eta_u = 4 - d - 2\eta, \quad (1.3)$$

where  $d$  is the dimension of the membrane. Therefore, we can focus on the determination of only one of the exponents, in our case,  $\eta$ . Let us remark that several other critical exponents can be defined for this model, but hyperscaling relations and Ward identities constrains them so that only one of them, *e.g.*,  $\eta$ , is enough to compute all the others. This is the case, for example, for the roughness exponent,

$$\zeta = (4 - d - \eta)/2, \quad (1.4)$$

which measures the fluctuations transverse to the flat directions. In short, the stiffness exponent  $\eta$  governs all infra-red properties of membranes in the flat phase, where parameters are length-scale-dependent, like the enhanced bending energy  $\kappa(p) \sim p^{-\eta}$  and the softened Lamé elastic moduli  $\mu(p) \sim \lambda(p) \sim p^{4-d-2\eta}$ , see *e.g.*, the reviews [11, 12].

A major challenge, in this context, is an accurate theoretical determination of the exponent  $\eta$  at the stable fixed point. In the (extreme) Gaussian approximation where no interactions are present, obviously,  $\eta = 0$ . Upon allowing interactions, the early seminal study by Nelson and Peliti [28] revealed that, in a mean field approximation, the anomalous stiffness yields  $\eta \approx 1$ . They further state that such a positive value stabilize the flat phase in the low temperature limit and that going beyond mean field, it is expected that the renormalization of the elastic constants will drag down the value of  $\eta$ . At that time, the question to address was then if higher-order corrections would be small enough so that  $\eta$  remains positive, in order for a flat phase to exist at long distances in crystalline membranes. Nowadays, we know the answer, which in short, is yes. Indeed, all the theoretical studies following [28] (that we present in the next paragraph) argue that beyond mean field,  $\eta$  should lie roughly in the range [0.6, 1], so that the flat phase is indeed stable. Nevertheless, to this day, there is no clear consensus on the precise value of  $\eta$ , despite the fact that it is a universal fundamental constant of tethered membranes, of uttermost interest in multiple areas of physics. In the following, we briefly present the various values obtained for  $\eta$  over more than three decades.

The first analytical theoretical study to follow [28] was the seminal perturbative one-loop computation by Aronovitz and Lubensky [29, 32] yielding  $\eta_{1\text{-loop}} = 0.96$ , that we will reproduce later in this chapter, with modern techniques. Due to the intricacy of the diagrammatic analysis involved in the perturbative approach, it became soon evident that higher-order loop computations would necessitate high automation of the computations. Moreover, one would naively expect the perturbative results to converge slowly (which we will see, is surprisingly wrong) due to the distance between the upper critical dimension,  $d_{\text{uc}} = 4$ , and the physical dimension,  $d = 2$ , which means that results are obtained in series of  $\varepsilon = 2 - d/2$  and the physical case is  $\varepsilon = 1$ . To circumvent the perturbative analysis, these pioneering works have been followed by various non-perturbative approaches, able to tackle the physics directly in dimension  $d = 2$ . Early approaches were carried out by means of an expansion in



the large embedding space ( $D=3$ ) dimension, by Gutter *et al.* [31, 33], yielding  $\eta_{\text{large-D}} = 2/D \approx 0.67$ , later followed by the similar  $1/d_c$  expansion [31–36], where  $d_c$  is the co-dimension of the membrane ( $d_c = D - d$ ), but it seems hard to estimate properly  $\eta$  numerically using this technique. The critical properties of membranes has also been studied by means of self-consistent approaches such as the self-consistent screening approximation (SCSA) [12, 37–40] as well as the so-called non-perturbative renormalization group (NPRG) [41–47]. The two last ones have produced roughly compatible results:  $\eta_{\text{SCSA}}^{\text{LO}} \simeq 0.821$  [12, 40] at leading order ( $\eta_{\text{SCSA}}^{\text{NLO}} \simeq 0.789$  at controversial next-to-leading order [37]) and  $\eta_{\text{NPRG}} = 0.849$  [41]. As for Monte Carlo simulations of membranes, they also led to scattered values, *e.g.*,  $\eta = 0.81(3)$  [48],  $\eta = 0.750(5)$  [49], and  $\eta = 0.795(10)$  [50] and Monte Carlo simulations of graphene to  $\eta \simeq 0.85$  [51]. See table 1.2, at the end of the chapter, for a summary of these results.

On the experimental side, the early study [16] showed evidence of a flat phase for red-blood cells membranes, measuring via small-angle x-ray techniques, a roughness exponent of  $\zeta = 0.65 \pm 0.10$ , which in terms of anomalous stiffness, using (1.4), yields  $\eta_{\text{blood-cells}} = 0.7 \pm 0.2$ . A similar result has been obtained using X-ray scattering on amphiphilic films (arachidic acid) [52] with the measure  $\eta_{\text{amphiphilic-films}} = 0.7 \pm 0.2$ . Still on the biophysics side, very recent measurement of nuclear wrinkling during egg development in the fruit fly (*Drosophila melanogaster*) [53] obtained measurements and numerical simulations compatible with  $\eta_{\text{vesicles}} \approx 0.8$ . On the condensed matter physics side, precision measurement of the elastic critical properties of flat materials seems difficult. In graphene and graphene-like materials, experimental estimations of the anomalous stiffness exponent usually lead to rough estimations in between  $\eta_{\text{graphene}} \approx 1$  and  $\eta_{\text{graphene}} \approx 0.8$ , see *e.g.*, the review [18]. A notable exception is the graphene experimental study [54] where they obtained  $\eta_{\text{graphene}} \approx 0.82$ .

In order to get a better understanding of the structure of the underlying field-theory, several groups have recently engaged in perturbative studies of both pure [47, 55] and disordered membranes [56] going beyond leading order. The two-loop order approach performed in particular in [47] has revealed an intriguing agreement between the perturbative and non-perturbative approaches in the vicinity of the upper critical dimension. Moreover, the value of the two-loop order anomalous dimension in  $d=2$ ,  $\eta_{2\text{-loop}} = 0.9139$  [47], when compared to the one-loop order one,  $\eta_{1\text{-loop}} = 0.96$  [29, 31–33], has been found to move in the right direction when referring to the generally accepted values that lie in the range [0.72, 0.88], see table eftab:mem:literatureeta at the end of the current chapter.

In this chapter, we reproduce the one and two-loop results obtained in [29, 31–33, 47], as well as the recent three-loop [1] ones, by means of a weak-coupling perturbative approach performed near the upper critical dimension  $d_{\text{uc}} = 4$ , within the modified minimal subtraction ( $\overline{\text{MS}}$ ) scheme. We will introduce the flexuron-phonon *two-field* model as well as the equivalent *effective flexural model* and compute the renormalization-group (RG) equations at this order in the effective flexural model. We determine the fixed points and the corresponding field anomalous dimensions at order  $\varepsilon^3$  and discuss them extensively. We finally use our results to benchmark those obtained within non-perturbative approaches, either re-expanded in powers of  $\varepsilon$  or directly in the physical dimensions  $d=2$ . Finally, we provide a (hopefully) exhaustive comparative table of all values obtained in the theoretical and numerical literature so far for the anomalous dimension  $\eta$ . As will be seen in the following, our analysis confirms unambiguously the order-by-order agreement between perturbative and non-perturbative approaches, that was suggested in the previous work [47]. Moreover, the value that we get for the three-loop order anomalous dimension in  $d=2$ ,  $\eta_{3\text{-loop}} = 0.8872$ , is compatible with non-perturbative results as well as results from numerical simulations. A striking feature of our results is that asymptotic series seem to be in a convergent regime, *i.e.*, the coefficients of the  $\varepsilon$  series are small and decreasing, such that setting  $\varepsilon = 1$  (physical  $d=2$  membrane in a  $D=3$  space) gives very good estimates of  $\eta$ . Soon after the publication of the three-loop results in [1], the four-loop computations have been performed in [57], obtaining  $\eta_{4\text{-loop}} = 0.8670$ , which allow us to provide even better results via the use of simple resummations and fits, yielding to our best estimates  $\eta = 0.8347$ .

## 1.2 Flat membranes model(s)

### 1.2.1 The two-field model

We consider a  $d$ -dimensional homogeneous and isotropic membrane embedded in an Euclidean  $D$ -dimensional space. Each mass point of the membrane is indexed by  $\vec{x} \in \mathbb{R}^d$ . In  $\mathbb{R}^D$ , the unperturbed state of the membrane is the flat phase where each of these mass points is indexed by  $\vec{R}^{(0)}(\vec{x}) = (\vec{x}, \vec{0}_{d_c})$  where  $\vec{0}_{d_c}$  is the null vector of dimension  $d_c = D - d$  (the co-dimension of the manifold). In the following, Latin indices will run from 1 to  $d$ , *e.g.*,  $\{a, b\} = 1, \dots, d$ . Similarly, Greek indices will run from 1 to  $d_c$ , *e.g.*,  $\{\alpha, \beta\} = 1, \dots, d_c$ .

The displacements inside the membrane are parameterized by a phonon field  $\vec{u}(\vec{x}) \in \mathbb{R}^d$  and a flexuron field  $\vec{h}(\vec{x}) \in \mathbb{R}^{d_c}$  such that the perturbed mass points are located at

$$\vec{R}(\vec{x}) = (\vec{x} + \vec{u}(\vec{x}), \vec{h}(\vec{x})), \quad (1.5)$$

which is the Monge parametrization. The induced metric is then defined as

$$g_{ab} = \partial_a \vec{R}(\vec{x}) \cdot \partial_b \vec{R}(\vec{x}), \quad (1.6)$$

where  $g_{ab}^{(0)} = \delta_{ab}$  in the unperturbed phase. To illustrate the parametrization of the membrane, we provide the figure 1.4, representing the special case of a physical membrane, *i.e.*, embedding space in  $D = 3$  and the membrane being a  $d = 2$  object (implying codimension  $d_c = D - d = 1$ ).

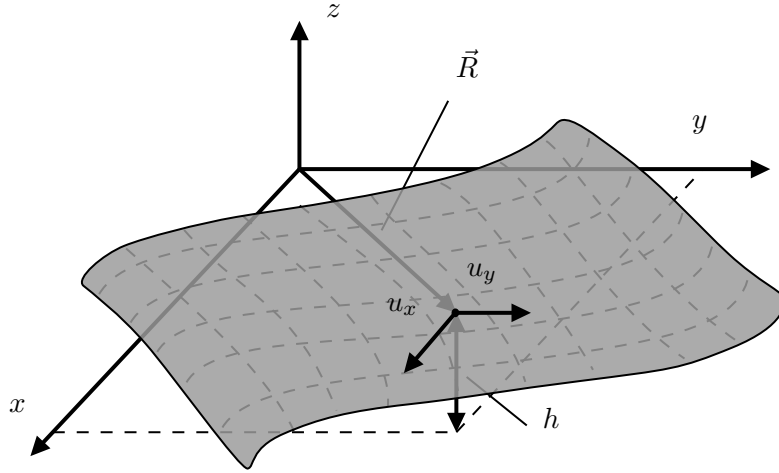


Figure 1.4: Parametrization of the membrane subject to thermal fluctuations in the physical Euclidean space, *i.e.*, embedding space in  $D = 3$ , membrane in  $d = 2$  (implying codimension  $d_c = D - d = 1$ ). For a given point of the membrane, the distance  $h$  parametrizes the height (transverse) fluctuations with respect to the reference point  $z = 0$  and  $\{u_x, u_y\}$  parametrizes the in-plane (longitudinal) fluctuations. The displaced point is then located at the new coordinates  $\vec{R} = (x + u_x, y + u_y, h)$ . Each point of the membrane, originally located at the coordinates  $\vec{x} = (x, y, 0)$ , is then fluctuating with its own quantities  $h(\vec{x})$ ,  $u_x(\vec{x})$ ,  $u_y(\vec{x})$  that we interpret as fields.

Nevertheless, in the following, we shall keep dimensions arbitrary. Indeed, since we work in dimensional regularization, we need to keep at least  $d$  arbitrary in order to perform expansions in  $d = 4 - 2\varepsilon$ . Moreover, it is also useful to keep  $d_c$  arbitrary to compare results with other methods such as large- $d_c$  techniques, see section 1.6.3.

The strain tensor  $T$  that encodes the local deformations with respect to the flat configuration  $\vec{R}^{(0)}(\vec{x}) = (\vec{x}, \vec{0}_{dc})$  is defined as

$$T_{ab} = \frac{1}{2} (g_{ab} - g_{ab}^{(0)}) = \frac{1}{2} (\partial_a \vec{R}(\vec{x}) \cdot \partial_b \vec{R}(\vec{x}) - \delta_{ab}) = \frac{1}{2} (\partial_a u_b + \partial_b u_a + \partial_a h_\alpha \partial_b h_\alpha + \partial_a u_c \partial_b u_c). \quad (1.7)$$

Neglecting the non-linearities in the phonon field (since they are irrelevant in the RG sense by simple canonical power counting) yields

$$T_{ab} \approx \frac{1}{2} (\partial_a u_b + \partial_b u_a + \partial_a h_\alpha \partial_b h_\alpha). \quad (1.8)$$

From there, the Euclidean low-energy action of the membrane, see, *e.g.*, the textbook [9], as well as [28, 29, 31–34, 47], reads

$$S[\vec{u}, \vec{h}] = \int d^d x \left[ \frac{\kappa}{2} (\partial^2 h_\alpha)^2 + \frac{\lambda}{2} T_{aa}^2 + \mu T_{ab}^2 \right], \quad (1.9)$$

where  $\kappa$  is the bending rigidity, which is not relevant in our case as it can be absorbed, by a simple rescaling of the couplings and fields. In (1.9),  $\lambda$  and  $\mu$  are the Lamé elastic moduli,  $\lambda$  being the first Lamé parameter and  $\mu$  is the shear modulus (second Lamé parameter). These two quantities will act as couplings for the field theory and are simply related to the other elastic moduli of the membrane via the relations (in arbitrary dimension)

$$\begin{aligned} \text{Bulk modulus: } B &= \lambda + 2\mu/d, & \text{Poisson ratio: } \nu &= \frac{\lambda}{(d-1)\lambda + 2\mu}, \\ \text{Young modulus: } Y &= \frac{2\mu(d\lambda + 2\mu)}{(d-1)\lambda + 2\mu}, & \text{p-wave modulus: } W &= \lambda + 2\mu. \end{aligned} \quad (1.10)$$

Using the action (1.9) in which quadratic (irrelevant in the RG sense) terms in the phonon field  $u$  are neglected, yields the expanded form<sup>1</sup>

$$\begin{aligned} S[\vec{u}, \vec{h}] &= \frac{1}{2} \int d^d x \left[ \kappa (\partial^2 h_\alpha)^2 + \lambda \left( (\partial_a u_a)^2 + \partial_a u_a (\partial_b h_\alpha)^2 + \frac{1}{4} (\partial_a h_\alpha)^4 \right) \right. \\ &\quad \left. + \mu \left( (\partial_a u_b)^2 + \partial_a u_b \partial_b u_a + 2\partial_a u_b (\partial_a h_\alpha \partial_b h_\alpha) + \frac{1}{2} (\partial_a h_\alpha \partial_b h_\beta)^2 \right) \right], \end{aligned} \quad (1.11)$$

which contains all relevant operators. Indeed, from canonical dimensional analysis, in  $d = 4 - 2\varepsilon$

$$[u] = d - 3 = 1 - 2\varepsilon, \quad [h] = \frac{d}{2} - 2 = -\varepsilon, \quad [\mu] = [\lambda] = 4 - d = 2\varepsilon. \quad (1.12)$$

In addition, a term  $(\Delta u_a)^2$  has been dropped as it is negligible in comparison with  $\lambda(\partial_a u_a)^2$  and  $\mu(\partial_a u_b)^2$  at small momenta. The action (1.11) is therefore a massless and highly derivative scalar two-field and two-coupling theory, which is very challenging computationally at high-loop order. For completeness, we provide a summary of its field content in table 1.1.

Field	index	excitations	physical deformations
$h_\alpha(x)$	$\alpha = 1, \dots, d_c = D - d$	flexurons	out-of-plan (transverse)
$u_a(x)$	$a = 1, \dots, d = 4 - 2\varepsilon$	phonons	in-plane (longitudinal)

Table 1.1: Field content of the two-field model.

<sup>1</sup>In principle, the action (1.11) should be  $O(D)$  invariant. However, we break it explicitly by neglecting irrelevant non-renormalizable interactions. What remains are the so-called linearized  $O(D)$  rotations [31]. It includes rigid fields translations,  $O(d)$  in-plane rotations,  $O(d_c)$  co-dimensional space rotations, and a set of non-local symmetries, see [58].

Instead of going further with this two field model (1.11), we will keep it aside for the next chapter, where we will perform computations in a disordered extension of this model. For the rest of this current chapter, we will consider an alternative path to obtain the results of the two-field model, which is the so-called effective flexural theory (EFT). Nevertheless, the calculation published in [1] were carried out both in the EFT and the two-field model.

### 1.2.2 Effective flexural theory (EFT)

Based on the fact that the action (1.11) is quadratic in the phonon field, we may integrate over it exactly. This leads to the so-called effective flexural theory (EFT) approach. The resulting effective action depends only on the flexuron field. In Fourier space, it reads [12, 40, 47]

$$\boxed{S_{\text{EFT}}[\vec{h}] = \frac{\kappa}{2} \int [d^d p] p^4 |h_\alpha(\vec{p})|^2 + \frac{1}{4} \int [d^d p_1][d^d p_2][d^d p_3][d^d p_4] h_\alpha(\vec{p}_1) h_\alpha(\vec{p}_2) R_{abcd}^{(0)}(\vec{p}) p_1^a p_2^b p_3^c p_4^d h_\beta(\vec{p}_3) h_\beta(\vec{p}_4),} \quad (1.13)$$

where the Euclidean momenta are  $\vec{p} = \vec{p}_1 + \vec{p}_2 = -\vec{p}_3 - \vec{p}_4$  and  $[d^d p] = d^d p / (4\pi)^d$  and obviously  $p_a p^a = p^2$ . The action (1.13) is the model we will consider in the rest of this chapter, which, in principle, is equivalent to the two-field model defined in (1.9). The rank-four tensor entering the four-flexuron term is given by

$$R_{abcd}^{(0)}(\vec{p}) = \mu M_{abcd}(\vec{p}) + b(d) N_{abcd}(\vec{p}), \quad (1.14)$$

which is a decomposition on the two  $M$  and  $N$  tensors reading

$$M_{abcd}(\vec{p}) = \frac{1}{2} \left[ P_{ac}^{(\perp)}(\vec{p}) P_{bd}^{(\perp)}(\vec{p}) + P_{ad}^{(\perp)}(\vec{p}) P_{bc}^{(\perp)}(\vec{p}) \right] - N_{abcd}(\vec{p}), \quad (1.15a)$$

$$N_{abcd}(\vec{p}) = \frac{1}{d-1} P_{ab}^{(\perp)}(\vec{p}) P_{cd}^{(\perp)}(\vec{p}), \quad P_{ab}^{(\perp)}(\vec{p}) = \delta_{ab} - \frac{p_a p_b}{p^2}. \quad (1.15b)$$

Using the definitions (1.15) it is straightforward to derive the full contractions

$$M_{abcd}(\vec{p}) M^{abcd}(\vec{p}) = \frac{(d+1)(d-2)}{2}, \quad N_{abcd}(\vec{p}) N^{abcd}(\vec{p}) = 1, \quad M_{abcd}(\vec{p}) N^{abcd}(\vec{p}) = 0, \quad (1.16)$$

from which we can define the normalized projectors

$$P_{abcd}^M(\vec{p}) = \frac{2}{(d+1)(d-2)} M_{abcd}(\vec{p}), \quad P_{abcd}^N(\vec{p}) = N_{abcd}(\vec{p}), \quad (1.17)$$

that are particularly handy to project out tensorial quantities onto their  $M$  and  $N$  components. Therefore, in the effective flexural theory, while  $\mu$ , the shear modulus, is still our first coupling, the second one is not  $\lambda$  anymore, but is replaced by  $b(d)$  that we introduced in (1.14) and reads

$$b(d) = \frac{\mu(d\lambda + 2\mu)}{\lambda + 2\mu}. \quad (1.18)$$

This new coupling is proportional to the  $d$ -dimensional bulk modulus  $B$ , or equivalently to the Young modulus  $Y$ , see (1.10), *i.e.*,

$$b(d) = \frac{\mu d}{W} B = \frac{\lambda}{2W\nu} Y. \quad (1.19)$$

Because the tensors  $M$  and  $N$  are mutually orthogonal projectors under tensor multiplication, we expect that  $\mu$  and  $b(d)$  will renormalize independently of each other. Therefore, we will consider in the following that  $\mu$  and  $b(d)$  are independent couplings. It seems that this is the correct procedure to follow. Indeed, as noticed by Gutter et al. [33], setting  $\mu = 0$  in (1.14) when expressed in terms of  $\mu$

and  $\lambda$  yields a zero vertex, *e.g.*, a free flexuron field. But we know from the two-field analysis (see the next chapter) that the  $\mu = 0$  limit leads to non-zero renormalization constants. It is by considering  $\mu$  and  $b(d)$  as independent couplings in the EFT that we shall overcome this inconsistency and match the two-field results. Moreover, we shall consider  $b(d)$  as independent of the dimension  $d$  and therefore set  $b(d) \rightarrow b$  as well as consider the co-dimension  $d_c$  fixed. For completeness, we also provide the other elastic moduli (1.10) of the membrane in terms of the new  $(\mu, b)$  variables in arbitrary dimension  $d$ , see (1.18)

$$\begin{aligned} \text{Bulk modulus: } B &= \frac{2b(d-1)\mu}{d(d\mu-b)}, & \text{Poisson ratio: } \nu &= \frac{b-\mu}{b(d-2)+\mu}, \\ \text{Young modulus: } Y &= \frac{2b(d-1)\mu}{b(d-2)+\mu}, & \text{p-wave modulus: } W &= \frac{2(d-1)\mu^2}{d\mu-b}, \end{aligned} \quad (1.20)$$

and the mechanical stability of the model is given by

$$\mu > 0, \quad b > 0. \quad (1.21)$$

In the following, we shall study the three-loop field theoretical renormalization of the model (1.13), at fixed co-dimension  $d_c$ , and near the upper critical dimension  $d_{uc} = 4$ , where the model is renormalizable [31, 33, 47]. We will work in  $d = 4 - 2\varepsilon$  and normalize all fields and coupling to remove the trivial bending rigidity,  $\kappa$ , *i.e.*

$$h_\alpha \rightarrow h_\alpha \kappa^{-1/2}, \quad \mu \rightarrow \mu \kappa^2, \quad b \rightarrow b \kappa^2, \quad (1.22)$$

which is equivalent to work in natural units and set  $\kappa = 1$  in the action (1.13). Retrospectively, we can also set  $u_a \rightarrow u_a \kappa^{-1}$  and  $\lambda \rightarrow \lambda \kappa^2$  in the original action (1.11) to get rid of  $\kappa$  in the same way.

## 1.3 Setup and conventions in the EFT

### 1.3.1 Feynman rules

The Feynman rules for the effective flexural model (1.13) can be derived using the correlation functions in Fourier space, defined via the functional derivative formula

$$\langle h_\alpha(\vec{p}_1) \cdots h_\omega(\vec{p}_n) \rangle_0 = \frac{\delta^n S_{\text{EFT}}[\vec{h}]}{\delta h_\alpha(\vec{p}_1) \cdots \delta h_\omega(\vec{p}_n)}. \quad (1.23)$$

The free massless flexuron propagator reads<sup>2</sup>

$$S_{\alpha\beta}^{(0)}(\vec{p}) = \langle h_\alpha(\vec{p}) h_\beta(-\vec{p}) \rangle_0 = \alpha \frac{\delta_{\alpha\beta}}{\vec{p}} \beta = \frac{\delta_{\alpha\beta}}{p^4}, \quad (1.24)$$

where  $\{\alpha, \beta\} = 1, \dots, d_c$  and the four-point flexuron vertex reads

$$V_{\alpha\beta\gamma\delta}^{(0)}(\vec{p}_1, \dots, \vec{p}_4) = \langle h_\alpha(\vec{p}_1) h_\beta(\vec{p}_2) h_\gamma(\vec{p}_3) h_\delta(\vec{p}_4) \rangle_0 = \begin{array}{c} \alpha \vec{p}_1 \\ \diagdown \\ \bullet \\ \diagup \\ \beta \vec{p}_2 \end{array} \text{---} \begin{array}{c} \delta \vec{p}_4 \\ \diagup \\ \bullet \\ \diagdown \\ \gamma \vec{p}_3 \end{array} \begin{array}{c} \vec{p} \\ \text{---} \\ \vec{p} \end{array} = -2R_{abcd}^{(0)}(\vec{p}) \delta_{\alpha\beta} \delta_{\gamma\delta} p_1^a p_2^b p_3^c p_4^d, \quad (1.25)$$

where  $\{a, b, c, d\} = 1, \dots, d$ . In (1.25), the front factor,  $-2$ , is made of three contributions. First, the usual minus associated with quartic interactions. Second, the  $1/4$  factor in the action (1.13). And

<sup>2</sup>In principle, the flexuron propagator is semi-massive, reading  $S_{\alpha\beta}^{(0)} = \delta_{\alpha\beta} / ((p^2 + m^2)p^2)$ . However the mass is not affecting the anomalous dimensions and the massless limit (1.24) is enough to access criticality, see related footnote 3.

third, the vertex factor, which is 8, so that  $-8/4 = -2$ . Let us remark that the vertex factor is indeed 8 and not  $4! = 24$ , as one might expect. This is due to the apparent asymmetry of the four-point coupling  $V_{\alpha\beta\gamma\delta}^{(0)}(\vec{p}_1, \vec{p}_2, \vec{p}_3, \vec{p}_4)$  that couple only bi-flexuron pairs. We represent graphically this particularity with a dashed line carrying momentum  $\vec{p} = \vec{p}_1 + \vec{p}_2 = -\vec{p}_3 - \vec{p}_4$  (all momenta are incoming).

In order to emphasize this asymmetry of the four-point coupling, one can decompose it and define new Feynman rules based on a three-point vertex. While the free flexuron propagator is kept identical, the vertex interaction is decomposed in two parts, the effective free  $R$ -propagator

$$R_{abcd}^{(0)}(\vec{p}) = ab \text{-----} cd = \mu M_{abcd}(\vec{p}) + b N_{abcd}(\vec{p}), \quad (1.26)$$

and a three-point interaction reading

$$\Gamma_{\alpha\beta}^{ab(0)}(\vec{p}_1, \vec{p}_2) = \begin{array}{c} \alpha \vec{p}_1 \\ \diagdown \\ \bullet \\ \diagup \\ \beta \vec{p}_2 \end{array} \text{-----} ab \vec{p}_3 = i\sqrt{2}\delta_{\alpha\beta} p_1^a p_2^b. \quad (1.27)$$

The factor  $i\sqrt{2}$  is designed in such a way that  $(i\sqrt{2})^2 = -8/4 = -2$  from (1.25). Therefore, the four-point interaction (vertex factor 8) is equivalent to a multiplication of two three-point interactions (vertex factor 2) and an effective  $R$ -propagator, *i.e.*

$$V_{\alpha\beta\gamma\delta}^{(0)}(\vec{p}_1, \vec{p}_2, \vec{p}_3, \vec{p}_4) = \Gamma_{\alpha\beta}^{ab(0)}(\vec{p}_1, \vec{p}_2) R_{abcd}^{(0)}(\vec{p}) \Gamma_{\gamma\delta}^{cd(0)}(\vec{p}_3, \vec{p}_4), \quad (1.28)$$

where  $\vec{p} = \vec{p}_1 + \vec{p}_2 = -\vec{p}_3 - \vec{p}_4$ . With these definitions, the two sets of Feynman rules are equivalent. The second set of Feynman rules, based on the three-point interaction (1.27) and the effective propagator (1.26), becomes very handy when noticing that every diagram will be exactly similar to, *e.g.*, QED, provided that one identifies the  $R$ -propagators with photons, and flexurons with fermions (as well as stripping off the legs in the four-point vertices to consider only the  $R$ -propagator ‘‘polarization’’ and identify it to a photon polarization). Thanks to this identification, we can conveniently automate the generation of the diagram expressions using codes very similar to QED (see the second part of this thesis), based on the use of the Fortran tool QGRAF [59, 60]. This is also why we use QED-like notations, *i.e.*,  $S$  and  $\Gamma$  for the Feynman rules as well as  $\Sigma$  and  $\Pi$  respectively for the self-energies and polarizations, see *e.g.*, [61]. The drawback of the use of the three-point Feynman rules is that it results in more contractions over the Euclidean space (Latin) indices to be performed, see (1.28). However, it is not an issue since we carry all our computations in a completely automated way using MATHEMATICA, with homemade codes to perform efficiently the contractions.

### 1.3.2 Fate of infra-red divergences

The form of the flexuron propagator ( $\sim 1/p^4$ ), see (1.24), suggests that the theory may be plagued by severe infra-red (IR) singularities, thus invalidating the renormalization prescription. It turns out that this is fortunately not the case and that the renormalization constants are determined by ultraviolet (UV) poles only.

In order to prove this statement in a non-perturbative way, let us temporarily define  $dh_\alpha^j(\vec{x}) = \partial_j h_\alpha(\vec{x})$  and its corresponding correlation function

$$G_{\alpha\beta}(\vec{p}) = \langle dh_\alpha^j(\vec{p}) dh_\beta^j(-\vec{p}) \rangle. \quad (1.29)$$

Obviously,  $G_{\alpha\beta}(\vec{p})$  is an IR-safe function with respect to loop integrals. It turns out that it is simply related to the flexuron propagator,  $S_{\alpha\beta}(\vec{p}) = \langle h_\alpha(\vec{p}) h_\beta(-\vec{p}) \rangle$  and the relation reads

$$G_{\alpha\beta}(\vec{p}) = p^2 S_{\alpha\beta}(\vec{p}). \quad (1.30)$$

This simple identity shows that the flexuron propagator is directly related to an IR-safe quantity. Hence, it is itself IR-safe.

At a more practical level, IR singularities do show up in the course of computing  $S_{\alpha\beta}(\vec{p})$ . Their appearance is due to the ambiguous nature of the massless tadpole, which is zero in dimensional regularization as a consequence of a subtle cancellation between IR and UV singularities. However, because the flexuron propagator is IR-safe these IR poles are harmless and do not require any special treatment as they simply cancel each-other order by order in perturbation theory. In this case, we may proceed with dimensional regularization in the conventional way as if all poles were of UV type, see, *e.g.*, [62] for a proof of this statement.

### 1.3.3 Dyson equations

We shall consider the Dyson equation for the dressed flexuron propagator reading

$$S_{\alpha\beta}(\vec{p}) = S_{\alpha\beta}^{(0)}(\vec{p}) + S_{\alpha\gamma}^{(0)}(\vec{p})\Sigma_{\gamma\delta}(\vec{p})S_{\delta\beta}(\vec{p}), \quad (1.31)$$

where  $\Sigma_{\alpha\beta}(\vec{p})$  is the 1-particle irreducible flexuron self-energy,  $S_{\alpha\beta}$  is the fully dressed flexuron propagator and  $S_{\alpha\beta}^{(0)}$  is its approximation at tree order, (1.24). It is convenient to project these quantities in a way consistent with their tensorial structure, reading

$$S_{\alpha\beta}(\vec{p}) = \delta_{\alpha\beta}S(\vec{p}), \quad \Sigma_{\alpha\beta}(\vec{p}) = \delta_{\alpha\beta}\Sigma(\vec{p}). \quad (1.32)$$

Then, the Dyson equation can be rearranged, yielding (forgetting about the momentum dependencies)

$$\begin{aligned} S &= S^{(0)} + S^{(0)}\Sigma S \\ &= S^{(0)} + S^{(0)}\Sigma S^{(0)} + S^{(0)}\Sigma S^{(0)}\Sigma S^{(0)} + \dots \\ &= S^{(0)}(1 + \Sigma S^{(0)} + (\Sigma S^{(0)})^2 + \dots) = \frac{S^{(0)}}{1 - \Sigma S^{(0)}}, \end{aligned} \quad (1.33)$$

and since  $S^{(0)}(p) = p^{-4}$ , it reads

$$S(\vec{p}) = \frac{1}{p^4} \frac{1}{1 - \tilde{\Sigma}(p^2)}, \quad \tilde{\Sigma}(p^2) = p^{-4}\Sigma(\vec{p}). \quad (1.34)$$

Similarly, the four-point vertex may be expressed with the help of the dressed  $R$ -propagator  $R_{abcd}(\vec{p})$  assuming that, to all orders, the following holds

$$\begin{aligned} V_{\alpha\beta\gamma\delta}(\vec{p}_1, \vec{p}_2, \vec{p}_3, \vec{p}_4) &= \Gamma_{\alpha\beta}^{ab(0)}(\vec{p}_1, \vec{p}_2)R_{abcd}(\vec{p})\Gamma_{\gamma\delta}^{cd(0)}(\vec{p}_3, \vec{p}_4) \\ &= -2R_{abcd}(\vec{p})\delta_{\alpha\beta}\delta_{\gamma\delta}p_1^a p_2^b p_3^c p_4^d. \end{aligned} \quad (1.35)$$

This implies that all corrections are in  $R_{abcd}(\vec{p})$  which satisfies the following Dyson equation

$$R_{abcd}(\vec{p}) = R_{abcd}^{(0)}(\vec{p}) + R_{abef}^{(0)}(\vec{p})\Pi_{efgh}(\vec{p})R_{ghcd}(\vec{p}), \quad (1.36)$$

where  $\Pi_{abcd}(\vec{p})$  is a 1-particle irreducible self-energy of the effective  $R$ -propagator, *i.e.*, corresponding to a vacuum polarization. As will be shown in the following, the fact that the Dyson equation for the four-point vertex is entirely encapsulated in (1.36) is not an approximation and allows reproducing exactly the non-trivial two-field results (see the results of the next chapter, where computations are carried out in the two-field model, in the more general disordered case). This also reinforces the use of the second set of Feynman rules that consist of a free flexuron propagator, a free  $R$ -propagator and the triple vertex made of a  $R$ -propagator and two flexuron propagators. At this point, it is convenient



to decompose the polarization operator and the vertex function on the basis of the tensors  $M$  and  $N$  (1.15) in order to solve the Dyson equation for the  $R$ -propagator (1.36). This yields

$$R_{abcd}(\vec{p}) = R_M(\vec{p})M_{abcd}(\vec{p}) + R_N(\vec{p})N_{abcd}(\vec{p}), \quad (1.37a)$$

$$\Pi_{abcd}(\vec{p}) = \Pi_M(\vec{p})M_{abcd}(\vec{p}) + \Pi_N(\vec{p})N_{abcd}(\vec{p}). \quad (1.37b)$$

Following a similar procedure as for the flexuron propagator, the dressed  $R$ -propagator decomposes as

$$R_M(\vec{p}) = \frac{\mu}{1 - \tilde{\Pi}_M(\vec{p})}, \quad \tilde{\Pi}_M(\vec{p}) = \mu\Pi_M(\vec{p}), \quad (1.38a)$$

$$R_N(\vec{p}) = \frac{b}{1 - \tilde{\Pi}_N(\vec{p})}, \quad \tilde{\Pi}_N(\vec{p}) = b\Pi_N(\vec{p}). \quad (1.38b)$$

### 1.3.4 Renormalization conventions

We are now in a position to introduce the renormalization constants associated with the effective flexural model (1.13)

$$\vec{h} = Z^{1/2}\vec{h}_r, \quad \mu = Z_\mu\mu_r M^{2\varepsilon}, \quad b = Z_b b_r M^{2\varepsilon}, \quad (1.39)$$

where the subscript  $r$  denotes renormalized quantities and the renormalization scale,  $M$ , has been introduced in such a way that  $\mu_r$  and  $b_r$  are dimensionless in  $d = 4 - 2\varepsilon$  dimensions. The latter is related to the corresponding parameter  $\overline{M}$  in the modified minimal subtraction ( $\overline{\text{MS}}$ ) scheme with the help of

$$\overline{M}^2 = 4\pi e^{-\gamma_E} M^2, \quad (1.40)$$

where  $\gamma_E$  is Euler's constant. In the MS scheme, the renormalization constants take the form of a Laurent series in  $\varepsilon$

$$Z_x(\mu_r, b_r) = 1 + \delta Z_x(\mu_r, b_r) = 1 + \sum_{l=1}^{\infty} \sum_{j=1}^l Z_x^{(l,j)}(\mu_r, b_r) \frac{1}{\varepsilon^j}, \quad (1.41)$$

where  $x \in \{\mu, b\}$  and they do not depend on momentum (or mass which is absent in the present model). Furthermore, the dependence on  $M$  is only through  $\mu_r$  and  $b_r$ . So the renormalization constants  $Z_x$  depend only on  $\mu_r(M)$ ,  $b_r(M)$  and  $\varepsilon$ . They also relate renormalized and bare propagators as follows

$$S_{\alpha\beta}(\vec{p}; \mu, b) = Z(\mu_r, b_r) S_{\alpha\beta,r}(\vec{p}; \mu_r, b_r, M), \quad (1.42a)$$

$$R_{abcd}(\vec{p}; \mu, b) = M^{2\varepsilon} Z^{-2}(\mu_r, b_r) R_{abcd,r}(\vec{p}; \mu_r, b_r, M), \quad (1.42b)$$

where the bare propagators do not depend on  $M$ . Then, decomposing into their respective tensors,  $\delta$ ,  $M$  and  $N$ , and forgetting about the functional dependencies, it reads

$$S = ZS_r \quad R_M = M^{2\varepsilon} Z^{-2} R_{M,r}, \quad R_N = M^{2\varepsilon} Z^{-2} R_{N,r}. \quad (1.43)$$

We may now explain our renormalization technique, *i.e.*, our method to determine the renormalization constants  $\{Z, Z_\mu, Z_b\}$ . It has to be underlined here that we are not using counter terms, or any other advanced renormalization method. Instead, for the whole manuscript, we will use a more pragmatic approach and directly derive relations relating the renormalization constants  $\{Z, Z_\mu, Z_b\}$  to the self-energy and polarization  $\{\Sigma, \Pi_M, \Pi_N\}$ , using respectively the propagators  $\{S, R_M, R_N\}$ . Let us detail this procedure once, *e.g.*, for the flexuron. Using the renormalization definitions (1.43) and the Dyson equation (1.34) reads

$$S = ZS_r \quad \implies \quad \frac{1}{p^4} \frac{1}{1 - \tilde{\Sigma}} = Z \frac{1}{p^4} \frac{1}{1 - \tilde{\Sigma}_r}. \quad (1.44)$$



Rearranging the equation and gather renormalized quantities on the left-hand side yields

$$\tilde{\Sigma}_r = 1 - (1 - \tilde{\Sigma})Z. \quad (1.45)$$

This relation is crucial as it allows to completely determine  $Z$  once  $\tilde{\Sigma}$  has been computed, since the left-hand side must be finite. Mathematically, this is achieved using the fact that  $\mathcal{K}[\tilde{\Sigma}_r(\vec{p})] = 0$ , where  $\mathcal{K}$  is the operator used to take the divergent part of the series, defined formally as

$$\mathcal{K} \left[ \sum_{n=-\infty}^{+\infty} \frac{c_n}{\varepsilon^n} \right] = \sum_{n=1}^{+\infty} \frac{c_n}{\varepsilon^n}. \quad (1.46)$$

It yields the relation

$$0 = \mathcal{K}[(1 - \tilde{\Sigma})Z], \quad (1.47)$$

which is the definition of  $Z$  as a function of  $\tilde{\Sigma}$ , order by order. Indeed, taking the parametrization,

$$\tilde{\Sigma} = \tilde{\Sigma}_1 + \tilde{\Sigma}_2 + \tilde{\Sigma}_3 + \dots, \quad (1.48a)$$

$$Z = 1 + \delta Z_1 + \delta Z_2 + \delta Z_3 + \dots, \quad (1.48b)$$

and solving (1.47) order by order in the loop expansion completely defines  $Z$  recursively as a function of  $\tilde{\Sigma}$ , yielding up to three loops

$$\text{1-loop: } \delta Z_1 = \mathcal{K}(\tilde{\Sigma}_1), \quad (1.49a)$$

$$\text{2-loop: } \delta Z_2 = \mathcal{K}(\delta Z_1 \tilde{\Sigma}_1) + \mathcal{K}(\tilde{\Sigma}_2), \quad (1.49b)$$

$$\text{3-loop: } \delta Z_3 = \mathcal{K}(\delta Z_2 \tilde{\Sigma}_1) + \mathcal{K}(\delta Z_1 \tilde{\Sigma}_2) + \mathcal{K}(\tilde{\Sigma}_3). \quad (1.49c)$$

This efficient renormalization technique greatly reduces the number of diagrams to be computed as compared to the traditional counter term technique.

Similarly, the computation of the renormalization constants  $Z_\mu$  and  $Z_b$  are derived from the renormalization of the vertex parts. From (1.37) and (1.39), we have

$$\tilde{\Pi}_{M,r}(\vec{p}) = 1 + \left(1 - \tilde{\Pi}_M(\vec{p})\right) Z_{\Gamma_\mu}^{-1}, \quad (1.50a)$$

$$\tilde{\Pi}_{N,r}(\vec{p}) = 1 + \left(1 - \tilde{\Pi}_N(\vec{p})\right) Z_{\Gamma_b}^{-1}, \quad (1.50b)$$

where we have introduced two intermediate renormalization functions

$$Z_{\Gamma_\mu} = Z_\mu Z^2, \quad Z_{\Gamma_b} = Z_b Z^2. \quad (1.51)$$

Then, similarly to the above procedure for  $Z$ , using the fact that  $\mathcal{K}[\tilde{\Pi}_{M,r}(\vec{p})] = 0$  and  $\mathcal{K}[\tilde{\Pi}_{N,r}(\vec{p})] = 0$ , it is possible to extract the general expression of  $Z_{\Gamma_\mu}$  and  $Z_{\Gamma_b}$

$$0 = \mathcal{K} \left[ \left(1 - \tilde{\Pi}_M(\vec{p})\right) Z_{\Gamma_\mu}^{-1} \right], \quad (1.52a)$$

$$0 = \mathcal{K} \left[ \left(1 - \tilde{\Pi}_N(\vec{p})\right) Z_{\Gamma_b}^{-1} \right]. \quad (1.52b)$$

By combining (1.52) with the expression of  $Z$  (1.49), we are able to deduce  $Z_\mu$  and  $Z_b$  from (1.51).

Once the renormalization constants are determined, we shall compute the renormalization-group functions reading

$$\beta_\mu = \left. \frac{d\mu_r}{d\log M} \right|_B, \quad \beta_b = \left. \frac{db_r}{d\log M} \right|_B, \quad \eta = \left. \frac{d\log Z}{d\log M} \right|_B, \quad (1.53)$$

where the subscript  $B$  indicates that bare parameters, which do not depend on the renormalization scale  $M$ , are fixed. More explicitly, the system of beta functions to be solved perturbatively is

$$\beta_\mu = -2\varepsilon\mu_r - \mu_r\mathcal{D}Z_\mu, \quad (1.54a)$$

$$\beta_b = -2\varepsilon b_r - b_r\mathcal{D}Z_b, \quad (1.54b)$$

where we introduced the differential operator

$$\mathcal{D}X = \beta_\mu \frac{\partial \log X}{\partial \mu_r} + \beta_b \frac{\partial \log X}{\partial b_r}. \quad (1.55)$$

The solution to the linear beta system is then, in matrix form

$$\begin{pmatrix} \beta_\mu \\ \beta_b \end{pmatrix} = -2\varepsilon \begin{pmatrix} \mu_r \frac{\partial \log \mu_r Z_\mu}{\partial \mu_r} & \mu_r \frac{\partial \log \mu_r Z_\mu}{\partial b_r} \\ b_r \frac{\partial \log b_r Z_b}{\partial \mu_r} & b_r \frac{\partial \log b_r Z_b}{\partial b_r} \end{pmatrix}^{-1} \begin{pmatrix} \mu_r \\ b_r \end{pmatrix}. \quad (1.56)$$

Finally, the field anomalous dimension associated with the flexuron field reads<sup>3</sup>

$$\eta = \mathcal{D}Z. \quad (1.57)$$

Let us recall that, physically, it corresponds to the anomalous stiffness induced by long-range correlations, such that the dressed flexuron propagator scales in the IR as

$$S(p) = \langle h_r(p)h_r(-p) \rangle \sim p^{-(4-\eta)}. \quad (1.58)$$

Upon solving perturbatively the RG-functions (1.54) and (1.57), it is well known that all of them are determined only by the coefficients of the simple poles of the renormalization constants. However, in the following we shall use a more pragmatic approach, consisting in computing the RG-functions ( $\beta_\mu$ ,  $\beta_b$ ,  $\eta$ ) directly with the complete (containing all kinds of poles) expressions of the renormalization constants ( $Z$ ,  $Z_\mu$ ,  $Z_b$ ). Then, if the RG-functions are finite (pole free), it implies that the full set of constraints is verified. The finiteness of the RG-functions constitutes a strong check of the results, together with the locality of the renormalization constants (no momentum dependency).

Finally, once the RG functions ( $\beta_\mu$ ,  $\beta_b$ ,  $\eta$ ) have been determined as a function of the renormalized couplings  $\mu_r$  and  $b_r$ , we will search for the fixed points of the theory. Indeed, since the beta functions characterize the scaling of the coupling with respect to the renormalization scale  $M$ , one can search for the specific points where the theory is scale invariant, *i.e.*, by solving the system

$$\beta_\mu(\mu^*, b^*) = 0, \quad \beta_b(\mu^*, b^*) = 0, \quad (1.59)$$

and obtain various fixed point coordinates  $(\mu^*, b^*)$  where the theory exhibits universal scaling behaviors and such that  $\eta(\mu^*, b^*)$  is a universal number characterizing the corresponding phase, *i.e.*, a critical exponent. Since canceling one of the couplings leads to trivial solutions, we expect to find 4 types of fixed points. First, a trivial Gaussian fixed point ( $P_1$ ) where  $\mu_1^* = b_1^* = 0$  such that the theory is non-interacting. Second, a shearless fixed point ( $P'_2$ ) (which we call  $P'_2$  instead of  $P_2$  because this name will be used in the two-field model), where  $\mu_2^* = 0$  and  $b_2^* \neq 0$ . Third, a fixed point  $P_3$  with  $\mu_3^*$  and  $b_3^* = 0$ , *i.e.*, a vanishing bulk modulus (infinitely compressible). And finally, a fourth, non-trivial fixed point ( $P_4$ ) where both couplings are non-zero,  $\mu_4^* \neq 0$  and  $b_4^* \neq 0$  which is the most interesting since it corresponds to the fully interacting theory. Moreover, the mechanical stability of the membranes, see (1.21), requires a positive shear modulus  $\mu^* > 0$  as well as a positive bulk modulus  $\lambda^* + 2\mu^*/d > 0$ ,

<sup>3</sup>The mass anomalous dimension  $\eta_m$  is trivial and reads  $\eta_m = 4 - d - \eta$ . See related footnote 2.

*i.e.*,  $b^* > 0$ . The RG stability of these fixed points can be studied by searching the eigenvalues of the stability matrix

$$\mathcal{S} = \begin{pmatrix} d\beta_\mu/d\mu_r & d\beta_\mu/db_r \\ d\beta_b/d\mu_r & d\beta_b/db_r \end{pmatrix}, \quad (1.60)$$

such that positive (respectively negative) eigenvalues indicates an IR stable (respectively unstable) fixed point. We recall that an IR stable fixed point is attractive as the theory renormalizes down to the IR and therefore controls the long range behavior of the model.

The questions are then the following. Are these fixed point existing? If so, are they located in the mechanically stable region? Which one is stable or unstable in the RG sense? And finally, how are these properties modified under higher-loop corrections, *i.e.*, at two, and three-loop order? Answering these questions will allow us to completely characterize the RG flow of the model and access its long-range properties.

## 1.4 Perturbative calculations up to three loops in the EFT

In this section, we compute the renormalization constants of the model  $Z, Z_\mu$  and  $Z_b$ , (1.39), at one, two and three-loop order. To do so, we compute order by order all the Feynman diagrams entering the self-energy of the flexuron propagator (1.34) and the polarization of the  $R$ -propagator (1.36).

### 1.4.1 One-loop analysis

The one-loop, two-point and four-point self-energy diagrams are displayed on figure 1.5, with their corresponding symmetry factors (S).



(a) Flexuron self-energy  $\Sigma_{\alpha\beta}^{(1)}(\vec{p})$ ,  $S = 1$ . (b) Vertex self-energy  $V_{\alpha\beta\gamma\delta}^{(1)}(\vec{p}_1, \vec{p}_2, \vec{p}_3, \vec{p}_4)$ ,  $S = 1/2$ .

Figure 1.5: One-loop diagrams and their associated symmetry factors (S).

### One-loop flexuron self-energy

The one-loop flexuron self-energy, figure 1.5a, has a symmetry factor of 1 and is defined as

$$\Sigma_{\alpha\beta}^{(1)}(\vec{p}) = \alpha \text{---} \begin{array}{c} \vec{p}-\vec{k} \\ \text{---} \\ \vec{p} \quad \vec{k} \end{array} \text{---} \beta = 1 \times \int [d^d k] V_{\alpha\alpha_1\beta_1\beta}^{(0)}(\vec{p}, -\vec{k}, \vec{k}, -\vec{p}) S_{\alpha_1\beta_1}^{(0)}(\vec{k}), \quad (1.61)$$

or equivalently with the second set of Feynman rules

$$\Sigma_{\alpha\beta}^{(1)}(\vec{p}) = 1 \times \int [d^d k] \Gamma_{\alpha\alpha_1}^{ab(0)}(\vec{p}, -\vec{k}) R_{abcd}^{(0)}(\vec{p}-\vec{k}) \Gamma_{\beta_1\beta}^{cd(0)}(\vec{k}, -\vec{p}) S_{\alpha_1\beta_1}^{(0)}(\vec{k}). \quad (1.62)$$

After using one of the two equivalent sets of Feynman rules and contracting part of the internal indices, the one-loop flexuron self-energy reads

$$\Sigma_{\alpha\beta}^{(1)}(\vec{p}) = -2\delta_{\alpha\beta} p^a p^b \int \frac{[d^d k]}{k^4} k^c k^d R_{abcd}^{(0)}(\vec{p}-\vec{k}). \quad (1.63)$$

The latter can be expressed in terms of the one-loop  $J$ -function, defined in Appendix A, and yields

$$\tilde{\Sigma}^{(1)}(p^2) = -\frac{(b+(d-2)\mu)}{8(d-1)} \left( 4J(d, \vec{p}, 1, 1) - 8p^2 J(d, \vec{p}, 2, 1) + p^4 J(d, \vec{p}, 2, 2) \right), \quad (1.64)$$

where we dropped all one-loop  $J$ -functions containing null or negative indices, since they are equally zero, see (A.14) in Appendix A. Then using the techniques of integration by part (IBP) reduction [63–65] discussed in Appendix A, we may express the remaining  $J$ -functions on a reduced basis of master integrals, the latter taking only ones and zeros as arguments, *i.e.*, in this simple case

$$J(d, \vec{p}, 2, 1) = -p^{-2}(d-3)J(d, \vec{p}, 1, 1), \quad (1.65a)$$

$$J(d, \vec{p}, 2, 2) = p^{-4}(d-6)(d-3)J(d, \vec{p}, 1, 1), \quad (1.65b)$$

which then reads

$$\tilde{\Sigma}^{(1)}(p^2) = -\frac{(b+(d-2)\mu)}{8(d-1)} \frac{(p^2)^{d/2-2}}{(4\pi)^{d/2}} (d+1)(d-2)G(d, 1, 1), \quad (1.66)$$

where  $g(d, \alpha, \beta)$  is the dimensionless master integral at one loop, also defined in Appendix A. Note that due to the presence of a  $d$ -dependent combination of coupling constants in (1.66), the intuitive combination  $b+2\mu$  does not factor in the expanded expression, and the finite term gets a non-trivial combination of coupling constants.

Upon expanding (1.66) in  $\varepsilon$ -series, the one-loop flexuron self-energy in  $\overline{\text{MS}}$ -scheme then reads

$$\tilde{\Sigma}^{(1)}(p^2) = \frac{5(b+2\mu)}{12(4\pi)^2 M^{2\varepsilon}} \left( \frac{-1}{\varepsilon} + L_p - \frac{4}{15} - \frac{b}{b+2\mu} + \text{O}(\varepsilon) \right), \quad (1.67)$$

where  $L_p = \log(p^2/\overline{M}^2)$ . Note that we display here only the first terms of the series expansion to keep it light. However, more terms of this expansion will be needed in the next sections in order to renormalize properly the theory to higher loops. Indeed, this is due to our renormalization method that does not require counter terms but instead makes uses of all previously computed diagrams expanded to higher orders. In general, at a given  $L$ -loop order, the diagrams of loop order  $l < L$  have to be expanded up to  $\text{O}(\varepsilon^{L-l-1})$  in order to compute the  $L$ -loop RG-functions and up to  $\text{O}(\varepsilon^{L-l})$  in order to compute the renormalized self-energies and polarizations. In the case of (1.67), one therefore needs to reach the term of  $\text{O}(\varepsilon)$  to be able to compute the three-loop RG-functions and up to  $\text{O}(\varepsilon^2)$  to compute the renormalized three-loop self-energies and polarizations in the latter stages of this work, see section 1.4.3.

Combining (1.67) and (1.49) yields the one-loop field renormalization constant

$$\delta Z^{(1)} = \mathcal{K} \left[ \tilde{\Sigma}^{(1)}(p^2) \right] = -\frac{5(b_r + 2\mu_r)}{12(4\pi)^2 \varepsilon}, \quad (1.68)$$

where we performed the trivial replacements  $\mu \rightarrow M^{2\varepsilon} \mu_r$  and  $b \rightarrow M^{2\varepsilon} b_r$ , that is enough at this order. Also, using (1.68) as well as the first terms of the expansion of (1.45), we have straightforward access to the renormalized flexuron self-energy

$$\tilde{\Sigma}_r^{(1)} = \tilde{\Sigma}^{(1)} - \delta Z^{(1)} = \frac{5(b_r + 2\mu_r)}{12(4\pi)^2} \left( L_p - \frac{4}{15} - \frac{b_r}{b_r + 2\mu_r} + \text{O}(\varepsilon) \right), \quad (1.69)$$

which, at this order, is trivially equal to (1.67) with bare quantities being renormalized and the pole removed.

### One-loop vertex self-energy

The one-loop vertex self-energy, figure 1.5b, has a symmetry factor of 1/2 and is defined as

$$V_{\alpha\beta\gamma\delta}^{(1)}(\vec{p}_1, \vec{p}_2, \vec{p}_3, \vec{p}_4) = \begin{array}{c} \alpha \vec{p}_1 \\ \vec{p} - \vec{k} \\ \delta \vec{p}_4 \\ \vec{p} \\ \vec{p} \\ \beta \vec{p}_2 \\ \vec{k} \\ \gamma \vec{p}_3 \end{array} = \frac{1}{2} \int [d^d k] V_{\alpha\beta\gamma_1\delta_1}^{(0)}(\vec{p}_1, \vec{p}_2, -\vec{k}, -\vec{p} + \vec{k}) S_{\delta_1\alpha_1}^{(0)}(\vec{p} - \vec{k}) \\ \times S_{\gamma_1\beta_1}^{(0)}(\vec{k}) V_{\alpha_1\beta_1\gamma\delta}^{(0)}(\vec{p} - \vec{k}, \vec{k}, \vec{p}_3, \vec{p}_4), \quad (1.70)$$

where all  $p_i$  are defined in-going, *i.e.*,  $\vec{p} = \vec{p}_1 + \vec{p}_2 = -\vec{p}_3 - \vec{p}_4$ . This diagram can equivalently be expressed with the second set of Feynman rules

$$V_{\alpha\beta\gamma\delta}^{(1)}(\vec{p}_1, \vec{p}_2, \vec{p}_3, \vec{p}_4) = \frac{1}{2} \int [d^d k] \Gamma_{\alpha\beta}^{ab(0)}(\vec{p}_1, \vec{p}_2) R_{abcd}^{(0)}(\vec{p}) \Gamma_{\delta_1\gamma_1}^{cd(0)}(-\vec{p} + \vec{k}, -\vec{k}) \\ \times S_{\delta_1\alpha_1}^{(0)}(\vec{p} - \vec{k}) S_{\gamma_1\beta_1}^{(0)}(\vec{k}) \Gamma_{\alpha_1\beta_1}^{ef(0)}(\vec{p} - \vec{k}, \vec{k}) R_{efgh}^{(0)}(\vec{p}) \Gamma_{\gamma\delta}^{gh(0)}(\vec{p}_3, \vec{p}_4), \quad (1.71)$$

which make obvious the factorization of the external legs out of the integration, *i.e.*

$$V_{\alpha\beta\gamma\delta}^{(1)}(\vec{p}_1, \vec{p}_2, \vec{p}_3, \vec{p}_4) = \Gamma_{\alpha\beta}^{ab(0)}(\vec{p}_1, \vec{p}_2) R_{abcd}^{(0)}(\vec{p}) \left[ \frac{1}{2} \int [d^d k] \Gamma_{\delta_1\gamma_1}^{cd(0)}(-\vec{p} + \vec{k}, -\vec{k}) \right. \\ \left. \times S_{\delta_1\alpha_1}^{(0)}(\vec{p} - \vec{k}) S_{\gamma_1\beta_1}^{(0)}(\vec{k}) \Gamma_{\alpha_1\beta_1}^{ef(0)}(\vec{p} - \vec{k}, \vec{k}) \right] R_{efgh}^{(0)}(\vec{p}) \Gamma_{\gamma\delta}^{gh(0)}(\vec{p}_3, \vec{p}_4). \quad (1.72)$$

Here, the central term, in the brackets, is by definition the polarization operator  $\Pi_{cdef}^{(1)}(\vec{p})$ . This procedure holds at all loop orders since only the polarization operator is taking loop corrections

$$V_{\alpha\beta\gamma\delta}^{(L)}(\vec{p}_1, \vec{p}_2, \vec{p}_3, \vec{p}_4) = \Gamma_{\alpha\beta}^{ab(0)}(\vec{p}_1, \vec{p}_2) R_{abcd}^{(0)}(\vec{p}) \Pi_{cdef}^{(L)}(\vec{p}) R_{efgh}^{(0)}(\vec{p}) \Gamma_{\gamma\delta}^{gh(0)}(\vec{p}_3, \vec{p}_4), \quad (1.73)$$

where  $L$  stands for the  $L$ -loop order. Using the Feynman rules and performing the contractions yields the one-loop integral

$$\Pi_1^{cdef}(\vec{p}) = -d_c \int \frac{[d^d k]}{k^4 (\vec{p} - \vec{k})^4} (\vec{p} - \vec{k})^c k^d (\vec{p} - \vec{k})^e k^f. \quad (1.74)$$

Then we are able to project the polarization on the basis of the  $M$  and  $N$  tensors, using a full contraction with the normalized projectors defined in (1.17). It reads

$$\Pi_M^{(1)}(p^2) = P_{abcd}^M \Pi_{abcd}^{(1)}, \quad (1.75a)$$

$$\Pi_N^{(1)}(p^2) = P_{abcd}^N \Pi_{abcd}^{(1)}. \quad (1.75b)$$

Performing the contractions, reduction and integration, yields

$$\tilde{\Pi}_M^{(1)}(p^2) = -\frac{d_c \mu}{8} \frac{(p^2)^{d/2-2}}{(4\pi)^{d/2}} \frac{d-2}{d-1} G(d, 1, 1), \quad (1.76a)$$

$$\tilde{\Pi}_N^{(1)}(p^2) = -\frac{d_c b}{16} \frac{(p^2)^{d/2-2}}{(4\pi)^{d/2}} \frac{(d-2)(d+1)}{d-1} G(d, 1, 1), \quad (1.76b)$$

where  $\tilde{\Pi}_M^{(1)}(p^2)$  and  $\tilde{\Pi}_N^{(1)}(p^2)$  were defined in (1.37). In expanded form, the one-loop polarization operator in the  $\overline{\text{MS}}$ -scheme then reads

$$\tilde{\Pi}_M^{(1)}(p^2) = \frac{d_c \mu}{12(4\pi M^\epsilon)^2} \left( -\frac{1}{\epsilon} + L_p - \frac{5}{3} + \text{O}(\epsilon) \right), \quad (1.77a)$$

$$\tilde{\Pi}_N^{(1)}(p^2) = \frac{5d_c b}{24(4\pi M^\epsilon)^2} \left( -\frac{1}{\epsilon} + L_p - \frac{19}{15} + \text{O}(\epsilon) \right). \quad (1.77b)$$

Combining (1.77) and (1.50) yields the one-loop intermediate renormalization constant

$$\delta Z_{\Gamma_\mu}^{(1)} = -\mathcal{K} \left[ \tilde{\Pi}_M^{(1)}(p^2) \right] = \frac{d_c \mu_r}{12(4\pi)^2 \varepsilon}, \quad (1.78a)$$

$$\delta Z_{\Gamma_b}^{(1)} = -\mathcal{K} \left[ \tilde{\Pi}_N^{(1)}(p^2) \right] = \frac{5d_c b_r}{24(4\pi)^2 \varepsilon}, \quad (1.78b)$$

and hence the field renormalization constants

$$\delta Z_\mu^{(1)} = \delta Z_{\Gamma_\mu}^{(1)} - 2\delta Z^{(1)} = \frac{10b_r + (d_c + 20)\mu_r}{12(4\pi)^2 \varepsilon}, \quad (1.79a)$$

$$\delta Z_b^{(1)} = \delta Z_{\Gamma_b}^{(1)} - 2\delta Z^{(1)} = \frac{5((d_c + 4)b_r + 8\mu_r)}{24(4\pi)^2 \varepsilon}. \quad (1.79b)$$

This allows us to compute the one-loop renormalized polarization operator. In projected form, it reads

$$\tilde{\Pi}_{M,r}^{(1)}(p^2) = \tilde{\Pi}_M^{(1)} + \delta Z_{\Gamma_\mu}^{(1)} = -\frac{d_c \mu_r (5 - 3L_p)}{36(4\pi)^2} + \mathcal{O}(\varepsilon), \quad (1.80a)$$

$$\tilde{\Pi}_{N,r}^{(1)}(p^2) = \tilde{\Pi}_N^{(1)} + \delta Z_{\Gamma_b}^{(1)} = -\frac{d_c b_r (19 - 15L_p)}{72(4\pi)^2} + \mathcal{O}(\varepsilon). \quad (1.80b)$$

Before computing the renormalization-group functions from the renormalization constants, we shall proceed with the two and three-loop calculation of the self-energies.

## 1.4.2 Two-loop analysis

### Two-loop flexuron self-energy

At two-loop, the flexuron self-energy has three corrections represented by the diagrams in figure 1.6, labeled (a), (b) and (c).

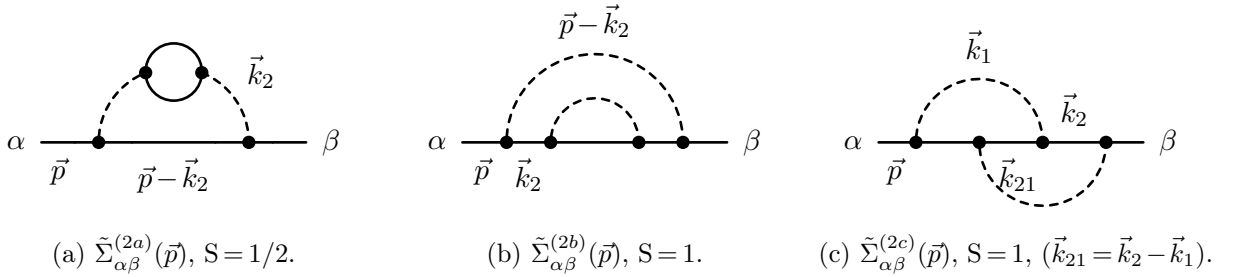


Figure 1.6: Two-loop flexuron self-energy diagrams and symmetry factors (S).

We first consider the diagram of figure 1.6a, defined as<sup>4</sup>

$$\begin{aligned} \Sigma_{\alpha\beta}^{(2a)}(\vec{p}) &= \text{Diagram (a)} \\ &= \frac{1}{2} \int [d^d k_1][d^d k_2] V_{\alpha\alpha_1\gamma_1\gamma_2}^{(0)}(\vec{p}, -\vec{p} + \vec{k}_2, \vec{k}_1 - \vec{k}_2, -\vec{k}_1) S_{\alpha_1\beta_1}^{(0)}(\vec{p} - \vec{k}_2) \\ &\quad \times V_{\delta_1\delta_2\beta_1\beta}^{(0)}(-\vec{k}_1 + \vec{k}_2, \vec{k}_1, \vec{p} - \vec{k}_2, -\vec{p}) S_{\gamma_1\delta_1}^{(0)}(-\vec{k}_1 + \vec{k}_2) S_{\gamma_2\delta_2}^{(0)}(\vec{k}_1). \end{aligned} \quad (1.81)$$

<sup>4</sup>Or equivalently as  $\Sigma_{\alpha\beta}^{(2a)}(\vec{p}) = \int [d^d k_2] V_{\alpha\gamma\delta\beta}^{(1)}(\vec{p}, -\vec{p} + \vec{k}_2, \vec{p} - \vec{k}_2, -\vec{p}) S_{\delta\gamma}^{(0)}(\vec{p} - \vec{k}_2)$

Performing the contractions, the reduction, and the integration, yields the exact result

$$\tilde{\Sigma}^{(2a)}(p^2) = -\frac{d_c}{24} \frac{(p^2)^{d-4}}{(4\pi)^d} \frac{(d-3)(d-2)(d+1)}{(d-1)(d-6)(d-4)} [(d+1)b^2 + 2(d-2)\mu^2] G(d,1,1)G(d,1,2-d/2). \quad (1.82)$$

Performing the  $\varepsilon$ -expansion in the  $\overline{\text{MS}}$ -scheme yields:

$$\tilde{\Sigma}^{(2a)}(p^2) = \frac{d_c(5b^2 + 4\mu^2)}{288(4\pi M\varepsilon)^4} \left[ \frac{1}{2\varepsilon^2} + \frac{1}{\varepsilon} \left( \frac{53}{60} - L_p + \frac{3b^2}{10b^2 + 8\mu^2} \right) + \mathcal{O}(\varepsilon^0) \right]. \quad (1.83)$$

We then consider the diagram of figure 1.6b, which has a symmetry factor of 1 and is defined as

$$\Sigma_{\alpha\beta}^{(2b)}(\vec{p}) = \alpha \begin{array}{c} \vec{p} - \vec{k}_2 \\ \text{---} \text{---} \text{---} \text{---} \\ \vec{p} \quad \vec{k}_2 \end{array} \beta = 1 \times \int [d^d k_1][d^d k_2] V_{\alpha\alpha_1\beta_2\beta}^{(0)}(\vec{p}, -\vec{k}_2, \vec{k}_2, -\vec{p}) S_{\alpha_1\alpha_2}^{(0)}(\vec{k}_2) \\ \times V_{\alpha_2\gamma_1\gamma_2\beta_1}^{(0)}(\vec{k}_2, -\vec{k}_1, \vec{k}_1, -\vec{k}_2) S_{\beta_1\beta_2}^{(0)}(\vec{k}_2) S_{\gamma_1\gamma_2}^{(0)}(\vec{k}_1). \quad (1.84)$$

Performing the contractions, the reduction, and the integration, yields the exact result

$$\tilde{\Sigma}^{(2b)}(p^2) = -\frac{(b + (d-2)\mu)^2}{12} \frac{(p^2)^{d-4}}{(4\pi)^d} \frac{(d-3)(d-2)(d+1)^2}{(d-6)(d-4)(d-1)} G(d,1,1)G(d,1,2-d/2), \quad (1.85)$$

and performing the  $\varepsilon$ -expansion in the  $\overline{\text{MS}}$ -scheme yields

$$\tilde{\Sigma}^{(2b)}(p^2) = \frac{25(b+2\mu)^2}{144(4\pi M\varepsilon)^4} \left[ \frac{1}{2\varepsilon^2} + \frac{1}{\varepsilon} \left( \frac{11}{60} - L_p + \frac{b}{b+2\mu} \right) + \mathcal{O}(\varepsilon^0) \right]. \quad (1.86)$$

Finally, we consider the diagram of figure 1.6c, which has a symmetry factor of 1 and is defined as

$$\Sigma_{\alpha\beta}^{(2c)}(\vec{p}) = \alpha \begin{array}{c} \vec{k}_1 \\ \text{---} \text{---} \text{---} \text{---} \\ \vec{p} \quad \vec{k}_2 \\ \vec{k}_{21} \end{array} \beta = 1 \times \int [d^d k_1][d^d k_2] V_{\alpha\alpha_1\beta_2\beta_3}^{(0)}(\vec{p}, -\vec{p} + \vec{k}_1, \vec{k}_2 - \vec{k}_1, -\vec{k}_2) S_{\alpha_1\alpha_2}^{(0)}(\vec{p} - \vec{k}_1) \\ \times V_{\alpha_2\alpha_3\beta_1\beta}^{(0)}(\vec{p} - \vec{k}_1, -\vec{k}_2 + \vec{k}_1, \vec{k}_2, -\vec{p}) S_{\alpha_3\beta_2}^{(0)}(\vec{k}_2 - \vec{k}_1) S_{\beta_3\beta_1}^{(0)}(\vec{k}_2). \quad (1.87)$$

Performing the contractions, the reduction, and the integration, yields

$$\tilde{\Sigma}^{(2c)}(p^2) = \frac{1}{256} \frac{(p^2)^{d-4}}{(4\pi)^d} \frac{1}{(d-6)(d-4)(d-1)^3} G^2(d,1,1) \\ \times \left[ (d^7 - 28d^6 + 313d^5 - 1686d^4 + 4388d^3 - 4864d^2 + 976d + 960)b^2 \right. \\ + 2(d^8 - 26d^7 + 277d^6 - 1556d^5 + 4956d^4 - 8832d^3 + 7680d^2 - 1408d - 1152)b\mu \\ \left. + (d^9 - 24d^8 + 245d^7 - 1394d^6 + 4936d^5 - 11464d^4 + 17008d^3 - 14048d^2 + 4032d + 768)\mu^2 \right] \\ - \frac{1}{12} \frac{(p^2)^{d-4}}{(4\pi)^d} \frac{d-3}{(d-6)^2(d-4)^2(d-1)^2} G(d,1,1)G(d,1,2-d/2) \\ \times \left[ (2d^6 - 26d^5 + 93d^4 + 35d^3 - 604d^2 + 524d + 336)b^2 \right. \\ \left. + 2(d^7 - 14d^6 + 64d^5 - 57d^4 - 366d^3 + 1012d^2 - 616d - 384)b\mu \right]$$

$$+ (d^8 - 15d^7 + 82d^6 - 188d^5 + 44d^4 + 788d^3 - 1776d^2 + 1232d + 192)\mu^2 \Big]. \quad (1.88)$$

Performing the  $\varepsilon$ -expansion in the  $\overline{\text{MS}}$ -scheme yields

$$\tilde{\Sigma}^{(2c)}(p^2) = \frac{5(121b^2 - 56b\mu + 52\mu^2)}{5184(4\pi M^\varepsilon)^4 \varepsilon} + \mathcal{O}(\varepsilon^0), \quad (1.89)$$

which contains only a simple pole and no non-local terms at this order. This comes from the fact that this diagram does not have any divergent subgraph.

### Two-loop field renormalization constant

Summing all the two-loop self-energy diagrams yields, in the expanded form, the following

$$\begin{aligned} \tilde{\Sigma}^{(2)} &= \tilde{\Sigma}^{(2a)} + \tilde{\Sigma}^{(2b)} + \tilde{\Sigma}^{(2c)} \\ &= \frac{5(5b^2(d_c + 2) + 40b\mu + 4\mu^2(d_c + 10))}{288(4\pi M^\varepsilon)^4} \left[ \frac{1}{2\varepsilon^2} \right. \\ &\quad \left. + \frac{1}{\varepsilon} \left( -L_p + \frac{5b^2(213d_c + 668) + 4360b\mu + 4\mu^2(159d_c + 460)}{180(5b^2(d_c + 2) + 40b\mu + 4\mu^2(d_c + 10))} \right) + \mathcal{O}(\varepsilon^0) \right]. \end{aligned} \quad (1.90)$$

In (1.90), it is enough to perform the trivial replacement  $\mu \rightarrow M^{2\varepsilon}\mu_r$ , and  $b \rightarrow M^{2\varepsilon}b_r$  to renormalize the couplings. More generally, at a given  $L$ -loop order, all the  $L$ -loop diagrams can be processed using this trivial map. However, non-trivial replacements including the renormalization constants, namely (1.39), are needed only for diagrams with  $l < L$  loops. Indeed, from (1.49), the definition of the field renormalization constant at this order reads

$$\delta Z^{(2)} = \mathcal{K} \left[ \tilde{\Sigma}^{(2)} \right] + \mathcal{K} \left[ \tilde{\Sigma}^{(1)} \delta Z^{(1)} \right], \quad (1.91)$$

where  $\tilde{\Sigma}^{(1)}$  is now needed up to  $\mathcal{O}(\varepsilon^0)$ , therefore requiring a non-trivial replacement of the bare quantities, *i.e.*,  $\mu \rightarrow Z_\mu^{(1)} M^{2\varepsilon}\mu_r$  and  $b \rightarrow Z_b^{(1)} M^{2\varepsilon}b_r$ . This is easily achieved from (1.66). Being careful with the loop and  $\varepsilon$  orders then leads to the two-loop contribution to the field renormalization constant

$$\begin{aligned} \delta Z^{(2)} &= \mathcal{K} \left[ \tilde{\Sigma}^{(2)} \right] + \mathcal{K} \left[ \tilde{\Sigma}^{(1)} \mathcal{K} \left[ \tilde{\Sigma}^{(1)} \right] \right] \\ &= \frac{-5}{576(4\pi)^4} \left[ \frac{1}{\varepsilon^2} \left( 5(d_c + 2)b_r^2 + 40b_r\mu_r + 4(d_c + 10)\mu_r^2 \right) \right. \\ &\quad \left. + \frac{1}{90\varepsilon} \left( 5(15d_c - 212)b_r^2 + 1160b_r\mu_r - 4(111d_c - 20)\mu_r^2 \right) \right], \end{aligned} \quad (1.92)$$

where all the non-local terms, *i.e.*, the  $L_p$  dependency, vanished as expected in the  $\overline{\text{MS}}$ -scheme. As mentioned earlier, the  $L_p$  cancellations in the renormalization constants is a strong check of the computations.

We are now in position to compute the two-loop contribution to the renormalized self-energy. Expanding (1.45) to two-loop order reads

$$\begin{aligned} \tilde{\Sigma}_r^{(2)} &= \tilde{\Sigma}^{(2)} - \delta Z^{(2)} + \delta Z^{(1)} \tilde{\Sigma}^{(1)} \\ &= \frac{1}{20736(4\pi)^4} \left[ (3239d_c - 6912\zeta_3 + 19024)b_r^2 + 8(432\zeta_3 + 1651)b_r\mu_r \right. \\ &\quad \left. + 4(805d_c - 6912\zeta_3 + 12708)\mu_r^2 + 180 \left( 5(d_c + 2)b_r^2 + 40b_r\mu_r + 4(d_c + 10)\mu_r^2 \right) L_p^2 \right. \\ &\quad \left. - 20 \left( 11(9d_c + 40)b_r^2 + 320b_r\mu_r + 4(27d_c + 44)\mu_r^2 \right) L_p \right], \end{aligned} \quad (1.93)$$

where an expansion of all the diagrams up to  $\mathcal{O}(\varepsilon^0)$  was needed. This reveals terms proportional to  $\zeta_3 \approx 1.202$ , which is the Apéry constant or equivalently the Riemann  $\zeta_n$  function at integer value  $n = 3$ .



### Two-loop vertex self-energy

At two-loop, the self-energy of the flexuron four-point interaction (or equivalently the  $R$ -propagator polarization) has two corrections represented by the diagrams in figure 1.7, labeled (a) and (b).

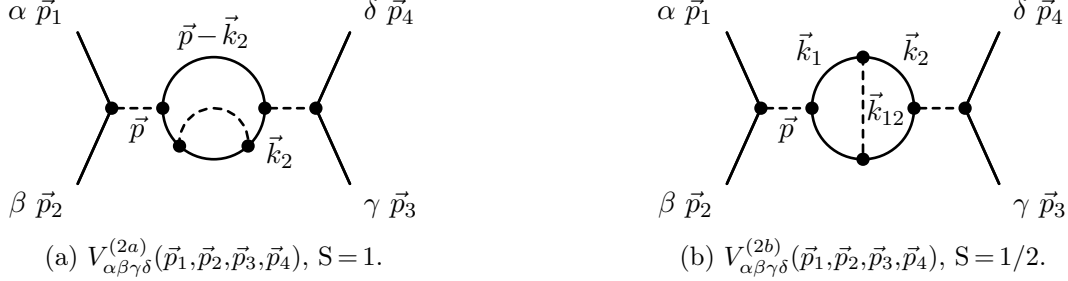


Figure 1.7: Two-loop vertex self-energy diagrams with their symmetry factors ( $S$ ).

Note that  $\vec{k}_{12} = \vec{k}_1 - \vec{k}_2$  and  $\vec{p} = \vec{p}_1 + \vec{p}_2 = -\vec{p}_3 - \vec{p}_4$ .

We first consider the diagram of figure 1.7a, which has a symmetry factor of 1 and is defined as

$$\begin{aligned}
 V_{\alpha\beta\gamma\delta}^{(2a)}(\vec{p}_1, \dots, \vec{p}_4) &= \int [d^d k_1][d^d k_2] V_{\alpha\beta\gamma\delta_1}^{(0)}(\vec{p}_1, \vec{p}_2, -\vec{p} + \vec{k}_2, -\vec{k}_2) S_{\delta_1\alpha_2}^{(0)}(\vec{k}_2) \\
 &\quad \times V_{\alpha_2\beta_2\gamma_2\delta_2}^{(0)}(\vec{k}_2, -\vec{k}_1, \vec{k}_1, -\vec{k}_2) S_{\beta_2\gamma_2}^{(0)}(\vec{k}_1) S_{\delta_2\alpha_1}^{(0)}(\vec{k}_2) \\
 &\quad \times V_{\alpha_1\beta_1\gamma\delta}^{(0)}(\vec{k}_2, \vec{p} - \vec{k}_2, \vec{p}_3, \vec{p}_4) S_{\gamma_1\beta_1}^{(0)}(\vec{p} - \vec{k}_2), \quad (1.94)
 \end{aligned}$$

where  $\vec{p} = \vec{p}_1 + \vec{p}_2 = -\vec{p}_3 - \vec{p}_4$ . It can be re-expressed in the following form

$$V_{\alpha\beta\gamma\delta}^{(2a)}(\vec{p}_1, \vec{p}_2, \vec{p}_3, \vec{p}_4) = \Gamma_{\alpha\beta}^{ab(0)}(\vec{p}_1, \vec{p}_2) R_{abcd}^{(2a)}(\vec{p}) \Gamma_{\gamma\delta}^{cd(0)}(\vec{p}_3, \vec{p}_4), \quad (1.95a)$$

$$R_{abcd}^{(2a)}(\vec{p}) = R_{abef}^{(0)}(\vec{p}) \Pi_{efgh}^{(2a)}(\vec{p}) R_{ghcd}^{(0)}(\vec{p}), \quad (1.95b)$$

where  $\Pi_{efgh}^{(2a)}(\vec{p})$  is the two-loop polarization associated with the diagram. Using the Feynman rules and performing the contractions leads to

$$\Pi_{efgh}^{(2a)}(\vec{p}) = 4d_c \int \frac{[d^d k_1][d^d k_2]}{k_1^8 (\vec{p} - \vec{k}_1)^4 (\vec{k}_1 - \vec{k}_2)^4} (\vec{k}_1 - \vec{p})_\epsilon (k_1)_f (\vec{k}_1 - \vec{p})_g (k_1)_h R_{ijkl}^{(0)}(-\vec{k}_2) k_1^i (\vec{k}_1 - \vec{k}_2)^j k_1^l (\vec{k}_1 - \vec{k}_2)^m. \quad (1.96)$$

Decomposing this self-energy on the basis of the irreducible tensors, performing the reduction of the integrals yields

$$\tilde{\Pi}_M^{(2a)}(p^2) = -\frac{d_c \mu (b + (d-2)\mu)}{6} \frac{(p^2)^{d-4}}{(4\pi)^d} \frac{(d-3)(d-2)(d+1)}{(d-6)(d-4)(d-1)} G(d, 1, 1) G(d, 1, 2-d/2), \quad (1.97a)$$

$$\tilde{\Pi}_N^{(2a)}(p^2) = -\frac{d_c b (b + (d-2)\mu)}{12} \frac{(p^2)^{d-4}}{(4\pi)^d} \frac{(d-3)(d-2)(d+1)^2}{(d-6)(d-4)(d-1)} G(d, 1, 1) G(d, 1, 2-d/2), \quad (1.97b)$$

where  $\tilde{\Pi}_M(p^2)$  and  $\tilde{\Pi}_N(p^2)$  were defined in (1.37). In expanded form, in  $\overline{\text{MS}}$ -scheme, it then read

$$\tilde{\Pi}_M^{(2a)}(p^2) = \frac{5d_c \mu (b + 2\mu)}{72(4\pi M^\epsilon)^4} \left[ \frac{1}{2\epsilon^2} + \frac{1}{\epsilon} \left( \frac{53}{60} - L_p + \frac{b}{2(b+2\mu)} \right) + \mathcal{O}(\epsilon^0) \right], \quad (1.98a)$$

$$\tilde{\Pi}_N^{(2a)}(p^2) = \frac{25d_c b (b + 2\mu)}{144(4\pi M^\epsilon)^4} \left[ \frac{1}{2\epsilon^2} + \frac{1}{\epsilon} \left( \frac{41}{60} - L_p + \frac{b}{2(b+2\mu)} \right) + \mathcal{O}(\epsilon^0) \right]. \quad (1.98b)$$

We then consider the diagram figure 1.7b which has a symmetry factor of 1/2 and is defined as

$$\begin{aligned}
 V_{\alpha\beta\gamma\delta}^{(2b)}(\vec{p}_1, \dots, \vec{p}_4) = & \text{Diagram} = \frac{1}{2} \int [d^d k_1][d^d k_2] V_{\alpha\beta\gamma_1\delta_1}^{(0)}(\vec{p}_1, \vec{p}_2, -\vec{k}_1, -\vec{p} + \vec{k}_1) S_{\delta_1\delta_2}^{(0)}(\vec{p} - \vec{k}_1) \\
 & \times V_{\gamma_2\alpha_2\delta_2\beta_2}^{(0)}(\vec{k}_1, -\vec{k}_2, \vec{p} - \vec{k}_1, -\vec{p} + \vec{k}_2) S_{\alpha_2\alpha_1}^{(0)}(\vec{k}_2) S_{\gamma_1\gamma_2}^{(0)}(\vec{k}_1) \\
 & \times V_{\alpha_1\beta_1\gamma\delta}^{(0)}(\vec{k}_2, \vec{p} - \vec{k}_2, \vec{p}_3, \vec{p}_4) S_{\beta_2\beta_1}^{(0)}(\vec{p} - \vec{k}_2), \quad (1.99)
 \end{aligned}$$

where  $\vec{p} = \vec{p}_1 + \vec{p}_2$ . Decomposing this self-energy on the basis of the irreducible tensors, performing the reduction and the integration, yields the two projections of the polarization

$$\begin{aligned}
 \tilde{\Pi}_M^{(2b)}(p^2) = & \frac{d_c \mu (p^2)^{d-4}}{128 (4\pi)^d} \frac{1}{(d-6)(d-4)(d-1)^3(d+1)} G^2(d, 1, 1) \\
 & \times [(d^5 - 13d^4 + 54d^3 + 60d^2 - 744d + 672)b \\
 & + (d^6 - 15d^5 + 80d^4 + 16d^3 - 608d^2 + 1456d - 960)\mu] \\
 & - \frac{d_c \mu (p^2)^{d-4}}{24 (4\pi)^d} \frac{d-3}{(d-6)^2(d-4)^2(d-1)^2(d+1)} G(d, 1, 1) G(d, 1, 2-d/2) \\
 & \times [(d^6 - 10d^5 + 27d^4 + 10d^3 - 164d^2 + 184d + 672)b \\
 & + (d^7 - 8d^6 + 39d^5 - 160d^4 + 208d^3 + 16d^2 - 240d - 576)\mu], \quad (1.100a)
 \end{aligned}$$

$$\begin{aligned}
 \tilde{\Pi}_N^{(2b)}(p^2) = & \frac{d_c b (p^2)^{d-4}}{512 (4\pi)^d} \frac{1}{(d-6)(d-4)(d-1)^3} G^2(d, 1, 1) \\
 & \times [(d^7 - 28d^6 + 313d^5 - 1686d^4 + 4388d^3 - 4864d^2 + 976d + 960)b \\
 & + (9d^8 - 174d^7 + 1377d^6 - 5768d^5 + 13784d^4 - 18936d^3 + 13584d^2 - 2784d - 1152)\mu] \\
 & - \frac{d_c b (p^2)^{d-4}}{24 (4\pi)^d} \frac{d-3}{(d-6)^2(d-4)^2(d-1)^2} G(d, 1, 1) G(d, 1, 2-d/2) \\
 & \times [(2d^6 - 26d^5 + 93d^4 + 35d^3 - 604d^2 + 524d + 336)b \\
 & + (2d^7 - 22d^6 + 57d^5 + 157d^4 - 982d^3 + 1700d^2 - 984d - 288)\mu]. \quad (1.100b)
 \end{aligned}$$

In expanded form and in  $\overline{\text{MS}}$ -scheme, these results read

$$\tilde{\Pi}_M^{(2b)}(p^2) = -\frac{5d_c \mu (b+2\mu)}{5184(4\pi M^\varepsilon)^4} \left[ \frac{1}{\varepsilon} + \text{O}(\varepsilon^0) \right], \quad (1.101a)$$

$$\tilde{\Pi}_N^{(2b)}(p^2) = \frac{5d_c b (b+2\mu)}{10368(4\pi M^\varepsilon)^4} \left[ \frac{121}{\varepsilon} + \text{O}(\varepsilon^0) \right]. \quad (1.101b)$$

Similarly to the diagram 2b in the flexuron self-energy, the results (1.101) shows only simple poles.

### Two-loop couplings renormalization constants

Summing the two contributions, (1.98) and (1.101), yields the total two-loop polarization projections

$$\begin{aligned}
 \tilde{\Pi}_M^{(2)}(p^2) = & \tilde{\Pi}_M^{(2a)}(p^2) + \tilde{\Pi}_M^{(2b)}(p^2) \\
 = & \frac{5d_c \mu (b+2\mu)}{72(4\pi M^\varepsilon)^4} \left[ \frac{1}{2\varepsilon^2} + \frac{1}{\varepsilon} \left( \frac{313}{360} - L_p + \frac{b}{2(b+2\mu)} \right) + \text{O}(\varepsilon^0) \right], \quad (1.102a)
 \end{aligned}$$

$$\begin{aligned}
 \tilde{\Pi}_N^{(2)}(p^2) = & \tilde{\Pi}_N^{(2a)}(p^2) + \tilde{\Pi}_N^{(2b)}(p^2) \\
 = & \frac{25d_c b (b+2\mu)}{144(4\pi M^\varepsilon)^4} \left[ \frac{1}{2\varepsilon^2} + \frac{1}{\varepsilon} \left( \frac{367}{360} - L_p + \frac{b}{2(b+2\mu)} \right) + \text{O}(\varepsilon^0) \right]. \quad (1.102b)
 \end{aligned}$$

From the above results, we compute the two-loop contribution to the intermediary renormalization constant

$$\begin{aligned}\delta Z_{\Gamma_\mu}^{(2)} &= -\mathcal{K}[\tilde{\Pi}_M^{(2)}] + \mathcal{K}[\delta Z_{\Gamma_\mu}^{(1)2}] + \mathcal{K}[\delta Z_{\Gamma_\mu}^{(1)}\tilde{\Pi}_M^{(1)}] \\ &= \frac{d_c\mu_r}{5184(4\pi)^4} \left[ \frac{36}{\varepsilon^2} (5b_r + (10+d_c)\mu_r) + \frac{1}{\varepsilon} (107b_r + 574\mu_r) \right],\end{aligned}\quad (1.103a)$$

$$\begin{aligned}\delta Z_{\Gamma_b}^{(2)} &= -\mathcal{K}[\tilde{\Pi}_N^{(2)}] + \mathcal{K}[\delta Z_{\Gamma_b}^{(1)2}] + \mathcal{K}[\delta Z_{\Gamma_b}^{(1)}\tilde{\Pi}_N^{(1)}] \\ &= \frac{d_c b_r}{576(4\pi)^4} \left[ \frac{25}{\varepsilon^2} ((2+d_c)b_r + 4\mu_r) - \frac{5}{18\varepsilon} (91b_r - 178\mu_r) \right].\end{aligned}\quad (1.103b)$$

Hence, we can compute the coupling renormalization constants

$$\begin{aligned}\delta Z_\mu^{(2)} &= \delta Z_{\Gamma_\mu}^{(2)} - 2\delta Z^{(2)} - 2\delta Z^{(1)}\delta Z_{\Gamma_\mu}^{(1)} + 3\delta Z^{(1)2} \\ &= \frac{1}{5184(4\pi)^4} \left[ \frac{18}{\varepsilon^2} (10(3d_c + 80)b_r\mu_r + 25(d_c + 8)b_r^2 + 2(d_c + 20)^2\mu_r^2) \right. \\ &\quad \left. + \frac{1}{\varepsilon} ((107d_c + 1160)b_r\mu_r + 5(15d_c - 212)b_r^2 + 10(13d_c + 8)\mu_r^2) \right],\end{aligned}\quad (1.104a)$$

$$\begin{aligned}\delta Z_b^{(2)} &= \delta Z_{\Gamma_b}^{(2)} - 2\delta Z^{(2)} - 2\delta Z^{(1)}\delta Z_{\Gamma_b}^{(1)} + 3\delta Z^{(1)2} \\ &= \frac{1}{576(4\pi)^4} \left[ \frac{5}{\varepsilon^2} (20(3d_c + 16)b_r\mu_r + 5(d_c + 4)^2b_r^2 + 8(d_c + 40)\mu_r^2) \right. \\ &\quad \left. + \frac{1}{18\varepsilon} (10(89d_c + 232)b_r\mu_r - 5(61d_c + 424)b_r^2 - 8(111d_c - 20)\mu_r^2) \right].\end{aligned}\quad (1.104b)$$

Similarly to the one-loop case, the cancellation of the  $L_p$  contributions is a strong check of our computations. These results also allow us to compute the two-loop contribution to the renormalized polarization projections

$$\begin{aligned}\tilde{\Pi}_{M,r}^{(2)}(p^2) &= \tilde{\Pi}_M^{(2)} + \delta Z_{\Gamma_\mu}^{(2)} - \delta Z_{\Gamma_\mu}^{(1)}\tilde{\Pi}_M^{(1)} - \delta Z_{\Gamma_\mu}^{(1)2} \\ &= -\frac{d_c\mu_r}{51840(4\pi)^4} \left[ 2(13187 + 260L_p + 1800L_p^2 - 12096\zeta_3)\mu_r \right. \\ &\quad \left. - (6863 - 3860L_p + 1800L_p^2 - 864\zeta_3)b_r \right],\end{aligned}\quad (1.105a)$$

$$\begin{aligned}\tilde{\Pi}_{N,r}^{(2)}(p^2) &= \tilde{\Pi}_N^{(2)} + \delta Z_{\Gamma_b}^{(2)} - \delta Z_{\Gamma_b}^{(1)}\tilde{\Pi}_N^{(1)} - \delta Z_{\Gamma_b}^{(1)2} \\ &= \frac{d_c b_r}{20736(4\pi)^4} \left[ 2(7065 - 2780L_p + 1800L_p^2 - 6048\zeta_3)\mu_r \right. \\ &\quad \left. + (12751 - 6380L_p + 1800L_p^2 - 3456\zeta_3)b_r \right].\end{aligned}\quad (1.105b)$$

### 1.4.3 Three-loop analysis

#### Three-loop flexuron self-energy

We now consider the three-loop flexuron self-energy that consists of 15 independent diagrams, all displayed in figure 1.8 and labeled in alphabetical order from  $a$  to  $o$ . There are 9 diagrams ( $a, b, c, d, e, i, j, m, n$ ) of the Ladder (L3) topology, 5 diagrams ( $f, g, h, k, l$ ) of the Benz (B3) topology and one diagram ( $o$ ) of the Non-planar (N3) topology. All of them are displayed with their corresponding symmetry factor (S) that are either 1, 1/2 or 1/4. Moreover, by symmetry, 3 diagrams ( $i, j, l$ ) should be taken into account twice. We therefore add an explicit factor 2 to their symmetry factor (S).

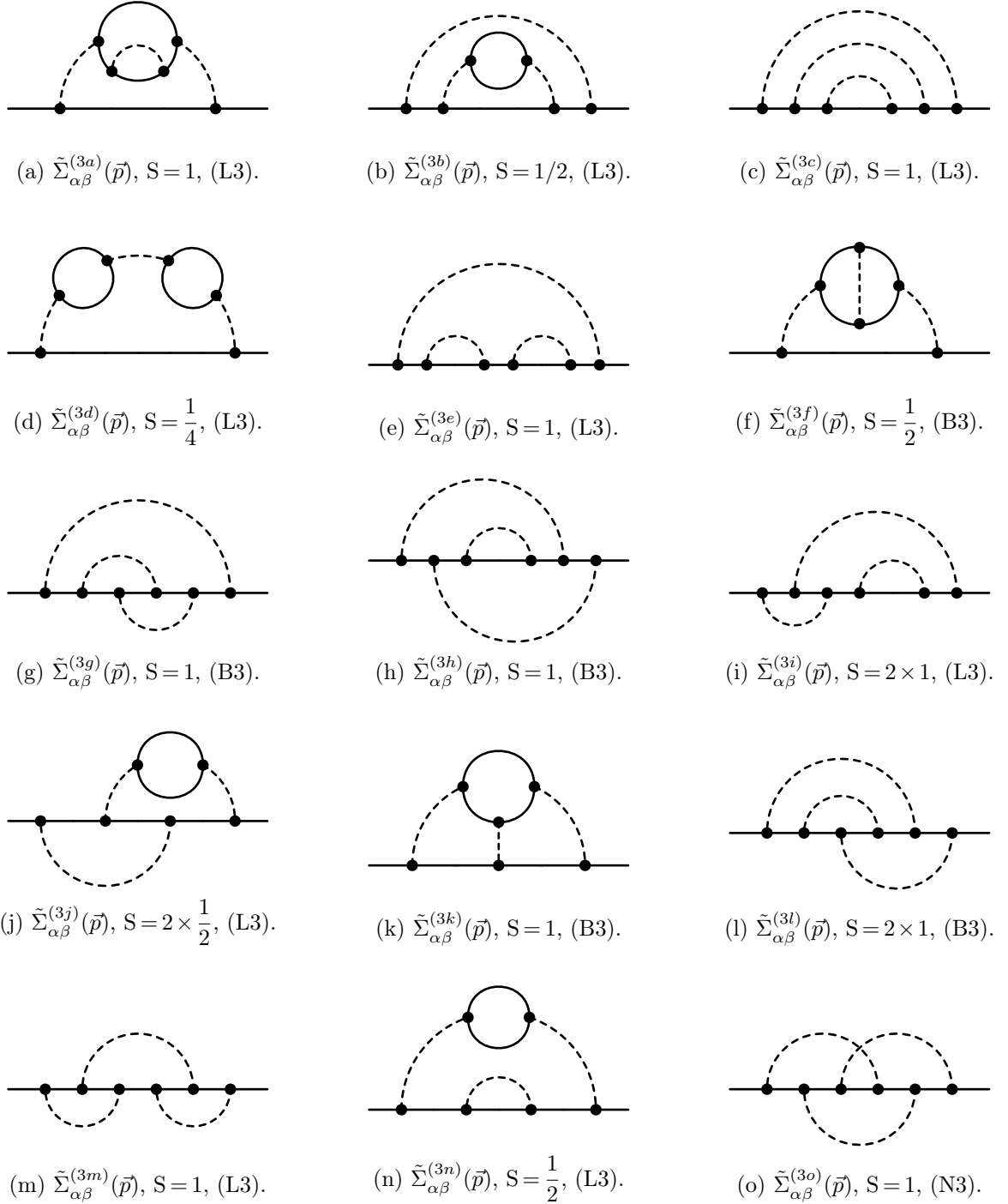


Figure 1.8: Three-loop flexuron self-energy diagrams and their associated symmetry factors ( $S$ ). Momenta arrows have been dropped to keep it light.

Proceeding along the lines of the one and two-loop cases, *i.e.*, performing carefully the contractions, reduction, integration, and  $\varepsilon$  expansion of the 15 diagrams as well as summing all of them together yields the complete three-loop flexuron self-energy

$$\begin{aligned}
\tilde{\Sigma}^{(3)}(p^2) &= \tilde{\Sigma}^{(3a)}(p^2) + \tilde{\Sigma}^{(3b)}(p^2) + \dots + \tilde{\Sigma}^{(3o)}(p^2) \\
&= -\frac{e^{-3\varepsilon L_p}}{20736(4\pi M\varepsilon)^6} \left[ \frac{5}{\varepsilon^3} \left( 50(5d_c + 18)b^2\mu + 25(d_c + 2)(d_c + 3)b^3 \right. \right. \\
&\quad \left. \left. + 100(d_c + 18)b\mu^2 + 8(d_c + 10)(d_c + 15)\mu^3 \right) \right. \\
&\quad \left. + \frac{4}{18\varepsilon^2} \left( 25(565d_c + 2604)b^2\mu + 50((39d_c + 265) + 442)d_c b^3 \right. \right. \\
&\quad \left. \left. + 20(296d_c + 2595)b\mu^2 + 4((147d_c + 2105) + 5050)d_c \mu^3 \right) \right. \\
&\quad \left. - \frac{1}{162\varepsilon} \left( (30375(d_c + 2)(d_c + 3)\zeta_2 + 2592(171d_c + 524)\zeta_3 - d_c(346320d_c + 2837779) - 5182746)b^3 \right. \right. \\
&\quad \left. \left. + 8(1215(d_c + 10)(d_c + 15)\zeta_2 + 648(48d_c + 2669)\zeta_3 - 2d_c(6516d_c + 152741) - 3328149)\mu^3 \right. \right. \\
&\quad \left. \left. + 12(10125(d_c + 18)\zeta_2 + 648(44d_c + 597)\zeta_3 - 144560d_c - 1933147)b\mu^2 \right. \right. \\
&\quad \left. \left. + 6(10125(5d_c + 18)\zeta_2 + 5184(5d_c + 71)\zeta_3 - 516735d_c - 2336048)b^2\mu \right) + \mathcal{O}(\varepsilon^0) \right], \quad (1.106)
\end{aligned}$$

where the  $L_p$  dependency has been factorized out in a front  $e^{-3\varepsilon L_p}$  term for the sake of brevity. However, it's worth stressing out that all computations were carried out with explicit  $L_p$  terms, such that their cancellation in the next steps provides a non-trivial check of the computations. Let us also emphasize that this computation required the computation of a total of  $\sim 130000$  three-loop integrals via the techniques of IBP reduction, provided in Appendix A.

We can now compute the three-loop contribution to the field renormalization constant

$$\begin{aligned}
\delta Z^{(3)} &= \mathcal{K} \left[ \tilde{\Sigma}^{(3)} \right] + \mathcal{K} \left[ \delta Z^{(2)} \tilde{\Sigma}^{(1)} \right] + \mathcal{K} \left[ \delta Z^{(1)} \tilde{\Sigma}^{(2)} \right] \\
&= -\frac{1}{20736(4\pi)^6} \left[ \frac{5}{\varepsilon^3} \left( 50(5d_c + 18)b_r^2\mu_r + 100(d_c + 18)b_r\mu_r^2 + 25(d_c + 2)(d_c + 3)b_r^3 \right. \right. \\
&\quad \left. \left. + 8(d_c + 10)(d_c + 15)\mu_r^3 \right) + \frac{1}{18\varepsilon^2} \left( 50(311d_c - 480)b_r^2\mu_r - 20(283d_c - 3000)b_r\mu_r^2 \right. \right. \\
&\quad \left. \left. + 25(15d_c^2 - 319d_c - 1060)b_r^3 - 8(3d_c + 5)(37d_c - 100)\mu_r^3 \right) \right. \\
&\quad \left. - \frac{1}{324\varepsilon} \left( 6(18144(5d_c + 2)\zeta_3 - 56445d_c + 221204)b_r^2\mu_r + 12(1296(50d_c + 57)\zeta_3 \right. \right. \\
&\quad \left. \left. - 82681d_c - 108974)b_r\mu_r^2 - (5184(9d_c + 16)\zeta_3 - 41625d_c^2 + 180563d_c + 516252)b_r^3 \right. \right. \\
&\quad \left. \left. + 8((1395d_c - 124416\zeta_3 + 188605)d_c + 659664\zeta_3 - 652398)\mu_r^3 \right) + \mathcal{O}(\varepsilon^0) \right]. \quad (1.107)
\end{aligned}$$

And finally computing the three-loop contribution to the renormalized flexuron self-energy

$$\begin{aligned}
\tilde{\Sigma}_r^{(3)}(p^2) &= \tilde{\Sigma}^{(3)} - \delta Z^{(3)} + \delta Z^{(2)} \tilde{\Sigma}^{(1)} + \delta Z^{(1)} \tilde{\Sigma}^{(2)} \\
&= \frac{1}{13436928(4\pi)^6} \left[ 2((41014512\zeta_3 + 816480\zeta_4 - 55987200\zeta_5 + 7390987)d_c \right. \\
&\quad \left. + 32(3750624\zeta_3 + 10206\zeta_4 - 6006960\zeta_5 + 1500773))b_r^2\mu_r \right. \\
&\quad \left. + 4((216345168\zeta_3 + 583200\zeta_4 - 324725760\zeta_5 + 75106109)d_c + 2(82306368\zeta_3 \right. \\
&\quad \left. + 332424\zeta_4 - 122472000\zeta_5 + 27546817))b_r\mu_r^2 - ((3(54000\zeta_3 + 52087)d_c - 4774032\zeta_3 \right. \\
&\quad \left. + 139968\zeta_4 + 11876687)d_c - 12(2260872\zeta_3 - 20736\zeta_4 - 1658880\zeta_5 - 2141599))b_r^3 \right. \\
&\quad \left. - 8((3(2160\zeta_3 + 7681)d_c - 243603504\zeta_3 + 373248\zeta_4 + 369515520\zeta_5 - 90673907)d_c \right.
\end{aligned}$$

$$\begin{aligned}
& -2(103991040\zeta_3 + 989496\zeta_4 - 164384640\zeta_5 + 44356427)\mu_r^3 \\
& -12\left(6(2592(15d_c + 52)\zeta_3 - 108355d_c - 452468)b_r^2\mu_r + 12(1944(16d_c + 79)\zeta_3 \right. \\
& - 67768d_c - 483607)b_r\mu_r^2 + (2592(51d_c + 164)\zeta_3 - 52065d_c^2 - 780274d_c - 1663086)b_r^3 \\
& - 8((2925d_c + 31104\zeta_3 + 12997)d_c - 796392\zeta_3 + 1183509)\mu_r^3\left.)L_p \right. \\
& - 540\left(30(91d_c + 632)b_r^2\mu_r + 12(163d_c + 820)b_r\mu_r^2 + 5(99d_c^2 + 813d_c + 1532)b_r^3 \right. \\
& + 8(3(9d_c + 91)d_c + 640)\mu_r^3\left.)L_p^2 + 3240\left(50(5d_c + 18)b_r^2\mu_r + 100(d_c + 18)b_r\mu_r^2 \right. \right. \\
& \left. \left. + 25(d_c + 2)(d_c + 3)b_r^3 + 8(d_c + 10)(d_c + 15)\mu_r^3\right)L_p^3\right]. \tag{1.108}
\end{aligned}$$

### Three-loop vertex polarization

Finally, we consider the three-loop vertex self-energy that consist of 11 independent diagrams, all displayed in figure 1.9 and labeled in alphabetical order from  $a$  to  $k$ . There are 7 diagrams ( $a, b, c, f, h, i, j$ ) of the Ladder (L3) topology, 3 diagrams ( $d, e, g$ ) of the Benz (B3) topology and one diagram ( $k$ ) of the Non-planar (N3) topology. All of them are displayed with their corresponding symmetry factor (S) that are either 1, 1/2 or 1/4. Moreover, by symmetry, one diagram ( $f$ ) should be taken into account twice. We therefore add an explicit factor 2 to its symmetry factor (S).

Proceeding as for the one and two-loop cases, *i.e.*, performing carefully the projections, contractions, reduction, integration, and the expansion of the 11 diagrams as well as summing all of them together yields the total result

$$\begin{aligned}
\tilde{\Pi}_M^{(3)}(p^2) &= \tilde{\Pi}_M^{(3a)}(p^2) + \tilde{\Pi}_M^{(3b)}(p^2) + \dots + \tilde{\Pi}_M^{(3k)}(p^2) \\
&= -\frac{5\mu d_c e^{-3\varepsilon L_p}}{5184(4\pi M^\varepsilon)^6} \left[ \frac{1}{2\varepsilon^3} \left( 5(d_c + 8)b^2 + 160b\mu + 4(d_c + 40)\mu^2 \right) \right. \\
&+ \frac{1}{45\varepsilon^2} \left( 5(82d_c + 739)b^2 + 9830b\mu + 2(137d_c + 3250)\mu^2 \right) \\
&- \frac{1}{8100\varepsilon} \left( (5d_c(6075\zeta_2 + 5832\zeta_3 - 89497) + 30(8100\zeta_2 + 15120\zeta_3 - 124853))b^2 \right. \\
&+ (240(4050\zeta_2 - 25731\zeta_3 - 10517) - 39200d_c)b\mu \\
&\left. + (4d_c(6075\zeta_2 - 81648\zeta_3 + 19591) + 360(2700\zeta_2 - 37404\zeta_3 + 21511))\mu^2 \right) + \mathcal{O}(\varepsilon^0) \left. \right], \tag{1.109a}
\end{aligned}$$

$$\begin{aligned}
\tilde{\Pi}_N^{(3)}(p^2) &= \tilde{\Pi}_N^{(3a)}(p^2) + \tilde{\Pi}_N^{(3b)}(p^2) + \dots + \tilde{\Pi}_N^{(3k)}(p^2) \\
&= -\frac{5bd_c e^{-3\varepsilon L_p}}{5184(4\pi M^\varepsilon)^6} \left[ \frac{5}{4\varepsilon^3} \left( 5(d_c + 8)b^2 + 160b\mu + 4(d_c + 40)\mu^2 \right) \right. \\
&+ \frac{1}{36\varepsilon^2} \left( 5(209d_c + 1838)b^2 + 26860b\mu + 8(91d_c + 2525)\mu^2 \right) \\
&- \frac{1}{3240\varepsilon} \left( (5d_c(6075\zeta_2 + 23328\zeta_3 - 131779) + 6(40500\zeta_2 + 165024\zeta_3 - 827623))b^2 \right. \\
&+ (120(8100\zeta_2 + 44280\zeta_3 - 126979) - 3920d_c)b\mu \\
&\left. + (4d_c(6075\zeta_2 + 40824\zeta_3 - 118343) + 288(3375\zeta_2 + 21204\zeta_3 - 42083))\mu^2 \right) + \mathcal{O}(\varepsilon^0) \left. \right], \tag{1.109b}
\end{aligned}$$

where, once again, the  $L_p$  dependency has been factorized out in a front  $e^{-3\varepsilon L_p}$  term for the sake of brevity, but all computations were carried out with explicit  $L_p$  terms, such that their cancellation in the next steps provides a non-trivial check of the computations. This complete computation required the use of the  $\sim 130000$  three-loop integrals computed in the previous section plus  $\sim 350000$  new ones, via the techniques of IBP reduction defined in Appendix A.

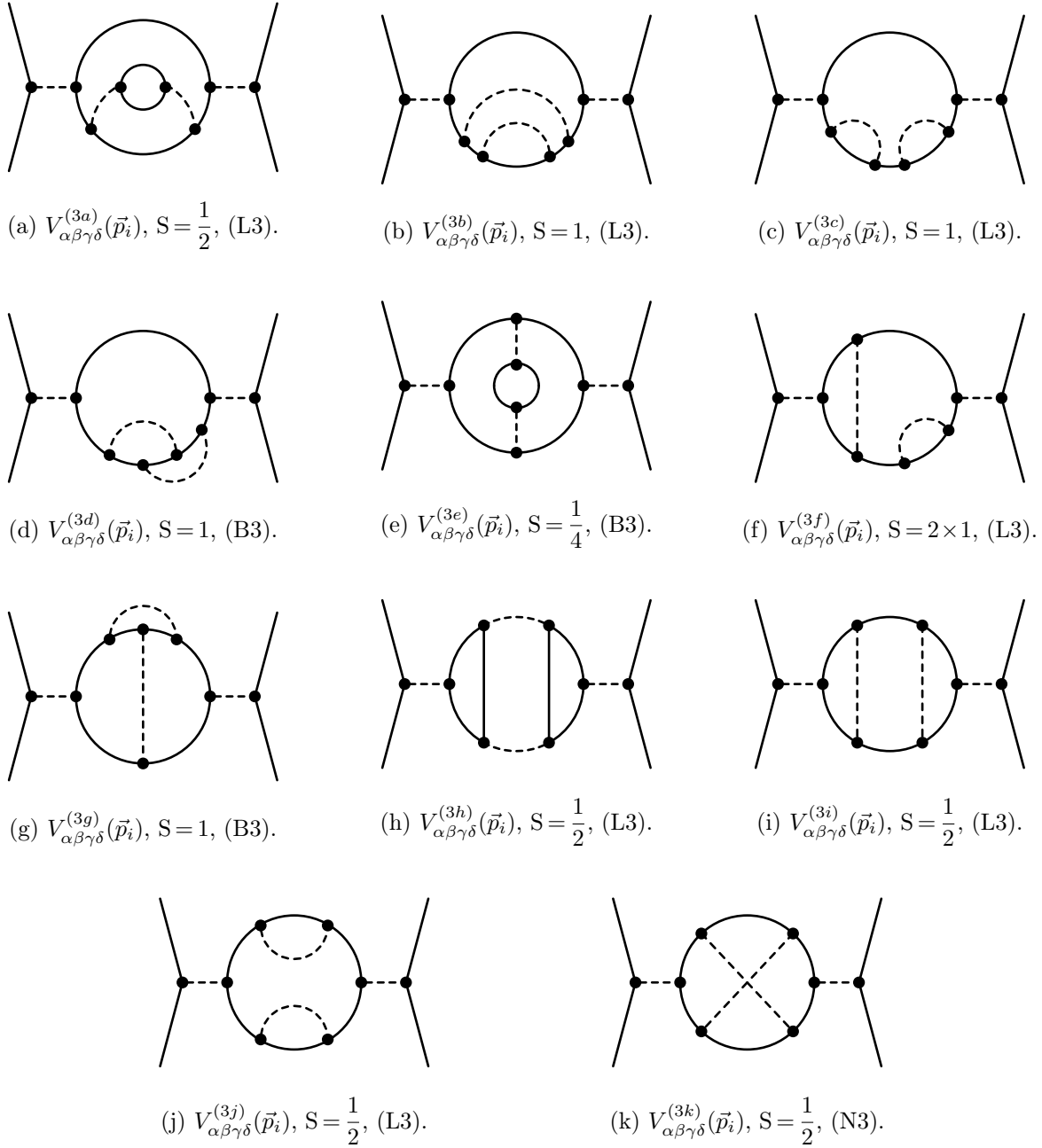


Figure 1.9: Three-loop vertex self-energy diagrams and their associated symmetry factors ( $S$ ). All momentum parametrizations and indices have been dropped to keep it light. All external momenta  $\vec{p}_i = \{\vec{p}_1, \vec{p}_2, \vec{p}_3, \vec{p}_4\}$  are defined incoming. One might be tempted to call them TIE diagrams, in reference to the similar-looking ships from Star Wars.

From all the previous results, we can now compute the three-loop contribution to the intermediary renormalization constants

$$\begin{aligned}
\delta Z_{\Gamma_\mu}^{(3)} &= -\mathcal{K} \left[ \tilde{\Pi}_M^{(3)} \right] + \mathcal{K} \left[ \delta Z_{\Gamma_\mu}^{(1)} \tilde{\Pi}_M^{(2)} \right] + \mathcal{K} \left[ \delta Z_{\Gamma_\mu}^{(2)} \tilde{\Pi}_M^{(1)} \right] - \mathcal{K} \left[ \delta Z_{\Gamma_\mu}^{(1)^2} \tilde{\Pi}_M^{(1)} \right] + 2\mathcal{K} \left[ \delta Z_{\Gamma_\mu}^{(1)} \delta Z_{\Gamma_\mu}^{(2)} \right] - \mathcal{K} \left[ \delta Z_{\Gamma_\mu}^{(1)^3} \right] \\
&= \frac{d_c \mu}{10368(4\pi)^6} \left[ \frac{1}{\varepsilon^3} \left( 20(3d_c + 40)b_r \mu_r + 25(d_c + 8)b_r^2 + 2(d_c + 10)(3d_c + 40)\mu_r^2 \right) \right. \\
&\quad + \frac{1}{36\varepsilon^2} \left( 4(321d_c + 9040)b_r \mu_r + 5(167d_c + 8)b_r^2 + 20(313d_c + 2312)\mu_r^2 \right) \\
&\quad + \frac{1}{648\varepsilon} \left( 32(980d_c + 2754\zeta_3 + 3801)b_r \mu_r + (34987d_c - 384(459\zeta_3 - 296))b_r^2 \right. \\
&\quad \left. \left. + 4(5317d_c + 80352\zeta_3 + 93600)\mu_r^2 + \mathcal{O}(\varepsilon^0) \right] \right], \tag{1.110a}
\end{aligned}$$

$$\begin{aligned}
\delta Z_{\Gamma_b}^{(3)} &= -\mathcal{K} \left[ \tilde{\Pi}_N^{(3)} \right] + \mathcal{K} \left[ \delta Z_{\Gamma_b}^{(1)} \tilde{\Pi}_N^{(2)} \right] + \mathcal{K} \left[ \delta Z_{\Gamma_b}^{(2)} \tilde{\Pi}_N^{(1)} \right] - \mathcal{K} \left[ \delta Z_{\Gamma_b}^{(1)^2} \tilde{\Pi}_N^{(1)} \right] + 2\mathcal{K} \left[ \delta Z_{\Gamma_b}^{(1)} \delta Z_{\Gamma_b}^{(2)} \right] - \mathcal{K} \left[ \delta Z_{\Gamma_b}^{(1)^3} \right] \\
&= \frac{d_c b_r}{41472(4\pi)^6} \left[ \frac{25}{\varepsilon^3} \left( 40(3d_c + 8)b_r \mu_r + 5(d_c + 2)(3d_c + 8)b_r^2 + 8(d_c + 40)\mu_r^2 \right) \right. \\
&\quad + \frac{25}{18\varepsilon^2} \left( 4(267d_c + 224)b_r \mu_r - (577d_c + 1576)b_r^2 - 4(71d_c - 728)\mu_r^2 \right) \\
&\quad + \frac{1}{324\varepsilon} \left( 2240(7d_c - 6(54\zeta_3 + 5))b_r \mu_r + (371495d_c - 228096\zeta_3 + 614832)b_r^2 \right. \\
&\quad \left. \left. + 4(87893d_c + 425088\zeta_3 - 248616)\mu_r^2 + \mathcal{O}(\varepsilon^0) \right] \right]. \tag{1.110b}
\end{aligned}$$

And then computing the three-loop contribution to the renormalization constant of the couplings

$$\begin{aligned}
\delta Z_\mu^{(3)} &= \delta Z_{\Gamma_\mu}^{(3)} - 2\delta Z^{(3)} - 2\delta Z^{(1)} \delta Z_{\Gamma_\mu}^{(2)} - 2\delta Z^{(2)} \delta Z_{\Gamma_\mu}^{(1)} + 3\delta Z^{(1)^2} \delta Z_{\Gamma_\mu}^{(1)} + 6\delta Z^{(1)} \delta Z^{(2)} - 4\delta Z^{(1)^3} \\
&= \frac{1}{10368(4\pi)^6} \left[ \frac{1}{\varepsilon^3} \left( 100(d_c + 10)(d_c + 36)b_r^2 \mu_r + 40((3d_c + 145)d_c + 1800)b_r \mu_r^2 \right) \right. \\
&\quad + 125(d_c + 6)(d_c + 8)b_r^3 + 6(d_c + 20)^3 \mu_r^3 \\
&\quad + \frac{1}{36\varepsilon^2} \left( 5((257d_c + 8940)d_c - 26880)b_r^2 \mu_r + 12((107d_c + 3260)d_c + 28000)b_r \mu_r^2 \right. \\
&\quad + 50((15d_c - 184)d_c - 2968)b_r^3 + 140(d_c + 20)(13d_c + 8)\mu_r^3 \\
&\quad - \frac{1}{648\varepsilon} \left( (20736(61d_c + 21)\zeta_3 - 34987d_c^2 - 791004d_c + 2654448)b_r^2 \mu_r \right. \\
&\quad + 8(648(283d_c + 342)\zeta_3 - 3920d_c^2 - 263247d_c - 326922)b_r \mu_r^2 \\
&\quad - 2(5184(9d_c + 16)\zeta_3 - 41625d_c^2 + 180563d_c + 516252)b_r^3 \\
&\quad \left. \left. + 4((263d_c - 578016\zeta_3 + 660820)d_c + 2638656\zeta_3 - 2609592)\mu_r^3 + \mathcal{O}(\varepsilon^0) \right] \right], \tag{1.111a}
\end{aligned}$$

$$\begin{aligned}
\delta Z_b^{(3)} &= \delta Z_{\Gamma_b}^{(3)} - 2\delta Z^{(3)} - 2\delta Z^{(1)} \delta Z_{\Gamma_b}^{(2)} - 2\delta Z^{(2)} \delta Z_{\Gamma_b}^{(1)} + 3\delta Z^{(1)^2} \delta Z_{\Gamma_b}^{(1)} + 6\delta Z^{(1)} \delta Z^{(2)} - 4\delta Z^{(1)^3} \\
&= \frac{1}{41472(4\pi)^6} \left[ \frac{5}{\varepsilon^3} \left( 160(d_c(d_c + 62) + 360)b_r \mu_r^2 + 400((3d_c + 29)d_c + 72)b_r^2 \mu_r \right) \right. \\
&\quad + 75(d_c + 4)^3 b_r^3 + 32(d_c + 30)(d_c + 40)\mu_r^3 \\
&\quad + \frac{1}{18\varepsilon^2} \left( 300((89d_c + 484)d_c - 896)b_r^2 \mu_r + 20((3972 - 1021d_c)d_c + 33600)b_r \mu_r^2 \right. \\
&\quad - 175(d_c + 4)(61d_c + 424)b_r^3 - 32((111d_c + 4880)d_c - 1400)\mu_r^3 \\
&\quad \left. - \frac{1}{324\varepsilon} \left( 8(36288(10d_c + 3)\zeta_3 - 1960d_c^2 - 160935d_c + 663612)b_r^2 \mu_r \right) \right] \right],
\end{aligned}$$



$$\begin{aligned}
& + 4(5184(68d_c + 171)\zeta_3 - 87893d_c^2 - 743556d_c - 1307688)b_r\mu_r^2 \\
& + (41472(d_c - 8)\zeta_3 - 204995d_c^2 - 1337084d_c - 2065008)b_r^3 \\
& + 32((1395d_c - 124416\zeta_3 + 188605)d_c + 659664\zeta_3 - 652398)\mu_r^3) + \mathcal{O}(\varepsilon^0)]. \quad (1.111b)
\end{aligned}$$

All the above results also allow us to compute the three-loop contribution to the  $R$ -propagator polarization projections:

$$\begin{aligned}
\tilde{\Pi}_{M,r}^{(3)}(p^2) &= \tilde{\Pi}_M^{(3)} + \delta Z_{\Gamma_\mu}^{(3)} - \delta Z_{\Gamma_\mu}^{(1)}\tilde{\Pi}_M^{(2)} + \left( \delta Z_{\Gamma_\mu}^{(1)2} - \delta Z_{\Gamma_\mu}^{(2)} \right) \tilde{\Pi}_M^{(1)} - 2\delta Z_{\Gamma_\mu}^{(1)}\delta Z_{\Gamma_\mu}^{(2)} + \delta Z_{\Gamma_\mu}^{(1)3} \\
&= \frac{\mu_r d_c}{67184640(4\pi)^6} \left[ 8(78783408\zeta_3 d_c - 77760(1545d_c + 812)\zeta_5 + 29826539d_c \right. \\
&+ 28920240\zeta_3 - 165240\zeta_4 + 30851634)b_r\mu_r + (28429488\zeta_3 d_c \\
&- 622080(63d_c + 146)\zeta_5 + 4895207d_c + 77296032\zeta_3 + 2643840\zeta_4 - 11407688)b_r^2 \\
&+ 4(9(43511376\zeta_3 - 66614400\zeta_5 + 16738993)d_c + 8(167805432\zeta_3 - 150660\zeta_4 \\
&- 275484240\zeta_5 + 84287719))\mu_r^2 + 12 \left( 80(980d_c + 53298\zeta_3 - 29007)b_r\mu_r \right. \\
&- 5(1296(3d_c + 92)\zeta_3 - 43877d_c - 367500)b_r^2 \\
&+ 4(1296(42d_c + 1835)\zeta_3 - 12749d_c - 2145660)\mu_r^2 \left. \right) L_p \\
&- 2700 \left( (163d_c + 1968)b_r^2 + 2832b_r\mu_r + 4(47d_c + 96)\mu_r^2 \right) L_p^2 \\
&+ 32400 \left( 5(d_c + 8)b_r^2 + 160b_r\mu_r + 4(d_c + 40)\mu_r^2 \right) L_p^3 \left. \right], \quad (1.112a)
\end{aligned}$$

$$\begin{aligned}
\tilde{\Pi}_{N,r}^{(3)}(p^2) &= \tilde{\Pi}_N^{(3)} + \delta Z_{\Gamma_b}^{(3)} - \delta Z_{\Gamma_b}^{(1)}\tilde{\Pi}_N^{(2)} + \left( \delta Z_{\Gamma_b}^{(1)2} - \delta Z_{\Gamma_b}^{(2)} \right) \tilde{\Pi}_N^{(1)} - 2\delta Z_{\Gamma_b}^{(1)}\delta Z_{\Gamma_b}^{(2)} + \delta Z_{\Gamma_b}^{(1)3} \\
&= \frac{b_r d_c}{26873856(4\pi)^6} \left[ 64(1235520\zeta_3 d_c - 77760(24d_c + 49)\zeta_5 + 450089d_c \right. \\
&+ 3847500\zeta_3 + 34020\zeta_4 - 933261)b_r\mu_r + (3(930672\zeta_3 + 622080\zeta_5 - 2835595)d_c \\
&+ 8(4245372\zeta_3 + 85536\zeta_4 - 2488320\zeta_5 - 5320957))b_r^2 + 4((144862128\zeta_3 - 219749760\zeta_5 \\
&+ 53345485)d_c + 8(22129200\zeta_3 - 159408\zeta_4 - 34972560\zeta_5 + 8943373))\mu_r^2 \\
&+ 12 \left( 160(49d_c - 23652\zeta_3 + 42723)b_r\mu_r - (5184(15d_c + 142)\zeta_3 - 455545d_c \right. \\
&- 2844276)b_r^2 - 4(1296(21d_c + 676)\zeta_3 - 101047d_c - 1142832)\mu_r^2 \left. \right) L_p \\
&- 540 \left( 5(289d_c + 2976)b_r^2 + 34320b_r\mu_r + 4(361d_c + 5520)\mu_r^2 \right) L_p^2 \\
&+ 32400 \left( 5(d_c + 8)b_r^2 + 160b_r\mu_r + 4(d_c + 40)\mu_r^2 \right) L_p^3 \left. \right]. \quad (1.112b)
\end{aligned}$$

## 1.5 Renormalization group and fixed points

In the previous section, we have computed explicitly and exactly up to three-loop order the renormalization constants of the flexuron field and the couplings. In this section, we will use them to derive the renormalization-group functions of the effective flexural model. To do so, we first derive the beta functions by solving the system (1.54) up to three-loop order, reading

$$\begin{aligned} \beta_\mu = & -2\mu_r\varepsilon + \frac{\mu_r(10b_r + (d_c + 20)\mu_r)}{6(4\pi)^2} + \frac{\mu_r(5(15d_c - 212)b_r^2 + (107d_c + 1160)b_r\mu_r + 10(13d_c + 8)\mu_r^2)}{1296(4\pi)^4} \\ & - \frac{\mu_r}{1119744(4\pi)^6} \left[ 2(d_c(41625d_c - 180563) - 516252 - 5184(9d_c + 16)\zeta_3)b_r^3 \right. \\ & \quad - (d_c(34987d_c + 791004) - 2654448 - 20736(61d_c + 21)\zeta_3)b_r^2\mu_r \\ & \quad - (8(d_c(3920d_c + 263247) + 326922) - 5184(283d_c + 342)\zeta_3)b_r\mu_r^2 \\ & \quad \left. + 4(d_c(263d_c + 660820) - 2609592 + 2592(1018 - 223d_c)\zeta_3)\mu_r^3 \right], \end{aligned} \quad (1.113a)$$

$$\begin{aligned} \beta_b = & -2b_r\varepsilon + \frac{5b_r(b_r(d_c + 4) + 8\mu_r)}{12(4\pi)^2} - \frac{b_r(5b_r^2(61d_c + 424) - 10b_r(89d_c + 232)\mu_r + 8(111d_c - 20)\mu_r^2)}{2592(4\pi)^4} \\ & + \frac{b_r}{2239488(4\pi)^6} \left[ (7d_c(29285d_c + 191012) + 2065008 - 41472(d_c - 8)\zeta_3)b_r^3 \right. \\ & \quad + 8(5d_c(392d_c + 32187) - 663612 - 36288(10d_c + 3)\zeta_3)b_r^2\mu_r \\ & \quad + 4(d_c(87893d_c + 743556) + 1307688 - 5184(68d_c + 171)\zeta_3)b_r\mu_r^2 \\ & \quad \left. - 32(5d_c(279d_c + 37721) - 652398 - 1296(96d_c - 509)\zeta_3)\mu_r^3 \right], \end{aligned} \quad (1.113b)$$

together with the anomalous dimension of the flexuron field

$$\begin{aligned} \eta = & \frac{5(b_r + 2\mu_r)}{6(4\pi)^2} + \frac{5b_r^2(15d_c - 212) + 1160b_r\mu_r + 4(20 - 111d_c)\mu_r^2}{2592(4\pi)^4} \\ & + \frac{1}{1119744(4\pi)^6} \left[ (d_c(180563 - 41625d_c) + 516252 + 5184(9d_c + 16)\zeta_3)b_r^3 \right. \\ & \quad + 6(56445d_c - 221204 - 18144(5d_c + 2)\zeta_3)b_r^2\mu_r \\ & \quad + 12(82681d_c + 108974 - 1296(50d_c + 57)\zeta_3)b_r\mu_r^2 \\ & \quad \left. - 8(5d_c(279d_c + 37721) - 652398 - 1296(96d_c - 509)\zeta_3)\mu_r^3 \right], \end{aligned} \quad (1.114)$$

which are the main result of this chapter<sup>5</sup>.

From the  $\beta$ -functions, we may now compute the fixed points up to three-loop by the system  $\beta_x(\mu^*, b^*) = 0$ ,  $x = \mu, b$ . The solving is indeed perturbative, *i.e.*, we suppose an ansatz of the form  $\mu = \mu^{(1)}\varepsilon + \mu^{(2)}\varepsilon^2 + \mu^{(3)}\varepsilon^3 + \dots$  and similarly for  $b$ , and solve order by order. From one to three-loop accuracy, there are 4 fixed points, as advertised in the discussion below equation (1.59).

### 1.5.1 Gaussian fixed point $P_1$

First, the Gaussian fixed point  $P_1$  reading

$$P_1: \left. \begin{aligned} \mu_1^* &= 0 + O(\varepsilon^4) \\ b_1^* &= 0 + O(\varepsilon^4) \end{aligned} \right\} \text{ (Gaussian),} \quad (1.115)$$

<sup>5</sup>We also computed the mass anomalous dimension and checked explicitly that  $\eta_m = 4 - d - \eta$ . See footnotes 2 and 3.

where both couplings are trivial. At this point the theory is completely free, *i.e.*, non-interacting. This point is twice unstable in the RG flow sense, *i.e.*, the eigenvalues of the stability matrix (1.60) are both negative, implying that this fixed point is repulsive in all directions as the renormalization flow goes to lower energies. In this trivial case, the corresponding flexuron anomalous dimension is also vanishing

$$\eta(P_1) = 0 + O(\varepsilon^4). \quad (1.116)$$

Indeed, no interaction means no anomalous scaling of the correlation functions, *i.e.*, no critical exponents.

### 1.5.2 Shearless fixed point $P'_2$

Second, the shearless fixed point  $P'_2$ , reading<sup>6</sup>

$$P'_2: \quad \mu_2^* = 0 + O(\varepsilon^4) \quad (\text{Shearless}), \quad (1.117a)$$

$$b_2^* = (4\pi)^2 \left[ \frac{24\varepsilon}{5(d_c+4)} + \left( \frac{96}{5(d_c+4)^3} + \frac{488}{75(d_c+4)^2} \right) \varepsilon^2 + \left( \frac{768}{5(d_c+4)^5} - \frac{32(10368\zeta_3 - 18371)}{5625(d_c+4)^4} + \frac{8(3456\zeta_3 + 37643)}{5625(d_c+4)^3} - \frac{81998}{3375(d_c+4)^2} \right) \varepsilon^3 + O(\varepsilon^4) \right], \quad (1.117b)$$

with vanishing shear modulus  $\mu_2^*$  and a non-trivial value for  $b_2^*$ . The absence of shear is a characteristic property of fluid membranes, although a dynamical connectivity would also be needed, which is not the case here [31]. The two-loop order correction to this fixed point has first been computed by Mauri and Katsnelson [55]. Let us remark that the Poisson ratio is not properly defined for this fixed point since it reads

$$\nu(P'_2) = \frac{b_2^* - \mu_2^*}{b_2^*(d-2) + \mu_2^*}, \quad (1.118)$$

which is singular as  $\mu_2^* \rightarrow 0$  and  $d \rightarrow 2$ . As for the eigenvalues of the stability matrix (1.60), it reveals that it is unstable in the  $\mu_r$  direction, and stable in the  $b_r$  direction. The anomalous dimension of the flexuron field is also non-trivial and reads

$$\eta(P'_2) = \frac{4\varepsilon}{d_c+4} + \left( \frac{16}{(d_c+4)^3} - \frac{20}{3(d_c+4)^2} + \frac{2}{3(d_c+4)} \right) \varepsilon^2 + \left( \frac{128}{(d_c+4)^5} - \frac{16(10368\zeta_3 + 2029)}{3375(d_c+4)^4} - \frac{4(5184\zeta_3 + 58177)}{3375(d_c+4)^3} + \frac{4(3888\zeta_3 + 27239)}{3375(d_c+4)^2} - \frac{37}{9(d_c+4)} \right) \varepsilon^3 + O(\varepsilon^4). \quad (1.119)$$

We then observe an interesting structure in the perturbative series with denominators in powers of  $1/(4+d_c)$ . Indeed, in the physical case  $d_c = 1$ ,

$$\eta(P'_2) = \frac{4\varepsilon}{5} - \frac{2\varepsilon^2}{375} + \frac{(119232\zeta_3 - 120079)\varepsilon^3}{2109375} + O(\varepsilon^4), \quad (1.120)$$

which mean that each term of the series gets divided by increasing powers of  $1/5$ . Numerically, this series reads

$$\eta(P'_2) = 0.8000\varepsilon - 0.005333\varepsilon^2 + 0.01102\varepsilon^3 + O(\varepsilon^4), \quad (1.121)$$

where we indeed observe very small coefficients. Naively, in perturbative multi-loop computations, one usually expect perturbative series to be manifestly asymptotic. However, in our case, we observe that the asymptotic nature of the series is alleviated, at least for the first terms, thanks to the apparent structure in  $1/(d_c+4)$ , allowing the first terms to be small and in some cases even decreasing. In the

<sup>6</sup>We recall that we named this fixed point  $P'_2$  instead of simply  $P_2$  because this name is reserved for the two-field case. As we will see in the next chapter, contrary to the other fixed points,  $P_2$  in the two-field model does not identify exactly with  $P'_2$  in the effective flexural model.

particular case of (1.121) we still observe that the third contribution is twice the second one. Therefore, we expect the asymptotic nature of the series to manifest at higher orders, such that resummations will be needed. As we will see in the following, structures in  $1/(n+d_c)$  will be also present for the next fixed points, with bigger values for  $n$ , such that the three-loop coefficient will be smaller than the two-loop one. In this case, we will follow the empiric ‘‘Optimal Truncation Rule’’ that if the first terms of an asymptotic series are small and decreasing, simply summing them provides a good approximation<sup>7</sup> of the series, see [66]. Indeed, taking raw  $\varepsilon = 1$ , in the series yields successively

$$\boxed{\eta_{1\text{-loop}}(P'_2) = 0.8000, \quad \eta_{2\text{-loop}}(P'_2) = 0.7947, \quad \eta_{3\text{-loop}}(P'_2) = 0.8057.} \quad (1.122)$$

The one-loop result has been first obtained in [29], the two-loop result (32 year later) in [47, 55], and the three-loop result in [1]. The four-loop result is still unknown, since the four-loop study [57] was carried out in the two-field model, where  $P_2$  is different from  $P'_2$ .

### 1.5.3 Infinitely compressible fixed point $P_3$

Third, the infinitely compressible fixed point  $P_3$  reading

$$P_3: \quad \mu_3^* = (4\pi)^2 \left[ \frac{12\varepsilon}{d_c + 20} + \left( \frac{1680}{(d_c + 20)^3} - \frac{260}{3(d_c + 20)^2} \right) \varepsilon^2 + \left( \frac{470400}{(d_c + 20)^5} \right. \right. \quad (1.123a)$$

$$\left. \left. + \frac{8(591624\zeta_3 - 709633)}{9(d_c + 20)^4} - \frac{4(144504\zeta_3 - 171025)}{27(d_c + 20)^3} + \frac{263}{27(d_c + 20)^2} \right) \varepsilon^3 + O(\varepsilon^4) \right],$$

$$b_3^* = 0 + O(\varepsilon^4) \quad (\text{Infinitely compressible}) \quad (1.123b)$$

with a non-trivial value for the shear modulus  $\mu_3^*$  but a vanishing coordinate  $b_3^*$ , *i.e.*, a vanishing bulk modulus since  $b \propto B = \lambda + 2\mu/d$ . In this case, the invariance under uniform compression can be interpreted as a conformal invariance [31, 58]. As for the stability, it is once unstable, *i.e.*, attractive in the  $\mu_r$  direction but repulsive in the  $b_r$  direction (which is exactly the opposite of  $P'_2$ ). Let us also note that the Poisson ratio is trivial for this fixed point since it reads

$$\nu(P_3) = \frac{b_3^* - \mu_3^*}{b_3^*(d-2) + \mu_3^*} = -1, \quad (1.124)$$

in any dimension. This implies that the membrane, in this infinitely compressible phase, exhibits maximum auxetic properties, *i.e.*, a longitudinal compression of an amount  $x$  will result in a transverse compression of the same amount  $x$ .

This infinitely compressible fixed point leads to a non-trivial value for the field anomalous dimension of the flexuron

$$\eta(P_3) = \frac{20\varepsilon}{d_c + 20} + \left( \frac{2800}{(d_c + 20)^3} + \frac{1060}{3(d_c + 20)^2} - \frac{74}{3(d_c + 20)} \right) \varepsilon^2 + \left( \frac{784000}{(d_c + 20)^5} \right. \quad (1.125)$$

$$\left. + \frac{40(591624\zeta_3 - 615553)}{27(d_c + 20)^4} - \frac{2(1006344\zeta_3 - 1024193)}{27(d_c + 20)^3} + \frac{2(20736\zeta_3 - 17105)}{27(d_c + 20)^2} - \frac{155}{9(d_c + 20)} \right) \varepsilon^3 + O(\varepsilon^4),$$

where the structure in  $d_c$  now displays denominators in powers of  $d_c + 20$ . We therefore expect the first terms of the series to be even more convergent than for  $P'_2$ . Indeed, in the physical case  $d_c = 1$ , it reads

$$\eta(P_3) = \frac{20\varepsilon}{21} - \frac{94\varepsilon^2}{1323} - \frac{(312336\zeta_3 - 9011)\varepsilon^3}{5250987} + O(\varepsilon^4), \quad (1.126)$$

<sup>7</sup>We can illustrate that results (1.122) are good approximations by showing that, up to three loops, resummations of the series (1.121) give results close to the raw ones. As an example, a simple Padé approximant yields either  $\eta^{[2/1]}(P'_2) = 0.7983$ , which is very close to (1.122), and  $\eta^{[1/2]}(P'_2) = 0.8057$ , where the first four digits are exactly the same as the three-loop result with raw  $\varepsilon = 1$ . Nevertheless, such oscillating series with small coefficients calls for a four-loop computation and a resummation with Padé approximant [2/2].

which numerically reads

$$\eta(\text{P}_3) = 0.9524\varepsilon - 0.07105\varepsilon^2 - 0.06978\varepsilon^3 + \mathcal{O}(\varepsilon^4). \quad (1.127)$$

This time, the first coefficients of the  $\varepsilon$ -series are small and decreasing such that taking raw  $\varepsilon = 1$  gives a very good approximation<sup>8</sup> to the series, *i.e.*, successively

$$\boxed{\eta_{1\text{-loop}}(\text{P}_3) = 0.9524, \quad \eta_{2\text{-loop}}(\text{P}_3) = 0.8813, \quad \eta_{3\text{-loop}}(\text{P}_3) = 0.8115.} \quad (1.128)$$

The one-loop result has been first obtained in [29], the two-loop result (32 year later) in [47], and the three-loop result in [1]. Let us remark that a few months after we released the three-loop result, the four-loop computation has been achieved (in the equivalent two-field model) in [57], leading to a new improved value  $\eta_{4\text{-loop}}(\text{P}_3) = 0.7368$ .

### 1.5.4 Non-trivial fixed point $\text{P}_4$

Finally and most importantly, the fourth, nontrivial, fixed point  $\text{P}_4$  is given by

$$\text{P}_4: \quad \mu_4^* = (4\pi)^2 \left[ \frac{12\varepsilon}{d_c + 24} + \left( \frac{1440}{(d_c + 24)^3} - \frac{616}{5(d_c + 24)^2} \right) \varepsilon^2 + \left( \frac{345600}{(d_c + 24)^5} + \frac{96(576288\zeta_3 - 812161)}{125(d_c + 24)^4} - \frac{144(12288\zeta_3 - 20401)}{125(d_c + 24)^3} - \frac{8168}{75(d_c + 24)^2} \right) \varepsilon^3 + \mathcal{O}(\varepsilon^4) \right], \quad (1.129a)$$

$$b_4^* = (4\pi)^2 \left[ \frac{24\varepsilon}{5(d_c + 24)} + \left( \frac{576}{(d_c + 24)^3} + \frac{1936}{25(d_c + 24)^2} \right) \varepsilon^2 + \left( \frac{138240}{(d_c + 24)^5} + \frac{4416(25056\zeta_3 - 31007)}{625(d_c + 24)^4} - \frac{48(71136\zeta_3 - 163967)}{625(d_c + 24)^3} - \frac{77512}{375(d_c + 24)^2} \right) \varepsilon^3 + \mathcal{O}(\varepsilon^4) \right], \quad (1.129b)$$

where both couplings are non-vanishing. This fixed point is fully stable, *i.e.*, attractive in the direction of  $\mu_r$  and  $b_r$  in the RG flow. In that sense, it fully controls the flat phase of the membrane in the long range. Interestingly, this scale invariant fixed point is believed to be non-conformal [58]. Let us also remark that at these coordinates, the Poisson ratio perturbatively reads

$$\begin{aligned} \nu(\text{P}_4) &= \frac{b_4^* - \mu_4^*}{b_4^*(d-2) + \mu_4^*} \\ &= -\frac{1}{3} + \left( \frac{88}{9(d_c + 24)} - \frac{4}{27} \right) \varepsilon + \left( \frac{3520}{3(d_c + 24)^3} + \frac{4(288\zeta_3 + 4349)}{75(d_c + 24)^2} - \frac{1406}{135(d_c + 24)} - \frac{16}{243} \right) \varepsilon^2 + \mathcal{O}(\varepsilon^3). \end{aligned} \quad (1.130)$$

However, we cannot do much with this series since numerically it reads

$$\nu(\text{P}_4) = -\frac{1}{3} (1 - 0.7289\varepsilon + 0.02006\varepsilon^2 + \mathcal{O}(\varepsilon^3)), \quad (1.131)$$

which is very hard to estimate in the limit  $\varepsilon \rightarrow 1$ , *i.e.*, we don't have enough terms for a resummation<sup>9</sup>.

Let us get back to our main goal, the anomalous dimension of the flexuron, which for this non-trivial fixed point takes the value

$$\eta(\text{P}_4) = \frac{24\varepsilon}{d_c + 24} + \left( \frac{2880}{(d_c + 24)^3} + \frac{456}{(d_c + 24)^2} - \frac{24}{(d_c + 24)} \right) \varepsilon^2 + \left( \frac{691200}{(d_c + 24)^5} \right) \varepsilon^3 + \mathcal{O}(\varepsilon^4) \quad (1.132)$$

<sup>8</sup>For completeness, resummations of the series (1.126) with simple Padé approximant reads  $\eta^{[1/2]}(\text{P}_3) = 0.8257$  and the [2/1] approximant is negative, hence unphysical. See the related footnote 7. Note that at four loops [57], the Padé approximant behaves badly, reading  $\eta^{[2/2]}(\text{P}_3) = 1.8695$ .

<sup>9</sup>Another approach is to use a Padé approximant [2/1] ([1/2] is unphysical) directly on the fixed point coordinates (1.129), yielding at  $d_c = 1$  and  $\varepsilon = 1$ , the values  $\mu_4^{*[1/2]} = 64.23$ , and  $b_4^{*[1/2]} = 51.59$  and then  $\nu^{[1/2]}(\text{P}_4) = -0.1968$ , which is smaller but quite close to  $\nu = -1/3$ . Note that the value  $\nu = -1/3$  has been obtained at leading order from multiple approaches, see, *e.g.*, the seminal paper [25], and in some cases is even argued to be exact [37], indicating that in the end, the contribution of the resummed perturbative series is expected to be small.

$$+ \frac{576(192096\zeta_3 - 234137)}{125(d_c + 24)^4} - \frac{8(923616\zeta_3 - 1031777)}{125(d_c + 24)^3} + \frac{4(86832\zeta_3 - 39029)}{375(d_c + 24)^2} - \frac{64}{3(d_c + 24)} \Big) \varepsilon^3 + \mathcal{O}(\varepsilon^4),$$

where the structure in  $d_c$  is now in  $d_c + 24$ , which we expect will alleviate even more the asymptotic aspect of the series. Indeed, in the physical case of codimension  $d_c = 1$ , it reads

$$\eta(\text{P}_4) = \frac{24\varepsilon}{25} - \frac{144\varepsilon^2}{3125} - \frac{4(1286928\zeta_3 - 568241)\varepsilon^3}{146484375} + \mathcal{O}(\varepsilon^4), \quad (1.133)$$

and numerically,

$$\eta(\text{P}_4) = 0.9600\varepsilon - 0.04608\varepsilon^2 - 0.02673\varepsilon^3 + \mathcal{O}(\varepsilon^4). \quad (1.134)$$

Again, the first coefficients of the  $\varepsilon$ -series are small and decreasing and taking raw  $\varepsilon = 1$  gives a very good approximation<sup>10</sup> to the series, *i.e.*, successively

$$\boxed{\eta_{1\text{-loop}}(\text{P}_4) = 0.9600, \quad \eta_{2\text{-loop}}(\text{P}_4) = 0.9139, \quad \eta_{3\text{-loop}}(\text{P}_4) = 0.8872.} \quad (1.135)$$

Similarly to  $\text{P}_3$ , the one-loop result has been first obtained in [29], the two-loop result (32 year later) in [47], the three-loop result in [1] and a few months after, the four-loop computation has been achieved (in the two-field model) in [57], yielding a new improved value  $\eta_{4\text{-loop}}(\text{P}_4) = 0.8670$ . Therefore, the perturbative value for the anomalous stiffness slowly decrease with the loop order. To illustrate this fact, we provide in figure 1.10 a plot of the values obtained versus the loop order, and provide an exponential fit to give an estimate of where the value is going at higher-loop order.

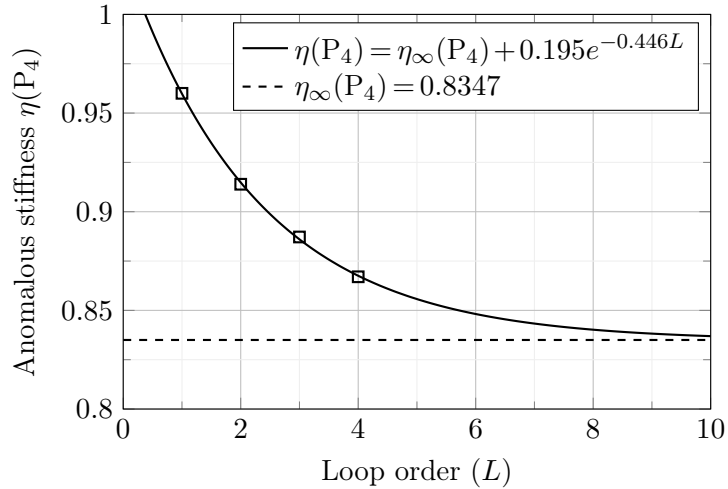


Figure 1.10: Exponential fit on the results found for  $\eta(\text{P}_4)$  from 1 to 4-loop. The values seem to slowly converge towards  $\eta_{\infty\text{-loop}}(\text{P}_4) = 0.8347$ .

Including the results from 1 to 4 loop order, this gives an estimated value at infinite loop order of

$$\boxed{\eta_{\infty\text{-loop}}(\text{P}_4) = 0.8347.} \quad (1.136)$$

This is our best estimate for the anomalous dimension of the flexuron field at the non-trivial fixed point governing the flat phase.

<sup>10</sup>For completeness, resummations of the series with simple Padé approximant reads  $\eta^{[1/2]}(\text{P}_4) = 0.8904$  and  $\eta^{[2/1]}(\text{P}_4) = 0.8503$ . See the related footnote 7. Note also that the four-loop results [57] yields a Padé approximant resummation of  $\eta^{[2/2]} = 0.8060$ .

### 1.5.5 Phase diagram

Finally, we provide in figure 1.11 the phase diagram obtained from all previous results. The picture is basically the same at one, two and three-loop order. The fixed points coordinates vary slightly with the loop order.  $P_1$ ,  $P'_2$  and  $P_3$  stay exactly on the mechanical stability lines imposed by positive shear modulus  $\mu_r > 0$  and positive bulk modulus  $b_r > 0$ . The scale on the axes is not displayed, as it depends on the choice of  $\varepsilon$  used for the plot (the picture is not substantially changed for reasonable values of  $\varepsilon$ , *i.e.*,  $0.001 < \varepsilon < 0.8$ ).

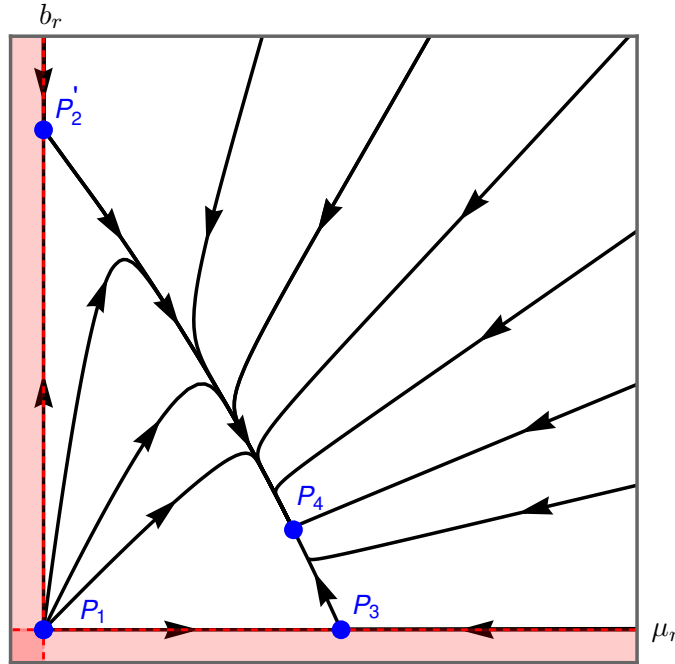


Figure 1.11: RG-flow diagram on the plane  $(\mu_r, b_r)$ . The mechanical stability of the model imposes  $\mu_r > 0$  and  $b_r > 0$ . The corresponding non-physical regions are indicated in red and delimited by the red dashed lines  $\mu_r = 0$ ,  $b_r = 0$ , on which lie the fixed points  $P_1$ ,  $P'_2$  and  $P_3$  at all loop orders. This plot has been obtained from the beta functions (1.113) and remain qualitatively the same for all values  $0.001 < \varepsilon < 0.8$ .

## 1.6 Comparisons with other approaches

Let us first recall that all the results that we have obtained so far were limited to a given order in the loop expansion, but are otherwise exact. In this section, we will use them to benchmark other results obtained in the literature using self-consistent equations or non-perturbative methods, but still relying on uncontrolled approximations (such as an ansatz or truncations) in order to perform actual computations. Here, it should be underlined that we do not pretend that our estimates for physical quantities at  $\varepsilon = 1$  should be closer to the experiments than the results obtained via another technique. However, the perturbative expansions in  $\varepsilon = (4-d)/2$  that we obtained in the previous sections are exact order by order. Therefore, if we take the results of a self-consistent or non-perturbative technique and re-expand it in  $\varepsilon$ , we can benchmark it order by order and observe if the corresponding technique is able to mimic the first terms of the true perturbative expansion given by our results.

### 1.6.1 Benchmarking the NPRG approach

We will first focus on the so called Non-Perturbative Renormalization Group (NPRG) technique. This method is based on solving the exact Wilsonian RG equation controlling the running of an effective action derived from the model one wants to study [67] (see [68–72] for reviews). For the Wilsonian equation to be solved, approximations are needed, and the effective action is often truncated in powers of the field derivatives present in the action, which is called a derivative expansion (see [73–75] for empirical validations of the method on the Ising model). The advantage of the NPRG is that it leads to solutions that remain non-perturbative both in  $\varepsilon$  and  $d_c$  as well as in the couplings at leading order. Nevertheless, one should keep in mind that this approach is not exact and is generally approximating starting at two-loop of the perturbative approaches (as it would require the knowledge of infinite series in the derivatives [76, 77], which can be partially achieved with the use of ansatz [42, 43]).

The renormalization-group functions for the effective flexural model at leading order in the NPRG technique has been obtained in [41–43]. We take the results of [41] that, in our conventions, reads

$$\beta_\mu^{\text{NPRG}} = \mu F\left(\frac{2\mu}{d+1}\right), \quad \beta_b^{\text{NPRG}} = bF(b), \quad \eta_{\text{NPRG}} = \frac{(d+4)A_d}{(d+2)(d+4)d^2 + A_d}, \quad (1.137)$$

where we defined the temporary functions

$$F(x) = d - 4 + 2\eta + \frac{d(d-\eta+8)d_c\eta}{(d+8)(d-\eta+4)(b+(d-2)\mu)}x, \quad A_d = \frac{16(d+1)(b+(d-2)\mu)}{(4\pi)^{d/2}\Gamma(d/2)}. \quad (1.138)$$

The first approach is to solve the system ( $\beta_\mu^{\text{NPRG}} = \beta_b^{\text{NPRG}} = 0$ ) non-perturbatively, *i.e.*, at exactly  $d=2$  and  $d_c=1$ . This yields two values for the anomalous dimension of the flexuron field, the Gaussian value  $\eta_{\text{NPRG}}=0$ , and  $\eta_{\text{NPRG}}=0.8491$ , which is the value for non-trivial coordinates of the fixed point, *i.e.*, at  $P_4$ . This value takes into account non-perturbative effects (an infinite number of diagrams) and in principle should be very precise. However, it relies on uncontrolled approximations and may be unreliable.

What we can do to increase our trust into this value is to benchmark the NPRG results by comparing them order by order with our perturbative results, that are exact order by order. We therefore solve the NPRG system perturbatively, *i.e.*, for  $d=4-2\varepsilon$ , yielding

$$\eta_{\text{NPRG}}(P_1) = 0, \quad (1.139a)$$

$$\eta_{\text{NPRG}}(P'_2) = \frac{4\varepsilon}{d_c+4} + \left( \frac{8}{3(d_c+4)^3} - \frac{14}{3(d_c+4)^2} + \frac{1}{d_c+4} \right) \varepsilon^2 \quad (1.139b)$$

$$+ \left( \frac{32}{9(d_c+4)^5} - \frac{76}{9(d_c+4)^4} + \frac{25}{3(d_c+4)^3} - \frac{65}{18(d_c+4)^2} + \frac{1}{2(d_c+4)} \right) \varepsilon^3 + \mathcal{O}(\varepsilon^4),$$

$$\eta_{\text{NPRG}}(P_3) = \frac{20\varepsilon}{d_c+20} + \left( \frac{1000}{3(d_c+20)^3} + \frac{1330}{3(d_c+20)^2} - \frac{23}{d_c+20} \right) \varepsilon^2 \quad (1.139c)$$

$$+ \left( \frac{100000}{9(d_c+20)^5} + \frac{204500}{9(d_c+20)^4} + \frac{26365}{3(d_c+20)^3} - \frac{10217}{18(d_c+20)^2} + \frac{7}{2(d_c+20)} \right) \varepsilon^3 + \mathcal{O}(\varepsilon^4),$$

$$\eta_{\text{NPRG}}(P_4) = \frac{24\varepsilon}{d_c+24} + \left( \frac{576}{(d_c+24)^3} + \frac{504}{(d_c+24)^2} - \frac{22}{d_c+24} \right) \varepsilon^2 \quad (1.139d)$$

$$+ \left( \frac{27648}{(d_c+24)^5} + \frac{37440}{(d_c+24)^4} + \frac{9192}{(d_c+24)^3} - \frac{546}{(d_c+24)^2} + \frac{4}{d_c+24} \right) \varepsilon^3 + \mathcal{O}(\varepsilon^4).$$

First, we observe that the NPRG is capable of mimicking accurately the  $1/(d_c+n)$  structure previously observed with  $n=4, 20, 24$ . As for the coefficients, the NPRG is, as expected, exact at one-loop and for higher orders, is approximating the loop expansion with rationals. Indeed, the true loop expansion, in dimensional regularization, contains the Riemann Zeta function evaluated at integer values, such as



$\zeta_3 \approx 1.202$  at three-loop order. The comparison of NPRG with our work is therefore easier numerically, and yields up to three-loop order

$$\eta_{\text{NPRG}}(P_1) = 0, \quad \eta(P_1) = 0, \quad (1.140a)$$

$$\eta_{\text{NPRG}}(P'_2) = 0.8000\varepsilon + 0.03467\varepsilon^2 + 0.00985\varepsilon^3, \quad \eta(P'_2) = 0.8000\varepsilon - 0.00533\varepsilon^2 + 0.01102\varepsilon^3, \quad (1.140b)$$

$$\eta_{\text{NPRG}}(P_3) = 0.9524\varepsilon - 0.05395\varepsilon^2 - 0.05192\varepsilon^3, \quad \eta(P_3) = 0.9524\varepsilon - 0.07105\varepsilon^2 - 0.06978\varepsilon^3, \quad (1.140c)$$

$$\eta_{\text{NPRG}}(P_4) = 0.9600\varepsilon - 0.03674\varepsilon^2 - 0.02663\varepsilon^3, \quad \eta(P_4) = 0.9600\varepsilon - 0.04608\varepsilon^2 - 0.02673\varepsilon^3, \quad (1.140d)$$

where the left part is the NPRG and the right part is our three-loop results that we reproduced for convenience. On the one hand, we observe that the NPRG fails to properly reproduce the anomalous dimension of the flexuron field in the case of  $P'_2$ . Indeed, the  $O(\varepsilon^2)$  term has the wrong sign and is  $\sim 6.5$  too large. On the other hand, it is evident that NPRG is very successful to reproduce the true loop expansion for both  $P_3$  and  $P_4$ . We believe that this success is partially due to the apparent convergent nature of the first terms of these asymptotic series.

## 1.6.2 Benchmarking the SCSA approach

We will now proceed with a similar analysis for the results obtained via the so-called Self Consistent Screening Approximation (SCSA) technique, originally introduced by Bray [78] for the  $O(N)$  model and then applied to membranes by le Doussal and Radzihovsky [40]. The SCSA is based on the self-consistent solution of the Schwinger-Dyson equations (the equations of motion of the correlation functions) via successive dressing approximations for the 2-point correlation functions, as well as neglecting the vertex corrections (in the gauge theory language, such an approximation is called the rainbow approximation). This method is generally employed using the effective flexural action (1.13) which is more suitable than the two field model (1.9) to establish self-consistent equations.

The SCSA results have been obtained at leading order in [12, 40], and in the conventions of the current manuscript, are given by the equations

$$P_1: \quad \eta = 0, \quad (1.141a)$$

$$P'_2: \quad 2F(d, \eta) - d_c = 0, \quad (1.141b)$$

$$P_3: \quad (d+1)(d-2)F(d, \eta) - d_c = 0, \quad (1.141c)$$

$$P_4: \quad d(d-1)F(d, \eta) - d_c = 0, \quad (1.141d)$$

that need to be solved for  $\eta$  and where we defined the function

$$F(d, \eta) = \frac{\Gamma(2-\eta)\Gamma(2-\eta/2)\Gamma(\eta/2)\Gamma(\eta+d)}{\Gamma(2-\eta-d/2)\Gamma((4-\eta+d)/2)\Gamma((\eta+d)/2)\Gamma(\eta+d/2)}. \quad (1.142)$$

Solving non-perturbatively these equations leads to the Gaussian value  $\eta_{\text{SCSA}} = 0$  and to the value  $\eta_{\text{SCSA}} = 0.8209$ , which is the self-consistent result at the equivalent of the fixed point  $P_4$  where the fixed point coordinates are non-trivial.

In order to benchmark the SCSA, we then expand in  $d = 4 - 2\varepsilon$  and solve perturbatively the SCSA system for each fixed point, in order to check the ability of the SCSA to reproduce the true perturbative expansion, reading

$$\eta_{\text{SCSA}}(P_1) = 0, \quad (1.143a)$$

$$\begin{aligned} \eta_{\text{SCSA}}(P'_2) &= \frac{4\varepsilon}{d_c+4} + \left( \frac{16}{(d_c+4)^3} - \frac{20}{3(d_c+4)^2} + \frac{2}{3(d_c+4)} \right) \varepsilon^2 \\ &+ \left( \frac{128}{(d_c+4)^5} + \frac{128}{3(d_c+4)^4} - \frac{400}{3(d_c+4)^3} + \frac{406}{9(d_c+4)^2} - \frac{37}{9(d_c+4)} \right) \varepsilon^3 + O(\varepsilon^4), \end{aligned} \quad (1.143b)$$

$$\begin{aligned} \eta_{\text{SCSA}}(\text{P}_3) &= \frac{20\varepsilon}{d_c+20} + \left( \frac{2000}{(d_c+20)^3} + \frac{1180}{3(d_c+20)^2} - \frac{74}{3(d_c+20)} \right) \varepsilon^2 \\ &+ \left( \frac{400000}{(d_c+20)^5} + \frac{584000}{3(d_c+20)^4} - \frac{18720}{(d_c+20)^3} + \frac{6694}{9(d_c+20)^2} - \frac{155}{9(d_c+20)} \right) \varepsilon^3 + \text{O}(\varepsilon^4), \end{aligned} \quad (1.143c)$$

$$\begin{aligned} \eta_{\text{SCSA}}(\text{P}_4) &= \frac{24\varepsilon}{d_c+24} + \left( \frac{3456}{(d_c+24)^3} + \frac{432}{(d_c+24)^2} - \frac{24}{(d_c+24)} \right) \varepsilon^2 \\ &+ \left( \frac{995328}{(d_c+24)^5} + \frac{345600}{(d_c+24)^4} - \frac{35520}{(d_c+24)^3} + \frac{1320}{(d_c+24)^2} - \frac{64}{3(d_c+24)} \right) \varepsilon^3 + \text{O}(\varepsilon^4). \end{aligned} \quad (1.143d)$$

For ease of comparison, we then provide numerically the results of the SCSA, alongside with our results, yielding, up to three-loop order

$$\eta_{\text{SCSA}}(\text{P}_1) = 0, \quad \eta(\text{P}_1) = 0, \quad (1.144a)$$

$$\eta_{\text{SCSA}}(\text{P}'_2) = 0.8000\varepsilon - 0.005333\varepsilon^2 + 0.02478\varepsilon^3, \quad \eta(\text{P}'_2) = 0.8000\varepsilon - 0.005333\varepsilon^2 + 0.01102\varepsilon^3, \quad (1.144b)$$

$$\eta_{\text{SCSA}}(\text{P}_3) = 0.9524\varepsilon - 0.06673\varepsilon^2 - 0.05602\varepsilon^3, \quad \eta(\text{P}_3) = 0.9524\varepsilon - 0.07105\varepsilon^2 - 0.06978\varepsilon^3, \quad (1.144c)$$

$$\eta_{\text{SCSA}}(\text{P}_4) = 0.9600\varepsilon - 0.04762\varepsilon^2 - 0.02796\varepsilon^3, \quad \eta(\text{P}_4) = 0.9600\varepsilon - 0.04608\varepsilon^2 - 0.02673\varepsilon^3. \quad (1.144d)$$

What we observe is that SCSA (on the left) seems very accurate to mimic numerically the true  $\varepsilon$  expansion obtained within our study (on the right). The first order is exact, as expected from such a technique, the second order is very close for both  $\text{P}_3$  and  $\text{P}_4$  and even exact for  $\text{P}'_2$ , and finally, the three-loop order is very close for both  $\text{P}_3$  and  $\text{P}_4$  but still differs by a factor two for  $\text{P}'_2$ .

Let us note that the results (1.143) can be obtained from our perturbative approach by neglecting all vertex corrections. To underline this fact, one can add a tracking factor  $V$  with  $V^2 = V$  in front of each diagram containing a vertex correction. In this case, our perturbative results yields numerically

$$\eta(\text{P}_1) = 0 + \text{O}(\varepsilon^4), \quad (1.145a)$$

$$\eta(\text{P}'_2) = 0.8000\varepsilon - 0.005333\varepsilon^2 + (0.02478 - 0.01376V)\varepsilon^3 + \text{O}(\varepsilon^4), \quad (1.145b)$$

$$\eta(\text{P}_3) = 0.9524\varepsilon - (0.06673 + 0.004319V)\varepsilon^2 - (0.05602 + 0.01376V)\varepsilon^3 + \text{O}(\varepsilon^4), \quad (1.145c)$$

$$\eta(\text{P}_4) = 0.9600\varepsilon - (0.04762 - 0.001536V)\varepsilon^2 - (0.02796 - 0.001230V)\varepsilon^3 + \text{O}(\varepsilon^4), \quad (1.145d)$$

which recover the SCSA results if one neglects the vertex corrections (in the limit  $V = 0$ ), and recover our results if allowing them (in the limit  $V = 1$ ). Each term which is  $V$ -independent is then exact in SCSA. The general results (1.145) also show that vertex correction terms ( $\propto V$ ) are small, explaining why SCSA is rather close numerically.

### 1.6.3 Comparison with large- $d_c$ approaches

In this last section, we compare our results to the values obtained from the large- $d_c$  approach in the SCSA technique (recalling that  $d_c = D - d$  is the codimension of the membrane which is  $d_c = 1$  in the physical case  $D = 3$ ,  $d = 2$ ). According to the SCSA approach in large  $d_c$  [12, 40], the field anomalous dimension is found to be

$$\eta_{\text{SCSA}}(d, d_c) = \frac{8}{d_c} \frac{d-1}{d+2} \frac{\Gamma(d)}{\Gamma^3(d/2)\Gamma(2-d/2)} + \text{O}(1/d_c^2), \quad (1.146)$$

which is exact for all  $d$ , at this order in  $d_c$ . Moreover, the fixed point correspondence in the conventions of the current chapter reads

$$\eta_{\text{SCSA}}(\text{P}_1) = 0, \quad (1.147a)$$

$$\eta_{\text{SCSA}}(\text{P}'_2) = \eta_{\text{SCSA}}\left(d, \frac{d_c d (d-1)}{2}\right), \quad (1.147b)$$

$$\eta_{\text{SCSA}}(\text{P}_3) = \eta_{\text{SCSA}}\left(d, \frac{d_c d(d-2)}{(d-1)(d+1)}\right), \quad (1.147c)$$

$$\eta_{\text{SCSA}}(\text{P}_4) = \eta_{\text{SCSA}}(d, d_c). \quad (1.147d)$$

Upon setting  $d = 4 - 2\varepsilon$  and expanding up to  $\mathcal{O}(\varepsilon^3)$  the large- $d_c$  results, it reads

$$\eta_{\text{SCSA}}(\text{P}_1) = 0, \quad (1.148a)$$

$$\eta_{\text{SCSA}}(\text{P}'_2) = \frac{1}{d_c} \left( 4\varepsilon + \frac{2\varepsilon^2}{3} - \frac{37\varepsilon^3}{9} + \mathcal{O}(\varepsilon^4) \right) + \mathcal{O}(1/d_c^2), \quad (1.148b)$$

$$\eta_{\text{SCSA}}(\text{P}_3) = \frac{1}{d_c} \left( 20\varepsilon - \frac{74\varepsilon^2}{3} - \frac{155\varepsilon^3}{9} + \mathcal{O}(\varepsilon^4) \right) + \mathcal{O}(1/d_c^2), \quad (1.148c)$$

$$\eta_{\text{SCSA}}(\text{P}_4) = \frac{1}{d_c} \left( 24\varepsilon - 24\varepsilon^2 - \frac{64\varepsilon^3}{3} + \mathcal{O}(\varepsilon^4) \right) + \mathcal{O}(1/d_c^2). \quad (1.148d)$$

These results are in perfect accordance with our results, see (1.119), (1.125), (1.132), re-expanded to the first large- $d_c$  order. For example, for  $\text{P}_4$ , it is very easy to see that the series of numbers  $\{+24, -24, -64/3\}$  exactly corresponds to the last term in  $1/(d_c + 24)$  at each order of the  $\varepsilon$  expansion in our result (1.132). As a conclusion, we note that this comparison has already been done, up to four loops and in the two-field model framework, in [57] for  $\text{P}_3$  and  $\text{P}_4$  only, since the two field model cannot access  $\text{P}'_2$ . Therefore the agreement between large- $d_c$  expansions and our EFT approach for  $\text{P}'_2$  is a new result.

Let us also emphasize that the leading-order result (1.146) yields in  $d = 2$ , for the fixed point  $\text{P}_4$ , the value  $\eta_{\text{SCSA}}(\text{P}_4) = 2/d_c + \mathcal{O}(1/d_c^2)$ . Moreover, the contribution at order  $1/d_c^2$  to  $\eta$  at the fixed point  $\text{P}_4$  has been computed recently analytically (exactly in  $d = 2$ ) in [36], taking into account beyond-SCSA contributions, and reads

$$\eta_{\text{large-}d_c}(\text{P}_4) = \frac{2}{d_c} + \frac{73 - 68\zeta_3}{27d_c^2} + \mathcal{O}(1/d_c^3). \quad (1.149)$$

Naively, we would expect the large  $d_c$  approximation combined with (beyond-) SCSA technique to be very accurate, as it resums an infinite number of diagrams self-consistently. However, very surprisingly, the series yields numerically the value  $\eta_{\text{large-}d_c}(\text{P}_4) = 2/d_c - 0.32/d_c^2 + \mathcal{O}(1/d_c^3)$ , for which, if we set raw  $d_c = 1$ , reads  $\eta_{\text{large-}d_c}(\text{P}_4) = 1.68$ , well over the usual range of results  $[0.7, 0.9]$ . This series then behaves very badly compared to the series we obtained in the loop expansion, and definitely needs higher-order calculations combined with resummations to give a correct estimate of  $\eta$ . Let us also note that the NLO SCSA result, at  $1/d_c^2$ , as been obtained semi-analytically in [37] and according to the author yields ultimately a value of  $\eta_{\text{SCSA}}^{\text{NLO}}(\text{P}_4) = 0.78922(5)$ . However, to our knowledge, this result is not available analytically, or for all dimension  $d$ , so we cannot further compare it with our results. As a conclusive remark on the large  $d_c$  approach, let us recall that early computations [31, 33] (see also [79]) considered a large- $D$  approach, which is strictly equivalent to large  $d_c$  at leading order since  $d_c = D - d$ , yielding the result

$$\eta_{\text{large-}D}(\text{P}_4) = \frac{2}{D} + \mathcal{O}(1/D^2). \quad (1.150)$$

The key difference is that this result in the physical case  $D = 3$  reads  $\eta_{\text{large-}D}(\text{P}_4) = 2/3 = 0.667$ , which is a much better approximation than for the large  $d_c$  approach. Therefore, it would be interesting to carry a next-to-leading order computation in a large  $D$  limit, though it is unclear if this would be possible with usual diagrammatic techniques.

### 1.6.4 Comparison of $\eta(\mathbf{P}_4)$ with the literature

As a final summary, we provide the table 1.2 of all the values obtained for the flexuron-field anomalous dimension, at the non-trivial fixed point  $\mathbf{P}_4$ , over more than three decades of literature in simulations and theoretical studies of membranes.

$\eta(\mathbf{P}_4)$	Method	Year/ref
$\approx 0.66$	Monte Carlo (membrane)	1990 [80] Abraham, Nelson
0.667	Large $D$ (LO)	1988 [31, 33] Gutter, <i>et al.</i>
$\approx 0.7$	Monte Carlo (vesicles)	1991 [81] Komura, Baumgärtner
0.72(4)	Monte Carlo (membrane)	1989 [82] Leibler, Maggs
0.75(5)	Monte Carlo (membrane)	1990 [83] Gutter <i>et al.</i>
0.750(5)	Monte Carlo (membrane)	1996 [49] Bowick <i>et al.</i>
0.789	SCSA (large- $d_c$ NLO, semi-numerical)	2009 [37] Gazit
0.795(10)	Monte Carlo (graphene)	2013 [50] Tröster
0.806	4-loop (Padé approximant [2/2])	2021 [57] Pikelner
0.81(3)	Monte Carlo (membrane)	1993 [48] Zhang <i>et al.</i>
$\approx 0.82$	Molecular dynamics simulations	1996 [84] Zhang <i>et al.</i>
$\approx 0.82$	SCSA (LO, semi-numerical)	2010 [38, 39] Zakharchenko <i>et al.</i>
0.821	SCSA (LO, analytical)	1992 [12, 40] Le Doussal, Radzihovsky
0.835	1 to 4-loop (exponential fit)	2023 [1, 57] Metayer <i>et al.</i> and Pikelner
0.849	NPRG (analytical)	2009 [41] Kownacki, Mouhanna
$\approx 0.85$	NPRG (semi-numerical)	2009 [42, 43] Braghin, Hasselmann
$\approx 0.85$	Monte Carlo (graphene)	2009 [51] Los <i>et al.</i>
0.850	3-loop (Padé approximant [2/1])	2021 [1] Metayer <i>et al.</i>
0.867	4-loop	2021 [57] Pikelner
0.887	3-loop	2021 [1] Metayer <i>et al.</i>
0.890	3-loop (Padé approximant [1/2])	2021 [1] Metayer <i>et al.</i>
0.90(4)	Molecular dynamics simulations	1993 [85] Petsche, Grest
0.914	2-loop	2020 [47] Coquand <i>et al.</i>
0.960	1-loop	1988 [29, 32] Aronovitz, Lubensky
1	Mean field	1987 [28] Nelson, Peliti

Table 1.2: Results for the anomalous stiffness of flat membranes, obtained from 1987 to 2023, ranging in the interval [0.7,0.9]. Shaded lines are the multi-loop results explicitly computed in this chapter. Note that some references evaluated the roughness exponent ( $\zeta$ ), which we converted to the anomalous stiffness using  $\eta = 2(1 - \zeta)$ , see (1.4). According to the multi-loop results, the value to retain is  $\eta(\mathbf{P}_4) = 0.835$ .

## 1.7 Conclusion

In this chapter, we have analytically investigated the flat phase of polymerized membranes at three-loop order by means of a weak-coupling, perturbative approach. We have determined the RG equations, the fixed points and the anomalous dimension,  $\eta(P_4)$ , of the flexuron field, from which all the scalings of the theory in the IR can be easily derived. Our best result (1.136) reads

$$\boxed{\eta(P_4) = 0.8347.} \quad (1.151)$$

A spectacular feature of our perturbative results is the smallness of the coefficients found in the  $\varepsilon$ -series, see the series expansion for  $P'_2$  (1.121),  $P_3$  (1.127) and  $P_4$  (1.134). As can be seen from (1.127) and (1.134), the coefficients even get smaller with increasing loop order, thus seemingly alleviating the asymptotic nature of the series, at least up to three loops. The case of (1.121) is particularly interesting because the first two coefficients are decreasing, but the second one slightly increases. This is an indication that the asymptotic nature of the series is expected to manifest at higher orders. As discussed in the main text, the smallness of the coefficients partly originates from the  $d_c$  structure of the series. Indeed, all series involve an expansion parameter of the form  $\varepsilon^l/(n+d_c)^{2l-1}$ , with  $l$  the loop order and  $n=4,20,24$ , which is small in  $\varepsilon=1$  and  $d_c=1$ . Thanks to this property, the first terms of the series appear to be effectively convergent, allowing us to provide precise estimates for the critical exponents with few orders and without the need for resummations. Such small and decreasing coefficients are very rare in field theory.

In this context, another remarkable feature of our results, with respect to the one- and two-loop order calculations, is that the value found for the three-loop order critical exponent  $\eta(P_4)$  in  $d=2$  (without any resummation of the  $\varepsilon$ -series) is in quantitative agreement with the usually accepted values from (all orders) non-perturbative methods and various Monte-Carlo simulation methods, see table 1.2. We also used our (exact order-by-order) results to benchmark several non-perturbative (truncated) approaches, such as NPRG and SCSA. We observe an order-by-order quantitative agreement between our perturbative approach and the non-perturbative ones when the later are re-expanded in powers of  $\varepsilon$ . We were also able to cross-check our results with the large- $d_c$  SCSA approach for arbitrary  $d$ , which is also an exact approach at LO.

Finally, one can note that recent attempts have been made to probe more deeply the non-perturbative structure of the theory, notably concerning the relation between scale invariance and conformal symmetry, see [58]. The result is that the scale invariance at the infrared fixed point is not being promoted to conformal invariance. Therefore, the use of methods such as conformal bootstrap techniques seems to be excluded.

This chapter was based on the so-called effective flexural theory (EFT). However, let us recall that the original computations in [1] have been carried out by means of two (equivalent and complementary) models, the EFT and the so-called two-field model. The latter will be of special interest in the next chapter, where we will perform similar computations, in the more general disordered case. The clean case will also be recovered. As we will see in the next chapter, the agreement between the results obtained from both models shows that we have obtained an unambiguous control of the renormalization procedure in these theories.





# Chapter 2

## Critical elastic properties of disordered flat membranes

This chapter is partly based on the publication

[3] S. Metayer and D. Mouhanna, *Phys. Rev. E* **106**, 064114,  
“Flat phase of quenched disordered membranes at three-loop order”.

We pursue our study of elastic planar systems with a generalization to the case of membranes subject to quenched disorder, such as partial polymerization or dilution. This is achieved by the introduction of additional couplings to the disorder and the use of the replica theory. We perform the complete RG calculation, from one to three loops. We then present the subtle analysis of the phase structure of this model and confirm the existence of a new non-trivial IR critical fixed point,  $P_c$ , seen for the first time in recent NPRG calculations, controlling a finite disorder and finite temperature wrinkling transition. Our study confirms the existence of a glassy phase at low temperatures in flat membranes. In such a state, experimentally accessible and interesting effects occur, such as the modulus of elasticity being paradoxically increased by the density of defects.

### Contents

---

2.1	Introduction and motivation . . . . .	<b>62</b>
2.2	Disordered flat membranes model . . . . .	<b>64</b>
2.2.1	Disordered model . . . . .	64
2.2.2	Scalings and exponents in the IR . . . . .	66
2.2.3	Replica algebra . . . . .	67
2.2.4	Feynman rules . . . . .	67
2.2.5	Dyson equations for the flexuron and phonon fields . . . . .	69
2.2.6	Renormalization conventions . . . . .	70
2.3	Perturbative calculations up to three loops . . . . .	<b>72</b>
2.3.1	One-loop analysis . . . . .	72
2.3.2	Two-loop analysis . . . . .	74
2.3.3	Three-loop analysis . . . . .	77
2.4	Renormalization group . . . . .	<b>80</b>
2.4.1	Renormalization constant derivation . . . . .	80
2.4.2	Renormalization group functions . . . . .	81
2.5	Fixed points and results . . . . .	<b>83</b>
2.5.1	Purely non-disordered fixed points . . . . .	83
2.5.2	How to find the disordered fixed points . . . . .	87
2.5.3	Disordered fixed points and results up to three loops . . . . .	91
2.5.4	Phase diagram . . . . .	94
2.6	Comparison with other approaches . . . . .	<b>96</b>
2.6.1	Benchmarking the NPRG approach . . . . .	96
2.6.2	Benchmarking the SCSA approach . . . . .	97
2.6.3	Comparison with large- $d_c$ approaches . . . . .	97
2.6.4	Non-perturbative comparison summary . . . . .	98
2.7	Conclusion . . . . .	<b>99</b>

---



## 2.1 Introduction and motivation

Elastic disorder is a phenomenon occurring in crystalline systems, where the lattice structure is not perfectly ordered but contains defects, such as dislocations, vacancies, or grain boundaries, see figure 2.1 for an illustration of some of them. These defects can cause local variations in the mechanical properties of the system, especially in two-dimensional systems. The study of elastic disorder has become increasingly important in recent years for the advancement of planar materials, a remarkable example being graphene [26]. In the following, we will consider *quenched* disorder, *i.e.*, frozen defects that are a background random potential for the thermally fluctuating elastic degrees of freedom. In other words, the defects are not dynamical, and we average over the possible disorder realizations.

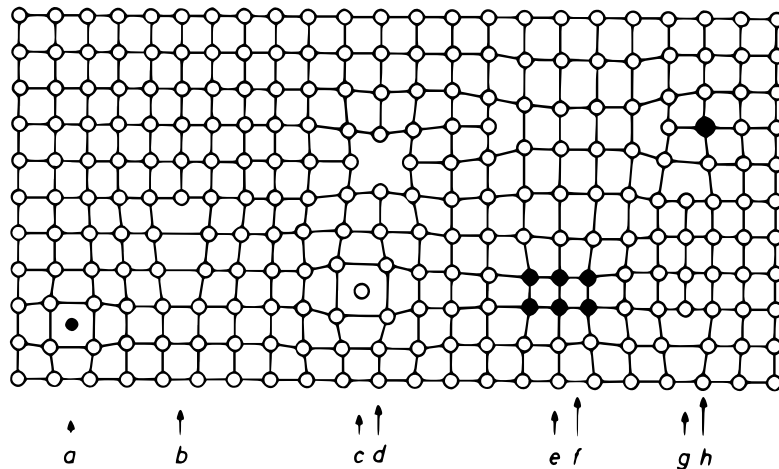


Figure 2.1: a) Interstitial impurity atom, b) Edge dislocation, c) Self interstitial atom, d) Vacancy, e) Precipitate of impurity atoms, f) Vacancy type dislocation loop, g) Interstitial type dislocation loop, h) Substitutional impurity atom. Original image from [86].

Understanding the effects of quenched disorder in the flat phase of polymerized membranes has become a major challenge with, as a priority target, unveiling new phenomena in the physics of graphene and graphene-like materials [18, 26, 87–89] going from mechanical ones — e.g., a paradoxical enhancement of elasticity modulus with the density of defects [54] — to electronic ones — e.g., the possibility to open a tunable band gap [90, 91]. However, the interest for quenched disorder in membranes has a longer history and goes back to the early experiments of Sackmann *et al.* [92] followed by those of Mutz *et al.* [93] and Chaieb *et al.* [94–97] on partially polymerized lipid membranes. These authors have shown that, upon cooling below the melting temperature, these systems undergo a phase transition from a smooth structure at low-disorder, or equivalently at high polymerization, into a wrinkled structure at high disorder, or equivalently at low polymerization.

These investigations have stimulated an important theoretical work aiming to identify precisely the nature of this weakly polymerized wrinkled phase that has been conjectured to coincide with a *glassy* phase, a phase mainly controlled by *disorder* fluctuations. Nelson and Radzihovsky [98, 99], using a *one-loop* perturbative approach in the vicinity of the upper critical dimension  $d=4$ , have shown the irrelevance of a disorder acting only on the internal metric of the membrane. They have shown that the renormalization group (RG) flow was driven toward the disorder-free fixed point, called  $P_4$  (studied perturbatively in the previous chapter), identified by Aronovitz and Lubensky [29] in their early RG approach of pure membranes. This result has then been confirmed by Radzihovsky and Le Doussal [100] in the context of a leading order self-consistent screening approximation (SCSA). Morse *et al.* [101, 102] have then extended the one-loop study of Nelson and Radzihovsky by adding a

curvature disorder with the metric disorder. They have confirmed the irrelevance of the disorder below  $d=4$  and discovered a new vanishing-temperature fixed point, called  $P_5$ . This fixed point has been identified, within the one-loop computation of Morse *et al.*, as being stable with respect to the disorders but unstable in the direction associated with the temperature, making the fixed point  $P_5$  non-pertinent in the prospect of a glassy phase. These works have then been followed by a new approach relying on the use of the so-called non-perturbative renormalization group (NPRG) by Coquand *et al.* [103] on the metric/curvature-disordered model initially considered by Morse *et al.* [101, 102]. A striking result obtained by means of this approach [103] is the discovery of a finite-temperature, finite-disorder, critical fixed point  $P_c$ , *unstable* with respect to the temperature, making the vanishing temperature fixed point  $P_5$  *fully attractive* at sufficiently low temperatures. This approach has, thus, confirmed theoretically the possibility of a whole glassy phase at low temperatures in quenched disordered membranes. Moreover, the various scaling laws observed by Chaieb *et al.* [94–97] in their investigations of partially polymerized lipid membranes have been qualitatively and quantitatively explained [104] on the basis of the analysis performed in [103].

Although convincing, the NPRG approach of Coquand *et al.* [103] has happened to be at odds with the results obtained from the SCSA approach of Le Doussal and Radzihovsky [12] that includes both metric and curvature disorders and in which the critical fixed point  $P_c$  is missing. This is notably for this reason that recently, a *two-loop order* perturbative approach in the vicinity of  $d=4$  has been performed by Coquand and Mouhanna [56], following the early one-loop order computation of Morse *et al.* [101, 102] and the two and three-loop order ones performed on disorder-free membranes, extensively described in the previous chapter. This approach has confirmed the existence of a critical fixed point  $P_c$  associated with a phase transition between a high-temperature phase<sup>1</sup> controlled by the disorder-free fixed point  $P_4$  and a low-temperature phase controlled by the vanishing-temperature, infinite-disorder, fixed point  $P_5$ . However, this approach was not conclusive as it led to an indeterminacy of the coordinates of the various fixed points  $P_5$  and  $P_c$  as well as of the corresponding anomalous dimensions.

In order to clarify this situation, our work [3] investigates the flat phase of quenched disorder membranes by means of a *three-loop* computation in the vicinity of  $d=4$ , following the very recent approach that we performed in the pure case [2]; see also [105] for a four-loop computation in the pure case. We showed that the indeterminacy discussed above was associated with an incorrect expression for the RG function of the curvature disorder. We provided the correct expressions of the RG functions at three-loop order and determined all physical quantities up to order  $\varepsilon^3$  without ambiguity. Our results confirmed, within the perturbative context, the existence of a new fixed point  $P_c$  in the flat phase of quenched polymerized membranes, even if it is found to be marginally — to order  $O(\varepsilon^2)$  — stable in contradiction with the result of the NPRG approach. However, the anomalous dimensions computed at the various fixed points  $P_5$  and  $P_c$  are in strong agreement with those predicted within the NPRG approach.

In the rest of this chapter, we provide a technical review on the perturbative loop computation performed in [3], at one, two and three loops. We first introduce the disordered version of the two-field model described early in the previous chapter. We also introduce all the machinery necessary to assess the critical exponents, such as the replica formalism and the technicalities induced by the disorder. We then proceed to a complete analytical calculation of the RG functions up to three loops. This allows us to discuss the various fixed points of the theory. First, we recover the pure (or equivalently clean or non-disordered) results of the previous chapter by means of the two-field model, which is an independent approach. Then, we extract the two relevant fixed points including disorder,  $P_5$  and  $P_c$ . We compute all the associated anomalous dimensions and provide the phase diagram of the theory. We then proceed in benchmarking the NPRG [103], as well as the small coupling SCSA [12] results. We also show accordance with the large- $d_c$  ( $\forall d$ ) LO results obtained in [12]. Note that the NLO large- $d_c$  has been performed in [106], but in  $d=2$  so that direct comparison is not possible.

---

<sup>1</sup>This phase should not be confused with the high-temperature, crumpled, phase of membranes.

## 2.2 Disordered flat membranes model

### 2.2.1 Disordered model

In this section, we derive a disordered version of the two field model introduced in the previous chapter. For convenience, we reproduce here the clean (non-disordered) action (1.9)

$$S[\vec{u}, \vec{h}] = \int d^d x \left[ \frac{\kappa}{2} (\partial^2 h_\alpha)^2 + \frac{\lambda}{2} T_{aa}^2 + \mu T_{ab}^2 \right], \quad (2.1)$$

where the strain tensor reads

$$T_{ab} \approx \frac{1}{2} (\partial_a u_b + \partial_b u_a + \partial_a h_\alpha \partial_b h_\alpha). \quad (2.2)$$

We recall that this action describes a  $d$ -dimensional flat membrane fluctuating in a bigger  $D$ -dimensional space, *i.e.*, with codimension  $d_c = D - d$ . The action (2.1) is made of two independent fields, the flexuron (or height) field  $h(x)$ , controlling the transversal modes of the membrane, as well as the phonon field  $u(x)$ , controlling the in-plane modes. The pure action (2.1), has two couplings, that are also the two elastic moduli,  $\lambda$  the first Lamé parameter and  $\mu$ , the shear modulus. It also contains the bending rigidity  $\kappa$  as an additional parameter. However, it is irrelevant, as it can be absorbed in a redefinition of the fields and couplings.

We will now add disorder to this model. In a crystalline membrane context, this can be understood as defects from partial polymerization. This generates several kinds of anomalies in the lattice structure like dislocations and disclinations, see figure 2.1. In a continuous field theory model, to account for the possible defects in the membrane lattice, we introduce additional random fields. First, a local random curvature  $c(x)$  coupled to the height field as well as a local random stress  $s(x)$ , coupled to the strain tensor. This yields to the most general action for a membrane subject to short-range disorder [101, 102]

$$S[\vec{u}, \vec{h}] = \int d^d x \left[ \frac{\kappa}{2} (\partial^2 h_\alpha)^2 + \frac{\lambda}{2} T_{aa}^2 + \mu T_{ab}^2 - \kappa \partial^2 h_\alpha c_\alpha - \lambda s_{aa} T_{bb} - 2\mu s_{ab} T_{ab} \right]. \quad (2.3)$$

We then need to average over the possible realizations of disorder, *i.e.*, over the random fields  $c(x)$  and  $s(x)$ . For simplicity, we take them as quenched<sup>2</sup> Gaussian distribution with zero mean, defined by the variances

$$\overline{c_\alpha(x) c_\beta(y)} = \Delta_\kappa \delta_{\alpha\beta} \delta(x - y), \quad (2.4a)$$

$$\overline{s_{ab}(x) s_{cd}(y)} = (\Delta_\lambda \delta_{ab} \delta_{cd} + \Delta_\mu (\delta_{ac} \delta_{bd} + \delta_{ad} \delta_{bc})) \delta(x - y), \quad (2.4b)$$

where overbars denote averages over disorder realizations. The newly introduced parameters  $\Delta_x$  are the variances associated with the elastic parameters  $x$ . Then, we want to perform the average directly at the level of the action, or more precisely, the partition function. This procedure (see, *e.g.*, the review part of [12] for a derivation) implies a Gaussian average over the log of the partition function  $\mathcal{Z}$ , *i.e.*,  $\overline{\log \mathcal{Z}}$ , which is very hard to compute. To simplify it, we then use the common formula

$$\overline{\log \mathcal{Z}} = \lim_{n \rightarrow 0} \frac{\overline{\mathcal{Z}^n} - 1}{n}, \quad (2.5)$$

and then assume that  $n$  is an integer, which is equivalent to averaging over  $n$  replicas of the system. This is known as the replica trick, see, *e.g.*, the textbook [107]. Concretely, it implies the introduction of an extra replica index for each field of the theory, reading

$$u_i \rightarrow u_i^A \quad \text{and} \quad h_\alpha \rightarrow h_\alpha^A \quad \text{with} \quad A = 1, 2, \dots, n \quad \text{and} \quad n \rightarrow 0. \quad (2.6)$$

<sup>2</sup>According to [12], an unquenched (therefore dynamical, also called “annealed”) disorder can be shown to be irrelevant in the RG sense, since it leads to only non-singular renormalization of the elastic coefficients.

The strain tensor (2.2) is then promoted to

$$T_{ab}^A \approx \frac{1}{2} (\partial_a u_b^A + \partial_b u_a^A + \partial_a h_\alpha^A \partial_b h_\alpha^A). \quad (2.7)$$

Note that the replica index  $A$  is not contracted in the last term! Therefore, the usual Einstein convention (not showing the sum symbol for indices appearing twice) is not reasonable for replica indices. After averaging over the quenched random Gaussian field, the action reads

$$S[\vec{u}, \vec{h}] = \int d^d x \left[ \sum_A \left[ \frac{\kappa}{2} (\partial^2 h_\alpha^A)^2 + \frac{\lambda}{2} (T_{aa}^A)^2 + \mu (T_{ab}^A)^2 \right] + \sum_{AB} \left[ \frac{\Delta_\kappa}{2} \partial^2 h_\alpha^A \partial^2 h_\alpha^B + \frac{\Delta_\lambda}{2} T_{aa}^A T_{bb}^A + \Delta_\mu T_{ab}^A T_{ab}^B \right] \right], \quad (2.8)$$

where the summations over replica indices ( $A, B, \dots$ ) are indicated, while the Einstein convention is understood for space indices ( $a, b, \dots$ ) and co-space indices ( $\alpha, \beta, \dots$ ). At this stage, it is important to summarize the parameters at play in this model, and underline some of their features,

$$\text{Fields: } \begin{cases} h \equiv \text{Flexuron field,} \\ u \equiv \text{Phonon field,} \end{cases} \quad (2.9a)$$

$$\text{Couplings: } \begin{cases} \lambda \equiv \text{1st Lamé parameter,} \\ \Delta_\lambda \equiv \text{Elastic disorder variance,} \\ \mu \equiv \text{Shear modulus (2nd Lamé parameter),} \\ \Delta_\mu \equiv \text{Shear disorder variance,} \end{cases} \quad (2.9b)$$

$$\text{Parameters: } \begin{cases} \kappa \equiv \text{Bending rigidity (not renormalizing),} \\ \Delta_\kappa \equiv \text{Curvature disorder variance.} \end{cases} \quad (2.9c)$$

The action (2.8) is then made of 2 fields and 4 couplings as well as two parameters and is a massless derivative field theory. The fate of the parameters  $\kappa$  and  $\Delta_\kappa$  is worth a little discussion. On the one hand, as for the pure case, the bending rigidity  $\kappa$  does not renormalize and, in principle, can be absorbed by a redefinition of the couplings and fields (which we won't do until the very end of the chapter). On the other hand, the curvature disorder variance  $\Delta_\kappa$  do renormalize. This parameter has no straightforward equivalent in the high energy physics language. First, it is not a mass, because it is dimensionless, and will enter the results of the anomalous dimensions (the minimal subtraction scheme prevent dimensionful parameters to appear in the anomalous dimensions, but not the dimensionless ones). Second, it is not a coupling, because we won't consider it as small in the loop expansion and because its energy dimension is exactly zero (whilst a renormalized coupling has dimension  $M^{2\epsilon}$  with  $M$  the renormalization scale). In this sense, it is similar to a gauge-fixing parameter in a gauge theory. We will simply call  $\Delta_\kappa$ , or more precisely  $\Delta_{\kappa r}$ , a running parameter. Note also that the temperature has been absorbed in a redefinition of the parameters, see, *e.g.*, [101, 102]. The scaling of the parameters with the temperature  $T$  then yields  $x \sim T$  and  $\Delta_x \sim 1/T$  with  $x = \kappa, \lambda, \mu$ .

Going further, the action (2.8) can be re-written in a more compact form

$$S[\vec{u}, \vec{h}] = \int d^d x \sum_{AB} \left[ \frac{1}{2} \kappa_-^{AB} \partial^2 h_\alpha^A \partial^2 h_\alpha^B + \frac{1}{2} \lambda_-^{AB} T_{aa}^A T_{bb}^B + \mu_-^{AB} T_{ab}^A T_{ab}^B \right], \quad (2.10)$$

with the tensorial parameters

$$\kappa_-^{AB} = \kappa \delta^{AB} - \Delta_\kappa J^{AB}, \quad (2.11a)$$

$$\mu_-^{AB} = \mu \delta^{AB} - \Delta_\mu J^{AB}, \quad (2.11b)$$

$$\lambda_{-}^{AB} = \lambda \delta^{AB} - \Delta_{\lambda} J^{AB}, \quad (2.11c)$$

where we introduced two tensors,  $\delta^{AB}$  the identity matrix and  $J^{AB}$ , a matrix where every entry is equal to one, both of size  $n \times n$ , *i.e.*, formally

$$J_{AB} = 1 \quad \forall A, B \quad \text{and} \quad \delta_{AB} = \begin{cases} 1 & \text{if } A = B \\ 0 & \text{otherwise} \end{cases}. \quad (2.12a)$$

In this form, the compact disordered action (2.10) is very similar to the pure (non-disordered) one (2.1) with all quantities generalized with replica indices. More generally, we define the six tensorial parameters

$$\alpha_{\pm}^{AB} = \alpha \delta^{AB} \pm \Delta_{\alpha} J^{AB} \quad \alpha \in \{\mu, \lambda, \kappa\}. \quad (2.13)$$

Note that their inverse are useful and easy to derive, reading

$$(\alpha_{\pm}^{AB})^{-1} = \frac{1}{\alpha} \delta^{AB} - \frac{\pm \Delta_{\alpha}}{\alpha^2} J^{AB} \quad \alpha \in \{\mu, \lambda, \kappa\}. \quad (2.14)$$

To summarize all the indices at play in this model, we also provide the Table 2.1.

	alphabet	index	physical limit	tensorial basis
space	Latin	$\{a, b, c, \dots\} = 1, 2, \dots, d$	$4 - 2\varepsilon = d \rightarrow 2$	$\{P_{ab}^{\parallel}(p), P_{ab}^{\perp}(p)\}$
co-space	Greek	$\{\alpha, \beta, \gamma, \dots\} = 1, 2, \dots, d_c$	$D - d = d_c \rightarrow 1$	$\{\delta_{\alpha\beta}\}$
replica	caps Latin	$\{A, B, C, \dots\} = 1, 2, \dots, n$	$n \rightarrow 0$	$\{\delta^{AB}, J^{AB}\}$

Table 2.1: Summary of the index content for the model (2.10) ( $d$ -dimensional quenched disordered membrane embedded in a  $D$ -dimensional space, *i.e.*, with codimension  $d_c = D - d$ ).

## 2.2.2 Scalings and exponents in the IR

Due to the use of the replica trick, the correlation functions, compared to the clean case, are promoted to tensorial quantities. Therefore, the exponents characterizing in the clean case the scaling of the two point correlation functions for the flexuron and the phonon,  $\eta$  and  $\eta_u$ , now need a disordered counterpart, that we name  $\eta'$  and  $\eta'_u$ . The scaling in the IR is then parameterized as

$$\langle h_r^A(p) h_r^B(-p) \rangle \sim c_1 \delta^{AB} p^{-(4-\eta)} + c_2 J^{AB} p^{-(4-\eta')}, \quad (2.15a)$$

$$\langle u_r^A(p) u_r^B(-p) \rangle \sim c_3 \delta^{AB} p^{-(2+\eta_u)} + c_4 J^{AB} p^{-(2+\eta'_u)}, \quad (2.15b)$$

where  $c_i$  are coefficient functions independent of the momentum  $p$ . Like in the clean case, the exponents  $\eta_u^{(l)}$  and  $\eta^{(l)}$  are related by Ward identities [101, 102]

$$\eta_u = 4 - d - 2\eta, \quad (2.16a)$$

$$\eta'_u = 4 - d - 2\eta', \quad (2.16b)$$

so that we can focus only on the determination of  $\eta$  and  $\eta'$ . More precisely, instead of  $\eta'$ , we will focus on the quantity

$$\phi = \eta' - \eta, \quad (2.17)$$

which is very useful to characterize what are the dominant fluctuations depending on its sign

$$\phi > 0 \equiv \text{Thermal fluctuations dominates (Clean phase)}, \quad (2.18a)$$

$$\phi < 0 \equiv \text{Disorder fluctuations dominates (Glassy phase)}, \quad (2.18b)$$

$$\phi = 0 \equiv \text{Both thermal and disorder fluctuations coexist (Marginal phase)}. \quad (2.18c)$$

In the rest of this chapter, we will focus on the determination, at different fixed points, of  $\eta$  and  $\phi$ , since these two anomalous dimensions are enough to compute all the critical exponents of the theory.

### 2.2.3 Replica algebra

Since sums over replica indices have to be specified, for the tensors  $\delta$  and  $J$ , we will distinguish two algebras. First, in the unsummed case

$$\delta^{AB}\delta^{AB} = \delta^{AB}, \quad J^{AB}J^{AB} = J^{AB}, \quad \delta^{AB}J^{AB} = \delta^{AB}, \quad (2.19a)$$

$$\delta^{AB} = \delta^{BA}, \quad J^{AB} = J^{BA}, \quad \delta^{AA} = J^{AA} = 1, \quad (2.19b)$$

and second, in the summed case

$$\sum_C \delta^{AC}\delta^{CB} = \delta^{AB}, \quad \sum_C J^{AC}J^{CB} = nJ^{AB}, \quad \sum_C \delta^{AC}J^{CB} = J^{AB}, \quad (2.20a)$$

$$\sum_A \delta^{AA} = n, \quad \sum_A J^{AA} = n, \quad \sum_A 1 = n. \quad (2.20b)$$

Although these rules look quite trivial, during the computations one can encounter confusing contractions, such as

$$\sum_A J^{AB}J^{AB}J^{AD}, \quad \sum_{AB} \delta^{AB}\delta^{AC}\delta^{AD}, \quad \sum_{AB} \delta^{AB}J^{AC}\delta^{AD}J^{AD}, \quad \sum_A J^{AB}(\delta^{AC} + J^{AC})J^{AD}, \quad \text{etc.} \quad (2.21)$$

In that case, an efficient way to perform the replica algebra is to

- 0) Apply the unsummed algebra (2.19) at all steps of the calculation.
- 1) Expand the expression fully to avoid any ambiguity.
- 2) Contract all the  $\delta$ 's with the rule  $\sum_A \delta^{AB}F(A) = F(B)$  with  $F(X)$  any tensor containing (possibly multiple times) the index  $X$ .
- 3) Contract all the  $J$ 's with the rule  $\sum_A J^{AB}F \propto n = 0$  assuming  $F$  is a tensor that does not contain any index  $A$  on a  $\delta$ , *i.e.*,  $\delta_{AX}$ .

Following this procedure, the examples showed in (2.21) reads

$$\sum_A J^{AB}J^{AB}J^{AD} \stackrel{0)}{=} \sum_A J^{AB}J^{AD} \stackrel{3)}{=} 0, \quad (2.22a)$$

$$\sum_{AB} \delta^{AB}\delta^{AC}\delta^{AD} \stackrel{2)}{=} \sum_B \delta^{BC}\delta^{BD} \stackrel{2)}{=} \delta^{CD}, \quad (2.22b)$$

$$\sum_{AB} \delta^{AB}J^{AC}\delta^{AD}J^{AD} \stackrel{0)}{=} \sum_{AB} \delta^{AB}J^{AC}\delta^{AD} \stackrel{2)}{=} J^{DC}, \quad (2.22c)$$

$$\sum_A J^{AB}(\delta^{AC} + J^{AC})J^{AD} \stackrel{1)}{=} \sum_A J^{AB}\delta^{AC}J^{AD} + \sum_A J^{AB}J^{AC}J^{AD} = \dots = J^{BC}J^{CD}. \quad (2.22d)$$

### 2.2.4 Feynman rules

The Feynman rules for the model (2.8) can be derived using the usual functional derivative formula

$$\langle \phi_1(\vec{p}_1) \cdots \phi_n(\vec{p}_n) \rangle_0 = \frac{\delta^n S[\phi]}{\delta \phi_1(\vec{p}_1) \cdots \delta \phi_n(\vec{p}_n)} \quad \text{with } \phi \equiv \{u, h\}, \quad (2.23)$$

The free flexuron propagator reads

$$S_{\alpha\beta}^{AB(0)}(\vec{p}) = \langle h_{\alpha}^A(\vec{p}) h_{\beta}^B(-\vec{p}) \rangle_0 = \alpha A \frac{\text{---}}{\vec{p}} \beta B = \frac{\delta_{\alpha\beta} \kappa_{+}^{AB}}{p^4 \kappa^2}. \quad (2.24)$$

The free phonon propagator is given by

$$D_{ab}^{AB(0)}(\vec{p}) = \langle u_a^A(\vec{p}) u_b^B(-\vec{p}) \rangle_0 = a A \text{---} \vec{p} \text{---} b B = \frac{1}{p^2} \left( \frac{\mu_{+}^{AB}}{\mu^2} P_{ab}^{\perp}(\vec{p}) + \frac{\lambda_{+}^{AB} + 2\mu_{+}^{AB}}{(\lambda + 2\mu)^2} P_{ab}^{\parallel}(\vec{p}) \right), \quad (2.25)$$

where the standard transverse and longitudinal projectors are defined, as usual, as

$$P_{ab}^{(\perp)}(\vec{p}) = \delta_{ab} - \frac{p_a p_b}{p^2}, \quad P_{ab}^{(\parallel)}(\vec{p}) = \frac{p_a p_b}{p^2}. \quad (2.26)$$

The 3-point phonon-flexuron vertex is given by (vertex factor 1/2)

$$\begin{aligned} \Gamma_{\alpha\beta c}^{ABC(0)}(\vec{p}_1, \vec{p}_2, \vec{p}_3) &= \langle h_{\alpha}^A(\vec{p}_1) h_{\beta}^B(\vec{p}_2) u_c^C(\vec{p}_3) \rangle_0 \\ &= c C \text{---} \vec{p}_3 \text{---} \begin{array}{l} \alpha A \vec{p}_1 \\ \beta B \vec{p}_2 \end{array} = -i\delta_{\alpha\beta} \delta^{BC} [\mu_{-}^{AB} (\vec{p}_3 \cdot \vec{p}_1 p_2^c + \vec{p}_3 \cdot \vec{p}_2 p_1^c) + \lambda_{-}^{AB} \vec{p}_1 \cdot \vec{p}_2 p_3^c]. \end{aligned} \quad (2.27)$$

Note that the replica index  $B$  is indeed not contracted! The 4-point (fully symmetrized) flexuron vertex yields (vertex factor  $1/4! = 1/24$ )

$$\begin{aligned} \Gamma_{\alpha\beta\gamma\delta}^{ABCD(0)}(\vec{p}_1, \dots, \vec{p}_4) &= \langle h_{\alpha}^A(\vec{p}_1) h_{\beta}^B(\vec{p}_2) h_{\gamma}^C(\vec{p}_3) h_{\delta}^D(\vec{p}_4) \rangle_0 \\ &= \begin{array}{l} \alpha A \vec{p}_1 \\ \delta D \vec{p}_4 \\ \beta B \vec{p}_2 \\ \gamma C \vec{p}_3 \end{array} \\ &= -\lambda_{-}^{AC} \delta^{AB} \delta^{CD} \delta_{\alpha\beta} \delta_{\gamma\delta} \vec{p}_1 \cdot \vec{p}_2 \vec{p}_3 \cdot \vec{p}_4 - \lambda_{-}^{AB} \delta^{AC} \delta^{BD} \delta_{\alpha\gamma} \delta_{\beta\delta} \vec{p}_1 \cdot \vec{p}_3 \vec{p}_2 \cdot \vec{p}_4 \\ &\quad - \lambda_{-}^{AB} \delta^{AD} \delta^{BC} \delta_{\alpha\delta} \delta_{\beta\gamma} \vec{p}_1 \cdot \vec{p}_4 \vec{p}_2 \cdot \vec{p}_3 \\ &\quad - \mu_{-}^{AC} \delta^{AB} \delta^{CD} \delta_{\alpha\beta} \delta_{\gamma\delta} \vec{p}_1 \cdot \vec{p}_3 \vec{p}_2 \cdot \vec{p}_4 - \mu_{-}^{AC} \delta^{AB} \delta^{CD} \delta_{\alpha\beta} \delta_{\gamma\delta} \vec{p}_1 \cdot \vec{p}_4 \vec{p}_2 \cdot \vec{p}_3 \\ &\quad - \mu_{-}^{AB} \delta^{AC} \delta^{BD} \delta_{\alpha\gamma} \delta_{\beta\delta} \vec{p}_1 \cdot \vec{p}_2 \vec{p}_3 \cdot \vec{p}_4 - \mu_{-}^{AB} \delta^{AC} \delta^{BD} \delta_{\alpha\gamma} \delta_{\beta\delta} \vec{p}_1 \cdot \vec{p}_4 \vec{p}_2 \cdot \vec{p}_3 \\ &\quad - \mu_{-}^{AB} \delta^{AD} \delta^{BC} \delta_{\alpha\delta} \delta_{\beta\gamma} \vec{p}_1 \cdot \vec{p}_2 \vec{p}_3 \cdot \vec{p}_4 - \mu_{-}^{AB} \delta^{AD} \delta^{BC} \delta_{\alpha\delta} \delta_{\beta\gamma} \vec{p}_1 \cdot \vec{p}_3 \vec{p}_2 \cdot \vec{p}_4, \end{aligned} \quad (2.28)$$

where all momenta are defined ingoing, such that  $\vec{p}_1 + \vec{p}_2 = -\vec{p}_3 - \vec{p}_4$ . Again, note that the replica indices repeated over are not contracted.

As a final remark, it has to be underlined that the subcase of non-disordered membranes can obviously be recovered by removing all replica indices as well as taking the limit  $\delta^{AB} \rightarrow 1$  and  $J^{AB} \rightarrow 0$ , which amount to take  $\alpha_{\pm}^{AB} \rightarrow \alpha$  for the parameters  $\alpha = \{\kappa, \mu, \lambda\}$ . Equivalently, it can be achieved by setting all the disorder variances to zero, *i.e.*,  $\Delta_{\mu} = \Delta_{\lambda} = \Delta_{\kappa} = 0$ . In this limit, we obtain the pure two-field model. In principle, we should recover the results of the previous chapter, carried out with the equivalent pure effective flexural model.



### 2.2.5 Dyson equations for the flexuron and phonon fields

Turning on interactions, the two Dyson equations for the flexuron and phonon fields, with all indices, read<sup>3</sup>

$$S_{\alpha\beta}^{AB}(\vec{p}) = S_{\alpha\beta}^{AB(0)}(\vec{p}) + S_{\alpha\gamma}^{AC(0)}(\vec{p})\Sigma_{\gamma\delta}^{CD}(\vec{p})S_{\delta\beta}^{DB}(\vec{p}), \quad (2.29a)$$

$$D_{ab}^{AB}(\vec{p}) = D_{ab}^{AB(0)}(\vec{p}) + D_{ac}^{AC(0)}(\vec{p})\Pi_{cd}^{CD}(\vec{p})D_{db}^{DB}(\vec{p}), \quad (2.29b)$$

where  $\Sigma_{\alpha\beta}^{AB}(\vec{p})$  is the 1-particle irreducible flexuron self-energy and  $\Pi_{ab}^{AB}(\vec{p})$  the 1-particle irreducible phonon polarization. It is convenient to decompose these self-energies in a way consistent with the tensorial structure of the propagators. Let us first settle the notations. For an arbitrary tensor  $F$  with two indices  $(a,b)$  or  $(\alpha,\beta)$  or  $(A,B)$ , its respective decompositions (we also provide the inverses for convenience) reads

$$F_{\alpha\beta} = F\delta_{\alpha\beta}, \quad (F_{\alpha\beta})^{-1} = \frac{1}{F}\delta_{\alpha\beta}, \quad (2.30a)$$

$$F_{ab} = F_{\perp}P_{ab}^{\perp} + F_{\parallel}P_{ab}^{\parallel}, \quad (F_{ab})^{-1} = \frac{1}{F_{\perp}}P_{ab}^{\perp} + \frac{1}{F_{\parallel}}P_{ab}^{\parallel}, \quad (2.30b)$$

$$F^{AB} = F_{\delta}\delta^{AB} + F_JJ^{AB}, \quad (F^{AB})^{-1} = \frac{1}{F_{\delta}}\delta^{AB} - \frac{F_J}{F_{\delta}^2}J^{AB}, \quad (2.30c)$$

where  $\{F, F_{\perp}, F_{\parallel}, F_{\delta}, F_J\}$  are scalar functions. In the case where a double pair of indices is present, a double decomposition is performed using the same notations. Therefore, for the flexuron propagator and its self-energy, their decomposition leads to

$$S_{\alpha\beta}^{AB} = \delta_{\alpha\beta}S^{AB} \quad \text{with} \quad S^{AB} = S_{\delta}\delta^{AB} + S_JJ^{AB}, \quad (2.31a)$$

$$\Sigma_{\alpha\beta}^{AB} = \delta_{\alpha\beta}\Sigma^{AB} \quad \text{with} \quad \Sigma^{AB} = \Sigma_{\delta}\delta^{AB} + \Sigma_JJ^{AB}, \quad (2.31b)$$

where we dropped the momentum dependence. Similarly, for the phonon propagator and its polarization, the decompositions read

$$D_{ab}^{AB} = D_{\perp}^{AB}P_{ab}^{\perp} + D_{\parallel}^{AB}P_{ab}^{\parallel} \quad \text{with} \quad \begin{cases} D_{\perp}^{AB} = D_{\delta}^{\perp}\delta^{AB} + D_J^{\perp}J^{AB} \\ D_{\parallel}^{AB} = D_{\delta}^{\parallel}\delta^{AB} + D_J^{\parallel}J^{AB} \end{cases}, \quad (2.32a)$$

$$\Pi_{ab}^{AB} = \Pi_{\perp}^{AB}P_{ab}^{\perp} + \Pi_{\parallel}^{AB}P_{ab}^{\parallel} \quad \text{with} \quad \begin{cases} \Pi_{\perp}^{AB} = \Pi_{\delta}^{\perp}\delta^{AB} + \Pi_J^{\perp}J^{AB} \\ \Pi_{\parallel}^{AB} = \Pi_{\delta}^{\parallel}\delta^{AB} + \Pi_J^{\parallel}J^{AB} \end{cases}. \quad (2.32b)$$

Therefore, we are left with 6 scalar quantities to be computed  $\{\Sigma_{\delta}, \Sigma_J, \Pi_{\delta}^{\perp}, \Pi_J^{\perp}, \Pi_{\delta}^{\parallel}, \Pi_J^{\parallel}\}$  respectively from the 6 propagators  $\{S_{\delta}, S_J, D_{\delta}^{\perp}, D_J^{\perp}, D_{\delta}^{\parallel}, D_J^{\parallel}\}$ . These will then be used to determine the renormalization of the 6 quantities<sup>4</sup>  $\{h, \Delta_{\kappa}, \mu, \Delta_{\mu}, \lambda, \Delta_{\lambda}\}$ , where we recall that  $h$  is the flexuron field. We can now derive the scalar Dyson equations for the flexuron propagator

$$S_{\delta}(\vec{p}) = \frac{1}{p^4\kappa - \Sigma_{\delta}(p^2)}, \quad S_J(\vec{p}) = \frac{1}{-p^4\Delta_{\kappa} - \Sigma_J(p^2)}, \quad (2.33)$$

and for the phonon propagator

$$D_{\delta}^{\perp}(\vec{p}) = \frac{1}{p^2\mu - \Pi_{\delta}^{\perp}(p^2)}, \quad D_J^{\perp}(\vec{p}) = \frac{1}{-p^2\Delta_{\mu} - \Pi_J^{\perp}(p^2)}, \quad (2.34a)$$

$$D_{\delta}^{\parallel}(\vec{p}) = \frac{1}{p^2(\lambda + 2\mu) - \Pi_{\delta}^{\parallel}(p^2)}, \quad D_J^{\parallel}(\vec{p}) = \frac{1}{-p^2(\Delta_{\lambda} + 2\Delta_{\mu}) - \Pi_J^{\parallel}(p^2)}. \quad (2.34b)$$

<sup>3</sup>The Dyson equations for the vertex parts won't be considered since the field and coupling renormalization can be determined only from (2.29), *i.e.*, from the 2-point functions.

<sup>4</sup>The phonon field  $u$  is not in the list because it renormalizes with the same function as  $h$ . The bending rigidity  $\kappa$  is neither in the list because it does not renormalize.



### 2.2.6 Renormalization conventions

We are now in a position to introduce the renormalization constants associated with the model (2.8)

$$u = Zu_r, \quad h = Z^{1/2}h_r, \quad (2.35a)$$

$$\Delta_\kappa = Z_{\Delta_\kappa}\Delta_{\kappa r}, \quad \alpha = Z_\alpha M^{2\varepsilon}\alpha_r \quad \forall \alpha = \{\mu, \Delta_\mu, \lambda, \Delta_\lambda\}, \quad (2.35b)$$

where we dropped field indices for shortness and where the subscript  $r$  denotes renormalized quantities. The renormalization scale,  $M$ , has been introduced in such a way that the couplings  $\alpha_r$  are dimensionless in  $d = 4 - 2\varepsilon$  dimensions. Note that  $\Delta_\kappa$  plays a very special role as it does not need the introduction of a renormalization scale. In that sense,  $\Delta_\kappa$  does not play the special role of a coupling. We recall that the renormalization scale  $M$  is related to the corresponding parameter  $\bar{M}$  in the modified minimal subtraction ( $\overline{\text{MS}}$ ) scheme with the help of

$$\bar{M}^2 = 4\pi e^{-\gamma_E} M^2, \quad (2.36)$$

where  $\gamma_E$  is Euler's constant. In the MS scheme, the renormalization constants take the form of a Laurent series in  $\varepsilon$

$$Z_x(\alpha_r, \Delta_{\kappa r}) = 1 + \delta Z_x(\alpha_r, \Delta_{\kappa r}) = 1 + \sum_{l=1}^{\infty} \sum_{j=1}^l Z_x^{(l,j)}(\alpha_r, \Delta_{\kappa r}) \frac{1}{\varepsilon^j}, \quad (2.37)$$

where  $x \in \{\alpha_r, \Delta_{\kappa r}\} = \{\mu_r, \Delta_{\mu r}, \lambda_r, \Delta_{\lambda r}, \Delta_{\kappa r}\}$ . Moreover, the  $Z_x$  do not depend on momentum (or mass, which is absent in the present model) and the dependence on  $M$  is only through  $\alpha_r$  and  $\Delta_{\kappa r}$ . So the  $Z_x$  functions depend only on  $\alpha_r(M)$ ,  $\Delta_{\kappa r}(M)$  and  $\varepsilon$ . They also relate renormalized and bare propagators as follows

$$S_x(\vec{p}; \alpha, \Delta_\kappa) = Z(\alpha_r, \Delta_{\kappa r}) S_x(\vec{p}; \alpha_r, \Delta_{\kappa r}, M), \quad \text{with } S_x = \{S_\delta, S_J\}, \quad (2.38a)$$

$$D_x(\vec{p}; \alpha, \Delta_\kappa) = Z(\alpha_r, \Delta_{\kappa r}) D_x(\vec{p}; \alpha_r, \Delta_{\kappa r}, M), \quad \text{with } D_x = \{D_\delta^\perp, D_J^\perp, D_\delta^\parallel, D_J^\parallel\}, \quad (2.38b)$$

where the bare propagators do not depend on  $M$ . Notice that, due to rotational symmetry, the two fields  $\vec{u}$  and  $\vec{h}$  renormalize with the same  $Z$ .

We can now establish the relations needed in order to determine the 6 renormalization constants  $\{Z, Z_{\Delta_\kappa}, Z_\mu, Z_{\Delta_\mu}, Z_\lambda, Z_{\Delta_\lambda}\}$  from the 6 self-energies and polarizations  $\{\Sigma_\delta, \Sigma_J, \Pi_\delta^\perp, \Pi_J^\perp, \Pi_\delta^\parallel, \Pi_J^\parallel\}$ . Along the lines of the procedure detailed in the previous chapter, we derive from the renormalization conventions (2.35) and the Dyson equations (2.33) and (2.34), all the renormalized self-energies and polarizations of the model, reading

$$\Sigma_{\delta r} = p^4(1 - Z)\kappa + Z\Sigma_\delta, \quad (2.39a)$$

$$\Sigma_{Jr} = -p^4(1 - ZZ_{\Delta_\kappa})\Delta_{\kappa r} + Z\Sigma_J, \quad (2.39b)$$

$$\Pi_{\delta r}^\perp = p^2(1 - M^{2\varepsilon}Z_\mu Z^2)\mu_r + Z^2\Pi_\delta^\perp, \quad (2.39c)$$

$$\Pi_{Jr}^\perp = -p^2(1 - M^{2\varepsilon}Z_{\Delta_\mu} Z^2)\Delta_{\mu r} + Z^2\Pi_J^\perp, \quad (2.39d)$$

$$\Pi_{\delta r}^\parallel = p^2[(\lambda_r + 2\mu_r) - (Z_\lambda\lambda_r + 2Z_\mu\mu_r)M^{2\varepsilon}Z^2] + Z^2\Pi_\delta^\parallel, \quad (2.39e)$$

$$\Pi_{Jr}^\parallel = -p^2[(\Delta_{\lambda r} + 2\Delta_{\mu r}) - (Z_{\Delta_\lambda}\Delta_{\lambda r} + 2Z_{\Delta_\mu}\Delta_{\mu r})M^{2\varepsilon}Z^2] + Z^2\Pi_J^\parallel. \quad (2.39f)$$

Applying the pole operator  $\mathcal{K}$  on these relations yields the following renormalization identities

$$Z: \quad \mathcal{K}[(\tilde{\Sigma}_\delta - 1)Z] = 0 \quad \text{with } \tilde{\Sigma}_\delta = \frac{\Sigma_\delta}{p^4\kappa}, \quad (2.40a)$$

$$Z_{\Delta_\kappa}: \quad \mathcal{K}[(\tilde{\Sigma}_J + Z_{\Delta_\kappa})Z] = 0 \quad \text{with } \tilde{\Sigma}_J = \frac{\Sigma_J}{p^4\Delta_{\kappa r}}, \quad (2.40b)$$

$$Z_\mu: \quad \mathcal{K} \left[ (\tilde{\Pi}_\delta^\perp - M^{2\varepsilon} Z_\mu) Z^2 \right] = 0 \quad \text{with } \tilde{\Pi}_\delta^\perp = \frac{\Pi_\delta^\perp}{p^2 \mu_r}, \quad (2.40c)$$

$$Z_{\Delta_\mu}: \quad \mathcal{K} \left[ (\tilde{\Pi}_J^\perp + M^{2\varepsilon} Z_{\Delta_\mu}) Z^2 \right] = 0 \quad \text{with } \tilde{\Pi}_J^\perp = \frac{\Pi_J^\perp}{p^2 \Delta_{\mu r}}, \quad (2.40d)$$

$$Z_\lambda: \quad \mathcal{K} \left[ \left( \tilde{\Pi}_\delta^\parallel - M^{2\varepsilon} \frac{Z_\lambda \lambda_r + 2Z_\mu \mu_r}{\lambda_r + 2\mu_r} \right) Z^2 \right] = 0 \quad \text{with } \tilde{\Pi}_\delta^\parallel = \frac{\Pi_\delta^\parallel}{p^2 (\lambda_r + 2\mu_r)}, \quad (2.40e)$$

$$Z_{\Delta_\lambda}: \quad \mathcal{K} \left[ \left( \tilde{\Pi}_J^\parallel + M^{2\varepsilon} \frac{Z_{\Delta_\lambda} \Delta_{\lambda r} + 2Z_{\Delta_\mu} \Delta_{\mu r}}{\Delta_{\lambda r} + 2\Delta_{\mu r}} \right) Z^2 \right] = 0 \quad \text{with } \tilde{\Pi}_J^\parallel = \frac{\Pi_J^\parallel}{p^2 (\Delta_{\lambda r} + 2\Delta_{\mu r})}, \quad (2.40f)$$

where we indicated which relation is used to derive which  $Z_x$ . Notice that all tilde self-energies and polarization  $\{\tilde{\Sigma}_\delta, \tilde{\Sigma}_J, \tilde{\Pi}_\delta^\perp, \tilde{\Pi}_J^\perp, \tilde{\Pi}_\delta^\parallel, \tilde{\Pi}_J^\parallel\}$  are now logarithmic and conveniently related to the renormalization constants  $Z_x$ .

Once all the renormalization constant are computed, one can use them to derive the renormalization-group functions. There are 6 of them. First, 4 beta functions associated with the four couplings  $\{\mu, \Delta_\mu, \lambda, \Delta_\lambda\}$ . Second, 2 anomalous dimensions associated respectively with the flexuron field  $h$  and the disorder parameter  $\Delta_\kappa$ . Let us first focus on the beta functions, reading

$$\beta_\alpha = \frac{d\alpha_r}{d\log M} = -2\varepsilon\alpha_r - \alpha_r \frac{d\log Z_\alpha}{d\log M}, \quad \alpha \in \{\mu, \Delta_\mu, \lambda, \Delta_\lambda\}, \quad (2.41)$$

where we recall that only renormalized parameters (with subscript  $r$ ) depend on  $M$ . In order to compute these beta functions, let us recall that the differentiation can be expanded such that

$$\frac{d\log f}{d\log M} = \sum_\alpha \frac{d\alpha_r}{d\log M} \frac{df}{d\alpha_r} = \sum_\alpha \beta_\alpha \frac{d\log f}{d\alpha_r}, \quad (2.42)$$

so that the  $\beta_\alpha$  form a linear system to be solved, and the solution is conveniently written in the matrix form

$$\begin{pmatrix} \beta_\mu \\ \beta_{\Delta_\mu} \\ \beta_\lambda \\ \beta_{\Delta_\lambda} \end{pmatrix} = -2\varepsilon \begin{pmatrix} \mu \bar{\partial}_\mu \mu Z_\mu & \mu \bar{\partial}_{\Delta_\mu} Z_\mu & \mu \bar{\partial}_\lambda Z_\mu & \mu \bar{\partial}_{\Delta_\lambda} Z_\mu \\ \Delta_\mu \bar{\partial}_\mu Z_{\Delta_\mu} & \Delta_\mu \bar{\partial}_{\Delta_\mu} \Delta_\mu Z_{\Delta_\mu} & \Delta_\mu \bar{\partial}_\lambda Z_{\Delta_\mu} & \Delta_\mu \bar{\partial}_{\Delta_\lambda} Z_{\Delta_\mu} \\ \lambda \bar{\partial}_\mu Z_\lambda & \lambda \bar{\partial}_{\Delta_\mu} Z_\lambda & \lambda \bar{\partial}_\lambda \lambda Z_\lambda & \lambda \bar{\partial}_{\Delta_\lambda} Z_\lambda \\ \Delta_\lambda \bar{\partial}_\mu Z_{\Delta_\lambda} & \Delta_\lambda \bar{\partial}_{\Delta_\mu} Z_{\Delta_\lambda} & \Delta_\lambda \bar{\partial}_\lambda Z_{\Delta_\lambda} & \Delta_\lambda \bar{\partial}_{\Delta_\lambda} \Delta_\lambda Z_{\Delta_\lambda} \end{pmatrix}_r^{-1} \begin{pmatrix} \mu \\ \Delta_\mu \\ \lambda \\ \Delta_\lambda \end{pmatrix}_r, \quad (2.43)$$

using the temporary notation  $\bar{\partial}_x = \partial \log / \partial x$  as well as assuming that the subscript  $r$  apply to all the quantities of the corresponding matrix.

Finally, the anomalous dimensions of the flexuron (height) field  $h$  and the disorder parameter  $\Delta_\kappa$  reads

$$\eta = \frac{d\log Z}{d\log M}, \quad \phi = -\frac{d\log Z_{\Delta_\kappa}}{d\log M}, \quad (2.44)$$

that can be conveniently computed using (2.42) once the beta functions have been computed.

In summary, the procedure is exactly the same as in the previous chapter, with three times as many quantities. Indeed, in order to characterize the renormalized quantities  $\{h_r, \Delta_{\kappa r}, \mu_r, \Delta_{\mu r}, \lambda_r, \Delta_{\lambda r}\}$  we want to compute their respective renormalization-group functions  $\{\eta, \phi, \beta_\mu, \beta_{\Delta_\mu}, \beta_\lambda, \beta_{\Delta_\lambda}\}$ . This is achieved by a study of the 2-point correlation functions  $\{S_\delta, S_J, D_\delta^\perp, D_J^\perp, D_\delta^\parallel, D_J^\parallel\}$ , or more specifically their respective self-energies and polarizations  $\{\Sigma_\delta, \Sigma_J, \Pi_\delta^\perp, \Pi_J^\perp, \Pi_\delta^\parallel, \Pi_J^\parallel\}$  and their pole structure, embedded in the renormalization constants  $\{Z, Z_{\Delta_\kappa}, Z_\mu, Z_{\Delta_\mu}, Z_\lambda, Z_{\Delta_\lambda}\}$ .

## 2.3 Perturbative calculations up to three loops

In this section, we compute all the Feynman diagrams necessary at one, two, and three loops, to evaluate later all the RG functions of the model (2.8). Since the computations are extremely lengthy, we will briefly sketch the derivation at one loop, give only the final results at two loops, and at three loops, only display the diagrams that we computed. All these computations have been carried out in a completely automated way.

### 2.3.1 One-loop analysis

At one loop, the two-point flexuron self-energy has only one diagrammatic contribution, with symmetry factor 1, reading

$$\begin{aligned} \Sigma_{\alpha\beta}^{AB(1)} &= \alpha A \text{---} \text{---} \text{---} \beta B \\ &= 1 \times M^{2\varepsilon} \int [d^d k] \sum_{CDEF} \Gamma_{\beta\gamma f}^{BCF(0)}(-\vec{p}, \vec{p}-\vec{k}, \vec{k}) D_{ef}^{EF(0)}(\vec{k}) \Gamma_{\alpha\delta e}^{ADE(0)}(\vec{p}, \vec{k}-\vec{p}, -\vec{k}) S_{\gamma\delta}^{DC(0)}(\vec{p}-\vec{k}). \end{aligned} \quad (2.45)$$

Its computation is not conceptually complicated, but it is lengthy. After caring out carefully all the algebra as well as removing all the vanishing integrals, its expression takes a surprisingly simple form reading

$$\Sigma_{\alpha\beta}^{AB(1)} = p^4 M^{2\varepsilon} \delta_{\alpha\beta} (X_1 \delta^{AB} + X_2 J^{AB}) (p^4 j(d, \vec{p}, 2, 2) - 8p^2 j(d, \vec{p}, 2, 1) + 4j(d, \vec{p}, 1, 1)), \quad (2.46)$$

where  $j(d, \vec{p}, \alpha, \beta)$  is the one-loop integral defined in Appendix A, and where

$$X_1 = \frac{\kappa \Delta_\mu (\lambda^2 + 2\lambda\mu + 2\mu^2) + \mu (\kappa\mu \Delta_\lambda - (\Delta_\kappa + \kappa)(\lambda + \mu)(\lambda + 2\mu))}{4\kappa^2 (\lambda + 2\mu)^2}, \quad (2.47a)$$

$$X_2 = \frac{\Delta_\kappa (\lambda^2 \Delta_\mu + \mu (\mu \Delta_\lambda + 2\Delta_\mu (\lambda + \mu)))}{4\kappa^2 (\lambda + 2\mu)^2}. \quad (2.47b)$$

After IBP reduction, it further simplifies to

$$\Sigma_{\alpha\beta}^{AB(1)} = p^4 M^{2\varepsilon} \delta_{\alpha\beta} (X_1 \delta^{AB} + X_2 J^{AB}) (d-2)(d+1) j(d, \vec{p}, 1, 1), \quad (2.48)$$

from which we can easily extract the two scalar parts, and expand in series around  $d = 4 - 2\varepsilon$ , reading

$$\Sigma_\delta^{(1)} = \frac{X_1 p^4}{(4\pi)^2} \left( \frac{p^2}{M^2} \right)^\varepsilon \left[ \frac{10}{\varepsilon} + 6 + \left( 16 - \frac{5\pi^2}{6} \right) \varepsilon + \mathcal{O}(\varepsilon^2) \right], \quad (2.49a)$$

$$\Sigma_J^{(1)} = \frac{X_2 p^4}{(4\pi)^2} \left( \frac{p^2}{M^2} \right)^\varepsilon \left[ \frac{10}{\varepsilon} + 6 + \left( 16 - \frac{5\pi^2}{6} \right) \varepsilon + \mathcal{O}(\varepsilon^2) \right]. \quad (2.49b)$$

We now turn to the evaluation of the phonon polarization at one loop. It also yields a single diagram, with symmetry factor 1/2, defined as

$$\Pi_{ab}^{AB(1)} = a A \text{---} \text{---} \text{---} b B \quad (2.50a)$$

$$= \frac{1}{2} \times M^{2\varepsilon} \int [d^d k] \sum_{CDEF} \Gamma_{\gamma\delta b}^{CDB(0)}(\vec{p}-\vec{k}, \vec{k}, -\vec{p}) S_{\tau\delta}^{FD(0)}(\vec{k}) \Gamma_{\rho\tau a}^{EFA(0)}(\vec{k}-\vec{p}, -\vec{k}, \vec{p}) S_{\gamma\rho}^{CE(0)}(\vec{k}-\vec{p}).$$

This diagram contains open momentum indices  $(a, b)$ , so it needs to be projected right away to obtain scalar integrals. Using the projectors (2.26), the transverse and longitudinal parts reads

$$\Pi_{\perp}^{AB(1)} = \frac{d_c}{d-1} p^2 M^{2\varepsilon} (Y_1 \delta^{AB} + Y_2 J^{AB}) j(d, \vec{p}, 1, 1), \quad (2.51a)$$

$$\begin{aligned} \Pi_{\parallel}^{AB(1)} = d_c p^2 M^{2\varepsilon} & \left[ (Y_7 p^4 j(d, \vec{p}, 2, 2) + Y_5 p^2 j(d, \vec{p}, 2, 1) + Y_3 j(d, \vec{p}, 1, 1)) \delta^{AB} \right. \\ & \left. + (Y_8 p^4 j(d, \vec{p}, 2, 2) + Y_6 p^2 j(d, \vec{p}, 2, 1) + Y_4 j(d, \vec{p}, 1, 1)) J^{AB} \right], \end{aligned} \quad (2.51b)$$

where we used the eight temporary polynomials

$$\begin{aligned} 4\kappa^3 Y_1 &= \mu^2 (2\Delta\kappa + \kappa), & 4\kappa^4 Y_2 &= \mu (\Delta\kappa^2 \mu - 2\Delta\mu\kappa (2\Delta\kappa + \kappa)), \\ 4\kappa^3 Y_3 &= (2\Delta\kappa + \kappa) (\lambda^2 + 2\lambda\mu + 2\mu^2), & 2\kappa^3 Y_5 &= -\lambda (2\Delta\kappa + \kappa) (\lambda + \mu), & 8\kappa^3 Y_7 &= (2\Delta\kappa + \kappa) (\lambda + \mu)^2, \\ 4\kappa^4 Y_4 &= \Delta\kappa^2 \lambda^2 + 2\Delta\kappa^2 \lambda\mu + 2\Delta\kappa^2 \mu^2 - 2\kappa\lambda (2\Delta\kappa + \kappa) (\Delta\lambda + \Delta\mu) - 2\kappa\mu (2\Delta\kappa + \kappa) (\Delta\lambda + 2\Delta\mu), \\ 2\kappa^4 Y_6 &= -\Delta\kappa^2 \lambda (\lambda + \mu) + 2\Delta\kappa\kappa (\Delta\lambda (2\lambda + \mu) + \Delta\mu\lambda) + \kappa^2 (\Delta\lambda (2\lambda + \mu) + \Delta\mu\lambda), \\ 8\kappa^4 Y_8 &= (\lambda + \mu) (\Delta\kappa^2 (\lambda + \mu) - 4\Delta\kappa\kappa (\Delta\lambda + \Delta\mu) - 2\kappa^2 (\Delta\lambda + \Delta\mu)). \end{aligned} \quad (2.52)$$

As we can see, the longitudinal part of the polarization is highly non-trivial as soon as one loop. Indeed, as opposed to the transverse part, the polynomials do not factorize nicely. This will be the case for the vast majority of the diagrams beyond one loop. Going further, after IBP reduction, the polarization projections read

$$\Pi_{\perp}^{AB(1)} = \frac{d_c}{d-1} p^2 M^{2\varepsilon} (Y_1 \delta^{AB} + Y_2 J^{AB}) j(d, \vec{p}, 1, 1), \quad (2.53a)$$

$$\Pi_{\parallel}^{AB(1)} = d_c p^2 M^{2\varepsilon} \left( ((d-3)((d-6)Y_7 - Y_5) + Y_3) \delta^{AB} + ((d-3)((d-6)Y_8 - Y_6) + Y_4) J^{AB} \right) j(d, \vec{p}, 1, 1), \quad (2.53b)$$

which, once expanded in  $d = 4 - 2\varepsilon$  reads

$$\Pi_{\delta}^{\perp(1)} = \frac{Y_1 d_c p^2}{(4\pi)^2} \left( \frac{p^2}{M^2} \right)^{\varepsilon} \left[ \frac{1}{3\varepsilon} + \frac{8}{9} + \left( \frac{52}{27} - \frac{\pi^2}{36} \right) \varepsilon + \mathcal{O}(\varepsilon^2) \right], \quad (2.54a)$$

$$\Pi_J^{\perp(1)} = \frac{Y_2 d_c p^2}{(4\pi)^2} \left( \frac{p^2}{M^2} \right)^{\varepsilon} \left[ \frac{1}{3\varepsilon} + \frac{8}{9} + \left( \frac{52}{27} - \frac{\pi^2}{36} \right) \varepsilon + \mathcal{O}(\varepsilon^2) \right], \quad (2.54b)$$

$$\Pi_{\delta}^{\parallel(1)} = \frac{d_c p^2}{(4\pi)^2} \left( \frac{p^2}{M^2} \right)^{\varepsilon} \left[ \frac{Y_3 - Y_5 - 2Y_7}{\varepsilon} + 2(Y_3 - Y_7) + \frac{1}{12} \varepsilon (\pi^2 (Y_5 + 2Y_7) - (\pi^2 - 48) Y_3) + \mathcal{O}(\varepsilon^2) \right], \quad (2.54c)$$

$$\Pi_J^{\parallel(1)} = \frac{d_c p^2}{(4\pi)^2} \left( \frac{p^2}{M^2} \right)^{\varepsilon} \left[ \frac{Y_4 - Y_6 - 2Y_8}{\varepsilon} + 2(Y_4 - Y_8) + \frac{1}{12} \varepsilon (\pi^2 (Y_6 + 2Y_8) - (\pi^2 - 48) Y_4) + \mathcal{O}(\varepsilon^2) \right]. \quad (2.54d)$$

As we can see, the polynomials  $Y_x$  contribute differently at each order of the  $\varepsilon$ -expansion. Therefore, the calculation of the integrals cannot be separated from the tensorial contractions generating the polynomials  $Y_x$  (unlike, *e.g.*, in QCD, where one may compute the integrals and the color factors independently).

## 2.3.2 Two-loop analysis

At two loops, the flexuron self-energy has five contributions represented by the diagrams in figure 2.2.

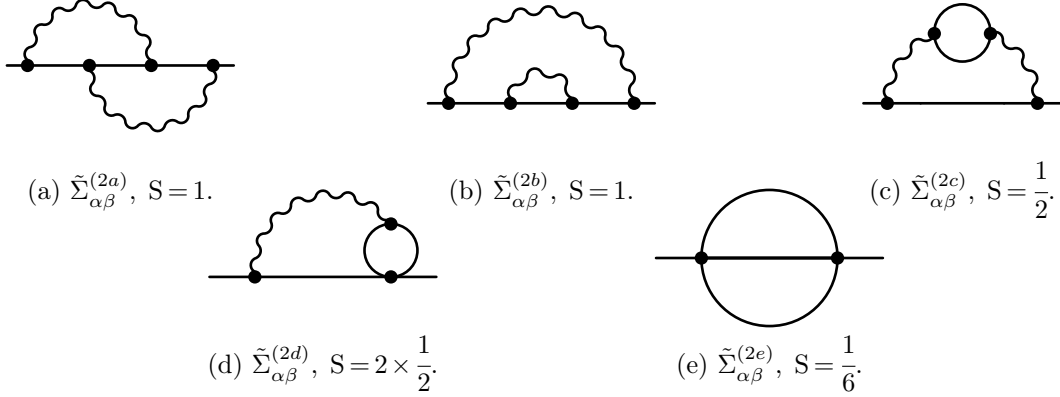


Figure 2.2: Two-loop flexuron self-energy diagrams and their symmetry factors ( $S$ ).

At this point, we won't give any details of the derivation and just provide the results obtained after computing and summing all the diagrams. We will use the notations

$$T_n = \frac{(p^2)^{n/2}}{48(4\pi)^4 \kappa^6 (\lambda + 2\mu)^n} \left( \frac{p^2}{M^2} \right)^{2\varepsilon}, \quad \alpha_{ijk}^{lmn} = \lambda^i \mu^j \kappa^k \Delta_\lambda^l \Delta_\mu^m \Delta_\kappa^n. \quad (2.55)$$

First, the  $\delta^{AB}$  part yields

$$\begin{aligned} \Sigma_\delta^{(2)} = & \frac{5\kappa T_4}{\varepsilon^2} \left[ 12(d_c + 10)\alpha_{062}^{000} + (44d_c + 360)\alpha_{152}^{000} + (63d_c + 390)\alpha_{242}^{000} + 36(d_c + 5)\alpha_{332}^{000} + (7d_c + 30)\alpha_{422}^{000} \right. \\ & + 36(d_c + 10)\alpha_{061}^{001} + 12(11d_c + 90)\alpha_{151}^{001} + 9(21d_c + 130)\alpha_{241}^{001} + 108(d_c + 5)\alpha_{331}^{001} + (21d_c + 90)\alpha_{421}^{001} \\ & + (36d_c + 240)\alpha_{060}^{002} + (132d_c + 720)\alpha_{150}^{002} + (189d_c + 780)\alpha_{240}^{002} + 36(3d_c + 10)\alpha_{330}^{002} + (21d_c + 60)\alpha_{420}^{002} \\ & - 24(d_c + 10)\alpha_{052}^{010} - (68d_c + 600)\alpha_{142}^{010} - (76d_c + 600)\alpha_{232}^{010} - 4(13d_c + 75)\alpha_{322}^{010} - 2(7d_c + 30)\alpha_{412}^{010} \\ & - 48(d_c + 10)\alpha_{051}^{011} - 8(17d_c + 150)\alpha_{141}^{011} - 8(19d_c + 150)\alpha_{231}^{011} - 8(13d_c + 75)\alpha_{321}^{011} - 4(7d_c + 30)\alpha_{411}^{011} \\ & - 20(d_c + 6)\alpha_{052}^{100} - 10(5d_c + 18)\alpha_{142}^{100} - 20(d_c + 3)\alpha_{232}^{100} - 40(d_c + 6)\alpha_{051}^{101} - 20(5d_c + 18)\alpha_{141}^{101} - 40(d_c + 3)\alpha_{231}^{101} \\ & \left. + 120\alpha_{042}^{020} + 240\alpha_{132}^{020} + 240\alpha_{222}^{020} + 120\alpha_{312}^{020} + 30\alpha_{402}^{020} + 120\alpha_{042}^{110} + 120\alpha_{132}^{110} + 60\alpha_{222}^{110} + 30\alpha_{042}^{200} \right] \\ & + \frac{\kappa T_4}{6\varepsilon} \left[ (756d_c + 4240)\alpha_{062}^{000} + (2532d_c + 13440)\alpha_{152}^{000} + (3129d_c + 15940)\alpha_{242}^{000} + (1608d_c + 7980)\alpha_{332}^{000} \right. \\ & + (291d_c + 1420)\alpha_{422}^{000} + (2268d_c + 12720)\alpha_{061}^{001} + (7596d_c + 40320)\alpha_{151}^{001} + (9387d_c + 47820)\alpha_{241}^{001} \\ & + 36(134d_c + 665)\alpha_{331}^{001} + (873d_c + 4260)\alpha_{421}^{001} + 36(63d_c + 250)\alpha_{060}^{002} + 36(211d_c + 810)\alpha_{150}^{002} \\ & + (9387d_c + 35730)\alpha_{240}^{002} + 72(67d_c + 255)\alpha_{330}^{002} + 9(97d_c + 370)\alpha_{420}^{002} - 8(189d_c + 1060)\alpha_{052}^{010} \\ & - 4(1011d_c + 5480)\alpha_{142}^{010} - 4(1077d_c + 5660)\alpha_{232}^{010} - 4(624d_c + 3145)\alpha_{322}^{010} - (582d_c + 2840)\alpha_{412}^{010} \\ & - 16(189d_c + 1060)\alpha_{051}^{011} - 8(1011d_c + 5480)\alpha_{141}^{011} - 8(1077d_c + 5660)\alpha_{231}^{011} - 8(624d_c + 3145)\alpha_{321}^{011} \\ & - 4(291d_c + 1420)\alpha_{411}^{011} - 20(51d_c + 248)\alpha_{052}^{100} - 30(65d_c + 308)\alpha_{142}^{100} - 20(36d_c + 169)\alpha_{232}^{100} \\ & - 40(51d_c + 248)\alpha_{051}^{101} - 60(65d_c + 308)\alpha_{141}^{101} - 40(36d_c + 169)\alpha_{231}^{101} + 4240\alpha_{042}^{020} + 8480\alpha_{132}^{020} \\ & \left. + 8840\alpha_{222}^{020} + 4600\alpha_{312}^{020} + 1420\alpha_{402}^{020} + 4960\alpha_{042}^{110} + 4960\alpha_{132}^{110} + 3380\alpha_{222}^{110} + 2140\alpha_{042}^{200} \right]. \quad (2.56) \end{aligned}$$

Second, the  $J^{AB}$  part yields

$$\Sigma_J^{(2)} = \frac{5\Delta_\kappa T_4}{\varepsilon^2} \left[ 12d_c \alpha_{060}^{002} + 44d_c \alpha_{150}^{002} + 63d_c \alpha_{240}^{002} + 36d_c \alpha_{330}^{002} + 7d_c \alpha_{420}^{002} - 24(d_c + 10)\alpha_{052}^{010} \right]$$

$$\begin{aligned}
& - (68d_c + 600)\alpha_{142}^{010} - (76d_c + 600)\alpha_{232}^{010} - 4(13d_c + 75)\alpha_{322}^{010} - 2(7d_c + 30)\alpha_{412}^{010} - 48(d_c + 5)\alpha_{051}^{011} \\
& - 8(17d_c + 75)\alpha_{141}^{011} - 8(19d_c + 75)\alpha_{231}^{011} - 4(26d_c + 75)\alpha_{321}^{011} - 4(7d_c + 15)\alpha_{411}^{011} - 20(d_c + 6)\alpha_{052}^{100} \\
& - 10(5d_c + 18)\alpha_{142}^{100} - 20(d_c + 3)\alpha_{232}^{100} - 40(d_c + 3)\alpha_{051}^{101} - 20(5d_c + 9)\alpha_{141}^{101} - 20(2d_c + 3)\alpha_{231}^{101} \\
& + 360\alpha_{042}^{020} + 720\alpha_{132}^{020} + 720\alpha_{222}^{020} + 360\alpha_{312}^{020} + 90\alpha_{402}^{020} + 360\alpha_{042}^{110} + 360\alpha_{132}^{110} + 180\alpha_{222}^{110} + 90\alpha_{042}^{200} \\
& + \frac{\Delta_\kappa T_4}{6\varepsilon} \left[ (756d_c + 520)\alpha_{060}^{002} + (2532d_c + 2280)\alpha_{150}^{002} + 7(447d_c + 550)\alpha_{240}^{002} + 24(67d_c + 100)\alpha_{330}^{002} \right. \\
& + (291d_c + 490)\alpha_{420}^{002} - 8(189d_c + 1060)\alpha_{052}^{010} - 4(1011d_c + 5480)\alpha_{142}^{010} - 4(1077d_c + 5660)\alpha_{232}^{010} \\
& - 4(624d_c + 3145)\alpha_{322}^{010} - (582d_c + 2840)\alpha_{412}^{010} - 112(27d_c + 85)\alpha_{051}^{011} - 8(1011d_c + 3155)\alpha_{141}^{011} \\
& - 8(1077d_c + 3335)\alpha_{231}^{011} - 52(96d_c + 305)\alpha_{321}^{011} - 4(291d_c + 955)\alpha_{411}^{011} - 20(51d_c + 248)\alpha_{052}^{100} \\
& - 30(65d_c + 308)\alpha_{142}^{100} - 20(36d_c + 169)\alpha_{232}^{100} - 40(51d_c + 155)\alpha_{051}^{101} - 300(13d_c + 43)\alpha_{141}^{101} \\
& - 20(72d_c + 245)\alpha_{231}^{101} + 12720\alpha_{042}^{020} + 25440\alpha_{132}^{020} + 26520\alpha_{222}^{020} + 13800\alpha_{312}^{020} + 4260\alpha_{402}^{020} \\
& \left. + 14880\alpha_{042}^{110} + 14880\alpha_{132}^{110} + 10140\alpha_{222}^{110} + 6420\alpha_{042}^{200} \right]. \tag{2.57}
\end{aligned}$$

Let us discuss briefly the notation  $\alpha_{ijk}^{lmn} = \lambda^i \mu^j \kappa^k \Delta_\lambda^l \Delta_\mu^m \Delta_\kappa^n$ . First, we recall that the loop expansion is performed into the couplings only, *i.e.*,  $\alpha = \{\lambda, \mu, \Delta_\lambda, \Delta_\mu\}$ , which excludes  $\kappa$  and  $\Delta_\kappa$ . Therefore, the two indices  $\{k, n\}$  does not count for the expansion. It is apparent in (2.56) and (2.57) since the order of the coupling in the expansion is 6, and we factorized a term  $(\lambda + 2\mu)^4$  in  $T_4$  so that the resulting order is indeed 2, as expected from a two-loop expansion. Let us also note that, by construction of  $\alpha_{ijk}^{lmn}$ , only terms with the same total number of indices ( $i + j + k + l + m + n$ ), as well as the same number of coupling indices ( $i + j + l + m$ ), and the same number of parameter indices ( $k + n$ ) can appear next to each other at a given order in the expansion. Interestingly, if we set  $a = i + j + l + m$  and  $b = k + n$ , for a given tuple  $a, b$ , there is a total of  $(b + 1)(1 + a)(2 + a)(3 + a)/6$  possible terms. Taking (2.56) as an example, the order in the couplings is  $i + j + l + m = 6$  and the order in the parameters is  $k + n = 2$ . This gives a total number of possible term of 252, although we observe an effective number of terms of 40. This is partially because the amount of disorder is always reduced, so that the sum  $l + m$  will never exceed 2, taking this into account, the number of possible terms simply yields  $(b + 1)(1 + 3a)$ , which is 57 for our example, much closer to 40. The takeaway of this little discussion is that for a given  $\alpha_{ijk}^{lmn} = \lambda^i \mu^j \kappa^k \Delta_\lambda^l \Delta_\mu^m \Delta_\kappa^n$ , the number of terms is of the order of  $(i + j + l + m + 1)(1 + 3(k + n))$ .

We now move on to the two-loop polarization of the phonon. It has three contributions, displayed in figure 2.3.

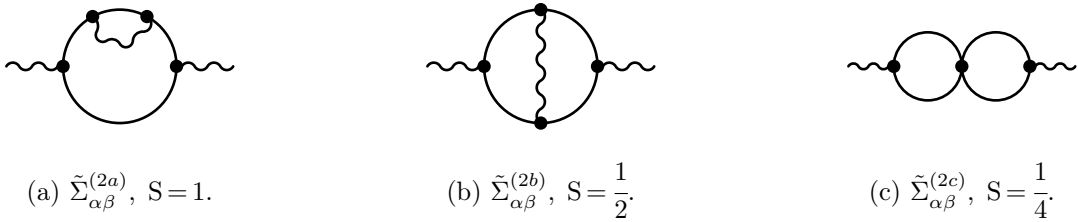


Figure 2.3: Two-loop phonon polarization diagrams and their symmetry factors (S).

All computations done, we obtain the following results. First for the transverse  $\delta^{AB}$  part

$$\begin{aligned}
\Pi_\delta^{\perp(2)} = & - \frac{d_c \mu^2 T_2}{3\varepsilon^2} \left[ 4(d_c + 15)\alpha_{032}^{000} + (4d_c + 90)\alpha_{122}^{000} + (d_c + 30)\alpha_{212}^{000} + 16(d_c + 15)\alpha_{031}^{001} \right. \\
& + 8(2d_c + 45)\alpha_{121}^{001} + 4(d_c + 30)\alpha_{211}^{001} + 4(4d_c + 45)\alpha_{030}^{002} + (16d_c + 270)\alpha_{120}^{002} + (4d_c + 90)\alpha_{210}^{002} \\
& - 60\alpha_{022}^{010} - 60\alpha_{112}^{010} - 30\alpha_{202}^{010} - 240\alpha_{021}^{011} - 240\alpha_{111}^{011} - 120\alpha_{201}^{011} - 30\alpha_{022}^{100} - 120\alpha_{021}^{101} \left. \right] \\
& - \frac{d_c \mu^2 T_2}{18\varepsilon} \left[ 2(64d_c + 733)\alpha_{032}^{000} + (128d_c + 2199)\alpha_{122}^{000} + (32d_c + 733)\alpha_{212}^{000} + 8(64d_c + 733)\alpha_{031}^{001} \right]
\end{aligned}$$

$$\begin{aligned}
& + (512d_c + 8796)\alpha_{121}^{001} + 4(32d_c + 733)\alpha_{211}^{001} + (512d_c + 4388)\alpha_{030}^{002} + (512d_c + 6582)\alpha_{120}^{002} \\
& + (128d_c + 2194)\alpha_{210}^{002} - 1466\alpha_{022}^{010} - 1466\alpha_{112}^{010} - 733\alpha_{202}^{010} - 5864\alpha_{021}^{011} - 5864\alpha_{111}^{011} - 2932\alpha_{201}^{011} \\
& - 733\alpha_{022}^{100} - 2932\alpha_{021}^{101} \Big]. \tag{2.58}
\end{aligned}$$

Then, for the transverse  $J^{AB}$  part

$$\begin{aligned}
\Pi_J^{\perp(2)} = & \frac{d_c \mu T_2}{3\kappa \varepsilon^2} \Big[ -8(d_c + 15)\alpha_{041}^{002} - 4(2d_c + 45)\alpha_{131}^{002} - 2(d_c + 30)\alpha_{221}^{002} - 8(2d_c + 15)\alpha_{040}^{003} \\
& - 4(4d_c + 45)\alpha_{130}^{003} - 4(d_c + 15)\alpha_{220}^{003} + 12(d_c + 10)\alpha_{033}^{010} + 12(d_c + 15)\alpha_{123}^{010} + 3(d_c + 20)\alpha_{213}^{010} \\
& + 48(d_c + 10)\alpha_{032}^{011} + 48(d_c + 15)\alpha_{122}^{011} + 12(d_c + 20)\alpha_{212}^{011} + (48d_c + 540)\alpha_{031}^{012} + 48(d_c + 15)\alpha_{121}^{012} \\
& + 6(2d_c + 45)\alpha_{211}^{012} - 120\alpha_{023}^{020} - 120\alpha_{113}^{020} - 60\alpha_{203}^{020} - 480\alpha_{022}^{021} - 480\alpha_{112}^{021} - 240\alpha_{202}^{021} + 90\alpha_{031}^{022} \\
& - 60\alpha_{023}^{110} - 240\alpha_{022}^{111} \Big] \\
& + \frac{d_c \mu T_2}{9\kappa \varepsilon} \Big[ -2(64d_c + 733)\alpha_{041}^{002} - (128d_c + 2199)\alpha_{131}^{002} - (32d_c + 733)\alpha_{221}^{002} - 16(16d_c + 91)\alpha_{040}^{003} \\
& - 8(32d_c + 273)\alpha_{130}^{003} - 8(8d_c + 91)\alpha_{220}^{003} + 2(96d_c + 733)\alpha_{033}^{010} + 3(64d_c + 733)\alpha_{123}^{010} + (48d_c + 733)\alpha_{213}^{010} \\
& + 8(96d_c + 733)\alpha_{032}^{011} + (768d_c + 8796)\alpha_{122}^{011} + 4(48d_c + 733)\alpha_{212}^{011} + (768d_c + 6582)\alpha_{031}^{012} \\
& + (768d_c + 8776)\alpha_{121}^{012} + (192d_c + 3291)\alpha_{211}^{012} - 1466\alpha_{023}^{020} - 1466\alpha_{113}^{020} - 733\alpha_{203}^{020} - 5864\alpha_{022}^{021} - 5864\alpha_{112}^{021} \\
& - 2932\alpha_{202}^{021} + 1097\alpha_{031}^{022} - 733\alpha_{023}^{110} - 2932\alpha_{022}^{111} \Big]. \tag{2.59}
\end{aligned}$$

Then, the longitudinal  $\delta^{AB}$  part

$$\begin{aligned}
\Pi_\delta^{\parallel(2)} = & -\frac{d_c T_2}{\varepsilon^2} \Big[ (8d_c + 60)\alpha_{052}^{000} + (44d_c + 210)\alpha_{142}^{000} + 110(d_c + 3)\alpha_{232}^{000} + 3(43d_c + 80)\alpha_{322}^{000} \\
& + (66d_c + 60)\alpha_{412}^{000} + 12d_c\alpha_{502}^{000} + (32d_c + 240)\alpha_{051}^{001} + (176d_c + 840)\alpha_{141}^{001} + 440(d_c + 3)\alpha_{231}^{001} \\
& + (516d_c + 960)\alpha_{321}^{001} + (264d_c + 240)\alpha_{411}^{001} + 48d_c\alpha_{501}^{001} + 4(8d_c + 45)\alpha_{050}^{002} + (176d_c + 630)\alpha_{140}^{002} \\
& + 110(4d_c + 9)\alpha_{230}^{002} + (516d_c + 720)\alpha_{320}^{002} + (264d_c + 180)\alpha_{410}^{002} + 48d_c\alpha_{500}^{002} - 60\alpha_{042}^{010} - 180\alpha_{132}^{010} - 270\alpha_{222}^{010} \\
& - 180\alpha_{312}^{010} - 60\alpha_{402}^{010} - 240\alpha_{041}^{011} - 720\alpha_{131}^{011} - 1080\alpha_{221}^{011} - 720\alpha_{311}^{011} - 240\alpha_{401}^{011} - 30\alpha_{042}^{100} - 60\alpha_{132}^{100} - 60\alpha_{222}^{100} \\
& - 120\alpha_{041}^{101} - 240\alpha_{131}^{101} - 240\alpha_{221}^{101} \Big] \\
& + \frac{d_c T_2}{6\varepsilon} \Big[ -2(100d_c + 923)\alpha_{052}^{000} - (632d_c + 4101)\alpha_{142}^{000} - (1130d_c + 3893)\alpha_{232}^{000} \\
& - 36(29d_c + 59)\alpha_{322}^{000} - 18(25d_c + 27)\alpha_{412}^{000} - 72d_c\alpha_{502}^{000} - 8(100d_c + 923)\alpha_{051}^{001} - 4(632d_c + 4101)\alpha_{141}^{001} \\
& - 4(1130d_c + 3893)\alpha_{231}^{001} - 144(29d_c + 59)\alpha_{321}^{001} - 72(25d_c + 27)\alpha_{411}^{001} - 288d_c\alpha_{501}^{001} - (800d_c + 5668)\alpha_{050}^{002} \\
& - 2(1264d_c + 6519)\alpha_{140}^{002} - 2(2260d_c + 6547)\alpha_{230}^{002} - 36(116d_c + 207)\alpha_{320}^{002} - 72(25d_c + 24)\alpha_{410}^{002} - 288d_c\alpha_{500}^{002} \\
& + 1846\alpha_{042}^{010} + 3178\alpha_{132}^{010} + 3227\alpha_{222}^{010} + 1638\alpha_{312}^{010} + 486\alpha_{402}^{010} + 7384\alpha_{041}^{011} + 12712\alpha_{131}^{011} + 12908\alpha_{221}^{011} \\
& + 6552\alpha_{311}^{011} + 1944\alpha_{401}^{011} + 923\alpha_{042}^{100} + 666\alpha_{132}^{100} + 486\alpha_{222}^{100} + 3692\alpha_{041}^{101} + 2664\alpha_{131}^{101} + 1944\alpha_{221}^{101} \Big]. \tag{2.60}
\end{aligned}$$

And finally, the longitudinal  $J^{AB}$  part

$$\begin{aligned}
\Pi_J^{\parallel(2)} = & -\frac{d_c T_2}{\kappa \varepsilon^2} \Big[ 8(2d_c + 15)\alpha_{051}^{002} + (88d_c + 420)\alpha_{141}^{002} + 220(d_c + 3)\alpha_{231}^{002} + 6(43d_c + 80)\alpha_{321}^{002} \\
& + (132d_c + 120)\alpha_{411}^{002} + 24d_c\alpha_{501}^{002} + 8(4d_c + 15)\alpha_{050}^{003} + (176d_c + 420)\alpha_{140}^{003} + 220(2d_c + 3)\alpha_{230}^{003} \\
& + (516d_c + 480)\alpha_{320}^{003} + 24(11d_c + 5)\alpha_{410}^{003} + 48d_c\alpha_{500}^{003} - 24(d_c + 5)\alpha_{043}^{010} - 12(8d_c + 25)\alpha_{133}^{010} - 30(5d_c + 8)\alpha_{223}^{010} \\
& - 30(3d_c + 2)\alpha_{313}^{010} - 18d_c\alpha_{403}^{010} - 96(d_c + 5)\alpha_{042}^{011} - 48(8d_c + 25)\alpha_{132}^{011} - 120(5d_c + 8)\alpha_{222}^{011} - 120(3d_c + 2)\alpha_{312}^{011} \\
& - 72d_c\alpha_{402}^{011} - 12(8d_c + 45)\alpha_{041}^{012} - 96(4d_c + 15)\alpha_{131}^{012} - 30(20d_c + 51)\alpha_{221}^{012} - 360(d_c + 2)\alpha_{311}^{012} - 36(2d_c + 5)\alpha_{401}^{012} \\
& + 120\alpha_{033}^{020} + 240\alpha_{123}^{020} + 180\alpha_{213}^{020} + 60\alpha_{303}^{020} + 480\alpha_{032}^{021} + 960\alpha_{122}^{021} + 720\alpha_{212}^{021} + 240\alpha_{302}^{021} - 12(3d_c + 10)\alpha_{043}^{100}
\end{aligned}$$

$$\begin{aligned}
& -60(3d_c + 7)\alpha_{133}^{100} - 3(99d_c + 140)\alpha_{223}^{100} - 60(3d_c + 2)\alpha_{313}^{100} - 36d_c\alpha_{403}^{100} - 48(3d_c + 10)\alpha_{042}^{101} \\
& - 240(3d_c + 7)\alpha_{132}^{101} - 12(99d_c + 140)\alpha_{222}^{101} - 240(3d_c + 2)\alpha_{312}^{101} - 144d_c\alpha_{402}^{101} - 18(8d_c + 25)\alpha_{041}^{102} \\
& - 720(d_c + 2)\alpha_{131}^{102} - 36(33d_c + 40)\alpha_{221}^{102} - 360(2d_c + 1)\alpha_{311}^{102} - 144d_c\alpha_{401}^{102} + 180\alpha_{033}^{110} + 420\alpha_{123}^{110} + 300\alpha_{213}^{110} \\
& + 120\alpha_{303}^{110} + 720\alpha_{032}^{111} + 1680\alpha_{122}^{111} + 1200\alpha_{212}^{111} + 480\alpha_{302}^{111} + 60\alpha_{033}^{200} + 120\alpha_{123}^{200} + 240\alpha_{032}^{201} + 480\alpha_{122}^{201} \Big] \\
& + \frac{d_c T_2}{3\kappa\varepsilon} \left[ -2(100d_c + 923)\alpha_{051}^{002} + (-632d_c - 4101)\alpha_{141}^{002} + (-1130d_c - 3893)\alpha_{231}^{002} - 36(29d_c + 59)\alpha_{321}^{002} \right. \\
& - 18(25d_c + 27)\alpha_{411}^{002} - 72d_c\alpha_{501}^{002} - 8(50d_c + 247)\alpha_{050}^{003} - 4(316d_c + 1209)\alpha_{140}^{003} - 4(565d_c + 1327)\alpha_{230}^{003} \\
& - 36(58d_c + 89)\alpha_{320}^{003} - 36(25d_c + 21)\alpha_{410}^{003} - 144d_c\alpha_{500}^{003} + (300d_c + 1846)\alpha_{043}^{010} + (732d_c + 3435)\alpha_{133}^{010} \\
& + (831d_c + 1922)\alpha_{223}^{010} + 9(48d_c + 37)\alpha_{313}^{010} + 81d_c\alpha_{403}^{010} + 8(150d_c + 923)\alpha_{042}^{011} + (2928d_c + 13740)\alpha_{132}^{011} \\
& + (3324d_c + 7688)\alpha_{222}^{011} + 36(48d_c + 37)\alpha_{312}^{011} + 324d_c\alpha_{402}^{011} + (1200d_c + 8502)\alpha_{041}^{012} + 16(183d_c + 992)\alpha_{131}^{012} \\
& + (3324d_c + 11649)\alpha_{221}^{012} + 108(16d_c + 37)\alpha_{311}^{012} + 108(3d_c + 8)\alpha_{401}^{012} - 1846\alpha_{033}^{020} - 2512\alpha_{123}^{020} - 1589\alpha_{213}^{020} \\
& - 333\alpha_{303}^{020} - 7384\alpha_{032}^{021} - 10048\alpha_{122}^{021} - 6356\alpha_{212}^{021} - 1332\alpha_{302}^{021} + (216d_c + 666)\alpha_{043}^{100} + 27(32d_c + 73)\alpha_{133}^{100} \\
& + 9(126d_c + 199)\alpha_{223}^{100} + 54(11d_c + 9)\alpha_{313}^{100} + 108d_c\alpha_{403}^{100} + 72(12d_c + 37)\alpha_{042}^{101} + 108(32d_c + 73)\alpha_{132}^{101} \\
& + (4536d_c + 7164)\alpha_{222}^{101} + 216(11d_c + 9)\alpha_{312}^{101} + 432d_c\alpha_{402}^{101} + (864d_c + 3685)\alpha_{041}^{102} + 216(16d_c + 37)\alpha_{131}^{102} \\
& + 378(12d_c + 19)\alpha_{221}^{102} + 216(11d_c + 8)\alpha_{311}^{102} + 432d_c\alpha_{401}^{102} - 1589\alpha_{033}^{110} - 1971\alpha_{123}^{110} - 1305\alpha_{213}^{110} \\
& \left. - 486\alpha_{303}^{110} - 6356\alpha_{032}^{111} - 7884\alpha_{122}^{111} - 5220\alpha_{212}^{111} - 1944\alpha_{302}^{111} - 333\alpha_{033}^{200} - 486\alpha_{123}^{200} - 1332\alpha_{032}^{201} - 1944\alpha_{122}^{201} \right].
\end{aligned} \tag{2.61}$$

### 2.3.3 Three-loop analysis

At three loops, the computation, as well as the results in themselves, are extremely lengthy (each result well over a page) so that we won't display any of them. We simply provide the diagrams that we have computed with similar techniques.

For the flexuron self-energy at three loops, it has 32 distinct contributions. All the diagrams are provided in figure 2.4. As for the topologies, it contains 23 Ladder (L3), 8 Benz (B3) topology, and 1 non-planar (N3). Similarly, the three-loop phonon polarization has 19 contributions. All the diagrams are provided in figure 2.5. It contains 13 L3 topologies, 5 B3 and a single N3. See Appendix A for details on these topologies, and why it is important to distinguish them.

After full computation and summation, we obtain the results (not displayed) for

$$\Sigma_{\delta}^{(3)}, \quad \Sigma_J^{(3)}, \quad \Pi_{\delta}^{\perp(3)}, \quad \Pi_J^{\perp(3)}, \quad \Pi_{\delta}^{\parallel(3)}, \quad \Pi_J^{\parallel(3)}. \tag{2.62}$$

See the diagrams on next pages.



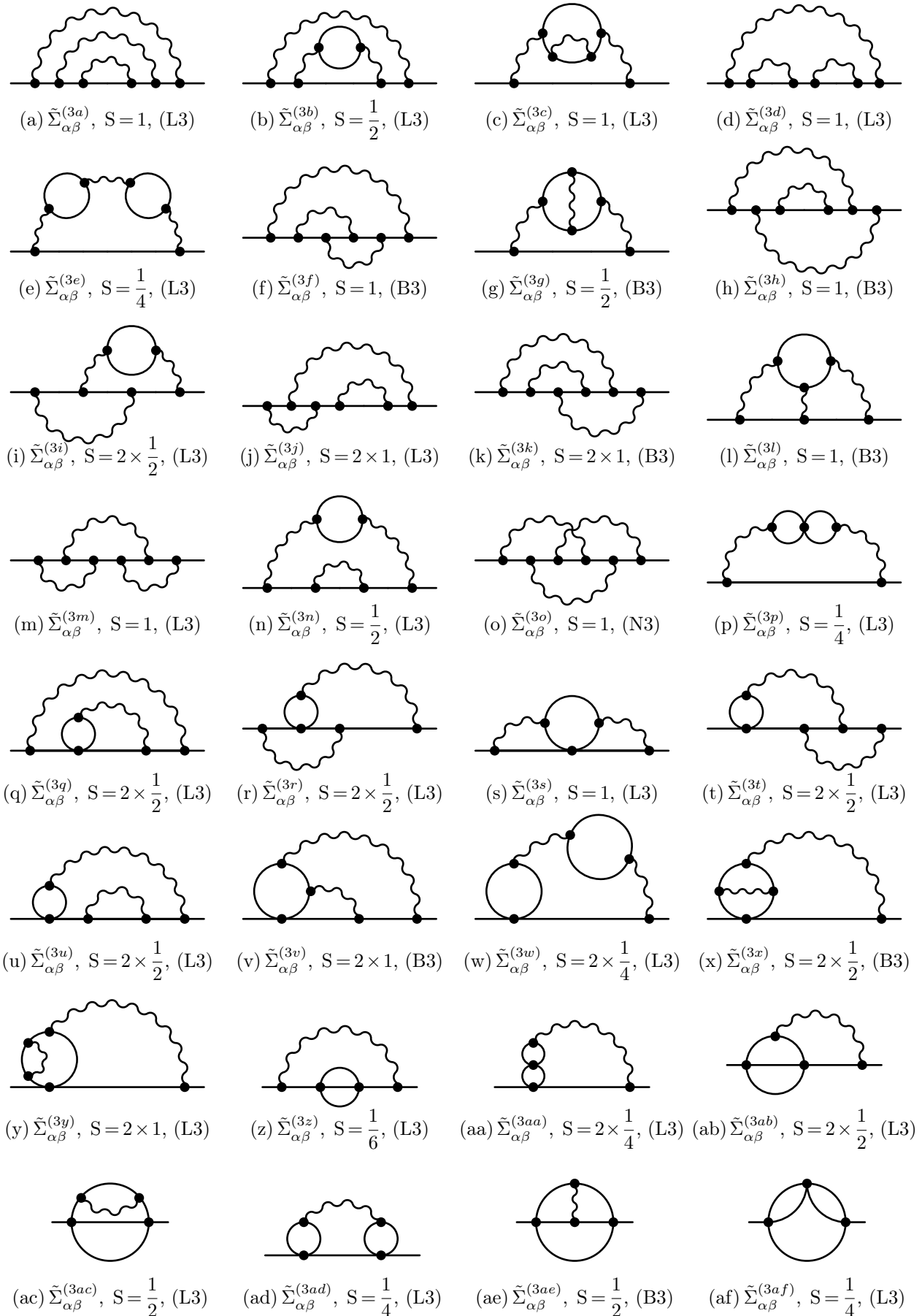


Figure 2.4: Three-loop self-energies for the flexuron propagator.

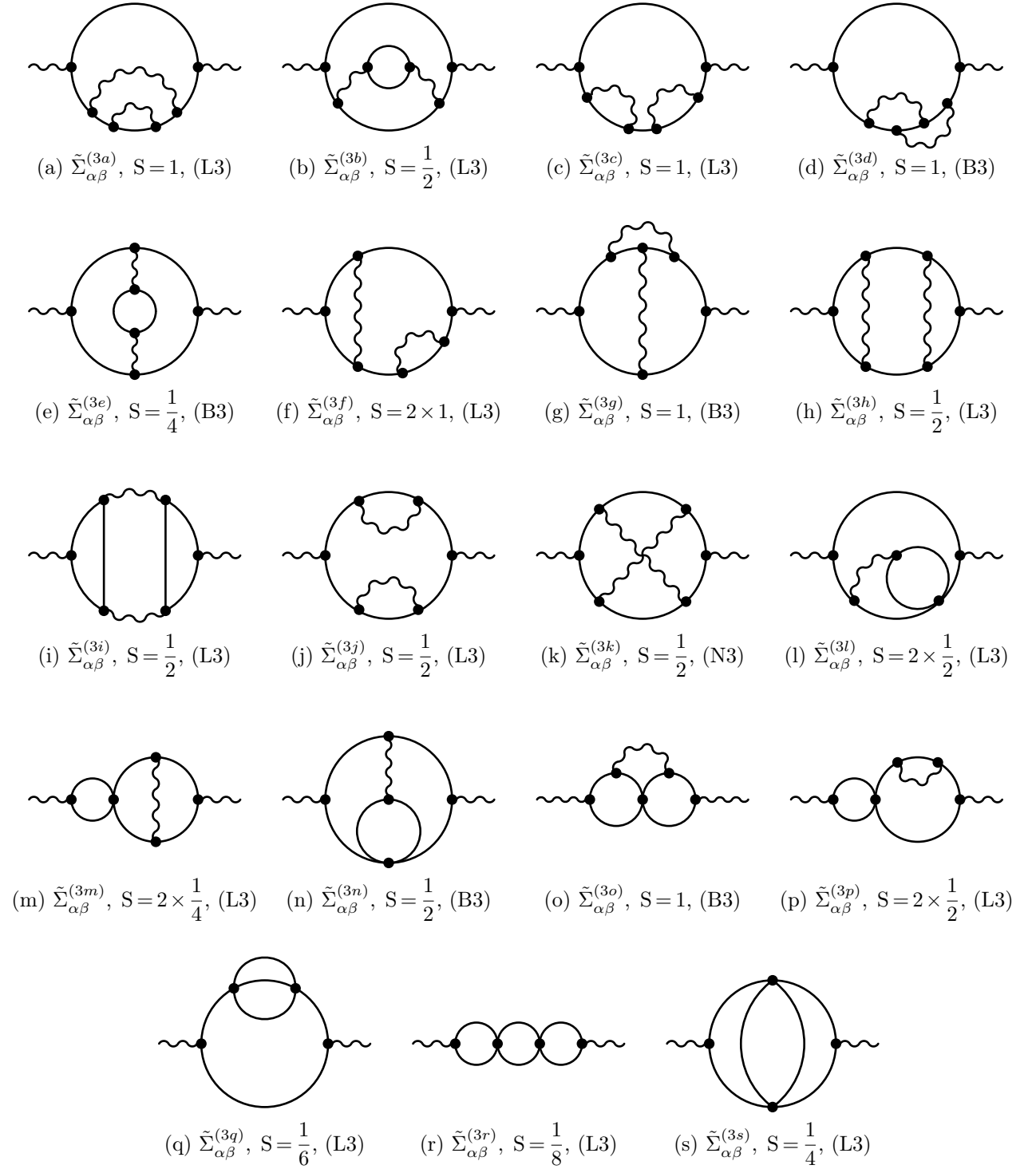


Figure 2.5: Three-loop polarizations for the photon propagator.

## 2.4 Renormalization group

### 2.4.1 Renormalization constant derivation

We are now in position to compute the renormalization constants, directly from the diagrammatic results of the previous section. First, we parameterize the renormalization constants as

$$Z = 1 + \delta Z^{(1)} + \delta Z^{(2)} + \delta Z^{(3)} + \dots \quad (2.63a)$$

$$Z_{\Delta\kappa} = 1 + \delta Z_{\Delta\kappa}^{(1)} + \delta Z_{\Delta\kappa}^{(2)} + \delta Z_{\Delta\kappa}^{(3)} + \dots \quad (2.63b)$$

$$Z_\mu = 1 + \delta Z_\mu^{(1)} + \delta Z_\mu^{(2)} + \delta Z_\mu^{(3)} + \dots \quad (2.63c)$$

$$Z_{\Delta\mu} = 1 + \delta Z_{\Delta\mu}^{(1)} + \delta Z_{\Delta\mu}^{(2)} + \delta Z_{\Delta\mu}^{(3)} + \dots \quad (2.63d)$$

$$Z_\lambda = 1 + \delta Z_\lambda^{(1)} + \delta Z_\lambda^{(2)} + \delta Z_\lambda^{(3)} + \dots \quad (2.63e)$$

$$Z_{\Delta\lambda} = 1 + \delta Z_{\Delta\lambda}^{(1)} + \delta Z_{\Delta\lambda}^{(2)} + \delta Z_{\Delta\lambda}^{(3)} + \dots \quad (2.63f)$$

Then, from the renormalization identities (2.40), it yields at one loop

$$\delta Z^{(1)} = \mathcal{K}(\tilde{\Sigma}_\delta^{(1)}), \quad (2.64a)$$

$$\delta Z_{\Delta\kappa}^{(1)} = -\delta Z^{(1)} - \mathcal{K}(\tilde{\Sigma}_J^{(1)}), \quad (2.64b)$$

$$\delta Z_\mu^{(1)} = -2\delta Z^{(1)} + \mathcal{K}(\tilde{\Pi}_\delta^{\perp(1)}), \quad (2.64c)$$

$$\delta Z_{\Delta\mu}^{(1)} = -2\delta Z^{(1)} - \mathcal{K}(\tilde{\Pi}_J^{\perp(1)}), \quad (2.64d)$$

$$\delta Z_\lambda^{(1)} = \frac{1}{\lambda_r} \left[ a_r \mathcal{K}(\tilde{\Pi}_\delta^{\parallel(1)}) - 2a_r \delta Z^{(1)} - 2\mu_r \delta Z_\mu^{(1)} \right], \quad (2.64e)$$

$$\delta Z_{\Delta\lambda}^{(1)} = -\frac{1}{\Delta_{\lambda r}} \left[ \Delta_{ar} \mathcal{K}(\tilde{\Pi}_J^{\parallel(1)}) + 2\Delta_{ar} \delta Z^{(1)} + 2\Delta_{\mu r} \delta Z_{\Delta\mu}^{(1)} \right], \quad (2.64f)$$

where  $a_r = \lambda_r + 2\mu_r$  and  $\Delta_{ar} = \Delta_{\lambda r} + 2\Delta_{\mu r}$  and obviously,  $\mathcal{K}(\delta Z_x) = \delta Z_x$  for any  $Z_x$ . Then at two loops

$$\delta Z^{(2)} = \mathcal{K}(\delta Z^{(1)} \tilde{\Sigma}_\delta^{(1)}) + \mathcal{K}(\tilde{\Sigma}_\delta^{(2)}), \quad (2.65a)$$

$$\delta Z_{\Delta\kappa}^{(2)} = -\delta Z^{(2)} - \mathcal{K}(\delta Z^{(1)} \delta Z_{\Delta\kappa}^{(1)}) - \mathcal{K}(\delta Z^{(1)} \tilde{\Sigma}_J^{(1)}) - \mathcal{K}(\tilde{\Sigma}_J^{(2)}), \quad (2.65b)$$

$$\delta Z_\mu^{(2)} = -\mathcal{K}(\delta Z^{(1)2}) - 2\delta Z^{(2)} - 2\mathcal{K}(\delta Z^{(1)} \delta Z_\mu^{(1)}) + 2\mathcal{K}(\delta Z^{(1)} \tilde{\Pi}_\delta^{\perp(1)}) + \mathcal{K}(\tilde{\Pi}_\delta^{\perp(2)}), \quad (2.65c)$$

$$\delta Z_{\Delta\mu}^{(2)} = -\mathcal{K}(\delta Z^{(1)2}) - 2\delta Z^{(2)} - 2\mathcal{K}(\delta Z^{(1)} \delta Z_{\Delta\mu}^{(1)}) - 2\mathcal{K}(\delta Z^{(1)} \tilde{\Pi}_J^{\perp(1)}) - \mathcal{K}(\tilde{\Pi}_J^{\perp(2)}), \quad (2.65d)$$

$$\begin{aligned} \delta Z_\lambda^{(2)} = & \frac{1}{\lambda_r} \left[ -a_r \mathcal{K}(\delta Z^{(1)2}) - 2a_r \delta Z^{(2)} - 2\mu_r \delta Z_\mu^{(2)} - 4\mu_r \mathcal{K}(\delta Z^{(1)} \delta Z_\mu^{(1)}) \right. \\ & \left. - 2\lambda_r \mathcal{K}(\delta Z^{(1)} \delta Z_\lambda^{(1)}) + 2a_r \mathcal{K}(\delta Z^{(1)} \tilde{\Pi}_\delta^{\parallel(1)}) + a_r \mathcal{K}(\tilde{\Pi}_\delta^{\parallel(2)}) \right], \end{aligned} \quad (2.65e)$$

$$\begin{aligned} \delta Z_{\Delta\lambda}^{(2)} = & \frac{1}{\Delta_{\lambda r}} \left[ -\Delta_{ar} \mathcal{K}(\delta Z^{(1)2}) - 2\Delta_{ar} \delta Z^{(2)} - 2\Delta_{\mu r} \delta Z_{\Delta\mu}^{(2)} - 4\Delta_{\mu r} \mathcal{K}(\delta Z^{(1)} \delta Z_{\Delta\mu}^{(1)}) \right. \\ & \left. - 2\Delta_{\lambda r} \mathcal{K}(\delta Z^{(1)} \delta Z_{\Delta\lambda}^{(1)}) - 2\Delta_{ar} \mathcal{K}(\delta Z^{(1)} \tilde{\Pi}_J^{\parallel(1)}) - \Delta_{ar} \mathcal{K}(\tilde{\Pi}_J^{\parallel(2)}) \right]. \end{aligned} \quad (2.65f)$$

And finally, at three loops

$$\delta Z^{(3)} = \mathcal{K}(\delta Z^{(1)} \tilde{\Sigma}_\delta^{(2)}) + \mathcal{K}(\delta Z^{(2)} \tilde{\Sigma}_\delta^{(1)}) + \mathcal{K}(\tilde{\Sigma}_\delta^{(3)}), \quad (2.66a)$$

$$\delta Z_{\Delta\kappa}^{(3)} = -\delta Z^{(3)} - \mathcal{K}(\delta Z^{(1)} \delta Z_{\Delta\kappa}^{(2)}) - \mathcal{K}(\delta Z^{(1)} \tilde{\Sigma}_J^{(2)}) - \mathcal{K}(\delta Z^{(2)} \delta Z_{\Delta\kappa}^{(1)}) - \mathcal{K}(\delta Z^{(2)} \tilde{\Sigma}_J^{(1)}) - \mathcal{K}(\tilde{\Sigma}_J^{(3)})$$

$$\begin{aligned} \delta Z_\mu^{(3)} = & -2\delta Z^{(3)} - \mathcal{K}(\delta Z^{(1)2} \delta Z_\mu^{(1)}) + \mathcal{K}(\delta Z^{(1)2} \tilde{\Pi}_\delta^{\perp(1)}) - 2\mathcal{K}(\delta Z^{(1)} \delta Z^{(2)}) \\ & - 2\mathcal{K}(\delta Z^{(1)} \delta Z_\mu^{(2)}) + 2\mathcal{K}(\delta Z^{(1)} \tilde{\Pi}_\delta^{\perp(2)}) - 2\mathcal{K}(\delta Z^{(2)} \delta Z_\mu^{(1)}) + 2\mathcal{K}(\delta Z^{(2)} \tilde{\Pi}_\delta^{\perp(1)}) + \mathcal{K}(\tilde{\Pi}_\delta^{\perp(3)}), \end{aligned} \quad (2.66b)$$

$$\begin{aligned} \delta Z_{\Delta_\mu}^{(3)} = & -\mathcal{K}(\delta Z^{(1)2} \delta Z_{\Delta_\mu}^{(1)}) - \mathcal{K}(\delta Z^{(1)2} \tilde{\Pi}_J^{\perp(1)}) - 2\delta Z^{(3)} - 2\mathcal{K}(\delta Z^{(1)} \tilde{\Pi}_J^{\perp(2)}) - 2\mathcal{K}(\delta Z^{(2)} \tilde{\Pi}_J^{\perp(1)}) \\ & - 2\mathcal{K}(\delta Z^{(1)} \delta Z^{(2)}) - 2\mathcal{K}(\delta Z^{(1)} \delta Z_{\Delta_\mu}^{(2)}) - 2\mathcal{K}(\delta Z^{(2)} \delta Z_{\Delta_\mu}^{(1)}) - \mathcal{K}(\tilde{\Pi}_J^{\perp(3)}), \end{aligned} \quad (2.66c)$$

$$\begin{aligned} \delta Z_\lambda^{(3)} = & \frac{1}{\lambda_r} \left[ a_r \mathcal{K}(\tilde{\Pi}_\delta^{\parallel(3)}) + 2a_r \mathcal{K}(\delta Z^{(2)} \tilde{\Pi}_\delta^{\parallel(1)}) + a_r \mathcal{K}(\delta Z^{(1)2} \tilde{\Pi}_\delta^{\parallel(1)}) + 2a_r \mathcal{K}(\delta Z^{(1)} \tilde{\Pi}_\delta^{\parallel(2)}) \right. \\ & - 2a_r \delta Z^{(3)} - 2\mu_r \delta Z_\mu^{(3)} - 2\mu_r \mathcal{K}(\delta Z^{(1)2} \delta Z_\mu^{(1)}) - 4\mu_r \mathcal{K}(\delta Z^{(1)} \delta Z_\mu^{(2)}) - 4\mu_r \mathcal{K}(\delta Z^{(2)} \delta Z_\mu^{(1)}) \\ & \left. - \lambda_r \mathcal{K}(\delta Z^{(1)2} \delta Z_\lambda^{(1)}) - 2a_r \mathcal{K}(\delta Z^{(1)} \delta Z^{(2)}) - 2\lambda_r \mathcal{K}(\delta Z^{(1)} \delta Z_\lambda^{(2)}) - 2\lambda_r \mathcal{K}(\delta Z^{(2)} \delta Z_\lambda^{(1)}) \right], \end{aligned} \quad (2.66d)$$

$$\begin{aligned} \delta Z_{\Delta_\lambda}^{(3)} = & -\frac{1}{\Delta_{\lambda r}} \left[ \Delta_{ar} \mathcal{K}(\tilde{\Pi}_J^{\parallel(3)}) + 2\Delta_{ar} \mathcal{K}(\delta Z^{(1)} \tilde{\Pi}_J^{\parallel(2)}) + \Delta_{ar} \mathcal{K}(\delta Z^{(1)2} \tilde{\Pi}_J^{\parallel(1)}) + 2\Delta_{ar} \mathcal{K}(\delta Z^{(2)} \tilde{\Pi}_J^{\parallel(1)}) \right. \\ & + 2\Delta_{ar} \delta Z^{(3)} + 2\Delta_{\mu r} \delta Z_{\Delta_\mu}^{(3)} + 2\Delta_{\mu r} \mathcal{K}(\delta Z^{(1)2} \delta Z_{\Delta_\mu}^{(1)}) + 4\Delta_{\mu r} \mathcal{K}(\delta Z^{(1)} \delta Z_{\Delta_\mu}^{(2)}) + 4\Delta_{\mu r} \mathcal{K}(\delta Z^{(2)} \delta Z_{\Delta_\mu}^{(1)}) \\ & \left. + \Delta_{\lambda r} \mathcal{K}(\delta Z^{(1)2} \delta Z_{\Delta_\lambda}^{(1)}) + 2\Delta_{ar} \mathcal{K}(\delta Z^{(1)} \delta Z^{(2)}) + 2\Delta_{\lambda r} \mathcal{K}(\delta Z^{(1)} \delta Z_{\Delta_\lambda}^{(2)}) + 2\Delta_{\lambda r} \mathcal{K}(\delta Z^{(2)} \delta Z_{\Delta_\lambda}^{(1)}) \right]. \end{aligned} \quad (2.66e)$$

All these relations completely determines the renormalization constants of the model as a function of the diagrams computed in the previous section.

### 2.4.2 Renormalization group functions

Now that we determined all the renormalization constants, we are in position to derive the renormalization-group functions.

First, the anomalous dimension of the fields, using the definition (2.44), reads

$$\begin{aligned} \eta = & \frac{5}{(4\pi)^2 \kappa^3 a_r^2} \left[ 2\alpha_{031}^{000} + 3\alpha_{121}^{000} + \alpha_{211}^{000} + 2\alpha_{030}^{001} + 3\alpha_{120}^{001} + \alpha_{210}^{001} - 2\alpha_{021}^{010} - 2\alpha_{111}^{010} - \alpha_{201}^{010} - \alpha_{021}^{100} \right] \\ & - \frac{1}{72(4\pi)^4 \kappa^6 a_r^4} \left[ (324d_c - 80)\alpha_{062}^{000} + (948d_c + 480)\alpha_{152}^{000} + (861d_c + 1900)\alpha_{242}^{000} + (312d_c + 1500)\alpha_{332}^{000} \right. \\ & + (39d_c + 340)\alpha_{422}^{000} + (972d_c - 240)\alpha_{061}^{001} + 36(79d_c + 40)\alpha_{151}^{001} + (2583d_c + 5700)\alpha_{241}^{001} + (936d_c + 4500)\alpha_{331}^{001} \\ & + 3(39d_c + 340)\alpha_{421}^{001} + (972d_c + 360)\alpha_{060}^{002} + 36(79d_c + 90)\alpha_{150}^{002} + 9(287d_c + 850)\alpha_{240}^{002} + 72(13d_c + 75)\alpha_{330}^{002} \\ & + 117(d_c + 10)\alpha_{420}^{002} + (160 - 648d_c)\alpha_{052}^{010} - 4(399d_c + 80)\alpha_{142}^{010} - 4(393d_c + 260)\alpha_{232}^{010} - 4(156d_c + 445)\alpha_{322}^{010} \\ & - (78d_c + 680)\alpha_{412}^{010} + (320 - 1296d_c)\alpha_{051}^{011} - 8(399d_c + 80)\alpha_{141}^{011} - 8(393d_c + 260)\alpha_{231}^{011} - 8(156d_c + 445)\alpha_{321}^{011} \\ & - 4(39d_c + 340)\alpha_{411}^{011} - 20(15d_c + 32)\alpha_{052}^{100} - 30(5d_c + 92)\alpha_{142}^{100} - 40(15d_c + 32)\alpha_{051}^{101} - 60(5d_c + 92)\alpha_{141}^{101} \\ & - 80\alpha_{042}^{020} - 160\alpha_{132}^{020} + 200\alpha_{222}^{020} + 280\alpha_{312}^{020} + 340\alpha_{402}^{020} - 1220\alpha_{232}^{100} - 2440\alpha_{231}^{101} + 640\alpha_{042}^{110} \\ & \left. + 640\alpha_{132}^{110} + 1220\alpha_{222}^{110} + 1060\alpha_{042}^{200} \right] \\ & + \frac{1}{5184(4\pi)^6 \kappa^9 a_r^6} \left[ -8(5(307d_c^2 - 199d_c - 42340) + 5184(2d_c + 45)\zeta_3)\alpha_{093}^{000} + \langle\langle 108 \rangle\rangle \right. \\ & \left. + (2154000d_c^2 - 33694602d_c + 2592(7307d_c + 11656)\zeta_3 - 66835964)\alpha_{441}^{012} \right] + \mathcal{O}(\alpha^4), \end{aligned} \quad (2.67)$$

where  $\langle\langle x \rangle\rangle$  indicates that  $x$  similar terms are not displayed here. Note that  $\alpha_{ijk}^{lmn}$  now stands for renormalized quantities, *i.e.*,  $\alpha_{ijk}^{lmn} = \lambda_r^i \mu_r^j \kappa^k \Delta_{\lambda r}^l \Delta_{\mu r}^m \Delta_{\kappa r}^n$ . We also recall that the expansion is in the couplings only, *i.e.*,  $\alpha_r = \{\lambda_r, \mu_r, \Delta_{\lambda r}, \Delta_{\mu r}\}$ , which excludes  $\kappa$  and  $\Delta_{\kappa r}$ . Therefore, the two indices  $\{k, n\}$  on the right does not count for the expansion. We shall then use the notation  $\alpha_{ijk}^{lmn} = \mathcal{O}(\alpha^{i+j+l+m})$ .

The anomalous dimension of the disorder parameter  $\Delta_\kappa$ , using the definition (2.44), reads

$$\phi = 2\eta - \frac{5}{(4\pi)^2 \kappa^3 a_r^2} \left[ 2\alpha_{031}^{000} + 3\alpha_{121}^{000} + \alpha_{211}^{000} + 2\alpha_{030}^{001} + 3\alpha_{120}^{001} + \alpha_{210}^{001} \right]$$

$$\begin{aligned}
& + \frac{1}{72(4\pi)^4 \kappa^6 a_r^4} \left[ (324d_c - 80)\alpha_{062}^{000} + (948d_c + 480)\alpha_{152}^{000} + (861d_c + 1900)\alpha_{242}^{000} + (312d_c + 1500)\alpha_{332}^{000} \right. \\
& + (39d_c + 340)\alpha_{422}^{000} + (972d_c - 240)\alpha_{061}^{001} + 36(79d_c + 40)\alpha_{151}^{001} + (2583d_c + 5700)\alpha_{241}^{001} + (936d_c + 4500)\alpha_{331}^{001} \\
& + 3(39d_c + 340)\alpha_{421}^{001} + 8(81d_c - 20)\alpha_{060}^{002} + 24(79d_c + 40)\alpha_{150}^{002} + (1722d_c + 3800)\alpha_{240}^{002} + (624d_c + 3000)\alpha_{330}^{002} \\
& + (78d_c + 680)\alpha_{420}^{002} + 1200\alpha_{051}^{011} + 3000\alpha_{141}^{011} + 3000\alpha_{231}^{011} + 1500\alpha_{321}^{011} + 300\alpha_{411}^{011} + 160\alpha_{042}^{020} + 320\alpha_{132}^{020} - 400\alpha_{222}^{020} \\
& \left. - 560\alpha_{312}^{020} - 680\alpha_{402}^{020} + 600\alpha_{051}^{101} + 900\alpha_{141}^{101} + 300\alpha_{231}^{101} - 1280\alpha_{042}^{110} - 1280\alpha_{132}^{110} - 2440\alpha_{222}^{110} - 2120\alpha_{042}^{200} \right] \\
& + \frac{1}{5184(4\pi)^6 \kappa^9 a_r^6} \left[ 8(5(307d_c^2 - 199d_c - 42340) + 5184(2d_c + 45)\zeta_3)\alpha_{093}^{000} + \langle\langle 108 \rangle\rangle \right. \\
& \left. + (2205600d_c^2 - 21720138d_c + 5184(2116d_c + 4265)\zeta_3 - 42576640)\alpha_{451}^{002} \right] + O(\alpha^4), \tag{2.68}
\end{aligned}$$

which is expressed as a function of  $\eta$  just for the sake of brevity.

Finally, the beta functions are determined by inverting the matrix (2.43) and reads

$$\begin{aligned}
\beta_\mu & = -2\varepsilon\mu_r + 2\eta\mu_r + \frac{d_c\mu_r^2}{6(4\pi)^2\kappa^3} \left[ \alpha_{001}^{000} + 2\alpha_{000}^{001} \right] \\
& + \frac{d_c\mu_r^2}{216(4\pi)^4\kappa^6 a_r^2} \left[ 454\alpha_{032}^{000} + 681\alpha_{122}^{000} + 227\alpha_{212}^{000} + 1816\alpha_{031}^{001} + 2724\alpha_{121}^{001} + 908\alpha_{211}^{001} + 1372\alpha_{030}^{002} + 2058\alpha_{120}^{002} \right. \\
& \left. + 686\alpha_{210}^{002} - 454\alpha_{022}^{010} - 454\alpha_{112}^{010} - 227\alpha_{202}^{010} - 1816\alpha_{021}^{011} - 1816\alpha_{111}^{011} - 908\alpha_{201}^{011} - 227\alpha_{022}^{100} - 908\alpha_{021}^{101} \right] \\
& \frac{d_c\mu_r^2}{31104(4\pi)^6\kappa^9 a_r^4} \left[ 4(8451d_c + 25920\zeta_3 + 67744)\alpha_{063}^{000} + (2421403d_c - 3022272\zeta_3 + 14993840)\alpha_{241}^{002} \right. \\
& \left. + \langle\langle 59 \rangle\rangle + (-165810d_c + 528768\zeta_3 - 893888)\alpha_{143}^{100} \right] + O(\alpha^5), \tag{2.69a}
\end{aligned}$$

$$\begin{aligned}
\beta_{\Delta_\mu} & = -2\varepsilon\Delta_{\mu r} + 2\eta\Delta_{\mu r} + \frac{d_c\mu_r}{6(4\pi)^2\kappa^4} \left[ -\alpha_{010}^{002} + 2\alpha_{002}^{010} + 4\alpha_{001}^{011} \right] \\
& - \frac{d_c\mu_r}{108(4\pi)^4\kappa^7 a_r^2} \left[ 454\alpha_{041}^{002} + 681\alpha_{131}^{002} + 227\alpha_{221}^{002} + 464\alpha_{040}^{003} + 696\alpha_{130}^{003} + 232\alpha_{220}^{003} - 454\alpha_{033}^{010} - 681\alpha_{123}^{010} \right. \\
& - 227\alpha_{213}^{010} - 1816\alpha_{032}^{011} - 2724\alpha_{122}^{011} - 908\alpha_{212}^{011} - 2058\alpha_{031}^{012} - 2744\alpha_{121}^{012} - 1029\alpha_{211}^{012} + 454\alpha_{023}^{020} + 454\alpha_{113}^{020} \\
& \left. + 227\alpha_{203}^{020} + 1816\alpha_{022}^{021} + 1816\alpha_{112}^{021} + 908\alpha_{202}^{021} - 343\alpha_{031}^{102} + 227\alpha_{023}^{110} + 908\alpha_{022}^{111} \right] \\
& - \frac{d_c\mu_r}{15552(4\pi)^6\kappa^{10} a_r^4} \left[ 12(2817d_c + 8640\zeta_3 + 24794)\alpha_{072}^{002} + (885822d_c + 1977354)\alpha_{250}^{004} + \langle\langle 83 \rangle\rangle \right. \\
& \left. + \alpha_{242}^{012}(-2818883d_c + 2607552\zeta_3 - 17574176) \right] + O(\alpha^5), \tag{2.69b}
\end{aligned}$$

$$\begin{aligned}
\beta_\lambda & = -2\varepsilon\lambda_r + 2\eta\lambda_r + \frac{d_c}{6(4\pi)^2\kappa^3} \left[ \alpha_{021}^{000} + 6\alpha_{111}^{000} + 6\alpha_{201}^{000} + 2\alpha_{020}^{001} + 12\alpha_{110}^{001} + 12\alpha_{200}^{001} \right] \\
& - \frac{d_c}{216(4\pi)^4\kappa^6 a_r^2} \left[ (24d_c - 34)\alpha_{052}^{000} + (168d_c - 375)\alpha_{142}^{000} + (366d_c + 253)\alpha_{232}^{000} + 36(7d_c + 27)\alpha_{322}^{000} \right. \\
& + 54(d_c + 7)\alpha_{412}^{000} + (96d_c - 136)\alpha_{051}^{001} + (672d_c - 1500)\alpha_{141}^{001} + 4(366d_c + 253)\alpha_{231}^{001} + 144(7d_c + 27)\alpha_{321}^{001} \\
& + 216(d_c + 7)\alpha_{411}^{001} + (96d_c + 308)\alpha_{050}^{002} + (672d_c + 1110)\alpha_{140}^{002} + (1464d_c + 5014)\alpha_{230}^{002} + 36(28d_c + 171)\alpha_{320}^{002} \\
& + 216(d_c + 9)\alpha_{410}^{002} + 34\alpha_{042}^{010} + 358\alpha_{132}^{010} - 415\alpha_{222}^{010} - 594\alpha_{312}^{010} - 378\alpha_{402}^{010} + 136\alpha_{041}^{011} + 1432\alpha_{131}^{011} - 1660\alpha_{221}^{011} \\
& - 2376\alpha_{311}^{011} - 1512\alpha_{401}^{011} + 17\alpha_{042}^{100} + 162\alpha_{132}^{100} - 378\alpha_{222}^{100} + 68\alpha_{041}^{101} + 648\alpha_{131}^{101} - 1512\alpha_{221}^{101} \left. \right] \\
& + \frac{d_c}{31104(4\pi)^6\kappa^9 a_r^4} \left[ 4(432d_c^2 + 18639d_c + 10368\zeta_3 - 52592)\alpha_{083}^{000} + \langle\langle 92 \rangle\rangle \right. \\
& \left. + (466560d_c^2 + 30611863d_c + 6853248\zeta_3 + 14054192)\alpha_{261}^{002} \right] + O(\alpha^5), \tag{2.69c}
\end{aligned}$$

$$\begin{aligned}
\beta_{\Delta_\lambda} = & -2\varepsilon\Delta_{\lambda r} + 2\eta\Delta_{\lambda r} + \frac{d_c}{6(4\pi)^2\kappa^4} \left[ -\alpha_{020}^{002} - 6\alpha_{110}^{002} - 6\alpha_{200}^{002} + 2\alpha_{012}^{010} + 6\alpha_{102}^{010} + 4\alpha_{011}^{011} + 12\alpha_{101}^{011} \right. \\
& + 6\alpha_{012}^{100} + 12\alpha_{102}^{100} + 12\alpha_{011}^{101} + 24\alpha_{101}^{101} \left. \right] \\
& + \frac{d_c}{108(4\pi)^4\kappa^7 a_r^2} \left[ (24d_c - 34)\alpha_{051}^{002} + (168d_c - 375)\alpha_{141}^{002} + (366d_c + 253)\alpha_{231}^{002} + 36(7d_c + 27)\alpha_{321}^{002} \right. \\
& + 54(d_c + 7)\alpha_{411}^{002} + 8(6d_c + 47)\alpha_{050}^{003} + (336d_c + 1860)\alpha_{140}^{003} + (732d_c + 4508)\alpha_{230}^{003} + (504d_c + 4212)\alpha_{320}^{003} \\
& + 108(d_c + 11)\alpha_{410}^{003} + (34 - 36d_c)\alpha_{043}^{010} + (213 - 180d_c)\alpha_{133}^{010} + (260 - 261d_c)\alpha_{223}^{010} + (81 - 144d_c)\alpha_{313}^{010} \\
& - 27d_c\alpha_{403}^{010} + (136 - 144d_c)\alpha_{042}^{011} + (852 - 720d_c)\alpha_{132}^{011} + (1040 - 1044d_c)\alpha_{222}^{011} + (324 - 576d_c)\alpha_{312}^{011} \\
& - 108d_c\alpha_{402}^{011} - 6(24d_c + 77)\alpha_{041}^{012} - 16(45d_c + 79)\alpha_{131}^{012} - 3(348d_c + 995)\alpha_{221}^{012} - 36(16d_c + 63)\alpha_{311}^{012} \\
& - 108(d_c + 9)\alpha_{401}^{012} - 34\alpha_{033}^{020} - 196\alpha_{123}^{020} - 179\alpha_{213}^{020} - 81\alpha_{303}^{020} - 136\alpha_{032}^{021} - 784\alpha_{122}^{021} - 716\alpha_{212}^{021} - 324\alpha_{302}^{021} \\
& + (162 - 72d_c)\alpha_{043}^{100} - 9(32d_c + 57)\alpha_{133}^{100} - 117(2d_c + 9)\alpha_{223}^{100} - 54(d_c + 7)\alpha_{313}^{100} + 72(9 - 4d_c)\alpha_{042}^{101} \\
& - 36(32d_c + 57)\alpha_{132}^{101} - 468(2d_c + 9)\alpha_{222}^{101} - 216(d_c + 7)\alpha_{312}^{101} - (288d_c + 401)\alpha_{041}^{102} - 72(16d_c + 63)\alpha_{131}^{102} \\
& - 18(52d_c + 387)\alpha_{221}^{102} - 216(d_c + 9)\alpha_{311}^{102} - 179\alpha_{033}^{110} + 513\alpha_{123}^{110} + 675\alpha_{213}^{110} + 378\alpha_{303}^{110} - 716\alpha_{032}^{111} \\
& + 2052\alpha_{122}^{111} + 2700\alpha_{212}^{111} + 1512\alpha_{302}^{111} - 81\alpha_{033}^{200} + 378\alpha_{123}^{200} - 324\alpha_{032}^{201} + 1512\alpha_{122}^{201} \left. \right] \\
& + \frac{d_c}{15552(4\pi)^6\kappa^{10}a_r^4} \left[ -12(216d_c^2 + 6009d_c + 3456\zeta_3 - 41998)\alpha_{082}^{002} + \langle\langle 158 \rangle\rangle \right. \\
& \left. + \alpha_{252}^{012}(622080d_c^2 + 22227815d_c + 7485696\zeta_3 - 14479264) \right] + O(\alpha^5). \tag{2.69d}
\end{aligned}$$

## 2.5 Fixed points and results

Back to the physics. We have computed all the renormalization constants of the system, namely,  $\eta$ ,  $\phi$ , and the beta functions  $\beta_\alpha$  for the couplings  $\alpha = \mu, \Delta_\mu, \lambda, \Delta_\lambda$ . Our next goal is to solve the system of equations  $\beta_\alpha = 0$ , in order to access the fixed points of the theory, where the system exhibits scale invariant behavior and therefore, universality. This allows us to compute the critical exponents of the system.

First, as a check on our computations, we will focus on the pure non-disordered fixed points and recover some results of the first chapter. Second, we will sketch the procedure for the search of fixed points that include disorder. Third, we will provide the complete three-loop results obtained for the two disordered fixed points we found, namely  $P_5$  and  $P_c$ .

### 2.5.1 Purely non-disordered fixed points

First, we focus on the case of pure (non-disordered) membranes, and then set all the variances to zero

$$\Delta_\mu = \Delta_\lambda = \Delta_\kappa = 0. \tag{2.70}$$

In this case, we are supposed to recover the results obtained in the previous chapter. Let us emphasize that in the current chapter, we use the two-field model, while in the previous chapter, we used the effective flexural model. Therefore, retrieving the results of previous chapter is a strong check.

In the pure case (2.70)  $\beta_{\Delta_\mu}$ ,  $\beta_{\Delta_\lambda}$  and  $\phi$  are irrelevant and therefore vanishing. Then, the non-vanishing RG functions tremendously simplify, and yields, up to three loops, the beta functions

$$\beta_\mu = -2\mu_r\varepsilon + 2\eta\mu_r + \frac{d_c\mu_r^2}{6(4\pi)^2} + \frac{227d_c\mu_r^3(\lambda_r + \mu_r)}{216(4\pi)^4(\lambda_r + 2\mu_r)}$$

$$\begin{aligned}
& + \frac{d_c \mu_r^4}{31104(4\pi)^6(\lambda_r + 2\mu_r)^2} \left[ \lambda_r^2(22839d_c - 59616\zeta_3 + 128672) \right. \\
& \left. + 8\lambda_r\mu_r(2975d_c + 36(713 - 63\zeta_3)) + \mu_r^2(8451d_c + 25920\zeta_3 + 67744) \right] + \mathcal{O}(\alpha^5), \tag{2.71a}
\end{aligned}$$

$$\begin{aligned}
\beta_\lambda = & -2\lambda_r\varepsilon + 2\eta\lambda_r + \frac{d_c(6\lambda_r^2 + 6\lambda_r\mu_r + \mu_r^2)}{6(4\pi)^2} \\
& - \frac{d_c\mu_r(54(d_c + 7)\lambda_r^3 + 72(2d_c + 3)\lambda_r^2\mu_r + (78d_c - 179)\lambda_r\mu_r^2 + (12d_c - 17)\mu_r^3)}{216(4\pi)^4(\lambda_r + 2\mu_r)} \\
& + \frac{d_c\mu_r^2}{31104(4\pi)^6(\lambda_r + 2\mu_r)^2} \left[ 36\lambda_r^4(27d_c^2 + 6498d_c - 3888\zeta_3 + 7876) + 54\lambda_r^3\mu_r(84d_c^2 + 9539d_c - 5184\zeta_3 + 8512) \right. \\
& + \lambda_r^2\mu_r^2(6588d_c^2 + 416667d_c - 51840\zeta_3 + 109400) + 2\lambda_r\mu_r^3(1512d_c^2 + 74309d_c + 648(52\zeta_3 - 99)) \\
& \left. + \mu_r^4(432d_c^2 + 18639d_c + 10368\zeta_3 - 52592) \right] + \mathcal{O}(\alpha^5), \tag{2.71b}
\end{aligned}$$

and the anomalous dimension of the flexuron field reads

$$\begin{aligned}
\eta = & \frac{5\mu_r(\lambda_r + \mu_r)}{(4\pi)^2(\lambda_r + 2\mu_r)} - \frac{\mu_r^2((39d_c + 340)\lambda_r^2 + 4(39d_c + 35)\lambda_r\mu_r + (81d_c - 20)\mu_r^2)}{72(4\pi)^4(\lambda_r + 2\mu_r)^2} \\
& - \frac{\mu_r^3}{5184(4\pi)^6(\lambda_r + 2\mu_r)^3} \left[ \lambda_r^3(12745d_c^2 + d_c(36288\zeta_3 - 97175) + 32400\zeta_3 - 135430) \right. \\
& + \lambda_r^2\mu_r(19020d_c^2 + 3d_c(45792\zeta_3 - 70043) + 231984\zeta_3 - 264058) \\
& + \lambda_r\mu_r^2(8640d_c^2 + 27d_c(4128\zeta_3 - 4531) + 409536\zeta_3 - 350372) \\
& \left. + \mu_r^3(1535d_c^2 + d_c(10368\zeta_3 - 995) + 233280\zeta_3 - 211700) \right] + \mathcal{O}(\alpha^4). \tag{2.72}
\end{aligned}$$

In order to solve for  $\beta_\alpha = 0$  order by order, we use a perturbative ansatz for the couplings  $\alpha_r = \mu_r, \lambda_r$ , *i.e.*,

$$\mu_r = \mu^{(1)}\varepsilon + \mu^{(2)}\varepsilon^2 + \mu^{(3)}\varepsilon^3 + \dots \tag{2.73a}$$

$$\lambda_r = \lambda^{(1)}\varepsilon + \lambda^{(2)}\varepsilon^2 + \lambda^{(3)}\varepsilon^3 + \dots \tag{2.73b}$$

and we solve order by order in perturbative series of  $\varepsilon$ . Note that in the following, we will use the notation

$$d_n = d_c + n. \tag{2.74}$$

With three-loop accuracy, like in the previous chapter, we find 4 fixed points. Their respective coordinates read

$$\text{P}_1: \left. \begin{array}{l} \mu_1^* = 0 + \mathcal{O}(\varepsilon^4) \\ \lambda_1^* = 0 + \mathcal{O}(\varepsilon^4) \end{array} \right\} \text{ (Gaussian),} \tag{2.75a}$$

$$\text{P}_2: \mu_2^* = 0 + \mathcal{O}(\varepsilon^4) \text{ (Shearless),} \tag{2.75b}$$

$$\lambda_2^* = (4\pi)^2 \frac{2}{d_c} \varepsilon + \mathcal{O}(\varepsilon^4), \tag{2.75c}$$

$$\begin{aligned}
\text{P}_3: \mu_3^* = & (4\pi)^2 \left[ \frac{12\varepsilon}{d_{20}} + \left( \frac{1680}{d_{20}^3} - \frac{20}{3d_{20}^2} \right) \varepsilon^2 \right. \\
& \left. + \left( \frac{470400}{d_{20}^5} + \frac{8(591624\zeta_3 - 684433)}{9d_{20}^4} - \frac{4(144504\zeta_3 - 167155)}{27d_{20}^3} + \frac{1985}{27d_{20}^2} \right) \varepsilon^3 + \mathcal{O}(\varepsilon^4) \right], \tag{2.75d}
\end{aligned}$$

$$\lambda_3^* = -(4\pi)^2 \left[ \frac{6\varepsilon}{d_{20}} + \left( \frac{840}{d_{20}^3} - \frac{190}{3d_{20}^2} + \frac{6}{d_{20}} \right) \varepsilon^2 \right] \tag{2.75e}$$

$$+ \left( \frac{235200}{d_{20}^5} + \frac{4(591624\zeta_3 - 722233)}{9d_{20}^4} - \frac{4(72252\zeta_3 - 95525)}{27d_{20}^3} - \frac{3791}{27d_{20}^2} + \frac{9}{d_{20}} \right) \varepsilon^3 + \mathcal{O}(\varepsilon^4) \Big],$$

$$\text{P}_4: \quad \mu_4^* = (4\pi)^2 \left[ \frac{12\varepsilon}{d_{24}} + \left( \frac{1440}{d_{24}^3} - \frac{376}{5d_{24}^2} \right) \varepsilon^2 \right. \quad (2.75f)$$

$$\left. + \left( \frac{345600}{d_{24}^5} + \frac{96(576288\zeta_3 - 797161)}{125d_{24}^4} - \frac{48(36864\zeta_3 - 59153)}{125d_{24}^3} - \frac{2766}{25d_{24}^2} \right) \varepsilon^3 + \mathcal{O}(\varepsilon^4) \right],$$

$$\lambda_4^* = -(4\pi)^2 \left[ \frac{4\varepsilon}{d_{24}} + \left( \frac{480}{d_{24}^3} - \frac{152}{5d_{24}^2} \right) \varepsilon^2 \right. \quad (2.75g)$$

$$\left. + \left( \frac{115200}{d_{24}^5} + \frac{288(64032\zeta_3 - 89129)}{125d_{24}^4} - \frac{8(225504\zeta_3 - 297083)}{375d_{24}^3} - \frac{746}{75d_{24}^2} \right) \varepsilon^3 + \mathcal{O}(\varepsilon^4) \right].$$

Note that  $\text{P}_2$  is not renormalized beyond one loop. For the sake of the comparison with the results of previous chapter, we can try to recover the value of the coupling  $b$  of the EFT from the coordinates of the two field model, *i.e.*, (2.75). We recall from (1.18) that  $b = \mu(d\lambda + 2\mu)/(\lambda + 2\mu)$ . It yields

$$b_1^* = 0, \quad (2.76a)$$

$$b_2^* = 0, \quad (2.76b)$$

$$b_3^* = (4\pi)^2 \left[ \left( \frac{160}{d_{20}^2} - \frac{8}{d_{20}} \right) \varepsilon^2 + \left( \frac{44800}{d_{20}^4} - \frac{12400}{3d_{20}^3} + \frac{468}{d_{20}^2} - \frac{56}{3d_{20}} \right) \varepsilon^3 + \mathcal{O}(\varepsilon^4) \right], \quad (2.76c)$$

$$b_4^* = (4\pi)^2 \left[ \frac{24\varepsilon}{5d_{24}} + \left( \frac{576}{d_{24}^3} - \frac{464}{25d_{24}^2} + \frac{24}{5d_{24}} \right) \varepsilon^2 \right. \quad (2.76d)$$

$$\left. + \left( \frac{138240}{d_{24}^5} + \frac{192(576288\zeta_3 - 788161)}{625d_{24}^4} - \frac{144(23712\zeta_3 - 53489)}{625d_{24}^3} - \frac{17524}{125d_{24}^2} \right) \varepsilon^3 + \mathcal{O}(\varepsilon^4) \right].$$

Comparing with the results of previous chapter, (1.117a), (1.123a), (1.129a), we observe that the values for  $b$  are not exactly recovered. Indeed, the leading order values for  $b_3^*$  and  $b_4^*$  are correct, but we observe deviations at two and three loops. Moreover, the value of  $b_2^*$  is different. This mismatch is not a real problem because it is known that the fixed point coordinates are not universal and that only the anomalous dimensions took at the fixed point are universal quantities. Indeed, taking the anomalous dimension of the flexuron field at these coordinates reads

$$\eta(\text{P}_1) = 0, \quad (2.77a)$$

$$\eta(\text{P}_2) = 0, \quad (2.77b)$$

$$\eta(\text{P}_3) = \frac{20\varepsilon}{d_{20}} + \left( \frac{2800}{d_{20}^3} + \frac{1060}{3d_{20}^2} - \frac{74}{3d_{20}} \right) \varepsilon^2 + \left( \frac{784000}{d_{20}^5} + \right. \quad (2.77c)$$

$$\left. + \frac{40(591624\zeta_3 - 615553)}{27d_{20}^4} - \frac{2(1006344\zeta_3 - 1024193)}{27d_{20}^3} + \frac{2(20736\zeta_3 - 17105)}{27d_{20}^2} - \frac{155}{9d_{20}} \right) \varepsilon^3 + \mathcal{O}(\varepsilon^4),$$

$$\eta(\text{P}_4) = \frac{24\varepsilon}{d_{24}} + \left( \frac{2880}{d_{24}^3} + \frac{456}{d_{24}^2} - \frac{24}{d_{24}} \right) \varepsilon^2 + \left( \frac{691200}{d_{24}^5} + \right. \quad (2.77d)$$

$$\left. + \frac{576(192096\zeta_3 - 234137)}{125d_{24}^4} - \frac{8(923616\zeta_3 - 1031777)}{125d_{24}^3} + \frac{4(86832\zeta_3 - 39029)}{375d_{24}^2} - \frac{64}{3d_{24}} \right) \varepsilon^3 + \mathcal{O}(\varepsilon^4).$$

Here, as expected, we recover exactly the results of the previous chapter, for the fixed points  $\text{P}_1$  (1.116),  $\text{P}_3$  (1.125) and  $\text{P}_4$  (1.132). As for the fixed point  $\text{P}_2$ , we find the anomalous dimension to be exactly zero. Therefore,  $\text{P}_2$  is indeed different of  $\text{P}'_2$ . We believe that this is an artifact of perturbation theory induced by the approximation  $b(d) = b$ .

The stability of the fixed points are the same as for the EFT case, after the change of variables from  $b_r$  to  $\lambda_r$ . Indeed,  $\text{P}_1$  is twice unstable (repulsive in all directions).  $\text{P}_2$  is stable in the direction



of  $\lambda_r$  but repulsive in  $\mu_r$ .  $P_3$  is the opposite, *i.e.*, stable in  $\mu_r$  but repulsive in  $\lambda_r$ . And finally,  $P_4$  is stable in all directions.  $P_4$  is then the relevant attractive fixed point controlling the flat phase at long distances.

We provide in figure 2.6 the flow diagram of the model. This flow diagram is in essence the same as for the EFT, see figure 1.11, up to two small differences. First, the change of variable from  $b_r$  to  $\lambda_r$  yields that the mechanical stability  $\mu_r > 0$ ,  $b_r > 0$ , is now

$$\mu_r > 0, \quad 2\lambda_r + \mu_r > 0, \quad (2.78)$$

therefore the corresponding forbidden regions appear tilted in the  $\lambda_r, \mu_r$  coordinates. Second, a key feature is that, going from one to two loops, the fixed point  $P_3$  is marginally ejected out of the stability region, see figure 2.6b. This feature is also conserved at three loops. However, we believe that it is an artifact of the perturbative expansion and that upon higher orders and resummations,  $P_3$  would eventually rest on the line  $2\lambda_r + \mu_r = 0$ , like in the EFT approach. In the end, the physically interesting, attractive fixed point  $P_4$  is the one controlling the flat phase at long distances. We expect it to be universal, which is indeed the case as it corresponds perfectly to the one obtained in the EFT case, both with its coordinates and the value of the critical exponent  $\eta$  found at this point.

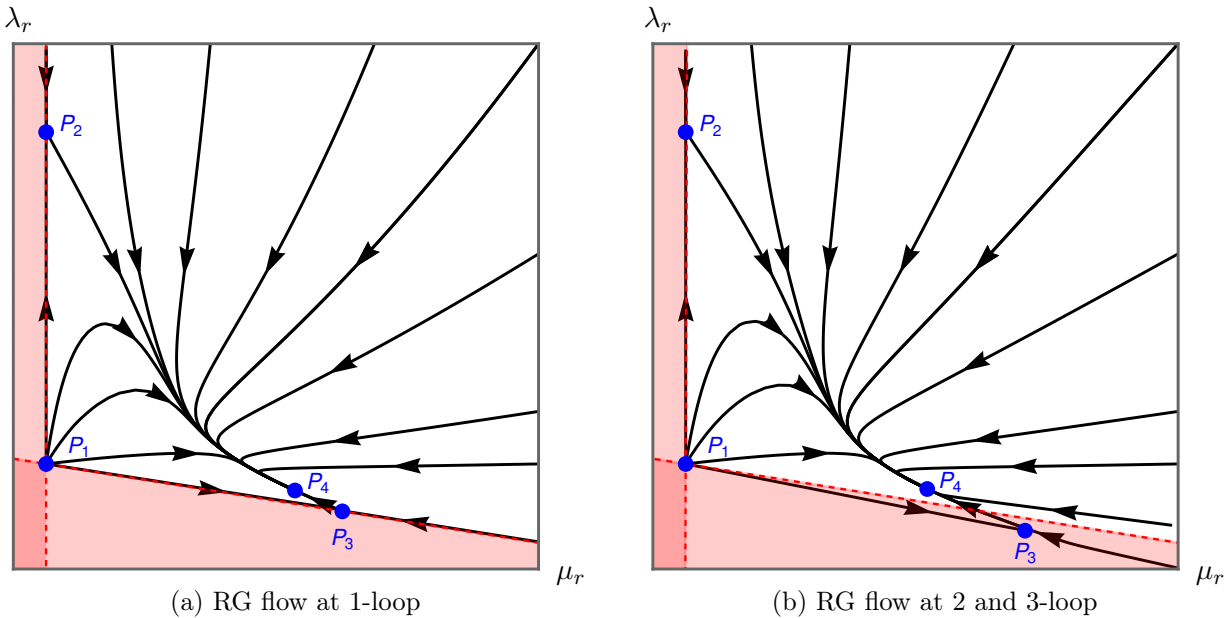


Figure 2.6: RG-flow diagram in the plane  $(\lambda_r, \mu_r)$ . The mechanical stability of the model is delimited by the conditions  $\mu_r > 0$  and  $2\lambda_r + \mu_r > 0$  (red is mechanically unstable). At one loop,  $P_2$  and  $P_3$  lies exactly on the border of these regions (red dashed lines), while  $P_4$  is located on the line  $3\lambda_r + \mu_r = 0$  (not represented). At two and three loops, the picture changes,  $P_2$  is still located at  $\mu_r = 0$ , but  $P_3$  is ejected out of the stability region, and  $P_4$  is located above the line  $3\lambda_r + \mu_r = 0$ . This plot has been obtained from the beta functions (2.71) and remain qualitatively the same for all values  $0.001 < \varepsilon < 0.8$ .

### 2.5.2 How to find the disordered fixed points

In this section, we investigate the fixed points with disorder, *i.e.*,  $\Delta_x > 0$  with  $x = \kappa, \mu, \lambda$ . To do so, we need to solve the system

$$\beta_\alpha = 0, \quad \alpha = \{\mu, \Delta_\mu, \lambda, \Delta_\lambda\}. \quad (2.79)$$

First, we will naively solve it to find the fixed points as a function of  $\Delta_{\kappa r}$  and  $\kappa$ . This will raise several issues. In order to avoid them, we proceed on showing how to derive the relevant fixed points by means of a change of variables, toward the so-called low-temperature variables. In this section, for the sake of brevity, we restrict demonstrations to two loops. The full three-loop result will be provided in the next section.

#### Search in high temperature variables

The first naive approach is to solve the system (2.79) for arbitrary parameters  $\kappa$ ,  $\Delta_{\kappa r}$  and  $d_c$ . It yields the following fixed points. First, a disordered version of the shearless fixed point  $P_2$ , noted  $P_2(\Delta_\kappa)$ , where the shear modulus and its variance are exactly vanishing, reading

$$\mu_2^*(\Delta_\kappa) = 0 + O(\varepsilon^3), \quad (2.80a)$$

$$\Delta_{\mu 2}^*(\Delta_\kappa) = 0 + O(\varepsilon^3), \quad (2.80b)$$

$$\frac{\lambda_2^*(\Delta_\kappa)}{(4\pi\kappa)^2} = \frac{2\kappa}{d_c(\kappa + 2\Delta_{\kappa r})} \varepsilon + O(\varepsilon^3), \quad (2.80c)$$

$$\frac{\Delta_{\lambda 2}^*(\Delta_\kappa)}{(4\pi\kappa)^2} = \frac{2\Delta_{\kappa r}^2}{d_c(\kappa + 2\Delta_{\kappa r})^2} \varepsilon + O(\varepsilon^3). \quad (2.80d)$$

Second, a disordered version of  $P_3$ , *i.e.*,  $P_3(\Delta_\kappa)$ , yielding

$$\frac{\mu_3^*(\Delta_\kappa)}{(4\pi\kappa)^2} = \frac{12\kappa(\kappa + 2\Delta_{\kappa r})}{x_1} \varepsilon - \frac{4\kappa(x_1(20\Delta_{\kappa r}^3 + 721\Delta_{\kappa r}^2\kappa + 252\Delta_{\kappa r}\kappa^2 + 5\kappa^3) - 20x_2)}{3x_1^3} \varepsilon^2 + O(\varepsilon^3), \quad (2.81a)$$

$$\frac{\Delta_{\mu 3}^*(\Delta_\kappa)}{(4\pi\kappa)^2} = \frac{12\Delta_{\kappa r}^2}{x_1} \varepsilon - \frac{8\Delta_{\kappa r}^2(\kappa x_1(5\Delta_{\kappa r}^2 - 333\Delta_{\kappa r}\kappa - 111\kappa^2) - 10x_2)}{3x_1^3(2\Delta_{\kappa r} + \kappa)} \varepsilon^2 + O(\varepsilon^3), \quad (2.81b)$$

$$\frac{\lambda_3^*(\Delta_\kappa)}{(4\pi\kappa)^2} = -\frac{6\kappa(\kappa + 2\Delta_{\kappa r})}{x_1} \varepsilon + \frac{2\kappa(x_1(200\Delta_{\kappa r}^3 + 1081\Delta_{\kappa r}^2\kappa + 612\Delta_{\kappa r}\kappa^2 + 95\kappa^3 - 9x_1(2\Delta_{\kappa r} + \kappa)) - 20x_2)}{3x_1^3} \varepsilon^2 + O(\varepsilon^3), \quad (2.81c)$$

$$\frac{\Delta_{\lambda 3}^*(\Delta_\kappa)}{(4\pi\kappa)^2} = -\frac{6\Delta_{\kappa r}^2}{x_1} \varepsilon + \frac{2\Delta_{\kappa r}^2(x_1(180\Delta_{\kappa r}^3 + 640\Delta_{\kappa r}^2\kappa + 54\Delta_{\kappa r}\kappa^2 - 42\kappa^3 - 9x_1(2\Delta_{\kappa r} + \kappa)) - 20x_2)}{3x_1^3(2\Delta_{\kappa r} + \kappa)} \varepsilon^2 + O(\varepsilon^3). \quad (2.81d)$$

And finally, a disordered version of  $P_4$ , namely  $P_4(\Delta_\kappa)$

$$\frac{\mu_4^*(\Delta_\kappa)}{(4\pi\kappa)^2} = \frac{12\kappa(\kappa + 2\Delta_{\kappa r})}{y_1} \varepsilon - \frac{8\kappa(y_1(104\Delta_{\kappa r}^3 + 1015\Delta_{\kappa r}^2\kappa + 462\Delta_{\kappa r}\kappa^2 + 47\kappa^3) - 12y_2)}{5y_1^3} \varepsilon^2 + O(\varepsilon^3), \quad (2.82a)$$

$$\frac{\Delta_{\mu 4}^*(\Delta_\kappa)}{(4\pi\kappa)^2} = \frac{12\Delta_{\kappa r}^2}{y_1} \varepsilon - \frac{32\Delta_{\kappa r}^2(y_1(21\Delta_{\kappa r}^3 + 76\Delta_{\kappa r}^2\kappa - 114\Delta_{\kappa r}\kappa^2 - 45\kappa^3) - 3y_2)}{5y_1^3(2\Delta_{\kappa r} + \kappa)} \varepsilon^2 + O(\varepsilon^3), \quad (2.82b)$$

$$\frac{\lambda_4^*(\Delta_\kappa)}{(4\pi\kappa)^2} = -\frac{4\kappa(\kappa + 2\Delta_{\kappa r})}{y_1} \varepsilon + \frac{8\kappa(y_1(88\Delta_{\kappa r}^3 + 395\Delta_{\kappa r}^2\kappa + 174\Delta_{\kappa r}\kappa^2 + 19\kappa^3) - 4y_2)}{5y_1^3} \varepsilon^2 + O(\varepsilon^3), \quad (2.82c)$$

$$\frac{\Delta_{\lambda 4}^*(\Delta_\kappa)}{(4\pi\kappa)^2} = -\frac{4\Delta_{\kappa r}^2}{y_1} \varepsilon - \frac{32\Delta_{\kappa r}^2(y_1(3\Delta_{\kappa r}^3 - 2\Delta_{\kappa r}^2\kappa + 48\Delta_{\kappa r}\kappa^2 + 15\kappa^3) + y_2)}{5y_1^3(2\Delta_{\kappa r} + \kappa)} \varepsilon^2 + O(\varepsilon^3). \quad (2.82d)$$

Note that we used the polynomials

$$x_1 = 4d_5\Delta_{\kappa r}^2 + 4d_{15}\Delta_{\kappa r}\kappa + d_{20}\kappa^2, \quad y_1 = 4d_6\Delta_{\kappa r}^2 + 4d_{18}\Delta_{\kappa r}\kappa + d_{24}\kappa^2, \quad (2.83a)$$

$$x_2 = 260\Delta_{\kappa r}^5 + 2738\Delta_{\kappa r}^4\kappa + 5863\Delta_{\kappa r}^3\kappa^2 + 3462\Delta_{\kappa r}^2\kappa^3 + 789\Delta_{\kappa r}\kappa^4 + 63\kappa^5, \quad (2.83b)$$

$$y_2 = 94\Delta_{\kappa r}^5 + 3295\Delta_{\kappa r}^4\kappa + 8042\Delta_{\kappa r}^3\kappa^2 + 4755\Delta_{\kappa r}^2\kappa^3 + 1035\Delta_{\kappa r}\kappa^4 + 75\kappa^5. \quad (2.83c)$$

The corresponding field anomalous dimensions reads

$$\eta(\text{P}_2(\Delta_\kappa)) = 0 + \text{O}(\varepsilon^3), \quad (2.84a)$$

$$\eta(\text{P}_3(\Delta_\kappa)) = \frac{20z_1}{x_1}\varepsilon - \frac{2(x_1 - 20z_1)(111x_1z_1(2\Delta_{\kappa r} + \kappa) + 10x_2)}{9x_1^3(2\Delta_{\kappa r} + \kappa)}\varepsilon^2 + \text{O}(\varepsilon^3), \quad (2.84b)$$

$$\eta(\text{P}_4(\Delta_\kappa)) = \frac{24z_1}{y_1}\varepsilon - \frac{8(y_1 - 24z_1)(15y_1z_1(2\Delta_{\kappa r} + \kappa) + y_2)}{5y_1^3(2\Delta_{\kappa r} + \kappa)}\varepsilon^2 + \text{O}(\varepsilon^3), \quad (2.84c)$$

and the anomalous dimension of  $\Delta_\kappa$  yields

$$\phi(\text{P}_2(\Delta_\kappa)) = 0 + \text{O}(\varepsilon^3), \quad (2.85a)$$

$$\phi(\text{P}_3(\Delta_\kappa)) = \frac{20\kappa z_2}{x_1}\varepsilon - \frac{2(10x_1x_3 + 111\kappa x_1^2z_2(2\Delta_{\kappa r} + \kappa) - 200\kappa x_2z_2)}{9x_1^3(2\Delta_{\kappa r}\varepsilon^2 + \kappa)}\varepsilon^2 + \text{O}(\varepsilon^3), \quad (2.85b)$$

$$\phi(\text{P}_4(\Delta_\kappa)) = \frac{24\kappa z_2}{y_1}\varepsilon + \frac{8(y_1y_3 - 15\kappa y_1^2z_2(2\Delta_{\kappa r} + \kappa) + 24\kappa y_2z_2)}{5y_1^3(2\Delta_{\kappa r} + \kappa)}\varepsilon^2 + \text{O}(\varepsilon^3), \quad (2.85c)$$

with the extra polynomials

$$z_1 = \Delta_{\kappa r}^2 + 3\Delta_{\kappa r}\kappa + \kappa^2, \quad z_2 = 3\Delta_{\kappa r} + \kappa, \quad (2.86a)$$

$$x_3 = 144\Delta_{\kappa r}^5 + 1054\Delta_{\kappa r}^4\kappa + 1375\Delta_{\kappa r}^3\kappa^2 - 1183\Delta_{\kappa r}^2\kappa^3 - 987\Delta_{\kappa r}\kappa^4 - 159\kappa^5, \quad (2.86b)$$

$$y_3 = 120\Delta_{\kappa r}^5 - 596\Delta_{\kappa r}^4\kappa - 800\Delta_{\kappa r}^3\kappa^2 + 2762\Delta_{\kappa r}^2\kappa^3 + 1845\Delta_{\kappa r}\kappa^4 + 285\kappa^5. \quad (2.86c)$$

These fixed points identify very well with the non-disordered case. Indeed, in the limit  $\Delta_{\kappa r} \rightarrow 0$  we perfectly recover the fixed points  $\{\text{P}_2, \text{P}_3, \text{P}_4\}$  of the pure non-disordered case and the corresponding anomalous dimensions described in the previous section. Formally,

$$\text{P}_2(0) = \text{P}_2 \quad \text{and} \quad \eta(\text{P}_2(0)) = \eta(\text{P}_2), \quad (2.87a)$$

$$\text{P}_3(0) = \text{P}_3 \quad \text{and} \quad \eta(\text{P}_3(0)) = \eta(\text{P}_3), \quad (2.87b)$$

$$\text{P}_4(0) = \text{P}_4 \quad \text{and} \quad \eta(\text{P}_4(0)) = \eta(\text{P}_4). \quad (2.87c)$$

Another limit that one might be interested in is the case of very large disorder, *i.e.*,  $\Delta_{\kappa r} \rightarrow \infty$ . In that case, a naive limit gives (in natural units  $\kappa = 1$ )

$$\eta = (\text{P}_2(\infty)) = 0 + \text{O}(\varepsilon^3), \quad (2.88a)$$

$$\eta = (\text{P}_3(\infty)) = \frac{5\varepsilon}{d_5} + \left( \frac{1625}{18d_5^3} + \frac{115}{9d_5^2} - \frac{37}{6d_5} \right) \varepsilon^2 + \text{O}(\varepsilon^3), \quad (2.88b)$$

$$\eta = (\text{P}_4(\infty)) = \frac{6\varepsilon}{d_6} + \left( \frac{141}{5d_6^3} + \frac{313}{10d_6^2} - \frac{6}{d_6} \right) \varepsilon^2 + \text{O}(\varepsilon^3). \quad (2.88c)$$

In this case, we observe new structures in  $d_n = d_c + n$  with  $n = 5, 6$  (in the non-disordered case it was  $n = 4, 20, 24$ ). This is a phenomenological evidence of the presence of new fixed points including disorder. However, in the limit  $\Delta_{\kappa r} \rightarrow \infty$  we have  $\phi \rightarrow \infty$  for  $\text{P}_3(\infty)$  and  $\text{P}_4(\infty)$ , which is non-physical. Moreover, it is unsure to us that this limit commutes properly with the  $\varepsilon$  series expansions. We therefore discard the results (2.88). We will try to access these fixed points by other means.

A very special point that one might want to identify is the point where  $\phi = 0$ , *i.e.*, where the theory is marginal (both thermal and disorder fluctuations being of the same order). In a sense, it amounts to interpret  $\phi$  as a beta function<sup>5</sup> and find its fixed point. The first naive ansatz to search

<sup>5</sup>In that case, we would use the coherent notations  $\beta_{\Delta_\kappa} = d\Delta_{\kappa r}/d\log M = \Delta_{\kappa r}\phi$ .

for a perturbative solution is  $\Delta_{\kappa r} = \Delta_{\kappa r}^{(0)} + \Delta_{\kappa r}^{(1)}\varepsilon + \dots$ . However, it naively leads to negative solutions for  $\Delta_{\kappa r}$ , such as

$$\Delta_{\kappa 3}^* = -\frac{\kappa}{3} + \frac{4\kappa\varepsilon}{81d_{20}} + \mathcal{O}(\varepsilon^2) \implies \eta(\Delta_{\kappa 3}^*) = \frac{20\varepsilon}{d_{20}} + \left( \frac{7600}{3d_{20}^3} + \frac{1100}{3d_{20}^2} - \frac{74}{3d_{20}} \right) \varepsilon^2 + \mathcal{O}(\varepsilon^3), \quad (2.89a)$$

$$\Delta_{\kappa 4}^* = -\frac{\kappa}{3} + \frac{4\kappa\varepsilon}{5d_{24}} + \mathcal{O}(\varepsilon^2) \implies \eta(\Delta_{\kappa 4}^*) = \frac{24\varepsilon}{d_{24}} + \left( \frac{3072}{d_{24}^3} + \frac{448}{d_{24}^2} - \frac{24}{d_{24}} \right) \varepsilon^2 + \mathcal{O}(\varepsilon^3), \quad (2.89b)$$

that are non-physical. Moreover, we observe a  $d_c$  structure in  $d_n = d_c + n$  with  $n = 20, 24$ , which phenomenologically means that these are in fact non-disordered solutions. In order to approach a regime where  $\Delta_{\kappa r}$  is very large, one can take a non-perturbative ansatz of the form  $\Delta_{\kappa r} = \Delta_{\kappa r}^{(-1)}/\varepsilon + \Delta_{\kappa r}^{(0)} + \varepsilon\Delta_{\kappa r}^{(1)} + \dots$ . In this case, the solution reads

$$\Delta_{\kappa 3}^* = \frac{-3d_5\kappa}{2\varepsilon} + \mathcal{O}(\varepsilon^0) \implies \eta(\Delta_{\kappa 3}^*) = \frac{5\varepsilon}{d_5} + \left( \frac{1025}{18d_5^3} + \frac{175}{9d_5^2} - \frac{37}{6d_5} \right) \varepsilon^2 + \mathcal{O}(\varepsilon^3), \quad (2.90a)$$

$$\Delta_{\kappa 4}^* = \frac{-3d_6\kappa}{\varepsilon} + \mathcal{O}(\varepsilon^0) \implies \eta(\Delta_{\kappa 4}^*) = \frac{6\varepsilon}{d_6} + \left( \frac{261}{5d_6^3} + \frac{273}{10(d_6)^2} - \frac{6}{d_6} \right) \varepsilon^2 + \mathcal{O}(\varepsilon^3). \quad (2.90b)$$

The first one is irrelevant because it is unstable in several directions. However, the second one is very interesting, because it is stable in most of the directions. This is a strong evidence that it exist a fixed at finite disorder, where the model is marginal ( $\phi = 0$ ). This fixed point should indicate the critical point below (respectively above) which the theory will flow toward a disordered (respectively non-disordered) fixed point. We will call it  $P_c$ . However, this approach can be easily criticized. First, the use of a non-perturbative ansatz is quite shaky. Second, the first-order contribution to  $\Delta_{\kappa r}$  for  $P_c$  is a negative pole, which prevents any conclusion towards its real value or its sign without resummations<sup>6</sup>. Third, even though we postulated  $\phi = 0$  to derive this fixed point, it is very hard to keep this equality true at all orders in  $\varepsilon$  while using a non-perturbative ansatz for  $\Delta_{\kappa r}$ . Indeed, in the non-perturbative approach it seems that  $\phi = 0 + x\varepsilon^2 + \dots$  where  $x$  is non-vanishing. As we will see in the following section, this is in fact due to the presence of a second fixed point  $P_5$ , for which  $\phi = x\varepsilon^2 + \dots$ . In this approach, we are not able to distinguish between  $P_c$  and  $P_5$  properly.

### Search in low temperature variables

Let us summarize what we learned in the previous section. We solved naively the system of beta functions in the variables  $\mu_r, \Delta_{\mu r}, \lambda_r, \Delta_{\lambda r}$ , for arbitrary  $\Delta_{\kappa r}$ , that we will call the high-temperature variables. This allowed us to recover the non-disordered results in the limit  $\Delta_{\kappa r} \rightarrow 0$ . Taking the limit  $\Delta_{\kappa r} \rightarrow \infty$ , or various ansatz for  $\Delta_{\kappa r}$  revealed the existence of an interesting fixed point with a flexuron anomalous dimension yielding  $\eta = 6\varepsilon/d_6 + \dots$ . However, for all approaches, the analysis was flawed in one way or another, which prevents us from making conclusions.

To circumvent these issue, in this section, we will perform the change of variables

$$g_{\mu r} = \Delta_{\kappa r}\mu_r \quad \text{and} \quad g_{\lambda r} = \Delta_{\kappa r}\lambda_r. \quad (2.91)$$

By doing so, we completely absorb  $\Delta_{\kappa r}$ . Moreover, we will work in natural units and set  $\kappa = 1$ , which is equivalent to redefining the couplings and fields of the theory to absorb it.

Moreover, the quantities  $g_\mu$  and  $g_\lambda$  can both be interpreted as couplings, so that the new set of couplings we will work with is then made of the five quantities

$$\mu_r, \quad g_{\mu r}, \quad \Delta_{\mu r}, \quad g_{\lambda r}, \quad \Delta_{\lambda r}. \quad (2.92)$$

<sup>6</sup>The sign of the pole does not give the sign of the true value obtained upon computing higher orders and using resummations

Taking the derivative with respect to the renormalization scale  $M$  on both sides of equations (2.91) leads to the following definitions for their respective beta functions

$$\beta_{g_\mu} = \Delta_{\kappa r} \beta_\mu + \mu_r \phi, \quad (2.93a)$$

$$\beta_{g_\lambda} = \Delta_{\kappa r} \beta_\lambda + \lambda_r \phi. \quad (2.93b)$$

The new system of beta to be solved is then

$$\beta_\alpha = 0, \quad \alpha = \{\mu_r, g_{\mu r}, \Delta_{\mu r}, g_{\lambda r}, \Delta_{\lambda r}\}. \quad (2.94)$$

Solving this system perturbatively (ansatz  $\alpha_r = \alpha^{(1)}\varepsilon + \dots$ ) leads to a total of 8 solutions. However, 7 of them are unstable in the RG sense or mechanically not allowed. We shall not display them here. More interestingly, the last solutions give a fixed point with an undetermined parameter. We will choose  $\mu_r^{(2)}$  as the undetermined parameter, and we define  $\mu_r^{(2)} = (4\pi)^2 C$  for brevity. Moreover, for the time being and for the sake of brevity, we limit our analysis to two loops (conclusions at three loops are the same). This fixed point, that we call  $P_x(C)$ , then reads

$$P_x(C): \quad \mu_x^*(C) = (4\pi)^2 \left[ 0 \times \varepsilon + C\varepsilon^2 + O(\varepsilon^3) \right], \quad (2.95a)$$

$$g_{\mu x}^*(C) = (4\pi)^2 \left[ \frac{6\varepsilon}{d_6} + \left( \frac{216}{d_6^4} + \frac{51}{5d_6^3} - \frac{52}{5d_6^2} + \left( \frac{108}{d_6^2} - \frac{21}{d_6} - \frac{1}{2} \right) C \right) \varepsilon^2 + O(\varepsilon^3) \right], \quad (2.95b)$$

$$\Delta_{\mu x}^*(C) = (4\pi)^2 \left[ \frac{3\varepsilon}{d_6} + \left( \frac{108}{d_6^4} + \frac{141}{10d_6^3} - \frac{21}{5d_6^2} + \left( \frac{54}{d_6^2} - \frac{6}{d_6} - \frac{1}{2} \right) C \right) \varepsilon^2 + O(\varepsilon^3) \right], \quad (2.95c)$$

$$g_{\lambda x}^*(C) = (4\pi)^2 \left[ -\frac{2\varepsilon}{d_6} + \left( -\frac{72}{d_6^4} - \frac{17}{5d_6^3} + \frac{44}{5d_6^2} + \left( -\frac{36}{d_6^2} + \frac{7}{d_6} + \frac{1}{6} \right) C \right) \varepsilon^2 + O(\varepsilon^3) \right], \quad (2.95d)$$

$$\Delta_{\lambda x}^*(C) = (4\pi)^2 \left[ -\frac{\varepsilon}{d_6} + \left( -\frac{36}{d_6^4} - \frac{47}{10d_6^3} - \frac{3}{5d_6^2} + \left( -\frac{18}{d_6^2} + \frac{2}{d_6} + \frac{1}{6} \right) C \right) \varepsilon^2 + O(\varepsilon^3) \right], \quad (2.95e)$$

with the corresponding anomalous dimensions

$$\eta(P_x(C)) = \frac{6\varepsilon}{d_6} + \left( \frac{216}{d_6^4} - \frac{39}{5d_6^3} + \frac{313}{10d_6^2} - \frac{6}{d_6} + \left( \frac{108}{d_6^2} - \frac{30}{d_6} + 2 \right) C \right) \varepsilon^2 + O(\varepsilon^3), \quad (2.96a)$$

$$\phi(P_x(C)) = 0 + \left( -\frac{36}{d_6^3} + \frac{6}{d_6^2} - \left( \frac{18}{d_6} - 3 \right) C \right) \varepsilon^2 + O(\varepsilon^3). \quad (2.96b)$$

The first interesting case is the disordered, shearless, fixed point  $\mu = 0$  (completely dominated by disorder) which we call  $P_5$ . It amounts to set  $C = 0$ , reading

$$\eta(P_5) = \frac{6\varepsilon}{d_6} + \left( \frac{216}{d_6^4} - \frac{39}{5d_6^3} + \frac{313}{10d_6^2} - \frac{6}{d_6} \right) \varepsilon^2 + O(\varepsilon^3), \quad (2.97a)$$

$$\phi(P_5) = 0 + \left( -\frac{36}{d_6^3} + \frac{6}{d_6^2} \right) \varepsilon^2 + O(\varepsilon^3). \quad (2.97b)$$

The second interesting case is to take  $\phi(P_x(C)) = 0$ , and solve for  $C$ , which simply leads to  $C = -2/d_6^2$ . We call this fixed point  $P_c$ , yielding the anomalous dimensions

$$\eta(P_c) = \frac{6\varepsilon}{d_6} + \left( \frac{261}{5d_6^3} + \frac{273}{10d_6^2} - \frac{6}{d_6} \right) \varepsilon^2 + O(\varepsilon^3), \quad (2.98a)$$

$$\phi(P_c) = 0 + O(\varepsilon^3). \quad (2.98b)$$

This fixed point is then marginal ( $\phi = 0$ ), so that both thermal fluctuations and disorder coexist. These results were first obtained in [56] but contained a mistake, preventing the author to conclude and to provide a numerical estimate of the anomalous dimensions. Before discussing further these results, we will extend our analysis to three loops.

### 2.5.3 Disordered fixed points and results up to three loops

At three loops the picture is unchanged and, following a very similar procedure, we extend to three loops the coordinates for the fixed points  $P_5$  and  $P_c$ .

#### Results for $P_5$

First, for  $P_5$ , the three-loop computation yields the following coordinates

$$\mu_5^* = 0 + O(\varepsilon^4) \quad (\text{Shearless}), \quad (2.99a)$$

$$g_{\mu_5}^* = (4\pi)^2 \left[ \frac{6\varepsilon}{d_6} + \left( \frac{216}{d_6^4} + \frac{51}{5d_6^3} - \frac{52}{5d_6^2} \right) \varepsilon^2 + \left( \frac{11664}{d_6^7} + \frac{30456}{5d_6^6} - \frac{6(2315304\zeta_3 - 3147523)}{125d_6^5} \right. \right. \\ \left. \left. + \frac{27(177984\zeta_3 - 240053)}{100d_6^4} + \frac{5084087 - 3558816\zeta_3 - 1589}{1000d_6^3} - \frac{1589}{50d_6^2} \right) \varepsilon^3 + O(\varepsilon^4) \right], \quad (2.99b)$$

$$\Delta_{\mu_5}^* = (4\pi)^2 \left[ \frac{3\varepsilon}{d_6} + \left( \frac{108}{d_6^4} + \frac{141}{10d_6^3} - \frac{21}{5d_6^2} \right) \varepsilon^2 + \left( \frac{5832}{d_6^7} + \frac{17658}{5d_6^6} - \frac{3(2315304\zeta_3 - 3159823)}{125d_6^5} \right. \right. \\ \left. \left. + \frac{4849308\zeta_3 - 6531701}{250d_6^4} + \frac{528815 - 384912\zeta_3 - 213}{300d_6^3} - \frac{213}{200d_6^2} \right) \varepsilon^3 + O(\varepsilon^4) \right], \quad (2.99c)$$

$$\lambda_5^* = 0 + O(\varepsilon^4) \quad (\text{Rigid}), \quad (2.99d)$$

$$g_{\lambda_5}^* = (4\pi)^2 \left[ -\frac{2\varepsilon}{d_6} + \left( -\frac{72}{d_6^4} - \frac{17}{5d_6^3} + \frac{44}{5d_6^2} \right) \varepsilon^2 + \left( -\frac{3888}{d_6^7} - \frac{10152}{5d_6^6} + \frac{2(2315304\zeta_3 - 3123523)}{125d_6^5} \right. \right. \\ \left. \left. + \frac{6485671 - 4805568\zeta_3}{300d_6^4} + \frac{3468096\zeta_3 - 4777447}{3000d_6^3} + \frac{1349}{150d_6^2} \right) \varepsilon^3 + O(\varepsilon^4) \right], \quad (2.99e)$$

$$\Delta_{\lambda_5}^* = (4\pi)^2 \left[ -\frac{\varepsilon}{d_6} + \left( -\frac{36}{d_6^4} - \frac{47}{10d_6^3} - \frac{3}{5d_6^2} \right) \varepsilon^2 + \left( -\frac{1944}{d_6^7} - \frac{5886}{5d_6^6} + \frac{2315304\zeta_3 - 3177823}{125d_6^5} \right. \right. \\ \left. \left. + \frac{6526601 - 4849308\zeta_3}{750d_6^4} + \frac{43578\zeta_3 - 57349}{75d_6^3} - \frac{2027}{600d_6^2} \right) \varepsilon^3 + O(\varepsilon^4) \right]. \quad (2.99f)$$

Since  $\mu_5^* = \lambda_5^*$ , this fixed point is indeed completely dominated by disorder. The corresponding anomalous dimensions read

$$\eta(P_5) = \frac{6\varepsilon}{d_6} + \left( \frac{216}{d_6^4} - \frac{39}{5d_6^3} + \frac{313}{10d_6^2} - \frac{6}{d_6} \right) \varepsilon^2 + \left( \frac{11664}{d_6^7} + \frac{25596}{5d_6^6} - \frac{6(2315304\zeta_3 - 3200773)}{125d_6^5} \right. \\ \left. + \frac{3(2388204\zeta_3 - 3246043)}{125d_6^4} + \frac{16228747 - 11992536\zeta_3}{1500d_6^3} + \frac{152928\zeta_3 - 194339}{600d_6^2} - \frac{16}{3d_6} \right) \varepsilon^3, \quad (2.100a)$$

$$\phi(P_5) = 0 \times \varepsilon + \left( -\frac{36}{d_6^3} + \frac{6}{d_6^2} \right) \varepsilon^2 + \left( -\frac{1944}{d_6^6} - \frac{2304}{5d_6^5} + \frac{243(19056\zeta_3 - 26257)}{250d_6^4} \right. \\ \left. - \frac{4(147177\zeta_3 - 209119)}{125d_6^3} + \frac{3(90144\zeta_3 - 134243)}{1000d_6^2} \right) \varepsilon^3, \quad (2.100b)$$

which the first set of main result in this chapter. Interestingly, in the physical case  $d_c = 1$ , the anomalous dimensions read

$$\eta(P_5) = \frac{6\varepsilon}{7} - \frac{3629\varepsilon^2}{24010} + \frac{(759884263 - 698184144\zeta_3)\varepsilon^3}{823543000} + O(\varepsilon^4), \quad (2.101a)$$

$$\phi(P_5) = \frac{6\varepsilon^2}{343} + \frac{(72599819 - 58508352\zeta_3)\varepsilon^3}{117649000} + O(\varepsilon^4), \quad (2.101b)$$

and numerically yields

$$\eta(P_5) = 0.8571\varepsilon - 0.1511\varepsilon^2 - 0.09638\varepsilon^3 + O(\varepsilon^4), \quad (2.102a)$$

$$\phi(P_5) = 0.01749\varepsilon^2 + 0.01929\varepsilon^3 + O(\varepsilon^4), \quad (2.102b)$$

which, at  $\varepsilon = 1$ , reads

$$\eta(P_5) = 0.6096, \quad \phi(P_5) = ?, \quad (2.103)$$

where “?” indicates that the situation is unclear at  $\varepsilon = 1$ . Indeed, for  $\eta(P_5)$ , the coefficients are small and decreasing so that  $\varepsilon = 1$  is a good approximation. However, for  $\phi(P_5)$ , the first coefficient of the series is zero, and the third one is bigger than the second one. Therefore, taking  $\varepsilon = 1$  is not reasonable here, and one cannot conclude on the sign of  $\phi(P_5)$ , see the related footnote 7. Therefore, we are not able to conclude from  $\phi$  yet if the fixed point  $P_5$  is dominated by disorder ( $\phi(P_5) > 0$ ) or by thermal fluctuations ( $\phi(P_5) < 0$ ). Nevertheless, since  $\mu_5^* = \lambda_5^* = 0$  and that these quantities scale linearly with the temperature  $T$ , we know that  $P_5$  must be disorder dominated and ultimately that  $\phi(P_5) < 0$ .

Going further, we provide in figure 2.7 a plot of the values obtained for  $\eta(P_5)$  versus the loop order, and provide an exponential fit to give an estimate of where the value is going at higher-loop order.

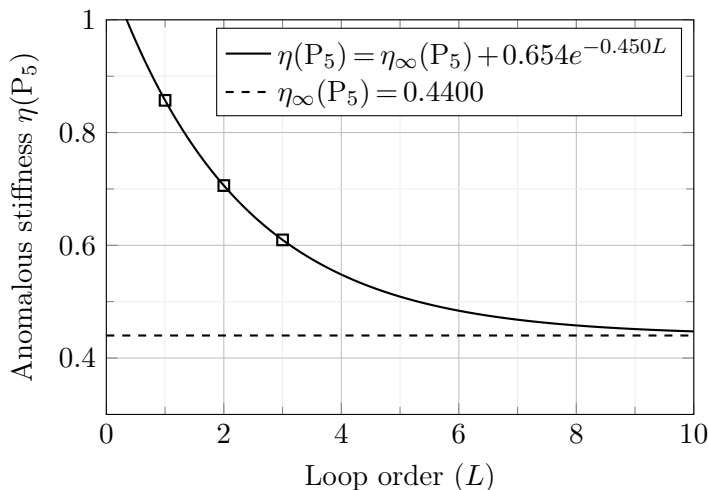


Figure 2.7: Exponential fit on the results found for  $\eta(P_5)$  from 1 to 3 loops. The values seem to slowly converge towards  $\eta_{\infty\text{-loop}}(P_5) = 0.4400$ .

Including the results from 1- to 3-loop order, a simple exponential fit gives an estimated value at infinite-loop order of  $\eta_{\infty\text{-loop}}(P_5) = 0.4400$ . Another way to resum this quantity is to use a simple Padé approximant. Interestingly, the first Padé approximant yields  $\eta^{[1/2]}(P_c) = 0.6494$ , which is close to the raw value (2.103) at  $\varepsilon = 1$  and the second possible Padé approximant yields  $\eta^{[2/1]}(P_c) = 0.4400$ , which is surprisingly the same value as the one obtained via exponential fit figure 2.7. Similarly, for  $\phi(P_5)$ , while a Padé [1/2] is not possible due to a pole (and would require higher-order computation), the Padé approximant [2/1] reads  $\phi^{[2/1]}(P_5) = -0.1703$ , which is indeed negative. Our best estimates for these two exponents are then

$$\eta^{[2/1]}(P_5) = 0.4400, \quad \phi^{[2/1]}(P_5) = -0.1703. \quad (2.104)$$

### Results for $P_c$

Second, for  $P_c$ , the three-loop computation lead to the following non-trivial coordinates

$$\mu_c^* = (4\pi)^2 \left[ 0 \times \varepsilon - \frac{2\varepsilon^2}{d_6^2} + \left( -\frac{174}{5d_6^4} + \frac{1543536\zeta_3 - 2103817}{1500d_6^3} - \frac{3(30048\zeta_3 - 44081)}{1000d_6^2} \right) \varepsilon^3 \right], \quad (2.105a)$$

$$g_{\mu c}^* = (4\pi)^2 \left[ \frac{6\varepsilon}{d_6} + \left( \frac{261}{5d_6^3} - \frac{47}{5d_6^2} \right) \varepsilon^2 + \left( \frac{22707}{25d_6^5} + \frac{4177656\zeta_3 - 5276807}{250d_6^4} + \frac{9056669 - 6540912\zeta_3}{3000d_6^3} + \frac{90144\zeta_3 - 195803}{2000d_6^2} \right) \varepsilon^3 \right], \quad (2.105b)$$

$$\Delta_{\mu c}^* = (4\pi)^2 \left[ \frac{3\varepsilon}{d_6} + \left( \frac{261}{10d_6^3} - \frac{16}{5d_6^2} \right) \varepsilon^2 + \left( \frac{22707}{50d_6^5} + \frac{4177656\zeta_3 - 5263757}{500d_6^4} + \frac{5021743 - 3770064\zeta_3}{3000d_6^3} + \frac{3(30048\zeta_3 - 44791)}{2000d_6^2} \right) \varepsilon^3 \right], \quad (2.105c)$$

$$\lambda_c^* = (4\pi)^2 \left[ 0 \times \varepsilon + \frac{2\varepsilon^2}{3d_6^2} + \varepsilon^3 \left( \frac{58}{5d_6^4} + \frac{2095817 - 1543536\zeta_3}{4500d_6^3} + \frac{30048\zeta_3 - 44081}{1000d_6^2} \right) \right], \quad (2.105d)$$

$$g_{\lambda c}^* = (4\pi)^2 \left[ -\frac{2\varepsilon}{d_6} + \left( \frac{127}{15d_6^2} - \frac{87}{5d_6^3} \right) \varepsilon^2 + \left( -\frac{7569}{25d_6^5} + \frac{5346407 - 4177656\zeta_3}{750d_6^4} + \frac{6268752\zeta_3 - 8121749}{9000d_6^3} + \frac{186203 - 90144\zeta_3}{6000d_6^2} \right) \varepsilon^3 \right], \quad (2.105e)$$

$$\Delta_{\lambda c}^* = (4\pi)^2 \left[ -\frac{\varepsilon}{d_6} + \left( -\frac{87}{10d_6^3} - \frac{14}{15d_6^2} \right) \varepsilon^2 + \left( -\frac{7569}{50d_6^5} + \frac{5211557 - 4177656\zeta_3}{1500d_6^4} + \frac{1716768\zeta_3 - 2205491}{3000d_6^3} + \frac{111973 - 90144\zeta_3}{6000d_6^2} \right) \varepsilon^3 \right]. \quad (2.105f)$$

At first glance, the result for  $\mu_c^*$  may seem non-physical, since the first non-vanishing contribution is negative. However, one cannot trust the sign of the second order term in a perturbative series starting by a vanishing first-order term<sup>7</sup>. In order to obtain a reliable value for such series, one need high order expansion and perform resummations, which is outside the scope of this chapter.

The anomalous dimensions associated with this fixed point reads

$$\eta(P_c) = \frac{6\varepsilon}{d_6} + \left( \frac{261}{5d_6^3} + \frac{273}{10d_6^2} - \frac{6}{d_6} \right) \varepsilon^2 + \left( \frac{22707}{25d_6^5} + \frac{2088828\zeta_3 - 2558581}{125d_6^4} - \frac{7(173178\zeta_3 - 209501)}{375d_6^3} + \frac{223776\zeta_3 - 166237}{3000d_6^2} - \frac{16}{3d_6} \right) \varepsilon^3 + \mathcal{O}(\varepsilon^4), \quad (2.106a)$$

$$\phi(P_c) = 0 + \mathcal{O}(\varepsilon^4) \quad (\text{marginal}), \quad (2.106b)$$

which is the second set of main results in this chapter. In the physical case  $d_c = 1$ , they read

$$\eta(P_c) = \frac{6\varepsilon}{7} - \frac{507\varepsilon^2}{3430} + \frac{(10463737 - 9504432\zeta_3)\varepsilon^3}{10084200} + \mathcal{O}(\varepsilon^4), \quad (2.107a)$$

$$\phi(P_c) = 0 + \mathcal{O}(\varepsilon^4). \quad (2.107b)$$

Equivalently, numerically

$$\eta(P_c) = 0.8571\varepsilon - 0.1478\varepsilon^2 - 0.09531\varepsilon^3 + \mathcal{O}(\varepsilon^4), \quad (2.108a)$$

$$\phi(P_c) = 0 + \mathcal{O}(\varepsilon^4), \quad (2.108b)$$

and at  $\varepsilon = 1$

$$\eta(P_c) = 0.6140, \quad \phi(P_c) = 0, \quad (2.109)$$

<sup>7</sup>Let us provide an example for the unconvinced reader. Let us imagine that we obtained a three-loop result for a quantity  $A$ , yielding  $A = 0 \times \varepsilon - \varepsilon^2 - 2\varepsilon^3 + \mathcal{O}(\varepsilon^4)$ , and that one wants to take the limit  $\varepsilon = 1$ . One would naively argue that  $A < 0$ . However, if the true non-perturbative result would be, *e.g.*,  $A = \varepsilon^2 / (2\varepsilon - 1)$ , it is clear that the true answer at  $\varepsilon = 1$  is indeed  $A = 1 > 0$ . Therefore, one cannot trust the sign of the  $\mathcal{O}(\varepsilon^2)$  term if the leading one, of  $\mathcal{O}(\varepsilon)$ , is vanishing.



where  $\phi(P_c) = 0$  indicates a marginal fixed point.

Going further we again provide in figure 2.8 a plot of the values obtained for  $\eta(P_c)$  versus the loop order with an exponential fit estimation.

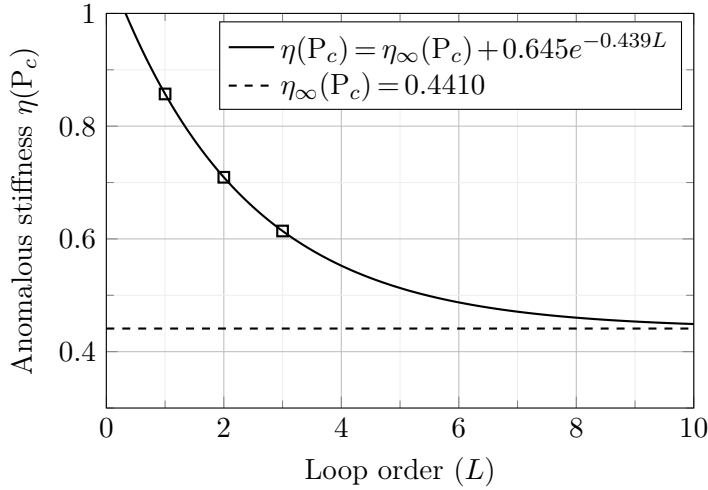


Figure 2.8: Exponential fit on the results found for  $\eta(P_c)$  from 1 to 3 loops. The values seem to slowly converge towards  $\eta_{\infty\text{-loop}}(P_c) = 0.4410$ .

Therefore, including the results from 1- to 3-loop order, the estimated value at infinite-loop order gives  $\eta_{\infty\text{-loop}}(P_c) = 0.4410$ . Again, interestingly, the first Padé approximant yields  $\eta^{[1/2]}(P_c) = 0.6526$  which is quite close to the raw result (2.109) at  $\varepsilon = 1$ , and the second Padé approximant yields  $\eta^{[2/1]}(P_c) = 0.4410$ , which is again surprisingly the same value as the one obtained via exponential fit in figure 2.8. Our best estimates for these exponents then reads

$$\boxed{\eta^{[2/1]}(P_c) = 0.4410, \quad \phi(P_c) = 0.} \quad (2.110)$$

### 2.5.4 Phase diagram

Since an image is worth a thousand words, instead of a long discussion about which directions these two fixed points are attractive or repulsive in the 6-dimensional space  $\{\mu_r, g_{\mu r}, \Delta_{\mu r}, g_{\lambda r}, \Delta_{\lambda r}\}$ , we provide a plot of the RG flow in figure 2.9. We represent the flow in three dimension, *i.e.*, restricting ourselves to the subspace  $\{\mu_r, \Delta_{\mu r}, g_{\mu r}\}$ , by setting  $\Delta_{\lambda r} = -\Delta_{\mu r}/3$  and  $g_{\lambda r} = -g_{\mu r}/3$ , which is a very good approximation at both  $P_5$  and  $P_c$ , as well as  $P_4$ , the pure (non-disordered) fixed point.

From the plots of figure 2.9, several comments are necessary. First and foremost, we see that going from one to two loops, the picture changes radically. Indeed, at one loop, the fixed point  $P_c$  is overlapping with  $P_5$  so that we can't distinguish it. In this case, in absence of shear  $\mu_r = 0$  (or equivalently at zero temperature  $T = 0$ ), all flow lines converges towards  $P_5$ , but as soon as  $\mu_r > 0$  (or equivalently  $T > 0$ ), all flow lines ultimately converge towards  $P_4$ , the fixed point controlling the flat phase without disorder. Therefore, if we limited our analysis to one loop, we would conclude that the disorder is always irrelevant in membranes, and that such systems are always dominated by thermal fluctuations. However, at two loops, the fixed point  $P_c$  emerges from  $P_5$  and they become two distinct fixed points. In this drastically different picture, all flow lines converges towards the attractive line formed by  $L = (P_5, P_c, P_4)$ . Moreover,  $P_c$  is itself attractive in all directions, except along the line  $L$ , where it is marginally repulsive. Therefore, if the system stands in between  $P_5$  and  $P_c$ , it will flow towards  $P_5$ , while if it stands between  $P_c$  and  $P_4$ , it will flow towards  $P_4$ .

Physically, the marginally unstable fixed point  $P_c$  is therefore controlling a phase transition between a thermally dominated phase ( $P_4$ ) and a disorder dominated phase ( $P_5$ ). In other words, a

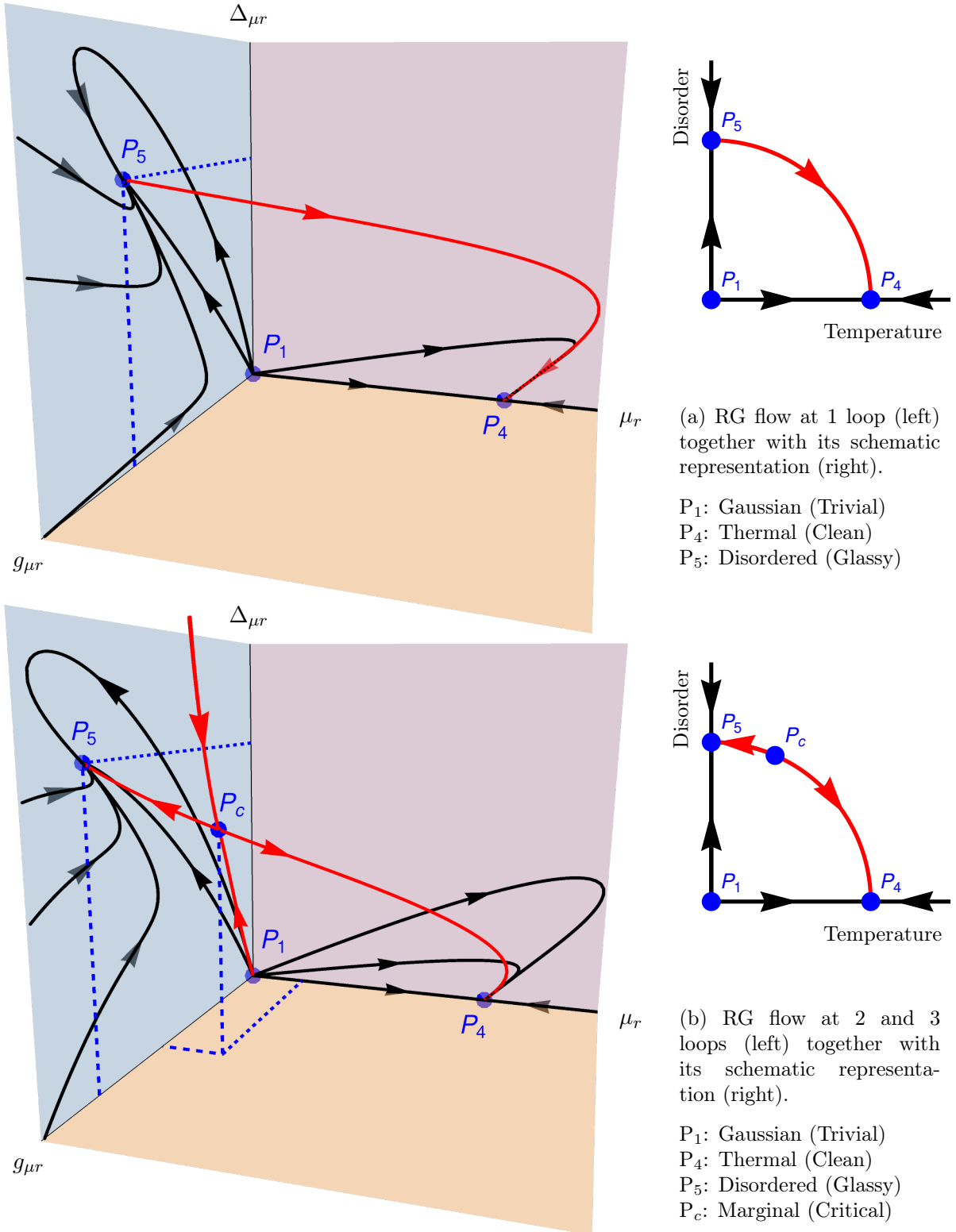


Figure 2.9: RG-flow diagram in the coordinates  $\mu_r$ ,  $\Delta_{\mu r}$ ,  $g_{\mu r}$ , and at  $\Delta_{\lambda r} = -\Delta_{\mu r}/3$  and  $g_{\lambda r} = -g_{\mu r}/3$ . At one loop, figure (a), the shearless fixed point  $P_5$  is attractive in the plane formed by  $\Delta_{\mu r}$  and  $g_{\mu r}$ . However, as soon as  $\mu_r > 0$ , all flow lines converges towards the disorderless non-trivial fixed point  $P_4$ . At two and three loops, figure (b), the picture changes dramatically with the emergence (from  $P_5$ ) of a new fixed point,  $P_c$ . In this case, all the flow lines converges towards the attractive line ( $P_5$ ,  $P_c$ ,  $P_4$ ) and, once there, the flow goes either to  $P_4$  or  $P_5$ , depending on whether it has passed the critical fixed point  $P_c$  or not. (Black lines are confined on the planes  $(\Delta_{\mu r}, g_{\mu r})$  and  $(\Delta_{\mu r}, \mu_r)$ , while red lines are on the bulk.) Since  $\mu_r \sim T$  can be considered as a measure of temperature and  $\Delta_{\mu r} \sim 1/T$  as a measure of disorder, we provide alongside the plots a schematic representation in the Disorder-Temperature axes.

possible transition towards a glassy phase, where the disorder is dominating the thermal fluctuations. It is a perturbative confirmation of the existence, at finite disorder and finite temperature, of a transition occurring in the phase diagram of quenched disordered membranes, as well as of the existence of a low-temperature glassy phase in these systems.

## 2.6 Comparison with other approaches

### 2.6.1 Benchmarking the NPRG approach

It is very instructive to compare our results with those obtained from the NPRG approach [103] when re-expanded in powers of  $\varepsilon$ . The results for  $\eta(P_5)$ , and  $\eta(P_c)$  in the NPRG approach [103] reads

$$\begin{aligned} \eta_{\text{NPRG}}(P_5) &= \frac{6\varepsilon}{d_6} + \left( \frac{108}{5d_6^4} - \frac{207}{5d_6^3} + \frac{264}{5d_6^2} - \frac{31}{4d_6} \right) \varepsilon^2 \\ &+ \left( \frac{2916}{25d_6^7} - \frac{7452}{25d_6^6} + \frac{41499}{50d_6^5} - \frac{400383}{400d_6^4} + \frac{89781}{160d_6^3} - \frac{33113}{400d_6^2} + \frac{215}{96d_6} \right) \varepsilon^3 + \text{O}(\varepsilon^4), \end{aligned} \quad (2.111a)$$

$$\begin{aligned} \phi_{\text{NPRG}}(P_5) &= 0 \times \varepsilon + \left( -\frac{18}{5d_6^3} + \frac{33}{5d_6^2} - \frac{1}{d_6} \right) \varepsilon^2 \\ &+ \left( -\frac{486}{25d_6^6} + \frac{2403}{50d_6^5} - \frac{2169}{20d_6^4} + \frac{10617}{100d_6^3} - \frac{441}{25d_6^2} + \frac{11}{24d_6} \right) \varepsilon^3 + \text{O}(\varepsilon^4), \end{aligned} \quad (2.111b)$$

$$\begin{aligned} \eta_{\text{NPRG}}(P_c) &= \frac{6\varepsilon}{d_6} + \left( \frac{3}{5d_6^3} + \frac{212}{5d_6^2} - \frac{85}{12d_6} \right) \varepsilon^2 \\ &+ \left( \frac{3}{25d_6^5} + \frac{15119}{1200d_6^4} + \frac{713483}{2400d_6^3} - \frac{222941}{3600d_6^2} + \frac{5197}{2592d_6} \right) \varepsilon^3 + \text{O}(\varepsilon^4), \end{aligned} \quad (2.111c)$$

$$\phi_{\text{NPRG}}(P_c) = 0. \quad (2.111d)$$

We observe that the NPRG is able to correctly recover the structure in  $d_6$ , but is not able to reproduce the  $\zeta_3$  structure. For simplicity, we compare numerically with our result, at  $d_c = 1$  (conveniently displayed on the right), reading

$$\eta_{\text{NPRG}}(P_5) = 0.8571\varepsilon - 0.1413\varepsilon^2 - 0.1034\varepsilon^3, \quad \eta(P_5) = 0.8571\varepsilon - 0.1511\varepsilon^2 - 0.09638\varepsilon^3, \quad (2.112a)$$

$$\phi_{\text{NPRG}}(P_5) = -0.01866\varepsilon^2 - 0.02746\varepsilon^3, \quad \phi(P_5) = 0.01749\varepsilon^2 + 0.01929\varepsilon^3, \quad (2.112b)$$

$$\eta_{\text{NPRG}}(P_c) = 0.8571\varepsilon - 0.1448\varepsilon^2 - 0.1054\varepsilon^3, \quad \eta(P_c) = 0.8571\varepsilon - 0.1478\varepsilon^2 - 0.09531\varepsilon^3, \quad (2.112c)$$

$$\phi_{\text{NPRG}}(P_c) = 0, \quad \phi(P_c) = 0. \quad (2.112d)$$

For  $\eta$ , the NPRG is very good to mimic numerically the exact loop expansion for both  $P_5$  and  $P_c$ . In the case of  $\phi(P_5)$ , the situation is unclear since the two series have a sign difference. However, both series are hard to resum with such few terms since they are in an asymptotic regime. The NPRG [103] also provides results exactly in  $d = 2$  ( $\varepsilon = 1$ ) reading

$$\eta_{\text{NPRG}}(P_c) = 0.492, \quad \eta_{\text{NPRG}}(P_5) = 0.449, \quad (2.113a)$$

$$\phi_{\text{NPRG}}(P_c) = 0, \quad \phi_{\text{NPRG}}(P_5) = -0.172, \quad (2.113b)$$

which are reasonably close to our best estimates (2.104) and (2.110). For  $P_5$ ,  $\phi < 0$  is in accordance with the fact that it must be disorder dominated.

### 2.6.2 Benchmarking the SCSA approach

In [12], a LO SCSA computation for arbitrary  $d$  in presence of quenched disorder has been performed. The results lead to a single fixed point, which is marginal, *i.e.*,  $\phi_{\text{SCSA}} = 0$  and the flexuron field anomalous dimension can be derived from the equation

$$1 = \frac{d(d-1)}{4d_c} \frac{\Gamma(2-\eta)\Gamma(2-\eta/2)\Gamma(\eta/2)\Gamma(d+\eta)}{\Gamma(2-\eta-d/2)\Gamma((d-\eta+4)/2)\Gamma(\eta+d/2)\Gamma((d+\eta)/2)}, \quad (2.114)$$

where  $\eta = \eta_{\text{SCSA}}$ . Solving this equation yields the non-perturbative result

$$\eta_{\text{SCSA}} = 0.449, \quad \phi_{\text{SCSA}} = 0. \quad (2.115)$$

Their finding of a single fixed point seems to indicate that, due to the LO approach, the SCSA is not able at this order to distinguish the fixed point  $P_c$  from  $P_5$ . The picture is therefore the one of figure 2.9a, where  $P_5$  is marginally stable, and all flow lines eventually converges towards  $P_4$ , so that the disorder is irrelevant as soon as  $\mu_r > 0$  (or equivalently  $T > 0$ ). Therefore, we denote  $\eta_{\text{SCSA}}$  as  $\eta_{\text{SCSA}}(P_x)$ . Solving perturbatively (2.114) at  $d = 4 - 2\varepsilon$  reads

$$\eta_{\text{SCSA}}(P_x) = \frac{6\varepsilon}{d_6} + \left( \frac{54}{d_6^3} + \frac{27}{d_6^2} - \frac{6}{d_6} \right) \varepsilon^2 + \left( \frac{972}{d_6^5} + \frac{1350}{d_6^4} - \frac{555}{d_6^3} + \frac{165}{2d_6^2} - \frac{16}{3d_6} \right) \varepsilon^3 + \text{O}(\varepsilon^4), \quad (2.116a)$$

$$\phi_{\text{SCSA}}(P_x) = 0. \quad (2.116b)$$

Interestingly, it seems that the structure in  $1/d_6$  resemble more to our result for  $P_c$  than for  $P_5$ . Moreover, if we compare numerically with our results (conveniently displayed on the right)

$$\eta_{\text{SCSA}}(P_x) = 0.8571\varepsilon - 0.1487\varepsilon^2 - 0.07621\varepsilon^3, \quad \begin{aligned} \eta(P_5) &= 0.8571\varepsilon - 0.1511\varepsilon^2 - 0.09638\varepsilon^3, \\ \eta(P_c) &= 0.8571\varepsilon - 0.1478\varepsilon^2 - 0.09531\varepsilon^3, \end{aligned} \quad (2.117)$$

it seems that the (single) fixed point captured by the SCSA has a flow structure compatible with  $P_5$ , but an anomalous dimension close to the one we have for  $P_c$ . This is a strong evidence that the LO SCSA computation seem not to be able to capture the whole physics of the system, *i.e.*, distinguishing the two fixed points found within our approach. This calls for a NLO SCSA computation.

### 2.6.3 Comparison with large- $d_c$ approaches

From [12], the SCSA technique at LO in the large- $d_c$  expansion, for arbitrary  $d$ , also yields a single fixed point, with anomalous dimensions

$$\eta_{\text{SCSA}}(P_x) = \frac{2}{d_c} \frac{d-1}{d+2} \frac{\Gamma(d)}{\Gamma^3(d/2)\Gamma(2-d/2)} + \text{O}(1/d_c^2), \quad (2.118a)$$

$$\phi_{\text{SCSA}}(P_x) = 0 + \text{O}(1/d_c^2), \quad (2.118b)$$

which is exact at this order. It is also remarkably exactly (up to a factor 4) the same result as for the clean case, see (1.146). These results can be directly compared to ours if we expand them in  $d = 4 - 2\varepsilon$ , reading

$$\eta_{\text{SCSA}}(P_x) = \frac{1}{d_c} \left( 6\varepsilon - 6\varepsilon^2 - \frac{16\varepsilon}{3}\varepsilon^3 + \text{O}(\varepsilon^4) \right) + \text{O}(1/d_c^2), \quad (2.119a)$$

$$\phi_{\text{SCSA}}(P_x) = 0 + \text{O}(1/d_c^2). \quad (2.119b)$$

Interestingly, the result  $\eta_{\text{SCSA}}$  corresponds to our results for both  $P_5$  and  $P_c$ . See the leading order terms  $\varepsilon^n/d_c$  in equations (2.100a) and (2.106a). It is again an indication that the SCSA is not able to distinguish between  $P_5$  and  $P_c$ .

Interestingly, the NLO large- $d_c$  computation has been performed in [106]<sup>8</sup>, directly in  $d=2$ , while taking infinite disorder ( $\Delta_\kappa \rightarrow \infty$ ). This reads

$$\eta_{\text{large-}d_c} = \frac{1}{2d_c} - \frac{612\zeta_3 - 265}{1728d_c^2} + \mathcal{O}(1/d_c^3), \quad (2.120a)$$

$$\phi_{\text{large-}d_c} = -\frac{68\zeta_3 - 31}{228d_c^2} + \mathcal{O}(1/d_c^3). \quad (2.120b)$$

Note that taking  $d_c = 1$  gives  $\eta_{\text{large-}d_c} = 0.2276$  and  $\phi_{\text{large-}d_c} = -0.2225$ . Again, the presence of a single fixed point seems to indicate that the large- $d_c$  approach is not able to distinguish  $P_5$  and  $P_c$ .

## 2.6.4 Non-perturbative comparison summary

As a summary, we recall our perturbative results directly at  $\varepsilon = 1$ , our resummations, as well as the non-perturbative results directly in  $d = 2$  provided by NPRG [103], SCSA [12] and the large- $d_c$  (NLO) [106] at  $d_c = 1$ .

$\varepsilon = 1$	This work					Other approaches		
	1-loop	2-loop	3-loop	Padé [1/2]	Padé [2/1]	NPRG [103]	SCSA [12]	large- $d_c$ [106]
$\eta(P_5)$	0.8571	0.7060	0.6096	0.6494	0.4400	0.449	0.449	0.2276
$\eta(P_c)$	0.8571	0.7093	0.6140	0.6526	0.4410	0.492		
$\phi(P_5)$	0	?	?	?	-0.1703	-0.172	0	-0.2225
$\phi(P_c)$	0	0	0	0	0	0		

Table 2.2: The “?” indicates that the result has been obtained as a series whose first terms behaves too badly to be resummed at this order, calling for a higher-order expansion. The values indicated  $L$ -loop with  $L = 1, 2, 3$  have been obtained taking raw  $\varepsilon = 1$  at the loop level  $L$ , from the results of this chapter. The Padé values [2/1] are the resummation extrapolations at  $\infty$ -loop order, which are our best estimates.

<sup>8</sup>In [106] the authors considered only a quenched random curvature.

## 2.7 Conclusion

In this chapter, we have analyzed quenched disordered membranes by means of a three-loop order perturbative approach. We have derived the all the RG functions for all the coupling constants and determined the fixed points relevant to the long-distance physics of quenched disordered membranes from one to three-loop orders. The main result of this work is that, beyond one loop, it clearly exists a new finite-temperatur , finite-disorder fixed point  $P_c$  in the RG-flow diagram. We provide in figure 2.10 a summary of our findings.

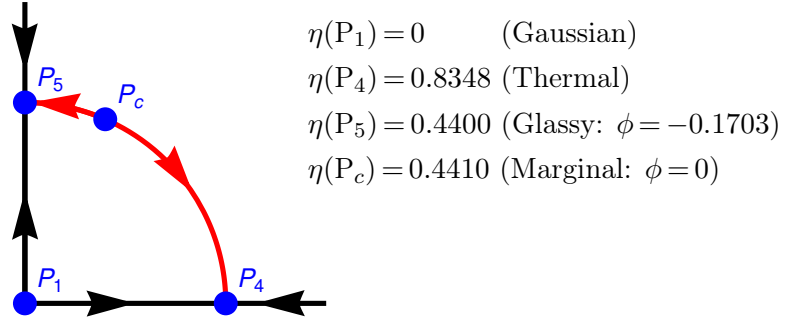


Figure 2.10: Schematic RG-flow diagram of quenched disordered flat membranes beyond one-loop, together with our best estimates for the flexuron field anomalous dimensions.

Therefore, beyond one loop, there exist two distinct fixed points including disorder,  $P_5$  and  $P_c$ . At the marginality, the critical exponent  $\phi$  of the disorder parameter  $\Delta_{\kappa_r}$  yields by definition  $\phi(P_c) = 0$ . As for its value at the fixed point  $P_5$ , our best estimates reveal  $\phi(P_5) < 0$ . Interestingly, the results that we obtained for  $\eta$  at the fixed points  $P_5$  and  $P_c$  exhibits a very peculiar asymptotic series structure, with small and decreasing coefficients. These series are then effectively convergent for the first terms, so that estimations at  $\varepsilon = 1$  should provide a good approximation of the series, even at low orders.

Admitting these arguments, our is a first perturbative confirmation of the existence of a finite disorder, finite temperature transition occurring in the phase diagram of quenched disordered membranes, as well as of the existence of a low-temperature glassy phase in these systems. The proximity between the values obtained for the anomalous dimensions at various fixed points within our perturbative results and the NPRG ones suggests that the fixed point  $P_c$  identified in the former approach coincides with that discovered within the latter one.

Let us underline that, in this chapter, we also recovered the results in the clean case, obtained in the last chapter. We recall that the clean results were obtained in the previous chapter by means of the effective flexural model. In this chapter, we used the independent, but equivalent and complementary, two-field model. The agreement of results in both models is a very strong check on our computations, and a proof that we acquired an unambiguous control on the renormalization procedure in these models.

It remains to confirm the present results by circumventing the difficulty encountered here, mainly due to the various series starting at  $O(\varepsilon^2)$ , thereby preventing us to conclude in some intermediary steps. Within the perturbative context, this may be achieved by changing the regularization and/or the renormalization scheme. Another method could be to enlarge the perturbative series by several orders and to use resummation techniques in order to extract reliable information about the position of the fixed points. Unfortunately, both solutions are far beyond the scope of this work, especially given the technical complexity of the model. In this respect, it would be of tremendous interest to revisit the SCSA approach in view of the present findings.



## Part II

# ELECTRONIC PROPERTIES OF MEMBRANES





# Chapter 3

## Critical properties of QED and reduced QED

This chapter is partly based on the publication

[4] S. Metayer and S. Teber, *JHEP* 09 (2021) 107,  
“Two-loop mass anomalous dimension in reduced quantum electrodynamics and application to dynamical fermion mass generation”.

We introduce the basics of Quantum Electrodynamics (QED) in four dimensions and then motivate the study of the more general reduced QED, where photons lives in a (possibly) bigger space-time than electrons. We compute the corresponding self-energies and polarizations up to two loops in a small coupling expansion and obtain all the anomalous dimensions. Our results are then applied for everyday QED as well as for a physical model of graphene, for which we compute the optical conductivity. We address the critical properties of reduced QEDs and study the eventuality of a phase transition from an insulating to a metallic phase in these models.

### Contents

---

3.1	Introduction . . . . .	<b>104</b>
3.1.1	Basics of QED in four dimensions (QED <sub>4</sub> ) . . . . .	104
3.1.2	Motivations for reduced QED . . . . .	107
3.2	The QED <sub>d<sub>γ</sub>,d<sub>e</sub></sub> model, conventions, and renormalization setup . . . . .	<b>111</b>
3.2.1	Model . . . . .	111
3.2.2	Perturbative setup . . . . .	112
3.2.3	Renormalization setup . . . . .	115
3.3	General perturbative calculations up to two loops in QED <sub>4,d<sub>e</sub></sub> . . . . .	<b>117</b>
3.3.1	One-loop calculations . . . . .	118
3.3.2	Two-loop calculations . . . . .	121
3.3.3	Electron field and mass anomalous dimensions . . . . .	126
3.4	Results for the different models of interest . . . . .	<b>128</b>
3.4.1	Results for QED <sub>4</sub> . . . . .	128
3.4.2	Results for reduced QED <sub>4,3</sub> (Graphene) . . . . .	128
3.4.3	Results for QED <sub>3</sub> (Large- $N_f$ ) . . . . .	131
3.4.4	Case of parity-odd mass term in QED <sub>4,3</sub> . . . . .	131
3.5	Critical properties . . . . .	<b>136</b>
3.5.1	Leading-order solution of SD equations for QED <sub>4,d<sub>e</sub></sub> . . . . .	136
3.5.2	Gap equation and criterion for dynamical mass generation . . . . .	137
3.5.3	Application to quenched QED <sub>4,d<sub>e</sub></sub> . . . . .	139
3.5.4	Application to unquenched QED <sub>4,d<sub>e</sub></sub> . . . . .	142
3.6	Conclusion . . . . .	<b>150</b>
3.A	QED <sub>4</sub> at three loops . . . . .	<b>151</b>

---

## 3.1 Introduction

### 3.1.1 Basics of QED in four dimensions (QED<sub>4</sub>)

Quantum electrodynamics (QED), first formulated by Paul Dirac in 1927 [108], is the relativistic quantum field theory describing how light (photons) and electrically charged particles (like electrons) behave and interact. QED is famous for its extremely accurate theoretical predictions of various quantities, two prominent examples being the anomalous magnetic moment of the electron and the Lamb shift of the energy levels of hydrogen, see, *e.g.*, [109]. QED is usually considered in the physical (3+1)-dimensional spacetime, *i.e.*, 3 space dimensions and 1 time dimension, that we shall name QED<sub>4</sub>.

Mathematically, the QED<sub>4</sub> model is derived from the principle of gauge invariance. It is an abelian gauge field theory with the unitary symmetry group U(1), defined on Minkowski space (flat spacetime). Formally, the QED<sub>4</sub> theory is made of a bosonic spin-1 field,  $A^\mu(x)$ , called the gauge field (or electromagnetic field) as well as (possibly multiple) charged spin-1/2 fields  $\Psi^i(x)$ . Excitations of the gauge field are called photons and mediate the interaction between the excitations of the matter field(s), called fermions, like, *e.g.*, electrons. See Table 3.1 for a summary of the field content and the usual vocabulary in QED<sub>4</sub>.

Field	index	spin	stat.	excitations	physical sense	mathematical definition
$\Psi^i(x)$	$\sigma = 1, \dots, N_f$	1/2	fermion	electrons ( $e^\pm$ )	matter	4-comp. Dirac spinor
$A^\mu(x)$	$\mu = 0, \dots, 3$	1	boson	photons ( $\gamma$ )	EM interaction	gauge covariant vector

Table 3.1: Summary of the field content in QED<sub>4</sub>.

The action, defining the model for this field content, can be written down considering that the theory should be invariant under some carefully chosen symmetries. The first ones are the usual relativistic spacetime symmetries, *i.e.*, invariance of the physics under rotations and boosts (Lorentz symmetry group) as well as translations, altogether forming the Poincaré symmetry group. The second ones are the internal symmetries of the theory, which in the QED case, is the internal unitary U(1) gauge group symmetry (circle group), directly related to the electric charge. While writing down the resulting action, one also needs to restrict to the terms that are relevant in the field theory sense, *i.e.*, renormalizable terms with a coupling parameter of canonical dimension between 0 and 1. Note that the vector field, mediating the gauge interactions, is naturally introduced by the generalization of the global gauge transformation to one that depends upon the local spacetime coordinate, while still requiring that the action remains invariant under all aforementioned symmetries. The obtained action can be written in a usual compact form, see, *e.g.*, the standard textbook [110], and reads

$$S_{\text{QED}_4} = \int d^4x \left[ \bar{\Psi}_i (i\not{D} - m) \Psi^i - \frac{1}{4} F^{\mu\nu} F_{\mu\nu} - \frac{1}{2\xi} (\partial_\mu A^\mu)^2 \right], \quad (3.1)$$

where we use natural units  $\hbar = c = 1$ . The notations require some unpacking. First,  $i = 1, 2, \dots, N_f$  are the  $N_f$  flavors of the massive (4-component) fermionic Dirac fields  $\Psi^i(x)$ , each of which has the same mass  $m$ . Note that in everyday life QED<sub>4</sub>,  $N_f = 1$ , nevertheless we keep  $N_f$  arbitrary in prevision of the next sections where  $N_f$  may be two, or even considered very large. Secondly,  $\{\mu, \nu\} = 0, 1, 2, 3$  are the 3+1 Lorentz spacetime indices of the gauge field  $A^\mu$ , *i.e.*, the covariant four-potential of the electromagnetic field generated by the fermions themselves. Also,  $\not{D} = \gamma^\mu D_\mu$  is the usual Feynman slash notation with the covariant derivative and the electromagnetic field tensor respectively defined as

$$D_\mu = \partial_\mu + ieA_\mu \quad \text{and} \quad F_{\mu\nu} = \partial_\mu A_\nu - \partial_\nu A_\mu, \quad (3.2)$$

with the coupling constant  $e$  standing for the electric charge, which is dimensionless in  $d=4$ . The 4 Dirac gamma matrices, of size  $4 \times 4$ , are noted  $\gamma^\mu$  and are defined so that they fulfill the so-called

Clifford algebra

$$\{\gamma^\mu, \gamma^\nu\} = \gamma^\mu \gamma^\nu + \gamma^\nu \gamma^\mu = 2g^{\mu\nu} I_4, \quad (3.3)$$

with  $I_n$  the  $n \times n$  identity matrix and  $g^{\mu\nu}$  the Minkowski flat space metric with, *e.g.*, the convention  $g^{\mu\nu} = \text{diag}(1, -1, -1, -1)$ . A usual representation for these four matrices is the Dirac basis

$$\gamma^0 = \begin{pmatrix} I_2 & 0 \\ 0 & -I_2 \end{pmatrix}, \quad \gamma^j = \begin{pmatrix} 0 & \sigma_j \\ -\sigma_j & 0 \end{pmatrix}, \quad (3.4)$$

where  $j = 1, 2, 3$  are the space indices and  $\sigma_i$  are the usual  $2 \times 2$  Pauli matrices. The gamma matrices are the fundamental objects that transform the 4-component Dirac spinor fields  $\Psi^i(x)$ . Indeed, the Dirac adjoint is defined as  $\bar{\Psi}^i(x) = (\Psi^i(x))^\dagger \gamma^0$ . Note that there exist also additional matrices that anticommutes with this set and generates the chiral and parity transformations of the model. We will describe precisely these matrices later in this chapter, in the devoted section 3.4.4.

Note also that instead of fixing the gauge by constraining the gauge field a priori, via an auxiliary equation, we added a gauge breaking term to the physical (gauge invariant) action, called the  $R_\xi$  gauge term, and parameterized by the gauge fixing parameter  $\xi$ . This term is also necessary to allow the inversion of the Lorentz tensorial structures while writing down the propagator for the photon. The choice of the parameter  $\xi$  determines the choice of gauge and by definition, physical results do not depend on the gauge fixing parameter  $\xi$ , *i.e.*, its value is an arbitrary choice. Several gauge fixing choices can be made, some more useful than other depending on the situation. Usual choices of gauge are named after physicists,

$$\text{Landau: } \xi = 0, \quad \text{Feynman/'t Hooft: } \xi = 1, \quad \text{Yennie: } \xi = 3, \quad \dots \quad (3.5)$$

To finish, let us remark that from trivial dimensional analysis on the action (3.1) we have

$$[\Psi] = 3/2, \quad [A] = 1, \quad [e] = 0, \quad [m] = 1, \quad [\xi] = 0, \quad (3.6)$$

where we used  $[\partial] = 1$ ,  $[d^4x] = -4$  and  $[S] = 0$ .

### Sketch of a perturbative computation in QED<sub>4</sub>

A typical perturbative computation in QED<sub>4</sub> goes as follows. First, write down all possible Feynman diagrams at a given loop order for the process of interest like, *e.g.*, a photon disintegrating into an electron-positron pair ( $\gamma \rightarrow e^+ e^-$ ). Then, write down the corresponding expressions using the Feynman rules of the model, compute all the diagrams and sum them! From the action (3.1), the Feynman rules in their simplest form (in the Feynman gauge and for  $N_f = 1$ ) read

$$\begin{array}{c} \longrightarrow \\ p \end{array} = \frac{i}{\not{p} - m}, \quad \mu \begin{array}{c} \nearrow \\ \bullet \\ \searrow \end{array} = -ie\gamma^\mu, \quad \mu \begin{array}{c} \sim \\ p \end{array} \nu = \frac{-i}{p^2} g^{\mu\nu}. \quad (3.7)$$

The first contributions to our example process,  $\gamma \rightarrow e^+ e^-$ , are the quantum corrections to the three-point vertex interaction

$$\Gamma^\mu = \mu \begin{array}{c} \sim \\ \bullet \\ \sim \end{array} = \left( \mu \begin{array}{c} \nearrow \\ \bullet \\ \searrow \end{array} + \mu \begin{array}{c} \nearrow \\ \bullet \\ \searrow \\ \nearrow \\ \bullet \\ \searrow \end{array} + \dots \right) = -ie(\gamma^\mu + \Gamma_1^\mu + \dots). \quad (3.8)$$

The physical process is then accurately described by the (infinite) sum of all the possible diagrams, that become more and more intricate with increasing loop order. Hopefully, if the coupling parameter is small, the more loops a diagram has (therefore the more complicated it is), the less it contributes. For QED<sub>4</sub>, in low energy conditions, the relevant expansion parameter is the fine structure constant  $\alpha = e^2/(4\pi\epsilon_0\hbar c)$  which reduces to  $\alpha = e^2/(4\pi) \approx 1/137$  in the natural units  $\hbar = c = \epsilon_0 = 1$ . The value of

$\alpha$  means that each loop order contributes  $1/137$  times less than the previous one. Therefore, taking into account the first few diagrams is already extremely precise in QED<sub>4</sub> at low energies.

Computing these Feynman diagrams involves integrations over the internal loop momenta, and generally leads to divergences. These are conveniently regularized using dimensional regularization, which is the most convenient regularization scheme for higher-order computations. Performing the computations in arbitrary dimension  $d$  allows regularizing the divergences that may appear in exactly  $d=4$ . Then, one can perform an expansion close to the convenient upper critical dimension, which is  $d_{uc}=4$  for QED<sub>4</sub>, the dimension where the theory is scale invariant, *i.e.*, where the coupling is dimensionless,  $[\alpha]=[e^2]=0$ . One usually takes the convention  $d=4-2\varepsilon$  with  $\varepsilon \rightarrow 0$ . After some appropriate projections, the result for the leading order (one-loop triangle) diagram in (3.8) takes the form

$$\Gamma_1 = \frac{A}{\varepsilon} + B + O(\varepsilon). \quad (3.9)$$

In a high energy physics context, one is usually interested on the so-called *probability amplitude* related to this diagram, *i.e.*, the probability of this peculiar process to happen. To extract this amplitude, we use renormalization, which is trivial at this order and basically removes the  $1/\varepsilon$  pole. This leads to the renormalized, *i.e.*, physical, amplitude  $\Gamma_{1r} = B$ . It turns out that this number is directly related to a famous physical quantity, the anomalous magnetic dipole moment of the electron  $a_e = (g-2)/2$ , which basically quantifies the difference between a classical spinning magnet and a true quantum electron. Our first order estimation of this quantity is, after computation,  $a_e = \alpha/2\pi$ . This result was first derived by Julian Schwinger in [111] and engraved on his headstone. Taking the fine structure constant to be  $\alpha \approx 1/137$  yields the value  $a_e = 0.001161$ . Thanks to the smallness of  $\alpha$ , this result is already accurate up to 4 digits. Indeed, recent precision experiments, *e.g.*, from quantum cyclotron orbits [112, 113] showed that  $a_e = 0.00115965218073(28)$  (recalling that the most recent measurements for the fine structure constant reads  $\alpha = 1/137.035999206(11)$  [114]). On the theoretical side, going further and including more diagrams increases the theoretical precision. Indeed, actual state-of-the-art numerical computations at five loops, see, *e.g.*, [115], involving several thousands of diagrams, gives the theoretical value  $a_e = 0.00115965218178(77)$  which is in accordance with the experiment up to 11 digits! This example is famous to be one of the most accurate theoretical prediction verified by an experiment.

Interestingly, in this analysis, renormalization was basically used to throw away (consistently) the divergent parts of the diagrams and obtain finite results. However, in a low energy physics context, *i.e.*, in statistical physics and more generally for condensed matter systems, this pole part is exactly what one wants to extract from this computation to access the so-called renormalization functions. Indeed, the pole  $A/\varepsilon$  is directly related to the asymptotics of Green's functions, thereby quantifying via anomalous scalings the violent features of the model, such as phase transitions. In this specific case, it is related to the running of the coupling of the theory with respect to the energy scale of observations, *i.e.*,  $\alpha(\mu)$  with  $\mu$  the renormalization scale. At low energies, we must recover the fine structure constant, so we define  $\alpha(m_e) \approx 1/137$  with  $m_e$  the electron mass, since it is the lightest particle charged electrically. The question is then if the coupling increases or decreases when the energy scale increases. The function quantifying this flow is called the beta function, defined as  $\beta(\alpha) = \partial\alpha/\partial\log\mu$ . At first order, a simple computation leads to  $\beta(\alpha) = -2A\alpha = 2\alpha^2/3\pi$ . This shows that the pole content of the theory is directly related to the beta function. Therefore, the running coupling  $\alpha(\mu)$  increases with  $\mu$ . Indeed, at higher scales such as the Z-boson mass ( $10^5$  times larger than  $m_e$ ), it has been measured as  $\alpha(m_Z) \approx 1/127$  [116]. Moreover, since the coupling flows with energy scale, one may ask the simple question; is there a special point where the coupling is scale invariant, *i.e.*,  $\beta(\alpha) = 0$ . Solving these equations leads to the so-called fixed points of the theory, where the theory exhibits peculiar universal features. One of the striking feature of theories taken at their fixed points is that they exhibit universal scaling for their correlation functions, that we call anomalous dimensions or equivalently critical exponents. Moreover, completely different theories, possibly arising from different physical models, can exhibit the same critical exponents. We call these categories of theories exhibiting

the same fixed points, universality classes. Unfortunately, in the high energy physics context, in 3+1 dimensions, there exist very few fixed points. Nevertheless, we will see in the following that this picture changes completely in lower dimensions and more specifically in 2+1 spacetime dimensions.

### 3.1.2 Motivations for reduced QED

Reduced quantum electrodynamics is a model describing fermions interacting via photons that live in a (possibly) bigger spacetime. Formally, the relativistic massive fermions lie in a  $d_e$ -dimensional spacetime and interact via the exchange of massless bosons in  $d_\gamma$ -dimensions ( $d_e \leq d_\gamma$ ), we then denote it  $\text{QED}_{d_\gamma, d_e}$ . At the level of the action, it simply amounts to split the Lagrangian of usual  $\text{QED}_4$  (3.1) into two parts and give two different dimensions to the spinor and vector fields, *i.e.*, schematically

$$S_{\text{QED}_{d_\gamma, d_e}} \equiv \int d^{d_e} x \left[ \bar{\Psi}_i (i\not{D} - m) \Psi^i \right] + \int d^{d_\gamma} x \left[ -\frac{1}{4} F^{\mu\nu} F_{\mu\nu} - \frac{1}{2\xi} (\partial_\mu A^\mu)^2 \right]. \quad (3.10)$$

Obviously, one should be careful with Lorentz indices in the model (3.10) since the interactions are limited to the  $d_e$  plane. We will give a more precise definition of this action in the next sections, see (3.12). The first trivial example of such model is to take the same dimension for fermions and bosons, *e.g.*,  $d_\gamma = d_e = 4$ , *i.e.*,  $\text{QED}_{4,4}$  which recovers  $\text{QED}_4$  see (3.1). A less trivial example is to take  $d_e = d_\gamma = 3$ , *i.e.*,  $\text{QED}_{3,3}$  that we denote  $\text{QED}_3$ . In this case, the coupling acquires a non-zero canonical dimension. Indeed, simple power counting on the action (3.10) yields in arbitrary dimensions

$$[\Psi] = \frac{d_e - 1}{2}, \quad [A] = \frac{d_\gamma - 2}{2}, \quad [e] = 2 - \frac{d_\gamma}{2}, \quad [m] = 1, \quad [\xi] = 0, \quad (3.11)$$

which, in  $\text{QED}_3$  implies  $[e] = 1/2$ , so that  $\alpha = e^2/4\pi$  has the dimension of a mass, making the theory superrenormalizable and therefore asymptotically free. Therefore, in  $\text{QED}_3$ ,  $\alpha$  is not suitable to be the “small parameter” and one has to choose another perturbative parameter, which is usually  $1/N_f$ , *i.e.*, considering the number of fermion-field flavors to be large. This is the so-called large- $N_f$  expansion technique, see [117] for a review. We will keep this model for the next chapter that will be devoted to the study of  $\text{QED}_3$  and some of its bosonic and supersymmetric variants using large- $N_f$  techniques. In the rest of this chapter we focus on the case  $d_\gamma = 4$ , *i.e.*,  $\text{QED}_{4, d_e}$  such that we keep the canonical dimension  $[e] = 0$ . This leads to the third prominent example of reduced QED models, in which fermions are confined in a  $d_e = 2 + 1$  plane, interacting via photons that are  $d_\gamma = 3 + 1$  dimensional, *i.e.*,  $\text{QED}_{4,3}$ , see figure 3.1. Since fermions are confined on a plane, the out of plane photons propagates freely, *i.e.*, are non-interacting. As we shall see in the following, this model is particularly accurate to describe electronic interactions in graphene [26, 27], and more generally Dirac planar liquids.

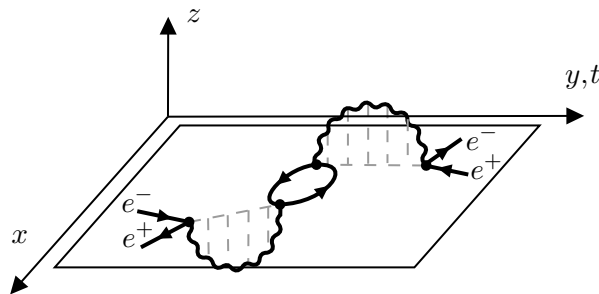


Figure 3.1: Illustration of an interaction event in  $\text{QED}_{4,3}$ . Electrons and positrons are confined on the  $d_e = 2 + 1$  plane  $(x, y, t)$  and interact via photons that eventually exit the plane in one extra dimension  $(z)$ . Photons propagates freely (no interactions) outside the plane  $(x, y, t)$ . Note that  $t$  and  $y$  axis are shrunk together for illustration purposes, the true event living on a  $3 + 1 = 4$  dimensional space.

Historically, the reduced  $\text{QED}_{d_e, d_\gamma}$  model (3.10) has been introduced motivated by the study of dynamical chiral symmetry breaking in brane-world theories, see, *e.g.*, [118, 119]). Soon after, a first application was devoted to the specially important case of conformal  $\text{QED}_{4,3}$  (also known as pseudo-QED from [120] and mixed-dimensional QED from the recent [121]) in relation with graphene [122]. Indeed, in condensed matter physics, an emergent relativity appears at low energies for systems with two stable Fermi points, see, *e.g.*, the textbook [123]. This is the case of pure (undoped) graphene, a one-atom thick layer of graphite, see, *e.g.*, [87, 124–126] for reviews. In such models, the quasiparticle spectrum is Dirac-like and massless at low-energies [127, 128]. Indeed,  $\text{QED}_{4,3}$  describes graphene in very particular energy conditions. More precisely, the renormalization group approach of [129] revealed the existence of a low energy (infrared) Lorentz invariant fixed point for graphene. Approaching this fixed point, electrons renormalize, *i.e.*, are dressed (shielded) by a cloud of other electrons and photons to become a collective electronic excitation called *quasiparticle*. These new quasi-electrons are the relevant degrees of freedom at low energy. Miraculously, the quasi-electrons are described by exactly the same dynamics as for bare electrons (the  $\text{QED}_{4,3}$  theory), but with different (renormalized) parameters. Flowing down from high to low energy in graphene, the speed of the (quasi)electrons, characterized by the Fermi velocity,  $v_F$ , flows to the velocity of light,  $c \approx 300v_F$ . Similarly, the fine structure constant of graphene,  $\alpha_g = e^2/4\pi\epsilon_0\hbar v_F$ , which is of order one, flows to the usual high-energy fine structure constant,  $\alpha = 1/137$ . These allow us to consider  $\text{QED}_{4,3}$  in its full relativistic (Lorentz invariant) form, and work in the natural units  $\hbar = c = 1$ . In short, relativistic  $\text{QED}_{4,3}$  seems to be the appropriate field theory to describe an ideally pure graphene sheet cooled down to very low temperatures, where (quasi-)electrons move at relativistic speeds, which simplifies tremendously the computations.

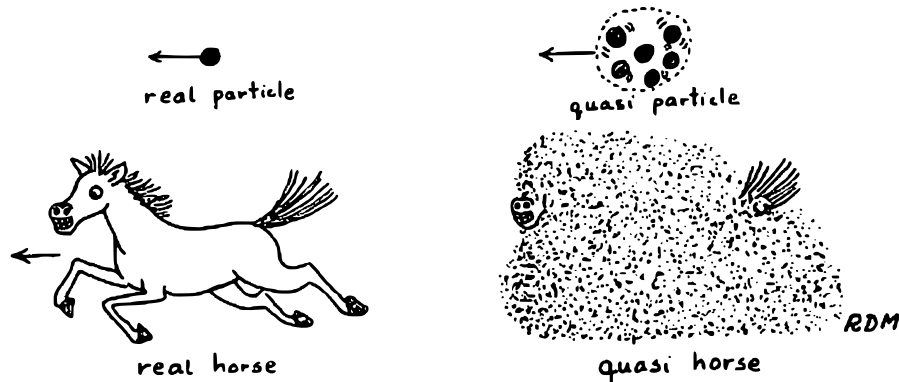


Figure 3.2: “Quasi particle concept” from R. Mattuck [130].

In this context, we compute theoretically several physical quantities of interest. The first one is the *optical conductivity* of graphene in the low energy regime, which is directly related to the physical (gauge invariant) *polarization operator of the photon*,  $\Pi(p^2)$ . This polarization admits corrections, and we will compute the physical (gauge-invariant) and universal (scale-invariant) first *quantum correction factor*,  $C_\gamma$ , which is a pure number, *i.e.*, a fundamental constant of graphene. As we will see in the following, our results compare accurately with optical experiments. Another quantity of interest is the *anomalous dimension of the electron mass*,  $\gamma_m$ , which is also physical and universal. This quantity is directly related to the phenomenon of dynamical mass generation in graphene. Indeed, since we consider a relativistic theory with a vanishing rest mass for the electrons, one natural question is to ask if the renormalized (quasi-)electrons are also massless or may become massive? Since the massless theory is chiral (or flavor) invariant, the appearance of a radiatively generated massive term breaks the chiral symmetry. One refers to this phenomenon as dynamical chiral/flavor symmetry breaking, sometimes shortened in the literature as  $\text{D}\chi\text{SB}$ . We will see in the following that the answer to this question depends on the coupling ( $\alpha_r$ ) considered and also on the number of fermions ( $N_f$ ). Indeed, for a given  $N_f$ , the coupling has to be large enough for dynamical electron mass generation to occur, which in turn implies that  $N_f$  has to be small enough. Therefore, this non-perturbative mechanism



relies on the existence of a critical coupling constant,  $\alpha_c$ , which is such that for  $\alpha_r < \alpha_c$  fermions are massless (assuming chiral invariance), while for  $\alpha_r > \alpha_c$  a dynamical fermion mass is generated at a given number of fermion flavors  $N_f$  (and chiral symmetry is dynamically broken). Alternatively, in the limit  $\alpha_c \rightarrow \infty$ , a dynamical mass is generated for  $N_f < N_c$  where  $N_c$  is the critical number of fermion flavors. Such a dynamical mass generated is directly determined by the so-called Miransky scaling as a function of the critical coupling, which is itself a function of the number of flavor  $N_f$ , *i.e.*,  $m_{\text{dyn}} \propto \exp(-2\pi/\sqrt{\alpha_r/\alpha_c - 1})$  [131]. The knowledge of  $\alpha_c$  and  $N_c$  therefore provides precious information on the phase structure of such gauge theories. See figure 3.3 for an illustration. In the condensed matter terminology, this mechanism corresponds to a (semi) metal to (excitonic) insulator transition, whereby a dynamical gap is generated at strong coupling and controlled by some parameters. This implies the opening of a tunable bandgap in the system and could lead, *e.g.*, to the development of graphene-based transistors [132], provided that one finds an experimental way to change on demand the control parameters, *i.e.*,  $\alpha_r$  and/or  $N_f$ . Such transistors could lead to groundbreaking applications, since graphene exhibits high performance conductivity, thermal dissipation, mechanical properties etc. [133]

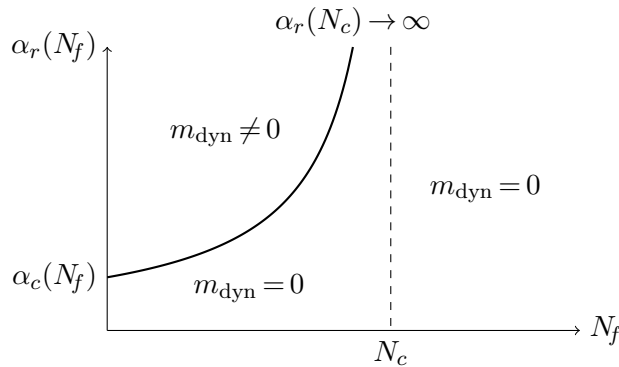


Figure 3.3: Phase diagram of  $\text{QED}_{d_\gamma, d_e}$  in the  $(\alpha_r, N_f)$  plane. Note that,  $m_{\text{dyn}} = 0$  implies a (semi-)metallic gapless phase while  $m_{\text{dyn}} \neq 0$  is a shorthand for  $m_{\text{dyn}} \propto \exp(-2\pi/\sqrt{\alpha_r/\alpha_c(N_f) - 1}) \neq 0$  and implies an (excitonic) insulating gaped phase.

To pursue with the motivations for reduced QED, it has been shown in [134] that it exists a mapping between  $\text{QED}_{4,3}$  and the well known three-dimensional QED ( $\text{QED}_3$ ) in the large- $N_f$  limit (where  $N_f$  is the number of Dirac spinors — see also [117] for a review on large- $N_f$  quantum field theories) which is a celebrated effective field theory for planar condensed matter physics systems exhibiting Dirac-like low-energy excitations such as, *e.g.*, high- $T_c$  superconductors [135–138], and quantum antiferromagnets [139]. The  $\text{QED}_{4,3}$  model also captures some universal features of a broader range of so-called planar Dirac liquids that have been discovered experimentally during the last decade and are under active study such as, *e.g.*, artificial graphene-like materials [140], surface states of topological insulators [141] quantum Hall effect [121, 142] and half-filled fractional quantum Hall systems [143].

Theoretically, there has been rather extensive studies of  $\text{QED}_{4,3}$  during the last decade with primary applications to Dirac liquids, *e.g.*, their transport and spectral properties [144–150] and dynamical symmetry breaking [134, 151] which we will focus on at the end of this chapter (see also [152] for a review on these topics). From a more field-theoretic point of view, the model was shown to be unitary [153], its properties were studied under the Landau-Khalatnikov-Fradkin transformation [154, 155] as well as under duality transformations [156]. Renewed interest in the model and its formal properties was triggered by the study [157] of interacting boundary conformal field theories, see, *e.g.*, [158–162] and supersymmetric extensions constructed and analyzed in [163, 164].

As for the study of dynamical mass generation in gauge theories, in the last four decades, the standard approaches were either based on lattice simulations [165–170] or solving partially the Schwinger-Dyson (SD) equations, see [171] for an early detailed review as well as the manuscripts [172, 173]. See



also [174] and references therein for a more recent publication. While initial interests were towards four-dimensional theories, the importance of QED<sub>3</sub> (and its large- $N_f$  limit with no running coupling) was recognized very early [175–177] because of its simpler UV structure and its similarities with Quantum Chromodynamics (QCD). Indeed, because of the absence of running of their coupling constants, QED<sub>4,3</sub> and large- $N_f$  QED<sub>3</sub> may be referred to as “standing” gauge theories. In contrast, QED<sub>4</sub> has a running of the coupling constant. It is only in the quenched approximation (where fermion loops are neglected) that the coupling constant of QED<sub>4</sub> does not renormalize. Nevertheless, because of the formidable complexity of the task of solving the SD equations, calculations were generally carried out only at the leading order (LO) in the coupling constant [131] or by including non-perturbative ansätze for the vertex function in one-loop-like SD equations [178–180]. Often, the resulting solutions displayed residual gauge variance, which is unsatisfactory for a physical quantity such as a critical coupling. Following early multi-loop works of Nash [181] and Kotikov [182, 183], a complete gauge-invariant prescription up to next-to-leading (NLO) of the  $1/N_f$ -expansion for QED<sub>3</sub> appeared only recently in [184] and [185, 186] (see also [187] for a recent review). In [134] the results were then mapped to QED<sub>4,3</sub>, thereby extending the LO results of [118] to the NLO in  $\alpha$ . The gauge-invariant prescriptions found in [184] and [186] for large- $N_f$  QED<sub>3</sub> alleviate doubts about the validity of the SD equation approach, though a similar prescription still has to be implemented for QED<sub>4</sub>. Considering the complexity of the calculations, simpler approaches are worthwhile investigating. An argument often invoked in the recent literature on QED<sub>3</sub>, see, *e.g.*, [188–197] (see also [198] for a review), is the fact that a fermion quadrilinear operator becomes relevant at criticality (this has actually been noted in the early literature on four-dimensional models, see, *e.g.*, [199–203]). The computation of the anomalous dimension of the corresponding composite operator allows then to derive a marginality crossing equation — as referred to in [196–198] — in order to extract the value of the critical coupling. Actually, as noticed in [184], the SD gap equation incorporates such a criterion in a rather simple and efficient way, *i.e.*, via the mass anomalous dimension (the anomalous dimension of the fermion bilinear mass operator) which is a gauge-invariant quantity governing the ultraviolet (UV) asymptotic behavior of the fermion propagator [204–207] (see also the textbook [208]).

The chapter is organized as follows. In section 3.2 we present the model, the perturbative setup as well as our renormalization conventions. In section 3.3, we present the complete one and two-loop calculations in the general model of reduced QED<sub>4, $d_e$</sub> . This includes the computation of the photon polarization  $\Pi$  as well as the field and mass anomalous dimensions, *i.e.*,  $\gamma_\Psi$  and  $\gamma_m$  at the second order in the small coupling expansion, *i.e.*, at  $O(\alpha^2)$ . This allows us to recover, in section 3.4, the full two-loop results for the subcases of QED<sub>4</sub> and QED<sub>4,3</sub> thereby generalizing recent results in QED<sub>4,3</sub> [161] and recovering well known ones in QED<sub>4</sub> (see the lectures [61]). We will discuss the optical conductivity of graphene and also recover the results of QED<sub>3</sub> in the large- $N_f$  expansion via mapping [134]. Then in the subsection 3.4.4 we will analyze the special case of a parity-odd electron mass term and clarify the different gamma matrices representations that we use in this manuscript, in dimensions 3+1 and 2+1. In section 3.5, the critical properties of the model are then analyzed. The gap equation is derived from the SD equations, and applied to QED<sub>4,3</sub> and QED<sub>4</sub>, where both the quenched and unquenched cases are provided, leading to gauge-dependant results. Following [184], we then construct a semi-phenomenological gap equation allowing us to study the critical properties of QED<sub>4, $d_e$</sub>  in a gauge invariant way. In the case of QED<sub>4,3</sub>, we straightforwardly recover the results of [134] for the NLO critical coupling and flavor number. As for QED<sub>4</sub>, our approach is semi-phenomenological, but our results are in good quantitative agreement with those obtained from numerical solutions of SD equations, see, *e.g.*, [172, 174]. The conclusion is given in section 3.6. As an Appendix, we provide in section 3.A the complete three-loop results that we derived for the QED<sub>4</sub> model.

## 3.2 The QED<sub>d<sub>γ</sub>,d<sub>e</sub></sub> model, conventions, and renormalization setup

### 3.2.1 Model

In Minkowski space, the QED<sub>d<sub>γ</sub>,d<sub>e</sub></sub> action [118, 144, 147] including (in order to compute  $\gamma_m$ ) a bare (parity-even<sup>1</sup>) fermion mass reads

$$S_{\text{QED}_{d_\gamma, d_e}} = \int d^{d_e} x [\bar{\Psi}_i (i\gamma^{\mu_e} D_{\mu_e} - m) \Psi^i] + \int d^{d_\gamma} x \left[ -\frac{1}{4} F^{\mu_\gamma \nu_\gamma} F_{\mu_\gamma \nu_\gamma} - \frac{1}{2\xi} (\partial_{\mu_\gamma} A^{\mu_\gamma})^2 \right], \quad (3.12)$$

where  $\Psi_i$  are  $N_f$  flavors of 4-component Dirac spinors ( $i = 1, \dots, N_f$ ) in  $d_e$  dimensions ( $\mu_e = 0, 1, \dots, d_e - 1$ ) of mass  $m$ , while the gauge field  $A^{\mu_\gamma}$  is  $d_\gamma$ -dimensional ( $\mu_\gamma = 0, 1, \dots, d_\gamma - 1$ ) with  $d_e \leq d_\gamma$ . The interactions are only allowed on the  $d_e$  subspace (the fermionic “plane”), such that the covariant derivative is defined as

$$D_{\mu_e} = \partial_{\mu_e} + ieA_{\mu_e}, \quad (3.13)$$

where it is understood that  $A_{\mu_e}$  are the  $d_e$  components of the gauge field, *i.e.*,  $A_{\mu_e}(x^{\mu_\gamma} = 0, x^{\mu_e})$ . In the following, we will use dimensional regularization and parameterize the dimensions as

$$d_\gamma = 4 - 2\varepsilon_\gamma, \quad d_e = 4 - 2\varepsilon_e - 2\varepsilon_\gamma, \quad (3.14)$$

where  $\varepsilon_\gamma$  is the regulator which is such that  $\varepsilon_\gamma \rightarrow 0$  for QED<sub>4,d<sub>e</sub></sub> while  $\varepsilon_e = (d_\gamma - d_e)/2$ . Note that the use of dimensional regularization preserves symmetries that are important to us for computations purposes, like translational invariance, see Appendix A.

Before going into computations, the mixed dimensional action (3.12) can be simplified and expressed fully from the point of view of the fermionic plane. Indeed, since photons propagate freely (no interactions with fermions) outside the plane, we are able to integrate exactly over all possible photonic propagations paths and project the result on the fermionic plane to obtain an effective, non-local, photon propagator living in the fermionic plane. See figure 3.4 for an illustration.

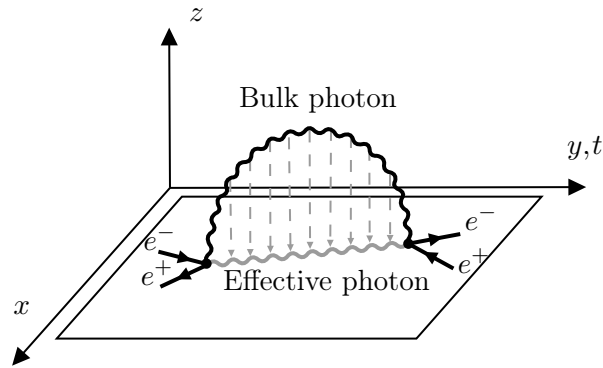


Figure 3.4: Illustration in QED<sub>4,3</sub> of the projection of a  $d_\gamma = 3+1$  ( $x, y, z, t$ ) free bulk photon onto the  $d_e = 2+1$  ( $x, y, t$ ) plane of interacting electrons. Note that  $t$  and  $y$  axis are shrunk together for illustration purposes.

Performing the exact integration over the free degrees of freedom of the photons in arbitrary dimension yields the following action

$$S_{\text{QED}_{d_\gamma, d_e}} = \int d^{d_e} x \left[ \bar{\Psi}_i (i\mathcal{D} - m) \Psi^i - \frac{1}{4} F^{\mu\nu} \mathcal{D} F_{\mu\nu} + \frac{1}{2\xi} A^\mu \mathcal{D} \partial_\mu \partial_\nu A^\nu \right], \quad (3.15)$$

<sup>1</sup>The parity-odd case is treated separately in subsection 3.4.4

where all Lorentz indices now run on the same  $d_e$  spacetime plane such that we dropped all the  $e$  indices for convenience, *i.e.*,  $\{\mu_e, \nu_e\} \rightarrow \{\mu, \nu\} = 0, \dots, d_e - 1$ . The field  $A^\mu$  now describes the effective (reduced) photons projected on the fermionic  $d_e$ -dimensional plane. Moreover, the reduced gauge-fixing parameter reads

$$\tilde{\xi} = \varepsilon_e + (1 - \varepsilon_e)\xi. \quad (3.16)$$

The model (3.15) is build from the differential operator  $\mathcal{D}$  reading

$$\mathcal{D} = \frac{(4\pi)^{2\varepsilon_e}}{\Gamma(1 - \varepsilon_e)(-\square)^{\varepsilon_e}}, \quad (3.17)$$

containing the d'Alembertian  $\square = \partial^\mu \partial_\mu$  with a fractional power. Note that the appearance of fractional d'Alembertian in (3.15) for  $\varepsilon_e > 0$  implies that the reduced theory is nonlocal. Fractional d'Alembertians (or Laplacians) appear in the field of fractional calculus, see [209] for an extended monograph.

An important remark is that since the action is  $d_e$ -dimensional, we now have  $d_e$  gamma matrices. In the case of QED<sub>4</sub>, *i.e.*,  $d_e = 4$ , it means that we have four gamma matrices, *e.g.*, the set described in (3.4), that we reproduce here for clarity

$$\gamma^0 = \begin{pmatrix} I_2 & 0 \\ 0 & -I_2 \end{pmatrix}, \quad \gamma^j = \begin{pmatrix} 0 & \sigma_j \\ -\sigma_j & 0 \end{pmatrix}, \quad (3.18)$$

where  $j = 1, 2, 3$  are the space indices and  $\sigma_j$  are the usual  $2 \times 2$  Pauli matrices. In striking contrast, in the case of QED<sub>4,3</sub>, *i.e.*,  $d_e = 3$ , there are three gamma matrices. A common representation is the set of  $4 \times 4$  matrices

$$\gamma^0 = \begin{pmatrix} \sigma_3 & 0 \\ 0 & -\sigma_3 \end{pmatrix}, \quad \gamma^1 = i \begin{pmatrix} \sigma_1 & 0 \\ 0 & -\sigma_1 \end{pmatrix}, \quad \gamma^2 = i \begin{pmatrix} \sigma_2 & 0 \\ 0 & -\sigma_2 \end{pmatrix}. \quad (3.19)$$

An important remark is that, in the three-dimensional case, it turns out that a smaller,  $2 \times 2$ , representation is possible and leads to different results as it amounts to consider an action that is different, *i.e.*, that may contain a parity-odd mass term. To avoid this, in the following, we will not specify the representation and just consider that for any dimension  $d_e$  of interest, it exists a set of gamma matrices of size  $4 \times 4$  that realizes the Clifford algebra. In this case, there is no subtlety and the mass term is parity preserving. These specificities will be discussed in detail in the devoted section 3.4.4, devoted to the parity-odd mass term and the other possible representation. In the rest of the chapter, our computations will anyway be performed without specifying the representation that we are using.

### 3.2.2 Perturbative setup

#### Feynman rules

From the action (3.15), the Feynman rules read

$$S_0(p) = \langle \bar{\Psi}(-p)\Psi(p) \rangle_0 = \begin{array}{c} \longrightarrow \\ p \end{array} = \frac{i}{\not{p} - m}, \quad (3.20a)$$

$$\Gamma_0^\mu = \langle A^\mu(p)\bar{\Psi}(p_1)\Psi(p_2) \rangle_0 = \begin{array}{c} \mu \text{ --- wavy line --- } \bullet \\ \swarrow \searrow \end{array} = -ie\gamma^\mu, \quad (3.20b)$$

$$D_0^{\mu\nu}(p) = \langle A^\mu(-p)A^\nu(p) \rangle_0 = \begin{array}{c} \mu \text{ --- wavy line --- } p \text{ --- wavy line --- } \nu \end{array} = \frac{i}{(4\pi)^{\varepsilon_e}} \frac{\Gamma(1 - \varepsilon_e)}{(-p^2)^{1 - \varepsilon_e}} \left( g^{\mu\nu} - (1 - \tilde{\xi}) \frac{p^\mu p^\nu}{p^2} \right). \quad (3.20c)$$

Together with the usual rule that each fermion loop should give an additional factor  $-1$  to the diagram considered. Note that the Feynman rules (3.20) are for  $N_f = 1$ , *i.e.*, without indices on the  $\Psi$  field. In

order to generalize for  $N_f$  fields, we are supposed to introduce trivial delta functions in (3.20a) and (3.20b) such that  $\delta_{\sigma\sigma} = N_f$ . This is the simplest way to proceed for automated calculations. However, for hand computations, we can equivalently drop all delta functions associated to  $\Psi$  replicas and simply add a factor  $-N_f$  for each fermion loop in a diagram instead of only  $-1$ . Note also that we hide the trivial identity matrix  $I_4$  next to the mass  $m$  and we make the usual notation abuse for the fermion propagator (3.20a), with inverse tensor notations used. Indeed, multiplying the numerator and denominator by the matrix  $(\not{p} + m)$  read  $S_0(p) = i(\not{p} + m)/(p^2 - m^2)$ , recalling the usual notations and definitions for the momentum

$$p^2 = p^\mu p_\mu, \quad |p| = \sqrt{p^2}, \quad \not{p} = \gamma^\mu p_\mu, \quad \not{p}^2 = p^2, \quad \frac{1}{\not{p}} = \frac{\not{p}}{p^2}, \quad p_E = \sqrt{-p^2} = i|p|, \quad k \cdot p = k^\mu p_\mu, \quad (3.21)$$

where  $p_E$  is the Euclidean momentum and  $p^\mu$  the Minkowski four-momentum, related via Wick rotation. In (3.20), the photon propagator (3.20c) is therefore reduced ( $d_e$ -dimensional), and is now non-local after integrating out the free photons degrees of freedom present on the bulk in  $d_\gamma - d_e$  dimensions. Let us remark that in the case of QED<sub>4</sub> ( $\varepsilon_e = 0$ ), the photon propagator reduces to its familiar form, while in the case of QED<sub>4,3</sub> ( $\varepsilon_e = 1/2$ ) the photon propagator acquires a branch cut reading

$$D_{0 \text{ QED}_4}^{\mu\nu}(p) = \frac{i}{-p^2} \left( g^{\mu\nu} - (1 - \xi) \frac{p^\mu p^\nu}{p^2} \right), \quad (3.22a)$$

$$D_{0 \text{ QED}_{4,3}}^{\mu\nu}(p) = \frac{i}{2\sqrt{-p^2}} \left( g^{\mu\nu} - \frac{1 - \xi}{2} \frac{p^\mu p^\nu}{p^2} \right). \quad (3.22b)$$

This inverse square root momentum dependence is responsible for the appearance of Feynman diagrams with non-integer indices and is a major source of technical difficulty to perform the integrations. As we will see in the next chapter, a similar momentum dependence can be found for QED<sub>3</sub> in the large- $N_f$  limit due to the infrared softening of the photon propagator. This is the essence of the existence of the mapping [134] between QED<sub>4,3</sub> and QED<sub>3</sub>.

### Numerator algebra

As for the numerator algebra, after suitable projections and contractions, we will only be left with traces over gamma matrices to compute. As discussed below the equation (3.18), we will not consider any specific representation. We will consider that we have an arbitrary number  $d_e$  of  $4 \times 4$  gamma matrices satisfying the Clifford algebra (3.3). In this case, the basic trace identities read

$$\text{Tr}(\gamma^\mu) = 0, \quad \text{Tr}(I_4) = 4, \quad \text{Tr}(\gamma^\mu \gamma^\nu) = 4g^{\mu\nu}. \quad (3.23)$$

From there, all traces with more than two matrices can be calculated with the following simple recursive algorithm

$$\text{Tr}(\gamma^{\mu_1} \gamma^{\mu_2} \dots \gamma^{\mu_m}) = \sum_{i=2}^m (-1)^i g^{\mu_1 \mu_i} \text{Tr}(\cancel{\gamma^{\mu_1}} \gamma^{\mu_2} \dots \cancel{\gamma^{\mu_i}} \dots \gamma^{\mu_m}), \quad m > 2, \quad (3.24)$$

where  $\cancel{\gamma^{\mu_i}}$  means removing  $\gamma^{\mu_i}$ . Dirac gamma traces can then be calculated simply in terms of the metric tensor, the size of the matrix representation, here 4, and eventually the dimension  $d_e$  appearing from Lorentz indices contractions since  $g_\mu^\mu = d_e$ . Here is an example with  $m = 6$

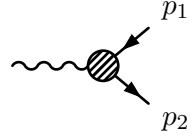
$$\begin{aligned} \text{Tr}(\gamma^\kappa \gamma^\lambda \gamma^\mu \gamma^\nu \gamma^\rho \gamma^\sigma) &= g^{\kappa\lambda} \text{Tr}(\gamma^\mu \gamma^\nu \gamma^\rho \gamma^\sigma) - g^{\kappa\mu} \text{Tr}(\gamma^\lambda \gamma^\nu \gamma^\rho \gamma^\sigma) + g^{\kappa\nu} \text{Tr}(\gamma^\lambda \gamma^\mu \gamma^\rho \gamma^\sigma) \\ &\quad - g^{\kappa\rho} \text{Tr}(\gamma^\lambda \gamma^\mu \gamma^\nu \gamma^\sigma) + g^{\kappa\sigma} \text{Tr}(\gamma^\lambda \gamma^\mu \gamma^\nu \gamma^\rho) \\ &= 4g^{\kappa\lambda} \left( g^{\mu\nu} g^{\rho\sigma} - g^{\mu\rho} g^{\nu\sigma} + g^{\mu\sigma} g^{\nu\rho} \right) - 4g^{\kappa\mu} \left( g^{\lambda\nu} g^{\rho\sigma} - g^{\lambda\rho} g^{\nu\sigma} + g^{\lambda\sigma} g^{\nu\rho} \right) + 4g^{\kappa\nu} \left( g^{\lambda\mu} g^{\rho\sigma} - g^{\lambda\rho} g^{\mu\sigma} + g^{\lambda\sigma} g^{\mu\rho} \right) \\ &\quad - 4g^{\kappa\rho} \left( g^{\lambda\mu} g^{\nu\sigma} - g^{\lambda\nu} g^{\mu\sigma} + g^{\lambda\sigma} g^{\mu\nu} \right) + 4g^{\kappa\sigma} \left( g^{\lambda\mu} g^{\nu\rho} - g^{\lambda\nu} g^{\mu\rho} + g^{\lambda\rho} g^{\mu\nu} \right), \end{aligned} \quad (3.25)$$



which can be usefully contrasted with the QED<sub>4</sub> case

$$d_{\perp}^{\text{QED}_4}(p^2) = \frac{-i}{p^2} \frac{1}{1 - \Pi(p^2)}. \quad (3.33)$$

As for the coupling, the Dyson equation reads

$$\Gamma^{\mu}(p_1, p_2) = \langle A^{\mu}(p) \bar{\Psi}(p_1) \Psi(p_2) \rangle = \mu \text{ (diagram) } = -ie(\gamma^{\mu} + \Lambda^{\mu}(p_1, p_2)) \quad (3.34)$$


with  $\Lambda^{\mu}$  the vertex correction function. However, as we shall see in the following, this function is not needed in the perturbative approach thanks to the Ward identity that relates  $\Gamma^{\mu}$  and the dressed fermion propagator  $S(p)$ .

### 3.2.3 Renormalization setup

The usual renormalization conventions for QED are

$$A^{\mu} = Z_A^{1/2} A_r^{\mu}, \quad \Psi = Z_{\Psi}^{1/2} \Psi_r, \quad \xi = Z_{\xi} \xi_r, \quad e = \mu^{\varepsilon_{\gamma}} Z_e e_r, \quad m = Z_m m_r, \quad (3.35)$$

where  $r$  stands for renormalized, *i.e.*, finite, quantities. All the divergences are contained in the bare quantities as well as in the renormalization constants in the form of poles in  $\varepsilon_{\gamma}$ . We also use the additional definitions

$$\alpha = \frac{e^2}{4\pi}, \quad \bar{\alpha} = \frac{\alpha}{4\pi}, \quad Z_{\alpha} = Z_e^2, \quad \alpha = \mu^{2\varepsilon_{\gamma}} Z_{\alpha} \alpha_r, \quad (3.36)$$

where  $\bar{\alpha}$  is the reduced, bare coupling constant, which is the natural expansion parameter of the theory. Moreover, we introduced the renormalization scale  $\mu$ , so that the coupling  $\alpha$  remains massless in  $d_{\gamma} = 4 - 2\varepsilon_{\gamma}$ . The latter is related to the corresponding parameter  $\bar{\mu}$  in the modified minimal subtraction ( $\overline{\text{MS}}$ ) scheme with the help of

$$\bar{\mu}^2 = 4\pi e^{-\gamma_E} \mu^2, \quad (3.37)$$

with  $\gamma_E$  the Euler constant. Notice that, in the  $\overline{\text{MS}}$ -scheme, the renormalization constants are Laurent series in  $\varepsilon_{\gamma}$  and can be written as

$$Z_X = 1 + \delta Z_X, \quad \delta Z_X = \sum_{l=1}^{\infty} \delta Z_{lX} \bar{\alpha}_r^l = \sum_{l=1}^{\infty} \sum_{j=1}^l Z_X^{(l,j)} \frac{\bar{\alpha}_r^l}{\varepsilon_{\gamma}^j} \quad (X = \{A, \Psi, m\}). \quad (3.38)$$

From the above definitions, the relation between the bare and renormalized dressed propagators and vertices are

$$D^{\mu\nu} = Z_A D_r^{\mu\nu}, \quad S = Z_{\Psi} S_r, \quad \Gamma^{\mu} = Z_{\Gamma} \Gamma_r^{\mu}, \quad (3.39)$$

where  $Z_{\Gamma}$  is a shorthand for  $Z_{\Gamma} = Z_{\alpha}^{-1/2} Z_{\Psi}^{-1} Z_A^{1/2}$ . Note that we omit the functional dependencies and that for a bare quantity  $X$ , we have in general

$$X(p, \alpha, \xi) = Z_X [p, \alpha_r(\mu), \xi_r(\mu)] X_r [p, \alpha_r(\mu), \xi_r(\mu)] \quad (3.40)$$

such that all renormalized quantities may “run” with the renormalization scale  $\mu$ . In particular,  $\alpha_r$  taken at the energy scale of the electron mass, is exactly the fine structure constant and is valued  $\alpha_r \approx 1/137$ .

An important addition to these definitions comes from an important Ward identities of the theory [110]

$$ie p_{\mu} \Gamma^{\mu}(p_1, p_2) = S^{-1}(p_2) - S^{-1}(p_1), \quad (3.41)$$

relating  $\Gamma^\mu$  is the dressed vertex function and  $S$  the dressed fermion propagator. After taking the limit  $p \rightarrow 0$ , it leads to the identities

$$Z_\Gamma = Z_\Psi^{-1}, \quad Z_\alpha = Z_A^{-1}, \quad Z_\xi = Z_A. \quad (3.42)$$

Therefore, only 3 renormalization factors are independent, and we choose  $\{Z_A, Z_\Psi, Z_m\}$  such that the new renormalization setup simplifies to

$$A^\mu = Z_A^{1/2} A_r^\mu, \quad \Psi = Z_\Psi^{1/2} \Psi_r, \quad \xi = Z_A \xi_r, \quad \alpha = \mu^{2\varepsilon_\gamma} Z_A^{-1} \alpha_r, \quad m = Z_m m_r, \quad (3.43a)$$

$$D^{\mu\nu} = Z_A D_r^{\mu\nu}, \quad S = Z_\Psi S_r, \quad \Gamma^\mu = Z_\Psi^{-1} \Gamma_r^\mu. \quad (3.43b)$$

From the definitions of the renormalized correlations functions (3.43b) and using previous results, we can simply derive the dressed renormalized self-energy, polarization, and vertex correction

$$\Pi_r = 1 - (1 - \Pi) Z_A, \quad (3.44a)$$

$$\Sigma_{Vr} = 1 - (1 - \Sigma_V) Z_\Psi, \quad (3.44b)$$

$$\Sigma_{Sr} = 1 - (1 - \Sigma_S) Z_\Psi Z_m, \quad (3.44c)$$

$$\Lambda_r^\mu = -\gamma^\mu - (\gamma^\mu - \Lambda^\mu) Z_\Psi, \quad (3.44d)$$

where we used the projectors (3.28) to separate  $\Sigma_{Vr}$  from  $\Sigma_{Sr}$ .

From there, the multiplicative renormalization constants  $Z_A$ ,  $Z_\Psi$  and  $Z_m$  can be computed respectively from the photon polarization and the two fermion self-energy parts ( $V/S$ ) by remarking that, to ensure finiteness of the above identities (3.44), we should necessarily have

$$(1 - \Pi) Z_A = \text{finite}, \quad (1 - \Sigma_V) Z_\Psi = \text{finite}, \quad \frac{1 + \Sigma_S}{1 - \Sigma_V} Z_m = \text{finite}. \quad (3.45)$$

where finite means no poles in  $\varepsilon_\gamma$ . One can clarify these identities by using the pole operator  $\mathcal{K}$  on both sides of the equations (3.45). Indeed,  $\mathcal{K}(x)$  is the operator that truncates the Laurent series in  $\varepsilon_\gamma$  to keep only the divergent part, *i.e.*, the poles of the series. These expressions can be extended in perturbation theory and completely fixes, order by order, the renormalization constants  $Z_A$ ,  $Z_\Psi$  and  $Z_m$ . At one loop, they read

$$Z_A = 1 + \mathcal{K}(\Pi_1) + \mathcal{O}(\bar{\alpha}_r^2), \quad (3.46a)$$

$$Z_\Psi = 1 + \mathcal{K}(\Sigma_{1V}) + \mathcal{O}(\bar{\alpha}_r^2), \quad (3.46b)$$

$$Z_m = 1 - \mathcal{K}(\Sigma_{1SV}) + \mathcal{O}(\bar{\alpha}_r^2), \quad (3.46c)$$

where we momentarily defined  $\Sigma_{1SV} = \Sigma_{1S} + \Sigma_{1V}$ . At two loops, the expansion reads

$$Z_A = 1 + \mathcal{K}(\Pi_1) + \mathcal{K}(\Pi_2) + \mathcal{K}(\Pi_1 \mathcal{K}(\Pi_1)) + \mathcal{O}(\bar{\alpha}_r^3), \quad (3.47a)$$

$$Z_\Psi = 1 + \mathcal{K}(\Sigma_{1V}) + \mathcal{K}(\Sigma_{2V}) + \mathcal{K}(\Sigma_{1V} \mathcal{K}(\Sigma_{1V})) + \mathcal{O}(\bar{\alpha}_r^3), \quad (3.47b)$$

$$Z_m = 1 - \mathcal{K}(\Sigma_{1SV}) - \mathcal{K}(\Sigma_{2SV}) + \mathcal{K}(\Sigma_{1S} \Sigma_{1SV}) - \mathcal{K}(\Sigma_{1SV}^2) + \mathcal{K}(\Sigma_{1SV} \mathcal{K}(\Sigma_{1SV})) + \mathcal{O}(\bar{\alpha}_r^3), \quad (3.47c)$$

where we observe an interesting asymmetry between  $S$  and  $V$  self-energies. This technique allows avoiding computing extra counter-terms diagrams explicitly, they are generated directly from the expressions (3.47).

Once the renormalization functions are computed, the corresponding anomalous dimensions and beta function of the theory can be calculated in a standard way with the help of

$$\gamma_X = \frac{d \log Z_X}{d \log \mu} \quad (X = \{A, \Psi, m\}), \quad \beta = \frac{d \bar{\alpha}_r}{d \log \mu} = -2\varepsilon_\gamma \bar{\alpha}_r + \gamma_A \bar{\alpha}_r, \quad (3.48)$$



where  $\beta \equiv \beta(\bar{\alpha}_r(\mu))$  characterizes the running of the coupling of theory with respect to the energy renormalization scale  $\mu$ . Also, substituting (3.38) in (3.48) yields

$$\gamma_X = \sum_{l=1}^{\infty} \gamma_{lX} \bar{\alpha}_r^l, \quad \gamma_{lX} = -2lZ_X^{(l,1)}, \quad (X = \{A, \Psi, m\}). \quad (3.49)$$

Note that the definitions (3.48) are chosen so that they allow to extract the scaling of the correlation functions with respect to the renormalization energy scale, *i.e.*,

$$D_r^{\mu\nu}(p) \sim p_E^{-2+2\varepsilon_e+\gamma_A}, \quad S_r(p) \sim p_E^{-1+\gamma_\Psi}, \quad m_r(p) \sim p_E^{1+\gamma_m}. \quad (3.50)$$

Additionally, from simple power counting [126], it is easy to show that the field anomalous dimension  $\gamma_A$  vanishes (as do the beta function) in QED<sub>4,3</sub>. We shall prove it perturbatively and comment on this behavior in the next sections.

### 3.3 General perturbative calculations up to two loops in QED<sub>4,d<sub>e</sub></sub>

In this section, we will compute all the renormalization-group functions of the general model QED<sub>4,d<sub>e</sub></sub>, up to two loops. This requires the computation of the polarization function for the photon, as well as the self-energy of the electron. From it, we will compute the gauge field anomalous dimension  $\gamma_A$  and the corresponding beta function, as well as the anomalous dimensions  $\gamma_\Psi$  and  $\gamma_m$ . This amounts to compute all the following diagrams

$$i\Pi^{\mu\nu}(p) = \mu \text{ [diagram 1]} + \mu \text{ [diagram 2]} + \mu \text{ [diagram 3]} + \nu + O(\alpha^3), \quad (3.51a)$$

$$-i\Sigma(p) = \text{[diagram 4]} + \text{[diagram 5]} + \text{[diagram 6]} + \text{[diagram 7]} + O(\alpha^3), \quad (3.51b)$$

which is the usual QED diagrammatic expansion for the photon polarization operator and the fermion self-energy up to two loops, *i.e.*, at  $O(\alpha^2)$ .

Let us note that  $\gamma_\Psi$  was already computed in [147] for QED<sub>4,d<sub>e</sub></sub> and we shall follow the notations of that paper. In particular, the following parameters will be useful

$$L_p = \log\left(\frac{-p^2}{\bar{\mu}^2}\right), \quad \bar{L}_p = L_p - \psi(2 - \varepsilon_e) + \psi(1), \quad K_1 = \frac{\Gamma^3(1 - \varepsilon_e)\Gamma(\varepsilon_e)}{\Gamma(2 - 2\varepsilon_e)}, \quad (3.52a)$$

$$\bar{\Psi}_1 = \psi(1 - \varepsilon_e) - \psi(1), \quad \bar{\Psi}_2 = \psi(\varepsilon_e) - 2\psi(1 - \varepsilon_e) + 2\psi(2 - 2\varepsilon_e) - \psi(1), \quad (3.52b)$$

where  $\psi(x)$  is the digamma function; see also Appendix A of [147] for the expansion of the relevant master integrals.

From [210], we recall that, in the  $\overline{\text{MS}}$ -scheme in the four-dimensional case, *i.e.*, for QED<sub>4</sub>, the anomalous dimensions can depend only on the Euler constant  $\gamma_E$  and the Riemann zeta function  $\zeta_n$ . However, in the QED<sub>4,3</sub> case, *i.e.*, in three dimensions, we expect new non-trivial transcendental numbers to occur, as illustrated in Appendix A.

In the following, we will provide the exact results and the  $\varepsilon_\gamma$ -expansion of individual diagrams contributing to the photon polarization  $\Pi$  and the electron  $\Sigma_V$  and  $\Sigma_S$  self-energies for arbitrary  $\varepsilon_e$ . Combined with (3.45) and (3.49), this will allow us to compute the renormalization constants and





Note that the first and last integrals are exactly zero by parity. Using the definitions of Appendix A, devoted to multi-loop integral computations in the Euclidean space, it can be written as

$$\Pi_1(p^2) = 2\mu^{2\varepsilon_\gamma} \frac{N_f e^2}{p_E^2} \frac{d_e - 2}{d_e - 1} \left[ j(d_e, p_E, 0, 1) - p^2 j(d_e, p_E, 1, 1) + j(d_e, p_E, 1, 0) \right], \quad (3.59)$$

from it, the exact result reads

$$\Pi_1(p^2) = -2N_f e^2 \mu^{2\varepsilon_\gamma} \frac{(-p^2)^{d_e/2-2}}{(4\pi)^{d_e/2}} \frac{d_e - 2}{d_e - 1} G(d_e, 1, 1), \quad (3.60)$$

where we switched back the external momentum  $p$  to Minkowski space with inverse Wick rotation. Then, it's  $\varepsilon_\gamma$ -expansion at arbitrary  $\varepsilon_e$  reads

$$\Pi_1(p^2) = -4\bar{\alpha} N_f \frac{1 - \varepsilon_e}{3 - 2\varepsilon_e} \left( \frac{4\pi}{-p^2} \right)^{\varepsilon_e} \frac{\Gamma^2(1 - \varepsilon_e) \Gamma(\varepsilon_e)}{\Gamma(2 - 2\varepsilon_e)} + \mathcal{O}(\varepsilon_\gamma), \quad (3.61)$$

which is a result unfortunately valid only, for QED<sub>4,3</sub>, *i.e.*,  $d_e = 3$  or equivalently  $\varepsilon_e = 1/2$ . In this case it yields a finite value

$$\Pi_1^{\text{QED}_{4,3}}(p^2) = -\frac{\bar{\alpha}}{\sqrt{-p^2}} \hat{\Pi}_1^{\text{QED}_{4,3}}, \quad \hat{\Pi}_1^{\text{QED}_{4,3}} = 2N_f \pi^2. \quad (3.62)$$

There is therefore nothing to renormalize here and leads to a trivial renormalization constant for the gauge field, *i.e.*,  $Z_A = 1 + \mathcal{O}(\bar{\alpha}_r^2)$ . In turn, the anomalous dimensions of the gauge field and the corresponding beta function of the QED<sub>4,3</sub> model can be computed from (3.48) and trivially reads

$$\gamma_A^{\text{QED}_{4,3}} = 0 + \mathcal{O}(\bar{\alpha}_r^2), \quad \beta^{\text{QED}_{4,3}} = -2\bar{\alpha}_r \varepsilon_\gamma + \mathcal{O}(\bar{\alpha}_r^3), \quad (3.63)$$

where  $-2\bar{\alpha}_r \varepsilon_\gamma$  is the trivial 0<sup>th</sup>-order (tree-level) value for the beta function. Since the beta function is trivial, the coupling is not running in QED<sub>4,3</sub>. We refer to this phenomenon as a ‘‘standing’’ gauge theory, as opposed to a theory where the coupling is ‘‘running’’, like in, *e.g.*, QED<sub>4</sub> as we will show in the next lines.

The fact that the result (3.61) is only valid for QED<sub>4,3</sub> is related to the fact that the coupling constant does not run in QED<sub>4,3</sub>. In striking contrast with QED<sub>4,3</sub>, we notice that (3.61) does not reproduce properly the pole structure of QED<sub>4</sub>. The correct result is obtained from (3.53) by first setting  $\varepsilon_e = 0$  and then performing the  $\varepsilon_\gamma$ -expansion. This yields

$$\Pi_1^{\text{QED}_4}(p^2) = -\bar{\alpha} \left[ \frac{4N_f}{3} \left( \frac{1}{\varepsilon_\gamma} - \frac{L_p}{3} \right) + \hat{\Pi}_1^{\text{QED}_4} + \mathcal{O}(\varepsilon_\gamma) \right], \quad \hat{\Pi}_1^{\text{QED}_4} = \frac{20N_f}{9}. \quad (3.64)$$

This non-commutativity of  $\varepsilon_e \rightarrow 0$  and  $\varepsilon_\gamma \rightarrow 0$  limits will also appear in the two-loop fermion self-energy diagrams with a fermion loop insertion (see 3.85a) thereby affecting the anomalous dimensions. We will discuss, in section 3.3.3, a way to obtain expansions valid in both QED<sub>4,3</sub> and QED<sub>3</sub>. From (3.64) and the definitions (3.46) and (3.48) it is straightforward to derive the first order renormalization constant for the gauge field in the QED<sub>4</sub> case,

$$\delta Z_A^{\text{QED}_4} = -\frac{4N_f}{3\varepsilon_\gamma} \bar{\alpha}_r. \quad (3.65)$$

Using (3.48), we derive the well known first order correction to the gauge field anomalous dimensions, that directly gives the first order correction to the QED<sub>4</sub> beta function. They both read

$$\gamma_A^{\text{QED}_4} = \frac{8N_f}{3} \bar{\alpha}_r + \mathcal{O}(\bar{\alpha}_r^2), \quad \beta^{\text{QED}_4} = -2\bar{\alpha}_r \varepsilon_\gamma + \frac{8N_f}{3} \bar{\alpha}_r^2 + \mathcal{O}(\bar{\alpha}_r^3). \quad (3.66)$$

### Fermion self-energy at one loop

Similarly, we now consider the one-loop fermion self-energy correction reading

$$-i\Sigma_1(p) = \text{Diagram} = \mu^{2\varepsilon_\gamma} \int [d^d k] \Gamma_0^\mu S_0(p-k) \Gamma_0^\nu D_{0\mu\nu}(k). \quad (3.67)$$

Using the Feynman rules (3.20) reads

$$\begin{aligned} -i\Sigma_1(p) &= \mu^{2\varepsilon_\gamma} \int [d^d k] (-ie\gamma^\mu) \frac{i}{\not{p}-\not{k}-m} (-ie\gamma^\nu) \frac{i}{(4\pi)^{\varepsilon_e}} \frac{\Gamma(1-\varepsilon_e)}{(-k^2)^{1-\varepsilon_e}} \left( g^{\mu\nu} - (1-\tilde{\xi}) \frac{k^\mu k^\nu}{k^2} \right) \\ &= \frac{\mu^{2\varepsilon_\gamma}}{(4\pi)^{\varepsilon_e}} \Gamma(1-\varepsilon_e) e^2 \int [d^d k] \left[ \frac{\gamma^\mu (\not{p}-\not{k}+m) \gamma_\mu}{(-k^2)^{1-\varepsilon_e} ((p-k)^2 - m^2)} - (1-\tilde{\xi}) \frac{\not{k}(\not{p}-\not{k}+m)\not{k}}{(-k^2)^{2-\varepsilon_e} ((p-k)^2 - m^2)} \right]. \end{aligned} \quad (3.68)$$

Using the parameterization (3.28), we extract the vector and scalar parts, perform the traces and then take the limit  $m=0$  without restricting the generality of the computation. This reads

$$\Sigma_{1V}(p) = i \frac{\mu^{2\varepsilon_\gamma}}{(4\pi)^{\varepsilon_e}} \Gamma(1-\varepsilon_e) e^2 (3-d_e-\tilde{\xi}) \left[ \int \frac{[d^d k] (k^2 p^2 - k^2 k \cdot p)}{(-k^2)^{2-\varepsilon_e} (p-k)^2} + \frac{2(1-\tilde{\xi})}{3-d_e-\tilde{\xi}} \int \frac{[d^d k] (k^2 k \cdot p - (k \cdot p)^2)}{(-k^2)^{2-\varepsilon_e} (p-k)^2} \right], \quad (3.69a)$$

$$\Sigma_{1S}(p) = i \frac{\mu^{2\varepsilon_\gamma}}{(4\pi)^{\varepsilon_e}} \Gamma(1-\varepsilon_e) e^2 (1-d_e-\tilde{\xi}+1) \int \frac{[d^d k]}{(-k^2)^{1-\varepsilon_e} (p-k)^2}. \quad (3.69b)$$

The integrals are then Wick rotated to Euclidean space, computed exactly using results of Appendix A and finally Wick rotated back, yielding the exact result

$$\Sigma_{1V}(p^2) = \frac{e^2}{(4\pi)^{d_\gamma/2}} \left( \frac{\mu^2}{-p^2} \right)^{\varepsilon_\gamma} \Gamma(1-\varepsilon_e) \frac{d_e-2}{2} \left( \frac{d_\gamma-d_e}{d_\gamma+d_e-4} - \xi \right) G(d_e, 1, 1-\varepsilon_e), \quad (3.70a)$$

$$\Sigma_{1S}(p^2) = \frac{e^2}{(4\pi)^{d_\gamma/2}} \left( \frac{\mu^2}{-p^2} \right)^{\varepsilon_\gamma} \Gamma(1-\varepsilon_e) \frac{d_\gamma+d_e-2-(d_\gamma-d_e-2)\xi}{2} G(d_e, 1, 1-\varepsilon_e). \quad (3.70b)$$

The resulting  $\varepsilon_\gamma$ -expansions at arbitrary  $\varepsilon_e$  then read

$$\begin{aligned} \Sigma_{1V}(p^2) &= \bar{\alpha} \left[ \left( \frac{\varepsilon_e}{2-\varepsilon_e} - \xi \right) \frac{1}{\varepsilon_\gamma} + \frac{2\varepsilon_e}{(2-\varepsilon_e)^2} - \left( \frac{\varepsilon_e}{2-\varepsilon_e} - \xi \right) \bar{L}_p \right. \\ &\quad \left. + \left( \frac{1}{2} \left( \frac{\varepsilon_e}{2-\varepsilon_e} - \xi \right) (\bar{L}_p^2 + 2\zeta_2 - 3\psi'(2-\varepsilon_e)) - \frac{2\varepsilon_e}{(2-\varepsilon_e)^2} \bar{L}_p + \frac{4\varepsilon_e}{(2-\varepsilon_e)^3} \right) \varepsilon_\gamma + \mathcal{O}(\varepsilon_\gamma^2) \right], \end{aligned} \quad (3.71a)$$

$$\begin{aligned} \Sigma_{1S}(p^2) &= \bar{\alpha} \left[ \left( \xi + \frac{3-\varepsilon_e}{1-\varepsilon_e} \right) \frac{1}{\varepsilon_\gamma} + \frac{1+\varepsilon_e+(1-\varepsilon_e)\xi}{(1-\varepsilon_e)^2} - \left( \xi + \frac{3-\varepsilon_e}{1-\varepsilon_e} \right) \bar{L}_p \right. \\ &\quad \left. + \left( \frac{1}{2} \left( \xi + \frac{3-\varepsilon_e}{1-\varepsilon_e} \right) (\bar{L}_p^2 + 2\zeta_2 - 3\psi'(1-\varepsilon_e)) - \frac{1+\varepsilon_e+(1-\varepsilon_e)\xi}{(1-\varepsilon_e)^2} \bar{L}_p + \frac{11-\varepsilon_e}{2(1-\varepsilon_e)^3} + \frac{5\xi}{2(1-\varepsilon_e)^2} \right) \varepsilon_\gamma + \mathcal{O}(\varepsilon_\gamma^2) \right], \end{aligned} \quad (3.71b)$$

where  $\bar{L}_p$  was defined in (3.52a) and  $\psi'(x)$  is the trigamma function. Note that all these results are valid in the general case  $\text{QED}_{4,d_e}$ . For completeness, we also provide these expansions in the  $\text{QED}_{4,3}$  case ( $\varepsilon_\gamma \rightarrow 0$  and  $\varepsilon_e = 1/2$ )

$$\Sigma_{1V}^{\text{QED}_{4,3}}(p^2) = \bar{\alpha} \left( \frac{\bar{\mu}^2}{-4p^2} \right)^{\varepsilon_\gamma} \left[ \frac{1-3\xi}{3\varepsilon_\gamma} + \left( \frac{10}{9} - 2\xi \right) + \left( \frac{112}{27} - 8\xi - \frac{7\pi^2}{36} (1-3\xi) \right) \varepsilon_\gamma + \mathcal{O}(\varepsilon_\gamma^2) \right], \quad (3.72a)$$

$$\Sigma_{1S}^{\text{QED}_{4,3}}(p^2) = \bar{\alpha} \left( \frac{\bar{\mu}^2}{-4p^2} \right)^{\varepsilon_\gamma} \left[ \frac{5+\xi}{\varepsilon_\gamma} + 4(4+\xi) + \left( 16(4+\xi) - \frac{7\pi^2}{12} (5+\xi) \right) \varepsilon_\gamma + \mathcal{O}(\varepsilon_\gamma^2) \right]. \quad (3.72b)$$

and, to fix notations, we also provide explicitly the well known QED<sub>4</sub> case ( $\varepsilon_\gamma \rightarrow 0$  and  $\varepsilon_e = 0$ )

$$\Sigma_{1V}^{\text{QED}_4}(p^2) = -\bar{\alpha}\xi \left( \frac{\bar{\mu}^2}{-p^2} \right)^{\varepsilon_\gamma} \left[ \frac{1}{\varepsilon_\gamma} + 1 + \frac{24 - \pi^2}{12} \varepsilon_\gamma + \mathcal{O}(\varepsilon_\gamma^2) \right], \quad (3.73a)$$

$$\Sigma_{1S}^{\text{QED}_4}(p^2) = \bar{\alpha} \left( \frac{\bar{\mu}^2}{-p^2} \right)^{\varepsilon_\gamma} \left[ \frac{3 + \xi}{\varepsilon_\gamma} + 2(2 + \xi) + \left( 4(2 + \xi) - (3 + \xi) \frac{\pi^2}{12} \right) \varepsilon_\gamma + \mathcal{O}(\varepsilon_\gamma^2) \right]. \quad (3.73b)$$

With the help of (3.45), the general results (3.71) allow for a straightforward derivation of the one-loop renormalization constants

$$\delta Z_{1\Psi} = \left( \frac{\varepsilon_e}{2 - \varepsilon_e} - \xi_r \right) \frac{1}{\varepsilon_\gamma}, \quad \delta Z_{1m} = - \frac{2(3 - 2\varepsilon_e)}{(1 - \varepsilon_e)(2 - \varepsilon_e)} \frac{1}{\varepsilon_\gamma}, \quad (3.74)$$

where the parameterization (3.38) was used. From (3.49), the corresponding one-loop anomalous dimensions read

$$\gamma_{1\Psi} = 2 \left( \xi_r - \frac{\varepsilon_e}{2 - \varepsilon_e} \right), \quad \gamma_{1m} = \frac{4(3 - 2\varepsilon_e)}{(2 - \varepsilon_e)(1 - \varepsilon_e)}, \quad (3.75)$$

that is valid in the general case of QED<sub>4,d<sub>e</sub></sub>. We will discuss their values for the cases of QED<sub>4</sub> and QED<sub>4,3</sub> once we have computed the two-loop contribution to these quantities.

### 3.3.2 Two-loop calculations

#### Photon polarization at two loops

We now focus on the two-loop photon polarization. It has two contributions that read

$$i\Pi_{2a}^{\mu\nu}(p) = \mu \text{ (diagram) } \nu = -2N_f \mu^{2\varepsilon_\gamma} \int [d^{d_e} k] \text{Tr} \left[ \Gamma_0^\nu S_0(k) (-i\Sigma_1(k)) S_0(k) \Gamma_0^\mu S_0(k-p) \right], \quad (3.76a)$$

$$i\Pi_{2b}^{\mu\nu}(p) = \mu \text{ (diagram) } \nu = -N_f \mu^{4\varepsilon_\gamma} \int [d^{d_e} k_1] [d^{d_e} k_2] \text{Tr} \left[ \Gamma_0^\nu S_0(k_2) \Gamma_0^\alpha S_0(k_1) \Gamma_0^\mu S_0(k_1-p) \Gamma_0^\beta \right. \\ \left. \times S_0(k_2-p) D_{0\alpha\beta}(k_2-k_1) \right], \quad (3.76b)$$

where we have used the (already computed) one-loop self-energy  $-i\Sigma_1(p)$ , defined in (3.67) as an insertion in the first diagram. We also added a factor 2 in  $\Pi_{2a}^{\mu\nu}$  because this diagram has equivalent topologies (one with the insertion of the self-energy on the top fermion propagator and one on the bottom propagator). After a complete computation that follows the lines of the one-loop case, while using the two-loop integrals techniques described in Appendix A, the exact result reads

$$\Pi_{2a}(p^2) = 4N_f e^4 \mu^{4\varepsilon_\gamma} \frac{(-p^2)^{\frac{d_e+d_\gamma}{2}-4}}{(4\pi)^{\frac{d_e+d_\gamma}{2}}} \frac{(d_e-2)^3 (d_e-d_\gamma + (d_e+d_\gamma-4)\xi)}{(d_e-1)(d_\gamma-4)(d_e+d_\gamma-4)} \Gamma(1-\varepsilon_e) G(d_e, 1, 1-\varepsilon_e) G(d_e, 1, \varepsilon_\gamma), \quad (3.77a)$$

$$\Pi_{2b}(p^2) = 4N_f e^4 \mu^{4\varepsilon_\gamma} \frac{(-p^2)^{\frac{d_e+d_\gamma}{2}-4}}{(4\pi)^{\frac{d_e+d_\gamma}{2}}} \frac{(d_e-2)\Gamma(1-\varepsilon_e)}{(d_e-1)(d_\gamma+d_e-6)(d_\gamma+d_e-4)^2(d_\gamma+2d_e-8)} \left[ \left( 4d_\gamma^4 - 92d_\gamma^3 + 776d_\gamma^2 \right. \right. \\ \left. \left. - 2880d_\gamma - d_e^5 - 5d_\gamma d_e^4 + 30d_e^4 - 8d_\gamma^2 d_e^3 + 110d_\gamma d_e^3 - 348d_e^3 - 5d_\gamma^3 d_e^2 + 120d_\gamma^2 d_e^2 - 848d_\gamma d_e^2 + 1848d_e^2 - d_\gamma^4 d_e + 44d_\gamma^3 d_e \right. \right. \\ \left. \left. - 544d_\gamma^2 d_e + 2640d_\gamma d_e - 4448d_e + 3968 - (d_e-2)^2 (d_\gamma+d_e-6)(d_\gamma+d_e-4)^2 \xi \right) G(d_e, 1, 1-\varepsilon_e) G(d_e, 1, 1+\varepsilon_\gamma) \right]$$

$$+ \frac{1}{2}(d_\gamma + d_e - 4)(d_\gamma + 2d_e - 8) \left( (d_\gamma - 2)d_e^2 - 4(d_\gamma - 4)^2 + ((d_\gamma - 12)d_\gamma + 28)d_e \right) G(d_e, 1, 1, 1, 1, 1 - \varepsilon_e) \Big]. \quad (3.77b)$$

As explained when we computed the one-loop photon polarization, the expansion in  $\varepsilon_\gamma$  does not commute with the limit  $\varepsilon_e \rightarrow 0$  for QED<sub>4</sub>. Therefore, we give the expansion in both cases separately. As for the QED<sub>4</sub> case ( $\varepsilon_e = 0$ ), the expansion in  $\varepsilon_\gamma \rightarrow 0$  reads

$$\Pi_{2a}^{\text{QED}_4}(p^2) = N_f \bar{\alpha}^2 \left( \frac{-p^2}{\bar{\mu}^2} \right)^{-2\varepsilon_\gamma} \left[ \frac{4\xi}{3\varepsilon_\gamma^2} + \frac{50\xi}{9\varepsilon_\gamma} + \frac{541 - 6\pi^2}{27} + \text{O}(\varepsilon_\gamma) \right], \quad (3.78a)$$

$$\Pi_{2b}^{\text{QED}_4}(p^2) = -N_f \bar{\alpha}^2 \left( \frac{-p^2}{\bar{\mu}^2} \right)^{-2\varepsilon_\gamma} \left[ \frac{4\xi}{3\varepsilon_\gamma^2} + \frac{2(9 + 25\xi)}{9\varepsilon_\gamma} + \left( \frac{55}{3} + \frac{541 - 6\pi^2}{27}\xi - 16\zeta_3 \right) + \text{O}(\varepsilon_\gamma) \right], \quad (3.78b)$$

and the sum of both diagrams then yields, for QED<sub>4</sub>

$$\Pi_2^{\text{QED}_4}(p^2) = \Pi_{2a}^{\text{QED}_4}(p^2) + \Pi_{2b}^{\text{QED}_4}(p^2) = -N_f \bar{\alpha}^2 \left( \frac{-p^2}{\bar{\mu}^2} \right)^{-2\varepsilon_\gamma} \left[ \frac{2}{\varepsilon_\gamma} + \frac{55}{3} - 16\zeta_3 + \text{O}(\varepsilon_\gamma) \right], \quad (3.79)$$

which is, as expected, completely gauge-independent, providing a strong check on our result. We observe that the second order pole cancel. However, as expected from QED<sub>4</sub>, the polarization exhibits a pole. From the result (3.79) and the definitions (3.47) and (3.48) it is straightforward to derive the gauge field anomalous dimensions and then the directly related beta function of QED<sub>4</sub> at two loops, reading

$$\gamma_A^{\text{QED}_4} = \bar{\alpha}_r \frac{8N_f}{3} + 8\bar{\alpha}_r^2 N_f + \text{O}(\bar{\alpha}_r^3), \quad \beta^{\text{QED}_4} = -2\bar{\alpha}_r \varepsilon_\gamma + \bar{\alpha}_r \frac{8N_f}{3} + 8\bar{\alpha}_r^3 N_f + \text{O}(\bar{\alpha}_r^4). \quad (3.80)$$

Now turning to the case of QED<sub>4,3</sub>, *i.e.*, first taking  $\varepsilon_e = 1/2$  and then  $\varepsilon_\gamma \rightarrow 0$  reads

$$\Pi_{2a}^{\text{QED}_{4,3}}(p^2) = N_f \frac{\alpha^2}{\sqrt{-p^2}} \left( \frac{-p^2}{\bar{\mu}^2} \right)^{-2\varepsilon_\gamma} \left[ -\frac{1 - 3\xi}{12\varepsilon_\gamma} - \frac{5 - 9\xi}{18} + \text{O}(\varepsilon_\gamma) \right], \quad (3.81a)$$

$$\Pi_{2b}^{\text{QED}_{4,3}}(p^2) = N_f \frac{\alpha^2}{\sqrt{-p^2}} \left( \frac{-p^2}{\bar{\mu}^2} \right)^{-2\varepsilon_\gamma} \left[ \frac{1 - 3\xi}{12\varepsilon_\gamma} - \frac{82 + 18\xi - 9\pi^2}{36} \text{O}(\varepsilon_\gamma) \right]. \quad (3.81b)$$

As expected, summing both contributions

$$\Pi_2^{\text{QED}_{4,3}}(p^2) = \Pi_{2a}^{\text{QED}_{4,3}}(p^2) + \Pi_{2b}^{\text{QED}_{4,3}}(p^2) = -N_f \frac{\alpha^2}{\sqrt{-p^2}} \frac{92 - 9\pi^2}{36} + \text{O}(\varepsilon_\gamma), \quad (3.82)$$

which is gauge-independent, providing a strong check on our results. It is also a finite result, which is a perturbative proof that the beta function of QED<sub>4,3</sub> is indeed vanishing. Using similar notations as in the one-loop case, we can then write, for QED<sub>4,3</sub>

$$\Pi^{\text{QED}_{4,3}}(p^2) = -\frac{\bar{\alpha}}{\sqrt{-p^2}} \left[ \hat{\Pi}_1^{\text{QED}_{4,3}} + \hat{\Pi}_2^{\text{QED}_{4,3}} \bar{\alpha} + \text{O}(\bar{\alpha}^3) \right], \quad (3.83a)$$

$$\text{with } \hat{\Pi}_1^{\text{QED}_{4,3}} = 2\pi^2 N_f \quad \text{and} \quad \hat{\Pi}_2^{\text{QED}_{4,3}} = \frac{4(92 - 9\pi^2)}{9} \pi^2 N_f, \quad (3.83b)$$

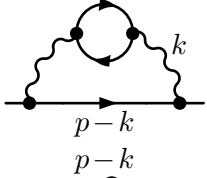
or in an even simpler form, *i.e.*, factorizing the one-loop contribution

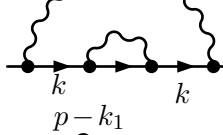
$$\Pi^{\text{QED}_{4,3}}(p^2) = \Pi_1^{\text{QED}_{4,3}}(p^2) \left[ 1 + C_\gamma^{\text{QED}_{4,3}} \alpha + \text{O}(\alpha^2) \right], \quad \text{with } C_\gamma^{\text{QED}_{4,3}} = \frac{92 - 9\pi^2}{18\pi}, \quad (3.84)$$

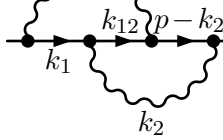
where  $C_\gamma^{\text{QED}_{4,3}}$  is the so-called interaction correction coefficient to the conductivity. Indeed, the polarization is closely related to the optical conductivity of the model, that we will discuss in section 3.4.2 devoted to the results for QED<sub>4,3</sub> and the closely related graphene material. The results (3.83) and (3.84) has been first computed in [144, 145, 212] and were also known to the authors of [182, 183, 213] (though it did not appear explicitly in these papers, the knowledge of  $\hat{\Pi}_2$  was required to perform the calculations carried out in these papers).

### Fermion self-energy at two loops

At two loops, three diagrams contribute to the fermion self-energies

$$-i\Sigma_{2a}(p) = \text{Diagram 1} = \mu^{2\varepsilon_\gamma} \int [d^{d_e} k] \Gamma_0^\alpha S_0(p-k) \Gamma_0^\beta D_{0\alpha\mu}(k) i\Pi_1^{\mu\nu}(k) D_{0\nu\beta}(k), \quad (3.85a)$$


$$-i\Sigma_{2b}(p) = \text{Diagram 2} = \mu^{2\varepsilon_\gamma} \int [d^{d_e} k] \Gamma_0^\mu S_0(k) (-i\Sigma_1(k)) S_0(k) \Gamma_0^\nu D_{0\mu\nu}(p-k), \quad (3.85b)$$


$$-i\Sigma_{2c}(p) = \text{Diagram 3} = \mu^{4\varepsilon_\gamma} \int [d^{d_e} k_1] [d^{d_e} k_2] \Gamma_0^\mu S_0(p-k_2) D_{0\beta\mu}(k_2) \Gamma_0^\alpha S_0(k_{12}) D_{0\alpha\nu}(p-k_1) \times \Gamma_0^\beta S_0(k_1) \Gamma_0^\nu. \quad (3.85c)$$


Using the parameterization (3.28), we extract the vector and scalar parts that are then computed exactly. For the vectorial part (first computed in [147]), it reads

$$\Sigma_{2Va}(p^2) = 2N \frac{e^4}{(4\pi)^{d_\gamma}} \left( \frac{\mu^2}{-p^2} \right)^{2\varepsilon_\gamma} \Gamma^2(1-\varepsilon_e) \frac{(d_e-2)^2}{2d_\gamma-d_e-6} G(d_e,1,1) G(d_e,1,\varepsilon_\gamma-\varepsilon_e), \quad (3.86a)$$

$$\Sigma_{2Vb}(p^2) = \frac{e^4}{(4\pi)^{d_\gamma}} \left( \frac{\mu^2}{-p^2} \right)^{2\varepsilon_\gamma} \Gamma^2(1-\varepsilon_e) \frac{(d_e-2)(d_\gamma-3)(d_\gamma+d_e-4)}{2(d_\gamma-4)} \left( \xi - \frac{d_\gamma-d_e}{d_\gamma+d_e-4} \right)^2 \times G(d_e,1,1-\varepsilon_e) G(d_e,1-\varepsilon_e,\varepsilon_\gamma), \quad (3.86b)$$

$$\begin{aligned} \Sigma_{2Vc}(p^2) = & -\frac{e^4}{(4\pi)^{d_\gamma}} \left( \frac{\mu^2}{-p^2} \right)^{2\varepsilon_\gamma} \Gamma^2(1-\varepsilon_e) \frac{d_e-2}{2} \left\{ \left[ d_e-4 + \frac{(d_e-2)(d_\gamma-3d_e+4)}{2(d_\gamma+d_e-4)} \right. \right. \\ & - \frac{(d_\gamma+d_e-6)(d_\gamma(d_e-4)+8)}{(2d_\gamma+d_e-10)(2d_\gamma+d_e-8)} - \frac{4(d_\gamma-d_e)}{d_\gamma+d_e-4} - \frac{d_\gamma-d_e}{2d_\gamma+d_e-8} \\ & \times \left( d_e-8 - \frac{4(d_\gamma+d_e-6)}{d_\gamma+d_e-4} \right) - \xi \frac{(d_e-2)(d_\gamma-d_e)}{d_\gamma+d_e-4} + \xi^2 \frac{d_e-2}{2} \left. \right] G(d_e,1,1-\varepsilon_e)^2 \\ & + \left[ 2d_e-d_\gamma-1 + \frac{4(d_e-2)(d_\gamma-1)}{d_\gamma+d_e-4} + \frac{8(d_\gamma-1)}{d_\gamma-4} + \frac{2(d_e-8)(d_\gamma-d_e)}{d_\gamma+d_e-6} \right. \\ & - \frac{4(d_\gamma-2)(d_\gamma-d_e)}{(d_\gamma-4)(d_\gamma+d_e-4)} + 2\xi \frac{(d_\gamma-3)(d_\gamma-d_e)}{d_\gamma+d_e-4} - \xi^2(d_\gamma-3) \left. \right] \\ & \times G(d_e,1,1-\varepsilon_e) G(d_e,1-\varepsilon_e,\varepsilon_\gamma) \\ & \left. - \frac{(d_\gamma-4)(d_\gamma(d_e-4)+8)}{(2d_\gamma+d_e-8)(2d_\gamma+d_e-10)} G(d_e,1-\varepsilon_e,1,1-\varepsilon_e,1,1) \right\}. \quad (3.86c) \end{aligned}$$

And for the scalar part it reads

$$\Sigma_{2Sa}(p^2) = -2N \frac{e^4}{(4\pi)^{d_\gamma}} \left( \frac{\mu^2}{-p^2} \right)^{2\varepsilon_\gamma} \Gamma^2(1-\varepsilon_e) \frac{(d_e-2)(2d_\gamma+d_e-8)}{2d_\gamma-d_e-4} G(d_e,1,1) G(d_e,1,\varepsilon_\gamma-\varepsilon_e), \quad (3.87a)$$

$$\begin{aligned} \Sigma_{2Sb}(p^2) = & \frac{e^4}{(4\pi)^{d_\gamma}} \left( \frac{\mu^2}{-p^2} \right)^{2\varepsilon_\gamma} \Gamma^2(1-\varepsilon_e) \frac{(d_\gamma-3)(2d_\gamma+d_e-8)(d_\gamma+d_e-2-(d_\gamma-d_e-2)\xi)}{2(d_\gamma-4)(d_\gamma+d_e-6)(d_\gamma+d_e-4)} \\ & \times \left( d_\gamma(d_\gamma-10) + d_e(4d_\gamma-d_e-2) + 8 - (d_\gamma+d_e-4)(d_\gamma+d_e-6)\xi \right) \\ & \times G(d_e,1,1-\varepsilon_e) G(d_e,1-\varepsilon_e,\varepsilon_\gamma), \quad (3.87b) \end{aligned}$$

$$\begin{aligned}
\Sigma_{2Sc}(p^2) = & -\frac{e^4}{(4\pi)^{d_\gamma}} \left( \frac{\mu^2}{-p^2} \right)^{2\varepsilon_\gamma} \Gamma^2(1-\varepsilon_e) \frac{d_e-2}{2} \left\{ \left[ d_\gamma + 3 - \frac{3d_e}{2} + \frac{2d_e(d_e-2)}{d_\gamma+d_e-4} + \frac{2d_e}{2d_\gamma+d_e-10} \right. \right. \\
& - \left. \left( 2d_\gamma - 2 - \frac{d_e(d_\gamma-d_e)}{d_\gamma+d_e-4} \right) \xi + \frac{2d_\gamma-d_e-6}{2} \xi^2 \right] G(d_e, 1, 1-\varepsilon_e)^2 \\
& - \frac{2(d_\gamma-3)}{d_e-2} \left[ d_\gamma - 4 + \frac{9d_e}{2} + \frac{2(d_e(d_e-2)(d_e+4)+8)}{(d_e-2)(d_\gamma-4)} + \frac{2(d_e-4)(d_e(d_e-2)+4)}{(d_e-2)(d_\gamma+d_e-6)} \right. \\
& \left. \left. - \frac{2(d_e-2)^2}{d_\gamma+d_e-4} - \frac{(2d_\gamma+d_e-8)(d_e(3d_\gamma-4)+d_\gamma(d_\gamma-8)+8)}{(d_\gamma-4)(d_\gamma+d_e-4)} \xi + \frac{2d_\gamma+d_e-8}{2} \xi^2 \right] \right. \\
& \times G(d_e, 1, 1-\varepsilon_e) G(1-\varepsilon_e, \varepsilon_\gamma) \\
& \left. - \frac{4(d_\gamma-5)-d_e(d_e+2(d_\gamma-7))}{2d_\gamma+d_e-10} G(d_e, 1-\varepsilon_e, 1, 1-\varepsilon_e, 1, 1) \right\}. \tag{3.87c}
\end{aligned}$$

For the vectorial part, the resulting  $\varepsilon_\gamma$ -expansions at arbitrary  $\varepsilon_e$  then read

$$\Sigma_{2Va}(p^2) = 2N\bar{\alpha}^2 K_1 \left[ \frac{-\varepsilon_e}{2-\varepsilon_e} \frac{1}{\varepsilon_\gamma} + \frac{2\varepsilon_e}{2-\varepsilon_e} \left( \bar{L}_p + \frac{1}{2}(\bar{\Psi}_1 - \bar{\Psi}_2) \right) + \frac{2}{1-\varepsilon_e} - \frac{6}{(2-\varepsilon_e)^2} + O(\varepsilon_\gamma) \right], \tag{3.88a}$$

$$\begin{aligned}
\Sigma_{2Vb}(p^2) = & \bar{\alpha}^2 \left[ \frac{(\varepsilon_e - (2-\varepsilon_e)\xi)^2}{2(2-\varepsilon_e)^2} \frac{1}{\varepsilon_\gamma^2} - \frac{1}{(2-\varepsilon_e)^2} \left( (\varepsilon_e - (2-\varepsilon_e)\xi)^2 \bar{L}_p \right. \right. \\
& - \left. \left. \frac{(\varepsilon_e - (2-\varepsilon_e)\xi)(5\varepsilon_e - (2-\varepsilon_e)\xi)}{2(2-\varepsilon_e)} \right) \frac{1}{\varepsilon_\gamma} + \frac{1}{(2-\varepsilon_e)^2} \left( (\varepsilon_e - (2-\varepsilon_e)\xi)^2 \bar{L}_p^2 \right. \right. \\
& - \left. \left. \left( \frac{5\varepsilon_e^2}{2-\varepsilon_e} - 6\varepsilon_e\xi + (2-\varepsilon_e)\xi^2 \right) \bar{L}_p + \frac{3}{2}(\varepsilon_e - (2-\varepsilon_e)\xi)^2 \zeta_2 + \frac{19\varepsilon_e^2}{2(2-\varepsilon_e)^2} - \frac{9\varepsilon_e}{2-\varepsilon_e} \xi \right. \right. \\
& \left. \left. - 2(\varepsilon_e - (2-\varepsilon_e)\xi)^2 \psi'(2-\varepsilon_e) + \frac{3\xi^2}{2} \right) + O(\varepsilon_\gamma) \right], \tag{3.88b}
\end{aligned}$$

$$\begin{aligned}
\Sigma_{2Vc}(p^2) = & -\bar{\alpha}^2 \left[ \frac{(\varepsilon_e - (2-\varepsilon_e)\xi)^2}{(2-\varepsilon_e)^2} \frac{1}{\varepsilon_\gamma^2} - \frac{1}{(2-\varepsilon_e)^2} \left( 2(\varepsilon_e - (2-\varepsilon_e)\xi)^2 \bar{L}_p \right. \right. \\
& + \frac{\varepsilon_e}{2}(\xi^2 + 10\xi + 1) - \xi^2 + 15 - \frac{20}{2-\varepsilon_e} - \frac{2}{1-\varepsilon_e} \left. \right) \frac{1}{\varepsilon_\gamma} + \frac{1}{(2-\varepsilon_e)^2} \left( 2(\varepsilon_e - (2-\varepsilon_e)\xi)^2 \bar{L}_p^2 \right. \\
& + (\varepsilon_e(\xi^2 + 10\xi + 1) - 2\xi^2 + 30 - \frac{40}{2-\varepsilon_e} - \frac{4}{1-\varepsilon_e}) \bar{L}_p \\
& + 2(\varepsilon_e^2(1+\xi)^2 - 4\varepsilon_e(\xi^2 + \xi + 1) + 4\xi^2 + 6) \zeta_2 + \frac{3(3\varepsilon_e^2 - 10\varepsilon_e + 9)}{2(1-\varepsilon_e)^2} \xi^2 \\
& - \left. \left( \frac{26}{2-\varepsilon_e} + \frac{6}{(1-\varepsilon_e)^2} - 19 \right) \xi + \frac{\varepsilon_e(\varepsilon_e(\varepsilon_e(13\varepsilon_e + 42) - 137) + 64) + 28}{2(2-\varepsilon_e)^2(1-\varepsilon_e)^2} \right. \\
& \left. - (3(2-\varepsilon_e)^2 \xi^2 - 6\varepsilon_e(2-\varepsilon_e)\xi - (\varepsilon_e(8-3\varepsilon_e) - 12)) \psi'(1-\varepsilon_e) \right) + O(\varepsilon_\gamma) \right], \tag{3.88c}
\end{aligned}$$

where the most complicated master integral  $G(4-2\varepsilon_e, 1-\varepsilon_e, 1, 1-\varepsilon_e, 1, 1)$  only contributes to the  $O(\varepsilon_\gamma)$  terms of (3.88c) and is therefore not displayed in this equation.

Similarly, for the scalar part, the resulting  $\varepsilon_\gamma$ -expansions at arbitrary  $\varepsilon_e$  then read

$$\Sigma_{2Sa}(p^2) = 2N\bar{\alpha}^2 K_1 \left[ -\frac{1}{\varepsilon_\gamma} + 2\bar{L}_p + \bar{\Psi}_1 - \bar{\Psi}_2 + O(\varepsilon_\gamma) \right], \tag{3.89a}$$

$$\begin{aligned}
\Sigma_{2Sb}(p^2) = & \frac{\bar{\alpha}^2}{(2-\varepsilon_e)(1-\varepsilon_e)^2} \left[ \frac{(\varepsilon_e - 3 - (1-\varepsilon_e)\xi)(\varepsilon_e(\varepsilon_e + 3 - (3-\varepsilon_e)\xi) - 6 + 2\xi)}{2\varepsilon_\gamma^2} \right. \\
& + \frac{1}{\varepsilon_\gamma} \left( -(\varepsilon_e - 3 - (1-\varepsilon_e)\xi)(\varepsilon_e(\varepsilon_e + 3 - (3-\varepsilon_e)\xi) - 6 + 2\xi) \bar{L}_p \right. \\
& \left. \left. + \frac{1}{2(2-\varepsilon_e)(1-\varepsilon_e)} \left( 60 - \varepsilon_e(\varepsilon_e(33 - 5\varepsilon_e(6-\varepsilon_e)) + 40) + 2\varepsilon_e(\varepsilon_e(7 + 3\varepsilon_e(2-\varepsilon_e)) - 22) \right) \xi \right. \right.
\end{aligned}$$

$$\begin{aligned}
& + 24\xi - (2 - \varepsilon_e)^2(1 - \varepsilon_e)^2\xi^2 \Big) \Big) + (\varepsilon_e - 3 - (1 - \varepsilon_e)\xi) (\varepsilon_e(\varepsilon_e + 3 - (3 - \varepsilon_e)\xi) - 6 + 2\xi) \bar{L}_p^2 \\
& - \frac{1}{(2 - \varepsilon_e)(1 - \varepsilon_e)} \left( 60 - \varepsilon_e(\varepsilon_e(33 - 5\varepsilon_e(6 - \varepsilon_e)) + 40) + 2\varepsilon_e(\varepsilon_e(7 + 3\varepsilon_e(2 - \varepsilon_e)) - 22) \right) \xi \\
& + 24\xi - (2 - \varepsilon_e)^2(1 - \varepsilon_e)^2\xi^2 \Big) \bar{L}_p + (\varepsilon_e - 3 - (1 - \varepsilon_e)\xi) (\varepsilon_e(\varepsilon_e + 3 - (3 - \varepsilon_e)\xi) - 6 + 2\xi) \\
& \times \left( \frac{3}{2} \zeta_2 - 2\psi'(2 - \varepsilon_e) \right) + \frac{\varepsilon_e(\varepsilon_e(\varepsilon_e(9\varepsilon_e^2 - 84\varepsilon_e + 209) - 86) - 268) + 248}{2(2 - \varepsilon_e)^2(1 - \varepsilon_e)^2} \\
& - \frac{\varepsilon_e(\varepsilon_e(\varepsilon_e(11\varepsilon_e - 35) + 10) + 64) - 56}{(2 - \varepsilon_e)^2(1 - \varepsilon_e)} \xi - \frac{2 - \varepsilon_e}{2} \xi^2 + \mathcal{O}(\varepsilon_\gamma) \Big], \tag{3.89b}
\end{aligned}$$

$$\begin{aligned}
\Sigma_{2Sc}(p^2) = & \frac{\bar{\alpha}^2}{(2 - \varepsilon_e)(1 - \varepsilon_e)} \left[ \frac{(\varepsilon_e - (2 - \varepsilon_e)\xi)(\varepsilon_e - 3 - (1 - \varepsilon_e)\xi)}{\varepsilon_\gamma^2} \right. \\
& + \frac{1}{\varepsilon_\gamma} \left( -2(\varepsilon_e - (2 - \varepsilon_e)\xi)(\varepsilon_e - 3 - (1 - \varepsilon_e)\xi) \bar{L}_p + \frac{5\varepsilon_e}{2} - \frac{\varepsilon_e(\varepsilon_e(\varepsilon_e + 6) - 23) + 18}{(2 - \varepsilon_e)(1 - \varepsilon_e)^2} \right. \\
& + \left( \frac{2(2 - \varepsilon_e^2)}{(2 - \varepsilon_e)(1 - \varepsilon_e)} - 3\varepsilon_e \right) \xi + \frac{3(2 - \varepsilon_e)}{2} \xi^2 \Big) + 2(\varepsilon_e - (2 - \varepsilon_e)\xi)(\varepsilon_e - 3 - (1 - \varepsilon_e)\xi) \bar{L}_p^2 \\
& - \left( 3(2 - \varepsilon_e)\xi^2 - \left( 6\varepsilon_e - \frac{8}{2 - \varepsilon_e} - \frac{4}{1 - \varepsilon_e} + 4 \right) \xi + 5\varepsilon_e - \frac{2(\varepsilon_e(\varepsilon_e(\varepsilon_e + 6) - 23) + 18)}{(2 - \varepsilon_e)(1 - \varepsilon_e)^2} \right) \bar{L}_p \\
& + \left( -3(2 - \varepsilon_e)(1 - \varepsilon_e)\xi^2 + 2(\varepsilon_e(7 - 3\varepsilon_e) - 6)\xi - \frac{2}{1 - \varepsilon_e} - 16 + \varepsilon_e(21 - 5\varepsilon_e) \right) \psi'(1 - \varepsilon_e) \\
& + 2 \left( (2 - \varepsilon_e)(1 - \varepsilon_e)\xi^2 + (3 - 2\varepsilon_e(2 - \varepsilon_e))\xi + 8 - \varepsilon_e(9 - 2\varepsilon_e) + \frac{1}{1 - \varepsilon_e} \right) \zeta_2 \\
& + \frac{9(2 - \varepsilon_e)}{2(1 - \varepsilon_e)} \xi^2 - \frac{\varepsilon_e(\varepsilon_e(\varepsilon_e(71 - 15\varepsilon_e) - 134) + 128) - 56}{(2 - \varepsilon_e)^2(1 - \varepsilon_e)^2} \xi - \frac{92}{(2 - \varepsilon_e)^2(1 - \varepsilon_e)^3} \\
& + \frac{\varepsilon_e(\varepsilon_e(\varepsilon_e(\varepsilon_e(28 + 3\varepsilon_e) - 133) + 94) + 172)}{2(2 - \varepsilon_e)^2(1 - \varepsilon_e)^3} \\
& \left. + 2(2 - \varepsilon_e)(1 - \varepsilon_e)(\varepsilon_e(1 - \varepsilon_e) + 1)\Gamma^2(1 - \varepsilon_e)G(4 - 2\varepsilon_e, 1 - \varepsilon_e, 1, 1 - \varepsilon_e, 1, 1) + \mathcal{O}(\varepsilon_\gamma) \right], \tag{3.89c}
\end{aligned}$$

where the parameters were defined in (3.52). Notice that, the most complicated master integral  $G(4 - 2\varepsilon_e, 1 - \varepsilon_e, 1, 1 - \varepsilon_e, 1, 1)$  only contributes to the finite part of the last graph, see (3.89c), and will therefore not affect the anomalous dimension.

In the QED<sub>4</sub> case ( $\varepsilon_\gamma \rightarrow 0$  and  $\varepsilon_e = 0$ ), the expansion for the vectorial part simplifies to

$$\Sigma_{2Va}^{\text{QED}_4}(p^2) = \bar{\alpha}^2 N_f \left( \frac{\bar{\mu}^2}{-p^2} \right)^{2\varepsilon_\gamma} \left[ \frac{1}{\varepsilon_\gamma} + \frac{7}{2} + \mathcal{O}(\varepsilon_\gamma) \right], \tag{3.90a}$$

$$\Sigma_{2Vb}^{\text{QED}_4}(p^2) = \bar{\alpha}^2 \xi^2 \left( \frac{\bar{\mu}^2}{-p^2} \right)^{2\varepsilon_\gamma} \left[ \frac{1}{2\varepsilon_\gamma^2} + \frac{5}{4\varepsilon_\gamma} + \frac{93 - 2\pi^2}{24} + \mathcal{O}(\varepsilon_\gamma) \right], \tag{3.90b}$$

$$\Sigma_{2Vc}^{\text{QED}_4}(p^2) = \bar{\alpha}^2 \left( \frac{\bar{\mu}^2}{-p^2} \right)^{2\varepsilon_\gamma} \left[ -\frac{\xi^2}{\varepsilon_\gamma^2} + \frac{3(1 - 3\xi^2)}{4\varepsilon_\gamma} + \frac{5}{8} + \frac{4\pi^2 - 141}{24} \xi + \mathcal{O}(\varepsilon_\gamma) \right], \tag{3.90c}$$

and similarly for the scalar part it simplifies to

$$\Sigma_{2Sa}^{\text{QED}_4}(p^2) = \bar{\alpha}^2 N_f \left( \frac{\bar{\mu}^2}{-p^2} \right)^{2\varepsilon_\gamma} \left[ -\frac{2}{\varepsilon_\gamma^2} - \frac{8}{\varepsilon_\gamma} - \frac{84 - \pi^2}{3} + \mathcal{O}(\varepsilon_\gamma) \right], \tag{3.91a}$$

$$\Sigma_{2Sb}^{\text{QED}_4}(p^2) = \bar{\alpha}^2 \left( \frac{\bar{\mu}^2}{-p^2} \right)^{2\varepsilon_\gamma} \left[ \frac{9 - \xi^2}{2\varepsilon_\gamma^2} + \frac{3((\xi - 2)\xi - 11)}{2\varepsilon_\gamma} + \frac{230 - 3\pi^2}{4} + 13\xi + \frac{\pi^2 - 54}{12} \xi^2 + \mathcal{O}(\varepsilon_\gamma) \right], \tag{3.91b}$$



$$\Sigma_{2Sc}^{\text{QED}_4}(p^2) = \bar{\alpha}^2 \left( \frac{\bar{\mu}^2}{-p^2} \right)^{2\varepsilon_\gamma} \left[ \frac{\xi(\xi+3)}{\varepsilon_\gamma^2} + \frac{-9+14\xi+7\xi^2}{2\varepsilon_\gamma} - \frac{41-24\xi_3}{2} + \frac{30-\pi^2}{2}\xi + \frac{57-\pi^2}{6}\xi^2 + \text{O}(\varepsilon_\gamma) \right]. \quad (3.91c)$$

In the QED<sub>4,3</sub> case ( $\varepsilon_\gamma \rightarrow 0$  and  $\varepsilon_e = 1/2$ ), the expansion for the vectorial part simplifies to

$$\Sigma_{2Va}^{\text{QED}_{4,3}}(p^2) = \bar{\alpha}^2 N_f \left( \frac{\bar{\mu}^2}{-p^2} \right)^{2\varepsilon_\gamma} \left[ -\frac{2\pi^2}{3\varepsilon_\gamma} + \text{O}(\varepsilon_\gamma) \right], \quad (3.92a)$$

$$\Sigma_{2Vb}^{\text{QED}_{4,3}}(p^2) = \bar{\alpha}^2 \left( \frac{\bar{\mu}^2}{-4p^2} \right)^{2\varepsilon_\gamma} \left[ \frac{(1-3\xi)^2}{18\varepsilon_\gamma^2} + \frac{(1-3\xi)(11-21\xi)}{27\varepsilon_\gamma} + \frac{206}{81} - 2\xi(6-7\xi) - \frac{\pi^2}{12}(1-3\xi)^2 + \text{O}(\varepsilon_\gamma) \right], \quad (3.92b)$$

$$\Sigma_{2Vc}^{\text{QED}_{4,3}}(p^2) = \bar{\alpha}^2 \left( \frac{\bar{\mu}^2}{-4p^2} \right)^{2\varepsilon_\gamma} \left[ -\frac{(1-3\xi)^2}{9\varepsilon_\gamma^2} - \frac{37-3\xi(34-39\xi)}{27\varepsilon_\gamma} - \frac{2}{81}(695-798\xi+891\xi^2) + \frac{\pi^2}{54}(71-21\xi(2-3\xi)) + \text{O}(\varepsilon_\gamma) \right], \quad (3.92c)$$

and similarly for the scalar part it simplifies to

$$\Sigma_{2Sa}^{\text{QED}_{4,3}}(p^2) = \bar{\alpha}^2 N \left( \frac{\bar{\mu}^2}{-p^2} \right)^{2\varepsilon_\gamma} \left[ -\frac{2\pi^2}{\varepsilon_\gamma} - 8\pi^2 + \text{O}(\varepsilon_\gamma) \right], \quad (3.93a)$$

$$\Sigma_{2Sb}^{\text{QED}_{4,3}}(p^2) = \bar{\alpha}^2 \left( \frac{\bar{\mu}^2}{-4p^2} \right)^{2\varepsilon_\gamma} \left[ \frac{(5+\xi)(17-3\xi)}{6\varepsilon_\gamma^2} + \frac{1073+118\xi-27\xi^2}{9\varepsilon_\gamma} + \frac{2}{27}(11605+1550\xi-243\xi^2) - \frac{\pi^2}{4}(5+\xi)(17-3\xi) + \text{O}(\varepsilon_\gamma) \right], \quad (3.93b)$$

$$\Sigma_{2Sc}^{\text{QED}_{4,3}}(p^2) = \bar{\alpha}^2 \left( \frac{\bar{\mu}^2}{-4p^2} \right)^{2\varepsilon_\gamma} \left[ -\frac{(5+\xi)(1-3\xi)}{3\varepsilon_\gamma} - \frac{305-206\xi-63\xi^2}{9\varepsilon_\gamma} - \frac{2}{27}(4507-1294\xi-513\xi^2) - \frac{\pi^2}{6}(27+22\xi+7\xi^2) + \frac{5\pi}{2}G(3,1/2,1,1/2,1,1) \right], \quad (3.93c)$$

where the non-trivial  $G(3,1/2,1,1/2,1,1)$  is a finite integral provided in Appendix A.

From (3.89) and (3.88) together with (3.45), the two-loop contributions to the renormalization constants read

$$\delta Z_{2\Psi} = \frac{(\varepsilon_e - (2-\varepsilon_e)\xi_r)^2}{2(2-\varepsilon_e)^2\varepsilon_\gamma^2} - \frac{2}{\varepsilon_\gamma} \left( \frac{N_f\varepsilon_e K_1}{2-\varepsilon_e} + \frac{(3-2\varepsilon_e)(\varepsilon_e(3-\varepsilon_e)-1)}{(1-\varepsilon_e)(2-\varepsilon_e)^3} \right), \quad (3.94a)$$

$$\delta Z_{2m} = \frac{2(3-2\varepsilon_e)^2}{(1-\varepsilon_e)^2(2-\varepsilon_e)^2\varepsilon_\gamma^2} + \frac{2}{\varepsilon_\gamma} \left( \frac{2N_f K_1}{2-\varepsilon_e} - \frac{3-2\varepsilon_e}{(1-\varepsilon_e)^2(2-\varepsilon_e)^3} \right). \quad (3.94b)$$

From (3.49), the corresponding two-loop contribution to the anomalous dimensions read

$$\gamma_{2\Psi} = 8 \left( \frac{N\varepsilon_e K_1}{2-\varepsilon_e} + \frac{(3-2\varepsilon_e)(\varepsilon_e(3-\varepsilon_e)-1)}{(1-\varepsilon_e)(2-\varepsilon_e)^3} \right), \quad (3.95a)$$

$$\gamma_{2m} = -8 \left( \frac{2NK_1}{2-\varepsilon_e} - \frac{3-2\varepsilon_e}{(1-\varepsilon_e)^2(2-\varepsilon_e)^3} \right). \quad (3.95b)$$

### 3.3.3 Electron field and mass anomalous dimensions

Combining the above derived one-loop (3.75) and two-loop (3.95) contributions to the anomalous dimensions yields

$$\gamma_\Psi = 2\bar{\alpha}_r \left( \xi_r - \frac{\varepsilon_e}{2-\varepsilon_e} \right) + 8\bar{\alpha}_r^2 \left( \frac{N\varepsilon_e K_1}{2-\varepsilon_e} + \frac{(3-2\varepsilon_e)(\varepsilon_e(3-\varepsilon_e)-1)}{(1-\varepsilon_e)(2-\varepsilon_e)^3} \right) + \text{O}(\bar{\alpha}_r^3), \quad (3.96a)$$

$$\gamma_m = 4\bar{\alpha}_r \frac{3-2\varepsilon_e}{(2-\varepsilon_e)(1-\varepsilon_e)} - 8\bar{\alpha}_r^2 \left( \frac{2NK_1}{2-\varepsilon_e} - \frac{3-2\varepsilon_e}{(1-\varepsilon_e)^2(2-\varepsilon_e)^3} \right) + \mathcal{O}(\bar{\alpha}_r^3), \quad (3.96b)$$

where  $\gamma_m$  is fully gauge invariant, as expected, while the gauge-variance of  $\gamma_\Psi$  is at one loop, in accordance with the Landau-Khalatnikov-Fradkin transformation, see, *e.g.*, [155]. Interestingly, (3.96a) and (3.96b) have similar structures. In particular, we see that in the limit of QED<sub>4,3</sub> ( $\varepsilon_e \rightarrow 1/2$ ) the factors of  $\pi^2$  arise from  $K_1$ , see (3.52a), and not from the  $\varepsilon_\gamma$ -expansion of  $\Gamma$ -functions. It turns out however that, because of these  $K_1$  terms, (3.96) (and similarly for the two-loop renormalization constants (3.94) and self-energies (3.89) and (3.88) above) do not apply to the case of QED<sub>4</sub>. As discussed below (3.61), this discrepancy (which is even more severe for  $\gamma_m$  than  $\gamma_\Psi$ ) originates from the fact that the limits  $\varepsilon_e \rightarrow 0$  and  $\varepsilon_\gamma \rightarrow 0$  do not commute for the one-loop polarization operator and hence for (3.89c) and (3.88c) where it appears as a subdiagram.<sup>2</sup> So (3.96) only apply to QED<sub>4,3</sub>.

The expressions (3.96) can then be improved in order to cover both cases of QED<sub>4</sub> and QED<sub>4,3</sub> at the expense of introducing an additional parameter  $z$  such that

$$L(\Sigma, d_e, z) = zL(\Sigma, d_e = 4) + (1-z)L(\Sigma, d_e < 4), \quad z = \delta_{\varepsilon_e, 0}, \quad (3.97)$$

where  $L(\Sigma, d)$  stands for Laurent expansion of  $\Sigma = \{\Pi_1, \Sigma_{2Va}, \Sigma_{2Sa}\}$  near the dimension  $d$ . All calculations done, the two-loop contributions to the renormalization constants (3.94) now take the form

$$\delta Z_{2\Psi} = \frac{(\varepsilon_e - (2-\varepsilon_e)\xi_r)^2}{2(2-\varepsilon_e)^2\varepsilon_\gamma^2} - \frac{2}{\varepsilon_\gamma} \left( \frac{(1-z)N_f\varepsilon_e K_1}{2-\varepsilon_e} - \frac{zN}{2} + \frac{(3-2\varepsilon_e)(\varepsilon_e(3-\varepsilon_e)-1)}{(1-\varepsilon_e)(2-\varepsilon_e)^3} \right), \quad (3.98a)$$

$$\delta Z_{2m} = \frac{2}{\varepsilon_\gamma^2} \left( \frac{(3-2\varepsilon_e)^2}{(1-\varepsilon_e)^2(2-\varepsilon_e)^2} - zN_f \right) + \frac{2}{\varepsilon_\gamma} \left( \frac{2(1-z)N_f K_1}{2-\varepsilon_e} + \frac{5zN}{6} - \frac{3-2\varepsilon_e}{(1-\varepsilon_e)^2(2-\varepsilon_e)^3} \right), \quad (3.98b)$$

where, in QED<sub>4</sub> the running of the coupling constant at one loop has been taken into account via  $\gamma_A = 8zN_f\bar{\alpha}_r/3 + \mathcal{O}(\bar{\alpha}_r^2)$ . Hence, we obtain one of the central results of this chapter in the form of improved expressions for the anomalous dimensions in QED<sub>4,d<sub>e</sub></sub>

$$\gamma_\Psi = 2\bar{\alpha}_r \left( \xi_r - \frac{\varepsilon_e}{2-\varepsilon_e} \right) + 8\bar{\alpha}_r^2 \left( \frac{(1-z)N_f\varepsilon_e K_1}{2-\varepsilon_e} - \frac{zN}{2} + \frac{(3-2\varepsilon_e)(\varepsilon_e(3-\varepsilon_e)-1)}{(2-\varepsilon_e)^3(1-\varepsilon_e)} \right) + \mathcal{O}(\bar{\alpha}_r^3), \quad (3.99a)$$

$$\gamma_m = 4\bar{\alpha}_r \frac{3-2\varepsilon_e}{(2-\varepsilon_e)(1-\varepsilon_e)} - 8\bar{\alpha}_r^2 \left( \frac{2(1-z)N_f K_1}{2-\varepsilon_e} + \frac{5zN}{6} - \frac{3-2\varepsilon_e}{(2-\varepsilon_e)^3(1-\varepsilon_e)^2} \right) + \mathcal{O}(\bar{\alpha}_r^3). \quad (3.99b)$$

A remark is in order here, in relation with (3.99a). Within the SD formalism, see, *e.g.*, the review [171], a common procedure to simplify the equations and minimize the gauge-variance of the solutions is to consider the gauge for which the fermion anomalous dimension vanishes,  $\gamma_\Psi(\xi_g) = 0$ . Such a gauge is referred to as the “good gauge”. At one loop, from (3.99a), the “good gauge” is simply

$$\xi_g = \frac{\varepsilon_e}{2-\varepsilon_e}, \quad (3.100)$$

which corresponds to the Landau gauge ( $\xi_g = 0$ ) in QED<sub>4</sub> and the Nash gauge ( $\xi_g = 1/3$ , see [181]) in QED<sub>4,3</sub>. Proceeding similarly at two loops, with the help of (3.99a), we find that the “good gauge” becomes

$$\xi_g = \frac{\varepsilon_e}{2-\varepsilon_e} + \bar{\alpha}_r \left( \frac{4(3-2\varepsilon_e)(1-3\varepsilon_e+\varepsilon_e^2)}{(2-\varepsilon_e)^3(1-\varepsilon_e)} - \frac{4N_f(1-z)\varepsilon_e K_1(\varepsilon_e)}{2-\varepsilon_e} + 2N_f z \right) + \mathcal{O}(\bar{\alpha}_r^3). \quad (3.101)$$

We may now proceed in applying our very general results (3.98), (3.99) and (3.101) to the various cases of interest.

<sup>2</sup>This problem will of course also appear at higher orders for each diagram containing a fermion loop.

### 3.4 Results for the different models of interest

In this section, we now apply our general results (3.98), (3.99) and (3.101) to the various cases of interest, *i.e.*, QED<sub>4</sub> and QED<sub>4,3</sub> where we discuss the absorbance of graphene, as well as the case of large- $N_f$  QED<sub>3</sub> via mapping [134]. Finally, we address the special case of the parity-odd mass term for QED<sub>4,3</sub>.

#### 3.4.1 Results for QED<sub>4</sub>

Let us first consider, as a check, the well-known case of QED<sub>4</sub>, see, *e.g.*, the textbook [61]. From (3.74) and (3.98a), this amounts to set  $z = 1$  and  $\varepsilon_e \rightarrow 0$  yielding

$$(3.102a)$$

$$Z_{\Psi}^{\text{QED}_4} = 1 - \frac{\bar{\alpha}_r \xi_r}{\varepsilon_\gamma} + \frac{\bar{\alpha}_r^2}{2} \left( \frac{\xi_r^2}{\varepsilon_\gamma^2} + \frac{4N_f + 3}{2\varepsilon_\gamma} \right) + \mathcal{O}(\bar{\alpha}_r^3), \quad (3.102b)$$

$$Z_m^{\text{QED}_4} = 1 - \frac{3\bar{\alpha}_r}{\varepsilon_\gamma} + \frac{\bar{\alpha}_r^2}{2} \left( \frac{9 - 4N_f}{\varepsilon_\gamma^2} + \frac{1}{2\varepsilon_\gamma} \left( \frac{20N_f}{3} - 3 \right) \right) + \mathcal{O}(\bar{\alpha}_r^3). \quad (3.102c)$$

Proceeding similarly from (3.99) together with previous results obtained, the anomalous dimensions in QED<sub>4</sub> reads

$$\gamma_{\Psi}^{\text{QED}_4} = 2\bar{\alpha}_r \xi_r - \bar{\alpha}_r^2 (4N_f + 3) + \mathcal{O}(\bar{\alpha}_r^3), \quad (3.103a)$$

$$\gamma_m^{\text{QED}_4} = 6\bar{\alpha}_r - \bar{\alpha}_r^2 \left( \frac{20N_f}{3} - 3 \right) + \mathcal{O}(\bar{\alpha}_r^3), \quad (3.103b)$$

$$\beta^{\text{QED}_4} = -2\bar{\alpha}_r \varepsilon_\gamma + \bar{\alpha}_r^2 \frac{8N_f}{3} + 8\bar{\alpha}_r^3 N_f + \mathcal{O}(\bar{\alpha}_r^4), \quad (3.103c)$$

$$\xi_g^{\text{QED}_4} = 0 + \bar{\alpha}_r \left( \frac{3}{2} + 2N_f \right) + \mathcal{O}(\bar{\alpha}_r^2). \quad (3.103d)$$

We also recall that  $N_f$  is here the number of 4-component spinors, so that the usual high energy physics QED<sub>4</sub> is recovered for  $N_f = 1$ . Focussing on the mass anomalous dimension, (3.103b), the one-loop contribution was probably first computed in [214], the quenched two-loop one in [215] and the unquenched two-loop contribution can be extracted from the QCD calculations of [216, 217] as we could learn from [218] where the three-loop QCD calculation was performed. Notice that, presently,  $\gamma_m$  is known up to five loops in QCD [219, 220] from which the corresponding QED result can be extracted (we shall use it in the next section). Note that, in the case of QED<sub>4</sub>, the good gauge (3.103d) is known since a long time (see, *e.g.*, eq. (B.1) in [214] for an early derivation in the quenched case) and can presently be extended to five loops thanks to state-of-the-art results for  $\gamma_{\Psi}$  [219, 220].

#### 3.4.2 Results for reduced QED<sub>4,3</sub> (Graphene)

Let us now consider the case of interest to us, *i.e.*, QED<sub>4,3</sub> which amounts to set  $z = 0$  and  $\varepsilon_e = 1/2$ . From (3.74) and (3.98a), the renormalization constants read

$$Z_{\Psi}^{\text{QED}_{4,3}} = 1 + \bar{\alpha}_r \frac{1 - 3\xi_r}{3\varepsilon_\gamma} + \bar{\alpha}_r^2 \left( \frac{(1 - 3\xi_r)^2}{18\varepsilon_\gamma^2} - \frac{4}{\varepsilon_\gamma} \left( N_f \zeta_2 + \frac{4}{27} \right) \right) + \mathcal{O}(\bar{\alpha}_r^3), \quad (3.104a)$$

$$Z_m^{\text{QED}_{4,3}} = 1 - \frac{16\bar{\alpha}_r}{3\varepsilon_\gamma} + \bar{\alpha}_r^2 \left( \frac{128}{9\varepsilon_\gamma^2} + \frac{16}{\varepsilon_\gamma} \left( N_f \zeta_2 - \frac{8}{27} \right) \right) + \mathcal{O}(\bar{\alpha}_r^3). \quad (3.104b)$$

And from (3.99), together with previous results obtained, the anomalous dimensions in QED<sub>4,3</sub> read

$$\gamma_{\Psi}^{\text{QED}_{4,3}} = -2\bar{\alpha}_r \frac{1-3\xi_r}{3} + 16\bar{\alpha}_r^2 \left( N_f \zeta_2 + \frac{4}{27} \right) + \mathcal{O}(\bar{\alpha}_r^3), \quad (3.105a)$$

$$\gamma_m^{\text{QED}_{4,3}} = \frac{32\bar{\alpha}_r}{3} - 64\bar{\alpha}_r^2 \left( N_f \zeta_2 - \frac{8}{27} \right) + \mathcal{O}(\bar{\alpha}_r^3), \quad (3.105b)$$

$$\Pi^{\text{QED}_{4,3}}(p^2) = -\frac{\pi N_f \alpha_r}{2p_E} \left( 1 + C_{\gamma}^{\text{QED}_{4,3}} \alpha_r + \mathcal{O}(\alpha_r^2) \right), \quad (3.105c)$$

$$C_{\gamma}^{\text{QED}_{4,3}} = \frac{92-9\pi^2}{18\pi} = 0.056, \quad (\beta^{\text{QED}_{4,3}} = 0), \quad (3.105d)$$

$$\xi_g^{\text{QED}_{4,3}} = \frac{1}{3} - 8\bar{\alpha}_r \left( N_f \zeta_2 + \frac{4}{27} \right) + \mathcal{O}(\bar{\alpha}_r^2), \quad (3.105e)$$

where (3.105a) agrees with the result of [147]. Our result (3.105b) is new and corresponds to the (parity-even) mass anomalous dimension of QED<sub>4,3</sub> for an arbitrary number  $N_f$  of 4-component spinors. We recall here that the correct value for graphene is  $N_f = 2$  flavor of 4-component spinors, because of the two inequivalent cones in the band structure, or equivalently, because of the two inequivalent lattices, see, *e.g.*, [126]. Note that the use of  $\alpha_r$  instead of  $\bar{\alpha}_r$  for the polarization is intended, and since this model is standing, we have trivially that  $\alpha = \mu^{2\varepsilon} \alpha_r$  and  $\xi = \xi_r$  since  $Z_{\xi} = Z_{\alpha}^{-1} = 1$  at all orders.

Going further, following [126], we can use our results to compute the optical conductivity of graphene. Indeed, the polarization of the photon  $\Pi^{\mu\nu}$ , finite and gauge invariant for QED<sub>4,3</sub> (hence physical), can be related to the optical (AC) conductivity of graphene with the Kubo formula

$$\sigma_g(p_0) = -\lim_{\vec{p} \rightarrow 0} \frac{ip_0}{|\vec{p}|^2} \Pi^{00}(p_0, \vec{p}), \quad (3.106)$$

where  $p^{\mu} = (p_0, \vec{p})$ . Since the parametrization (3.31) for the photon polarization reads  $\Pi^{\mu\nu} = (p^2 g^{\mu\nu} - p^{\mu} p^{\nu}) \Pi$  and  $\Pi^{\text{QED}_{4,3}} \sim 1/p_E$ , the formula (3.106) simply yields

$$\sigma_g = -p_E \Pi^{\text{QED}_{4,3}}, \quad (3.107)$$

which, after restoring momentarily the dimensions  $\hbar$ ,  $c$  and  $\varepsilon_0$  for clarity, reads

$$\sigma_g = \sigma_{0g} \left( 1 + C_{\gamma}^{\text{QED}_{4,3}} \alpha_r + \mathcal{O}(\alpha_r^2) \right), \quad \sigma_{0g} = \frac{N_f e^2}{8\hbar} = \frac{\pi N_f e^2}{4h}, \quad (3.108)$$

where  $\sigma_{0g}$  is the well known universal minimal AC conductivity<sup>3</sup> of graphene. Moreover, following [221], the optical conductivity of graphene is related to its transmittance ( $T_g$ ) and its absorbance ( $A_g$ ) (at half-filling) via the relation

$$T_g = 1 - A_g = \left( 1 + \frac{\sigma_g}{2\varepsilon_0 c} \right)^{-2} \approx 1 - \frac{\sigma_{0g}}{\varepsilon_0 c} = 1 - \frac{\pi N_f \alpha_r}{2}, \quad (3.109)$$

where  $\alpha_r = e^2/(4\pi\varepsilon_0 \hbar c)$ . At first order, since  $N_f = 2$  and  $\alpha_r = 1/137$  for graphene in its relativistic limit, we obtain an absorbance of

$$A_{0g} = \pi \alpha_r = 0.0229. \quad (3.110)$$

Moreover,  $C_{\gamma}^{\text{QED}_{4,3}}$  is the interaction correction coefficient to this quantity and so that we can expand the leading order absorbance to compute corrections, reading

$$A_g = \pi \alpha_r \left[ 1 + \alpha_r \left( C_{\gamma}^{\text{QED}_{4,3}} - \frac{3\pi}{4} \right) + \mathcal{O}(\alpha_r^2) \right]. \quad (3.111)$$

<sup>3</sup>The DC case is still under debate, partly because its value is sensitive to the disorder., see, *e.g.*, the review [221].

From perturbation theory, we expect the next corrections to be even smaller, so that the first one can be taken as an error bar for the next ones, *i.e.*, multiplying the NLO factor by  $\pm 1$ , and since  $\alpha_r = 1/137$ , we have numerically that pure standing relativistic graphene have an optical absorbance of

$$A_g = (2.29 \pm 0.04)\%. \quad (3.112)$$

In simple words, this implies that graphene, even though being one atom thick, can be seen bare eyes under white light. See figure 3.5 where graphene (middle) and bilayer graphene (right) are clearly visible under a simple optical microscope. Indeed, analyzing the image, provides a drop of  $A_g \approx 2.3\%$  for each layer of graphene, in accordance with our results.

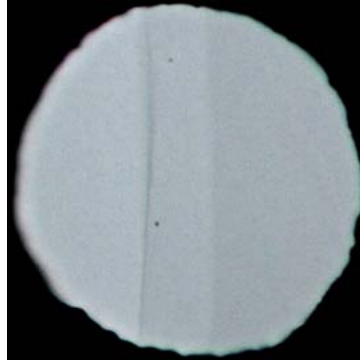


Figure 3.5: An optical image of an aperture partially covered with graphene and its bilayer (from left to right: air/graphene/bilayer), taken in a white light transmission experiment. Luminosity absorbance from left to right is  $A_{\text{air}} \approx 0\%$ ,  $A_{\text{graphene}} \approx 2.3\%$  and  $A_{\text{bi-layer graphene}} \approx 4.6\%$ . Image from [221, 222].

What is very surprising is that this value,  $A_g \approx 2.3\%$ , which is computed at the relativistic fixed point of graphene, is verified experimentally when measured in the pseudo-relativistic limit ( $v_F \approx c/300$ ) [223, 224]. Indeed, the uncertainty computed in (3.112) is for graphene in the infra-red regime, where the coupling is exactly the fine structure constant  $\alpha_r = 1/137$  (relativistic regime). However, in the case of graphene in ambient conditions (pseudo relativistic regime), the universal minimal conductivity ( $\sigma_{0g}$ ) is the same, but the correction coefficient is different and reads  $C_\gamma^{\text{QED}4,3} = (19 - 6\pi)/12 = 0.013$  (see [126, 225] and reference therein), which is 4 times smaller than in the relativistic case (3.105d). Obtaining this value require computations that break Lorentz invariance and are therefore beyond the scope of this thesis. Moreover, in the pseudo-relativistic regime,  $\alpha_r$  depends on the Fermi-velocity  $v_F \approx c/300$  such that the coupling in ambient condition graphene is  $\alpha_g \approx 2.2$ , leading to a much bigger correction to the minimal conductivity, corresponding to an absorbance of  $A_g = \pi\alpha_r \left[ 1 \pm \alpha_g \left( C_\gamma^{\text{QED}4,3} - 3\pi/4 \right) \right] = (2.3 \pm 12)\%$ , *i.e.*, with a very big uncertainty. This is however rude to put  $\alpha_r = 2.2$  in a perturbative series, and in principle, one should compute higher-order corrections and perform series resummations to be able to compute a proper value, which is extremely challenging in this case. At the end, we expect that, either the higher-order corrections will cancel each others, or all corrections coefficients will be small enough to compensate for  $\alpha_r = 2.2$ , so that we recover at the end the experimental value  $A_g \approx 2.3\%$ , such that the relativistic regime, where  $\alpha_r = 1/137$  was indeed a good approximation.

### 3.4.3 Results for QED<sub>3</sub> (Large- $N_f$ )

As a second check, in order to get more confidence in our results, we proceed on showing that the results we obtained for QED<sub>4,3</sub>, equations (3.105) can be mapped to the known results of QED<sub>3</sub> [226] at NLO in the expansion in the large number  $N_f$  of 4-components fermion with the help of the mapping [134]

$$\bar{\alpha}_r \rightarrow \frac{1}{N_f \pi^2}, \quad \hat{\Pi}_1^{\text{QED}_{4,3}} = 2N_f \pi^2 \rightarrow \hat{\Pi}_2^{\text{QED}_3} = \frac{4(92 - 9\pi^2)}{9}, \quad (3.113)$$

where  $\hat{\Pi}_1^{\text{QED}_{4,3}}$  was defined in (3.62) and  $\hat{\Pi}_2^{\text{QED}_3}$  needs to be computed separately, which we will do in the next chapter. Indeed, we will see that QED<sub>3</sub> has more diagrams than QED<sub>4,3</sub> so that we need to inject the NLO polarization in place of the one-loop one. Substituting (3.113) in our QED<sub>4,3</sub> results (3.105b) yields the QED<sub>3</sub> results

$$\gamma_\Psi^{\text{QED}_3} = -\frac{4(2-3\xi)}{3\pi^2 N_f} - \frac{16(2-3\xi)}{27\pi^4 N_f^2} \left( \zeta_2 - \frac{2(16-23\xi)}{9(2-3\xi)} \right) + \mathcal{O}(1/N_f^3), \quad (3.114a)$$

$$\gamma_m^{\text{QED}_3} = \frac{32}{3\pi^2 N_f} + \frac{128}{\pi^4 N_f^2} \left( \zeta_2 - \frac{14}{9} \right) + \mathcal{O}(1/N_f^3), \quad (3.114b)$$

$$\Pi^{\text{QED}_3} = -\frac{N_f e^2}{8p_E} \left[ 1 + \frac{C_\gamma^{\text{QED}_3}}{N_f} + \mathcal{O}(1/N_f^3) \right], \quad (3.114c)$$

$$C_\gamma^{\text{QED}_3} = \frac{2(92-9\pi^2)}{9\pi^2} = 0.07146, \quad (\beta^{\text{QED}_3} = 0), \quad (3.114d)$$

$$\xi_g^{\text{QED}_3} = \frac{2}{3} \left( 1 - \frac{8}{9\pi^2 N_f} + \mathcal{O}(1/N_f^2) \right), \quad (3.114e)$$

which corresponds exactly to the results first obtained by Gracey with another method; the field anomalous dimension in the Landau gauge in [213] and in an arbitrary covariant gauge in [226] as well as the mass anomalous dimension in [226], which indeed required the knowledge of (3.114d). Note that an advanced mapping [134] has been used here to recover properly the gauge dependence in the NLO part of the field anomalous dimension, see chapter 4 section 4.5.4 where the inverse mapping (from QED<sub>3</sub> to QED<sub>4,3</sub>) is explicitly detailed. Hence, all results are in complete agreement. Note that from (3.114a) we also display the “good gauge”, in large- $N_f$  QED<sub>3</sub> at NLO, leading to (3.114e), in agreement with equation (4.8) in [184], which is a first correction to the Nash gauge ( $\xi = 2/3$ ).

### 3.4.4 Case of parity-odd mass term in QED<sub>4,3</sub>

Until now, we have only considered 4-component Dirac spinors  $\Psi$  with a parity invariant action, *i.e.*, containing a parity-even mass term of the form  $m\bar{\Psi}_i\Psi^i$ , where  $i=1, \dots, N_f$ . In this section, we will treat the special case of a parity-odd mass term. To do so, we first recall the formalism in 4-component spinors in four and three dimensions and then introduce the case of three-dimensional 2-component gamma matrices. We therefore consider an arbitrary  $d_e$  number of gamma matrices of size  $n \times n$  satisfying the general Clifford algebra

$$\{\gamma^\mu, \gamma^\nu\} = \gamma^\mu \gamma^\nu + \gamma^\nu \gamma^\mu = 2g^{\mu\nu} I_n, \quad (3.115)$$

where  $\mu=0, 1, \dots, d_e-1$  and  $I_n$  the identity matrix of size  $n \times n$ .

### Four-dimensional $4 \times 4$ gamma matrices

In the four-dimensional case, the common Weyl (irreducible) chiral representation for the algebra (3.115) are the four matrices (see (3.4) for the complementary Dirac representation)

$$\gamma^0 = \begin{pmatrix} 0 & I_2 \\ I_2 & 0 \end{pmatrix}, \quad \gamma^j = \begin{pmatrix} 0 & \sigma_j \\ -\sigma_j & 0 \end{pmatrix}, \quad (3.116)$$

where  $j = 1, 2, 3$  are the space indices and  $\sigma_i$  are the usual  $2 \times 2$  Pauli matrices. In four dimensions, it exists a fifth matrix that anticommutes with the set (3.116), reading

$$\gamma^5 = i\gamma^0\gamma^1\gamma^2\gamma^3 = \begin{pmatrix} -I_2 & 0 \\ 0 & I_2 \end{pmatrix}, \quad (3.117)$$

such that  $\{\gamma^\mu, \gamma^5\} = 0$ . This matrix is the natural generator for chirality as it is the building block for the chiral projectors

$$\Psi_{L/R} = \frac{I_4 \mp \gamma^5}{2} \Psi, \quad \Psi = \begin{pmatrix} \psi_L \\ \psi_R \end{pmatrix}, \quad (3.118)$$

with  $\Psi_L = (\psi_L, 0)$  and  $\Psi_R = (0, \psi_R)$ . Indeed, the chiral transformation reads  $\Psi \rightarrow e^{i\beta\gamma^5} \Psi$  and, similarly, the parity transformation reads  $\Psi(\vec{x}, t) \rightarrow \gamma^0 \Psi(-\vec{x}, t)$  or equivalently  $\psi_{L/R}(\vec{x}, t) \rightarrow \psi_{R/L}(-\vec{x}, t)$ . There are two possible scalar bilinears related to mass terms, reading

$$\bar{\Psi}\Psi = \psi_L^\dagger \psi_R + \psi_R^\dagger \psi_L, \quad (\text{parity-even}) \quad (3.119a)$$

$$\bar{\Psi}\gamma^5\Psi = \psi_L^\dagger \psi_R - \psi_R^\dagger \psi_L, \quad (\text{parity-odd}) \quad (3.119b)$$

where we recall that  $\bar{\Psi} = \Psi^\dagger \gamma^0$ . Let us underline here that terms of the form  $\psi_L^\dagger \psi_R$  are flavor mixing and are therefore not bilinears in themselves. Therefore, the symmetry group of the QED<sub>4</sub> action is indeed  $U(1)$ , possibly enhanced to  $U(N_f)$  with a generalization to  $N_f$  4-component spinors  $\Psi^i$ . The massless action is chiral and parity invariant, and the introduction of a mass term may break the parity invariance depending on the mass choice, see (3.119).

### Three-dimensional $4 \times 4$ gamma matrices

In the three-dimensional case, it is natural to first consider matrices that are still of size  $4 \times 4$ . In this case, the common (reducible) representation for the algebra (3.115) are the three matrices (see (3.19))

$$\gamma^0 = \begin{pmatrix} \sigma_3 & 0 \\ 0 & -\sigma_3 \end{pmatrix}, \quad \gamma^1 = i \begin{pmatrix} \sigma_1 & 0 \\ 0 & -\sigma_1 \end{pmatrix}, \quad \gamma^2 = i \begin{pmatrix} \sigma_2 & 0 \\ 0 & -\sigma_2 \end{pmatrix}. \quad (3.120)$$

With this  $4 \times 4$  representation comes two additional matrices that anticommutes with the  $\gamma^\mu$  set, reading

$$\gamma^3 = \begin{pmatrix} 0 & I_2 \\ -I_2 & 0 \end{pmatrix}, \quad \gamma^5 = i\gamma^0\gamma^1\gamma^2\gamma^3 = \begin{pmatrix} 0 & I_2 \\ I_2 & 0 \end{pmatrix}, \quad (3.121)$$

where  $\{\gamma^\mu, \gamma^3\} = \{\gamma^\mu, \gamma^5\} = 0$ . Another useful matrix to introduce is

$$\gamma^{35} = \gamma^3\gamma^5 = \frac{1}{2} [\gamma^3, \gamma^5] = \begin{pmatrix} -I_2 & 0 \\ 0 & I_2 \end{pmatrix}. \quad (3.122)$$

In this case, the ‘‘chiral’’ transformations<sup>4</sup> are given by  $\Psi \rightarrow e^{i\beta\gamma^3} \Psi$  and  $\Psi \rightarrow e^{i\beta\gamma^5} \Psi$  and the parity transformation by  $\Psi(t, x, y) \rightarrow \gamma^5 \Psi(t, -x, y)$ . In this case, the massless QED<sub>3</sub> and QED<sub>4,3</sub> models

<sup>4</sup>In three-dimensions, *i.e.*, 2 space dimensions plus time, it is abusive to speak about chirality. Here we will refer to it as ‘‘flavor’’ transformations, as in general  $N_f$ , it amounts to exchange the first  $N_f/2$  flavors (left) with the second  $N_f/2$  flavors (right).



enjoys a full  $U(2)$  symmetry and is parity-even. The “chiral” projector is then defined as

$$\Psi_{L/R} = \frac{I_4 \mp \gamma^{35}}{2} \Psi, \quad \Psi = (\psi_L, \psi_R), \quad (3.123)$$

with  $\Psi_L = (\psi_L, 0)$  and  $\Psi_R = (0, \psi_R)$ . With this set of matrices, there are 2 possible<sup>5</sup> scalar fermion bilinears associated to mass terms in three dimensions, reading

$$\bar{\Psi}\Psi = \bar{\psi}_L\psi_L - \bar{\psi}_R\psi_R, \quad (\text{parity-even and breaks } U(2) \rightarrow U(1) \times U(1)) \quad (3.124a)$$

$$\bar{\Psi}\gamma^{35}\Psi = \bar{\psi}_L\psi_L + \bar{\psi}_R\psi_R, \quad (\text{parity-odd and } U(2) \text{ invariant}) \quad (3.124b)$$

where we recall that  $\bar{\Psi} = \Psi^\dagger \gamma^0$  and we defined  $\bar{\psi}_{L/R} = \psi_{L/R}^\dagger \sigma_3$ . What is very interesting here is that the terms  $\bar{\psi}_x \psi_x$  ( $x = L/R$ ) are themselves bilinears. In the case of (3.124b), the symmetry  $U(2)$  is obvious, and in the case of (3.124a), the sign difference of the two terms induces a breaking  $U(2) \rightarrow U(1) \times U(1)$ . As for a generalization to  $N_f$  4-component spinors  $\Psi$ , the global symmetry  $U(2)$  is raised to  $U(2N_f)$  and eventually breaks like  $U(2N_f) \rightarrow U(N_f) \times U(N_f)$ . Therefore, (3.124a) is the parity-even mass that we considered in the previous computations of this chapter, and (3.124b), the parity-odd mass term that we shall study in this specific section. In the  $N_f$  4-component spinor generalization, these two terms can be written as

$$\sum_{i=1}^{N_f} \bar{\Psi}_i \Psi^i = \sum_{i=1}^{N_f} \bar{\psi}_i \psi^i - \sum_{i=1+N_f}^{2N_f} \bar{\psi}_i \psi^i, \quad (\text{parity-even}), \quad (3.125a)$$

$$\sum_{i=1}^{N_f/2} \bar{\Psi}_i \Psi^i - \sum_{i=1+N_f/2}^{N_f} \bar{\Psi}_i \Psi^i = \sum_{i=1}^{2N_f} \bar{\psi}_i \psi^i, \quad (\text{parity-odd}). \quad (3.125b)$$

Note that since the parity-odd mass term is  $U(2N_f)$  invariant, it is then irrelevant for dynamical chiral breaking.

### Three-dimensional $2 \times 2$ gamma matrices

In three spacetime dimensions, in order to better appreciate the  $U(2N_f)$  “chiral” symmetry, it is possible to use a smaller representation for the Clifford algebra (3.115). Indeed, the minimal  $n \times n$  representation in arbitrary dimension  $d$  is  $n = 2^{\lfloor d/2 \rfloor}$ , with  $\lfloor x \rfloor$  the floor function. For  $d=3$ , it exists then a  $2 \times 2$  representation. One usually takes the gamma matrices as

$$\gamma^0 = \sigma_2, \quad \gamma^1 = i\sigma_3, \quad \gamma^2 = i\sigma_1. \quad (3.126)$$

Note that it exist a second inequivalent representation with opposite signs so that the combination of the two inequivalent  $2 \times 2$  representation gives the  $4 \times 4$  one (3.19). With this representation comes no additional matrix that anticommutes with the set (3.126). Therefore, the chirality is here undefined. One can only perform computations with two component spinors ( $L$  or  $R$ , we do not specify it). In this case, there is only one mass term, the scalar bilinear  $\bar{\psi}\psi$ , where  $\bar{\psi} = \psi^\dagger \sigma_3$ . For  $2N_f$  2-component spinors, it generalizes as

$$\sum_{i=1}^{2N_f} \bar{\psi}_i \psi^i. \quad (3.127)$$

Note that by comparison with the  $4 \times 4$  representation, this term can correspond to both a parity-even or odd mass term depending on the sign choice. What is very tricky with this choice of representation is that, in striking opposition with the  $4 \times 4$  representation, the traces over an odd number of gamma matrices is not zero! See more details in the next section.

<sup>5</sup>There is also two additional scalar terms, the parity-odd  $\bar{\Psi}\gamma^3\Psi = \bar{\psi}_L\psi_R + \bar{\psi}_R\psi_L$  and the parity-even  $\bar{\Psi}\gamma^5\Psi = \bar{\psi}_L\psi_R - \bar{\psi}_R\psi_L$ . However, we do not consider them because both are completely flavor breaking.



### Parity-odd mass in QED<sub>4,3</sub>

Notations being clarified, we will now consider the case of a parity-odd mass term for QED<sub>4,3</sub>, *i.e.*, of the form (3.125b). The simplest way to perform the computations is to avoid specifying any representation. We will then assume that it exist a  $n \times n$  representation for  $d_e$  Dirac matrices and use the following basic properties

$$\text{Tr}(\gamma^\mu) = 0, \quad \text{Tr}(I_n) = n, \quad \text{Tr}(\gamma^\mu \gamma^\nu) = n g^{\mu\nu}. \quad (3.128)$$

What is crucial here is the trace of 3 gamma matrices. Indeed, if one uses a  $4 \times 4$  representation like (3.120), it is well known and easy to show that  $\text{Tr}(\gamma^\mu \gamma^\nu \gamma^\rho) = 0$ , and then that all traces with an odd number of gamma matrices vanishes using the recursive formula (3.24). However, if one uses the  $2 \times 2$  representation (3.126), it is easy to show that these traces are non-vanishing and read  $\text{Tr}(\gamma^\mu \gamma^\nu \gamma^\rho) = 2i \varepsilon^{\mu\nu\rho}$ , with  $\varepsilon^{\mu\nu\rho}$  the rank-3 totally antisymmetric tensor, *i.e.*, the Levi-Civita symbol in three dimensions. Therefore, to keep track of both cases and work in arbitrary  $n \times n$  representation, we can define

$$\text{Tr}(\gamma^\mu \gamma^\nu \gamma^\rho) = ni \mathcal{T}_n \varepsilon^{\mu\nu\rho}, \quad (3.129)$$

where  $\mathcal{T}_n$  is an additional binary parameter allowing or not the vanishing of the odd traces, *i.e.*, defined as

$$\mathcal{T}_n = \begin{cases} 0 & \text{if } n = 4 \\ 1 & \text{if } n = 2 \end{cases}, \quad \mathcal{T}_n^2 = \mathcal{T}_n. \quad (3.130)$$

From these properties it is straightforward to show that in fact  $n\mathcal{T}_n = 4 - n$  so that one can alternatively work with the definition  $\text{Tr}(\gamma^\mu \gamma^\nu \gamma^\rho) = i(4 - n)\varepsilon^{\mu\nu\rho}$ . Nevertheless, in the following we will keep the  $\mathcal{T}_n$  notation to emphasize terms affected by the odd traces.

From there, all traces over a higher number (even or odd) of gamma matrices can be computed using the algorithm (3.24). On the computational side, the following identities are useful

$$\varepsilon^{\mu\nu\rho} \varepsilon^{\alpha\beta\gamma} = \det \begin{pmatrix} g^{\mu\alpha} & g^{\mu\beta} & g^{\mu\gamma} \\ g^{\nu\alpha} & g^{\nu\beta} & g^{\nu\gamma} \\ g^{\rho\alpha} & g^{\rho\beta} & g^{\rho\gamma} \end{pmatrix}, \quad \varepsilon^{\mu\nu\rho} g_{\mu\nu} = 0, \quad \varepsilon^{\mu\nu\rho} p_\mu p_\nu = 0, \quad (3.131)$$

where the two last identities are due to the fact that contracting completely  $\varepsilon^{\mu\nu\rho}$  with a symmetric tensor is zero. It also implies that contracting  $\varepsilon^{\mu\nu\rho}$  with the photon propagator or polarization is also vanishing. Here is an example of contraction identity to fix notations

$$\varepsilon^{\mu\nu\rho} \text{Tr}(\gamma^\mu \gamma^\nu \gamma^\rho) = ind(d-1)(d-2)\mathcal{T}_n. \quad (3.132)$$

These new traces, proportional to Levi-Civita tensors are obviously related to the famous Chern-Simons terms of the form  $\theta \varepsilon_{\mu\nu\rho} A_\mu \partial_\nu A_\rho$  (see, *e.g.*, [120, 227–229] for related works) and the eventuality of an axial anomaly (see, *e.g.*, the seminal papers [230, 231]), that may give a (bare of radiatively generated) mass  $\theta$  to the photon. However, in this whole manuscript, we completely neglect any Chern-Simons terms, *i.e.*,  $\theta = 0$ .

We now re perform all the computations for QED<sub>4,3</sub> with an arbitrary number  $\mathcal{N}_f$  of  $n$ -component spinors<sup>6</sup>, and a parity-odd mass term. It turns out that most of the diagrams are unchanged, up to the trivial generalization to arbitrary  $n$  via  $N_f \rightarrow n\mathcal{N}_f/4$  (and not forgetting to generalize the projectors (3.28) with  $4 \rightarrow n$ ). This implies that the odd traces do not contribute to the vast majority of the diagrams. Up to two loops, the only diagram affected by odd traces is the first contribution (a) to the two-loop scalar part of the electron self-energy, *i.e.*,  $\Sigma_{2Sa}(p^2)$ . Recomputing this diagram with an

<sup>6</sup>Using  $\mathcal{N}_f(n)$   $n$ -component spinors, we have that  $\mathcal{N}_f(4) = N_f$  and  $\mathcal{N}_f(2) = n_f = 2N_f$ .



### 3.5 Critical properties

As explained in the Introduction, a standard approach to study the critical properties of gauge theories is by solving the SD equations. Truncating these equations at LO is the simplest, but generally unsatisfactory, as the resulting critical coupling may be strongly gauge-dependant. The fully gauge-invariant procedure advocated in the recent [184] and [186] for large- $N_f$  QED<sub>3</sub> requires computing NLO corrections and then performing a so-called Nash resummation (following the seminal work of Nash [181]) in order to properly cancel the gauge dependence both at LO and NLO. The simplicity of the resulting gap equation (from which the gauge-invariant critical coupling is extracted) drastically contrasts with the complexity of the calculations that need to be performed in order to derive it. Following [184], in this section we provide a semi-phenomenological construction of the gap equation for QED<sub>4,d<sub>e</sub></sub> and apply it to our cases of interest. Before that, we would like nevertheless to apply the SD formalism at LO for QED<sub>4,d<sub>e</sub></sub>. This allows us to illustrate some of the difficulties we have just mentioned, and underline the importance of the “good gauge” introduced in the previous section.

#### 3.5.1 Leading-order solution of SD equations for QED<sub>4,d<sub>e</sub></sub>

The SD equation for the fermion self-energy in QED<sub>4,d<sub>e</sub></sub> reads

$$-i\Sigma(p) = \text{Diagram} = \mu^{2\varepsilon_\gamma} \int [d^{d_e} k] \Gamma^\mu(k, p) S(k) \Gamma_0^\nu D_{\mu\nu}(p-k), \quad (3.136)$$

where  $S(p)$ ,  $\Gamma^\mu(p_1, p_2)$  and  $D_{\mu\nu}(p)$  are respectively the full fermion propagator, the full vertex function and the full photon propagator, all represented by enlarged lines (and a blob for the vertex). In general, (3.136) is coupled to the Dyson equation for the polarization operator, reading

$$i\Pi^{\mu\nu}(p) = \mu \text{Diagram} \nu = -\mu^{2\varepsilon_\gamma} N_f \int [d^{d_e} k] \text{Tr} \left[ \Gamma^\mu(k, k-p) S(k) \Gamma_0^\nu S(k-p) \right], \quad (3.137)$$

and the vertex function  $\Gamma^\mu(p_1, p_2)$  defined as

$$\Gamma^\mu(p_1, p_2) = \mu \text{Diagram} = -ie\gamma^\mu - ie\Lambda^\mu(p_1, p_2), \quad (3.138a)$$

$$\Lambda^\mu(p_1, p_2) = \mu \text{Diagram} = \int [d^{d_e} k] S(k-p_1) \Gamma^\mu(k-p_1, k-p_2) S(k-p_1) K(p_1, k-p_2, k-p_1, p_2), \quad (3.138b)$$

with  $K$  is the four-fermion interaction scattering kernel, which is highly non-trivial. A dynamical mass arises as a non-trivial solution of this system of coupled equations for  $\Sigma_S(p^2)$ , that needs to be determined self-consistently.

Focusing on the LO approximation in the coupling constant, all equations decouple as both the vertex function and the photon propagators are taken as the free ones;  $\Gamma^\mu = \Gamma_0^\mu$  and  $D^{\mu\nu}(p) = D_0^{\mu\nu}(p)$ . Moreover, the wave-function renormalization is neglected, *i.e.*,  $\Sigma_V = 0$ , which implies that  $S(p) = i(\not{p} - \Sigma_S)^{-1}$  where  $\Sigma_S$  is now the dynamically generated parity-conserving mass (for convenience, the mass parameter has been absorbed in  $\Sigma_S$ ). With the help of the parametrization (3.28), the equation (3.136) decouples and significantly simplifies, yielding

$$\Sigma_S(p^2) = \frac{-ie^2 \Gamma(1 - \varepsilon_e)}{(4\pi)^{\varepsilon_e}} (d_e - 1 + \tilde{\xi}) \mu^{2\varepsilon_\gamma} \int \frac{[d^{d_e} k] \Sigma_S(k^2)}{(-k^2 + \Sigma_S^2(k^2))(-p-k)^2)^{1-\varepsilon_e}}. \quad (3.139)$$

At the critical point, (3.139) can be linearized in the limit  $\Sigma_S^2(k^2) \ll k^2$  and a power-law ansatz can be taken for the mass function  $\Sigma_S(p^2)$  such that

$$\Sigma_S(p^2) = m_{\text{dyn}}(-p^2)^{-b/2}, \quad (3.140)$$

where the mass is assumed to be dynamical in origin and the index  $b$  has to be self-consistently determined. As first noticed by Kotikov [182, 183], together with (3.140), the linearized equation (3.139) is now a massless integral which is easily solved in dimensional regularization with the help of the massless techniques described in Appendix A. The solution being finite for all  $d_e$ , one can set  $\varepsilon_\gamma = 0$  and straightforwardly derive the LO gap equation

$$b(d_e - 2 - b) = 4\bar{\alpha}(3 - \varepsilon_e + (1 - \varepsilon_e)\xi) + \mathcal{O}(\bar{\alpha}^2). \quad (3.141)$$

Solving it yields two values for the index  $b$

$$b_\pm = (1 - \varepsilon_e) \left( 1 \pm \sqrt{1 - 4\bar{\alpha} \frac{3 - \varepsilon_e + (1 - \varepsilon_e)\xi}{(1 - \varepsilon_e)^2}} \right). \quad (3.142)$$

Dynamical mass generation takes place for complex values of  $b$ , *i.e.*, for  $\alpha > \alpha_c$  with

$$\alpha_c(\xi) = \frac{\pi(1 - \varepsilon_e)^2}{3 - \varepsilon_e + (1 - \varepsilon_e)\xi}. \quad (3.143)$$

Notice that, in the case of QED<sub>4,3</sub> ( $\varepsilon_e = 1/2$ ), (3.143) leads to  $\alpha_c = \pi/(2(5 + \xi))$ , in agreement with [134]. On the other hand, in the case of QED<sub>4</sub> ( $\varepsilon_e = 0$ ), we obtain  $\alpha_c = \pi/(3 + \xi)$ , which exactly corresponds to the result of Rembiesa [234] according to [235].

As anticipated, (3.143) has a strong gauge dependence, which is not satisfactory, as  $\alpha_c$  is supposed to be a physical quantity. In order to minimize the gauge dependence, we consider the “good gauge” which is given by (3.100) at one loop. This yields

$$\alpha_c(\xi_g) = \frac{\pi(2 - \varepsilon_e)(1 - \varepsilon_e)^2}{2(3 - 2\varepsilon_e)}, \quad (3.144)$$

which is  $\alpha_c^{\text{QED}_4} = \pi/3$  and  $\alpha_c^{\text{QED}_{4,3}} = 3\pi/32$ . We shall come back to these results and discuss them in detail in the next subsections. At this point, let us note that the LO gap equation itself, (3.141), can also be written in the “good gauge” where it may be expressed in the form

$$b(d_e - 2 - b) = (d_e - 2)(\gamma_{1m}\bar{\alpha} + \mathcal{O}(\bar{\alpha}^2)). \quad (3.145)$$

Interestingly, the right-hand side of (3.145) involves the one-loop mass anomalous dimension (3.75) — a gauge-invariant quantity — as the only input.

The powerful technique of Kotikov [182, 183], that we have used here to easily solve the LO SD equation in dimensional regularization, can possibly be extended to higher orders for QED<sub>4</sub>, along the lines of the recent [186]. Of course, an NLO computation is more complicated and is out of the scope of the present manuscript. Instead, in the following subsection, we will present general arguments allowing us to build a fully gauge-invariant gap equation that is valid at any order in the coupling constant, thereby generalizing (3.145).

### 3.5.2 Gap equation and criterion for dynamical mass generation

We start by recalling that, from the operator product expansion, the scalar part of the fermion self-energy has two asymptotes in the UV [204–207] (see also the textbook [208] section 12.3):

$$\Sigma_S(p) \sim m p_E^{-\gamma_m} + m_{\text{dyn}} p_E^{-(d_e - 2 - \gamma_m)}, \quad (3.146)$$

where  $p_E^2 = -p^2$  is the Euclidean momentum,  $m$  is the bare mass of the fermion and  $m_{\text{dyn}}$  the dynamical one. As noticed in [207], dynamical mass generation arises from the coalescence of these two asymptotes. In particular, deep in the UV,  $p_E^2 \rightarrow \infty$ , the dynamical mass is favored over the bare mass provided the mass anomalous dimension is large enough;  $\gamma_m > (d_e - 2)/2$ . The non-perturbative criterion for dynamical mass generation is therefore given by  $\gamma_m(\alpha_c) = (d_e - 2)/2$  which requires the knowledge of the exact  $\gamma_m$ .

In our case, we only have access to a perturbative expansion for  $\gamma_m$ . Hence, we would like to find a criterion for dynamical mass generation (which is intrinsically a non-perturbative mechanism) that could be truncated at a given order of the perturbative expansion of  $\gamma_m$ . This can be achieved with the help of the gap equation found from the SD formalism. Actually, as we saw in the previous subsection, we know that the all order ansatz (valid at the critical point) for the fermion self-mass is given by  $\Sigma_S(p) \sim p_E^{-b}$  (see (3.140)) where the index  $b$  is determined self-consistently. Comparing this ansatz to (3.146), and in particular to the second asymptote of this equation, we see that  $b = d_e - 2 - \gamma_m$  and is therefore related to the mass anomalous dimension. From [184], we learn that the gap equation (which is quadratic in  $b$ ) is built up from the two asymptotes of (3.146) (at least for large- $N_f$  QED<sub>3</sub> at NLO in the  $1/N_f$ -expansion). Extending the result of Gusynin and Pyatkovskiy [184] to arbitrary  $d_e$ , we therefore assume that, for QED<sub>4, $d_e$</sub> , the gap equation is quadratic in  $b$  at all loop orders and takes the form

$$b(d_e - 2 - b) = \gamma_m(d_e - 2 - \gamma_m), \quad (3.147)$$

with  $\gamma_m$  as the only input. As we saw in the previous subsection, in the SD formalism, the dynamical mass is generated when  $b$  becomes complex, *i.e.*, for  $(b - (d_e - 2)/2)^2 < 0$ . In terms of the mass anomalous dimension and at the critical point, this criterion translates into

$$K(\alpha) = \left( \gamma_m(\alpha) - \frac{d_e - 2}{2} \right)^2, \quad \text{and} \quad K(\alpha_c) = 0, \quad (3.148)$$

from which the critical coupling  $\alpha_c$  can be computed. Note that, if  $\gamma_m$  would be known exactly, the gap equation would then simply yield  $\gamma_m(\alpha_c) = (d_e - 2)/2$ . However, when the mass anomalous dimension is known only perturbatively up to a certain loop order, the gap equation (3.148) accordingly needs to be properly truncated, *i.e.*, with  $\gamma_m = \gamma_{1m} + \gamma_{2m} + \dots$ , it reads

$$K(\alpha) = \frac{(d_e - 2)^2}{4} - (d_e - 2)\gamma_{1m} + (\gamma_{1m}^2 - (d_e - 2)\gamma_{2m}) + \dots, \quad (3.149)$$

and then solved with  $K(\alpha_c) = 0$ . Since  $\gamma_m$  is gauge invariant by construction, the resulting critical coupling will automatically be gauge invariant too. Moreover, as it is built from the SD formalism, it can be truncated to the accuracy at which  $\gamma_m$  is known (Equation (3.147) reduces to (3.145) at the LO in  $\alpha$ ). From this polynomial equation, we will obtain multiple solutions for  $\alpha_c$ . The physical  $\alpha_c$  will be taken as the smallest positive real solution that is found, in accordance with perturbation theory.

At this point, we would like to comment on the fact that the large mass anomalous dimension required for dynamical mass generation also affects the dimension of the quartic fermion operator  $\Delta[(\bar{\Psi}\Psi)^2] = 2d_e - 2 - \gamma_{(\bar{\Psi}\Psi)^2}$  where  $\gamma_{(\bar{\Psi}\Psi)^2}$  is the associated anomalous dimension. Indeed, assuming that  $\gamma_{(\bar{\Psi}\Psi)^2} = 2\gamma_m$ , we have  $\Delta[(\bar{\Psi}\Psi)^2] = 2d_e - 2 - 2\gamma_m \leq d_e$  for  $\gamma_m \geq (d_e - 2)/2$ , *i.e.*, the quartic fermion operator is marginal at the critical point and becomes relevant once the dynamical mass is generated. However, from these arguments, the marginality of the quartic fermion operator at criticality appears as a consequence of (3.148) and holds only in an approximate way. According to the literature on QED<sub>4</sub>, see, *e.g.*, the review [171] as well as [199–202], the assumption  $\gamma_{(\bar{\Psi}\Psi)^2} = 2\gamma_m$  is supposed to be valid in the quenched and rainbow approximation.<sup>8</sup> In the case of QED<sub>4</sub>, there is evidence that

<sup>8</sup>In the rainbow (or ladder) approximation, the full vertex  $\Gamma^\mu$  entering the SD equations is taken as the free vertex,  $\Gamma^\mu \rightarrow \Gamma_0^\mu = -ie\gamma^\mu$ . Note that our (two-loop) perturbative calculations do take into account of vertex corrections and our analysis is therefore beyond the rainbow approximation.

it still holds beyond the rainbow approximation [235]. Note also that the quenched approximation significantly affects QED<sub>4</sub> because in this approximation the coupling does not run. But its effect is weaker for a “standing” theory such as QED<sub>4,3</sub>. These arguments suggest that the marginality of the quartic fermion operator at criticality may hold even beyond the quenched (especially for QED<sub>4,3</sub>) and rainbow approximations. A more careful study of the validity of this approximation goes beyond the scope of this paper.

In the next sections, we will apply (3.148) to the study of the critical properties of QED<sub>4,d<sub>e</sub></sub> with applications to QED<sub>4,3</sub> and QED<sub>4</sub>. For the case of QED<sub>4,3</sub>, we will find perfect agreement with the SD formalism [134] which is natural since (3.148) is built from the SD formalism for large- $N_f$  QED<sub>3</sub> [184] which can be mapped to QED<sub>4,3</sub> [134]. As for QED<sub>4</sub>, our approach is more phenomenological, since it amounts to extrapolate an equation valid for QED<sub>4,3</sub> to the more subtle case of a “running” theory.

### 3.5.3 Application to quenched QED<sub>4,d<sub>e</sub></sub>

“Quenched” is the (extreme) approximation that completely neglects the fermion, *i.e.*,  $N_f = 0$ . Though unphysical, it is a convenient limit where computations are much simpler. As we will see in the following, this approximation appears as the natural solution to our equations beyond one loop.

#### Quenched QED<sub>4,d<sub>e</sub></sub> at one loop

We first consider QED<sub>4,d<sub>e</sub></sub> at one loop. Substituting the one-loop expression of  $\gamma_m$ , (3.75), in (3.148) yields the following critical coupling constant:

$$\alpha_c = \frac{\pi(2 - \varepsilon_e)(1 - \varepsilon_e)^2}{2(3 - 2\varepsilon_e)}, \quad (3.150)$$

which corresponds exactly to the result (3.144), obtained via the SD approach in the “good gauge” (3.100). Note that it is also independent of  $N_f$  at this order. In the case of QED<sub>4,3</sub> ( $\varepsilon_e = 1/2$ ), (3.150) yields

$$\alpha_c^{\text{QED}_{4,3}} = \frac{3\pi}{32} = 0.2945, \quad (1\text{-loop}), \quad (3.151)$$

which agrees with the result of [118, 134]. Note that from the mapping (3.113) to large- $N_f$  QED<sub>3</sub>, the corresponding critical fermion flavor number reads

$$N_c^{\text{QED}_3} = \frac{128}{3\pi^2} = 4.3230, \quad (\text{LO}), \quad (3.152)$$

where LO stands for leading order, *i.e.*, at  $O(1/N_f)$ . This result is in agreement with [118, 181, 184, 186].

In the case of QED<sub>4</sub> ( $\varepsilon_e = 0$ ), we recover the celebrated result

$$\alpha_c^{\text{QED}_4} = \frac{\pi}{3} = 1.0472, \quad (1\text{-loop}), \quad (3.153)$$

which was obtained via the rainbow approximation in the Landau gauge (which is the “good gauge” for QED<sub>4</sub> at one loop, see (3.103d)) in the early papers [236–238]. In [235], a numerical solution of SD equations with Curtis-Pennington vertex (and hard cut-off regularization) led to  $\alpha_c^{\text{QED}_4}(\xi) \approx 0.93$  with variations of the critical coupling of only a couple of percents over a wide range of the gauge fixing parameter; such a result deviates by 11% from  $\pi/3$ . In [239], calculations using dimensional regularization, which is a gauge-invariant regularization scheme, were found to agree with the hard cut-off regularization ones to within numerical precision. Moreover, in [240] the result  $\alpha_c^{\text{QED}_4} = \pi/3$  was extracted analytically from dimensionally regularized SD equations in the Landau gauge in perfect



agreement with our own calculation of section 3.5.1. Based on (3.148), we obtained in a very simple way that  $\alpha_c^{\text{QED}_4} = \pi/3$  is actually the fully gauge-invariant result at LO. This motivates us to include higher-order corrections, which is quite straightforward in our formalism, provided  $\gamma_m$  is known.

### Quenched QED<sub>4,d<sub>e</sub></sub> at two loops

We therefore consider QED<sub>4,d<sub>e</sub></sub> at two loops. Substituting the two-loop expression of  $\gamma_m$ , (3.99b), in (3.148), and selecting as a physical critical coupling the smallest value obtained, yields the following result

$$\alpha_c(N_f) = \frac{\pi(2-\varepsilon_e)(1-\varepsilon_e)^2}{3-2\varepsilon_e + \sqrt{\Delta_{N_f}}}, \quad (3.154)$$

where

$$\Delta_{N_f} = \frac{(1-\varepsilon_e)(3-2\varepsilon_e)}{2-\varepsilon_e} - 2N_f(1-z)(2-\varepsilon_e)(1-\varepsilon_e)^3 K_1 - \frac{10N_f z}{3}, \quad (3.155)$$

see (3.52a) for the definition of  $K_1$ . It turns out that  $\alpha_c$  in (3.154) is actually complex and hence nonphysical for all integer values of  $N_f$  except  $N_f=0$ . This comes from the fact that  $\Delta_{N_f}$  in (3.155) is positive only for values of  $N_f$  which are smaller than

$$N_{\max} = \frac{3(3-2\varepsilon_e)}{2(10z+3(1-z)(1-\varepsilon_e)^2(2-\varepsilon_e)^2 K_1)}, \quad (3.156)$$

and this maximal value is smaller than 1 for  $d_e \leq 4$ . Thus, the critical coupling (3.154) is defined only in the case of quenched QED<sub>4,d<sub>e</sub></sub> where its expression simplifies. We display it explicitly for clarity

$$\alpha_c(N_f=0) = \frac{\pi(2-\varepsilon_e)(1-\varepsilon_e)^2}{3-2\varepsilon_e + \sqrt{\Delta_0}}, \quad \Delta_0 = \frac{(1-\varepsilon_e)(3-2\varepsilon_e)}{2-\varepsilon_e}, \quad (3.157)$$

where, together with  $N_f$ , all the  $z$ -dependence dropped out. In the case of QED<sub>4,3</sub> ( $\varepsilon_e = 1/2$ ), (3.157) yields

$$\alpha_c^{\text{QED}_{4,3}}(N_f=0) = \frac{9\pi}{8(6+\sqrt{6})} = 0.4183, \quad (2\text{-loop}), \quad (3.158)$$

in agreement with [134]. Note that from the mapping (3.113) to large- $N_f$  QED<sub>3</sub>, the corresponding critical fermion flavor number reads

$$N_c^{\text{QED}_3} = \frac{16(4+\sqrt{3\pi^2-28})}{3\pi^2} = 2.8470, \quad (\text{NLO}), \quad (3.159)$$

where NLO stands for next to leading order, *i.e.*, of order  $1/N_f^2$ . This result is in agreement with [184, 186]. In the case of QED<sub>4</sub> ( $\varepsilon_e = 0$ ), (3.157) yields

$$\alpha_c^{\text{QED}_4}(N_f=0) = \frac{4\pi}{6+\sqrt{6}} = 1.4872, \quad (2\text{-loop}), \quad (3.160)$$

which is a new result and deviates substantially from the one-loop one (about 40% increase).

### Quenched QED<sub>4</sub> at higher loops

Actually, we can go beyond two loops in QED<sub>4</sub>, since computations are already known up to five loops. We first consider three loops (see the three-loop computations for QED<sub>4</sub> are presented in the appendix 3.A) where the corresponding mass anomalous dimension, from our calculations, yields

$$\gamma_m^{\text{QED}_4} = 6\bar{\alpha}_r + \bar{\alpha}_r^2 \left( 3 - \frac{20N_f}{3} \right) - \bar{\alpha}_r^3 \left( 129 + 4N_f(23 - 24\zeta_3) - \frac{280N_f^2}{27} \right) + \mathcal{O}(\bar{\alpha}^4), \quad (3.161)$$

in accordance with the literature, see, *e.g.*, [219, 220]. We can then use (3.161) to solve the effective gap equation (3.148) at three loops, reading

$$\alpha_c^{\text{QED}_4}(N_f=0) = \frac{2\pi}{111} (10 - 788s^{-1} + s) = 1.1322, \quad (3\text{-loop}), \quad (3.162)$$

where  $s^3 = 2(6161 + 111\sqrt{13009})$ . Going even further, we can use state-of-the-art results for  $\gamma_m$  at four and five loops [219, 220]<sup>9</sup> that reads

$$\begin{aligned} \gamma_m^{\text{QED}_4} = & 6\bar{\alpha}_r + \bar{\alpha}_r^2 \left( 3 - \frac{20N_f}{3} \right) + \bar{\alpha}_r^3 \left( 129 - 4N_f(23 - 24\zeta_3) - \frac{280N_f^2}{27} \right) \\ & + \bar{\alpha}_r^4 \left( -\frac{1}{4}(1261 + 2688\zeta_3) - \frac{16}{3}N_f(11 - 27\zeta_3 + 180\zeta_5) + \frac{32}{27}N_f^2(19 - 270\zeta_3 + 162\zeta_4) - \frac{16}{81}N_f^3(83 - 144\zeta_3) \right) \\ & + \bar{\alpha}_r^5 \left( \frac{1}{4}(50995 + 6784\zeta_3 + 16640\zeta_5) - \frac{1}{18}N_f(61469 - 70560\zeta_3 + 24192\zeta_4 + 17760\zeta_5 - 241920\zeta_7) \right. \\ & \quad + \frac{1}{27}N_f^2(3877 - 98880\zeta_3 + 48384\zeta_3^2 + 28944\zeta_4 + 103680\zeta_5 - 86400\zeta_6) \\ & \quad \left. + \frac{4}{81}N_f^3(4483 + 4752\zeta_3 - 12960\zeta_4 + 6912\zeta_5) - \frac{32}{81}N_f^4(65 + 80\zeta_3 - 144\zeta_4) \right) + \mathcal{O}(\bar{\alpha}^6), \quad (3.163) \end{aligned}$$

thereby confirming our three-loop result (3.161). Solving the effective gap equation (3.148) at four-loop order leads to a non-physical complex result, so we discard it. As for the five-loop solving, it can only be carried out numerically, as it amounts to find the roots of is a fifth order polynomial, and reads

$$\alpha_c^{\text{QED}_4}(N_f=0) = 1.0941, \quad (5\text{-loop}). \quad (3.164)$$

Our results for quenched QED<sub>4</sub> up to five loops are then summarized numerically in table 3.2.

loops	1	2	3	4	5
$\alpha_c(N_f=0)$	1.0472	1.4872	1.1322	—	1.0941

Table 3.2: Critical couplings of quenched QED<sub>4</sub> computed from (3.148) up to 5 loops (the symbol “—” indicates that no physical solution is found).

Though we do not find any physical solution at four loops, we observe that, beyond two loops, the critical coupling decreases reaching 1.0941 at five loops which deviates by only 4% from the one-loop result.

### Literature comparison for quenched QED<sub>4,de</sub>

We shall compare the results obtained via our method, summarized in the table 3.2, with the quenched QED<sub>4</sub> literature. We take as a reference the table II in [174], that we reproduce here in table 3.3 for convenience. We recall that our results should correspond to the results of the literature in the good gauge, which in the case of QED<sub>4</sub> is close to the Landau gauge, *i.e.*,  $\xi = 0$ . We therefore generate the table 3.4, of the relative deviations (in %) of our results as compared to the literature in Landau gauge. We sort the results from the literature in two categories; the bare approach, giving  $\approx \pi/3$  and the CP approach giving  $\approx 0.93$ .

Our new five-loop result (3.164), yielding  $\alpha_c(N_f=0) = 1.0941 \forall \xi$ , is therefore in quantitative agreement with other estimates from numerical solutions of SD equations in quenched QED<sub>4</sub> with various vertex ansätze, see, *e.g.*, [172, 174], that lead to  $\alpha_c(N_f=0) \approx 0.93$  in the Landau gauge<sup>10</sup>, *i.e.*, a 15% deviation from our result.

<sup>9</sup>We used the results of the ancillary files of both [241] and [242].

<sup>10</sup>In quenched QED<sub>4</sub>, up to five loops, the “good gauge” is very close (at most 0.18) to the Landau gauge. It is then reasonable to compare our gauge invariant results to those calculated in the Landau gauge.



Reference	$\xi = 0$	$\xi = 1$	$\xi = 3$	Vertex
Miransky [238] (1984)	$\pi/3$	NA	NA	Bare
CP [243] (1993)	$1.003 * \pi/3$	NA	NA	Bare
Bloch [172] (1995)	1.047	1.690	2.040	Bare
CP [243] (1993)	0.9344	0.9240	0.9218	CP
Atkinson <i>et al.</i> [235] (1993)	0.933667	0.923439	0.921272	CP
Bloch [172] (1995)	0.933667	0.890712	0.832927	modified CP
BBCR [244] (2011)	0.934	NA	NA	BBCR Ansatz

Table 3.3: Reproduced from [174]. Critical (gauge-dependent) coupling results from the literature. CP  $\equiv$  Curtis-Pennington, BBCR  $\equiv$  Bashir-Bermudez-Chang-Roberts. NA indicates “not available”.

QED <sub>4</sub> Literature		rel. diff. to our work				
Vertex model	$\alpha_c(N_f = 0)$	1l	2l	3l	4l	5l
Bare [172, 238, 243]	$\sim \pi/3$ ( $\xi = 0$ )	0%	30%	8%	–	4%
CP [172, 235, 243, 244]	$\sim 0.93$ ( $\xi = 0$ )	11%	37%	17%	–	15%
This work (1-loop)	1.0472 $\forall \xi$	0%	42%	8%	–	4%
This work (2-loop)	1.4872 $\forall \xi$	30%	0%	24%	–	26%
This work (3-loop)	1.1322 $\forall \xi$	8%	31%	0%	–	3%
This work (4-loop)	–	–	–	–	–	–
This work (5-loop)	1.0941 $\forall \xi$	4%	36%	3%	–	0%

Table 3.4: Comparative table for the critical quenched ( $N_f = 0$ ) coupling result obtained in this work vs the literature in Landau gauge, which has been sorted into two categories, Bare and CP  $\equiv$  Curtis-Pennington vertices

### 3.5.4 Application to unquenched QED<sub>4,d<sub>e</sub></sub>

In this section, we now consider the unquenched QED<sub>4,d<sub>e</sub></sub> case, *i.e.*,  $N_f > 0$ .

#### General remarks and naive approach

In order to be able to consider the more physical case of unquenched QED<sub>4,d<sub>e</sub></sub>, we shall follow [118, 122, 134, 245, 246] and include a dynamical screening of the interaction. In the case of QED<sub>4,3</sub>, this can be done with the help of the random phase approximation (RPA) that amounts to a simple redefinition of the coupling constant [118, 144] because, for this “standing” model, the polarization operator is finite (see (3.62) combined with (3.32)). This procedure resums exactly all the  $N_f$ -dependence in  $\gamma_m$  allowing us to go beyond the quenched approximation [134].

Following the QED<sub>4,3</sub> case [134], we shall proceed with a generalization to QED<sub>4,d<sub>e</sub></sub> by enforcing the resummation of the  $N_f$ -dependence of  $\gamma_m$  at each loop order in an effective coupling constant. As we shall see below, such a procedure does not correspond to RPA in the case of QED<sub>4</sub>. Indeed, applying RPA to QED<sub>4</sub> within our formalism does not allow to fully resum the  $N_f$ -dependence in  $\gamma_m$ . This originates from the running of the coupling constant, which arises from the UV divergent polarization operator (see (3.64)) and renders the QED<sub>4</sub> case more subtle to treat than the QED<sub>4,3</sub> one. Enforcing the resummation of the  $N_f$ -dependence of  $\gamma_m$  in QED<sub>4</sub> is a semi-phenomenological prescription. But, as we shall see, it will provide results that are in quantitative agreement with those obtained from numerical solutions of SD equations. Moreover, this effective coupling method allows us to compute a critical fermion flavor number,  $N_c$ , such that  $\alpha_c \rightarrow \infty$ , *i.e.*, a clearly non-perturbative quantity that requires the resummation of the  $N_f$ -dependence of  $\gamma_m$ .

Within our formalism, an interesting fact about studying QED<sub>4</sub> is that it allows to consider higher orders in the loop expansion which are presently inaccessible in QED<sub>4,3</sub>. We already exploited this in the last subsection related to the quenched case. As we saw there, in both cases of QED<sub>4,3</sub> and QED<sub>4</sub>, there is no solution to the two-loop gap equation for  $N_f > 0$ . It turns out that, for QED<sub>4</sub>, solutions of (3.148) appear at higher loops for non-zero  $N_f$  values without any need to introduce an effective coupling constant. We do not find these results satisfactory but, for completeness, we summarize them in table 3.5 and discuss them briefly.

loops	1	2	3	4	5
$N_{\max}$	$\infty$	0.45	5.4738	0	18.4653
$\alpha_c(N_f = 0)$	1.0472	1.4872	1.1322	—	1.0941
$\alpha_c(N_f = 1)$	1.0472	—	1.1635	—	1.0703
$\alpha_c(N_f = 2)$	1.0472	—	1.2302	—	1.0629
$\alpha_c(N_f = 3)$	1.0472	—	1.3536	—	1.0601
$\alpha_c(N_f = 4)$	1.0472	—	1.6037	—	1.0570
$\alpha_c(N_f = 5)$	1.0472	—	2.2669	—	1.0510
$\alpha_c(N_f = 6)$	1.0472	—	—	—	1.0414
$\alpha_c(N_f = 7)$	1.0472	—	—	—	1.0281

Table 3.5: Naive (and unsatisfactory) results for critical couplings of unquenched QED<sub>4</sub> computed from (3.148) up to 5 loops (“—” indicates that no physical solution is found).

First, as can be seen from table 3.5, a parity effect is observed, as no solution is obtained at two and four loops for  $N_f > 0$ . At three and five loops, we obtain solutions over a range of  $N_f$ -values smaller than some  $N_{\max}$  which is now larger than 1. However, this  $N_{\max}$  is not related to  $N_c$  and its physical interpretation is not clear; it is close to the  $N_c$  found from the effective coupling approach at three loops but deviates substantially from it at five loops, see table 3.6 for the results of the effective coupling approach. Moreover, at five loops the critical coupling obtained this way decreases with increasing  $N_f$  while the opposite behavior is observed at three loops. Actually, on physical grounds, we expect that  $\alpha_c$  should increase with increasing  $N_f$ . This comes from the fact that screening increases with  $N_f$ , thus effectively weakening interaction effects which in turn requires a larger value of the coupling constant in order to dynamically generate a mass. The effective coupling approach seems to overcome these difficulties (as far as our semi-phenomenological approach can tell) and we shall therefore focus on it in the following.

### Unquenched QED<sub>4,d<sub>e</sub></sub> at one loop

In order to include dynamical screening in QED<sub>4,d<sub>e</sub></sub>, we define the following effective (reduced) coupling constant

$$\bar{g}_r = \frac{\bar{\alpha}_r}{1 + \hat{\Pi}_{1\text{eff}}\bar{\alpha}_r}, \quad (3.165)$$

where  $\bar{g}_r = g_r/(4\pi)$ . All the  $N_f$ -dependence, *i.e.*, the effect of fermion loops (or screening), is then by definition in  $\hat{\Pi}_{1\text{eff}}$ . Substituting (3.165) in the mass anomalous dimension, (3.99b), and expanding the resulting expression up to second order in  $\bar{g}_r$ , we require that  $\hat{\Pi}_{1\text{eff}}$  cancels the two-loop  $N_f$ -dependent terms in (3.99b). This yields

$$\hat{\Pi}_{1\text{eff}} = 4(1-z)N_f \frac{(1-\varepsilon_e)K_1}{3-2\varepsilon_e} + \frac{10zN_f}{9}, \quad (3.166)$$

together with

$$\gamma_m = 4\bar{g}_r \frac{3-2\varepsilon_e}{(2-\varepsilon_e)(1-\varepsilon_e)} + 8\bar{g}_r^2 \frac{3-2\varepsilon_e}{(2-\varepsilon_e)^3(1-\varepsilon_e)^2} + \mathcal{O}(\bar{g}_r)^3. \quad (3.167)$$

From (3.166), in the case of QED<sub>4,3</sub> ( $z=0$  and  $\varepsilon_e \rightarrow 1/2$ ), we recover the fact that

$$\hat{\Pi}_{1\text{eff}}^{\text{QED}_{4,3}} = \hat{\Pi}_1^{\text{QED}_{4,3}}/2, \quad (3.168)$$

where  $\hat{\Pi}_1^{\text{QED}_{4,3}}$  was defined in (3.62). In this case, the procedure exactly corresponds to RPA (random phase approximation) in agreement with (3.32). In the case of QED<sub>4</sub> ( $z=1$  and  $\varepsilon_e \rightarrow 0$ ), we find from (3.166) that

$$\hat{\Pi}_{1\text{eff}}^{\text{QED}_4} = \hat{\Pi}_1^{\text{QED}_4}/2, \quad (3.169)$$

where  $\hat{\Pi}_1^{\text{QED}_4}$  was defined in (3.64). As we anticipated, in the case of QED<sub>4</sub>, the procedure is not RPA (the expected result for the RPA case would be  $\hat{\Pi}_{1\text{eff}}^{\text{QED}_4} = \hat{\Pi}_1^{\text{QED}_4}$ , see (3.33)) as it corresponds to a resummation of half of an effective one-loop renormalized polarization operator (and moreover  $L_p = 0$ ).

We may now proceed on solving (3.148) with (3.167) truncated at one-loop order. The effective critical coupling  $g_c$  that we obtain is equal to the one-loop critical coupling given by (3.150). With the help of (3.165), this result can be generalized to the unquenched case and yields

$$\alpha_c(N_f) = \frac{\pi(2-\varepsilon_e)(1-\varepsilon_e)^2}{2(3-2\varepsilon_e) - \hat{\Pi}_{1\text{eff}}(2-\varepsilon_e)(1-\varepsilon_e)^2/4}. \quad (3.170)$$

Note that we can deduce, from (3.170), a critical fermion flavor number,  $N_c$ , such that  $\alpha_c \rightarrow \infty$ , reading

$$N_c = \frac{6(3-2\varepsilon_e)^2}{3(1-z)(2-\varepsilon_e)(1-\varepsilon_e)^3 K_1 + 5z}. \quad (3.171)$$

We now apply our general one-loop results to specific cases starting from QED<sub>4,3</sub> ( $z=0$  and  $\varepsilon_e \rightarrow 1/2$ ). In this case, (3.170) and (3.171) yield

$$\boxed{\alpha_c^{\text{QED}_{4,3}}(N_f) = \frac{12\pi}{128-3\pi^2 N_f}, \quad N_c^{\text{QED}_{4,3}} = \frac{128}{3\pi^2} = 4.3230, \quad (1\text{-loop}),} \quad (3.172)$$

and, for the range of allowed non-zero values of  $N_f$ , (3.172) yields

$$\alpha_c(N_f=1) = 0.3832, \quad \alpha_c(N_f=2) = 0.5481, \quad \alpha_c(N_f=3) = 0.9624, \quad \alpha_c(N_f=4) = 3.9415, \quad (3.173)$$

with  $\alpha_c = \alpha_c^{\text{QED}_{4,3}}$ , and thereby recovering in a simple and straightforward way the results of [118]. Following [118], the result  $\alpha_c^{\text{QED}_{4,3}}(N_f)$  in (3.172) defines a critical line in the  $(\alpha, N_f)$  plane that separates the broken and symmetric phases. Moreover, in this one-loop case,  $N_c^{\text{QED}_{4,3}} = 4.3230$  is equal to the LO gauge-invariant critical fermion flavor number of large- $N_f$  QED<sub>3</sub> (see discussion below (3.150)).

Similarly, in the case of QED<sub>4</sub> ( $z=1$  and  $\varepsilon_e \rightarrow 0$ ), (3.170) and (3.171) yield

$$\boxed{\alpha_c^{\text{QED}_4}(N_f) = \frac{18\pi}{54-5N_f}, \quad N_c^{\text{QED}_4} = \frac{54}{5} = 10.8, \quad (1\text{-loop}),} \quad (3.174)$$

and, for the range of allowed values of  $N_f$ , (3.174) yields

$$\begin{aligned} \alpha_c(N_f=1) &= 1.1541, & \alpha_c(N_f=2) &= 1.2852, & \alpha_c(N_f=3) &= 1.4500, & \alpha_c(N_f=4) &= 1.6632, \\ \alpha_c(N_f=5) &= 1.9500, & \alpha_c(N_f=6) &= 2.3562, & \alpha_c(N_f=7) &= 2.9763, & \alpha_c(N_f=8) &= 4.0392, \\ \alpha_c(N_f=9) &= 6.2832, & \alpha_c(N_f=10) &= 14.1372, \end{aligned} \quad (3.175)$$

with  $\alpha_c = \alpha_c^{\text{QED}_4}$ . Note that the one-loop SD equation in the rainbow approximation and including the polarization operator in the LAK-approximation (following the work of Landau, Abrikosov and Khalatnikov [247]) was approximately solved in the Landau gauge in [248] with the results  $\alpha_c^{\text{QED}_4}(N_f=1) = 1.95$  (see also [172] for a review of other results as well as discussions below). It deviates by about 69% from our result,  $\alpha_c^{\text{QED}_4}(N_f=1) = 1.1541$ .

### Unquenched QED<sub>4,d<sub>e</sub></sub> at two loops

Next, in order to access the two-loop case, we solve (3.148) with the full (3.167) as the input. This yields the critical coupling  $g_c = \alpha_c(N_f = 0)$  where  $\alpha_c(N_f = 0)$  is the quenched critical coupling given by (3.157). With the help of (3.165), this result can be generalized to the unquenched case and yields

$$\alpha_c(N_f) = \frac{\pi(2 - \varepsilon_e)(1 - \varepsilon_e)^2}{3 - 2\varepsilon_e + \sqrt{\Delta_0} - \hat{\Pi}_{1\text{eff}}(2 - \varepsilon_e)(1 - \varepsilon_e)^2/4}. \quad (3.176)$$

Proceeding as in the one-loop case, we deduce from (3.176) a critical fermion flavor number,  $N_c$ , such that  $\alpha_c \rightarrow \infty$ . Its expression reads

$$N_c = \frac{3(3 - 2\varepsilon_e)(3 - 2\varepsilon_e + \sqrt{\Delta_0})}{3(1 - z)(2 - \varepsilon_e)(1 - \varepsilon_e)^3 K_1 + 5z}. \quad (3.177)$$

We now apply our general two-loop results to specific cases starting from QED<sub>4,3</sub> ( $z = 0$  and  $\varepsilon_e \rightarrow 1/2$ ). In this case, (3.176) and (3.177) yield

$$\alpha_c^{\text{QED}_{4,3}}(N_f) = \frac{36\pi}{32(6 + \sqrt{6}) - 9\pi^2 N_f}, \quad N_c^{\text{QED}_{4,3}} = \frac{32}{9\pi^2} (6 + \sqrt{6}) = 3.0440, \quad (2\text{-loop}), \quad (3.178)$$

and, for the range of allowed non-zero values of  $N_f$ , (3.178) yields

$$\alpha_c(N_f = 1) = 0.6230, \quad \alpha_c(N_f = 2) = 1.2196, \quad \alpha_c(N_f = 3) = 28.967, \quad (3.179)$$

with  $\alpha_c = \alpha_c^{\text{QED}_{4,3}}$ , and thereby recovering in a simple and straightforward way all the results of [134]. See figure 3.7a in the next pages for a graphical representation of the phase diagram. As already noticed in [134], we see from (3.178) that the two-loop  $N_c$  in QED<sub>4,3</sub> is slightly higher than the corresponding one in NLO large- $N_f$  QED<sub>3</sub> (for which  $N_c = 2.8470$ , see discussion below (3.157)).

Similarly, in the case of QED<sub>4</sub> ( $z = 1$  and  $\varepsilon_e \rightarrow 0$ ), (3.176) and (3.177) yield

$$\alpha_c^{\text{QED}_4}(N_f) = \frac{36\pi}{9(6 + \sqrt{6}) - 10N_f}, \quad N_c^{\text{QED}_4} = \frac{9}{10} (6 + \sqrt{6}) = 7.6045, \quad (2\text{-loop}), \quad (3.180)$$

and, for the range of allowed values of  $N_f$ , (3.180) yields, with  $\alpha_c = \alpha_c^{\text{QED}_4}$

$$\begin{aligned} \alpha_c(N_f = 1) &= 1.7124, & \alpha_c(N_f = 2) &= 2.0180, & \alpha_c(N_f = 3) &= 2.4562, & \alpha_c(N_f = 4) &= 3.1376, \\ \alpha_c(N_f = 5) &= 4.3423, & \alpha_c(N_f = 6) &= 7.0486, & \alpha_c(N_f = 7) &= 18.7080. \end{aligned} \quad (3.181)$$

### Unquenched QED<sub>4</sub> at higher loops

In the case of QED<sub>4</sub>, We can go further and use the three-loop mass anomalous dimension (3.161) that we have computed in Appendix 3.A. Proceeding with the same approach as in the two-loop case yields

$$\alpha_c^{\text{QED}_4}(N_f) = \frac{5994\pi t}{332667 + 3(4(9\zeta_3 - 8)t - 555)tN_f - 20t^2 N_f^2}, \quad N_c^{\text{QED}_4} = 5.3298, \quad (3\text{-loop}) \quad (3.182)$$

with  $t = 10 - 788s^{-1} + s$  and  $s^3 = 2(6161 + 111\sqrt{13009})$ . Going even further, we can again use state-of-the-art results for  $\gamma_m$  up to five loops [219, 220]<sup>11</sup>. Like in the quenched case, no physical solution is found at four loops (all solutions are complex) and therefore we effectively have  $N_c = 0$  in this case.

<sup>11</sup>We used the results of the ancillary files of both [241] and [242].

For five loops, the solving is numerical, as it amounts to find the roots of is a fifth order polynomial, and reads

$$\alpha_c^{\text{QED}_4}(N_f) = \frac{861.59}{787.51 - 43.28N_f - 35.748N_f^2 - 2.44N_f^3 + N_f^4}, \quad N_c^{\text{QED}_4} = 3.3954, \quad (5\text{-loop}). \quad (3.183)$$

Note that, at each order, the effective dynamical coupling is determined in such a way that it resums all the  $N_f$ -dependence of  $\gamma_m$ . This allows us to deduce a critical flavor fermion number,  $N_c$ , and the critical values of the coupling,  $\alpha_c(N_f)$  for  $N_f < N_c$  at higher loops. Our results for unquenched QED<sub>4</sub> (as well as the results of QED<sub>4,3</sub> for clarity) are summarized in table 3.6. See also figure 3.7b for a graphical representation of the QED<sub>4</sub> phase diagram from the state of the art five-loop results.

In addition to these results, in QED<sub>4</sub> at 1, 2, 3 and 5 loops, a finite non-zero value of  $N_c$  is obtained, which decreases with increasing loop order. In agreement with our physical intuition, at 1, 2, 3 and 5 loops the critical coupling is seen to increase with  $N_f$  (because of the increase of screening) and diverges at  $N_c$ . Moreover, provided that the apparent decrease of  $N_c$  with increasing loop order is smooth, we are able to extrapolate its value to infinite loop order using a simple decreasing exponential fit (discarding the four-loop order), see figure 3.6. This yields

$$N_c^{\text{QED}_4} \approx 2.0663, \quad (\infty\text{-loop}), \quad (3.184)$$

that we added to table 3.6. We therefore conjecture that, in the non-perturbative regime (infinite loop order), the critical coupling is defined only up to  $N_f = 2$ . Moreover, we can also infer that,  $\alpha_c(N_f = 2)$  may be extremely large since  $N_f = 2$  is very close to  $N_c = 2.0663$ . This last value is a strong evidence that at  $N_f = 1$  and at high coupling, QED<sub>4</sub> may be in an (excitonic) insulating phase.

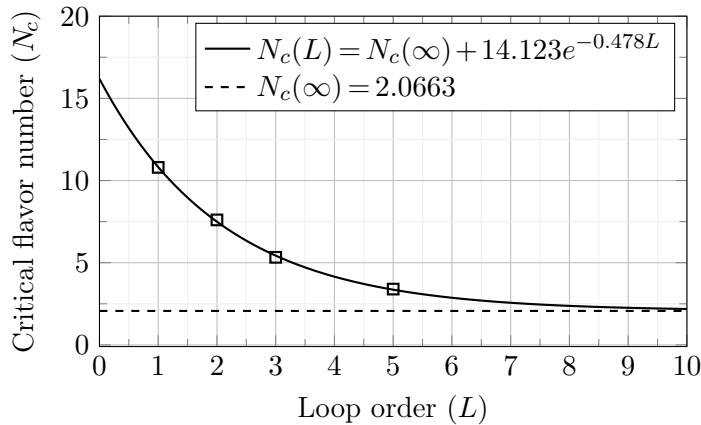


Figure 3.6: Exponential fit on the values found for  $N_c$  from 1 to 5-loop in QED<sub>4</sub>.

### Results summary

In this section we present, for both QED<sub>4,3</sub> and QED<sub>4</sub>, a summary of our results for the critical coupling  $\alpha_c$  depending on the fermion flavor number  $N_f$  and real up to the critical flavor number  $N_c$ . We also provide a graphical representation of our best results in a phase diagram for both models, figure 3.7. Note that all these numerical results were obtained analytically in the previous sections.

Model	QED <sub>4,3</sub>		QED <sub>4</sub>						
loops	1	2	1	2	3	4	5	...	$\infty$
$N_c$	4.3230	3.0440	10.8	7.6045	5.3298	0	3.3954	...	2.0663
$\alpha_c(N_f = 0)$	0.2945	0.4183	1.0472	1.4872	1.1322	—	1.0941		??
$\alpha_c(N_f = 1)$	0.3832	0.6229	1.1541	1.7124	1.2353	—	1.2221		??
$\alpha_c(N_f = 2)$	0.5481	1.2196	1.2852	2.0180	1.4424	—	1.6492		??
$\alpha_c(N_f = 3)$	0.9624	28.967	1.4500	2.4562	1.8707	—	4.5576		—
$\alpha_c(N_f = 4)$	3.9415	—	1.6632	3.1376	2.9997	—	—	...	—
$\alpha_c(N_f = 5)$	—	—	1.9500	4.3423	11.150	—	—		—
$\alpha_c(N_f = 6)$	—	—	2.3562	7.0486	—	—	—		—
$\alpha_c(N_f = 7)$	—	—	2.9763	18.708	—	—	—		—
$\alpha_c(N_f = 8)$	—	—	4.0392	—	—	—	—		—
$\alpha_c(N_f = 9)$	—	—	6.2832	—	—	—	—		—
$\alpha_c(N_f = 10)$	—	—	14.137	—	—	—	—		—

Table 3.6: Critical couplings of unquenched QED<sub>4,3</sub> and QED<sub>4</sub>, computed from (3.148) together with the effective dynamical coupling (3.165) up to 5 loops (the symbol “—” indicates that no physical solution is found and the symbol “??” indicates that we could not compute the corresponding value).

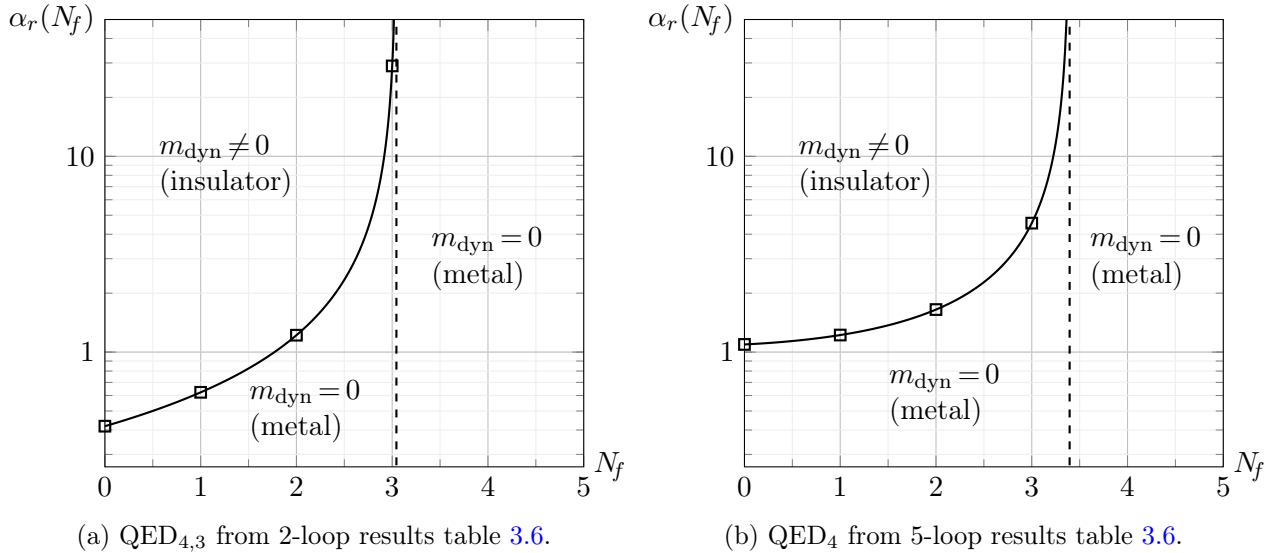


Figure 3.7: QED<sub>4,3</sub> and QED<sub>4</sub> dynamical mass generation phase diagrams in the plane  $(\alpha_r, N_f)$  from the best results of table 3.6. Here, insulator refers to an excitonic insulating phase, while metal refers to a semimetallic phase.

We recall here that graphene is described by QED<sub>4,3</sub> at  $N_f = 2$  and  $\alpha_r \approx 1/137$  in the IR limit, for which the plot 3.7a has been obtained<sup>12</sup>. Therefore, graphene at low-temperatures is indeed metallic,

<sup>12</sup>in ambient – pseudo-relativistic – conditions,  $\alpha_r \approx 2.2$ , but obtaining a phase diagram in this case would require Lorentz breaking computations, see, e.g., [126] and references therein.

in accordance with experimentation. Nevertheless, our results tend to show that if one manage to experimentally tune the coupling towards a sufficiently high value, it may undergo a phase transition towards an insulating phase. This could possibly be achieved with a well-chosen substrate, ideally tunable, such that the transition can be controlled on demand, thereby creating a graphene transistor.

Similarly, usual QED<sub>4</sub> from high energy physics is retrieved for  $N_f = 1$  and  $\alpha_r \approx 1/137$  in figure 3.7b. Therefore, it is also in a metallic phase in ambient conditions, and similarly, a phase transition towards an insulating phase may be possible at very large coupling. As explained in the introduction, in QED<sub>4</sub>,  $\alpha_r$  is running, and increases with the energy scale. The question is then, at what energy scale the coupling is  $\alpha_r \sim 1$ , such that QED<sub>4</sub> may be in a metallic state? The answer is that, if it happens, it would be at a tremendous energy scale. Indeed, the growth of  $\alpha_r$  is extremely slow: at the electron mass scale (in eV)  $\alpha_r(m_e \sim 10^6) \approx 1/137$ , at the Z-boson mass scale,  $\alpha_r(m_Z \sim 10^{11}) \approx 1/127$  and at the largest scale one could think of, the Grand Unification Theory (GUT) scale, it is roughly estimated as  $\alpha_r(m_{\text{GUT}} \sim 10^{25}) \approx 1/30$ , see [116]. Therefore, in particle physics, QED<sub>4</sub> is metallic at all reasonable energy scales. Nevertheless, in an eventual condensed matter system suitably described by QED<sub>4</sub>, with  $N_f = 1$  or 2 and  $\alpha_r \sim 1$ , such a phase transition is likely to be possible.

### Literature comparison for unquenched QED<sub>4,3</sub>

In this section, we provide a summary of the results obtained in the literature for D $\chi$ SB in graphene, *i.e.*, for  $\alpha_c(N_f = 2)$  and the corresponding  $N_c$ . Results are provided in table 3.7.

$\alpha_c(N_f = 2)$	$N_c$	Method	Year
7.65		SD (LO, dynamic RPA, running $v$ )	2013 [249]
3.7		FRG, Bethe-Salpeter	2016 [250]
$3.2 < \alpha_c < 3.3$		SD (LO, dynamic RPA, running $v$ )	2012 [251]
3.1		SD (LO, bare vertex approximation)	2015 [252]
2.06		SD (LO, dynamic RPA, running $v$ )	2017 [253]
1.62		SD (LO, static RPA)	2002 [122]
	3.52	SD (LO)	2009 [246]
1.22	3.04	SD (NLO, RPA, resummation, $v/c \rightarrow 1, \forall \xi$ )	2016 [134]
1.22	3.04	Effective gap eq. (2-loop, RPA, $v/c \rightarrow 1, \forall \xi$ )	2021 [4]
1.13	3.6	SD (LO, static RPA, running $v$ )	2008 [245]
$1.11 \pm 0.06$		Lattice simulations	2008 [254]
$1.03 < \alpha_c < 1.08$	$3.17 < N_c < 3.24$	SD (NLO, RPA, resummation, $v/c \rightarrow 1$ )	2016 [134]
1.02		SD (LO, dynamic RPA, running $v$ )	2011 [255]
$0.94 < \alpha_c < 1.02$	$3.24 < N_c < 3.36$	SD (NLO, RPA, $v/c \rightarrow 1$ )	2016 [134]
0.99		RG study	2012 [256]
0.92		SD (LO, dynamic RPA)	2009 [257]
$0.9 \pm 0.2$		Lattice simulations	2012 [258]
0.833		RG study	2008 [259]
0.5481	4.3230	Effective gap eq. (1-loop, RPA, $v/c \rightarrow 1, \forall \xi$ )	2021 [4]

Table 3.7: Reproduced from [126] and updated. D $\chi$ SB in graphene: some values of  $\alpha_c(N = 2)$  and  $N_c$  obtained over the years together with elements of the different methods used. The double line corresponds to  $\alpha_r = 2.2$ , the observed coupling value in physical graphene. Values presented in this manuscript are in gray. The values to be retained are the gauge-invariant ones,  $\alpha_c = 1.22$  and  $N_c = 3.04$ .



Literature comparison for unquenched QED<sub>4</sub>

In order to numerically compare our results with the ones of the literature, we should first discuss some “good gauge” issues. Indeed, at a given loop order greater than 1, a numerical evaluation of the “good gauge” parameter,  $\xi_g(\alpha_c, N_f)$ , shows substantial deviations from the Landau gauge as  $N_f$  increases and even diverges as  $N_f$  approaches  $N_c$ . At  $N_f = 1$ , a comparison with the Landau gauge results is justified since the “good gauge” is reasonably small,  $0.28 < \xi_g < 0.48$ . On the other hand, at  $N_f = 2$ , a comparison with the Feynman gauge becomes more relevant ( $0.41 < \xi_g < 0.89$ ). However, most of the unquenched SD results found in the literature are derived only in the Landau gauge. For these reasons, we are restricted to a comparison of only our  $N_f = 1$  results with the  $N_f = 1$  results of the literature in the Landau gauge.

Taking the review part of [174], table III, as a reference, a wide range of results have been found for  $\alpha_c(N_f = 1)$  in the Landau gauge over the last 30 years. For convenience, we reproduce this table in table 3.8 together with the relative differences to our results at each given loop order.

QED <sub>4</sub> Literature			rel. diff. to our work				
Reference	$\alpha_c(N_f = 1)$	Vertex model	1l	2l	3l	4l	5l
Kondo <i>et al.</i> [260] (1990)	1.9997 ( $\xi = 0$ )	Bare	91%	17%	62%	–	64%
Gusynin [248] (1989)	1.95 ( $\xi = 0$ )	Bare	86%	14%	58%	–	60%
Kondo [261] (1990)	1.9989 ( $\xi = 0$ )	Bare	91%	17%	62%	–	64%
Kondo [261] (1990)	2.0728 ( $\xi = 0$ )	Bare	98%	21%	68%	–	70%
Oliensis <i>et al.</i> [262] (1990)	1.9995 ( $\xi = 0$ )	Bare	91%	17%	62%	–	64%
Rakow [263] (1990)	2.25 ( $\xi = 0$ )	Bare	114%	31%	82%	–	84%
Atkinson <i>et al.</i> [264] (1990)	2.10028 ( $\xi = 0$ )	Bare	101%	23%	70%	–	72%
Kondo <i>et al.</i> [265] (1991)	2.084 ( $\xi = 0$ )	Bare	99%	22%	69%	–	71%
Ukita <i>et al.</i> [266] (1990)	2.0944	NA	100%	22%	70%	–	71%
Kondo <i>et al.</i> [267] (1993)	1.9995	NA	91%	17%	62%	–	64%
Bloch [172] (1995)	1.99953 ( $\xi = 0$ )	Bare	91%	17%	62%	–	64%
Bloch [172] (1995)	1.7410 @ $\Lambda^2$ ( $\xi = 0$ )	Bare	66%	2%	41%	–	42%
Bloch [172] (1995)	1.6322 @ $\Lambda^2$ ( $\xi = 0$ )	BC	56%	5%	32%	–	34%
Bloch [172] (1995)	1.6199 @ $\Lambda^2$ ( $\xi = 0$ )	modified CP	55%	5%	31%	–	33%
Bashir <i>et al.</i> [244] (2011)	2.27(Anal.) ( $\xi = 0$ )	BC+KP+A	117%	33%	84%	–	86%
Bashir <i>et al.</i> [244] (2011)	2.46(Num.) ( $\xi = 0$ )	BC+KP+A	135%	44%	99%	–	101%
Akram <i>et al.</i> [268] (2012)	0.9553 ( $\xi = 0$ )	BC+Ansatz	9%	44%	23%	–	22%
This work (1-loop) (2022)	1.1541 $\forall \xi$	Bare	0%	48%	7%	–	6%
This work (2-loop) (2022)	1.7124 $\forall \xi$	Perturbative	33%	0%	28%	–	29%
This work (3-loop) (2022)	1.2351 $\forall \xi$	Perturbative	7%	39%	0%	–	1%
This work (4-loop) (2022)	–	Perturbative	–	–	–	–	–
This work (5-loop) (2022)	1.2221 $\forall \xi$	Perturbative	6%	40%	1%	–	0%

Figure 3.8: Critical couplings from previous studies at  $N_f = 1$  with relative difference comparison with our results from 1 to 5 loop order. The top left part of the table is reproduced from [174]. Gray lines are the studies that compare best with our results. CP≡Curtis-Pennington, BC≡Ball-Chiu, KP≡Kizilersu-Pennington.

Most of the first order approaches (that neglect one or more equations of the SD system) presented in [174], lead to results that are far from the results of our paper, *e.g.*, a relative difference of 60% up to 101% by comparing with our five loops approach. However, better agreements are found when comparing our results with more sophisticated numerical approaches, especially the results of Bloch [172], that solve the full system of one-loop like SD equations with various vertex ansätze (bare, Ball-Chiu and modified CP as referred to in [172]). These various approaches lead to results that are very



close to each other in the  $N_f = 1$  case. Of course, the non-perturbative nature of the vertex ansätze used in these approaches does not have (to the best of our knowledge) a clear correspondence in terms of loops (such as in our case). Nevertheless, from these results, we find deviations of 2%–5% with respect to our two-loop results and deviations of 31%–42% with respect to our four and five-loop results. We also note a smaller deviation of 22% upon comparing our five-loop  $N_f = 1$  result with the most recent results of [268].

### 3.6 Conclusion

In this chapter, we have computed the two-loop mass anomalous dimension of  $\text{QED}_{4,d_e}$  with  $N_f$  flavors of four-component Dirac fermions. Our main formulas, (3.99), for  $\gamma_m$  and also the field anomalous dimension  $\gamma_\Psi$ , take into account the non-commutativity of  $\varepsilon_\gamma \rightarrow 0$  and  $\varepsilon_e \rightarrow 0$  limits and are valid in both cases of  $\text{QED}_{4,3}$  (which applies to graphene at its IR Lorentz invariant fixed point) and  $\text{QED}_4$ . For  $\text{QED}_{4,3}$ , our formula for  $\gamma_m$ , (3.134b), generalizes the one obtained in [161] to an arbitrary number of (2-component) fermion flavors, but our interest was mostly focused on the parity-even case (3.105b). When the latter is mapped to large- $N_f$   $\text{QED}_3$  [134], it corresponds exactly to the result obtained by Gracey in [226] thereby strengthening our result.

We then proceeded on studying the critical properties (dynamical generation of a parity-conserving fermion mass) of  $\text{QED}_{4,d_e}$  (both in the quenched and the unquenched cases) with the help of the gap equation (3.147) (and its solution (3.148)). The latter was derived in a semi-phenomenological way on the basis of the modern approach of Gusynin and Pyatkovskiy [184]. It matches exactly the NLO gap equation of large- $N_f$   $\text{QED}_3$  [184, 186] as well as that of  $\text{QED}_{4,3}$  [134] and its range of application was extended to cover the case of  $\text{QED}_4$ . Its only input being the mass anomalous dimension, it is fully gauge invariant by construction and allows deriving the gauge-invariant critical coupling constants and critical fermion flavor numbers of  $\text{QED}_{4,d_e}$  models with the help of (3.99b). We also underlined the fact that quantities derived with the help of this gauge-invariant method do match (at one-loop from our SD analysis) with gauge-dependent computations evaluated in the “good gauge” (a gauge where the fermion anomalous dimension vanishes order by order in perturbation theory). In the case of  $\text{QED}_{4,3}$ , we have explicitly checked that (3.148) does allow us to recover in a simple and straightforward way all the NLO results of [134]. In the case of  $\text{QED}_4$ , we have first recovered the celebrated  $\alpha_c = \pi/3$  (now exactly gauge-invariant, see (3.150) with  $\varepsilon_e = 0$ ) at LO in agreement with the result obtained from solving the SD equations in the “good gauge” (see (3.144) with  $\varepsilon_e = 0$ ). We have then used state-of-the-art expressions for  $\gamma_m$  up to five loops in  $\text{QED}_4$ , to access the critical properties of the model. The unquenched case was considered first, and our results are summarized in table 3.2. The latter shows that, at five loops, our value for the critical coupling,  $\alpha_c(N_f = 0) = 1.0941$ , deviates by only 4% from  $\pi/3$  and by 15% from the results of [172, 174] where numerical solution of SD equations in the Landau gauge with various vertex ansätze lead to  $\alpha_c(N_f = 0) \approx 0.93$ . The unquenched case is more subtle due to the running of the  $\text{QED}_4$  coupling constant (in contrast to  $\text{QED}_{4,3}$  which is a “standing” gauge theory). Nevertheless, a resummation of the  $N_f$ -dependence of  $\gamma_m$  into an effective coupling constant gave us access to  $N_c$  which is such that  $\alpha_{e \rightarrow \infty}$  together with all values of  $\alpha_c(N)$  for  $N_f < N_c$ . Our results are summarized in table 3.6. At five loops, we find that  $N_c = 3.3954$  with  $\alpha_c(N_f = 1) = 1.2221$ . Comparing our results to the ones of the literature, we find deviations of 2%–5% of our two-loop results with respect to the results of [172] and deviations of 31%–42% of our four and five-loop results with respect to the results of [172]. We also note an interestingly smaller deviation of 22% upon comparing our five-loop  $N_f = 1$  result with the most recent results of [268]. From our results, we could extrapolate  $N_c$  to infinite loop order finding  $N_c = 2.0663$ , see (3.184). This suggests that dynamical mass generation in  $\text{QED}_4$  may take place only for  $N_f \leq 2$ .

Our work has shown that (3.147) (and its solution (3.148)) allow for a simple and straightforward study of the critical properties of  $\text{QED}_{4,d_e}$ . In the case of  $\text{QED}_{4,3}$ , we were limited to two-loop order as, to the best of our knowledge,  $\gamma_m$  is still unknown for this model at three-loop and beyond. It

would be very interesting to compute  $\gamma_m$  at three-loop for QED<sub>4,3</sub> and use it as an input to (3.148). It would also be very instructive to solve the NNLO SD equations for QED<sub>4,3</sub> along the lines of [186] for the NLO case, in order to have a solid proof that (3.147) does hold at this order. But such analytic computations may be quite tedious at this order, and it remains to be seen if they can even be carried out (let us recall that it took approximately 30 years since the seminal work of Nash [181] for the gauge-invariant NLO calculation in large- $N_f$  QED<sub>3</sub> to be achieved in [184, 186]). In the case of QED<sub>4</sub>, our straightforward solution of the LO SD equations with the method of Kotikov [182, 183] is a good indication that this method might be extended to NLO along the lines of [186] (but now for a running theory in the unquenched case). We leave all these projects for future investigations.

### 3.A QED<sub>4</sub> at three loops

In this appendix section, we derive the three-loop renormalization group equations of QED<sub>4</sub>.

We first focus on the three-loop correction to the photon polarization operator. The corresponding Feynman diagrams are displayed in figure 3.9. It is composed of 11 diagrams labeled in alphabetical order; 7 of the Ladder (L3) topology labeled ( $a, b, c, f, h, i, j$ ), 3 of the Benz (B3) topology labeled ( $d, e, g$ ) and 1 of the Non-planar (N3) topology labeled ( $k$ ). Computing all these diagrams using the same techniques as describe in the main text (using Appendix A), and summing all the contributions leads to the three-loop correction

$$\Pi_3^{\text{QED}_4}(p^2) = 2N_f \bar{\alpha}^3 \left( \frac{\bar{\mu}^2}{-p^2} \right)^{3\varepsilon_\gamma} \left[ \frac{8N_f}{9\varepsilon_\gamma^2} + \frac{-288\zeta_3 N_f + 352N_f + 9}{27\varepsilon_\gamma} + 80\zeta_5 - 16\zeta_4 N_f - \frac{4\zeta_2 N_f}{3} + \frac{4}{9}\zeta_3(111 - 152N_f) + \frac{8834N_f}{81} + \frac{143}{9} + \mathcal{O}(\varepsilon_\gamma) \right], \quad (3.185)$$

which is again gauge-independent, providing a strong check of our result. The corresponding renormalization constant can then be derived using the third order expansion of (3.45), reading

$$\delta Z_{3A} = \mathcal{K}(\Pi_2 \mathcal{K}(\Pi_1)) + \mathcal{K}(\Pi_1 \mathcal{K}(\Pi_2)) + \mathcal{K}(\Pi_1 \mathcal{K}(\Pi_1 \mathcal{K}(\Pi_1))) + \mathcal{K}(\Pi_3), \quad (3.186)$$

and therefore, in the QED<sub>4</sub> case, using all previously computed results

$$\delta Z_{3A}^{\text{QED}_4} = N_f \bar{\alpha}_r^3 \left[ -\frac{8N_f}{9\varepsilon_\gamma^2} + \frac{2(22N_f + 9)}{27\varepsilon_\gamma} + \mathcal{O}(\varepsilon_\gamma^0) \right]. \quad (3.187)$$

We then focus on the three-loop correction to the fermion self-energy. The corresponding Feynman diagrams are displayed in figure 3.10. It is composed of 15 diagrams labeled in alphabetical order; 9 of the Ladder (L3) topology labeled ( $a, b, c, d, e, i, j, m, n$ ), 5 of the Benz (B3) topology labeled ( $f, g, h, k, l$ ) and 1 of the Non-planar (N3) topology labeled ( $o$ ). Computing all these diagrams and summing all the contributions leads to the three-loop corrections

$$\Sigma_{3V}^{\text{QED}_4}(p^2) = \bar{\alpha}^3 \left( \frac{\bar{\mu}^2}{-p^2} \right)^{3\varepsilon_\gamma} \left[ -\frac{\xi^3}{6\varepsilon_\gamma^3} - \frac{18\xi^3 - 9\xi(4N_f + 3) + 16N_f(4N_f + 3)}{36\varepsilon_\gamma^2} + \frac{54\zeta_2 \xi^3 - 216\xi^3 + 27\xi(36N_f + 11) - 64N_f(34N_f + 9) - 108}{216\varepsilon_\gamma} + \mathcal{O}(\varepsilon_\gamma^0) \right], \quad (3.188a)$$

$$\Sigma_{3S}^{\text{QED}_4}(p^2) = \bar{\alpha}^3 \left( \frac{\bar{\mu}^2}{-p^2} \right)^{3\varepsilon_\gamma} \left[ \frac{3(\xi + 3)^3 + 32N_f^2 - 36(\xi + 3)N_f}{18\varepsilon_\gamma^3} + \frac{27(\xi + 2)(\xi + 3)^2 + 320N_f^2 - 54(6\xi + 17)N_f}{27\varepsilon_\gamma^2} + \frac{4}{324\varepsilon_\gamma} \left[ 81(3\xi^3 + 27\xi^2 + 79\xi + 97) + 4816N_f^2 - 324\zeta_3(4N_f - 3(\xi + 3)) - 27(156\xi + 503)N_f - 27\zeta_2(3(\xi + 3)^3 + 32N_f^2 - 36(\xi + 3)N_f) \right] + \mathcal{O}(\varepsilon_\gamma^0) \right]. \quad (3.188b)$$

The corresponding renormalization constant can then be derived using the third order expansion of the eqs. (3.45), reading

$$\delta Z_{3\Psi} = \mathcal{K}(\Sigma_{2V}\mathcal{K}(\Sigma_{1V})) + \mathcal{K}(\Sigma_{1V}\mathcal{K}(\Sigma_{2V})) + \mathcal{K}(\Sigma_{1V}\mathcal{K}(\Sigma_{1V}\mathcal{K}(\Sigma_{1V}))) + \mathcal{K}(\Sigma_{3V}), \quad (3.189a)$$

$$\begin{aligned} \delta Z_{3m} = & -\mathcal{K}(\Sigma_{1S}^2\Sigma_{1SV}) + 2\mathcal{K}(\Sigma_{1S}\Sigma_{1SV}^2) - \mathcal{K}(\Sigma_{1S}\Sigma_{1SV}\mathcal{K}(\Sigma_{1SV})) - \mathcal{K}(\Sigma_{1SV}\mathcal{K}(\Sigma_{1S}\Sigma_{1SV})) \\ & + \mathcal{K}(\Sigma_{1S}\Sigma_{2SV}) + \mathcal{K}(\Sigma_{2S}\Sigma_{1SV}) - \mathcal{K}(\Sigma_{1SV}^3) + \mathcal{K}(\Sigma_{1SV}^2\mathcal{K}(\Sigma_{1SV})) + \mathcal{K}(\Sigma_{1SV}\mathcal{K}(\Sigma_{1SV}^2)) \\ & - 2\mathcal{K}(\Sigma_{1SV}\Sigma_{2SV}) + \mathcal{K}(\Sigma_{2SV}\mathcal{K}(\Sigma_{1SV})) + \mathcal{K}(\Sigma_{1SV}\mathcal{K}(\Sigma_{2SV})) - \mathcal{K}(\Sigma_{1SV}\mathcal{K}(\Sigma_{1SV}\mathcal{K}(\Sigma_{1SV}))) - \mathcal{K}(\Sigma_{3SV}), \end{aligned} \quad (3.189b)$$

where  $\Sigma_{lSV} = \Sigma_{lS} + \Sigma_{lV}$ , with  $l$  the loop order. Therefore, using all the previous results for QED<sub>4</sub>, we derive

$$\delta Z_{3\Psi}^{\text{QED}_4} = \bar{\alpha}_r^3 \left[ -\frac{\xi_r^3}{6\varepsilon_\gamma^3} + \frac{(4N_f + 3)(8N_f - 9\xi_r)}{36\varepsilon_\gamma^2} - \frac{40N_f^2 + 54N_f + 27}{54\varepsilon_\gamma} + \mathcal{O}(\varepsilon_\gamma^0) \right], \quad (3.190a)$$

$$\delta Z_{3m}^{\text{QED}_4} = \bar{\alpha}_r^3 \left[ -\frac{(4N_f - 9)(8N_f - 9)}{18\varepsilon_\gamma^3} + \frac{160N_f^2 - 1044N_f + 243}{108\varepsilon_\gamma^2} + \frac{280N_f^2 - 2592N_f\zeta_3 + 2484N_f - 3483}{162\varepsilon_\gamma} + \mathcal{O}(\varepsilon_\gamma^0) \right]. \quad (3.190b)$$

Note that  $\delta Z_{3m}$  is completely gauge-independent, which is again a strong check on our results. The full three-loop renormalization-group functions can then be derived using the definitions (3.48), reading

$$\gamma_\Psi^{\text{QED}_4} = 2\bar{\alpha}_r\xi_r - \bar{\alpha}_r^2(4N_f + 3) + \bar{\alpha}_r^3 \left( \frac{40N_f^2}{9} + 6N_f + 3 \right) + \mathcal{O}(\bar{\alpha}_r^4), \quad (3.191a)$$

$$\gamma_m^{\text{QED}_4} = 6\bar{\alpha}_r + \bar{\alpha}_r^2 \left( 3 - \frac{20N_f}{3} \right) + \bar{\alpha}_r^3 \left( -\frac{280N_f^2}{27} + 96N_f\zeta_3 - 92N_f + 129 \right) + \mathcal{O}(\bar{\alpha}_r^4), \quad (3.191b)$$

$$\beta^{\text{QED}_4} = -2\bar{\alpha}_r\varepsilon_\gamma + \frac{8\bar{\alpha}_r^2 N_f}{3} + 8\bar{\alpha}_r^3 N_f - \bar{\alpha}_r^4 \frac{4N_f(22N_f + 9)}{9} + \mathcal{O}(\bar{\alpha}_r^5), \quad (3.191c)$$

which is in accordance with the usual literature, see, *e.g.*, the textbook [61]. This complete three-loop result required the analytical calculation (by reduction) of a total of 14304 Feynman integrals, see table 3.8.

QED <sub>4</sub>	1-loop	2-loop	3-loop		
Topology	Bubble	Diamond	Ladder (L3)	Benz (B3)	Non-planar (N3)
Number of integrals	6	76	5377	7482	1363

Table 3.8: Number of integrals computed up to three loops for a given topology in QED<sub>4</sub>.

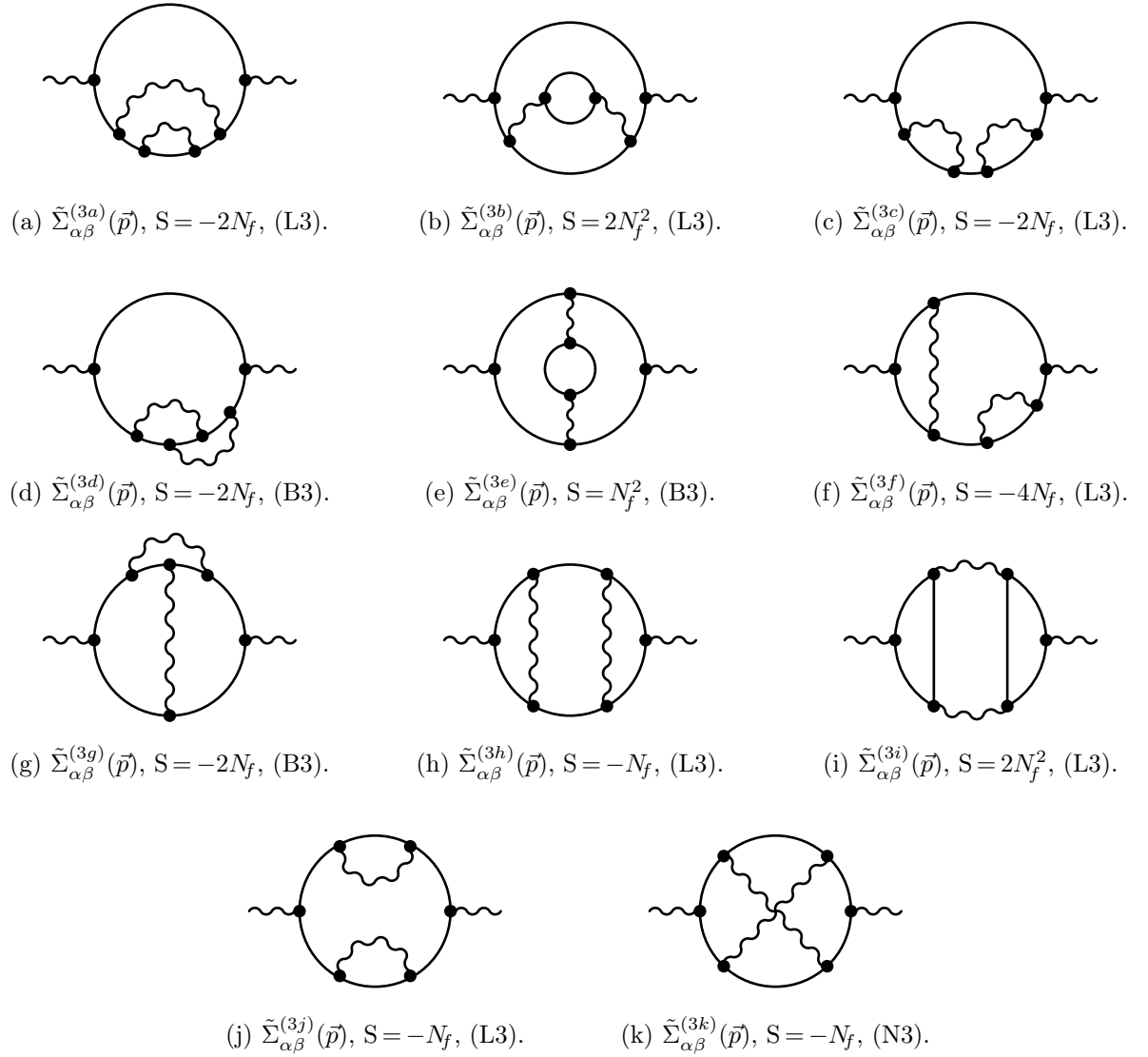


Figure 3.9: The 11 three-loop photon polarization diagrams for QED<sub>4</sub> in the small coupling expansion. Fermion arrow have been dropped to keep it light. S indicates the extra factor needed for each graph, *i.e.*, the  $-N_f$  factors due to fermion loops and an eventual multiplicative factor if the diagram have multiple equivalent topologies regarding different fermion flows (20 diagrams in total).

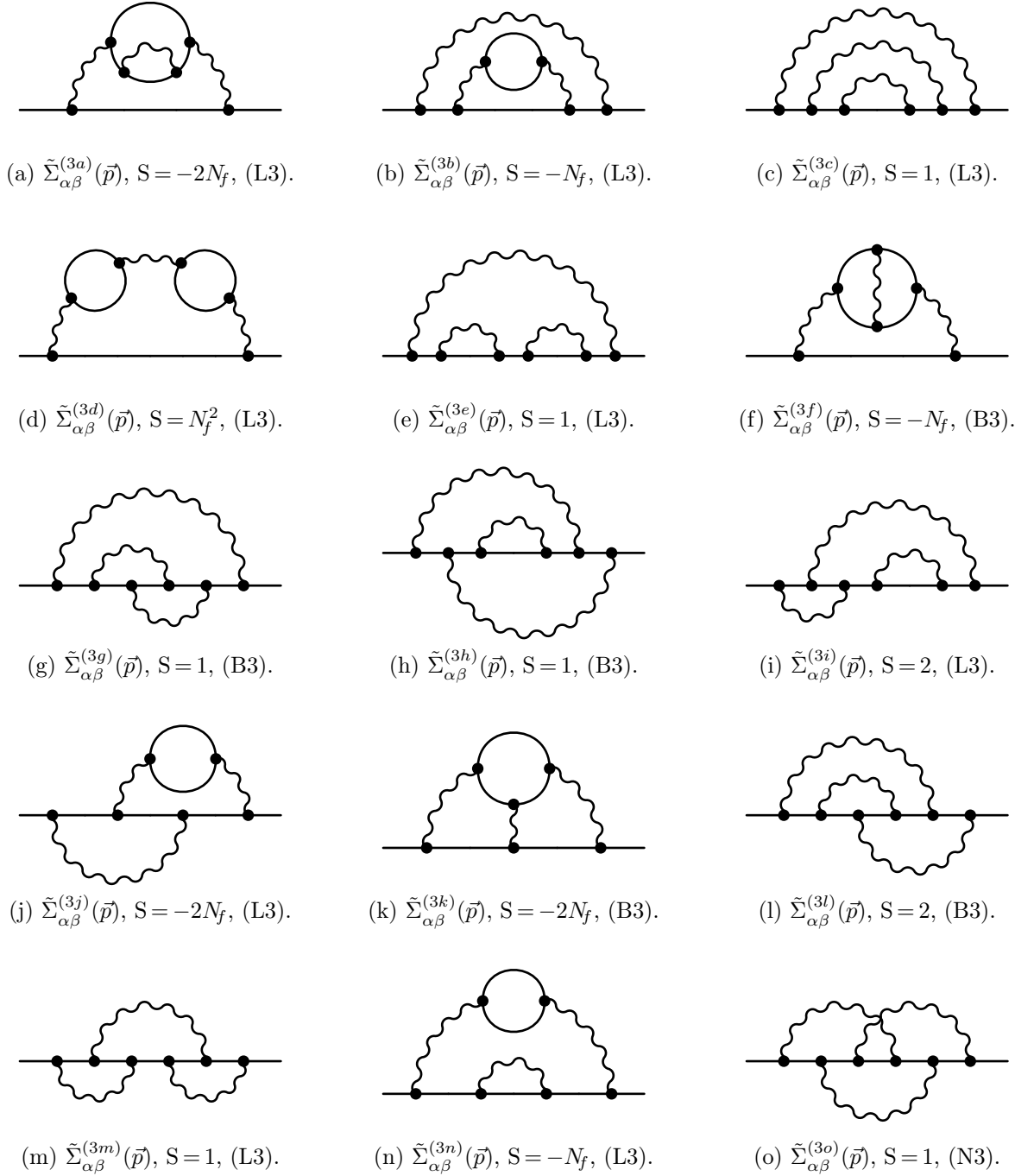


Figure 3.10: The 15 three-loop fermion self-energy diagrams for QED<sub>4</sub> in the small coupling expansion. Fermion arrows have been dropped to keep it light.  $S$  indicates the extra factor needed for each graph, *i.e.*, the  $-N_f$  factors due to fermion loops and an eventual multiplicative factor if the diagram have multiple equivalent topologies regarding different fermion flows (20 diagrams in total).





# Chapter 4

## Critical properties of many flavor QEDs in three dimensions

This chapter is partially based on the papers

- [5] S. Metayer and S. Teber, *Symmetry*. 2023; 15(9):1806,  
“Critical Properties of Three-Dimensional Many-Flavor QEDs”,
- [6] S. Metayer and S. Teber, *Phys. Lett. B* 838 (2023) 137729,  
“Electron mass anomalous dimension at  $O(1/N_f^2)$  in three-dimensional  $\mathcal{N}=1$  supersymmetric QED”,
- [7] A. James, S. Metayer and S. Teber, [arXiv:2102.02722](https://arxiv.org/abs/2102.02722),  
“ $\mathcal{N}=1$  supersymmetric three-dimensional QED in the large- $N_f$  limit and applications to super-graphene”.

We study several abelian gauge theories, the prototype of which is three-dimensional Quantum Electrodynamics, QED<sub>3</sub>. After motivating such study, we introduce a general model encompassing several of its variants, including the fermionic, bosonic and minimally supersymmetric QED<sub>3</sub>. We compute the corresponding self-energies and polarizations up to next-to-leading order in a large number of fermion flavors expansion, and compute exactly all the anomalous dimensions at that order. Our results are mapped to a model of super-graphene, for which we compute the optical conductivity. From the study of their critical properties, we address the phase structure of these gauge theories.

### Contents

---

4.1	Motivations for QED <sub>3</sub> and its supersymmetric extension. . . . .	<b>158</b>
4.2	Models of three-dimensional QEDs in large- $N_f$ . . . . .	<b>161</b>
4.2.1	Three-dimensional (fermionic) Quantum Electrodynamics (QED <sub>3</sub> ) . . . . .	161
4.2.2	Bosonic Quantum Electrodynamics (bQED <sub>3</sub> ) . . . . .	165
4.2.3	Minimally supersymmetric Quantum Electrodynamics ( $\mathcal{N}=1$ SQED <sub>3</sub> ) . . . . .	165
4.2.4	Super-graphene model (SQED <sub>4,3</sub> ) . . . . .	167
4.3	Presentation of the general gQED <sub>3</sub> model . . . . .	<b>168</b>
4.4	Perturbative calculations at NLO in gQED <sub>3</sub> . . . . .	<b>177</b>
4.4.1	Gauge-multiplet polarizations at LO . . . . .	177
4.4.2	Matter-multiplet self-energies at LO . . . . .	181
4.4.3	Vanishing contributions and generalized Furry theorem . . . . .	184
4.4.4	Gauge-multiplet polarizations at NLO . . . . .	187
4.4.5	Matter-multiplet self-energies at NLO . . . . .	191
4.4.6	Renormalized self-energies . . . . .	196
4.5	Results summary and discussion . . . . .	<b>197</b>
4.5.1	Results for QED <sub>3</sub> . . . . .	197
4.5.2	Results for $\mathcal{N}=1$ SQED <sub>3</sub> . . . . .	198
4.5.3	Results for bosonic bQED <sub>3</sub> . . . . .	199
4.5.4	Results for reduced QED <sub>4,3</sub> (Graphene) . . . . .	199
4.5.5	Results for reduced $\mathcal{N}=1$ SQED <sub>4,3</sub> (Super-Graphene) . . . . .	200
4.5.6	Discussion of the stability of the fixed point . . . . .	202
4.6	Critical $N_f$ for dynamical electron mass generation . . . . .	<b>202</b>
4.6.1	Schwinger Dyson equations at LO . . . . .	203
4.6.2	Semi-phenomenological gap equation . . . . .	204
4.7	Conclusion . . . . .	<b>210</b>

---



## 4.1 Motivations for QED<sub>3</sub> and its supersymmetric extension.

In this introductory section, we motivate the study of three-dimensional Quantum Electrodynamics, QED<sub>3</sub>, and its minimally supersymmetric variant, SQED<sub>3</sub>. On the fly, we will introduce briefly the minimally supersymmetric version of QED<sub>4,3</sub>, which is, by extension, a model of “super-graphene”, *i.e.*, SQED<sub>4,3</sub>, as well as the bosonic version of the non-SUSY model, bQED<sub>3</sub>.

### Three-dimensional QED (QED<sub>3</sub>)

QED<sub>3</sub> is a gauge field theory model of strongly interacting relativistic planar fermions that has been attracting continuous interest for the past four decades. An original motivation [175, 176] came from the idea that QED<sub>3</sub> might serve as a prototype for the more intricate four-dimensional Quantum Chromodynamics (QCD<sub>4</sub>), the non-abelian gauge theory of quarks and gluons. Indeed, QED<sub>3</sub> and QCD<sub>4</sub> share multiple features, such as asymptotic freedom and confinement, as well as dynamical chiral symmetry breaking (DχSB) induced by the radiative generation of a fermion mass. It is indeed easier to study these phenomena in QED<sub>3</sub> where computations are much shorter, but similar in essence. From QED to QCD, the Lie symmetry group is enhanced from  $U(1)$  to  $SU(3)$ , giving rise to a strong colored charge and additional gluon self interactions.

As underlined in the previous chapter, three-dimensional gauge theories are in general superrenormalizable with dimensionful coupling  $[e^2] = 1$ , which is not suitable as perturbative parameter. Early studies [175, 176, 269] realized that, within a  $1/N_f$  expansion, where  $N_f$  is the number of electron flavors, the super-renormalizable QED<sub>3</sub> model acquires an interacting fixed point in the low energy limit and becomes effectively renormalizable in the infrared (IR). In the following, we will compute higher-order corrections to this fixed point for several QED<sub>3</sub> variants and eventually address its stability with respect to higher-order quantum corrections. Indeed, the fate of IR singularities are ubiquitous to superrenormalizable models and the QED<sub>3</sub> often serve as a toy model for such studies [270–274] (see recent progress in [105, 275, 276]). Large- $N_f$  techniques (see [117] for a review) allow for an arbitrary large coupling and are therefore extremely useful to access the critical properties of the model, usually occurring in a non-perturbative coupling regime. In this chapter, about QED<sub>3</sub> and its variants, our main interest will be on the field and mass anomalous dimensions, that encode the renormalization of the composite operator  $\bar{\psi}\psi$  [213, 226], the simplest fermion bilinear. As showed in the previous chapter, such quantities play a crucial role in the study of fundamental quantum field theory mechanisms such as, *e.g.*, dynamical (flavor) symmetry breaking and electron mass generation [131, 177, 181–183, 269, 277–282] (see recent progress in [184–187, 283]).

In the last three decades, considerable revival in interest in QED<sub>3</sub> also arose from its applications to condensed matter physics systems with relativistic-like (Dirac-like) gapless quasiparticle excitations at low-energies such as high- $T_c$  superconductors [135–138], planar antiferromagnets [139] and graphene [26, 128] (for graphene, see reviews in refs. [87, 124–126]). As we have seen in the previous chapter, a universal quantity of interest to compute in graphene-like systems is the optical conductivity in the collisionless regime. Indeed, we have computed, in QED<sub>4,3</sub> up two-loop order in the (dimensionless) fine structure constant expansion, the optical conductivity of a monolayer freestanding graphene sheet in the ultra-relativistic limit and obtained from it an optical absorbance of  $A_g = (2.29 \pm 0.04)\%$ , a result first obtained in [144, 145, 150] (These authors also derived the result in the pseudo-relativistic regime). This quantity is derived from the minimal conductivity of graphene,  $\sigma_{0g} = N_f e^2 / 8$ , and from the first interaction correction coefficient to this quantity,  $C_\gamma^{\text{QED}_{4,3}}$ . We also showed that this universal (flavor independent) coefficient can actually be related to  $C_\gamma^{\text{QED}_3}$  with the help of a mapping [134]. Moreover, the most recent NLO results [134, 184, 186, 187] show that QED<sub>3</sub> has a gauge-invariant  $N_c = 2.847$ . In the following chapter, we will recover these results and slightly improve them with resummations to obtain  $N_c = 2.270$ . This won't change the big picture, and we will therefore confirm the possibility of a dynamical mass generation in this model for small  $N_f$  in QED<sub>3</sub>.

### Three-dimensional minimally supersymmetric QED (SQED<sub>3</sub>)

In this chapter, one of our main focuses will be the study of the minimal ( $\mathcal{N}=1$ ) supersymmetric (SUSY) extension of the QED<sub>3</sub> model. First, let us recall that, in a supersymmetric model, for each existing particle is introduced a new particle called superpartner that possesses the opposite spin statistics. In other words, for each matter particle, we introduce a new force and vice versa. In the case of QED, it amounts to introduce the bosonic (Bose–Einstein statistics) super-electron, called *selectron* as well as the fermionic (Fermi–Dirac statistics) super-photon, called the *photino*. As we will see in the following, some additional fields may be required to keep the supersymmetric field theory consistent, but they usually don't have any dynamics, *i.e.*, no particle excitations. There are several reasons to explore supersymmetric extensions of a model. In quantum field theory, SUSY is usually introduced for its mathematical convenience in the context of exact computations, as well as being the only allowed extension of the Poincaré symmetry group, as stated by the Coleman–Mandula theorem [284]. However, we will see in the following that in a perturbative context, additional supersymmetric fields make computations lengthy and possibly more difficult. Indeed, several complications come together with SUSY. First, we need to preserve SUSY, as it is naively not the case, since it is broken both by dimensional regularization and the usual  $R_\xi$  gauge fixing term. Second, supersymmetric theories often mixes Dirac and Majorana spinors, that behave unusually in three dimensions. We will address these technical issues in the rest of the chapter while using the large- $N_f$  expansion technique, see [117] for a review.

Supersymmetric variants of QED<sub>3</sub> have attracted continuous interest through the last decades. This has been partly motivated by the fact that the enhanced symmetry may simplify the resolution and, perhaps, even lead to an exact solution. As a matter of fact, the case of (non-minimal)  $\mathcal{N}=2$  SQED<sub>3</sub> has been studied in an early seminal paper of Pisarski [177] by dimensional reduction from the case of (minimal)  $\mathcal{N}=1$  four-dimensional supersymmetric QED (SQED<sub>4</sub>), with focus on dynamical electron mass generation along the lines of the non-supersymmetric case. Actually, in  $\mathcal{N}=1$  SQED<sub>4</sub>, a non-perturbative non-renormalization theorem forbids dynamical mass generation [285], and it was then argued in [286] that it, therefore, extends by dimensional reduction to  $\mathcal{N}=2$  SQED<sub>3</sub>. Further evidence for the absence of dynamical mass generation in  $\mathcal{N}=2$  SQED<sub>3</sub> came from numerical simulations [287] and a refined analytic treatment [288].

The situation in  $\mathcal{N}=1$  SQED<sub>3</sub> is more subtle because of the absence of non-renormalization theorem in this case. The model was first considered by Koopmans and Steringa [286] along the lines set by Appelquist et al. for standard fQED<sub>3</sub> [131]. Their truncated (to leading order (LO) in  $1/N_f$ -expansion) Schwinger–Dyson equations approach resulted in a critical fermion flavor number,  $N_c=1.62$ . This implies that a dynamical (parity-invariant) mass generation may occur for  $N_f=1$ , *i.e.*, one four-component Dirac spinor. A decade later, additional evidence for the generation of dynamical electron mass in minimal SQED<sub>3</sub> was also found in [289]. There is, however, no rigorous statement for electron mass generation for minimally supersymmetric SQED<sub>3</sub> [286, 289].

In the last two decades,  $\mathcal{N}=1$  SQED<sub>3</sub> has attracted significant attention (together with other supersymmetric and non-supersymmetric gauge theories) in the context of the study of IR dualities and renormalization group flows (see, e.g., [290–295]). Interestingly, it was argued in [197] that  $\mathcal{N}=1$  SQED<sub>3</sub> at  $N_f=1$  is dual to a conformal field theory in the IR. This suggests that no dynamical mass for the electron should be generated in contrast to the previously mentioned early (leading order) calculations [286, 289]. In this chapter, we will present a refined, next-to-leading order (NLO) analysis. We will show that, at NLO,  $N_c=0.39$ , which is strong evidence that no electron mass is radiatively generated in  $\mathcal{N}=1$  SQED<sub>3</sub>, which is in agreement with the analysis based on dualities [197].

At the interface with condensed matter physics, there have also been proposals during the last years that SUSY may emerge in the low-energy limit of various lattice models (see, e.g., [296–303]). To this day, there is still no evidence that SUSY is realized in nature, and an emergent SUSY should certainly be difficult to detect in the lab [304]. Nevertheless, computing critical exponents in the

corresponding models is certainly valuable in order to assess the potential impact of supersymmetry on experimentally measurable observables. In this context, some condensed-matter physics models describing planar relativistic Dirac fermions were supersymmetrized. Such is the case for the so-called super-graphene model that has been (for both  $\mathcal{N} = 1$  and  $\mathcal{N} = 2$  cases) first introduced in [157, 163] via superconformal techniques on the boundary. See also [164] for related non-perturbative computations of transport properties in the  $\mathcal{N} = 2$  case, as well as [305, 306] in which a  $\mathcal{N} = 2$  model for super-graphene has been proposed and also references therein in which the possible manifestation of SUSY in a theory for graphene has already been raised, even though they remained at the level of supersymmetric quantum mechanics and corresponding SUSY features of the energy spectrum. Notice that, similarly to the large- $N_f$  limit of QED<sub>3</sub>, the (non-SUSY) model of graphene is a conformal-invariant field theory that corresponds to the IR Lorentz-invariant fixed point of (non-relativistic) graphene [144] (see [129] where this fixed point was first discovered). We therefore refer to the super-graphene model as SQED<sub>4,3</sub> which is the minimal supersymmetric extension of the QED<sub>4,3</sub> graphene model studied in the previous chapter. In super-graphene, the matter (electrons and selectrons) is localized in the (2+1)-dimensional plane while gauge interactions (photons and photinos) propagate in the larger (3+1)-dimensional bulk. We recall that in the non SUSY case, such a (conformal) brane-world model (as such, initially introduced in [118] with a first application to graphene in [122], see also [120, 135, 136] in relation with high- $T_c$  superconductors and the quantum Hall effect) and its variants has attracted significant interest in the last years, see, e.g., [134, 147, 150, 153, 156–158, 160–162]. As we will see in the following, like in the non-SUSY case, it exists a mapping relation between SQED<sub>3</sub> in the large- $N_f$  expansion and SQED<sub>4,3</sub> in the small coupling expansion. We will use this to compute the properties of the eventual super-graphene from the NLO results we will obtain in SQED<sub>3</sub>.

Before going further into the supersymmetric case, we will introduce briefly the simpler case of bosonic QED. This textbook model has been granted many names through the years; Abelian Higgs, CP<sup>*N*−1</sup>, scalar QED, bosonic QED etc. For short, we will call it bQED. Our interest for this model is natural<sup>1</sup> since it is a subcase of SQED. Indeed, bQED is the gauge theory of the interaction of bosonic, or more specifically, scalar, particles via photons. This model has been extensively studied in four dimensions since many decades, see, e.g., the seminal papers [307, 308] (See also the recent four-loop computations carried out in [309] and references therein), as well as in three-dimensions, see, e.g., [175, 176]. In the following, we will focus our interest on “pure” bQED, *i.e.*, neglecting  $\phi^4$ -type (and eventually higher) interactions between scalar particles, since they are not present in the SUSY case. Moreover, we will consider the massless (or quasi massless) case such that the scalar potential is zero, and that all interactions are of pure gauge origin. Note that this pure gauge case is indeed a fixed point of the case with a non-vanishing scalar potential. This fixed point is often called in the literature tricritical bQED [196, 198, 310]. We shall refer to this pure case simply as bQED in the following, and consider it in the large- $N_f$  expansion.

## Outline of the chapter

Having set the background material together with the contemporary frame of activity, our primary concern in this chapter will be the critical properties of minimal SQED<sub>3</sub>. In a first section 4.2, we will introduce first the QED<sub>3</sub> and bQED<sub>3</sub> models and their specificities, as well as introducing briefly the large- $N_f$  technique graphically. We will then introduce the (minimal) associated three-dimensional supersymmetric model,  $\mathcal{N} = 1$  SQED<sub>3</sub> together with the technicalities necessary for perturbative computations, such as the dimensional reduction scheme (DRED) [311–313] (see also [314] for a review) that is the most convenient regularization scheme for practical calculations in supersymmetric theories. We will also introduce briefly a model of super-graphene, SQED<sub>4,3</sub>, to which our SQED<sub>3</sub> results can be mapped. To keep track of all these models, we will introduce in section 4.3 a general model, with additional parameters, that we will call gQED<sub>3</sub> and that encompasses all the previously described

<sup>1</sup>We warmly thank John Gracey for pointing out that bQED<sub>3</sub> computations had never been done at  $1/N_f^2$ .

model. In section 4.4, we will then perform the full LO and NLO computations in the large- $N_f$  expansion, in the general gQED<sub>3</sub> model, of all the polarizations and self-energies in order to compute the corresponding anomalous dimensions. This will lead us to discuss a generalized version of the Furry theorem for these models. As for the results, we will find that the electron and selectron critical exponents are highly constrained and that the related identities (by analogy with four-dimensional supersymmetric Slavnov-Taylor identities [315, 316]) are achieved thanks to a subtle role played by the particles associated with the DRED scheme, the so-called epsilon-scalars. In section 4.5 we present how our results map to all the models of interest, *i.e.*, QED<sub>3</sub>, bQED<sub>3</sub>, SQED<sub>3</sub>, and finally SQED<sub>4,3</sub>, where we compute the optical conductivity of an eventual super-graphene material. In section 4.6, we discuss the criteria for dynamical mass generation and the opening of a bandgap in the corresponding systems.

## 4.2 Models of three-dimensional QEDs in large- $N_f$

In this section we introduce various models, namely (fermionic) QED<sub>3</sub>, (bosonic) bQED<sub>3</sub>, supersymmetric  $\mathcal{N} = 1$  SQED<sub>3</sub>, the super-graphene model  $\mathcal{N} = 1$  SQED<sub>4,3</sub>, and finally a generalized version of SQED<sub>3</sub>, called gQED<sub>3</sub>, allowing us to consider all these models at the same time.

### 4.2.1 Three-dimensional (fermionic) Quantum Electrodynamics (QED<sub>3</sub>)

#### QED<sub>3</sub> model and specificities

Three-dimensional Quantum Electrodynamics (QED<sub>3</sub>) is an archetypal ultra-relativistic abelian gauge-field theory model describing strongly interacting planar fermions. In Minkowski space, it is described, in its simplest form, by the Lagrangian density

$$S_{\text{QED}_3} = \int d^3x \left[ i\bar{\psi}_i \not{D}\psi^i - \frac{1}{4} F_{\mu\nu} F^{\mu\nu} - \frac{1}{2\xi} (\partial_\mu A^\mu)^2 \right], \quad (4.1)$$

where  $\psi^i$  are  $2N_f$  flavors ( $i = 1, \dots, 2N_f$ ) of 2-component massless Dirac fermions (or equivalently  $N_f$  flavors of 4-component massless Dirac fermions  $\Psi^i$ ) and  $A^\mu$  the covariant three-dimensional gauge field with  $\mu = 0, 1, 2$ . As advertised earlier in this manuscript, this model is a subcase of reduced QED <sub>$d_e, d_\gamma$</sub> , the theory introduced in the previous chapter, see (3.12), with  $d \equiv d_e = d_\gamma = 3$ , *i.e.*, with electrons and photons all confined in the same  $d = 2 + 1$  plane. See figure 4.1, for an illustration of an event in QED<sub>3</sub> to fix ideas. In the model (4.1), the covariant derivative is defined as previously as

$$D_\mu = \partial_\mu + ieA_\mu, \quad \text{with} \quad \not{D} = \gamma^\mu D_\mu, \quad (4.2)$$

with the major difference that the electric coupling constant  $e$  is now dimensionful, as compared to the models considered in the previous chapter. Indeed, in the case of a three-dimensional gauge field, we have the canonical dimensions

$$[\psi] = 1, \quad [A] = \frac{1}{2}, \quad [e] = \frac{1}{2}, \quad [\xi] = 0, \quad (4.3)$$

implying that the coupling have positive mass dimension  $[e^2] = 1$  (see (3.11) in the previous chapter 3). This theory is then super-renormalizable, and hence asymptotically free, in striking contrast with the models of QED <sub>$4, d_e$</sub> , *e.g.*, QED<sub>4,3</sub> and QED<sub>4</sub>, considered in chapter 3. Since the coupling  $e$  or equivalently  $\alpha$  is not suitable to be the small parameter in QED<sub>3</sub>, we will introduce the large- $N_f$  technique in the following section.

Another key difference in the three-dimensional case, compared to the four dimensional case, is the choice of representation for the Dirac gamma matrices. Indeed, as already discussed in section 3.4.4

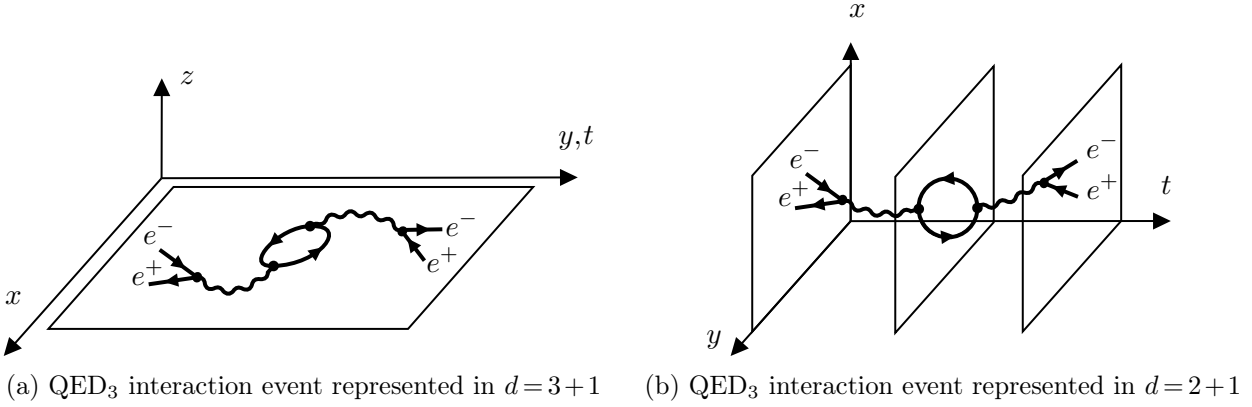


Figure 4.1: Two equivalent illustration of the same interaction event in QED<sub>3</sub>. All particles, electrons, positrons and photons, are confined on the  $d = 2 + 1$  plane  $(x, y, t)$ . Note that on the left image, the  $t$  and  $y$  axes are shrunk together for illustration purposes.

in the previous chapter, for a given dimension  $d$ , the minimal size for  $n \times n$  Dirac gamma matrices to realize the Clifford algebra

$$\{\gamma^\mu, \gamma^\nu\} = \gamma^\mu \gamma^\nu + \gamma^\nu \gamma^\mu = 2g^{\mu\nu} I_n, \quad (4.4)$$

is  $n = 2^{\lfloor d/2 \rfloor}$ , with  $\lfloor x \rfloor$  the floor function. This implies that for  $d = 3$ , it is enough to take 3 matrices of size  $2 \times 2$  as a representation. One can take, *e.g.*, the irreducible representation

$$\gamma^0 = \sigma_2, \quad \gamma^1 = i\sigma_3, \quad \gamma^2 = i\sigma_1, \quad (4.5)$$

with  $\sigma_j$  the usual Pauli matrices. As a matter of fact, as showed in sec 3.4.4 of the previous chapter, a (reducible)  $4 \times 4$  representation is also possible for QED<sub>3</sub>. However, in the following chapter, we will favor the  $2 \times 2$  (or more generally  $n \times n$ ) representation for ease of comparison with the supersymmetric case, where  $n = 2$  will be mandatory to preserve supersymmetry.

Note that the action (4.1) is massless. Actually, several mass terms can be considered in three-dimensional gauge theories. As demonstrated in section 3.4.4 in the previous chapter, two mass terms may be relevant in the three-dimensional case, *i.e.*, the parity-even and parity-odd masses

$$\mathcal{L}_{m_{\text{even}}} = m_{\text{even}} \left( \sum_{i=1}^{N_f} \bar{\psi}_i \psi^i - \sum_{i=1+2N_f}^{2N_f} \bar{\psi}_i \psi^i \right), \quad \mathcal{L}_{m_{\text{odd}}} = m_{\text{odd}} \left( \sum_{i=1}^{N_f} \bar{\psi}_i \psi^i + \sum_{i=1+2N_f}^{2N_f} \bar{\psi}_i \psi^i \right). \quad (4.6a)$$

In the following chapters, we will focus on the parity preserving (even) mass term. Indeed, it has been showed that no parity-odd mass term can be dynamically generated in such theories [317, 318], which makes sense since the odd term does not break the  $U(2N_f)$  symmetry of the model, while the parity-even mass term breaks it into  $U(2N_f) \rightarrow U(N_f) \times U(N_f)$ .

### Large- $N_f$ expansion

In this section, we briefly introduce graphically the idea of the large- $N_f$  expansion, see, *e.g.*, [117] for complete a review. We first recall that, in the loop expansion, the Dyson equation for the photon yields graphically, in its exact form

$$\text{wavy line} = \text{wavy line} + \text{wavy line} \text{---} \text{circle} \text{---} \text{wavy line}, \quad (4.7)$$

where the double wiggly line represents the fully dressed photon,  $D^{\mu\nu}(p)$ , the single wiggly line the bare photon,  $D_0^{\mu\nu}(p)$ , and the blob represent the polarization of the photon,  $\Pi^{\mu\nu}(p)$ . This recursive equation can then be developed and leads to the following series

$$\text{double wiggly} = \text{single wiggly} + \text{single wiggly} \text{---} \text{blob} \text{---} \text{single wiggly} + \text{single wiggly} \text{---} \text{blob} \text{---} \text{blob} \text{---} \text{single wiggly} + \dots \quad (4.8)$$

In the loop expansion, the blob, representing the polarization of the photon, has the usual diagrammatic expansion

$$\text{blob} = \text{circle} + \text{circle with wavy line} + \text{circle with wavy line and blob} + \dots, \quad (4.9)$$

where we display the diagrams up to two loops, and we dropped the fermion arrows for simplicity (we also dropped a factor of 2 in front of the third diagram). Using this expanded polarization, the dressed propagator can be written in the series form

$$\begin{aligned} \text{double wiggly} &= \text{single wiggly} \\ &+ \text{single wiggly} \text{---} \text{circle} \text{---} \text{single wiggly} \\ &+ \text{single wiggly} \text{---} \text{circle} \text{---} \text{single wiggly} \text{---} \text{circle} \text{---} \text{single wiggly} + \text{single wiggly} \text{---} \text{circle with wavy line} \text{---} \text{single wiggly} + \text{single wiggly} \text{---} \text{circle with wavy line and blob} \text{---} \text{single wiggly} \\ &+ \text{single wiggly} \text{---} \text{circle} \text{---} \text{single wiggly} \text{---} \text{circle} \text{---} \text{single wiggly} \text{---} \text{circle} \text{---} \text{single wiggly} + \text{single wiggly} \text{---} \text{circle} \text{---} \text{single wiggly} \text{---} \text{circle with wavy line} \text{---} \text{single wiggly} + \text{single wiggly} \text{---} \text{circle} \text{---} \text{single wiggly} \text{---} \text{circle with wavy line and blob} \text{---} \text{single wiggly} \\ &+ \dots \end{aligned} \quad (4.10)$$

The order in the coupling constant  $e$  can be found easily by counting the vertices of each diagram. Indeed, in the loop expansion, the perturbative series in the coupling  $e$  is well-defined because it takes into account in a perturbative way all the diagrams combinations, and then, one only has to compute the diagrams involved in the blob (4.9).

When the coupling  $e$  is not suitable as the expansion parameter, *e.g.*, in superrenormalizable theories, one can use the so-called large- $N_f$  expansion technique. In this case, we naively see that the series (4.10) is not perturbative at all since each fermion loop gives a factor proportional to  $N_f$ , thereby increasing with the complexity of the diagram. The trick to perform the  $1/N_f$  expansion is then to resum the infinite chain of simple matter loops in force field propagators, and rearrange the series expansion, making the theory effectively renormalizable in the IR [269]. Hence, considering the first term of each line in (4.10), *i.e.*, the simple bubble chains, we can define the new propagator

$$\begin{aligned} \text{double wiggly} &= \text{single wiggly} + \text{single wiggly} \text{---} \text{circle} \text{---} \text{single wiggly} + \text{single wiggly} \text{---} \text{circle} \text{---} \text{circle} \text{---} \text{single wiggly} + \dots \\ &= \text{single wiggly} \times \left( 1 + \text{circle} + \left( \text{circle} \right)^2 + \dots \right) \\ &= \text{single wiggly} \times \frac{1}{1 - \text{circle}}. \end{aligned} \quad (4.11)$$

Going further, we recall that the bare photon propagator has momentum dependence  $\sim p^{-2}$  and the fermionic simple bubble diagram yields<sup>2</sup>  $\sim e^2 N_f p_E$  (with  $p_E = i|p|$ , the Euclidean momentum). There-

<sup>2</sup>Note that  $\Pi_\gamma \sim e^2 N_f / p_E$  implying  $\Pi_\gamma^{\mu\nu} \sim p^2 \Pi_\gamma \sim e^2 N_f p_E$ .



fore, the new propagator (4.11), in the large- $N_f$  limit, reads

$$\text{---}\textcircled{1}\text{---} \sim \left( \text{---}\textcircled{1}\text{---} \right)^{-1} \sim \frac{1}{e^2 N_f p_E}. \quad (4.12)$$

This new photon propagator is then said to be softened, since its behavior in the infrared is attenuated. Moreover, it behaves properly in the large- $N_f$  limit since, in combination with the QED vertex which is  $\sim e$ , it gives

$$\text{---}\textcircled{1}\text{---} \sim \frac{1}{N_f p_E}, \quad (4.13)$$

where the coupling  $e^2$  drops in favor of  $1/N_f$ . Therefore, in the large- $N_f$  limit, QED<sub>3</sub> becomes renormalizable with dimensionless coupling  $1/N_f$ . Using this softened propagator, the first contribution to the electron self-energy is therefore

$$\text{---}\textcircled{1}\text{---} \sim \frac{1}{N_f}, \quad (4.14)$$

which takes into account an infinite number of diagrams! Moreover, the expansion for the dressed photon (4.10) can be rewritten as

$$\text{---}\textcircled{1}\text{---} = \text{---}\textcircled{1}\text{---} + \text{---}\textcircled{1}\text{---}\textcircled{1}\text{---} + \text{---}\textcircled{1}\text{---}\textcircled{1}\text{---}\textcircled{1}\text{---} + \dots \quad (4.15)$$

which is well-defined since  $\text{---}\textcircled{1}\text{---}$  is of order  $1/N_f$ , *i.e.*, the first two corrections displayed in (4.15) are now indeed of order  $1/N_f^2$ . Similarly, at the next-to-leading order (NLO) one can resum the two-loop contributions, yielding a new propagator  $\text{---}\textcircled{2}\text{---} \sim 1/N_f^2$  in the IR limit, which allow computing NLO corrections to the electron self-energy at  $1/N_f^2$ , etc. So the strategy goes as follows, at leading order (LO):

- 1) Compute the one-loop polarization using bare Feynman rules and compute the LO softened photon by resumming the one-loop polarization,
- 2) Compute the other diagrams of the theory at  $O(1/N_f)$  using the LO softened photon only.

Then at next-to-leading order (NLO):

- 3) Compute the two-loop polarizations using the LO softened photon propagator and compute the new NLO softened photon propagator by resumming the two-loop polarization,
- 4) Compute the other diagrams of the theory at NLO, *i.e.*,  $O(1/N_f^2)$  using both the LO and NLO softened photon propagators.

and pursue similarly at NNLO if desired (and motivated enough!). Note that using this technique, one should be careful not to take into account diagrams twice. In general, large- $N_f$  techniques are expected to be very powerful as they resum an infinite number of diagrams. Moreover, since the new coupling of the theory is  $1/N_f$ , the value of  $\alpha = e^2/(4\pi)$  can be arbitrarily large, which is extremely useful to study the critical properties of the corresponding field theories that originates from non-perturbative effects.

### 4.2.2 Bosonic Quantum Electrodynamics (bQED<sub>3</sub>)

Bosonic QED, also called scalar QED, is the gauge theory model mimicking the usual fermionic QED by means of electrically charged scalar particles instead of the fermionic (spinorial) one. Mathematically, the action is built from a gauged complex pseudo-scalar field  $\phi$ . The massless action in three dimensions then yields [110]

$$S_{\text{bQED}_3} = \int d^3x \left[ |D_\mu \phi_i|^2 - \frac{1}{4} F_{\mu\nu} F^{\mu\nu} - \frac{1}{2\xi} (\partial_\mu A^\mu)^2 \right], \quad (4.16)$$

with  $|X|^2 = X^* X$  and  $D_\mu = \partial_\mu + ieA_\mu$ . Similarly to fermionic QED<sub>3</sub>, this theory is super-renormalizable. The fields  $\phi_i$  are the  $2N_f$  flavors<sup>3</sup> ( $i = 1, \dots, 2N_f$ ) of the complex pseudo-scalar field  $\phi$ , *i.e.*, getting a minus sign under parity transformations so that the action stays parity-even. Let us remark that the term including the covariant derivative  $D_\mu$  deserves some unpacking, *i.e.*,

$$|D_\mu \phi_i|^2 = |\partial_\mu \phi_i|^2 + ieA^\mu \phi^i \partial_\mu \phi_i^* - ieA^\mu \phi_i^* \partial_\mu \phi^i + e^2 |A_\mu \phi_i|^2. \quad (4.17)$$

The first term in (4.17) is the expected kinetic term for a complex scalar field. The next two interaction terms in (4.17) are QED-like, *i.e.*, three-point interactions ( $A$ - $\phi$ - $\phi$ ) with the tweak that they include a derivative. This will give rise, after Fourier transform, to a momentum dependent three point interaction, thereby increasing the complexity of the theory. More interestingly, the last term in (4.17) is specific to bQED, as it is the interaction term describing the scattering of a photon with a scalar, *i.e.*, a four point interaction ( $A$ - $A$ - $\phi$ - $\phi$ ).

An important remark is that the action (4.16) is what we call the “pure” bosonic QED, *i.e.*, without  $\phi^4$ -type interactions. Indeed, in the literature exposed in the introduction, bosonic/scalar QED is usually studied in the case where the action (4.16) is augmented with interactions terms of the type  $\lambda_\pm (|\phi_i|^2 \pm |\phi_j|^2)^2$ . Note that the case of “pure” bQED is then the fixed point where  $\lambda_\pm = 0$ , often called tri-critical QED, that we will simply call bQED in the following. We also neglect eventual  $\phi^6$  interactions.

Similarly to the fermionic case, two mass terms can be considered, reading

$$\mathcal{L}_{m_\pm} = m_\pm^2 \left( \sum_{i=1}^{N_f} |\phi_i|^2 \pm \sum_{i=1+N_f}^{2N_f} |\phi_i|^2 \right). \quad (4.18)$$

On the one hand, it is important to notice that, in this scalar case, both terms are parity preserving, even though the field  $\phi$  is itself a pseudo-scalar. On the other hand, the  $m_+$  term preserves the  $U(2N_f)$  symmetry while the  $m_-$  term breaks it like  $U(2N_f) \rightarrow U(N_f) \times U(N_f)$ , such that half of the scalar degrees of freedom propagates with positive mass and the other half with negative mass. In the following, we will consider either massless bQED<sub>3</sub>, or the limit of a small mass (therefore neglecting all tadpoles, see the discussion in 4.3) to be able to compute its mass anomalous dimensions as well as addressing the eventuality of the dynamical generation of a small parity-even mass in the model. Since we consider  $\lambda_\pm = 0$  and the small (even) mass limit, we work with a vanishing scalar potential, dominated by gauge interactions.

As we will see in the following, from a supersymmetric point of view, the action of bQED<sub>3</sub> (4.16) is the exactly bosonic sector associated with the selectron, *i.e.*, the scalar superpartner of the electron.

### 4.2.3 Minimally supersymmetric Quantum Electrodynamics ( $\mathcal{N} = 1$ SQED<sub>3</sub>)

In the rest of this chapter, one of our main focuses will be a supersymmetric (SUSY) variant of QED<sub>3</sub>, namely the (minimal)  $\mathcal{N} = 1$  supersymmetric three-dimensional QED (SQED<sub>3</sub>). This model can be

<sup>3</sup>Taking  $N_b$  bosons flavors would have been more suitable, but we set  $N_b = 2N_f$  to anticipate the supersymmetric case.



obtained naively by combining the fermionic and bosonic QED<sub>3</sub> models described above, together with a superpartner for the photon, the photino. Mathematically, the degrees of freedom of  $\mathcal{N} = 1$  SQED<sub>3</sub> are the  $2N_f$  matter multiplets  $\{\phi^j, \psi^j, F^j\}$  and a gauge multiplet  $\{A^\mu, \lambda\}$ . Here,  $\phi^j$  are  $2N_f$  complex pseudo-scalars,  $\psi^j$  are  $2N_f$  2-component Dirac fermions and  $F^j$  are complex auxiliary scalar fields without any dynamics (they are here to ensure the equality of the degrees of freedom in the matter and gauge multiplet). The gauge multiplet, after choosing the Wess-Zumino gauge [319], contains the  $U(1)$  gauge field  $A^\mu$  as well as its superpartner, the photino  $\lambda$ , which is a 2-component Majorana field (and no extra auxiliary field, unlike in 3+1 dimensions). Following [286] and the notation already used in the previous fermionic and bosonic QED<sub>3</sub> sections, the microscopic action of  $\mathcal{N} = 1$  massless SQED<sub>3</sub> is then given by

$$S_{\text{SQED}_3} = \int d^3x \left[ i\bar{\psi}_i \not{D}\psi^i - \frac{1}{4} F_{\mu\nu} F^{\mu\nu} - \frac{1}{2\xi} (\partial_\mu A^\mu)^2 + |D_\mu \phi_i|^2 + \frac{i}{2} \bar{\lambda} \not{\partial} \lambda - ie(\bar{\psi}^i \lambda \phi_i - \bar{\lambda} \psi^i \phi_i^*) + |F_i|^2 \right], \quad (4.19)$$

where the covariant derivative is still defined as  $D_\mu = \partial_\mu + ieA_\mu$  and  $\not{X} = \gamma^\mu X_\mu$ . Similarly to fermionic and bosonic QED<sub>3</sub> described above, this theory is super-renormalizable, since its unique gauge coupling,  $e$ , still has the canonical dimension  $[e] = 1/2$ . The first three terms are of pure fermionic QED<sub>3</sub> origin (4.1). It is followed by the gauge term of pure bQED<sub>3</sub> origin (4.17) which is here interpreted as the supersymmetric counterpart of the electron, *i.e.*, the selectron  $\phi$ . The next two terms are the supersymmetric counterpart of the photon, *i.e.*, photino  $\lambda$ , including the interaction terms mixing the electron, the selectron and the photino. Finally, the last term is the one for the auxiliary field  $F$ , which is included even though it does not contribute to the dynamics and has no excitations. Before going further with this action, we need to define a regularization scheme suitable for the supersymmetric case, which will force us to introduce additional fields, the so-called  $\varepsilon$ -scalars.

### Dimensional reduction scheme (DRED)

Dimensional reduction (DRED) was introduced by Siegel [311] in 1979 as a way of regulating supersymmetric gauge theories while maintaining manifest supersymmetry and the nice features of dimensional regularization (DREG). It is the most convenient regularization scheme for practical calculations in supersymmetric theories. Indeed, in SUSY gauge theories, the usual DREG scheme breaks SUSY. This can be easily seen in the gauge multiplet, containing the photino with 2 degrees of freedom, and the gauge field, which has  $d-1$  degrees of freedom. Therefore, in dimensions other than 3, *e.g.*,  $d = 3 - 2\varepsilon$  for DREG, a mismatch exists in the degrees of freedom and SUSY is explicitly broken. We shall then briefly introduce (see [313] for an early pedagogical treatment and [320–323] for more recent reviews) and follow the DRED scheme along with modified minimal subtraction  $\overline{\text{DRED}}$ .

In DRED, the continuation from the physical space-time dimension 3 to  $d = 3 - 2\varepsilon < 3$  dimensions can be interpreted as a compactification. In this case, the metric, the scalar fields and the fermionic fields preserves their 3-dimensional nature, while the gauge field  $A^\mu$  that formally splits as

$$A^\mu = \hat{A}^\mu + \bar{A}^\mu, \quad (4.20)$$

where we follow the notation of [322]. Here the  $A^\mu$  field has 3 components, the hatted  $\hat{A}^\mu$  field has  $d = 3 - 2\varepsilon$  components and the  $\bar{A}_\mu$  field has  $2\varepsilon$  components to compensate. The excitations of the hatted field are the dimensionally regularized photons, and the excitations of the barred field are called  $\varepsilon$ -scalars. The  $\varepsilon$ -scalars thus account for the degrees of freedom lost by the gauge bosons during the dimensional reduction procedure. Similarly, all quantities with Lorentz indices are split. This is the case of the metric tensor, the  $\gamma$ -matrices, the momentum 3-vector and the covariant derivative, reading

$$g^{\mu\nu} = \hat{g}^{\mu\nu} + \bar{g}^{\mu\nu}, \quad \gamma^\mu = \hat{\gamma}^\mu + \bar{\gamma}^\mu, \quad p^\mu = \hat{p}^\mu + \cancel{p}^\mu, \quad \partial^\mu = \hat{\partial}^\mu + \cancel{\partial}^\mu, \quad (4.21)$$

where the metrics reads

$$g^\mu{}_\mu = 3, \quad \hat{g}^\mu{}_\mu = d = 3 - 2\varepsilon, \quad \bar{g}^\mu{}_\mu = 2\varepsilon. \quad (4.22)$$

Let us remark that  $\bar{p}^\mu = 0$  and  $\bar{\partial}^\mu = 0$  since the momentum and position three-vectors are living in the  $d$ -dimensional space. Nevertheless, we will keep the hat on the momentum if the Lorentz index is explicit. In that case, the notations related to the momentum trivially reads

$$p^2 = \hat{p}^\mu \hat{p}_\mu, \quad |p| = \sqrt{p^2}, \quad \not{p} = \hat{\gamma}^\mu \hat{p}_\mu, \quad \not{p}^2 = \hat{p}^2, \quad \frac{1}{\not{p}} = \frac{\not{p}}{p^2}, \quad p_E = \sqrt{-p^2} = i|p|, \quad k \cdot p = \hat{k}^\mu \hat{p}_\mu, \quad (4.23)$$

where  $p_E$  is the Euclidean momentum. At the level of the action (4.19), the decomposition of the gauge field yields

$$S_{d=3} = S_{d=3-2\varepsilon} + S_{\varepsilon\text{-scalars}}, \quad (4.24)$$

where  $S_{d=3-2\varepsilon}$  takes the same form as the original action (4.19) but with all vector indices restricted to  $d=3-2\varepsilon$  dimensions, *i.e.*, with hatted indices. On the other hand, additional terms from  $S_{\varepsilon\text{-scalars}}$  appear in the action due to the extra  $\varepsilon$ -scalar field. From (4.20), (4.21), the new DRED action then reads

$$\begin{aligned} S_{\text{SQED}_3} = \int d^d x \left[ i\bar{\psi}_i \not{D}\psi^i - \frac{1}{4} \hat{F}^{\mu\nu} \hat{F}_{\mu\nu} - \frac{1}{2\xi} (\hat{\partial}_\mu \hat{A}^\mu)^2 \right. \\ \left. + |\hat{D}_\mu \phi_i|^2 + \frac{i}{2} \bar{\lambda} \not{\partial} \lambda - ie(\bar{\psi}^i \lambda \phi_i - \bar{\lambda} \psi^i \phi_i^*) + |F_i|^2 \right. \\ \left. - \frac{1}{2} (\hat{\partial}_\mu \bar{A}_\nu)^2 - e\bar{\psi}_i \hat{\gamma}^\mu \bar{A}_\mu \psi^i + e^2 \bar{A}^2 |\phi_i|^2 \right]. \quad (4.25) \end{aligned}$$

Let us emphasize that the  $\varepsilon$ -scalar part of the Lagrangian, the last line of (4.25), does not appear in usual dimensional regularization (DREG) and is specific to the dimensional reduction (DRED) scheme. Thus,  $\varepsilon$ -scalars give rise to additional cubic and quartic couplings. The equality of the matter couplings for  $\hat{A}_\mu$  and  $\bar{A}_\mu$  has been assumed, as a consequence of supersymmetry [314, 324]. We provide in table 4.1 a summary of the field content for the  $\mathcal{N}=1$  SQED<sub>3</sub> in the DRED scheme.

Field	index	spin	stat.	excitations	multiplet	mathematical definition
$\psi_i(x)$	$i=1, \dots, N_f$	1/2	fermion	electrons ( $e^\pm$ )	matter	2-component Dirac spinor
$\hat{A}^\mu(x)$	$\mu=0, \dots, d-1$	1	boson	photons ( $\gamma$ )	gauge int.	gauge covariant vector
$\bar{A}^\mu(x)$	$\mu=0, \dots, 2\varepsilon-1$	1	boson	$\varepsilon$ -scalar ( $\varepsilon$ )	gauge int.	gauge covariant vector
$\phi_i(x)$	$i=1, \dots, N_f$	0	boson	selectrons ( $\tilde{e}^\pm$ )	matter	complex pseudo scalar
$\lambda$	none	1/2	fermion	photinos ( $\lambda$ )	gauge int.	2-component Majorana spinor
$F_i$	$i=1, \dots, N_f$	0	boson	none	matter	auxiliary complex scalar

Table 4.1: Summary of the field content in SQED<sub>3</sub> in the DRED scheme.

Before going further with the action (4.25), we briefly introduce the case of super-graphene (SQED<sub>4,3</sub>) and then the SQED<sub>3</sub> model (4.25) so that it explicitly allows us to recover the subcases of fermionic QED<sub>3</sub> and bosonic bQED<sub>3</sub>, as well as the super-graphene case via mapping.

#### 4.2.4 Super-graphene model (SQED<sub>4,3</sub>)

Similarly to the mapping that exists between large- $N_f$  QED<sub>3</sub> and small coupling QED<sub>4,3</sub> exposed in the previous chapter, there also exists a similar mapping for the minimally supersymmetric versions of these theories, *i.e.*, between large- $N_f$   $\mathcal{N}=1$  SQED<sub>3</sub> and small coupling  $\mathcal{N}=1$  SQED<sub>4,3</sub>. Since QED<sub>4,3</sub> describes (suspended) graphene at its IR Lorentz invariant fixed point [144], by analogy, SQED<sub>4,3</sub> describes what we call (suspended) super-graphene at its IR Lorentz invariant fixed point [163]. This model is then characterized by matter (electron and selectron fields) localized on a three-dimensional membrane and interacting via gauge interactions (photons and photinos) that are allowed

to propagate in the full four dimensional space-time. Let us emphasize that in this thesis we always consider *suspended* (super)-graphene, as opposed to a model defined on the boundary, as considered in, *e.g.*, [163]. In our case the boundary is considered as a transparent interface while the model of [163] considers a purely reflecting boundary (graphene on a substrate). Nevertheless, the two models can be simply related by doubling the interaction,  $\alpha_{\text{bdry}} = \alpha/2$ .

By analogy with the non-SUSY case, see chapter 3 equation (3.12), the action for  $\mathcal{N}=1$  (suspended) super-graphene can be written by splitting the action of SQED, (4.19), into two parts, while being careful about the indices and the spinor dimensions. Following [163], it yields

$$S_{\text{SQED}_{4,3}} = \int d^{d_e} x \left[ i\bar{\psi}_i \gamma^{\mu_e} D_{\mu_e} \psi^i + |D_{\mu_e} \phi_i|^2 + |F_i|^2 - ie(\bar{\psi}^i \lambda \phi_i - \bar{\lambda} \psi^i \phi_i^*) \right] \\ + \int d^{d_\gamma} x \left[ -\frac{1}{4} F_{\mu_\gamma \nu_\gamma} F^{\mu_\gamma \nu_\gamma} - \frac{1}{2\xi} (\partial_{\mu_\gamma} A^{\mu_\gamma})^2 + \frac{i}{2} \bar{\Lambda} \Gamma^{\mu_\gamma} \partial_{\mu_\gamma} \Lambda + \frac{1}{2} D^2 \right], \quad (4.26)$$

where  $d_e = 3 - 2\varepsilon$  and  $d_\gamma = 4 - 2\varepsilon$  with the corresponding Lorentz indices are  $\mu_e = 0, \dots, d_e - 1$ ,  $\mu_\gamma = 0, \dots, d_\gamma - 1$  with the covariant derivative defined on the  $d_e$  plane, *i.e.*,  $D_{\mu_e} = \partial_{\mu_e} + ieA_{\mu_e}$  where  $A_{\mu_e} = A_{\mu_e}(z=0)$  such that  $z$  is the collective coordinate of the  $d_\gamma - d_e$  codimensional space. In this case,  $\Gamma^{\mu_\gamma}$  are the four  $4 \times 4$  gamma matrices while  $\gamma^{\mu_e}$  are the three  $2 \times 2$  gamma matrices. Moreover,  $\Lambda$  denotes a four-component Majorana field. Note that  $D$  is a real auxiliary field, *i.e.*, without dynamics, present in the gauge multiplet to equate the degrees of freedom with the matter multiplet and preserve SUSY. At this point, similarly to the SQED<sub>3</sub> case, one should perform a dimensional reduction that introduces hatted and barred objects together with an additional propagator for the (bulk)  $\varepsilon$ -scalar. We will not explain this procedure here. Furthermore, by analogy with the non-SUSY case, one can integrate out the free bulk degrees of freedom and obtain an action projected on the  $d_e$ -dimensional manifold with effective non-local photons. Note that in the case of the bulk four-component photino,  $\Lambda$ , this procedure is accompanied by projecting out two of its components to identify it with the boundary two-component photino  $\lambda$ , see [163] where this has been carefully carried out. It is then possible to derive the effective gauge propagators on the three-dimensional plane, and compare them to the IR-softened propagators of the SQED<sub>3</sub> model to deduce a mapping. We will discuss briefly this comparison in section 4.5.5 devoted to super-graphene results. As one might expect, the end result is that the mapping is very similar to the non-SUSY case up to a factor two from SUSY, reading

$$\text{SQED}_3 \rightarrow \text{SQED}_{4,3} = \left\{ \frac{1}{\pi^2 2N_f} \rightarrow \bar{\alpha}_r, \xi \rightarrow \frac{1+\xi}{2} \right\}. \quad (4.27)$$

As in the non-SUSY case, this mapping is only the naive low-order one, and several tweaks have to be added to cope with the use of a non-local gauge and the additional higher loop order resummed diagrams in the large- $N_f$  case. This will be discussed in section 4.5.5 devoted to the super-graphene results.

### 4.3 Presentation of the general gQED<sub>3</sub> model

In the previous section, we introduced formally a total of 4 models, namely QED<sub>3</sub>, bQED<sub>3</sub>, SQED<sub>3</sub> and finally SQED<sub>4,3</sub>. In the following we will build a more general model that encompass QED<sub>3</sub>, bQED<sub>3</sub>, and SQED<sub>3</sub> with the help of two additional parameters,  $S$  and  $n$ . The case of SQED<sub>4,3</sub>, *i.e.*, super-graphene, will simply be recovered via mapping in the devoted super-graphene section 4.5.5. An additional parameter,  $\mathcal{E}$ , will also be introduced to study the effect of DRED on the results. This very general large- $N_f$  model will be denoted as gQED<sub>3</sub>.

### The massless gQED<sub>3</sub> model

We first introduce a new parameter  $S$ , standing for supersymmetry, that will highlight SUSY effects in our computations. To this end, each superpartner field will be associated with a tracking factor  $S \in \{0,1\}$  such that

$$\Phi \rightarrow S\Phi, \quad \forall \Phi \in \{\phi, \lambda, \bar{A}^\mu\}, \quad (4.28)$$

and  $S^2 = S$ . Hence, at any step of the calculation, we may turn on (respectively off) SUSY by setting  $S = 1$  (respectively  $S = 0$ ). This allows us to check our expressions by recovering known results for the corresponding non-SUSY theory, such as large- $N_f$  QED<sub>3</sub> [213, 226].

Secondly, we will work with  $2N_f$  arbitrary  $n$ -component spinors<sup>4</sup>. In the SQED<sub>3</sub> case,  $n = 2$  is necessary to ensure the equality of the matter and gauge degrees of freedom. Nevertheless, working with arbitrary  $n$  component spinors will allow us to take the case of  $n = 0$ -component spinors, *i.e.*, no fermions, which corresponds to the case of bQED<sub>3</sub>. Indeed, by killing the spinorial degrees of freedom with  $n = 0$ , one exactly recover the action of bQED<sub>3</sub>, (4.17). In order to keep track of both cases while limiting the complexity of our formulas, one can notice that the identity  $n^2 S = 2nS$  holds in both cases. We shall therefore use the constraint

$$n(n-2)S = 0, \quad (4.29)$$

to simplify our computations. Similarly, to better appreciate the effects of DRED during the computations, the  $\varepsilon$ -scalar field will be associated with a tracking factor  $\mathcal{E} \in \{0,1\}$  such that

$$\bar{A}^\mu \rightarrow \mathcal{E}\bar{A}^\mu, \quad (4.30)$$

and  $\mathcal{E}^2 = \mathcal{E}$ . Indeed, as we shall see in the following, though  $\varepsilon$ -scalars affect only few quantities at NLO, their effect is crucial to ensure the validity of supersymmetric identities. Implementing these parameters to (4.25), gives the general massless action

$$\begin{aligned} S_{\text{gQED}_3} = \int d^3x \left[ & i\bar{\psi}_i \not{D}\psi^i - \frac{1}{4} \hat{F}^{\mu\nu} \hat{F}_{\mu\nu} - \frac{1}{2\xi} (\hat{\partial}_\mu \hat{A}^\mu)^2 \right. \\ & + S |\hat{D}_\mu \phi_i|^2 + \frac{iS}{2} \bar{\lambda} \not{\partial} \lambda - ieS (\bar{\psi}^i \lambda \phi_i - \bar{\lambda} \psi^i \phi_i^*) + S |F_i|^2 \\ & \left. - S \mathcal{E} \frac{1}{2} (\hat{\partial}_\mu \bar{A}_\nu)^2 - e \mathcal{E} S \bar{\psi}_i \bar{\gamma}^\mu \bar{A}_\mu \psi^i + e^2 \mathcal{E} S \bar{A}^2 |\phi_i|^2 \right]. \end{aligned} \quad (4.31)$$

This is the general model we will work with in the rest of this chapter. The action (4.31) completely describes  $\mathcal{N} = 1$  supersymmetric QED in the DRED scheme with suitable parameters  $(S, \mathcal{E}, n)$  that allow to recover the subcases of QED<sub>3</sub> and bQED<sub>3</sub> (and SQED<sub>4,3</sub> case via a mapping) as well as study the effect of DRED by turning it on (or off) with  $\mathcal{E} = 1$  or 0. Explicitly, the SQED<sub>3</sub> case corresponds to  $S = 1$ ,  $n = 2$ ,  $\mathcal{E} = 1$ , the bQED<sub>3</sub> case is obtained from  $S = 1$ ,  $n = 0$ ,  $\mathcal{E} = 0$  and finally the QED<sub>3</sub> case is  $S = 0$ ,  $\mathcal{E} = 0$  and  $n = 2$ . These parametrizations are summed up in table 4.2.

In concluding this part, we summarize the notations of the action (4.31). The field strength tensor is given by  $\hat{F}_{\mu\nu} = \hat{\partial}_\mu \hat{A}_\nu - \hat{\partial}_\nu \hat{A}_\mu$  together with the covariant derivative  $\hat{D}_\mu = \hat{\partial}_\mu + ie\hat{A}_\mu$  and  $\not{t} = \hat{\gamma}^\mu \hat{t}_\mu$  for any  $d$ -vector  $t$ . The model is built from  $2N_f$  matter multiplets  $\{\psi_i, \phi_i, F_i\}$ , where each  $\psi_i$  is a 2-component Dirac fermion (electron), each  $\phi_i$  a complex pseudo-scalar (selectron) and each  $F_i$  a complex auxiliary scalar field, as well as a gauge multiplet  $\{\hat{A}_\mu, \bar{A}_\mu, \lambda\}$ , where  $\hat{A}_\mu$  is the  $d$ -dimensional  $U(1)$  gauge field (photons),  $\bar{A}_\mu$  is the  $2\varepsilon$ -dimensional  $U(1)$  gauge field ( $\varepsilon$ -scalar), and  $\lambda$  a 2-component Majorana fermion (photino), using the notations of the review [322] where hatted (respectively barred) quantities have

<sup>4</sup>Let us details our notations for the fermion flavor components. In principle, we consider  $2N_f(n)$  spinors in  $n$  components. Then, the natural notations are  $2N_f(4) = N_f$ ,  $2N_f(2) = n_f = 2N_f$  and  $2N_f(0) = 2N_b = 2N_f$  (where 0-comp. spinors are bosons and we consider  $N_b = N_f$  by SUSY). In order to keep it light, we abuse notations and denote  $\mathcal{N}_f(n)$  as  $N_f$ , which is natural for both  $n = 0$  and  $n = 2$ . Setting  $n = 4$  in our equations then also requires  $N_f \rightarrow N_f/2$ , giving the same result as  $n = 2$ .

Model	$S$	$n$	$\mathcal{E}$
$\mathcal{N} = 1$ SQED <sub>3</sub>	1	2	1
bosonic bQED <sub>3</sub>	1	0	0
fermionic QED <sub>3</sub>	0	2	0

Table 4.2: Parameter values used to recover the different large- $N_f$  models from the gQED<sub>3</sub> action (4.31).

$d$  (respectively  $2\varepsilon = 3 - d$ ) components. Additionally, in (4.31),  $\xi$  is the  $R_\xi$  covariant gauge fixing parameter and  $e^2$  is the coupling constant of the theory with the canonical dimension of a mass, so that the theory is superrenormalizable. Also, we recall that the gauge fixing term is SUSY breaking (Wess-Zumino gauge), therefore only the physical gauge-invariant quantities will be SUSY invariant. From naive dimensional analysis, the canonical dimensions read

$$[\psi] = [\lambda] = \frac{d-1}{2}, \quad [\hat{A}^\mu] = [\bar{A}^\mu] = [\phi] = \frac{d-2}{2}, \quad [F] = \frac{d}{2}, \quad [e] = 2 - \frac{d}{2}, \quad [\xi] = 0. \quad (4.32)$$

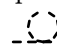
### About the masses and the fate of the tadpoles

Let us remark that the action (4.31) is completely massless. In the following, in order to compute the mass anomalous dimensions of the model, we will introduce a mass term for the matter multiplet, *i.e.*, for the electron and the selectron. Since we are interested in dynamical mass generation, we will choose the parity-even mass terms, *i.e.*, of the form,

$$\mathcal{L}_m = m_\psi \left( \sum_{i=1}^{N_f} \bar{\psi}_i \psi^i - \sum_{i=1+N_f}^{2N_f} \bar{\psi}_i \psi^i \right) + m_\phi^2 \left( \sum_{i=1}^{N_f} |\phi_i|^2 + \sum_{i=1+N_f}^{2N_f} |\phi_i|^2 \right). \quad (4.33)$$

Moreover, we will work in the limit of *small masses*, *i.e.*,

$$m_x \ll p_E \ll e^2 N_f, \quad (m_x = m_\psi, m_\phi). \quad (4.34)$$

This will have several advantages. First, this limit will remove all the tadpoles in the theory. We recall that tadpoles are diagrams with a scaleless closed loop (graphically ) , *i.e.*, proportional to  $\int d^d k (k^2 - m^2)^\beta$  that vanishes in the massless limit in DREG (and by extension, in DRED). In bQED<sub>3</sub> and SQED<sub>3</sub> (and therefore SQED<sub>4,3</sub>) the Feynman rules indeed give rise to tadpoles, as opposed to the case of QED<sub>3</sub> where no tadpole is present since the theory only has a three-point coupling. Second, because we are ultimately interested in the small masses limit, we may consider the  $+m_\psi$  term only, as the  $-m_\psi$  term will give the same result. This will simplify the computations and the mass term (4.33) effectively take the simple form

$$\mathcal{L}_m = m_\psi \bar{\psi}_i \psi^i + m_\phi^2 |\phi_i|^2, \quad (4.35)$$

where  $i = 1, \dots, 2N_f$ . These masses will therefore enter the electron and selectrons propagators as small IR regulative masses to allow the computation of their corresponding mass anomalous dimensions.

In summary, in this chapter, all our calculations will be carried out using massless techniques, which is entirely justified by the fact we restrict our study to the vicinity of the critical point, where  $m_x \ll p_E \ll e^2 N_f$ . Nevertheless, we will manage to compute the mass anomalous dimensions in the limit of a small mass by neglecting tadpole effects, and from these quantities, we will study the eventuality of the dynamical generation of small masses in the matter multiplet.

### Feynman rules

The gQED<sub>3</sub> model (4.31) contains both Dirac and Majorana fermions. Therefore, one has to be extremely careful to properly define the Feynman rules of the model in order to avoid sign mistakes. In the following, we will use a method based on the conventions of [325, 326]. We first derive the bare gauge-multiplet propagators from the general action (4.31), reading

$$\text{photon: } \hat{D}_{0AA}^{\mu\nu}(p) = \langle \hat{A}^\mu(-p) \hat{A}^\nu(p) \rangle_0 = \mu \begin{array}{c} \text{~~~~~} \\ \xrightarrow{p} \\ \text{~~~~~} \end{array} \nu = \frac{-i}{p^2} \hat{d}^{\mu\nu}(p), \quad (4.36a)$$

$$\varepsilon\text{-scalar: } \bar{D}_{0AA}^{\mu\nu}(p) = \langle \bar{A}^\mu(-p) \bar{A}^\nu(p) \rangle_0 = \mu \begin{array}{c} \text{.....} \\ \xrightarrow{p} \\ \text{.....} \end{array} \nu = \frac{-iS\mathcal{E}}{p^2} \bar{g}^{\mu\nu}, \quad (4.36b)$$

$$\text{photino: } D_{0\lambda\bar{\lambda}}(p) = \langle \lambda(-p) \bar{\lambda}(p) \rangle_0 = \begin{array}{c} \text{~~~~~} \\ \xrightarrow{p} \\ \text{~~~~~} \end{array} = \frac{iS}{\not{p}}, \quad (4.36c)$$

with  $\hat{d}^{\mu\nu}(p) = \hat{g}^{\mu\nu} - (1 - \xi)(\hat{p}^\mu \hat{p}^\nu / p^2)$ , like in usual QED. It is important to remark that the photino line (4.36c) carries a fermion-flow, but is not represented with a dedicated arrow. We also derive from (4.31) the bare matter-multiplet propagators, reading

$$\text{electron: } S_{0\psi\bar{\psi}}(p) = \langle \psi(-p) \bar{\psi}(p) \rangle_0 = \begin{array}{c} \text{-----} \\ \xrightarrow{p} \\ \text{-----} \end{array} = \frac{i}{\not{p} - m_\psi}, \quad (4.37a)$$

$$\text{selectron: } S_{0\phi\phi^*}(p) = \langle \phi(-p) \phi^*(p) \rangle_0 = \begin{array}{c} \text{-----} \\ \xrightarrow{p} \\ \text{-----} \end{array} = \frac{iS}{p^2 - m_\phi^2}. \quad (4.37b)$$

Note that the arrow on the Dirac fermion ( $\psi$ ) and the pseudo scalar ( $\phi$ ) propagators indicates the charge-flow or equivalently the matter flow. Like for the photino (4.36c), the fermion-flow on the Dirac fermion line (4.37a) is not indicated. Together with these gauge and matter propagators comes additional rules for the loops

- Each matter-field loop ( $\psi$  and  $\phi$  fields charge-flow) gives a factor  $2N_f$ , *i.e.*, graphically

$$\begin{array}{ccc} \begin{array}{c} \text{-----} \\ \text{-----} \end{array} \equiv 2N_f, & \begin{array}{c} \text{-----} \\ \text{-----} \end{array} \equiv 2N_f, & \begin{array}{c} \text{-----} \\ \text{-----} \end{array} \equiv 2N_f. \end{array} \quad (4.38)$$

- Each fermion loop ( $\psi$  and  $\lambda$  fields fermion-flow) gives a factor  $(-1)$  and a trace over the spinorial indices, *i.e.*, graphically

$$\begin{array}{ccc} \begin{array}{c} \text{-----} \\ \text{-----} \end{array} \equiv -\text{Tr}, & \begin{array}{c} \text{-----} \\ \text{-----} \end{array} \equiv -\text{Tr}, & \begin{array}{c} \text{-----} \\ \text{-----} \end{array} \equiv -\text{Tr}. \end{array} \quad (4.39)$$

Lastly, we provide all the vertices of the theory, derived from the action (4.31), in graphical form

$$\hat{\Gamma}_{0A\psi\bar{\psi}}^\mu = \mu \begin{array}{c} \text{~~~~~} \\ \bullet \\ \text{-----} \\ \text{-----} \end{array} = -ie\hat{\gamma}^\mu, \quad (4.40a)$$

$$\hat{\Gamma}_{0A\phi\phi^*}^\mu(p, k) = \mu \begin{array}{c} \text{~~~~~} \\ \bullet \\ \text{-----} \\ \text{-----} \end{array} = -ieS(\hat{p} + \hat{k})^\mu, \quad \hat{\Gamma}_{0AA\phi\phi^*}^{\mu\nu} = \begin{array}{c} \text{~~~~~} \\ \bullet \\ \text{~~~~~} \\ \text{-----} \\ \text{-----} \end{array} = 2ie^2 S \hat{g}^{\mu\nu}, \quad (4.40b)$$

$$\bar{\Gamma}_{0A\psi\bar{\psi}}^\mu = \mu \begin{array}{c} \text{.....} \\ \bullet \\ \text{-----} \\ \text{-----} \end{array} = -ie\mathcal{E}S\bar{\gamma}^\mu, \quad \bar{\Gamma}_{0AA\phi\phi^*}^{\mu\nu} = \begin{array}{c} \text{.....} \\ \bullet \\ \text{.....} \\ \text{-----} \\ \text{-----} \end{array} = 2ie^2 \mathcal{E}S\bar{g}^{\mu\nu}, \quad (4.40c)$$

$$\Gamma_{0\bar{\lambda}\psi\phi^*} = \begin{array}{c} \text{~~~~~} \\ \bullet \\ \text{-----} \\ \text{-----} \end{array} = eS, \quad \Gamma_{0\bar{\psi}\lambda\phi} = \begin{array}{c} \text{~~~~~} \\ \bullet \\ \text{-----} \\ \text{-----} \end{array} = -eS. \quad (4.40d)$$



Note that the first vertex (4.40a) is purely of fermionic QED origin, the second line (4.40b) are the vertices of bosonic bQED origin, then the vertices (4.40c) comes from the  $\varepsilon$ -scalar contributions and finally the vertices (4.40d) are of pure SQED origin.

In addition to all these rules, one should be extremely careful about fermion-flows when both Dirac and Majorana fermions are present. This usually results in a multitude of additional Feynman rules to cope with all the possible flow cases in order to obtain the correct minus signs everywhere. In the following, we will use the compact Feynman rules of [325, 326] that are based on assigning an additional fermion-flow line on diagrams (when necessary) along fermionic lines to obtain the correct signs. The additional Feynman rules are then written down by specifying the fermion-flow (arrow above) and, for the fermionic propagators (recalling that the middle arrow is the charge/matter flow and the bottom arrow is the momentum), they read

$$\begin{array}{c} \xrightarrow{\quad} \\ \xrightarrow{p} \end{array} = S_{0\psi\bar{\psi}}(p), \quad \begin{array}{c} \xrightarrow{\quad} \\ \xleftarrow{p} \end{array} = S_{0\psi\bar{\psi}}(-p), \quad (4.41a)$$

$$\begin{array}{c} \xleftarrow{\quad} \\ \xrightarrow{p} \end{array} = S_{0\psi\bar{\psi}}(-p), \quad \begin{array}{c} \xleftarrow{\quad} \\ \xleftarrow{p} \end{array} = S_{0\psi\bar{\psi}}(p), \quad (4.41b)$$

$$\begin{array}{c} \xrightarrow{\quad} \\ \xrightarrow{p} \end{array} = D_{0\lambda\bar{\lambda}}(p), \quad \begin{array}{c} \xrightarrow{\quad} \\ \xleftarrow{p} \end{array} = D_{0\lambda\bar{\lambda}}(-p), \quad (4.41c)$$

which amounts to add a minus sign on the flowing momentum for each opposite arrows. Similarly, for the fermionic Dirac vertices (fermion-flow indicated with the arrow on the right) they read

$$\mu \begin{array}{c} \nearrow \\ \bullet \\ \searrow \end{array} \left( = -ie\hat{\gamma}^\mu, \quad \mu \begin{array}{c} \nearrow \\ \bullet \\ \swarrow \end{array} \left( = +ie\hat{\gamma}^\mu, \quad (4.42a)$$

$$\mu \begin{array}{c} \dots \\ \bullet \\ \searrow \end{array} \left( = -ie\mathcal{E}S\bar{\gamma}^\mu, \quad \mu \begin{array}{c} \dots \\ \bullet \\ \swarrow \end{array} \left( = +ie\mathcal{E}S\bar{\gamma}^\mu, \quad (4.42b)$$

which amount to complex conjugate (charge conjugation) the vertex if the fermion-flow goes backward with respect to the charge-/matter-flow. Note that the other vertices mixing both Majorana and Dirac fermion (see (4.40d)) are real and are therefore unchanged under the inversion of the fermion-flow.

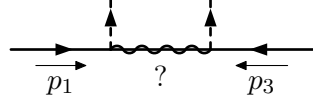
Actually, for the vast majority of the cases, the simple rules (4.36) to (4.40), *i.e.*, without the additional fermion-flow lines (4.41) and (4.42), are sufficient. This comes from the fact that most of the diagrams that we consider are such that the charge-flow can follow naturally the fermion-flow, both being continuous and unidirectional, *i.e.*, graphically

$$\begin{array}{c} \xrightarrow{\quad} \\ \xrightarrow{p_1} \end{array} \begin{array}{c} \uparrow \\ \xrightarrow{\quad} \\ \xrightarrow{p_2} \end{array} \begin{array}{c} \downarrow \\ \xrightarrow{\quad} \\ \xrightarrow{p_3} \end{array} \quad , \quad (4.43)$$

where the hidden fermion-flow goes from left to right, *i.e.*, through the Dirac fermion, then the Majorana fermion then the Dirac fermion again so that all arrows are properly aligned (reversing any of the arrow in this diagram would generate non-trivial minus signs not accounted for in simple the Feynman rules above). In such a case, provided that the momentum arrows follow the (hidden) fermion-flow and the charge-flow, one can safely use the simple Feynman rules without sign corrections shown above, (4.36), (4.38), (4.39) and (4.42).

Nevertheless, the advanced Feynman rules (4.41) and (4.42) will be required for a few diagrams,

where one encounters a configuration of the type


(4.44)

In such a case, we are forced to use the advanced Feynman rules (4.41) and (4.42). In the following chapter, this will be the case for only one diagram, which is the seventh (labeled (g)) diagram of the two-loop contribution to the fermion self-energy at NLO, *i.e.*,  $\Sigma_2^{\psi(g)}$ , see (4.140e).

Note that, in principle, these advanced Feynman rules are also needed for the computation of the photino polarization because of the Majorana external legs. However, these diagrams are always appearing in pairs (with respect to opposite charge-flows) that are exactly equal, such that we can consider only the case where all arrows are aligned and double the result. See discussion below (4.84) for an example.

We conclude this section by a brief warning to the reader that would like to use the software Qgraf [59, 60] (as we did) to generate the diagram expressions of any theory involving both Dirac and Majorana fermions. First, Qgraf does not seem to be able to provide the correct minus signs from the fermionic loops in (4.39). The simplest solution we found is to include additional trivial delta functions  $\delta^{\alpha\beta}$  in the propagators for  $\psi$  and  $\lambda$ , where  $\alpha, \beta$  are the spinor indices, such that  $\delta^{\alpha\alpha} = -1$ . Similarly, one can implement in an automated way the inclusion of the factors  $2N_f$  for (4.39) with a similar delta functions on the fields  $\psi^i$  and  $\phi^j$ , *i.e.*,  $\delta^{ij}$  such that  $\delta^{ii} = 2N_f$ . Moreover, Qgraf may have trouble to generate diagram expressions with continuous and unidirectional fermion-flows in rare cases. More specifically, the software seems to always generate the flow properly (*i.e.*, the indices generated by Qgraf that we use to orient the charge and fermion-flows are aligned with the momenta arrows), except when there is an isolated fermion between two Majorana or the reverse, *i.e.*, a chain of the form (4.44). In this particular case, we need additional routines to check the Qgraf output and possibly correct these fermionic flows by using the rules (4.41) and (4.42). As advertised before, our routine has corrected only one diagram in the NLO computations, which is  $\Sigma_2^{\psi(g)}$ , see (4.140e).

### Numerator algebra

We work in a three-dimensional Minkowski space with metric  $g^{\mu\nu} = \text{diag}(+, -, -)$ . The three,  $n \times n$  Dirac  $\gamma$ -matrices satisfy the usual Clifford algebra  $\{\gamma^\mu, \gamma^\nu\} = 2g^{\mu\nu} I_n$ , with  $\text{Tr}(I_n) = n$ . Since we work in the DRED scheme, we recall from (4.21) that the metric tensor and  $\gamma$ -matrices are decomposed as

$$g^{\mu\nu} = \hat{g}^{\mu\nu} + \bar{g}^{\mu\nu}, \quad \gamma^\mu = \hat{\gamma}^\mu + \bar{\gamma}^\mu, \quad (4.45)$$

so that there are  $d = 3 - 2\varepsilon$  matrices  $\hat{\gamma}^\mu$  and  $2\varepsilon$  matrices  $\bar{\gamma}^\mu$ , in order to keep a total integer number of 3 matrices  $\gamma^\mu$ . All of these matrices are of arbitrary size  $n \times n$  to be able to take the limits  $n = 0$  for bQED<sub>3</sub>, as well as  $n = 2$  for SQED<sub>3</sub> and QED<sub>3</sub>. In DRED scheme, the following intuitive properties hold

$$g^\mu{}_\mu = 3, \quad \hat{g}^\mu{}_\mu = d = 3 - 2\varepsilon, \quad \bar{g}^\mu{}_\mu = 2\varepsilon, \quad (4.46a)$$

$$\{\gamma^\mu, \gamma^\nu\} = 2g^{\mu\nu} I_n, \quad \{\hat{\gamma}^\mu, \hat{\gamma}^\nu\} = 2\hat{g}^{\mu\nu} I_n, \quad \{\bar{\gamma}^\mu, \bar{\gamma}^\nu\} = 2\bar{g}^{\mu\nu} I_n, \quad (4.46b)$$

as well as the very important case of the mixed dimensional anticommutator

$$\{\hat{\gamma}^\mu, \bar{\gamma}^\nu\} = 0. \quad (4.47)$$

As expected, the Dirac trace computations will be modified but in a somewhat trivial way thanks to the property (4.47). In the following, we will have to compute traces involving gamma matrices living in two different spacetimes such as, *e.g.*,  $\text{Tr}(\hat{\gamma}^\mu \bar{\gamma}^\nu \hat{\gamma}^\rho \bar{\gamma}^\sigma)$ . This requires some care. In practice, one first





where the polarizations  $\Pi_x$  respectively for the photon ( $\Pi_\gamma$ ), the  $\varepsilon$ -scalar ( $\Pi_\varepsilon$ ), and the photino ( $\Pi_\lambda$ ) are parameterized via the following projections

$$\hat{\Pi}^{\mu\nu}(p) = (p^2 \hat{g}^{\mu\nu} - \hat{p}^\mu \hat{p}^\nu) \Pi_\gamma(p^2) \implies \Pi_\gamma(p^2) = \left. \frac{\hat{\Pi}^\mu{}_\mu(p)}{(d-1)p^2} \right|_{m_x=0}, \quad (4.55a)$$

$$\bar{\Pi}^{\mu\nu}(p) = p^2 \bar{g}^{\mu\nu} \Pi_\varepsilon(p^2) \implies \Pi_\varepsilon(p^2) = \left. \frac{\bar{\Pi}^\mu{}_\mu(p)}{2\varepsilon p^2} \right|_{m_x=0}, \quad (4.55b)$$

$$\Pi_\lambda(p) = \not{p} \Pi_\lambda(p^2) \implies \Pi_\lambda(p^2) = \left. \frac{\text{Tr}[\not{p} \Pi_\lambda(p)]}{np^2} \right|_{m_x=0}. \quad (4.55c)$$

Using this setup<sup>5</sup>, all integrals can be carried out in the massless limit, *i.e.*,  $m_x \rightarrow 0$  for  $x = \{\psi, \phi\}$ , as an IR rearrangement.

An important remark is that in (4.54a), the tensorial structure still yields  $\hat{d}^{\mu\nu}(p) = \hat{g}^{\mu\nu} - (1 - \xi)(\hat{p}^\mu \hat{p}^\nu / p^2)$  because we are using a non-local gauge, *i.e.*, we took

$$\xi \rightarrow \xi(p^2) = \frac{\xi}{1 - \Pi_\gamma(p^2)}, \quad (4.56)$$

that we will still call  $\xi$  in the following by abuse of notation. This trick is widely used in the QED<sub>3</sub> literature to keep computations light, see *e.g.*, [213] (see also for the SUSY case [327–329]). We recall that the use of the non-local gauge (4.56) is possible without affecting the physical results because the gauge fixing parameter  $\xi$  is a mathematical artifact and does not appear in any physical results.

As we will prove explicitly in the next sections, all the polarizations (4.55) are finite. Indeed, we recall that, in the large- $N_f$  limit, SQED<sub>3</sub> [286], similarly to bQED<sub>3</sub> [175, 176] and QED<sub>3</sub> [177, 269], is a non-running (“standing”) gauge theory, *i.e.*, the coupling is not renormalized, implying finite polarizations and therefore vanishing beta functions. This leads to the triviality of the renormalization constants for the coupling, gauge-multiplet fields and gauge-fixing parameter, formally

$$Z_x = 1, \quad \text{and} \quad \gamma_x = 0 \quad \text{with} \quad x \in \{e, \gamma, \varepsilon, \lambda, \xi\}. \quad (4.57)$$

which imply a trivial beta function for the running of the coupling  $e$  reading

$$\beta = -2\varepsilon \bar{\alpha}_r, \quad (4.58)$$

where  $\alpha = e^2/(4\pi)$  and  $\bar{\alpha} = \alpha/(4\pi)$ . In this case, the coupling trivially renormalizes as  $\alpha = \mu^{2\varepsilon} \alpha_r$ , with  $\mu$  the renormalization scale. In the following, like in the previous sections, we will work in the modified minimal subtraction scheme, where the renormalization scale is defined as

$$\bar{\mu}^2 = 4\pi e^{-\gamma_E} \mu^2, \quad (4.59)$$

and further ( $\overline{\text{MS}}$  scheme) subtracts  $4\pi$  and  $\gamma_E$ . We will refer to this modified version of the dimensional reduction scheme as  $\overline{\text{DRED}}$ .

Now considering the matter multiplet, turning on the interactions leads to the following dressed propagators

$$S_{\psi\bar{\psi}}(p) = \frac{\text{---}\blacktriangleright\text{---}}{p} = \frac{i}{1 - \Sigma_p^\psi(p^2)} \frac{1}{\not{p}}, \quad (4.60a)$$

$$S_{\phi\phi^*}(p) = \frac{\text{====}\blacktriangleright\text{====}}{p} = \frac{iS}{1 - \Sigma_p^\phi(p^2)} \frac{1}{p^2}, \quad (4.60b)$$

<sup>5</sup>The term “polarization” for the photino is a bit abusive, but we will keep it for clarity. Note also that we slightly abuse notations in (4.55c) and we consider that the difference between the matrix  $\Pi_\lambda(p)$  and the scalar function  $\Pi_\lambda(p^2)$  is understood.

where the matter-multiplet self-energies are parameterized as

$$\Sigma^\psi(p) = \not{p}\Sigma_p^\psi(p^2) + m_\psi\Sigma_m^\psi(p^2), \quad (4.61a)$$

$$\Sigma^\phi(p) = p^2\Sigma_p^\phi(p^2) + m_\phi^2\Sigma_m^\phi(p^2). \quad (4.61b)$$

From these, the components  $p$  and  $m$  can be extracted with the following projectors

$$\Sigma_p^\psi(p^2) = \frac{\text{Tr}[\not{p}\Sigma^\psi(p)]}{np^2} \Big|_{m_x=0}, \quad \Sigma_m^\psi(p^2) = \frac{\text{Tr}[\Sigma^\psi(p)]}{nm_\psi} \Big|_{m_x=0}, \quad (4.62a)$$

$$\Sigma_p^\phi(p^2) = \frac{\Sigma^\phi(p)}{p^2} \Big|_{m_x=0}, \quad \Sigma_m^\phi(p^2) = \frac{\partial\Sigma^\phi(p)}{\partial m_\phi^2} \Big|_{m_x=0}, \quad (4.62b)$$

with  $m_x = \{m_\phi, m_\psi\}$ . As for the gauge polarizations, using this setup allows all integrals to be computed in the  $m_x \rightarrow 0$  limit, *i.e.*, completely massless, as an IR rearrangement.

The renormalization conventions for the non-trivial renormalization constants are defined as

$$\psi = Z_\psi^{1/2}\psi_r, \quad \phi = Z_\phi^{1/2}\phi_r, \quad m_\psi = Z_{m_\psi}m_{\psi r}, \quad m_\phi = Z_{m_\phi}m_{\phi r}. \quad (4.63)$$

Similarly to the previous chapters, the renormalization constants can be extracted from the bare self-energies thanks to the expression of the renormalized self-energies

$$\Sigma_{pr}^\psi = 1 - (1 - \Sigma_p^\psi)Z_\psi, \quad \Sigma_{mr}^\psi = 1 - (1 + \Sigma_m^\psi)Z_\psi Z_{m_\psi}, \quad (4.64a)$$

$$\Sigma_{pr}^\phi = 1 - (1 - \Sigma_p^\phi)Z_\phi, \quad \Sigma_{mr}^\phi = 1 - (1 + \Sigma_m^\phi)Z_\phi Z_{m_\phi}^2, \quad (4.64b)$$

leading to the following simple set of relations

$$\left(1 - \Sigma_p^\psi\right)Z_\psi = \text{finite}, \quad \left(1 - \Sigma_p^\phi\right)Z_\phi = \text{finite}, \quad \frac{1 + \Sigma_m^\psi}{1 - \Sigma_p^\psi}Z_{m_\psi} = \text{finite}, \quad \frac{1 + \Sigma_m^\phi}{1 - \Sigma_p^\phi}Z_{m_\phi}^2 = \text{finite}, \quad (4.65)$$

where “finite” means of the order of  $\varepsilon^0$ , so that no additional counter diagrams needs to be computed. Finally, the associated anomalous dimensions are defined as

$$\gamma_x = \frac{d\log Z_x}{d\log \mu}, \quad x \in \{\psi, \phi, m_\psi, m_\phi\}, \quad (4.66)$$

and correspond to the critical exponents of the theory that we want to compute. The latter govern the asymptotic behavior of renormalized correlators and parameters as

$$S_{\psi\bar{\psi},r}(p) \sim p_E^{-1+\gamma_\psi}, \quad S_{\phi\phi^*,r}(p) \sim p_E^{-2+2\gamma_\phi}, \quad (4.67a)$$

$$m_{\psi,r} \sim p_E^{1+\gamma_{m_\psi}}, \quad m_{\phi,r} \sim p_E^{1+\gamma_{m_\phi}}. \quad (4.67b)$$

Since the theory has no running coupling, no quantity will depend on the renormalization scale  $\mu$ . Nevertheless, we will still obtain some  $\mu^{2\varepsilon}$  factors when solving the integrals in dimensional regularization. These can be absorbed by considering that the coupling  $1/N_f$  depends on the renormalization scale  $\mu$  so that it trivially renormalize as  $N_{f,r}(\mu) = \mu^{2\varepsilon}N_f$  so that in the limit  $\varepsilon \rightarrow 0$  we have simply  $N_{f,r} = N_f$ . Therefore, one can generally use the more practical formula

$$\gamma_x = 2\varepsilon \frac{\partial \log Z_x}{\partial \log N_f}, \quad x \in \{\psi, \phi, m_\psi, m_\phi\}. \quad (4.68)$$

We now have all the required materials to start the complete perturbative computations up to NLO in the gQED<sub>3</sub> model.



$$\Pi_{1\gamma}^{(b)}(p^2) = -\frac{N_f e^2}{(4\pi)^{3/2} p_E} \left( \frac{\bar{\mu}^2}{-p^2} \right)^\varepsilon \frac{2S}{d-1} e^{\gamma_E \varepsilon} G(d, 1, 1), \quad (4.73b)$$

where we recall that  $\bar{\mu}^2 = 4\pi e^{-\gamma_E} \mu^2$  and  $G(d, \alpha, \beta)$  was defined in Appendix A. Performing the  $\varepsilon$ -expansion

$$\Pi_{1\gamma}^{(a)}(p^2) = -\frac{n N_f e^2}{16 p_E} \left( 1 - (1 - 2 \log 2 + L_p) \varepsilon + \mathcal{O}(\varepsilon^2) \right), \quad (4.74a)$$

$$\Pi_{1\gamma}^{(b)}(p^2) = -\frac{S N_f e^2}{8 p_E} \left( 1 + (1 + 2 \log 2 - L_p) \varepsilon + \mathcal{O}(\varepsilon^2) \right), \quad (4.74b)$$

where we recall that  $L_p = \log(-p^2/\bar{\mu}^2)$ . As expected, in the QED<sub>3</sub> case ( $S=0$ ,  $n=2$ ), only the first diagram, which is purely fermionic, contributes. Oppositely, in the bQED<sub>3</sub> case ( $S=1$ ,  $n=0$ ), only the second diagram, which is purely bosonic, contributes. Moreover, in the SQED<sub>3</sub> case ( $S=1$ ,  $n=2$ ), both diagrams equally contribute in the limit  $\varepsilon \rightarrow 0$ . From these results, the total photon polarization function at LO is therefore given by

$$\Pi_{1\gamma}(p^2) = \Pi_{1\gamma}^{(a)}(p^2) + \Pi_{1\gamma}^{(b)}(p^2) = -\frac{N_f e^2}{(4\pi)^{3/2} p_E} \left( \frac{\bar{\mu}^2}{-p^2} \right)^\varepsilon \frac{(d-2)n + 2S}{d-1} e^{\gamma_E \varepsilon} G(d, 1, 1), \quad (4.75)$$

and since it is completely finite in  $d=3$ , its expression yields exactly

$$\Pi_{1\gamma}(p^2) = -\frac{(n+2S)N_f e^2}{16 p_E}. \quad (4.76)$$

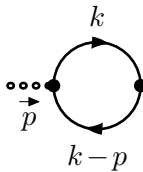
Interestingly, in the cases of SQED<sub>3</sub> ( $S=1$ ,  $n=2$ ), QED<sub>3</sub> ( $S=0$ ,  $n=2$ ) and bQED<sub>3</sub> ( $S=1$ ,  $n=0$ ), it reads

$$\Pi_{1\gamma}^{\text{SQED}_3}(p^2) = -\frac{N_f e^2}{4 p_E}, \quad \Pi_{1\gamma}^{\text{QED}_3}(p^2) = -\frac{N_f e^2}{8 p_E}, \quad \Pi_{1\gamma}^{\text{bQED}_3}(p^2) = -\frac{N_f e^2}{8 p_E}. \quad (4.77)$$

In this very simple case, the SQED<sub>3</sub> photon polarization is simply the sum of the fermionic and bosonic parts, since there is no one-loop diagram involving a mixture of both. Therefore, the SQED<sub>3</sub> photon polarization is twice the value for QED<sub>3</sub>, which was first obtained in [175, 176]. Note that our result for SQED<sub>3</sub> coincides with the earlier one-loop result given in ref. [286], but now obtained in the dimensional reduction scheme.

### $\varepsilon$ -scalar polarization at LO

Next, we proceed similarly for the  $\varepsilon$ -scalar propagator (4.54b), and compute the LO  $\varepsilon$ -scalar polarization function which consists of a single non-vanishing diagram, defined as

$$i\bar{\Pi}_1^{\mu\nu}(p) = \mu \begin{array}{c} \bullet \cdots \bullet \\ \uparrow p \\ \bullet \cdots \bullet \end{array} \nu = -\mu^{2\varepsilon} 2N_f \int [d^d k] \text{Tr} \left[ \bar{\Gamma}_{0A\psi\bar{\psi}}^\mu S_{0\psi\bar{\psi}}(k-p) \bar{\Gamma}_{0A\psi\bar{\psi}}^\nu S_{0\psi\bar{\psi}}(k) \right]. \quad (4.78)$$


Using the Feynman rules for the vertices (4.40) and the matter (electrons and selectrons) propagators (4.37) leads to the following expression

$$i\bar{\Pi}_1^{\mu\nu}(p) = -\mu^{2\varepsilon} 2N_f \mathcal{E} S e^2 \int [d^d k] \frac{\text{Tr}[\bar{\gamma}^\mu (\not{k} - \not{p} + m_\psi) \bar{\gamma}^\nu (\not{k} + m_\psi)]}{((k-p)^2 - m_\psi^2)(k^2 - m_\psi^2)}. \quad (4.79)$$

Using the projector defined in (4.55b), and performing the trace in the  $2\varepsilon$ -dimensional (barred) space with the help of the recursive formula (4.50) yields

$$\Pi_{1\varepsilon}(p^2) = -4i\mu^{2\varepsilon} \frac{N_f e^2}{p^2} \mathcal{E} S \int [d^d k] \frac{k^2 - k \cdot p}{k^2 (k-p)^2}. \quad (4.80)$$

After wick rotation and the calculation of the integral using the results of Appendix A, we have

$$\Pi_{1\varepsilon}(p^2) = -\frac{N_f e^2}{(4\pi)^{3/2} p_E} \left( \frac{\bar{\mu}^2}{-p^2} \right)^\varepsilon 2\mathcal{E} S e^{\gamma_E \varepsilon} G(d, 1, 1). \quad (4.81)$$

Since this result is again finite in  $d=3$ , it can be written as

$$\Pi_{1\varepsilon}(p^2) = -\frac{\mathcal{E} S N_f e^2}{4p_E}. \quad (4.82)$$

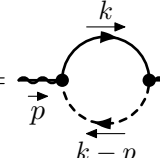
Let us note that in the case of bQED<sub>3</sub> ( $S=1$ ,  $n=0$ ,  $\mathcal{E}=0$ ) as well as in the case of QED<sub>3</sub> ( $S=0$ ,  $n=2$ ,  $\mathcal{E}=0$ ) this polarization is obviously zero. Indeed, the  $\varepsilon$ -scalars are relevant only in the case of SQED<sub>3</sub> ( $S=1$ ,  $n=2$ ,  $\mathcal{E}=1$ ), yielding

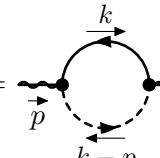
$$\Pi_{1\varepsilon}^{\text{SQED}_3}(p^2) = -\frac{N_f e^2}{4p_E}, \quad (4.83)$$

which is interestingly exactly equal to the polarization of the photon in the same case,  $\Pi_{1\gamma}^{\text{SQED}_3}(p^2)$  calculated in (4.77). As we will comment later on, such an equality is expected from SUSY.

### Photino polarization at LO

Lastly, we proceed in the same way for the photino propagator (4.54c), and compute the LO photino self-energy, which consists of two non-vanishing diagrams with opposite charge-flows. Since it is a photino (Majorana) polarization, in principle we need to follow the advanced Feynman rules (4.41) and (4.42), leading to

$$-i\Pi_{1\lambda}^{(a)}(p) = \text{Diagram (a)} = \mu^{2\varepsilon} 2N_f \int [d^d k] \Gamma_{0\bar{\psi}\lambda\phi} S_{0\psi\bar{\psi}}(k) \Gamma_{0\bar{\lambda}\psi\phi^*} S_{0\phi\phi^*}(k-p), \quad (4.84a)$$


$$-i\Pi_{1\lambda}^{(b)}(p) = \text{Diagram (b)} = \mu^{2\varepsilon} 2N_f \int [d^d k] \Gamma_{0\bar{\lambda}\psi\phi^*} S_{0\psi\bar{\psi}}(k) \Gamma_{0\bar{\psi}\lambda\phi} S_{0\phi\phi^*}(k-p), \quad (4.84b)$$


where we assigned a continuous and unidirectional fermion-flow that goes from left to right. In the case of diagram (a), the fermion-flow, charge-flow and momentum flow are all in the same direction. Moreover, the vertices (given by (4.40d)) are proportional to the unit matrix. Therefore, there is no reversed propagator or vertex. In the case of diagram (b), the fermion-flow is opposite to the fermion number flow so that the Dirac propagator gets reversed. However, the fermion number flow is also opposite to the momentum flow so that the momentum gets an additional minus sign. All together, the Dirac propagator remains unchanged (as  $S(-(-k)) = S(k)$ ) and diagram (b) is therefore equal to diagram (a). The resulting contribution is then defined as twice the configuration where all flows are aligned, *i.e.*,

$$-i\Pi_{1\lambda}(p) = 2 \times \mu^{2\varepsilon} 2N_f \int [d^d k] \Gamma_{0\bar{\psi}\lambda\phi} S_{0\psi\bar{\psi}}(k) \Gamma_{0\bar{\lambda}\psi\phi^*} S_{0\phi\phi^*}(k-p). \quad (4.85)$$



### 4.4.2 Matter-multiplet self-energies at LO

In this section we compute in detail the first correction to the self-energies of the matter multiplet, *i.e.*, for the electron and the selectron, at LO in the  $1/N_f$  expansion, *i.e.*, at  $O(1/N_f)$ .

#### Electron self-energy at LO

We start with the electron propagator (4.61) and compute it's LO correction which consists of three contributions

$$\Sigma_1^\psi(p) = \Sigma_1^{\psi(a)}(p) + \Sigma_1^{\psi(b)}(p) + \Sigma_1^{\psi(c)}(p), \quad (4.93)$$

one for each gauge interaction, that are respectively defined as

$$-i\Sigma_1^{\psi(a)}(p) = \begin{array}{c} \text{Diagram: Electron line with momentum } p \text{ entering from the left and } p-k \text{ exiting to the right. A loop is formed by a photon propagator (curly line) and a scalar propagator (dotted line). The loop contains a vertex labeled '1'. The loop momentum is } k. \end{array} = \mu^{2\varepsilon} \int [d^d k] \hat{\Gamma}_{0A\psi\bar{\psi}}^\mu S_{0\psi\bar{\psi}}(k) \hat{\Gamma}_{0A\psi\bar{\psi}}^\nu \hat{D}_{1AA,\mu\nu}(p-k), \quad (4.94a)$$

$$-i\Sigma_1^{\psi(b)}(p) = \begin{array}{c} \text{Diagram: Electron line with momentum } p \text{ entering from the left and } p-k \text{ exiting to the right. A loop is formed by a photon propagator (curly line) and a scalar propagator (dotted line). The loop contains a vertex labeled '1'. The loop momentum is } k. \end{array} = \mu^{2\varepsilon} \int [d^d k] \bar{\Gamma}_{0A\psi\bar{\psi}}^\mu S_{0\psi\bar{\psi}}(k) \bar{\Gamma}_{0A\psi\bar{\psi}}^\nu \bar{D}_{1AA,\mu\nu}(p-k), \quad (4.94b)$$

$$-i\Sigma_1^{\psi(c)}(p) = \begin{array}{c} \text{Diagram: Electron line with momentum } p \text{ entering from the left and } p-k \text{ exiting to the right. A loop is formed by a photon propagator (curly line) and a scalar propagator (dotted line). The loop contains a vertex labeled '1'. The loop momentum is } k. \end{array} = \mu^{2\varepsilon} \int [d^d k] \Gamma_{0\bar{\lambda}\psi\phi^*} S_{0\phi\phi^*}(k) \Gamma_{0\bar{\psi}\lambda\phi} D_{1\lambda\bar{\lambda}}(p-k), \quad (4.94c)$$

where the photon,  $\varepsilon$ -scalar and photino propagators are indeed the IR-softened ones at first order (4.92). Using the simple Feynman rules is here enough, *i.e.*, using equations (4.36) to (4.40), we obtain

$$-i\Sigma_1^{\psi(a)}(p) = -\frac{16i}{(n+2S)} \frac{\mu^{2\varepsilon}}{N_f} \int [d^d k] \frac{\hat{\gamma}^\mu (\not{k} + m_\psi) \hat{\gamma}^\nu \hat{d}_{\mu\nu}(p-k)}{(k^2 - m_\psi^2) |p-k|}, \quad (4.95a)$$

$$-i\Sigma_1^{\psi(b)}(p) = -4i\varepsilon S \frac{\mu^{2\varepsilon}}{N_f} \int [d^d k] \frac{\bar{\gamma}^\mu (\not{k} - m_\psi) \bar{\gamma}^\nu}{(k^2 - m_\psi^2) |p-k|}, \quad (4.95b)$$

$$-i\Sigma_1^{\psi(c)}(p) = i4S \frac{\mu^{2\varepsilon}}{N_f} \int [d^d k] \frac{\not{p} - \not{k}}{(k^2 - m_\phi^2) |p-k|}. \quad (4.95c)$$

Note that in (4.95) the (dimensionful) electric constant  $e$  drops out in favor of the new coupling  $1/N_f$  thanks to the softening of the gauge-multiplet propagators. These diagrams are then split into the part proportional to the external momentum  $p$  (also called vectorial part since proportional to  $\not{p}$ ) and the one proportional to the mass  $m_\psi$  (also called scalar part) using the projectors (4.62). First, focusing on the vectorial part, using the projector (4.62a) and computing these three diagrams with projection, trace calculation, wick rotation, integral evaluation, and wick rotate back, we find the following exact results

$$\Sigma_{1p}^{\psi(a)}(p^2) = \frac{4}{(4\pi)^{3/2} N_f} \left( \frac{\bar{\mu}^2}{-p^2} \right)^\varepsilon \frac{4(d-2)}{n+2S} \left( \frac{d-1}{2d-3} - \xi \right) e^{\gamma_E \varepsilon} G(d,1,1/2), \quad (4.96a)$$

$$\Sigma_{1p}^{\psi(b)}(p^2) = \frac{4}{(4\pi)^{3/2} N_f} \left( \frac{\bar{\mu}^2}{-p^2} \right)^\varepsilon \frac{2(d-3)(d-2)\varepsilon S}{n(2d-3)} e^{\gamma_E \varepsilon} G(d,1,1/2), \quad (4.96b)$$

$$\Sigma_{1p}^{\psi(c)}(p^2) = -\frac{4}{(4\pi)^{3/2} N_f} \left( \frac{\bar{\mu}^2}{-p^2} \right)^\varepsilon \frac{(d-1)S}{2d-3} e^{\gamma_E \varepsilon} G(d,1,1/2), \quad (4.96c)$$



where  $\Sigma_{1p}^{\psi(b)}$  is finite due to the  $\varepsilon$ -scalar, while the two other contributions are singular in the limit  $d \rightarrow 3$ . Secondly, focusing on the scalar part, using the projector (4.62b) and computing these three diagrams with the same approach yields the following exact results

$$\Sigma_{1m}^{\psi(a)}(p^2) = \frac{4}{(4\pi)^{3/2}N_f} \left( \frac{\bar{\mu}^2}{-p^2} \right)^\varepsilon \frac{4(d-1+\xi)}{n+2S} e^{\gamma_E \varepsilon} G(d,1,1/2), \quad (4.97a)$$

$$\Sigma_{1m}^{\psi(b)}(p^2) = -\frac{4}{(4\pi)^{3/2}N_f} \left( \frac{\bar{\mu}^2}{-p^2} \right)^\varepsilon \frac{2(d-3)\mathcal{E}S}{n} e^{\gamma_E \varepsilon} G(d,1,1/2), \quad (4.97b)$$

$$\Sigma_{1m}^{\psi(c)}(p^2) = 0, \quad (4.97c)$$

where the first contribution is singular in the limit  $d \rightarrow 3$  while the second diagram vanishes in  $d = 3$  and the last graph (c) is exactly zero because of the gamma matrix trace.

Summing all the contributions, the total vectorial and scalar electron self-energies are therefore given, expanded in  $d = 3 - 2\varepsilon$ , by

$$\Sigma_{1p}^\psi(p^2) = \frac{4}{3(n+2S)\pi^2 N_f} \left( \frac{\bar{\mu}^2}{-4p^2} \right)^\varepsilon \left( \frac{2-3\xi-2S}{\varepsilon} + \frac{2}{3} (7 - (13+3\mathcal{E}) - 9\xi) + \mathcal{O}(\varepsilon) \right), \quad (4.98a)$$

$$\Sigma_{1m}^\psi(p^2) = \frac{4}{3(n+2S)\pi^2 N_f} \left( \frac{\bar{\mu}^2}{-4p^2} \right)^\varepsilon \left( \frac{3(2+\xi)}{\varepsilon} + 6(3+\mathcal{E}S+2\xi) + \mathcal{O}(\varepsilon) \right). \quad (4.98b)$$

Note that some  $\log(2)$  have been resummed by adding a 4 next to the momentum  $p^2$ . From this result, we extract straightforwardly, with (4.65), the LO electron wave-function and mass renormalization

$$Z_\psi = 1 + \frac{4(2-3\xi-2S)}{3(n+2S)\pi^2 N_f \varepsilon} + \mathcal{O}(1/N_f^2), \quad Z_m = 1 + \frac{8(S-4)}{3(n+2S)\pi^2 N_f \varepsilon} + \mathcal{O}(1/N_f^2). \quad (4.99)$$

As expected, the general mass renormalization factor is completely gauge invariant, which is a strong check on our results. From the definition of the anomalous dimension (4.68), we have the general anomalous dimensions

$$\gamma_\psi = -\frac{8(2-3\xi-2S)}{3(n+2S)\pi^2 N_f} + \mathcal{O}(1/N_f^2), \quad \gamma_{m_\psi} = \frac{16(4-S)}{3(n+2S)\pi^2 N_f} + \mathcal{O}(1/N_f^2). \quad (4.100)$$

In the relevant cases of SQED<sub>3</sub> ( $S=1, n=2$ ) and QED<sub>3</sub> ( $S=0, n=2$ ), it reads

$$\gamma_\psi^{\text{SQED}_3} = \frac{2\xi}{\pi^2 N_f} + \mathcal{O}(1/N_f^2), \quad \gamma_{m_\psi}^{\text{SQED}_3} = \frac{4}{\pi^2 N_f} + \mathcal{O}(1/N_f^2), \quad (4.101a)$$

$$\gamma_\psi^{\text{QED}_3} = -\frac{4(2-3\xi)}{3\pi^2 N_f} + \mathcal{O}(1/N_f^2), \quad \gamma_{m_\psi}^{\text{QED}_3} = \frac{32}{3\pi^2 N_f} + \mathcal{O}(1/N_f^2). \quad (4.101b)$$

Also,  $\gamma_\psi^{\text{SQED}_3}$  vanishes in the Landau gauge ( $\xi=0$ ), which is then the good gauge at LO. This is to be contrasted with the non-supersymmetric case,  $\gamma_\psi^{\text{QED}_3}$  (first obtained in [213]) that vanishes in the so-called Nash gauge [181],  $\xi=2/3$ . Note also that the bosonic bQED<sub>3</sub> case is obviously irrelevant here, since we consider the anomalous dimension of the electron field and mass. We will further discuss the quantities (4.101) once we obtained their supersymmetric counterpart in the next section and their NLO correction after that.

### Selectron self-energy at LO

We proceed similarly for the electron superpartner, the selectron, which is the scalar propagator and compute its LO scalar self-energy which consists of the sum of the two diagrams

$$\Sigma_1^\phi(p) = \Sigma_1^{\phi(a)}(p) + \Sigma_1^{\phi(b)}(p), \quad (4.102)$$

that are defined as

$$-i\Sigma_1^{\phi(a)}(p) = \text{Diagram (a)} = \mu^{2\varepsilon} \int [d^d k] \hat{\Gamma}_{0A\phi\phi^*}^\mu(k, p) S_{0\phi\phi^*}(k) \hat{\Gamma}_{0A\phi\phi^*}^\nu(p, k) \hat{D}_{1AA, \mu\nu}(k-p), \quad (4.103a)$$

$$-i\Sigma_1^{\phi(b)}(p) = \text{Diagram (b)} = -\mu^{2\varepsilon} \int [d^d k] \text{Tr} \left[ \Gamma_{0\bar{\psi}\lambda\phi} S_{0\psi\bar{\psi}}(k) \Gamma_{0\lambda\psi\phi^*} D_{1\lambda\bar{\lambda}}(k-p) \right], \quad (4.103b)$$

where the photon and photino propagators are indeed the IR-softened ones (4.92) and  $\Sigma_{1b}^\phi$  contains a hybrid (Dirac/Majorana) fermion loop. Note that for the diagram (b), we can assign a counter-clockwise fermion-flow and momentum flows that follows the fermion loop consisting of the Dirac and Majorana fermions. Therefore, using the simple Feynman rules given by (4.36) to (4.40) is indeed enough and leads to

$$-i\Sigma_1^{\phi(a)}(p) = -\frac{16iS}{n+2S} \frac{\mu^{2\varepsilon}}{N_f} \int [d^d k] \frac{(\hat{k} + \hat{p})^\mu (\hat{k} + \hat{p})^\nu \hat{d}_{\mu\nu}(k-p)}{(k^2 - m_\phi^2) |k-p|}, \quad (4.104a)$$

$$-i\Sigma_1^{\phi(b)}(p) = -4iS \frac{\mu^{2\varepsilon}}{N_f} \int [d^d k] \frac{\text{Tr}[(\hat{k} + m_\psi)(\hat{k} - \hat{p})]}{(k^2 - m_\psi^2) |k-p|}. \quad (4.104b)$$

Performing the traces and using the projection (4.62b) yields the two LO contributions to the momentum part of the selectron self-energy

$$\Sigma_{1p}^{\phi(a)}(p^2) = \frac{4}{(4\pi)^{3/2} N_f} \left( \frac{\bar{\mu}^2}{-p^2} \right)^\varepsilon \frac{4S}{(n+2S)} \left( \frac{4(d-1)(d-2)}{2d-3} - (2d-5)\xi \right) e^{\gamma_{E\varepsilon}} G(d, 1, 1/2), \quad (4.105a)$$

$$\Sigma_{1p}^{\phi(b)}(p^2) = -\frac{4}{(4\pi)^{3/2} N_f} \left( \frac{\bar{\mu}^2}{-p^2} \right)^\varepsilon \frac{n(d-2)S}{2d-3} e^{\gamma_{E\varepsilon}} G(d, 1, 1/2), \quad (4.105b)$$

as well as the two LO contributions to the mass part of the selectron self-energy

$$\Sigma_{1m}^{\phi(a)}(p^2) = -\frac{4}{(4\pi)^{3/2} N_f} \left( \frac{\bar{\mu}^2}{-p^2} \right)^\varepsilon \frac{2S}{n+2S} \left( 4(d-3)(d-1) - \frac{2d-5}{d-4} (2d^2 - 13d + 19)\xi \right) e^{\gamma_{E\varepsilon}} G(d, 1, 1/2), \quad (4.106a)$$

$$\Sigma_{1m}^{\phi(b)}(p^2) = \frac{4}{(4\pi)^{3/2} N_f} \left( \frac{\bar{\mu}^2}{-p^2} \right)^\varepsilon \frac{n(d-1)S}{2} e^{\gamma_{E\varepsilon}} G(d, 1, 1/2). \quad (4.106b)$$

The total selectron momentum and mass self-energy are then given, in  $\varepsilon$ -expanded form, by

$$\Sigma_{1p}^\phi(p^2) = \frac{4S}{3(n+2S)\pi^2 N_f} \left( \frac{\bar{\mu}^2}{-4p^2} \right)^\varepsilon \left( \frac{8-3\xi-n}{\varepsilon} + \frac{2}{3}(28-5n) + \mathcal{O}(\varepsilon) \right), \quad (4.107a)$$

$$\Sigma_{1m}^\phi(p^2) = \frac{4S}{3(n+2S)\pi^2 N_f} \left( \frac{\bar{\mu}^2}{-4p^2} \right)^\varepsilon \left( \frac{3(\xi+n)}{\varepsilon} + 3(8-3\xi+3n) + \mathcal{O}(\varepsilon) \right). \quad (4.107b)$$

From these results, we extract the LO scalar wave-function and mass renormalization

$$Z_\phi = 1 + \frac{4(8-3\xi-n)S}{3(n+2)\pi^2 N_f \varepsilon} + \mathcal{O}(1/N_f^2), \quad Z_{m_\phi} = 1 - \frac{4(n+4)S}{3(n+2)\pi^2 N_f \varepsilon} + \mathcal{O}(1/N_f^2). \quad (4.108)$$

As expected from such a physical quantity, the general mass renormalization factor is completely gauge invariant. We can now derive the anomalous dimensions for the selectron field and mass using the definition (4.68), yielding

$$\gamma_\phi = -\frac{8(8-3\xi-n)S}{3(n+2)\pi^2 N_f} + \mathcal{O}(1/N_f^2), \quad \gamma_{m_\phi} = \frac{8(n+4)S}{3(n+2)\pi^2 N_f} + \mathcal{O}(1/N_f^2). \quad (4.109)$$

Note that in the relevant cases of SQED<sub>3</sub> ( $S = 1, n = 2$ ) and bQED<sub>3</sub> ( $S = 1, n = 0$ ), they read

$$\gamma_{\phi}^{\text{SQED}_3} = -\frac{2(2-\xi)}{\pi^2 N_f} + \mathcal{O}(1/N_f^2), \quad \gamma_{m_{\phi}}^{\text{SQED}_3} = \frac{4}{\pi^2 N_f} + \mathcal{O}(1/N_f^2), \quad (4.110a)$$

$$\gamma_{\phi}^{\text{bQED}_3} = -\frac{4(8-3\xi)}{3\pi^2 N_f} + \mathcal{O}(1/N_f^2), \quad \gamma_{m_{\phi}}^{\text{bQED}_3} = \frac{16}{3\pi^2 N_f} + \mathcal{O}(1/N_f^2). \quad (4.110b)$$

A few remarks are necessary here. First, we observe that for SQED<sub>3</sub>, the mass anomalous dimension for the selectron (4.110a) is identical to the one of the electron (4.101a), *i.e.*,

$$\gamma_{m_{\psi}}^{\text{SQED}_3} = \gamma_{m_{\phi}}^{\text{SQED}_3} = \frac{4}{\pi^2 N_f} + \mathcal{O}(1/N_f^2), \quad (4.111)$$

as expected from supersymmetry. In striking contrast, the field anomalous dimensions for the selectron (4.110a) and the electron (4.101a) are different. This is due to the use of a gauge fixing term that breaks supersymmetry (Wess-Zumino gauge). This is not an issue since the breaking of SUSY will occur only for gauge-dependant quantities that are, by definition, nonphysical. Secondly, let us remark that in the SQED<sub>3</sub> case, the field anomalous dimension of the selectron vanishes for  $\xi = 2$ . Since for the fermionic part of SQED<sub>3</sub>, the good gauge was the Landau gauge  $\xi = 0$ , it is therefore not possible to cancel both matter-field's anomalous dimensions at the same time. This may cause trouble for computations of the critical properties of the model using the Schwinger-Dyson equations, see the devoted section 4.6. As for the bQED case (4.110b), we see that the good gauge is then  $\xi = 8/3$ . We will discuss further these results again after improving them to NLO.

### 4.4.3 Vanishing contributions and generalized Furry theorem

Before going to higher orders and compute any NLO diagrams, we first need to discuss some additional diagrams that may enter the incoming NLO computations as subdiagrams. These LO diagrams are made of matter bubbles and triangles, and are of uttermost interest because a lot of them are vanishing, either exactly or in pairs. On the one hand, this will tremendously reduce the number of diagrams to be computed at NLO, but will also ensure that matter bubbles are connected to each other in a way suitable for the large- $N_f$  expansion.

We first focus on three one-loop diagrams made out of a matter bubble that are exactly vanishing, see figure 4.2.

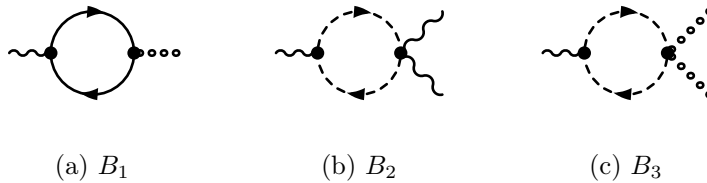


Figure 4.2: Exactly vanishing one-loop bubbles diagrams

The first vanishing bubble contribution is the mixed polarization  $B_1$  (ongoing photon and outgoing  $\varepsilon$ -scalar), displayed in figure 4.2a. Since this diagram is proportional to  $\text{Tr}(\tilde{\gamma}^{\mu}) = 0$ , it reads  $B_1 = 0$ . More generally, we conjecture that every diagram with an odd number of  $\varepsilon$ -scalar external is exactly zero, although one has to be careful in the case of diagrams also containing electrons and photino external legs that may generate non-trivial gamma traces. Instead of making all-order proofs, we limit ourselves to explicitly compute the diagrams we need and prove that they vanish. The two other contributions, given by figures 4.2b and 4.2c, are also exactly vanishing by parity on the internal momentum integral, *i.e.*,  $B_2 = B_3 = 0$ .

Multiple other vanishing contributions come from matter triangles. These are built from triangles of electrons and selectrons together with external legs of any allowed kinds, *i.e.*, taken in the gauge multiplet {photon, photino,  $\varepsilon$ -scalar}. In total, there are 8 triangles (disregarding the possible charge-flows), see figure 4.3. In the following, we will explicitly check that all these diagrams (all proportional to  $N_f$ ) are indeed vanishing.

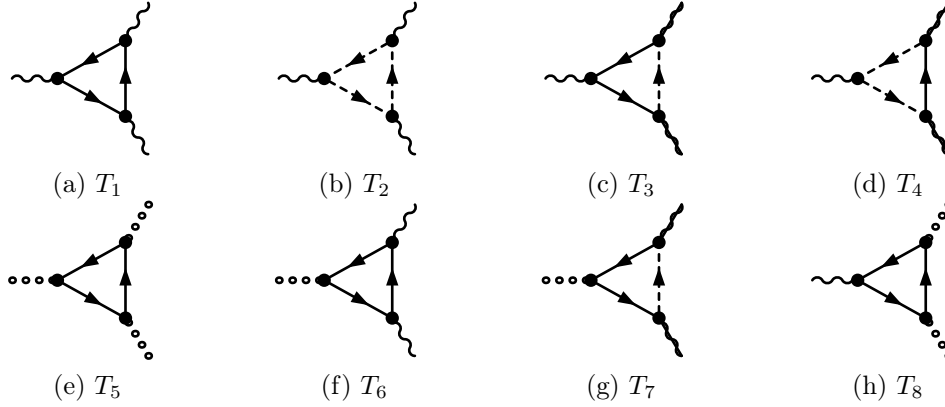


Figure 4.3: All one-loop matter triangles in gQED<sub>3</sub>.

The first one is the pure QED diagram  $T_1$  and is vanishing because it always appears paired up with its mirror conjugate diagram with opposite charge/matter flow. Indeed, a straightforward computation reads

$$T_1 + \tilde{T}_1 = \text{[Diagram 1]} + \text{[Diagram 2]} = 0, \quad (4.112)$$

where the tilde indicates that we reverse the charge/matter flow, which is equivalent to a charge conjugation. Note that the inner circular arrows denote momentum parametrization. This computation is an explicit check at first order of the so-called Furry theorem in QED, [330], which is the all-order proof that in QED, any diagram with an odd number of photon legs can be discarded since they will cancel with their opposite flow diagrams, as a direct consequence of the conservation of energy and charge conjugation symmetry. In the following, we will prove that the Furry theorem, generalized for gQED<sub>3</sub>, holds at least at the leading order, *i.e.*, for diagrams made of matter triangles and three external legs taken in the gauge multiplet.

The second vanishing contribution is the pure bQED diagram  $T_2$  and also vanishes with its opposite charge-flow counterpart

$$T_2 + \tilde{T}_2 = \text{[Diagram 3]} + \text{[Diagram 4]} = 0. \quad (4.113)$$

This calculation therefore generalizes Furry's theorem to the case of bQED<sub>3</sub>.

The third and fourth vanishing diagrams are the supersymmetric triangles made of mixed electron and selectrons, and yield (after careful parametrization and evaluation)

$$T_3 + \tilde{T}_3 = \text{[Diagram 5]} + \text{[Diagram 6]} = 0, \quad (4.114)$$

$$T_4 + \tilde{T}_4 = \text{[Diagram 1]} + \text{[Diagram 2]} = 0, \quad (4.115)$$

thereby generalizing Furry’s theorem to SQED<sub>3</sub> without  $\varepsilon$ -scalars.

Finally, as for the diagrams containing  $\varepsilon$ -scalars, we have the three contributions  $T_5$ ,  $T_6$  and  $T_7$  that are exactly zero, *i.e.*,

$$T_5 = \text{[Diagram 3]} = 0, \quad T_6 = \text{[Diagram 4]} = 0, \quad T_7 = \text{[Diagram 5]} = 0, \quad (4.116)$$

for any momentum or charge-flow direction. This is because they contain an odd number of  $\varepsilon$ -scalar external legs, *i.e.*, they are ultimately related to  $\text{Tr}(\bar{\gamma}^\mu) = 0$ . We are left with a last triangle,  $T_8$ , made of an electron loop together with one photon plus two  $\varepsilon$ -scalars external legs. This diagram is different since it is not vanishing because of  $\varepsilon$ -scalars, as in this case it is ultimately proportional to  $\text{Tr}(\bar{\gamma}^\mu \bar{\gamma}^\nu) \neq 0$ . In that case we have to consider the diagrams with the two opposite charge-flows, yielding after simple calculations

$$T_8 + \tilde{T}_8 = \text{[Diagram 6]} + \text{[Diagram 7]} = 0. \quad (4.117)$$

We have then check explicitly that every matter triangle does indeed vanish, either exactly or with respect to their (reversed matter flow) twin diagrams. This completes the perturbative leading order proof that the generalized Furry theorem holds in SQED<sub>3</sub> withing the DRED scheme, and therefore as subcases, also in QED<sub>3</sub> and bQED<sub>3</sub>. It means that every diagram containing a matter triangle can be set to zero in gQED<sub>3</sub>, *i.e.*, in SQED<sub>3</sub>, QED<sub>3</sub> and bQED<sub>3</sub>.

Some prominent examples of diagrams that we can (thankfully) drop are the Aslamazov-Larkin type diagrams in QED, *i.e.*,

$$\text{[Diagram 8]} + \text{[Diagram 9]} = 0. \quad (4.118)$$

From the definitions above, one can then generalize the Aslamazov-Larkin diagrams to gQED<sub>3</sub>, yielding

$$\text{[Diagram 10]} + \text{[Diagram 11]} = 0, \quad \text{where } \begin{cases} \text{[Wavy Line]} = \{\gamma, \lambda, \varepsilon\} \\ \text{[Arrow]} = \{\psi, \phi\} \end{cases} \quad (4.119)$$

provided that the vertices are allowed. These include a large number of diagrams that we can discard.

Taking into account of these various vanishing contributions tremendously reduces the number of diagrams that has to be computed at NLO. Indeed, as we shall see in the following, it ensures that up to NLO, not a single diagram of three-loop type needs to be computed. This is crucial because the three-loop master integrals with half integer indices are still unknown and are a big challenge to compute due to the inherent branch-cut structure of the integrals, that results into intricate hypergeometric functions and transcendental numbers (Catalan number, Clausen function etc...), see, *e.g.*, [331, 332].

Moreover, the generalized Furry theorem at LO also guarantees that matter loops are connected by simple chains of force field propagators, like in the simpler QED<sub>3</sub> case, in accordance with our starting assumption, ensuring that the large- $N_f$  expansion is reliable. We can now go forward and proceed with the NLO computations.

#### 4.4.4 Gauge-multiplet polarizations at NLO

In this section, we compute the NLO polarizations of the gauge multiplet, *i.e.*, for the photon, the  $\varepsilon$ -scalar and the photino at NLO in the  $1/N_f$  expansion, *i.e.*, at  $O(1/N_f^0)$ . We will show that all of these polarizations are finite and gauge invariant for gQED<sub>3</sub>. In the following, we shall use the shorthand notation for the polarization results

$$\Pi_{2X}^{(y)}(p^2) = \frac{e^2}{2(n+2S)p_E} \left( \frac{\bar{\mu}^2}{-p^2} \right)^{2\varepsilon} \tilde{\Pi}_{2X}^{(y)}, \quad \forall X \in \{\gamma, \varepsilon, \lambda\}. \quad (4.120)$$

#### Photon polarization at NLO

We first consider the NLO correction to the photon polarization that consists of 20 Feynman diagrams labeled  $(a, b, \dots, t)$ . Taking into account of the fact that mirror conjugate graphs take the same value, we are left with 11 distinct graphs to evaluate. This can be done exactly for all the diagrams, following the same procedure as for the one-loop case. Their expressions read

$$\frac{1}{2} \times \text{Diagram (a)} : \tilde{\Pi}_{2\gamma}^{(a)} = -\frac{4S(2+\xi)}{\pi^2} + O(\varepsilon), \quad (4.121a)$$

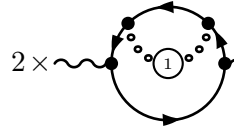
$$4 \times \text{Diagram (b)} : \tilde{\Pi}_{2\gamma}^{(bcde)} = \frac{16S}{3\pi^2} \left( \frac{1}{\varepsilon} + \frac{19}{3} + \frac{3\xi}{2} \right) + O(\varepsilon), \quad (4.121b)$$

$$2 \times \text{Diagram (c)} : \tilde{\Pi}_{2\gamma}^{(fg)} = -\frac{2S}{3\pi^2} \left( \frac{8-3\xi}{\varepsilon} + \frac{128}{3} - 9\xi \right) + O(\varepsilon), \quad (4.121c)$$

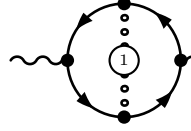
$$\text{Diagram (d)} : \tilde{\Pi}_{2\gamma}^{(h)} = -\frac{2S}{\pi^2} \left( \frac{\xi}{\varepsilon} + \frac{70}{9} - 3\zeta_2 + 5\xi \right) + O(\varepsilon), \quad (4.121d)$$

$$2 \times \text{Diagram (e)} : \tilde{\Pi}_{2\gamma}^{(ij)} = -\frac{n}{3\pi^2} \left( \frac{2-3\xi}{\varepsilon} + \frac{14}{3} - 6\xi \right) + O(\varepsilon), \quad (4.121e)$$

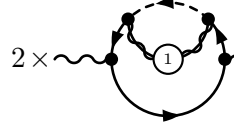
$$\text{Diagram (f)} : \tilde{\Pi}_{2\gamma}^{(k)} = \frac{n}{3\pi^2} \left( \frac{2-3\xi}{\varepsilon} - \frac{32}{3} + 9\zeta_2 - 6\xi \right) + O(\varepsilon), \quad (4.121f)$$



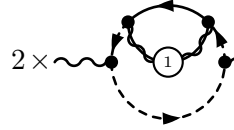
$$2 \times \text{diagram} : \tilde{\Pi}_{2\gamma}^{(lm)} = \frac{4S\mathcal{E}}{3\pi^2} + \mathcal{O}(\varepsilon), \quad (4.121g)$$



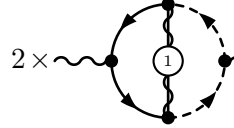
$$\text{diagram} : \tilde{\Pi}_{2\gamma}^{(n)} = -\frac{4S\mathcal{E}}{3\pi^2} + \mathcal{O}(\varepsilon), \quad (4.121h)$$



$$2 \times \text{diagram} : \tilde{\Pi}_{2\gamma}^{(op)} = \frac{2nS}{3\pi^2} \left( \frac{1}{\varepsilon} + \frac{13}{3} \right) + \mathcal{O}(\varepsilon), \quad (4.121i)$$



$$2 \times \text{diagram} : \tilde{\Pi}_{2\gamma}^{(qr)} = \frac{2nS}{3\pi^2} \left( \frac{1}{\varepsilon} + \frac{19}{3} \right) + \mathcal{O}(\varepsilon), \quad (4.121j)$$



$$2 \times \text{diagram} : \tilde{\Pi}_{2\gamma}^{(st)} = -\frac{4nS}{3\pi^2} \left( \frac{1}{\varepsilon} + \frac{11}{3} \right) + \mathcal{O}(\varepsilon). \quad (4.121k)$$

Summing all the contributions (4.121), all poles cancel, and the final result is finite, reading

$$\tilde{\Pi}_{2\gamma} = \frac{1}{18\pi^2} \left( (40S - 92 + 9\pi^2)n - 2(164 - 9\pi^2)S \right) + \mathcal{O}(\varepsilon). \quad (4.122)$$

Several remarks are in order here. First, the  $\varepsilon$ -scalars does not contribute (the corresponding tracking factor  $\mathcal{E}$  is absent) because the contributions  $\tilde{\Pi}_{2lm}^\gamma$  and  $\tilde{\Pi}_{2n}^\gamma$  cancel each others. Second, the result is completely gauge invariant, providing a strong check on our result. Lastly, the finiteness of the results ensure that the theory is still standing at NLO, *i.e.*, the coupling does not renormalize.

Since the NLO result is finite and has the same form as the LO one (4.76), we can write the photon polarization in the form

$$\Pi_\gamma(p^2) = \Pi_{1\gamma}(p^2) \left[ 1 + \frac{C_\gamma}{N_f} + \mathcal{O}(1/N_f^2) \right], \quad \text{recalling} \quad \Pi_{1\gamma}(p^2) = -\frac{(n+2S)N_f e^2}{16p_E}, \quad (4.123)$$

and where the interaction correction coefficient to the photon polarization reads

$$C_\gamma = \frac{4n(92 - 9\pi^2)}{9(n+2S)^2\pi^2} + \frac{8(164 - 20n - 9\pi^2)S}{9(n+2)^2\pi^2}. \quad (4.124)$$

In the different cases of interest, *i.e.*, SQED<sub>3</sub> ( $S=1$ ,  $n=2$ ), QED<sub>3</sub> ( $S=0$ ,  $n=2$ ) and bQED<sub>3</sub> ( $S=1$ ,  $n=0$ ), it yields the correction coefficients

$$C_\gamma^{\text{SQED}_3} = \frac{12 - \pi^2}{\pi^2}, \quad C_\gamma^{\text{QED}_3} = \frac{2(92 - 9\pi^2)}{9\pi^2}, \quad C_\gamma^{\text{bQED}_3} = \frac{2(164 - 9\pi^2)}{9\pi^2}. \quad (4.125)$$

As advertised in the previous Furry theorem section, 4.4.3, it turns out that all the diagrams considered are of two-loop type. Indeed, since we are in the large- $N_f$  expansion, higher-loop diagrams could have contributions at the same order in  $1/N_f$ . However, this is fortunately not the case. As a proof, we have explicitly checked that, up to NLO, no three-loop diagram contributes to the photon polarization, either because they contain a vanishing contribution, see section 4.4.3 or because they are of order  $1/N_f^2$  or higher. This required the check of 361 diagrams in an automated way. This has been done by generating the expressions for each diagram and then computing only what is the order in,  $1/N_f$  as well detecting subdiagram expressions that vanish because of the generalized Furry's theorem.

**$\varepsilon$ -scalar polarization at NLO**

We now consider the NLO correction to the  $\varepsilon$ -scalar polarization that consists of 9 Feynman diagrams labeled  $(a, b, \dots, i)$ . Taking into account of the fact that mirror conjugate graphs take the same value, we are left with 6 distinct graphs to evaluate. This can be done exactly for all the diagrams and reads

$$\frac{1}{2} \times \text{diagram (a)} : \tilde{\Pi}_{2\varepsilon}^{(a)} = -\frac{8S\mathcal{E}}{\pi^2} + \mathcal{O}(\varepsilon), \quad (4.126a)$$

$$2 \times \text{diagram (bc)} : \tilde{\Pi}_{2\varepsilon}^{(bc)} = \frac{8S\mathcal{E}}{3\pi^2} + \mathcal{O}(\varepsilon), \quad (4.126b)$$

$$\text{diagram (d)} : \tilde{\Pi}_{2\varepsilon}^{(d)} = \frac{8S\mathcal{E}}{\pi^2} \left( \frac{1}{\varepsilon} + 2 \right) + \mathcal{O}(\varepsilon), \quad (4.126c)$$

$$2 \times \text{diagram (ef)} : \tilde{\Pi}_{2\varepsilon}^{(ef)} = -\frac{4S\mathcal{E}}{3\pi^2} \left( \frac{2-3\xi}{\varepsilon} + \frac{20}{3} - 9\xi \right) + \mathcal{O}(\varepsilon), \quad (4.126d)$$

$$\text{diagram (g)} : \tilde{\Pi}_{2\varepsilon}^{(g)} = -\frac{4S\mathcal{E}}{\pi^2} \left( \frac{2+\xi}{\varepsilon} + 10 - 3\zeta_2 + 3\xi \right) + \mathcal{O}(\varepsilon), \quad (4.126e)$$

$$2 \times \text{diagram (hi)} : \tilde{\Pi}_{2\varepsilon}^{(hi)} = \frac{8S\mathcal{E}}{3\pi^2} \left( \frac{1}{\varepsilon} + \frac{16}{3} \right) + \mathcal{O}(\varepsilon). \quad (4.126f)$$

Summing all the contributions yields the complete result

$$\tilde{\Pi}_{2\varepsilon} = -\frac{2(12-\pi^2)S\mathcal{E}}{\pi^2} + \mathcal{O}(\varepsilon), \quad (4.127)$$

which is, as expected, completely gauge invariant and finite, providing a strong check on our result. Similarly to the photon case, we can rewrite the LO+NLO  $\varepsilon$ -scalar polarization as

$$\Pi_\varepsilon(p^2) = \Pi_{1\varepsilon}(p^2) \left[ 1 + \frac{C_\varepsilon}{N_f} + \mathcal{O}(1/N_f^2) \right], \quad \text{recalling} \quad \Pi_{1\varepsilon}(p^2) = -\frac{\mathcal{E}SN_f e^2}{4p_E}, \quad (4.128)$$

and where the interaction correction coefficient to the  $\varepsilon$ -scalar polarization reads

$$C_\varepsilon = \frac{(12-\pi^2)\mathcal{E}S}{\pi^2}. \quad (4.129)$$

Note that in the only case of interest here, SQED<sub>3</sub> ( $S=1$ ,  $n=2$ ), this result trivially reads

$$C_\varepsilon^{\text{SQED}_3} = \frac{12-\pi^2}{\pi^2}, \quad (4.130)$$

which is exactly the same result as the photon correction coefficient in the SQED<sub>3</sub> case, see (4.125), as expected from such a supersymmetric gauge invariant quantity.

Again, we have explicitly checked that, none of the 147 three-loop diagrams contributes to the  $\varepsilon$ -scalar polarization due to the generalized Furry theorem and the resummed one-loop contributions.



### Photino polarization at NLO

The last polarization to consider is the NLO correction to the photino polarization that consists of 14 Feynman diagrams labeled  $(a,b,\dots,n)$ . Taking into account of the fact that mirror conjugate graphs take the same value, we are left with 7 distinct graphs to evaluate. This can be done exactly for all the diagrams and reads

$$2 \times \text{Diagram (a)} : \tilde{\Pi}_{2\lambda}^{(ab)} = -\frac{2S}{3\pi^2} \left( \frac{8-3\xi}{\varepsilon} + \frac{80}{3} - 3\xi \right) + \mathcal{O}(\varepsilon), \quad (4.131a)$$

$$2 \times \text{Diagram (b)} : \tilde{\Pi}_{2\lambda}^{(cd)} = -\frac{2S}{3\pi^2} \left( \frac{2-3\xi}{\varepsilon} + \frac{8}{3} - 3\xi \right) + \mathcal{O}(\varepsilon), \quad (4.131b)$$

$$2 \times \text{Diagram (c)} : \tilde{\Pi}_{2\lambda}^{(ef)} = -\frac{4S}{\pi^2} \left( \frac{\xi}{\varepsilon} + 6 - 3\zeta_2 + \xi \right) + \mathcal{O}(\varepsilon), \quad (4.131c)$$

$$2 \times \text{Diagram (d)} : \tilde{\Pi}_{2\lambda}^{(gh)} = \frac{4S\mathcal{E}}{3\pi^2} + \mathcal{O}(\varepsilon), \quad (4.131d)$$

$$2 \times \text{Diagram (e)} : \tilde{\Pi}_{2\lambda}^{(ij)} = \frac{4S}{3\pi^2} \left( \frac{1}{\varepsilon} + \frac{13}{3} \right) + \mathcal{O}(\varepsilon), \quad (4.131e)$$

$$2 \times \text{Diagram (f)} : \tilde{\Pi}_{2\lambda}^{(kl)} = \frac{4S}{3\pi^2} \left( \frac{1}{\varepsilon} + \frac{10}{3} \right) + \mathcal{O}(\varepsilon), \quad (4.131f)$$

$$2 \times \text{Diagram (g)} : \tilde{\Pi}_{2\lambda}^{(mn)} = \frac{4S}{\pi^2} \left( \frac{1}{\varepsilon} + 2 \right) + \mathcal{O}(\varepsilon). \quad (4.131g)$$

Summing all the contributions yields the gauge invariant and finite result

$$\tilde{\Pi}_{2\lambda} = \frac{2S(3\pi^2 - 38 + 2\mathcal{E})}{3\pi^2} + \mathcal{O}(\varepsilon). \quad (4.132)$$

Note that this result depends non trivially on the parameter  $\mathcal{E}$  which implies that the  $\varepsilon$ -scalars are crucial here to ensure that the result is correct, as we will see in the following. The LO+NLO result for the photino polarization can again be written in the form

$$\Pi_\lambda(p^2) = \Pi_{1\lambda}(p^2) \left[ 1 + \frac{C_\lambda}{N_f} + \mathcal{O}(1/N_f^2) \right], \quad \text{recalling} \quad \Pi_{1\lambda}(p^2) = -\frac{SN_f e^2}{4p_E}, \quad (4.133)$$

where the interaction coefficient to the photino polarization reads

$$C_\lambda = \frac{(38 - 2\mathcal{E} - 3\pi^2)S}{3\pi^2}. \quad (4.134)$$

Note that this result is only of interest in the case of SQED<sub>3</sub> ( $S=1$ ,  $n=2$ ), where it reduces to

$$C_\lambda^{\text{SQED}_3} = \frac{12 - \pi^2}{\pi^2}, \quad (4.135)$$

provided that we allow for the  $\varepsilon$ -scalars ( $\mathcal{E}=1$ ). This is again the same result as for the photon and the  $\varepsilon$ -scalar correction coefficient in SQED<sub>3</sub>. Therefore, we have explicitly checked that, up to NLO,

$$\Pi_\gamma^{\text{SQED}_3} = \Pi_\varepsilon^{\text{SQED}_3} = \Pi_\lambda^{\text{SQED}_3}, \quad (4.136)$$

meaning that all polarization of the gauge multiplet are equal, as expected from supersymmetry for such gauge-invariant and finite quantities.

Again, we have explicitly checked that, none of the 234 three-loop diagrams contribute to the photino polarization due to the generalized Furry theorem and the resummed one-loop contributions.

### IR-softened gauge multiplet at NLO

We are now in a position to compute the NLO softened propagators, *i.e.*, of order  $1/N_f^2$ . Their expressions read

$$\hat{D}_{2AA}^{\mu\nu}(p) = \mu \text{---} \textcircled{2} \text{---} \nu = \frac{-16iC_\gamma}{(n+2S)N_f^2 e^2} \frac{\hat{d}^{\mu\nu}(p)}{p_E}, \quad (4.137a)$$

$$\bar{D}_{2AA}^{\mu\nu}(p) = \mu \text{---} \textcircled{2} \text{---} \nu = \frac{-4i\mathcal{E}S C_\varepsilon}{N_f^2 e^2} \frac{\bar{g}^{\mu\nu}}{p_E}, \quad (4.137b)$$

$$D_{2\lambda\bar{\lambda}}(p) = \text{---} \textcircled{2} \text{---} = \frac{4iS C_\lambda}{N_f^2 e^2} \frac{\not{p}}{p_E}. \quad (4.137c)$$

where we took the infrared limit  $p_E \ll e^2 N_f$ , as advertised in (4.34). Interestingly, we observe the nice property that the LO (4.92) and NLO (4.137) softened gauge-multiplet propagators are simply related via their polarization correction coefficients, *i.e.*,

$$\hat{D}_{2AA}^{\mu\nu}(p) = -C_\gamma \times \hat{D}_{1AA}^{\mu\nu}(p)/N_f, \quad (4.138a)$$

$$\bar{D}_{2AA}^{\mu\nu}(p) = -C_\varepsilon \times \bar{D}_{1AA}^{\mu\nu}(p)/N_f, \quad (4.138b)$$

$$D_{2\lambda\bar{\lambda}}(p) = -C_\lambda \times D_{1\lambda\bar{\lambda}}(p)/N_f, \quad (4.138c)$$

where the tensorial structure of the photon is still given by  $\hat{d}^{\mu\nu}(p) = \hat{g}^{\mu\nu} - (1-\xi)(\hat{p}^\mu \hat{p}^\nu / p^2)$  thanks to the use of the non-local gauge, see (4.56).

### 4.4.5 Matter-multiplet self-energies at NLO

In this section, we compute the NLO self-energies of the matter multiplet, *i.e.*, for the electron and the selectron at NLO in the  $1/N_f$  expansion, *i.e.*, at  $\mathcal{O}(1/N_f^2)$  in gQED<sub>3</sub>. In the following, we shall use the shorthand notation for the self-energies

$$\Sigma_{2z}^{X(y)}(p^2) = \frac{4}{(n+2S)^2 N_f^2} \left( \frac{\bar{\mu}^2}{-4p^2} \right)^{2\varepsilon} \tilde{\Sigma}_{2z}^{X(y)}, \quad \forall X \in \{\psi, \phi\}, z \in \{p, m\}. \quad (4.139)$$

#### Electron self-energy at NLO

We first consider the NLO correction to the electron self-energy that consists of 15 two-loop and 3 one-loop Feynman diagrams, all together labeled  $(a, b, \dots, r)$ . Indeed, contributions of the same order

in  $N_f$  with different loop order are possible now that we have at our disposal both the LO (4.92) and NLO (4.137) softened propagators. Taking into account of the fact that mirror conjugate graphs take the same value, we are left with a total of 16 distinct graphs to evaluate. For each one of them, we extract both the momentum and mass parts using the parametrization (4.61a). All computations done, we obtain the results

$$2 \times \begin{array}{c} \text{Diagram (a)} \\ \text{Diagram (b)} \end{array} : \begin{cases} \tilde{\Sigma}_{2p}^{\psi(ab)} = \frac{16S}{9\pi^4} \left( \frac{1-3\xi}{\varepsilon^2} + \frac{13-60\xi}{3\varepsilon} \right) + O(\varepsilon^0) \\ \tilde{\Sigma}_{2m}^{\psi(ab)} = \frac{8S}{3\pi^4} \left( \frac{2+\xi}{\varepsilon^2} + \frac{50+31\xi}{3\varepsilon} \right) + O(\varepsilon^0) \end{cases}, \quad (4.140a)$$

$$\begin{array}{c} \text{Diagram (c)} \\ \text{Diagram (d)} \end{array} : \begin{cases} \tilde{\Sigma}_{2p}^{\psi(c)} = -\frac{4}{9\pi^4} \left( \frac{(2-3\xi)^2}{\varepsilon^2} + \frac{64-3\xi(56-39\xi)}{3\varepsilon} \right) + O(\varepsilon^0) \\ \tilde{\Sigma}_{2m}^{\psi(c)} = -\frac{4}{3\pi^4} \left( \frac{(2+\xi)(2-3\xi)}{\varepsilon^2} + \frac{112-\xi(40+63\xi)}{3\varepsilon} \right) + O(\varepsilon^0) \end{cases}, \quad (4.140b)$$

$$2 \times \begin{array}{c} \text{Diagram (e)} \\ \text{Diagram (f)} \end{array} : \begin{cases} \tilde{\Sigma}_{2p}^{\psi(de)} = -\frac{16S\mathcal{E}(2+3\xi)}{9\pi^4\varepsilon} + O(\varepsilon^0) \\ \tilde{\Sigma}_{2m}^{\psi(de)} = \frac{32S\mathcal{E}(2+\xi)}{3\pi^4\varepsilon} + O(\varepsilon^0) \end{cases}, \quad (4.140c)$$

$$\begin{array}{c} \text{Diagram (g)} \\ \text{Diagram (h)} \end{array} : \begin{cases} \tilde{\Sigma}_{2p}^{\psi(f)} = \frac{16S\mathcal{E}}{3\pi^4\varepsilon} + O(\varepsilon^0) \\ \tilde{\Sigma}_{2m}^{\psi(f)} = -\frac{16S\mathcal{E}}{\pi^4\varepsilon} + O(\varepsilon^0) \end{cases}, \quad (4.140d)$$

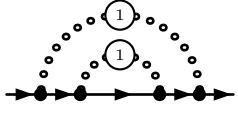
$$\begin{array}{c} \text{Diagram (i)} \\ \text{Diagram (j)} \end{array} : \begin{cases} \tilde{\Sigma}_{2p}^{\psi(g)} = \frac{4S}{3\pi^4} \left( \frac{2}{\varepsilon^2} + \frac{17}{\varepsilon} \right) + O(\varepsilon^0) \\ \tilde{\Sigma}_{2m}^{\psi(g)} = -\frac{4S}{\pi^4\varepsilon} + O(\varepsilon^0) \end{cases}, \quad (4.140e)$$

$$\begin{array}{c} \text{Diagram (k)} \\ \text{Diagram (l)} \end{array} : \begin{cases} \tilde{\Sigma}_{2p}^{\psi(h)} = \frac{2}{9\pi^4} \left( \frac{(2-3\xi)^2}{\varepsilon^2} + \frac{2(2-3\xi)(16-21\xi)}{3\varepsilon} \right) + O(\varepsilon^0) \\ \tilde{\Sigma}_{2m}^{\psi(h)} = \frac{2}{3\pi^4} \left( \frac{(2+\xi)(10-3\xi)}{\varepsilon^2} + \frac{2(232+86\xi-27\xi^2)}{3\varepsilon} \right) + O(\varepsilon^0) \end{cases}, \quad (4.140f)$$

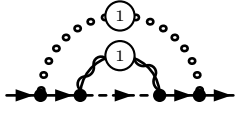
$$\begin{array}{c} \text{Diagram (m)} \\ \text{Diagram (n)} \end{array} : \begin{cases} \tilde{\Sigma}_{2p}^{\psi(i)} = -\frac{4S\mathcal{E}(2-3\xi)}{9\pi^4\varepsilon} + O(\varepsilon^0) \\ \tilde{\Sigma}_{2m}^{\psi(i)} = \frac{4S\mathcal{E}(2+\xi)}{3\pi^4\varepsilon} + O(\varepsilon^0) \end{cases}, \quad (4.140g)$$

$$\begin{array}{c} \text{Diagram (o)} \\ \text{Diagram (p)} \end{array} : \begin{cases} \tilde{\Sigma}_{2p}^{\psi(j)} = -\frac{4S}{9\pi^4} \left( \frac{2-3\xi}{\varepsilon^2} + \frac{44-63\xi}{3\varepsilon} \right) + O(\varepsilon^0) \\ \tilde{\Sigma}_{2m}^{\psi(j)} = -\frac{8S}{3\pi^4} \left( \frac{2+\xi}{\varepsilon^2} + \frac{56+31\xi}{3\varepsilon} \right) + O(\varepsilon^0) \end{cases}, \quad (4.140h)$$

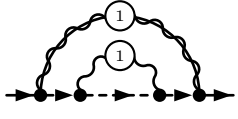
$$\begin{array}{c} \text{Diagram (q)} \\ \text{Diagram (r)} \end{array} : \begin{cases} \tilde{\Sigma}_{2p}^{\psi(k)} = -\frac{4S\mathcal{E}(2-3\xi)}{9\pi^4\varepsilon} + O(\varepsilon^0) \\ \tilde{\Sigma}_{2m}^{\psi(k)} = \frac{4S\mathcal{E}(10-3\xi)}{3\pi^4\varepsilon} + O(\varepsilon^0) \end{cases}, \quad (4.140i)$$



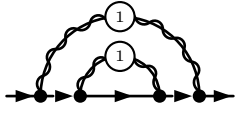
$$: \left\{ \begin{array}{l} \tilde{\Sigma}_{2p}^{\psi(l)} = \frac{8\mathcal{E}S}{9\pi^4} + \mathcal{O}(\varepsilon^1) \\ \tilde{\Sigma}_{2m}^{\psi(l)} = \frac{8\mathcal{E}S}{3\pi^4} + \mathcal{O}(\varepsilon^1) \end{array} \right\}, \quad (4.140j)$$



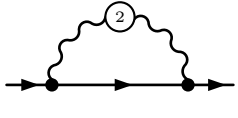
$$: \left\{ \begin{array}{l} \tilde{\Sigma}_{2p}^{\psi(m)} = \frac{8S\mathcal{E}}{9\pi^4\varepsilon} + \mathcal{O}(\varepsilon^0) \\ \tilde{\Sigma}_{2m}^{\psi(m)} = -\frac{16S\mathcal{E}}{3\pi^4\varepsilon} + \mathcal{O}(\varepsilon^0) \end{array} \right\}, \quad (4.140k)$$



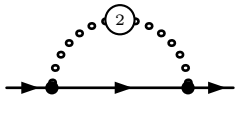
$$: \left\{ \begin{array}{l} \tilde{\Sigma}_{2p}^{\psi(n)} = -\frac{4S}{9\pi^2} \left( \frac{8-3\xi}{\varepsilon^2} + \frac{7(32-9\xi)}{3\varepsilon} \right) + \mathcal{O}(\varepsilon^0), \\ \tilde{\Sigma}_{2m}^{\psi(n)} = 0 \end{array} \right\}, \quad (4.140l)$$



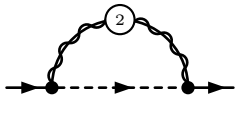
$$: \left\{ \begin{array}{l} \tilde{\Sigma}_{2p}^{\psi(o)} = \frac{8S}{9\pi^4} \left( \frac{1}{\varepsilon^2} + \frac{31}{3\varepsilon} \right) + \mathcal{O}(\varepsilon^0), \\ \tilde{\Sigma}_{2m}^{\psi(o)} = 0 \end{array} \right\}, \quad (4.140m)$$



$$: \left\{ \begin{array}{l} \tilde{\Sigma}_{2p}^{\psi(p)} = -\frac{2(2-3\xi)}{\pi^4\varepsilon} (n+2S)\zeta_2 C_\gamma + \mathcal{O}(\varepsilon^0), \\ \tilde{\Sigma}_{2m}^{\psi(p)} = -\frac{6(2+\xi)}{\pi^4\varepsilon} (n+2S)\zeta_2 C_\gamma + \mathcal{O}(\varepsilon^0) \end{array} \right\}, \quad (4.140n)$$



$$: \left\{ \begin{array}{l} \tilde{\Sigma}_{2p}^{\psi(q)} = \frac{4\mathcal{E}S}{\pi^4} \zeta_2 C_\varepsilon + \mathcal{O}(\varepsilon^1) \\ \tilde{\Sigma}_{2m}^{\psi(q)} = -\frac{12\mathcal{E}S}{\pi^4} \zeta_2 C_\varepsilon + \mathcal{O}(\varepsilon^1) \end{array} \right\}, \quad (4.140o)$$



$$: \left\{ \begin{array}{l} \tilde{\Sigma}_{2p}^{\psi(r)} = \frac{4S}{\pi^4\varepsilon} \zeta_2 C_\lambda + \mathcal{O}(\varepsilon^0) \\ \tilde{\Sigma}_{2m}^{\psi(r)} = 0 \end{array} \right\}. \quad (4.140p)$$

Note that the computation of the three last diagrams leads to the trivial result that they are simply their LO equivalents times their corresponding correction coefficient with a sign, *i.e.*, a factor  $-C_x/N_f$ , thanks to the equality (4.138). Moreover,  $C_\varepsilon$  will not contribute to the anomalous dimensions, because the diagram (4.140o)  $\tilde{\Sigma}_{p2}^{\psi(q)}$  is finite. Similarly,  $C_\lambda$  does not contribute to the mass anomalous dimension because the diagram  $\tilde{\Sigma}_{m2}^{\psi(r)}$  is exactly zero. Again, we also have explicitly checked that, none of the 390 three-loop diagrams contributes to the electron self-energy at NLO.

Summing all the NLO contributions (4.140), yields the following results

$$\Sigma_p^\psi = -\frac{2(S-\bar{\xi})}{RN_f\varepsilon} - \frac{2(S-\bar{\xi})^2}{R^2N_f^2\varepsilon^2} - \frac{1}{3R^2N_f^2\varepsilon} \left[ 4 + (77+6\mathcal{E})S + 4(1-(19+3\mathcal{E})S+6\bar{\xi})\bar{\xi} - 6R(SC_\lambda - \bar{\xi}C_\gamma) \right] + \mathcal{O}(\varepsilon^0), \quad (4.141a)$$

$$\Sigma_m^\psi = \frac{3(2+\xi)}{RN_f\varepsilon} + \frac{9(2+\xi)^2}{2R^2N_f^2\varepsilon^2} + \frac{1}{R^2N_f^2\varepsilon} \left[ 220 - 21S - 4(29-4\bar{\xi})\bar{\xi} + 3(2+\xi)(6\mathcal{E}S - RC_\gamma) \right] + \mathcal{O}(\varepsilon^0), \quad (4.141b)$$

where we introduced the useful notation

$$\bar{\xi} = (2-3\xi)/2, \quad R = A(-4p^2/\bar{\mu}^2)^\varepsilon, \quad A = 3\pi^2(n+2S)/4. \quad (4.142)$$

We can now compute the renormalization functions up to NLO for the electron, reading<sup>6</sup>

$$Z_\psi = 1 - \frac{2(S - \bar{\xi})}{A\mu^{2\varepsilon}N_f\varepsilon} + \frac{2(S - 2\bar{\xi}S + \bar{\xi}^2)}{A^2\mu^{4\varepsilon}N_f^2\varepsilon^2} - \frac{4 + (29 - 6\varepsilon)S - 6A\mu^{2\varepsilon}(SC_\lambda - \bar{\xi}C_\gamma)}{3A^2\mu^{4\varepsilon}N_f^2\varepsilon} + \mathcal{O}(1/N_f^3), \quad (4.143a)$$

$$Z_{m_\psi} = 1 - \frac{2(4 - S)}{A\mu^{2\varepsilon}N_f\varepsilon} + \frac{2(16 - 7S)}{A^2\mu^{4\varepsilon}N_f^2\varepsilon^2} - \frac{2(16 - (46 - 3\varepsilon)S + 3A\mu^{2\varepsilon}(SC_\lambda - 4C_\gamma))}{3A^2\mu^{4\varepsilon}N_f^2\varepsilon} + \mathcal{O}(1/N_f^3). \quad (4.143b)$$

From these, the anomalous dimensions read

$$\gamma_\psi = \frac{4(S - \bar{\xi})}{AN_f} + \frac{4}{3A^2N_f^2} \left[ 4 + (29 - 6\varepsilon)S - 3A(SC_\lambda - \bar{\xi}C_\gamma) \right] + \mathcal{O}(1/N_f^3), \quad (4.144a)$$

$$\gamma_{m_\psi} = \frac{4(4 - S)}{AN_f} + \frac{8}{3A^2N_f^2} \left[ 16 - (46 - 3\varepsilon)S + \frac{3}{2}A(SC_\lambda - 4C_\gamma) \right] + \mathcal{O}(1/N_f^3). \quad (4.144b)$$

We will discuss these results once the anomalous dimensions of the superpartner are computed.

### Selectron self-energy at NLO

We next consider the NLO correction to the selectron self-energy that consist into 15 two-loop and 2 one-loop Feynman diagrams labeled  $(a, b, \dots, p)$ . Taking into account of the fact that mirror conjugate graphs take the same value, we are left with a total of 14 distinct graphs to evaluate. For each of them, we extract both the momentum and mass parts using the parametrization (4.61b). All computations done, we obtain the results

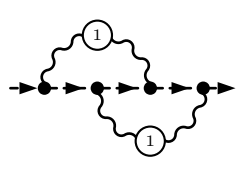
$$\frac{1}{2} \times \text{Diagram (a)} : \begin{cases} \tilde{\Sigma}_{2p}^{\phi(a)} = -\frac{4S(4 - \xi(4 - 3\xi))}{3\pi^4\varepsilon} + \mathcal{O}(\varepsilon^0) \\ \tilde{\Sigma}_{2m}^{\phi(a)} = -\frac{4S(4 - \xi(4 - 3\xi))}{\pi^4\varepsilon} + \mathcal{O}(\varepsilon^0) \end{cases}, \quad (4.145a)$$

$$\frac{1}{2} \times \text{Diagram (b)} : \begin{cases} \tilde{\Sigma}_{2p}^{\phi(b)} = -\frac{8\varepsilon S}{3\pi^4} + \mathcal{O}(\varepsilon^1) \\ \tilde{\Sigma}_{2m}^{\phi(b)} = -\frac{8\varepsilon S}{\pi^4} + \mathcal{O}(\varepsilon^1) \end{cases}, \quad (4.145b)$$

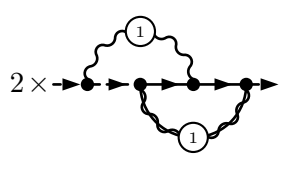
$$2 \times \text{Diagram (c)} : \begin{cases} \tilde{\Sigma}_{2p}^{\phi(cd)} = -\frac{16S}{9\pi^2} \left( \frac{2(4 - 3\xi)}{\varepsilon^2} + \frac{(4 - 3\xi)(32 + 9\xi)}{3\varepsilon} \right) + \mathcal{O}(\varepsilon^0) \\ \tilde{\Sigma}_{2m}^{\phi(cd)} = -\frac{16S}{3\pi^4} \left( \frac{2\xi}{\varepsilon^2} + \frac{48 + \xi(32 - 9\xi)}{3\varepsilon} \right) + \mathcal{O}(\varepsilon^0) \end{cases}, \quad (4.145c)$$

$$\text{Diagram (e)} : \begin{cases} \tilde{\Sigma}_{2p}^{\phi(e)} = -\frac{128S}{9\pi^4} \left( \frac{1}{\varepsilon^2} + \frac{14 + 9\xi}{3\varepsilon} \right) + \mathcal{O}(\varepsilon) \\ \tilde{\Sigma}_{2m}^{\phi(e)} = -\frac{256S(1 - \xi)}{3\pi^4\varepsilon} + \mathcal{O}(\varepsilon^0) \end{cases}, \quad (4.145d)$$

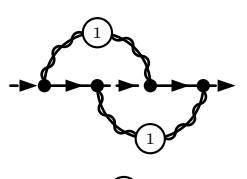
<sup>6</sup>The factors  $\mu^{2\varepsilon}$  appear in multiple places and are kept unexpanded in power of epsilon. This is to emphasize that the last terms of the expressions, containing the factors  $C_x$ , have an unusual  $\mu^{2\varepsilon}$  dependency because of the one-loop diagrams that are of the same order ( $1/N_f^2$ ) than the two-loop diagrams. In that sense, it is more simple to keep the  $\mu$  dependency to later take the derivative with respect to  $\mu$  in order to extract the anomalous dimension, *i.e.*, using the definition (4.66) instead of (4.68). If one wants to hide the factors  $\mu^{2\varepsilon}$  it is possible to use the natural notation  $N_{f_r} = N_f\mu^{2\varepsilon}$ , this would make the LO term  $\sim 1/N_{f_r}$ , and the NLO term would be a combination of a term  $\sim 1/N_{f_r}$ , and weird terms  $\sim C_x/(N_f N_{f_r})$ , so that later one should take the derivative with respect to  $N_{f_r}$ , in order to extract the anomalous dimension, *i.e.*, using (4.68).



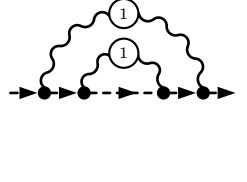
$$: \left\{ \begin{array}{l} \tilde{\Sigma}_{2p}^{\phi(f)} = \frac{4S}{3\pi^4} \left( \frac{8-3\xi}{\varepsilon^2} + \frac{64+9\xi(80-17\xi)}{18\varepsilon} \right) + O(\varepsilon^0) \\ \tilde{\Sigma}_{2m}^{\phi(f)} = \frac{4\xi S}{\pi^4} \left( \frac{\xi}{\varepsilon^2} + \frac{32-13\xi}{2\varepsilon} \right) + O(\varepsilon^0) \end{array} \right. , \quad (4.145e)$$



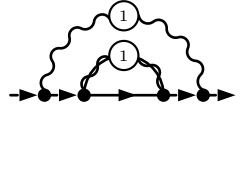
$$2 \times : \left\{ \begin{array}{l} \tilde{\Sigma}_{2p}^{\phi(gh)} = \frac{8nS}{9\pi^4} \left( \frac{4-3\xi}{\varepsilon^2} + \frac{104-75\xi}{6\varepsilon} \right) + O(\varepsilon^0) \\ \tilde{\Sigma}_{2m}^{\phi(gh)} = \frac{4nS}{3\pi^4} \left( \frac{4\xi}{\varepsilon^2} + \frac{48+31\xi}{3\varepsilon} \right) + O(\varepsilon^0) \end{array} \right. , \quad (4.145f)$$



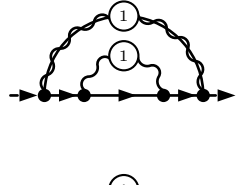
$$: \left\{ \begin{array}{l} \tilde{\Sigma}_{2p}^{\phi(i)} = \frac{4nS}{3\pi^4} \left( \frac{1}{\varepsilon^2} + \frac{15}{2\varepsilon} \right) + O(\varepsilon^0) \\ \tilde{\Sigma}_{2m}^{\phi(i)} = -\frac{4nS}{\pi^4} \left( \frac{1}{\varepsilon^2} + \frac{17}{2\varepsilon} \right) + O(\varepsilon^0) \end{array} \right. , \quad (4.145g)$$



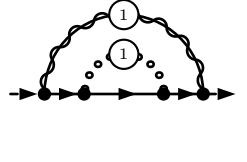
$$: \left\{ \begin{array}{l} \tilde{\Sigma}_{2p}^{\phi(j)} = \frac{2S}{9\pi^4} \left( \frac{(8-3\xi)^2}{\varepsilon^2} + \frac{(8-3\xi)(128+3\xi)}{3\varepsilon} \right) + O(\varepsilon^0) \\ \tilde{\Sigma}_{2m}^{\phi(j)} = \frac{2S}{3\pi^4} \left( \frac{(16-3\xi)\xi}{\varepsilon^2} + \frac{768-344\xi+45\xi^2}{3\varepsilon} \right) + O(\varepsilon^0) \end{array} \right. , \quad (4.145h)$$



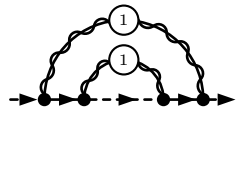
$$: \left\{ \begin{array}{l} \tilde{\Sigma}_{2p}^{\phi(k)} = -\frac{2nS}{9\pi^4} \left( \frac{8-3\xi}{\varepsilon^2} + \frac{152-27\xi}{3\varepsilon} \right) + O(\varepsilon^0) \\ \tilde{\Sigma}_{2m}^{\phi(k)} = \frac{2nS}{3\pi^4} \left( \frac{\xi}{\varepsilon^2} + \frac{48-17\xi}{3\varepsilon} \right) + O(\varepsilon^0) \end{array} \right. , \quad (4.145i)$$



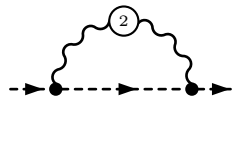
$$: \left\{ \begin{array}{l} \tilde{\Sigma}_{2p}^{\phi(l)} = -\frac{2nS}{9\pi^4} \left( \frac{2-3\xi}{\varepsilon^2} + \frac{44-63\xi}{3\varepsilon} \right) + O(\varepsilon^0) \\ \tilde{\Sigma}_{2m}^{\phi(l)} = \frac{2nS}{\pi^4} \left( \frac{6-\xi}{\varepsilon^2} + \frac{128-15\xi}{3\varepsilon} \right) + O(\varepsilon^0) \end{array} \right. , \quad (4.145j)$$



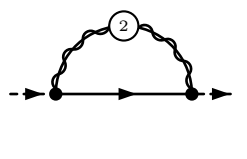
$$: \left\{ \begin{array}{l} \tilde{\Sigma}_{2p}^{\phi(m)} = \frac{4nS\mathcal{E}}{9\pi^4\varepsilon} + O(\varepsilon^0) \\ \tilde{\Sigma}_{2m}^{\phi(m)} = \frac{4nS\mathcal{E}}{\pi^4\varepsilon} + O(\varepsilon^0) \end{array} \right. , \quad (4.145k)$$



$$: \left\{ \begin{array}{l} \tilde{\Sigma}_{2p}^{\phi(n)} = \frac{4nS}{9\pi^4} \left( \frac{1}{\varepsilon^2} + \frac{28}{3\varepsilon} \right) + O(\varepsilon^0) \\ \tilde{\Sigma}_{2m}^{\phi(n)} = -\frac{4nS}{\pi^4} \left( \frac{1}{\varepsilon^2} + \frac{22}{3\varepsilon} \right) + O(\varepsilon^0) \end{array} \right. , \quad (4.145l)$$



$$: \left\{ \begin{array}{l} \tilde{\Sigma}_{2p}^{\phi(o)} = -\frac{(2+n)(8-3\xi)}{4\pi^4\varepsilon} \zeta_2 C_\gamma + O(\varepsilon^0) \\ \tilde{\Sigma}_{2m}^{\phi(o)} = -\frac{3(2+n)S\xi}{4\pi^4\varepsilon} \zeta_2 C_\gamma + O(\varepsilon^0) \end{array} \right. , \quad (4.145m)$$



$$: \left\{ \begin{array}{l} \tilde{\Sigma}_{2p}^{\phi(p)} = \frac{nS}{\pi^4\varepsilon} \zeta_2 C_\lambda + O(\varepsilon^0) \\ \tilde{\Sigma}_{2m}^{\phi(p)} = -\frac{3nS}{\pi^4\varepsilon} \zeta_2 C_\lambda + O(\varepsilon^0) \end{array} \right. . \quad (4.145n)$$

Again, note that the computation of the last two graph leads to the trivial results that they are simply the one-loop diagram result times the corresponding interaction correction coefficient with a sign  $-C_x$ ,

thanks to the identities (4.137). Interestingly,  $C_\varepsilon$  does not contribute at all to the selectron self-energy since there is no one-loop diagram containing an  $\varepsilon$ -scalar polarization at this order, due to the absence of a direct coupling between the selectron and the  $\varepsilon$ -scalar. Again, we also have explicitly checked that, none of the 297 three-loop diagrams contributes to the electron self-energy at NLO.

Summing all the contributions (4.145) reads

$$\Sigma_p^\phi = \frac{(6-n+2\bar{\xi})S}{RN_f\varepsilon} - \frac{(6-n+2\bar{\xi})^2S}{2R^2N_f^2\varepsilon^2} - \frac{S}{6R^2N_f^2\varepsilon} \left[ 8(85+28\bar{\xi}) - n(163+40\bar{\xi}) - 12\mathcal{E} - 6R(nC_\lambda - 2(3+\bar{\xi})C_\gamma) \right] + \mathcal{O}(\varepsilon^0), \quad (4.146a)$$

$$\Sigma_m^\phi = \frac{3(n+\xi)S}{RN_f\varepsilon} + \frac{9(n+\xi)^2S}{2R^2N_f^2\varepsilon^2} + \frac{3S}{2R^2N_f^2\varepsilon} \left[ 81n+12\mathcal{E} - 8(2+\bar{\xi})\bar{\xi} - 2R(nC_\lambda + \xi C_\gamma) \right] + \mathcal{O}(\varepsilon^0), \quad (4.146b)$$

where we again used the useful notation

$$\bar{\xi} = (2-3\xi)/2, \quad R = A(-4p^2/\bar{\mu}^2)^\varepsilon, \quad A = 3\pi^2(n+2S)/4. \quad (4.147)$$

We note that  $\varepsilon$ -scalars contribute to the self-energies in part from the polarization correction  $C_\lambda$  (this time for the selectron only) but not from  $C_\varepsilon$ , see (4.129). We can now compute the renormalization functions up to NLO for the selectron field and mass using the defining equations (4.65), reading

$$Z_\phi = 1 + \frac{(6-n+2\bar{\xi})S}{A\mu^{2\varepsilon}N_f\varepsilon} + \frac{(2(3+\bar{\xi})^2 - n(5+2\bar{\xi}))S}{A^2\mu^{4\varepsilon}N_f^2\varepsilon^2} - \frac{(8-12\mathcal{E}+29n-6A\mu^{2\varepsilon}(nC_\lambda-2(3+\bar{\xi})C_\gamma))S}{6A^2\mu^{4\varepsilon}N_f^2\varepsilon} + \mathcal{O}(1/N_f^3), \quad (4.148a)$$

$$Z_{m_\phi} = 1 - \frac{(4+n)S}{A\mu^{2\varepsilon}N_f\varepsilon} + \frac{(8+5n)S}{A^2\mu^{4\varepsilon}N_f^2\varepsilon^2} + \frac{2(28-15\mathcal{E}+7n+\frac{3}{2}A\mu^{2\varepsilon}(nC_\lambda+2C_\gamma))S}{3A^2\mu^{4\varepsilon}N_f^2\varepsilon} + \mathcal{O}(1/N_f^3). \quad (4.148b)$$

The factors  $\mu^{2\varepsilon}$  are discussed under equation (4.143). Using the definition of the anomalous dimensions (4.68), we derive the anomalous dimensions for the selectron field and mass, reading

$$\gamma_\phi = \frac{2(n-6-2\bar{\xi})S}{AN_f} + \frac{2S}{3A^2N_f^2} \left[ 8+29n-12\mathcal{E} - 3A(nC_\lambda - (8-3\xi)C_\gamma) \right] + \mathcal{O}(1/N_f^3), \quad (4.149a)$$

$$\gamma_{m_\phi} = \frac{2(4+n)S}{AN_f} - \frac{8S}{3A^2N_f^2} \left[ 28-15\mathcal{E}+7n+\frac{3}{4}A(nC_\lambda+4C_\gamma) \right] + \mathcal{O}(1/N_f^3). \quad (4.149b)$$

We will discuss the results for the different cases in the next to next section.

#### 4.4.6 Renormalized self-energies

In order to complete our analysis of gQED<sub>3</sub>, we provide in here the exact expressions of the renormalized matter self-energies at  $\mathcal{O}(1/N_f^2)$ . They can be derived from the relations (4.64), requiring the computation of the finite parts, *i.e.*, of  $\mathcal{O}(\varepsilon^0)$ , of the (bare) matter self-energies and from which one can straightforwardly recover the corresponding renormalized matter propagators. All calculations done, exactly up to  $\mathcal{O}(1/N_f^2)$ , the renormalized matter self-energies of  $\mathcal{N} = 1$  SQED<sub>3</sub> ( $S = \mathcal{E} = 1$ ,  $n = 2$ ) read

$$\Sigma_{pr}^\psi = -\frac{1}{\pi^2N_f} \left[ 2 + (2-\tilde{L})\xi \right] + \frac{2}{\pi^4N_f^2} \left[ 3 + 10\xi + \left( 1 - (5-\xi)\xi - \frac{1}{4}\xi^2\tilde{L} \right) \tilde{L} - \left( 4 + \frac{1}{2}(12+\xi)\xi - 3\xi\tilde{L} \right) \zeta_2 \right] + \mathcal{O}(\varepsilon), \quad (4.150a)$$

$$\Sigma_{mr}^\psi = -\frac{1}{\pi^2N_f} \left[ (2+\xi)(4-\tilde{L}) \right] + \frac{2}{\pi^4N_f^2} \left[ 37 - 16C_4 + 2(4-\xi)\xi - \left( 5 - 2(1+\xi)\xi + \frac{1}{4}(2+\xi)^2\tilde{L} \right) \tilde{L} - \left( 18 + 4C_2 + \frac{1}{2}(28+\xi)\xi - 3(2+\xi)\tilde{L} \right) \zeta_2 \right] + \mathcal{O}(\varepsilon), \quad (4.150b)$$

$$\Sigma_{pr}^\phi = \frac{1}{\pi^2N_f} \left[ 4 - (2-\xi)\tilde{L} \right] - \frac{2}{\pi^4N_f^2} \left[ 35 - 8C_4 - \left( 17 - 8\xi - \frac{1}{4}(2-\xi)^2\tilde{L} \right) \tilde{L} \right]$$

$$- \left( 9 + 2C_2 + \frac{1}{2}(4 - \xi)\xi - 3(2 - \xi)\tilde{L} \right) \zeta_2 \Big] + \mathcal{O}(\varepsilon), \quad (4.150c)$$

$$\Sigma_{mr}^{\phi} = -\frac{1}{\pi^2 N_f} \left[ 14 - 3\xi - (2 + \xi)\tilde{L} \right] + \frac{1}{\pi^4 N_f^2} \left[ 123 - 46C_4 - 2(12 + \xi)\xi - \left( 2 + (4 + 3\xi)\xi + \frac{1}{2}(2 + \xi)^2 \tilde{L} \right) \tilde{L} \right. \\ \left. - \frac{1}{4} \left( 227 + 46C_2 - 4(14 - \xi)\xi - 24(2 + \xi)\tilde{L} \right) \zeta_2 \right] + \mathcal{O}(\varepsilon), \quad (4.150d)$$

with  $\tilde{L} = \log(-4p^2/\bar{\mu}^2)$  and  $\zeta_2 = \pi^2/6$ , as well as  $C_2 = \text{CL}_2(\pi/2) = 0.916$  the Catalan number and  $C_4 = \text{CL}_4(\pi/2) = 0.989$  where  $\text{CL}_n(z)$  is the Clausen function, see Appendix A. For completeness, we also provide the bQED<sub>3</sub> ( $n = \mathcal{E} = 0$ ,  $S = 1$ ) case

$$\Sigma_{pr}^{\phi(b)} = \frac{2}{9\pi^2 N_f} \left[ 56 - 3(8 - 3\xi)\tilde{L} \right] - \frac{8}{81\pi^4 N_f^2} \left[ 5455 - 648C_4 - 3 \left( 884 - 330\xi - \frac{3}{4}(8 - 3\xi)^2 \tilde{L} \right) \tilde{L} \right. \\ \left. - 27 \left( 39 + 6C_2 + \frac{1}{2}(16 - 3\xi)\xi - 3(8 - 3\xi)\tilde{L} \right) \zeta_2 \right] + \mathcal{O}(\varepsilon), \quad (4.151a)$$

$$\Sigma_{mr}^{\phi(b)} = -\frac{2}{\pi^2 N_f} \left[ 8 - 3\xi - \xi\tilde{L} \right] + \frac{4}{9\pi^4 N_f^2} \left[ 1513 - 630C_4 - 6(86 + 3\xi)\xi - \left( 4(18 + 23\xi) + \frac{9}{2}(6 + \tilde{L})\xi^2 \right) \tilde{L} \right. \\ \left. - \frac{3}{4} \left( 365 + 210C_2 - 72(3 + \tilde{L})\xi + 12\xi^2 \right) \zeta_2 \right] + \mathcal{O}(\varepsilon), \quad (4.151b)$$

as well as the non-SUSY QED<sub>3</sub> case ( $S = 0$ ,  $n = 2$ ), reading

$$\Sigma_{pr}^{\psi(f)} = \frac{2}{9\pi^2 N_f} \left[ 2 + 3(2 - 3\xi)(2 - \tilde{L}) \right] - \frac{8}{81\pi^4 N_f^2} \left[ 787 - 846\xi - 3 \left( 110 - 3(59 - 9\xi)\xi - \frac{3}{4}(2 - 3\xi)^2 \tilde{L} \right) \tilde{L} \right. \\ \left. - 27 \left( 16 - \frac{1}{2}(32 + 3\xi)\xi - 3(2 - 3\xi)\tilde{L} \right) \zeta_2 \right] + \mathcal{O}(\varepsilon), \quad (4.152a)$$

$$\Sigma_{mr}^{\psi(f)} = -\frac{2}{\pi^2 N_f} \left[ 6 + 4\xi - (2 + \xi)\tilde{L} \right] + \frac{8}{9\pi^4 N_f^2} \left[ 5(23 - 36C_4) + 2(26 - 9\xi)\xi - \left( 26 - (17 + 18\xi)\xi + \frac{9}{4}(2 + \xi)^2 \tilde{L} \right) \tilde{L} \right. \\ \left. - \frac{9}{2} \left( 17 + 10C_2 + (28 + \xi)\xi - 6(2 + \xi)\tilde{L} \right) \zeta_2 \right] + \mathcal{O}(\varepsilon). \quad (4.152b)$$

## 4.5 Results summary and discussion

In this section, we summarize the obtained general results and discuss them in the different cases of interest. These include for the polarizations of the gauge multiple and their corresponding interaction correction coefficients,

### 4.5.1 Results for QED<sub>3</sub>

As a check of our computations, we will first recover the well known results of large- $N_f$  QED<sub>3</sub> at two loops. This can be achieved by considering our results without supersymmetry ( $S = 0$ ,  $n = 2$ ), reading

$$\gamma_{\psi}^{\text{QED}_3} = -\frac{4(2 - 3\xi)}{3\pi^2 N_f} + \frac{8(64 - 92\xi - (6 - 9\xi)\pi^2)}{9\pi^4 N_f^2} + \mathcal{O}(1/N_f^3), \quad (4.153a)$$

$$\gamma_{m_{\Psi}}^{\text{QED}_3} = \frac{32}{3\pi^2 N_f} - \frac{64(28 - 3\pi^2)}{9\pi^4 N_f^2} + \mathcal{O}(1/N_f^3), \quad (4.153b)$$

$$\Pi_{\gamma}^{\text{QED}_3} = -\frac{N_f e^2}{8p_E} \left[ 1 + \frac{C_{\gamma}^{\text{QED}_3}}{N_f} + \mathcal{O}(1/N_f^2) \right], \quad (4.153c)$$

$$C_{\gamma}^{\text{QED}_3} = \frac{2(92 - 9\pi^2)}{9\pi^2} = 0.07146. \quad (4.153d)$$

Therefore, we recover exactly our results of the previous chapter, see (3.114), that were first obtained in [213, 226], thus providing a strong check on our computations.



### 4.5.2 Results for $\mathcal{N} = 1$ SQED<sub>3</sub>

We now consider the main case of interest,  $\mathcal{N} = 1$  SQED<sub>3</sub>, *i.e.*, taking  $S = 1$ ,  $n = 2$ . First, it is interesting to consider the results with arbitrary  $\mathcal{E}$  to study the effect of DRED. In this case, the anomalous dimensions, together with the other results, then reads

$$\gamma_\psi = \frac{2\xi}{\pi^2 N_f} + \frac{2(2 - (12 - \pi^2)\xi)}{\pi^4 N_f^2} + \mathcal{O}(1/N_f^3), \quad (4.154a)$$

$$\gamma_\phi = -\frac{2(2 - \xi)}{\pi^2 N_f} + \frac{2(26 - (2 - \xi)\pi^2 - 12\xi)}{\pi^4 N_f^2} + \mathcal{O}(1/N_f^3), \quad (4.154b)$$

$$\gamma_{m_\psi} = \frac{4}{\pi^2 N_f} - \frac{4(14 - \pi^2)}{\pi^4 N_f^2} + \mathcal{O}(1/N_f^3), \quad (4.154c)$$

$$\gamma_{m_\phi} = \frac{4}{\pi^2 N_f} - \frac{4(46 - 4\mathcal{E} - 3\pi^2)}{3\pi^4 N_f^2} + \mathcal{O}(1/N_f^3), \quad (4.154d)$$

$$C_\gamma = \frac{12 - \pi^2}{\pi^2}, \quad C_\varepsilon = \frac{(12 - \pi^2)\mathcal{E}}{\pi^2}, \quad C_\lambda = \frac{38 - 2\mathcal{E} - 3\pi^2}{3\pi^2}, \quad (4.154e)$$

which is very interesting because the effect of the  $\varepsilon$ -scalar is stiff but still crucial. Indeed, the quantities  $\gamma_\psi$ ,  $\gamma_\phi$  as well as  $\gamma_{m_\psi}$  and  $C_\gamma$  are  $\mathcal{E}$ -independent up to NLO, but not  $C_\lambda$  and  $\gamma_{m_\phi}$ . Therefore taking  $\mathcal{E} = 1$ , so that DRED is allowed, is necessary the supersymmetric identities on these quantities and reads

$$\gamma_\psi^{\text{SQED}_3} = \frac{2\xi}{\pi^2 N_f} + \frac{2(2 - (12 - \pi^2)\xi)}{\pi^4 N_f^2} + \mathcal{O}(1/N_f^3), \quad (4.155a)$$

$$\gamma_\phi^{\text{SQED}_3} = -\frac{2(2 - \xi)}{\pi^2 N_f} + \frac{2(26 - (2 - \xi)\pi^2 - 12\xi)}{\pi^4 N_f^2} + \mathcal{O}(1/N_f^3), \quad (4.155b)$$

$$\gamma_{m_\psi}^{\text{SQED}_3} = \frac{4}{\pi^2 N_f} - \frac{4(14 - \pi^2)}{\pi^4 N_f^2} + \mathcal{O}(1/N_f^3), \quad (4.155c)$$

$$\gamma_{m_\phi}^{\text{SQED}_3} = \frac{4}{\pi^2 N_f} - \frac{4(14 - \pi^2)}{\pi^4 N_f^2} + \mathcal{O}(1/N_f^3), \quad (4.155d)$$

$$\Pi_x^{\text{SQED}_3} = -\frac{N_f e^2}{4p_E} \left[ 1 + \frac{C_x^{\text{SQED}_3}}{N_f} + \mathcal{O}(1/N_f^2) \right], \quad x = \{\gamma, \varepsilon, \lambda\}, \quad (4.155e)$$

$$C_x^{\text{SQED}_3} = \frac{12 - \pi^2}{\pi^2} = 0.2159, \quad x = \{\gamma, \varepsilon, \lambda\}. \quad (4.155f)$$

Several comments are needed here. First, we recall that we have the identity

$$\Pi_\gamma^{\text{SQED}_3}(p^2) = \Pi_\varepsilon^{\text{SQED}_3}(p^2) = \Pi_\lambda^{\text{SQED}_3}(p^2), \quad (4.156)$$

as well as the identity

$$\gamma_{m_\psi}^{\text{SQED}_3} = \gamma_{m_\phi}^{\text{SQED}_3}, \quad (4.157)$$

both verified up NLO. This is a behavior expected from SUSY that physical (gauge invariant) quantities are identical in the same multiplet. On the other hand, the field anomalous dimensions for the electron and the selectron are not equal, neither at LO nor at NLO. This is indeed due to the use of a gauge fixing term that breaks supersymmetry (Wess-Zumino gauge). We recall here that this expected and not an issue since the breaking of SUSY is occurring only for gauge-dependant quantities that are, by definition, non-physical.

### 4.5.3 Results for bosonic bQED<sub>3</sub>

We now consider the second subcase of interest in this chapter, which is bosonic bQED<sub>3</sub>, *i.e.*, taking  $S=1$ ,  $n=0$  and  $\mathcal{E}=0$ . It reads

$$\gamma_\phi^{\text{bQED}_3} = -\frac{4(8-3\xi)}{3\pi^2 N_f} + \frac{8(440-164\xi-3\pi^2(8-3\xi))}{9\pi^4 N_f^2} + \mathcal{O}(1/N_f^3), \quad (4.158a)$$

$$\gamma_{m_\phi}^{\text{bQED}_3} = \frac{16}{3\pi^2 N_f} - \frac{32(64-3\pi^2)}{9\pi^4 N_f^2} + \mathcal{O}(1/N_f^3), \quad (4.158b)$$

$$\Pi_\gamma^{\text{bQED}_3} = -\frac{N_f e^2}{8p_E} \left[ 1 + \frac{C_\gamma^{\text{bQED}_3}}{N_f} + \mathcal{O}(1/N_f^2) \right], \quad (4.158c)$$

$$C_\gamma^{\text{bQED}_3} = \frac{2(164-9\pi^2)}{9\pi^2} = 1.6926, \quad (4.158d)$$

the LO results are in accordance with [196, 198, 310] and, to our knowledge, the NLO results are new.

### 4.5.4 Results for reduced QED<sub>4,3</sub> (Graphene)

As another check, we will recover some results of the previous chapter, *i.e.*, for QED<sub>4,3</sub>. We recall that this model is a suitable description of graphene in its ultra-relativistic limit. These results can be obtained from the QED<sub>3</sub> case via a mapping. Indeed, comparing the LO softened photon in QED<sub>3</sub> (4.92a) with the bare propagator in QED<sub>4,3</sub> (3.22), that we reproduce here for clarity

$$D_{1AA}^{\mu\nu\text{QED}_3}(p) = \frac{8i}{N_f e^2 p_E} \left( g^{\mu\nu} - (1-\xi) \frac{p^\mu p^\nu}{p^2} \right), \quad D_0^{\mu\nu\text{QED}_{4,3}}(p) = \frac{i}{2p_E} \left( g^{\mu\nu} - \frac{1-\xi}{2} \frac{p^\mu p^\nu}{p^2} \right), \quad (4.159)$$

yields the following naive map

$$\text{QED}_3 \rightarrow \text{QED}_{4,3} = \left\{ \frac{1}{\pi^2 N_f} \rightarrow \bar{\alpha}_r, \quad \xi \rightarrow \frac{1+\xi}{2} \right\}. \quad (4.160)$$

This map is enough to recover the results for the polarization at one and two loops for QED<sub>4,3</sub> from the polarization of QED<sub>3</sub>, and therefore the corresponding correction coefficient  $C_\gamma$ . This map is also sufficient to recover the one-loop anomalous dimensions of the QED<sub>4,3</sub> model from the LO result of the QED<sub>3</sub> model. However, it breaks at two loops. Indeed, these models, though very similar, have two major differences that manifest at NLO.

First, QED<sub>3</sub> at NLO is expressed in a non-local gauge, while the QED<sub>4,3</sub> is not. To compensate this effect, it is enough to consider that if the two-loop polarization of QED<sub>3</sub> is next to the gauge parameter  $\xi$ , it should not be present in the QED<sub>4,3</sub> case. Since the two-loop polarization is proportional to  $C_\gamma$ , one can use the additional rule

$$\xi \times C_\gamma^{\text{QED}_3} \rightarrow 0, \quad (4.161)$$

to recover the proper gauge dependence at two loops in the anomalous dimensions of QED<sub>4,3</sub>.

Secondly, in QED<sub>3</sub>, we have softened the photon propagator at NLO and computed additional (one-loop but NLO) diagrams, see equations (4.140n) (4.140o) (4.140p) and (4.145m) (4.145n). These diagrams were not present in QED<sub>4,3</sub> and are replaced by diagrams with a simple fermion loop. To take this into account, we should replace the NLO softened propagator in QED<sub>3</sub> by the LO one times the regular factor for a fermion loop in QED<sub>4,3</sub>, *i.e.*,  $-N_f$ . Since the relation between the two propagator is exactly  $-C_\gamma^{\text{QED}_3}/N_f$ , see (4.138a), the additional needed mapping is trivial and reads

$$C_\gamma^{\text{QED}_3} \rightarrow N_f, \quad (4.162)$$

to be applied on the anomalous dimensions only.

Performing carefully this mapping yields the following results for QED<sub>4,3</sub>

$$\gamma_{\Psi}^{\text{QED}_{4,3}} = -2\bar{\alpha}_r \frac{1-3\xi}{3} + 16\bar{\alpha}_r^2 \left( N_f \zeta_2 + \frac{4}{27} \right) + \mathcal{O}(\bar{\alpha}_r^3), \quad (4.163a)$$

$$\gamma_m^{\text{QED}_{4,3}} = \frac{32\bar{\alpha}_r}{3} - 64\bar{\alpha}_r^2 \left( N_f \zeta_2 - \frac{8}{27} \right), \quad (4.163b)$$

$$\Pi_{\gamma}^{\text{QED}_{4,3}} = -\frac{\pi N_f \alpha_r}{2p_E} \left[ 1 + C_{\gamma}^{\text{QED}_{4,3}} \alpha_r + \mathcal{O}(\alpha_r^2) \right], \quad (4.163c)$$

$$C_{\gamma}^{\text{QED}_{4,3}} = \frac{92 - 9\pi^2}{18\pi} = 0.05612, \quad (4.163d)$$

which perfectly recover the results of previous chapter, see results (3.105). Note that the use of  $\alpha_r$  instead of  $\bar{\alpha}_r$  for the polarization is on purpose. We recall that in the previous chapter, we obtained from these results the optical conductivity of pure suspended graphene in the ultra-relativistic limit, which yielded an optical absorbance of

$$A_g = (2.293 \pm 0.002)\%, \quad (4.164)$$

see section 3.4.2 for the corresponding discussion. In the following, we will compute similarly the optical absorption of the super-graphene model.

#### 4.5.5 Results for reduced $\mathcal{N} = 1$ SQED<sub>4,3</sub> (Super-Graphene)

As a non-trivial application of our results, we will map our results for SQED<sub>3</sub> to a model of super-graphene, *i.e.*, for SQED<sub>4,3</sub>, see the action (4.26). We recall that this model is a suitable description of an eventual pure suspended super-graphene material in its ultra-relativistic limit. As advertised in the introduction, we will obtain the results in the SQED<sub>3</sub> case via a mapping similar to the non-SUSY case. Indeed, comparing the LO IR-softened gauge propagators of SQED<sub>3</sub> (4.92) with the propagators of SQED<sub>4,3</sub> derived, *e.g.*, from [163], reads

$$\hat{D}_{1AA}^{\mu\nu\text{SQED}_3}(p) = \frac{4i}{N_f e^2 p_E} \left( \hat{g}^{\mu\nu} + (1-\xi) \frac{\hat{p}^{\mu} \hat{p}^{\nu}}{p^2} \right), \quad \hat{D}_{0AA}^{\mu\nu\text{SQED}_{4,3}}(p) = \frac{i}{2p_E} \left( \hat{g}^{\mu\nu} + \frac{1-\xi}{2} \frac{\hat{p}^{\mu} \hat{p}^{\nu}}{p^2} \right), \quad (4.165a)$$

$$\bar{D}_{1AA}^{\mu\nu\text{SQED}_3}(p) = \frac{4i}{N_f e^2 p_E} \bar{g}_{\mu\nu}, \quad \bar{D}_{0AA}^{\mu\nu\text{SQED}_{4,3}}(p) = \frac{i}{2p_E} \bar{g}_{\mu\nu}, \quad (4.165b)$$

$$D_{1\lambda\bar{\lambda}}^{\mu\nu\text{SQED}_3}(p) = -\frac{4i\not{p}}{N_f e^2 p_E}, \quad D_{0\lambda\bar{\lambda}}^{\mu\nu\text{SQED}_{4,3}}(p) = -\frac{i\not{p}}{2p_E}. \quad (4.165c)$$

It is then straightforward to deduce the following naive mapping

$$\text{SQED}_3 \rightarrow \text{SQED}_{4,3} = \left\{ \frac{1}{\pi^2 2N_f} \rightarrow \bar{\alpha}_r, \xi \rightarrow \frac{1+\xi}{2} \right\}, \quad (4.166)$$

which is the same as the non-SUSY case up to a factor two. Similarly, this map is enough to access the polarization of SQED<sub>4,3</sub> up to two loops and also the anomalous dimensions up to one loop. In order to access the correct two-loop contribution to the anomalous dimensions for this model, like in the non-SUSY case we first have to cancel the effect of the non-local gauge by using

$$\xi \times C_{\gamma}^{\text{SQED}_3} = 0, \quad (4.167)$$

and then cancel the effect of the NLO softening of the gauge propagators by taking

$$C_x \rightarrow N_f \quad \forall x = \{\gamma, \varepsilon, \lambda\}, \quad (4.168)$$

in the anomalous dimensions. Performing carefully this mapping yields the following results

$$\gamma_\psi^{\text{SQED}_{4,3}} = 2(1 + \xi)\bar{\alpha}_r + 16\bar{\alpha}_r^2 + \mathcal{O}(\bar{\alpha}_r^3), \quad (4.169a)$$

$$\gamma_\phi^{\text{SQED}_{4,3}} = -2(3 - \xi)\bar{\alpha}_r + 16(1 + 6N_f\zeta_2)\bar{\alpha}_r^2 + \mathcal{O}(\bar{\alpha}_r^3), \quad (4.169b)$$

$$\gamma_{m_\psi}^{\text{SQED}_{4,3}} = 8\bar{\alpha}_r - 32(1 + 3N_f\zeta_2)\bar{\alpha}_r^2 + \mathcal{O}(\bar{\alpha}_r^3), \quad (4.169c)$$

$$\gamma_{m_\phi}^{\text{SQED}_{4,3}} = 8\bar{\alpha}_r - 32(1 + 3N_f\zeta_2)\bar{\alpha}_r^2 + \mathcal{O}(\bar{\alpha}_r^3), \quad (4.169d)$$

$$\Pi_\gamma^{\text{SQED}_{4,3}} = -\frac{\pi N_f \alpha_r}{p_E} \left[ 1 + C_\gamma^{\text{SQED}_{4,3}} \alpha_r + \mathcal{O}(\alpha_r^2) \right], \quad (4.169e)$$

$$C_\gamma^{\text{SQED}_{4,3}} = \frac{12 - \pi^2}{2\pi} = 0.3391. \quad (4.169f)$$

Note that use of  $\alpha_r$  instead of  $\bar{\alpha}_r$  for the polarization is on purpose. These results are in accordance with [163] at one loop. To our knowledge, the two-loop contributions are a new result. Note that in [163] is considered a super-graphene model on the boundary (on a substrate) such that the coupling  $\alpha_{\text{bdry}}$  is twice smaller than in our case, *i.e.*,  $\alpha_{\text{bdry}} = \alpha/2$ .

Similarly to the non-supersymmetric case, we can derive the optical conductivity of the hypothetical super-graphene. Indeed, the polarization of the photon  $\hat{\Pi}_\gamma^{\mu\nu}$ , for SQED<sub>4,3</sub>, can be related to the optical (AC) conductivity of graphene with the formula

$$\sigma_{sg}(p_0) = -\lim_{\vec{p} \rightarrow 0} \frac{ip_0}{|\vec{p}|^2} \hat{\Pi}_\gamma^{00}(p_0, \vec{p}), \quad (4.170)$$

where  $\hat{p}^\mu = (p_0, \vec{p})$ . Since the parametrization for the photon polarization reads  $\hat{\Pi}_\gamma^{\mu\nu} = (p^2 \hat{g}^{\mu\nu} - \hat{p}^\mu \hat{p}^\nu) \Pi_\gamma$  and  $\Pi_\gamma^{\text{SQED}_{4,3}} \sim 1/p_E$ , this simply yield  $\sigma_{sg} = -p_E \Pi_\gamma^{\text{SQED}_{4,3}}$  which, after restoring momentarily the dimensions  $\hbar$ ,  $c$  and  $\varepsilon_0$  in the following for clarity, reads

$$\sigma_{sg} = \sigma_{0sg} \left( 1 + C_\gamma^{\text{SQED}_{4,3}} \bar{\alpha}_r + \mathcal{O}(\bar{\alpha}_r^2) \right), \quad \sigma_{0sg} = \frac{N_f e^2}{4\hbar} = \frac{\pi N_f e^2}{2h}, \quad (4.171)$$

where  $\sigma_{0sg}$  is the minimal AC conductivity of super-graphene, which is twice bigger as the non-SUSY case. Following [221], like in the non-SUSY case, the optical conductivity of super-graphene is related to its transmittance ( $T_{sg}$ ) and its absorbance ( $A_{sg}$ ) (at half-filling) via the relation

$$T_{sg} = 1 - A_{sg} = \left( 1 + \frac{\sigma_{sg}}{2\varepsilon_0 c} \right)^{-2} \approx 1 - \frac{\sigma_{0sg}}{\varepsilon_0 c} = 1 - \pi N_f \alpha_r, \quad (4.172)$$

where  $\alpha_r = e^2/(4\pi\varepsilon_0\hbar c)$ . For SQED<sub>4,3</sub>, the physical super-graphene model is recovered for  $N_f = 2$  (*i.e.*, 8 elementary spinors) and  $\alpha_r = 1/137$  in its ultra-relativistic limit, we obtain an absorbance of

$$A_{sg} = 2\pi\alpha_r \left[ 1 + \alpha_r \left( C_\gamma^{\text{SQED}_{4,3}} - \frac{3\pi}{2} + \mathcal{O}(\alpha_r^2) \right) \right], \quad (4.173)$$

from which we can estimate the uncertainty by adding  $\pm$  in front the NLO contribution leading numerically to

$$A_{sg} = (4.59 \pm 0.15)\%. \quad (4.174)$$

Therefore, the absorbance of ultra-relativistic freestanding super-graphene is twice the value of normal graphene in the same conditions. Amusingly, a very similar opacity can be observed for bilayer (non-SUSY) graphene, which is experimentally also twice the absorbance of non-SUSY graphene, *i.e.*,  $A_g \approx 4.6\%$ . See the image 3.5 in the previous chapter, where the right part is basically a picture of bilayer graphene under white light, which would look exactly like super-graphene.

### 4.5.6 Discussion of the stability of the fixed point

At this point, let recall the crucial importance of the presence of an interacting IR fixed point in SQED<sub>3</sub> and all the variants we are studying. Following the QED<sub>3</sub> case [131], in such super-renormalizable theories, one can define a dimensionless effective charge

$$g_r(p_E) = \frac{g}{p_E(1 - \Pi_\gamma(p_E))}, \quad g = e^2 N_f. \quad (4.175)$$

In our case, for gQED<sub>3</sub>, we have that the photon polarization operator is given by

$$\Pi_\gamma(p_E) = X \frac{g}{p_E} \quad \text{with} \quad X = -\frac{n+2S}{16} \left( 1 + \frac{C_\gamma}{N_f} + \mathcal{O}(1/N_f^2) \right). \quad (4.176)$$

One can then define the corresponding beta function for the effective coupling  $g_r$ , reading

$$\beta(g_r) = \frac{dg_r}{d \log p_E} = -g_r(1 + X g_r). \quad (4.177)$$

The theory then yields two fixed points. A first Gaussian (trivial) non-interacting fixed point, and a second non-trivial IR fixed point which is stable (attractive) and where the coupling is non-vanishing. They read

$$g_r^* = \begin{cases} 0 & \text{asymptotic UV fixed point,} \\ -1/X & \text{interacting IR fixed point.} \end{cases} \quad (4.178)$$

Therefore, in the gQED<sub>3</sub> case, the non-trivial IR fixed point reads

$$g_r^* = \frac{16}{n+2S} \left( 1 - \frac{C_\gamma}{N_f} + \mathcal{O}(1/N_f^2) \right) = \begin{cases} \text{SQED}_3: & 4(1 - 0.216/N_f + \mathcal{O}(1/N_f^2)) \\ \text{QED}_3: & 8(1 - 0.071/N_f + \mathcal{O}(1/N_f^2)) \\ \text{bQED}_3: & 8(1 - 1.693/N_f + \mathcal{O}(1/N_f^2)) \end{cases} \quad (4.179)$$

We see that for both QED<sub>3</sub> and SQED<sub>3</sub> the IR fixed point is reasonably affected by higher-order corrections. However, in the bQED<sub>3</sub> case, the first correction is strong. This calls for a NNLO computation, which is outside the scope of this manuscript.

## 4.6 Critical $N_f$ for dynamical electron mass generation

As an application of our results, we now turn to an estimate of  $N_c$ , the critical number of (s)electron flavors which is such that for  $N_f > N_c$  the (s)electron is massless while for  $N_f < N_c$  a dynamical mass, with a Miransky scaling [131], is generated, reading

$$\left. \begin{array}{c} m_{\text{dyn}} \neq 0 \\ | \\ 0 \end{array} \right\} \begin{array}{c} m_{\text{dyn}} = 0 \\ | \\ N_c \end{array} \rightarrow N_f, \quad m_{\text{dyn}} \propto \exp\left(\frac{-2\pi}{\sqrt{N_c/N_f - 1}}\right). \quad (4.180)$$

As discussed in the introduction, at the level of the action, the potentially generated parity-even mass terms (parity-odd masses cannot be dynamically generated [318]) are of the form (4.33), that we reproduce here for clarity,

$$\mathcal{L}_{m_{\text{dyn}}} = m_{\text{dyn}_\psi} \left( \sum_{i=1}^{N_f} \bar{\psi}_i \psi^i - \sum_{i=1+N_f}^{2N_f} \bar{\psi}_i \psi^i \right) + m_{\text{dyn}_\phi}^2 \left( \sum_{i=1}^{N_f} |\phi_i|^2 + \sum_{i=1+N_f}^{2N_f} |\phi_i|^2 \right). \quad (4.181)$$

Let us remark that only the electron mass term breaks the global flavor symmetry. From SUSY, we also expect that  $m_{\text{dyn}_\psi} = m_{\text{dyn}_\phi}$ , which we will simply call  $m_{\text{dyn}}$ .

In the next section, we will first derive the critical number of fermion in gQED<sub>3</sub> via the conventional Schwinger-Dyson (SD) method at leading order. We will then use the semi-phenomenological gap equation technique developed in the previous chapter to estimate  $N_c$  directly from the gauge invariant anomalous dimension.

### 4.6.1 Schwinger Dyson equations at LO

In order to compute  $N_c$ , it is enough to focus on the critical properties of SQED<sub>3</sub>, *i.e.*, to work at the non-trivial IR fixed point. The conventional approach is to solve self consistently the Schwinger-Dyson (SD) equations, either for the electron or the selectron, since thanks to SUSY invariance, both sets of SD equations should yield the same criterion for mass generation. This has already been considered in [286], and we will reproduce their result using a more straightforward approach based on massless techniques [182, 183, 187], like in the previous chapter.

Following the previous notations, we will set the bare masses exactly to zero:  $m_\psi = m_\phi = 0$ , and parameterize the electron and scalar self-energies as

$$\Sigma^\psi(p) = \not{p}\Sigma_p^\psi(p^2) + \Sigma_m^\psi(p^2), \quad \Sigma^\phi(p) = p^2\Sigma_p^\phi(p^2) + \Sigma_m^\phi(p^2), \quad (4.182)$$

where now  $\Sigma_p^\psi(p^2)$  and  $\Sigma_p^\phi(p^2)$  are dynamically generated, *i.e.*, they are obtained as non-trivial solutions of the SD equations. The dressed electron and selectron propagators then read

$$S_{\psi\bar{\psi}}(p) = \frac{1}{1 - \Sigma_p^\psi(p^2)} \frac{i}{\not{p} - M_\psi(p^2)}, \quad M_\psi(p^2) = \frac{\Sigma_m^\psi(p^2)}{1 - \Sigma_p^\psi(p^2)}, \quad (4.183a)$$

$$S_{\phi\phi^*}(p) = \frac{1}{1 - \Sigma_p^\phi(p^2)} \frac{i}{p^2 - M_\phi(p^2)}, \quad M_\phi(p^2) = \frac{\Sigma_m^\phi(p^2)}{1 - \Sigma_p^\phi(p^2)}. \quad (4.183b)$$

We then consider the SD equations for the electron propagator, reading

$$-i\Sigma^{\psi(a)}(p) = \text{Diagram (a)} = \mu^{2\varepsilon} \int [d^d k] \hat{\Gamma}_{0A\psi\bar{\psi}}^\mu S_{\psi\bar{\psi}}(k) \hat{\Gamma}_{A\psi\bar{\psi}}^\nu \hat{D}_{AA,\mu\nu}(p-k), \quad (4.184a)$$

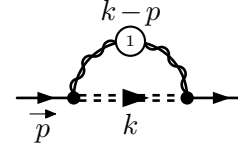
$$-i\Sigma^{\psi(b)}(p) = \text{Diagram (b)} = \mu^{2\varepsilon} \int [d^d k] \bar{\Gamma}_{0A\psi\bar{\psi}}^\mu S_{\psi\bar{\psi}}(k) \bar{\Gamma}_{A\psi\bar{\psi}}^\nu \bar{D}_{AA,\mu\nu}(p-k), \quad (4.184b)$$

$$-i\Sigma^{\psi(c)}(p) = \text{Diagram (c)} = \mu^{2\varepsilon} \int [d^d k] \Gamma_{0\bar{\lambda}\psi\phi^*} S_{\phi\phi^*}(k) \Gamma_{0\bar{\psi}\lambda\phi} D_{\lambda\bar{\lambda}}(p-k), \quad (4.184c)$$

which, in principle, are associated with other SD equations associated with the vertices and all the gauge propagators. We do not display them here because we will neglect them for a first estimation of  $N_c$ . Indeed, in the LO approximation of the  $1/N_f$ -expansion, we take the photon,  $\varepsilon$ -scalar and photino propagators as the LO IR softened ones, as well as all the vertices bare and finally  $\Sigma_p^\psi = 0$  so that  $M_x \rightarrow \Sigma_m^x$  with  $x = \psi, \phi$ . In this approximation, the set (4.184) tremendously simplifies and reads

$$-i\Sigma^{\psi(a)}(p) = \text{Diagram (a)} = \mu^{2\varepsilon} \int [d^d k] (-ie\hat{\gamma}^\mu) S_{\psi\bar{\psi}}(k) (-ie\hat{\gamma}^\nu) \hat{D}_{1\mu\nu}(k-p), \quad (4.185a)$$

$$-i\Sigma^{\psi(b)}(p) = \text{Diagram (b)} = \mu^{2\varepsilon} \mathcal{E}\mathcal{S} \int [d^d k] (-ie\bar{\gamma}^\mu) S_{\psi\bar{\psi}}(k) (-ie\bar{\gamma}^\nu) \bar{D}_{1AA,\mu\nu}(k-p), \quad (4.185b)$$



$$-i\Sigma^{\psi(c)}(p) = \text{---} \text{---} \text{---} = \mu^{2\varepsilon} S \int [d^d k] (-e) S_{\phi\phi^*}(k) (+e) D_{1\lambda\bar{\lambda}}(k-p). \quad (4.185c)$$

These equations are now decoupled and depends only self-consistently on the self-energy functions. The unknown function  $\Sigma_m^{\psi}(p^2)$  may further be parameterized as

$$\Sigma_m^{\psi}(p^2) = m_{\text{dyn}} \times (-p^2)^{-b/2}, \quad (4.186)$$

where the index  $b$  has to be self-consistently determined.

Together with (4.186), the scalar part of equations (4.185) in the linearized approximation significantly simplify and read

$$\Sigma_{1m}^{\psi(a)}(p^2) = m_{\text{dyn}} (-p^2)^{-b/2} \frac{4(2+\xi)}{n\pi^2 N_f b(1-b)}, \quad (4.187a)$$

$$\Sigma_1^{\psi(b)}(p^2) = m_{\text{dyn}} (-p^2)^{-b/2} \frac{2(3-d)\mathcal{E}S}{\pi^2 N_f b(1-b)}, \quad (4.187b)$$

$$\Sigma_{1m}^{\psi(c)}(p^2) = 0, \quad (4.187c)$$

where  $\Sigma_{1m}^{\psi(b)}$  vanishes in the limit  $d \rightarrow 3$  and  $\Sigma_{1m}^{\psi(c)}$  vanishes exactly from the fermionic trace. The total LO scalar self-energy is therefore given by  $\Sigma_{1m}^{\psi(a)}$  which is equal to (4.186). From this identity, we deduce the LO gap equation

$$b(1-b) = \frac{4(2+\xi)}{n\pi^2 N_f}. \quad (4.188)$$

Note that since only the (a) contribution is not vanishing, the dynamical mass generation for SQED<sub>3</sub> is of pure QED<sub>3</sub> origin. This is obvious from the fact that  $S$  does not appear in the gap equation. Solving the gap equation yields two values for the index  $b$

$$b_{\pm} = \frac{1}{2} \left( 1 \pm \sqrt{1 - \frac{16(2+\xi)}{n\pi^2 N_f}} \right). \quad (4.189)$$

Dynamical symmetry breaking takes place for complex values of the index  $b$ , *i.e.*, for  $N_f < N_c$  with

$$N_c = \frac{16(2+\xi)}{n\pi^2}, \quad (\text{LO}), \quad (4.190)$$

which is valid for both SQED<sub>3</sub> ( $S=1, n=2$ ) and QED<sub>3</sub> ( $S=0, n=2$ ), reading

$$N_c^{\text{SQED}_3} = \frac{8(2+\xi)}{\pi^2}, \quad N_c^{\text{QED}_3} = \frac{8(2+\xi)}{\pi^2}, \quad (4.191)$$

In the Landau gauge ( $\xi=0$ ), we recover the result for SQED<sub>3</sub> first obtained in [286], and for QED<sub>3</sub>, in [131]. As we will see in the following, the Landau gauge is the good gauge (cancel the electron field anomalous dimension) for both QED<sub>3</sub> and SQED<sub>3</sub> at LO. Nevertheless, the gauge-dependence of (4.190) is not satisfactory, especially because the critical number of fermion is a physical observable. Following the approach of the previous chapter, we will therefore consider an alternative derivation based on the use of the anomalous mass dimensions of either the electron or the selectron.

## 4.6.2 Semi-phenomenological gap equation

Proceeding along the lines of the previous chapter, we then consider that the electron gap equation for  $\mathcal{N}=1$  SQED<sub>3</sub> takes the same form as for QED<sub>3</sub>, see equation (3.148), reading

$$K(N_f) = \left( \gamma_m(N_f) - \frac{1}{2} \right)^2, \quad \text{and} \quad K(N_c) = 0, \quad (4.192)$$

where  $\gamma_m$  is either  $\gamma_{m_\psi}$  or  $\gamma_{m_\phi}$  depending on the model considered. Note that within an all-order estimate of  $\gamma_m$ , the gap equation indeed simply reads  $\gamma_m(N_c) = 1/2$ . However, if  $\gamma_m$  is known only from its perturbative expansion up to a certain order, the criterion function  $K(N_f)$  accordingly needs to be properly truncated at the desired order of the  $1/N_f$ -expansion, *i.e.*,

$$K(N_f) = \frac{1}{4} - \gamma_{1m} + \gamma_{1m}^2 - \gamma_{2m} + \dots, \quad \text{with} \quad \gamma_m = \gamma_{1m} + \gamma_{2m} + \dots \quad (4.193)$$

and only after expanding and truncating, solve for  $N_c$  with  $K(N_c) = 0$ . Though semi-phenomenological, such an approach is straightforward and completely gauge invariant. For completeness, we provide numerically the mass anomalous dimensions that we obtained in table 4.3.

QED <sub>3</sub>	$\gamma_{m_\psi} = 1.0808/N_f + 0.1174/N_f^2 + \mathcal{O}(1/N_f^3)$
SQED <sub>3</sub>	$\gamma_{m_\psi} = 0.4053/N_f - 0.1696/N_f^2 + \mathcal{O}(1/N_f^3)$
bQED <sub>3</sub>	$\gamma_{m_\phi} = 0.5404/N_f - 1.2553/N_f^2 + \mathcal{O}(1/N_f^3)$

Table 4.3: Numerical mass anomalous dimensions

### Case of bQED<sub>3</sub>

In the following, we shall only focus on the electron mass generation, and not its superpartner. Indeed, in the case of bQED<sub>3</sub> with  $N_f$  scalars, we did not find any evidence for dynamical scalar mass generation in bQED<sub>3</sub>, suggesting that

$$\boxed{N_c^{\text{bQED}_3} = 0, \quad (\text{all-order}),} \quad (4.194)$$

for that model, either via the SD method or via the effective gap equation method. Note that the picture seems different if one allows a non-zero quartic coupling  $\lambda(|\phi|^2)^2$  in three dimensions, see, *e.g.*, [309], where they obtained  $N_c^{\text{bQED}_3}(\lambda \neq 0) = 6.1 \pm 1.95$  from fixed point collision in a four-loop expansion combined with advanced resummations techniques. The situation seems to be also different in 4-dimensions, see [333].

### Case of SQED<sub>3</sub>

On the other hand, for SQED<sub>3</sub> (similarly to the 4-dimensional case, see [334, 335]) we find a possibility that a selectron mass can be induced by the electron condensate, if the latter exists. As we will see in the following, our results suggest that electrons do not condense in SQED<sub>3</sub>.

Truncating the gap equation at the LO of the  $1/N_f$  expansion, yields the gauge-invariant value

$$\boxed{N_c^{\text{SQED}_3} = \frac{16}{\pi^2} = 1.6211, \quad (\text{LO}),} \quad (4.195)$$

that coincides with the Landau gauge result of [286], which is indeed the good gauge for SQED<sub>3</sub> electrons. This LO result suggests that an electron mass is generated for  $N_f = 1$  thus seemingly breaking both flavor and SUSY symmetries. We find that higher-order corrections dramatically change this picture. Indeed, truncating the gap equation at the NLO of the  $1/N_f$  expansion, we find that

$$N_c^{\text{SQED}_3} = \frac{4}{\pi^2} \left( 2 \pm i\sqrt{14 - \pi^2} \right) = 0.8106(1 \pm 1.02i), \quad (4.196)$$

Such a complex value arises because of the negative NLO contribution (due to the selectron) to the mass anomalous dimension (4.155c), see table 4.3, that prevents the gap equation from having any real



valued solution. This calls for a  $1/N_f^3$  computation that is clearly outside the scope of this thesis. So, in order to overcome this difficulty, we shall proceed with a resummation of the seemingly alternating asymptotic series. A simple Padé approximant  $[1/1]$  of (4.155c) leads to

$$\gamma_{m_\psi}^{\text{SQED}_3} = \gamma_{m_\phi}^{\text{SQED}_3} = \frac{4}{14 + (N_f - 1)\pi^2}, \quad (\text{NLO } [1/1]). \quad (4.197)$$

Using this new improved value to solve the gap equation non-perturbatively, *i.e.*,  $\gamma_{m_\psi}(N_c) = 1/2$ , yields

$$N_c^{\text{SQED}_3} = \frac{\pi^2 - 6}{\pi^2} = 0.3921, \quad (\text{NLO } [1/1]). \quad (4.198)$$

This result is a strong evidence that, beyond the LO of the  $1/N_f$  expansion, no dynamical (parity-even) mass is generated for the electron in  $\mathcal{N} = 1$  SQED<sub>3</sub>. Though a dynamical breaking of SUSY may take place in SQED<sub>3</sub> (the Witten index is not well-defined with massless matter-fields, see, *e.g.*, [336] and references therein), the absence of any electron condensate suggests that SUSY is preserved, in accordance with our perturbative result  $\gamma_{m_\psi} = \gamma_{m_\phi}$  up to NLO.

### Case of QED<sub>3</sub>

We then focus on the case of QED<sub>3</sub> ( $S = 0$ ,  $n = 2$ ), for which the gap equation is known exactly up to NLO [184, 186, 187]. The same procedure, this time using (4.153b) for the mass anomalous dimension, leads at LO to

$$N_c^{\text{QED}_3} = \frac{128}{3\pi^2} = 4.32, \quad (\text{LO}), \quad (4.199)$$

and at NLO to

$$N_c^{\text{QED}_3} = \frac{16}{3\pi^2} \left( 4 + \sqrt{3\pi^2 - 28} \right) = 2.85, \quad (\text{NLO}), \quad (4.200)$$

in accordance with [184, 186, 187] and with the results of the previous chapter, found by mapping from QED<sub>4,3</sub>. Although the problem of a complex  $N_c$  is not encountered in this case (because the NLO term in (4.153b) is positive, see table 4.3), we still provide for completeness the improved  $N_c$  value obtained with resummation, *i.e.*,

$$N_c^{\text{QED}_3} = \frac{2(4 + 3\pi^2)}{3\pi^2} = 2.27, \quad (\text{NLO } [1/1]). \quad (4.201)$$

As expected from the effect of radiative corrections, this value is smaller than the exact NLO one but still quite close to it in accordance with the stability of the critical point. In striking contrast with both SQED<sub>3</sub> and bQED<sub>3</sub>, this suggests that a dynamical (flavor breaking and parity-even) mass is radiatively generated for the electron in QED<sub>3</sub> for small values of  $N_f$ , *i.e.*, for  $N_f = 1$  and 2. This new improved value  $N_c^{\text{QED}_3} = 2.27$ , is to compare with the extensive literature related to D $\chi$ SB in QED<sub>3</sub>, see table 4.4, where seemingly all values between 0 and 4 (even infinite in some early studies) has been obtained over four decades.

$N_c$ in QED <sub>3</sub>	Method	Year
$\infty$	Schwinger-Dyson (LO)	1984 [177]
$\infty$	Schwinger-Dyson (non-perturbative, Landau gauge)	1990, 1992 [278, 337]
$\infty$	RG study	1991 [338]
$\infty$	lattice simulations	1993, 1996 [339, 340]
$< 4.4$	F-theorem	2015 [189]
$(4/3)(32/\pi^2) = 4.32$	Schwinger-Dyson (LO, resummation)	1989 [181]
4.422	RG study (one-loop) ( $N_c^{\text{conf}} \approx 6.24$ )	2016 [191]
4	functional RG ( $4.1 < N_c^{\text{conf}} < 10.0$ )	2014 [341]
$3 < N_c < 4$	RG study	2001 [342]
$3.5 \pm 0.5$	lattice simulations	1988, 1989 [165, 166]
3.31	Schwinger-Dyson (NLO, Landau gauge)	1993 [182, 183]
3.29	Schwinger-Dyson (NLO, Landau gauge)	2016 [185]
$32/\pi^2 \approx 3.24$	Schwinger-Dyson (LO, Landau gauge)	1988 [131]
$3.0084 - 3.0844$	Schwinger-Dyson (NLO, resummation)	2016 [186]
2.89	RG study (one-loop)	2016 [192]
2.85	Schwinger-Dyson (NLO, resummation, $\forall \xi$ )	2016 [184, 186]
2.85	Effective gap equation (NLO, resummation, $\forall \xi$ )	2022 [4]
$1 + \sqrt{2} = 2.41$	F-theorem	2016 [343]
2.27	Effective gap equation (NLO, double resummation, $\forall \xi$ )	2022 [4]
$< 9/4 = 2.25$	RG study (one-loop)	2015 [188]
$< 3/2$	Free energy constraint	1999 [344]
$1 < N_c < 4$	lattice simulations	2004, 2008 [167, 168]
0	Schwinger-Dyson (non-perturbative, Landau gauge)	1990 [277]
0	lattice simulations	2015, 2016 [169, 170]

Table 4.4: Reproduced from [126] and updated.  $D\chi\text{SB}$  in  $f\text{QED}_3$ : some values of  $N_c$  obtained over the years with different methods. The value obtained with our method is grayed. Note that recent analytical methods (including ours) converge to a value of  $N_c$  in the range  $]2,3[$  such that a dynamical mass is generated for  $N_f \leq 2$ . On the other hand, results from lattice simulations are inconsistent. This may partly be due to the fact that, as  $N_f = 2$  is close to  $N_c$ , the dynamically generated mass is so small, see estimate and discussion in [184], that it is difficult to extract from lattice simulations.

### Case of SQED<sub>4,3</sub> (super-graphene)

Finally, using the mapping discussed in section 4.5.5, we can derive from the SQED<sub>4,3</sub> the critical number of fermion for the SQED<sub>4,3</sub> model, corresponding to the ultra-relativistic limit of freestanding super-graphene. In the quenched case, the critical coupling then reads

$$\alpha_c^{\text{SQED}_{4,3}}(N_f = 0) = \frac{\pi}{8} = 0.393, \quad (1\text{-loop}). \quad (4.202)$$

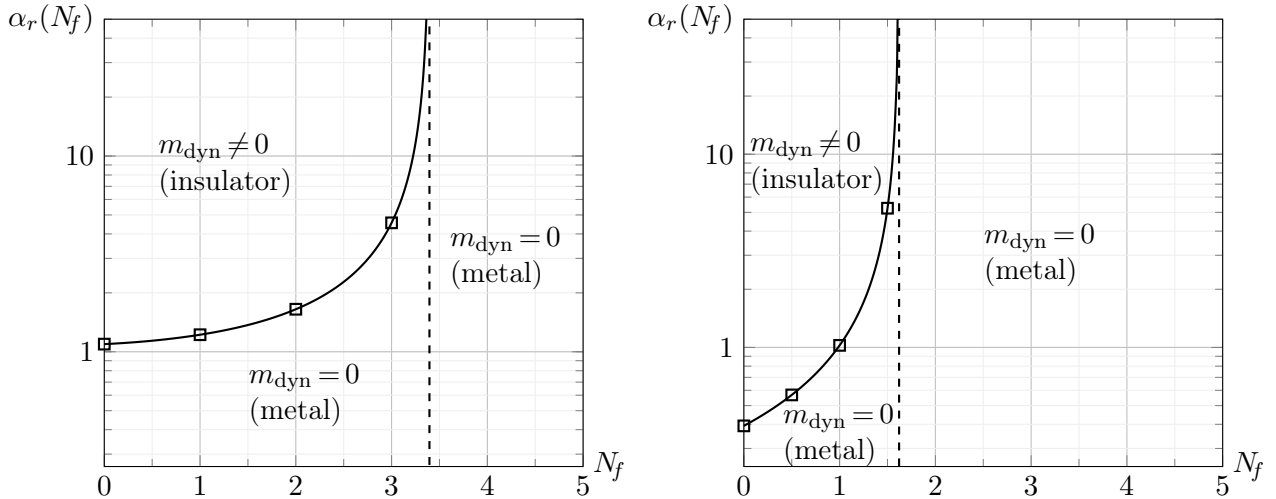
In the unquenched case, following the RPA-like procedure introduced in the previous chapter 3, which consist in resumming the two-loop  $N_f$  dependency, we obtain

$$\alpha_c^{\text{SQED}_{4,3}}(N_f) = \frac{2\pi}{16 - \pi^2 N_f}, \quad N_c^{\text{SQED}_{4,3}} = \frac{16}{\pi^2} = 1.6211, \quad (1\text{-loop}). \quad (4.203)$$

For the range of allowed values of  $N_f$ , it leads numerically to

$$\alpha_c^{\text{SQED}_{4,3}}(N_f = 0) = 0.3927, \quad \alpha_c^{\text{SQED}_{4,3}}(N_f = 1) = 1.0249. \quad (4.204)$$

At two loops, the result is complex, already in the quenched case. It follows that results are also complex in the unquenched case, despite trying RPA-like or Padé resummations. This is probably a parity effect (like the four-loop approach in QED<sub>4</sub>). We will then settle for the one-loop approach. We recall that, to obtain the case of super-graphene, we are interested in  $N_f = 2$ , because (super)graphene have a total of 8 spinors (2 cones/sub-lattices  $\times$  2 valley/chirality  $\times$  2 spins). Since  $N_c^{\text{SQED}_{4,3}} = 1.6211$  at one loop, and that we expect higher-order corrections to lower  $N_c$ , we can already tell that  $N_f = 2$  will always be above  $N_c$  in SQED<sub>4,3</sub>. This is a strong evidence that super-graphene is always in a metallic phase, in striking contrast with non-SUSY graphene, where we observed that a phase transition to an excitonic insulator was possible for large value of  $\alpha$ , *i.e.*, ( $\alpha > \alpha_c^{\text{QED}_{4,3}}(N_f = 2) \approx 1.2$ ). We provide in figure 4.4 the phase diagram of super-graphene together with the phase diagram of graphene that we already obtained in the previous chapter for comparison.



(a) Graphene (QED<sub>4,3</sub>) reproduced from chapter 3 (b) Super-graphene (SQED<sub>4,3</sub>) from results (4.204)

Figure 4.4: Phase diagrams for dynamical mass generation in graphene and super-graphene. Note that the relevant case for both graphene and super-graphene is  $N_f = 2$ . Here, insulator refers to an excitonic insulating phase, while metal refers to a semimetallic phase.

### Meta analysis of $N_c$ results in QEDs

For completeness and ease of comparison, we provide in figure 4.5 a comparative plot of all the  $N_c$  values found for all the QED models studied in this thesis.

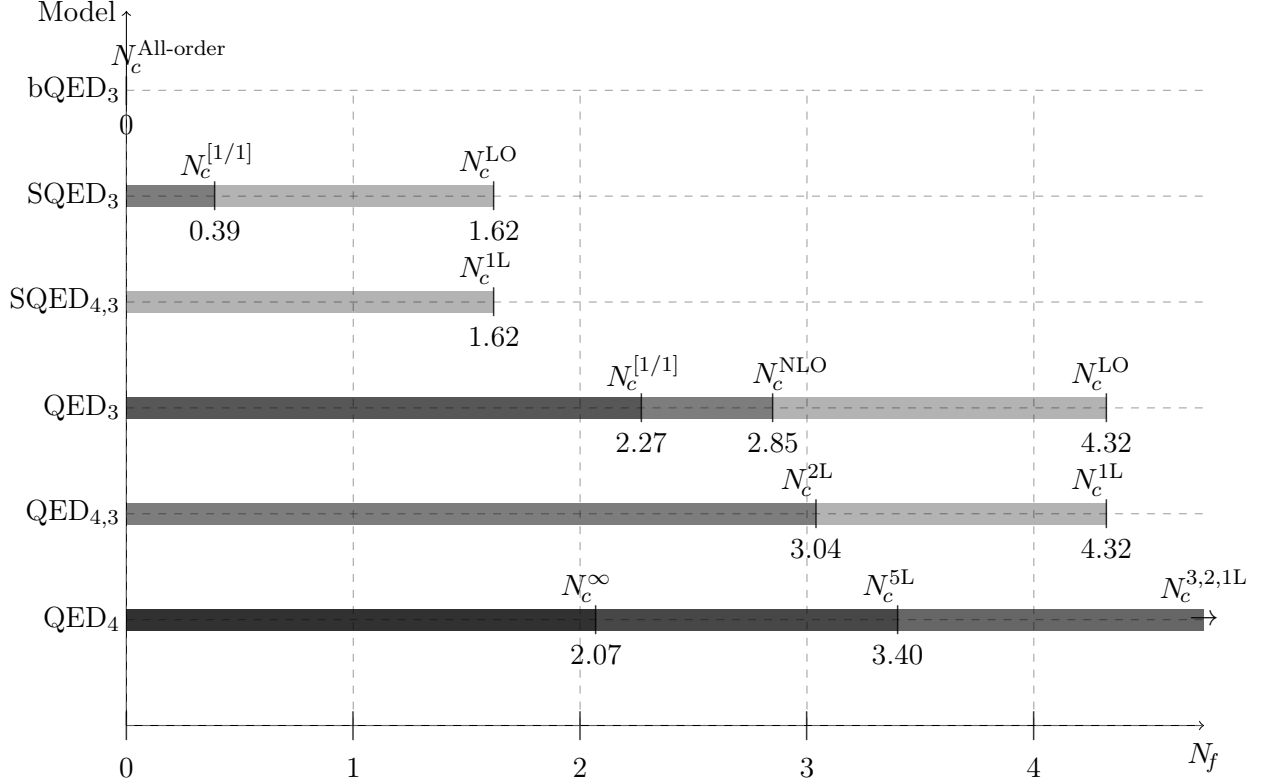


Figure 4.5: All results obtained in this thesis, for the critical number of fermion below which a dynamical mass is generated in various QED models. The darker it is, the more likely the corresponding model is massive for a given  $N_f$ . Note that the case of interest is generally  $N_f = 1$  for QED<sub>4</sub> and all the QED<sub>3</sub> variants. For the QED<sub>4,3</sub> variants, the case of interest is usually  $N_f = 2$  for graphene (QED<sub>4,3</sub>) and super-graphene (SQED<sub>4,3</sub>), because (super-)graphene have an additional factor 2 for cone (or sublattices) degeneracy.

In the three-dimensional case, this meta analysis shows that on one hand, dynamical mass generation is likely to occur in QED<sub>3</sub> while in the other hand, bQED<sub>3</sub> does not show any sign of boson condensation. Therefore, in SQED<sub>3</sub>, the fermionic part tries to generate a mass, in competition with the bosonic part that tries to prevent it. In the end, the selectronic part seems to overcome the electronic part such that no mass is radiatively generated in SQED<sub>3</sub>, thereby staying in a conformal phase. As for the reduced QED models, the QED<sub>4,3</sub> theory seems to allow mass generation for small values of the fermion number, which is enough for a metal to insulating phase transition to occur in (freestanding, ultra-relativistic, pure) graphene. In striking opposition, for the supersymmetric case, SQED<sub>4,3</sub>, mass generation seems to be allowed only for very small values of  $N_f$ , such that a metallic to insulating phase transition in super-graphene seems prevented. Finally, in usual high energy physics QED<sub>4</sub>, such a phase transition seems likely to be possible. In conclusion, we see that adding SUSY to an abelian gauge theory seems to prevent dynamical symmetry breaking.

## 4.7 Conclusion

In this chapter, we investigated the critical properties of minimal  $\mathcal{N} = 1$  supersymmetric QED<sub>3</sub>. To be complete, we introduced the more general gQED<sub>3</sub> model, encompassing the supersymmetric SQED<sub>3</sub>, the bosonic bQED<sub>3</sub> and the fermionic QED<sub>3</sub> cases. We also introduced a model of super-graphene, SQED<sub>4,3</sub>, to which our SQED<sub>3</sub> results can be mapped. In the general framework provided by the gQED<sub>3</sub> model, we performed a complete perturbative computation at LO and NLO in the large- $N_f$  expansion, in the DRED scheme, for an arbitrary covariant gauge fixing. We computed analytically the anomalous dimensions associated to the electron and selectron field and (parity-even) mass anomalous dimensions, as well as all the renormalized polarizations and self-energies. All these quantities correspond to the critical exponents of the considered models at the non-trivial IR fixed point that arises in the large- $N_f$  limit. Along the way, we provided a perturbative proof of the Furry theorem, generalized for these models. We also studied thoroughly the effect of DRED and showed its crucial importance in ensuring that the theory remains SUSY invariant.

As a first application of our results, we addressed the critical properties of those models. We showed that on the one hand, D $\chi$ SB is likely to be possible in purely fermionic models in specific conditions (at large coupling, small  $N_f$  and ultra-relativistic conditions), such as QED<sub>4</sub>, QED<sub>3</sub> and graphene (QED<sub>4,3</sub>). On the other hand, the presence of scalar particles, possibly via SUSY, seems to prevent dynamical mass generation, such as in bQED<sub>3</sub>, SQED<sub>3</sub> and super-graphene (SQED<sub>4,3</sub>). As a second application of our results, we also computed the optical conductivity of super-graphene, and we showed that it has an optical absorbance of  $\sim 4.6\%$  (like non-SUSY bilayer graphene). These properties are in striking opposition with the results for non-SUSY graphene (QED<sub>4,3</sub>) obtained in the previous chapter, where we showed that such regular graphene has an optical absorbance of  $\sim 2.3\%$  and is likely to possess a transition from a metallic to insulating phase at large electric coupling. Broadly speaking, the addition of scalar particles in a fermionic model seems to prevent D $\chi$ SB and then dynamical mass generation for the matter. While our computations tends to show that a graphene based transistor is likely to be possible (*e.g.*, using a substrate inducing a large tunable effecting coupling between the quasi-electrons), it seems hopeless if, instead of graphene, one decides to use a planar material exhibiting (emergent) SUSY, such as an eventual super-graphene.





# Appendix A

## Multi-loop massless techniques

This Appendix provides a review of multi-loop massless techniques for Feynman diagram computations, and more specifically, techniques devoted to the computation of two-point massless integrals via the powerful IBP-reduction technique in dimensional regularization. It is based partially on the review [211].

In the following, we will focus on one, two and three-loop integrals that are massless and of propagator type (specific to two-point functions) with generalized denominator powers. These are enough to cover all the computations carried out in this manuscript, from integrals found in elastic (disordered) membranes up to (supersymmetric) abelian gauge theory. Indeed, since our interest is on the renormalization group, massless computations are most of the time enough to access the UV structure of the theory and, if massive computations seem necessary, we may circumvent them by IR rearrangement or clever derivatives. Moreover, the theories we will consider may generate integrals with large numerators, made of momentum scalar products, but these can always be expressed as linear combination of integrals with generalized denominator indices. Lastly, we assume that all integrals have been projected out properly so that no open Lorentz indices are present. Therefore, in this manuscript, at one, two, and three loops, the integrals we have to compute take the following forms

$$J(d, \vec{p}, \alpha_1, \alpha_2) = \int \frac{[d^d k_1]}{k_1^{2\alpha_1} (\vec{p} - \vec{k}_1)^{2\alpha_2}}, \quad (1\text{-loop}), \quad (\text{A.1})$$

$$J(d, \vec{p}, \alpha_1, \dots, \alpha_5) = \int \frac{[d^d k_1][d^d k_2]}{k_1^{2\alpha_1} k_2^{2\alpha_2} (\vec{p} - \vec{k}_2)^{2\alpha_3} (\vec{p} - \vec{k}_1)^{2\alpha_4} (\vec{k}_{12})^{2\alpha_5}}, \quad (2\text{-loop}), \quad (\text{A.2})$$

$$J(d, \vec{p}, \alpha_1, \dots, \alpha_9) = \int \frac{[d^d k_1][d^d k_2][d^d k_3]}{k_1^{2\alpha_1} k_2^{2\alpha_2} k_3^{2\alpha_3} (\vec{p} - \vec{k}_3)^{2\alpha_4} (\vec{p} - \vec{k}_2)^{2\alpha_5} (\vec{p} - \vec{k}_1)^{2\alpha_6} (\vec{k}_{12})^{2\alpha_7} (\vec{k}_{23})^{2\alpha_8} (\vec{k}_{13})^{2\alpha_9}}, \quad (3\text{-loop}), \quad (\text{A.3})$$

with  $\vec{k}_{ij} = \vec{k}_i - \vec{k}_j$ . These integrals are extremely challenging and, beyond one loop, are not known for arbitrary indices  $\alpha_i$ . The purpose of this appendix is to introduce diagrammatic and reduction techniques to compute these integrals for some chosen sets of  $\alpha_i$  indices.



## A.1 One loop

We consider an Euclidean space of dimension  $d$  and follow most of the notations of the review [211]. The one-loop massless propagator-type master topology is given by the so-called *bubble* integral

$$J(d, \vec{p}, \alpha, \beta) = \text{---} \circlearrowleft \text{---} = \int \frac{[d^d k]}{k^{2\alpha} (\vec{p} - \vec{k})^{2\beta}} = \frac{(p^2)^{d/2 - \alpha - \beta}}{(4\pi)^{d/2}} G(d, \alpha, \beta), \quad (\text{A.4})$$

where  $[d^d k] = d^d k / (2\pi)^d$  and  $\alpha, \beta$  are the so-called indices of the propagators. For the diagrammatic representation of the integral, we used the propagator line with a generalized index

$$\text{---} \frac{1}{\alpha} \text{---} = \frac{1}{(p^2)^\alpha}. \quad (\text{A.5})$$

In (A.4),  $G$  is the dimensionless function left after factorization of the trivial dependence in  $p$  of the integral. At one loop,  $G$  is known exactly and can be easily derived using, *e.g.*, the generalized Feynman parametrization

$$\frac{1}{A^\alpha B^\beta} = \frac{\Gamma(\alpha + \beta)}{\Gamma(\alpha)\Gamma(\beta)} \int_0^1 \frac{u^{\alpha-1} (1-u)^{\beta-1}}{(uA + (1-u)B)^{\alpha+\beta}}, \quad (\text{A.6})$$

with  $A = k^2$  and  $B = (\vec{p} - \vec{k})^2$  together with the shift  $\vec{k} \rightarrow \vec{k} + (1-u)\vec{p}$ , we obtain the scalar integral

$$J(d, \vec{p}, \alpha, \beta) = \frac{\Gamma(\alpha + \beta)}{\Gamma(\alpha)\Gamma(\beta)} \int_0^1 du \int [d^d k] \frac{u^{\alpha-1} (1-u)^{\beta-1}}{(k^2 - u(1-u)p^2)^{\alpha+\beta}}. \quad (\text{A.7})$$

It can now be directly integrated over  $k$  using

$$\int d^d k f(k^2) = \Omega_d \int_0^\infty dk k^{d-1} f(k^2), \quad (\text{A.8})$$

with  $\Omega_d = 2\pi^{d/2} / \Gamma(d/2)$ , reading

$$J(d, \vec{p}, \alpha, \beta) = \frac{(p^2)^{d/2 - \alpha - \beta}}{(4\pi)^{d/2}} \frac{\Gamma(\alpha + \beta - d/2)}{\Gamma(\alpha)\Gamma(\beta)} \int_0^1 \frac{du}{u^{\beta+1-d/2} (1-u)^{\alpha+1-d/2}}. \quad (\text{A.9})$$

A direct integration over the Feynman parameter  $u$  then yields

$$J(d, \vec{p}, \alpha, \beta) = \frac{(p^2)^{d/2 - \alpha - \beta}}{(4\pi)^{d/2}} \frac{\Gamma(d/2 - \alpha)\Gamma(d/2 - \beta)\Gamma(\alpha + \beta - d/2)}{\Gamma(\alpha)\Gamma(\beta)\Gamma(d - \alpha - \beta)}. \quad (\text{A.10})$$

The dimensionless function  $G$  has then a simple expression in terms of Euler  $\Gamma$ -functions

$$G(d, \alpha, \beta) = \frac{a(d, \alpha)a(d, \beta)}{a(d, \alpha + \beta - d/2)}, \quad a(d, \alpha) = \frac{\Gamma(d/2 - \alpha)}{\Gamma(\alpha)}. \quad (\text{A.11})$$

To fix notations, we recall that  $\Gamma(x) = (x-1)!$  and its usual analytic continuation is defined by

$$\Gamma(1 - \varepsilon) = \exp\left(\gamma_E \varepsilon + \sum_{n=2}^{\infty} \frac{\varepsilon^n}{n} \zeta_n\right) = e^{\gamma_E \varepsilon} \left(1 + \frac{\zeta_2}{2} \varepsilon^2 + \frac{\zeta_3}{3} \varepsilon^3 + \frac{9\zeta_4}{16} \varepsilon^4 + \left(\frac{\zeta_2 \zeta_3}{6} + \frac{\zeta_5}{5}\right) \varepsilon^5 + \mathcal{O}(\varepsilon^6)\right), \quad (\text{A.12})$$

with  $\gamma_E = 0.577$  the Euler–Mascheroni constant and  $\zeta_n$  the Riemann zeta function

$$\zeta_n = \sum_{s=1}^{\infty} \frac{1}{s^n}, \quad (\text{A.13})$$

with,  $\zeta_2 = \pi^2/6$ ,  $\zeta_3 = 1.202$  the Apéry constant,  $\zeta_4 = \pi^4/90$  and  $\zeta_5 = 1.037$ . Therefore, the term of order  $\varepsilon^n$  in (A.12) is given by a polynomial in the  $\prod \zeta_i$  of weight  $n = \sum i$ .

Note that, at one loop, by construction and in any dimension,  $G$  is vanishing exactly if one index is negative or zero as well as being symmetrical under index exchange, *i.e.*,

$$G(d, \alpha, \beta) = 0, \text{ if } \alpha \leq 0 \text{ or } \beta \leq 0, \quad \text{and} \quad G(d, \alpha, \beta) = G(d, \beta, \alpha). \quad (\text{A.14})$$

An important example of evaluation of this function is for all indices being one, that we provide here evaluated in the dimensions of interest in this manuscript, *i.e.*, in  $d = 4 - 2\varepsilon$  and  $d = 3 - 2\varepsilon$ , reading

$$G(4 - 2\varepsilon, 1, 1) = e^{-\gamma_E \varepsilon} \left( \frac{1}{\varepsilon} + 2 + \left( 4 - \frac{\zeta_2}{2} \right) \varepsilon^2 + \left( 8 - \zeta_2 - \frac{7}{3} \zeta_3 \right) \varepsilon^3 + \mathcal{O}(\varepsilon^3) \right), \quad (\text{A.15a})$$

$$G(3 - 2\varepsilon, 1, 1) = 4^\varepsilon \pi^{3/2} e^{-\gamma_E \varepsilon} \left( 1 + \frac{5}{2} \zeta_2 \varepsilon^2 - \frac{1}{3} \zeta_3 \varepsilon^3 + \mathcal{O}(\varepsilon^4) \right). \quad (\text{A.15b})$$

In general, the  $\gamma_E$  factors can be trivially factorized in an exponential form thanks to (A.12). Since, at one loop,  $G$  is made up of  $\Gamma$  functions, all series expansions are only functions of the Riemann zeta functions  $\zeta_n$  with integer  $n$ .

## A.2 Introduction to IBP reduction

Knowing  $G(d, \alpha, \beta)$  at one loop for any values of the indices  $\alpha, \beta$  and in any dimension allows computing any one-loop two-point diagram without further technique. Nevertheless, in prevision of higher-loop computations, we introduce the so called integration-by-part (IBP) reduction technique, originally introduced in [63–65]. This method allows us to reduce any integral  $J(d, \vec{p}, \alpha, \beta)$  as a rational polynomial coefficient (in the dimension  $d$  and the indices  $\alpha, \beta$ ) times the so called master integral at one loop,  $J(d, \vec{p}, 1, 1)$ .

The IBP reduction relations are based on the translational invariance of dimensionally regularized Feynman integrals<sup>1</sup>

$$\int d^d k f(k) = \int d^d k f(k+q), \quad (\text{A.16})$$

where  $q$  can be chosen arbitrary small such that

$$f(k+q) = f(k) + q^\mu \frac{\partial}{\partial k^\mu} f(k). \quad (\text{A.17})$$

This yields the intuitive relation

$$0 = \int d^d k q^\mu \frac{\partial}{\partial k^\mu} f(k), \quad (\text{A.18})$$

where the derivative  $\partial/\partial k^\mu$  can be performed using the useful identities

$$\frac{\partial k^\nu}{\partial k^\mu} = g^\nu_\mu, \quad g^\mu_\mu = d, \quad \frac{\partial (k-p)^{-2\alpha}}{\partial k^\mu} = -2\alpha \frac{(k-p)_\mu}{(k-p)^{2(\alpha+1)}}, \quad k \cdot p = \frac{1}{2}(k^2 + p^2 - (k-p)^2). \quad (\text{A.19})$$

Then, taking  $f(k) = k^{-2\alpha} (\vec{p} - \vec{k})^{-2\beta}$  and choosing, *e.g.*,  $q = p$  in (A.18), it is easy to derive the identity

$$0 = \int d^d k \left[ \frac{-\beta}{k^{2(\alpha-1)} (\vec{p} - \vec{k})^{2(\beta+1)}} + \frac{d-2\alpha-\beta}{k^{2\alpha} (\vec{p} - \vec{k})^{2\beta}} + \frac{\beta p^2}{k^{2\alpha} (\vec{p} - \vec{k})^{2(\beta+1)}} \right], \quad (\text{A.20})$$

which can be re-written simply

$$0 = -\beta J(d, \vec{p}, \alpha-1, \beta+1) + (d-2\alpha-\beta) J(d, \vec{p}, \alpha, \beta) + \beta p^2 J(d, \vec{p}, \alpha, \beta+1). \quad (\text{A.21})$$

<sup>1</sup>Using a hard cutoff (like an upper bound  $\Lambda$ ) would break translational invariance and prevent the use of IBP reduction.

Taking the shift  $\beta \rightarrow \beta - 1$  and rearranging the identity yields the very useful relation

$$J(d, \vec{p}, \alpha, \beta) = \frac{1}{p^2} J(d, \vec{p}, \alpha - 1, \beta) + \frac{1 - 2\alpha - \beta + d}{(1 - \beta)p^2} J(d, \vec{p}, \alpha, \beta - 1) \quad (\beta \neq 1). \quad (\text{A.22})$$

From here, in principle, we can apply repetitively this identity to reduce any one-loop integral until reaching the lowest non-zero integral(s). In case of integer indices, it is simply  $J(d, \vec{p}, 1, 1)$  since we recall from (A.14) that  $J(d, \vec{p}, \alpha, \beta) = 0 \forall \alpha, \beta \leq 0$ . However, note that the above IBP identity does not work for  $\beta = 1$ . To cure this issue, we can use another identity that can be derived using the other natural choice  $q = k$  in (A.18) and, after some algebra, reads

$$0 = -\beta J(d, \vec{p}, \alpha - 1, \beta + 1) + \alpha J(d, \vec{p}, \alpha + 1, \beta - 1) - (\alpha - \beta) J(d, \vec{p}, \alpha, \beta) + \beta p^2 J(d, \vec{p}, \alpha, \beta + 1) - \alpha p^2 J(d, \vec{p}, \alpha + 1, \beta). \quad (\text{A.23})$$

Since we already covered all the cases but  $\beta = 1$  with the IBP (A.22), we can specialize this second IBP identity to take care only of the  $\beta = 1$  case, reading

$$0 = -J(d, \vec{p}, \alpha - 1, 2) + (\alpha - 1) J(d, \vec{p}, \alpha, 1) + p^2 J(d, \vec{p}, \alpha, 2) - \alpha p^2 J(d, \vec{p}, \alpha + 1, 1). \quad (\text{A.24})$$

Then, it can be simplified further using (A.22) on  $J(d, \vec{p}, \alpha, 2)$ , and together with the shift  $\alpha \rightarrow \alpha - 1$ , this identity takes the simple form

$$J(d, \vec{p}, \alpha, 1) = \frac{1 + \alpha - d}{(\alpha - 1)p^2} J(d, \vec{p}, \alpha - 1, 1) \quad (\alpha \neq 1). \quad (\text{A.25})$$

At this point, we can summarize the two reduction rules (A.22) and (A.25) graphically, yielding

$$\begin{array}{c} \alpha \\ \circ \\ \beta \end{array} = \frac{1}{p^2} \begin{array}{c} \alpha - 1 \\ \circ \\ \beta \end{array} + \frac{1 - 2\alpha - \beta + d}{(1 - \beta)p^2} \begin{array}{c} \alpha \\ \circ \\ \beta - 1 \end{array} \quad (\beta \neq 1), \quad (\text{A.26a})$$

$$\begin{array}{c} \alpha \\ \circ \\ 1 \end{array} = \frac{1 + \alpha - d}{(\alpha - 1)p^2} \begin{array}{c} \alpha - 1 \\ \circ \\ 1 \end{array} \quad (\alpha \neq 1). \quad (\text{A.26b})$$

Applied repetitively, these reduction rules allow us to reduce any one-loop integral  $J(d, \vec{p}, \alpha, \beta)$  with integer indices  $\alpha, \beta$  onto the simpler integral  $J(d, \vec{p}, 1, 1)$  already computed in the previous section. This integral is called the *master integral* at one loop. Here is an example of application

$$J(d, \vec{p}, 2, 2) = \frac{6 - d}{p^2} J(d, \vec{p}, 1, 2) = \frac{(6 - d)(3 - d)}{p^4} J(d, \vec{p}, 1, 1). \quad (\text{A.27})$$

Therefore, at one loop, for integer indices (the case of non integer indices is discussed in section A.5), only one master integral is needed to compute all other integrals, *i.e.*,  $J(d, \vec{p}, 1, 1)$ , that we computed exactly above. We provide a minimal Mathematica implementation for integer indices reduction

```
In[1]:= Clear[j]
j[_, alpha_, _] := 0 /; alpha <= 0
j[alpha_, beta_] := (1 + alpha - d) j[alpha - 1, beta] /; beta == 1 && alpha != 1
j[alpha_, beta_] := j[alpha - 1, beta] / p^2 + (1 - 2 alpha - beta + d) j[alpha, beta - 1] /; beta != 1
j[5, 5] // FullSimplify
Out[5]= 1 / (576 p^16) (-18 + d) (-16 + d) (-14 + d) (-12 + d) (-9 + d) (-7 + d) (-5 + d) (-3 + d) j[1, 1]
```

### A.3 Two loops

At two loops, one can encounter various massless propagator-type topologies. Nevertheless, all two-loop topologies can be encompassed by a general topology, the *diamond diagram*. It is the two-loop massless propagator-type master-topology integral and is given by

$$J(d, \vec{p}, \alpha_1, \dots, \alpha_5) = \text{Diagram} = \int \frac{[d^d k_1][d^d k_2]}{k_1^{2\alpha_1} k_2^{2\alpha_2} (\vec{p} - \vec{k}_2)^{2\alpha_3} (\vec{p} - \vec{k}_1)^{2\alpha_4} (\vec{k}_{12})^{2\alpha_5}} = \frac{(p^2)^{d - \sum \alpha_i}}{(4\pi)^d} G(d, \alpha_1, \dots, \alpha_5), \quad (\text{A.28})$$

where  $\vec{k}_{12} = \vec{k}_1 - \vec{k}_2$  and  $G(d, \alpha_1, \dots, \alpha_5)$  is dimensionless and unknown for arbitrary indices  $\{\alpha_i\}_{i=1-5}$ . This integral has two kinds of symmetries: first under the exchange  $k_1 \leftrightarrow k_2$  and second under the shifts  $k_1 \rightarrow k_1 - p$  and  $k_2 \rightarrow k_2 - p$ . This generates the following relations

$$J(d, \vec{p}, \alpha_1, \alpha_2, \alpha_3, \alpha_4, \alpha_5) = J(d, \vec{p}, \alpha_2, \alpha_1, \alpha_4, \alpha_3, \alpha_5) \quad (k_1 \leftrightarrow k_2), \quad (\text{A.29a})$$

$$J(d, \vec{p}, \alpha_1, \alpha_2, \alpha_3, \alpha_4, \alpha_5) = J(d, \vec{p}, \alpha_4, \alpha_3, \alpha_2, \alpha_1, \alpha_5) \quad (k_1 \rightarrow k_1 - p \text{ and } k_2 \rightarrow k_2 - p), \quad (\text{A.29b})$$

or equivalently, graphically,

$$\text{Diagram} = \text{Diagram} \quad (k_1 \leftrightarrow k_2), \quad (\text{A.30a})$$

$$\text{Diagram} = \text{Diagram} \quad (k_1 \rightarrow k_1 - p \text{ and } k_2 \rightarrow k_2 - p). \quad (\text{A.30b})$$

The first relation is then a mirror reflection along the vertical axis, *i.e.*, it exchanges  $\alpha_1 \leftrightarrow \alpha_2$  and  $\alpha_3 \leftrightarrow \alpha_4$  while the second one is the mirror reflection along the horizontal axis, *i.e.*, it exchanges  $\alpha_1 \leftrightarrow \alpha_4$  and  $\alpha_2 \leftrightarrow \alpha_3$ .

This diamond integral is the only one we have to consider at two loops for two-point massless diagrams, as it encompasses all the other two-loop topologies. Indeed, since lines with zero index contract like

$$\text{Diagram} = \text{Diagram} = \text{Diagram}, \quad (\text{A.31})$$

we have that all possible two-loop sub-topologies can be written using the diamond diagram with well-chosen zero indices

$$\text{Diagram} = J(d, \vec{p}, \alpha_1, \alpha_2, \alpha_3, \alpha_4, 0) = \text{Diagram} \quad (\text{double-bubble}), \quad (\text{A.32a})$$

$$\text{Diagram} = J(d, \vec{p}, 0, \alpha_1, \alpha_2, \alpha_3, \alpha_4) = \text{Diagram} \quad (\text{eye}), \quad (\text{A.32b})$$

$$\text{Diagram} = J(d, \vec{p}, 0, \alpha_1, 0, \alpha_2, \alpha_3) = \text{Diagram} \quad (\text{sunset}). \quad (\text{A.32c})$$

Moreover, these three sub-topologies are in fact reducible to one-loop diagrams. Indeed, the first one (double-bubble) obviously looks like the multiplications of two one-loop bubbles and upon closer inspection, the two others (eye and sunset) are in fact convolutions of one-loop bubbles. To make this evident, we can first remark that, using (A.5), the one-loop bubble is

$$\text{Bubble}(\alpha_1, \alpha_2) = \frac{(p^2)^{d/2-\alpha-\beta}}{(4\pi)^{d/2}} G(d, \alpha, \beta) = \frac{1}{(4\pi)^{d/2}} \times \frac{1}{\alpha+\beta-d/2} \times G(d, \alpha, \beta), \quad (\text{A.33})$$

so that we can build the following graphical replacement rule

$$\text{Graph} \left[ \text{Bubble}(\alpha, \beta) \right] = G(d, \alpha, \beta) \times \text{Graph} \left[ \frac{1}{\alpha+\beta-d/2} \right], \quad (\text{A.34})$$

which mean that if a diagram contains somewhere a simple one-loop bubble (no matter the number of legs attached to the two vertices) with indices  $\alpha, \beta$ , one can replace it by a simple line with index  $\alpha + \beta - d/2$  while extracting a factor  $G(d, \alpha, \beta)$  of the diagram. Using this technique, we can easily express the all the two-loop sub topologies as a function of the known one-loop bubble function  $G(d, \alpha, \beta)$ , yielding

$$\text{Diagram 1} = \frac{(p^2)^{d-\sum \alpha_i}}{(4\pi)^d} G(d, \alpha_1, \alpha_4) \times G(d, \alpha_2, \alpha_3), \quad (\text{A.35a})$$

$$\text{Diagram 2} = \frac{(p^2)^{d-\sum \alpha_i}}{(4\pi)^d} G(d, \alpha_1, \alpha_2 + \alpha_3 + \alpha_4 - d/2) \times G(d, \alpha_3, \alpha_4), \quad (\text{A.35b})$$

$$\text{Diagram 3} = \frac{(p^2)^{d-\sum \alpha_i}}{(4\pi)^d} G(d, \alpha_1, \alpha_2 + \alpha_3 - d/2) \times G(d, \alpha_2, \alpha_3). \quad (\text{A.35c})$$

These integrals are then called one-loop reducible and can be computed for any  $\alpha_i$  in any dimension  $d$  since  $G(d, \alpha, \beta)$  is known exactly. Therefore, as soon as any index is zero, the general diamond integral (A.28) can be computed exactly. We are then left with the case where all  $\alpha_i$  are non-zero, like, for example,  $J(d, \vec{p}, 1, 1, 1, 1)$ . In this case, IBP techniques are welcome and, following the one-loop approach we derived carefully earlier, we are able to derive IBP identities of the form

$$\text{Diagram 4} = \frac{1}{2\alpha_1 + \alpha_4 + \alpha_5 - d} \left[ p^2 \alpha_4 \times \text{Diagram 5} - \alpha_4 \times \text{Diagram 6} + \alpha_5 \times \text{Diagram 7} - \alpha_5 \times \text{Diagram 8} \right] \quad (\text{A.36})$$

where  $\alpha_i^\pm = \alpha_i \pm 1$ . Several similar IBP identities can be derived and, all together, they form a powerful reduction algorithm. One can show that, ultimately, every two-loop integral  $J(d, \vec{p}, \alpha_1, \alpha_2, \alpha_3, \alpha_4, \alpha_5)$ ,

with integer indices  $\alpha_i$ , can be reduced as a linear combination of two master integrals, the double bubble and the sunset with all indices to one, *i.e.*,  $J(d, \vec{p}, 1, 1, 1, 1, 0)$  and  $J(d, \vec{p}, 0, 1, 0, 1, 1)$ , that we already computed for arbitrary indices, *i.e.*

- the double bubble diagram: it corresponds to  $\alpha_2 = 0$  and reads

$$J(d, \vec{p}, 1, 1, 1, 1, 0) = \text{Diagram} = \frac{(p^2)^{d-4}}{(4\pi)^d} G^2(d, 1, 1), \quad (\text{A.37})$$

- the sunset diagram: it corresponds to  $\alpha_1 = \alpha_3 = 0$  (or  $\alpha_4 = \alpha_2 = 0$ ) and reads

$$J(d, \vec{p}, 0, 1, 0, 1, 1) = \text{Diagram} = \frac{(p^2)^{d-3}}{(4\pi)^d} G(d, 1, 1) G(d, 1, 2-d/2). \quad (\text{A.38})$$

Therefore, all two-loop propagator-type integrals, with integer indices, can be reduced to the trivial  $G(d, \alpha, \beta)$  one-loop function! There is no need to compute explicitly a single new integral. In, *e.g.*,  $d = 4 - 2\varepsilon$ , the master integrals then read

$$G(d, 1, 1, 1, 1, 0) = \text{Diagram} = \frac{\Gamma^2(2-d/2)\Gamma^4(d/2-1)}{\Gamma^2(d-2)} \stackrel{d=4-2\varepsilon}{=} e^{-2\gamma_E\varepsilon} \left[ \frac{1}{\varepsilon^2} + \frac{4}{\varepsilon} + (12 - \zeta_2) + \mathcal{O}(\varepsilon) \right], \quad (\text{A.39a})$$

$$G(d, 0, 1, 0, 1, 1) = \text{Diagram} = \frac{\Gamma(3-d)\Gamma^3(d/2-1)}{\Gamma(3d/2-3)} \stackrel{d=4-2\varepsilon}{=} e^{-2\gamma_E\varepsilon} \left[ -\frac{4}{\varepsilon} - \frac{13}{8} - \frac{1}{48}(345 - 12\zeta_2)\varepsilon + \mathcal{O}(\varepsilon^2) \right]. \quad (\text{A.39b})$$

The implementation of the IBP identities and the reduction process can be conveniently automated with the MATHEMATICA versatile package LITERED by Roman Lee [345, 346]. Here is an example of minimal implementation of this package together with a reduction example for  $J(d, \vec{p}, 1, 1, 1, 1, 1)$

```

SetDirectory[NotebookDirectory[]];
Import["RNL/LiteRed184.m"];
SetDim[d];
Declare[{k1, k2, p}, Vector];
NewBasis[T2, {k1, k2, p - k2, p - k1, k1 - k2},
  {k1, k2},
  GenerateIBP -> True,
  AnalyzeSectors -> True,
  FindSymmetries -> True
];
SolvejSector /@ UniqueSectors[T2];

***** LiteRed v1.83 *****
Author: Roman N. Lee, Budker Institute of Nuclear Physics, Novosibirsk.
Release Date: 11.01.2020
LiteRed stands for Loop INTEgrals REDuction.
The package is designed for the search and application of the Integration-By-Part reduction rules.
Input file timestamp: Mon 11 Jan 2021 11:19:15
See ?LiteRed` for a list of functions.

1 master integrals found: j[T2, 0, 1, 0, 1, 1].
1 master integrals found: j[T2, 1, 1, 1, 1, 0].

j[T2, 1, 1, 1, 1, 1] // IBPReduce

2(-10+3d)(-8+3d)j[T2, 0, 1, 0, 1, 1] - 2(-3+d)j[T2, 1, 1, 1, 1, 0]
-----
(-4+d)^2(p.p)^2

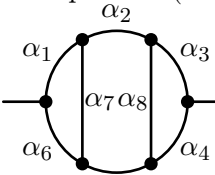
```

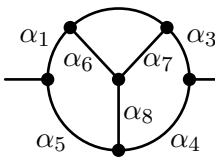
## A.4 Three loops

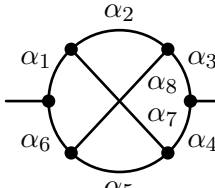
At three loops, the most general propagator-type integral one could think of is, *e.g.*,

$$J(d, \vec{p}, \alpha_1, \dots, \alpha_9) = \int \frac{[d^d k_1][d^d k_2][d^d k_3]}{k_1^{2\alpha_1} k_2^{2\alpha_2} k_3^{2\alpha_3} (\vec{p} - \vec{k}_3)^{2\alpha_4} (\vec{p} - \vec{k}_2)^{2\alpha_5} (\vec{p} - \vec{k}_1)^{2\alpha_6} (\vec{k}_{12})^{2\alpha_7} (\vec{k}_{23})^{2\alpha_8} (\vec{k}_{13})^{2\alpha_9}}, \quad (\text{A.40})$$

with  $\vec{k}_{ij} = \vec{k}_i - \vec{k}_j$ . However, contrary to the one and two-loop general propagator-type integrals, Eq. (A.40) does not correspond to a drawable diagram. This results from the fact that a propagator-type diagram with 3 loops and 9 internal lines does not exist. Therefore, for three loops and above, it is necessary to introduce multiple nonequivalent topologies with 8 internal lines only. At three loops, there are three different topologies for the propagator-type master integral, namely Ladder<sup>2</sup> (L3), Benz<sup>3</sup> (B3) and non-planar<sup>4</sup> (N3). These are respectively defined as

$$J_{\text{L3}}(d, \vec{p}, \alpha_i) = \int \frac{[d^d k_1][d^d k_2][d^d k_3]}{k_1^{2\alpha_1} k_2^{2\alpha_2} k_3^{2\alpha_3} (\vec{p} - \vec{k}_3)^{2\alpha_4} (\vec{p} - \vec{k}_2)^{2\alpha_5} (\vec{p} - \vec{k}_1)^{2\alpha_6} (\vec{k}_{12})^{2\alpha_7} (\vec{k}_{23})^{2\alpha_8}}, \quad (\text{A.41a})$$


$$J_{\text{B3}}(d, \vec{p}, \alpha_i) = \int \frac{[d^d k_1][d^d k_2][d^d k_3]}{k_1^{2\alpha_1} k_2^{2\alpha_2} k_3^{2\alpha_3} (\vec{p} - \vec{k}_3)^{2\alpha_4} (\vec{p} - \vec{k}_1)^{2\alpha_5} (\vec{k}_{12})^{2\alpha_6} (\vec{k}_{23})^{2\alpha_7} (\vec{k}_{13})^{2\alpha_8}}, \quad (\text{A.41b})$$


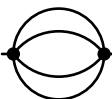
$$J_{\text{N3}}(d, \vec{p}, \alpha_i) = \int \frac{[d^d k_1][d^d k_2][d^d k_3]}{k_1^{2\alpha_1} k_2^{2\alpha_2} k_3^{2\alpha_3} (\vec{p} - \vec{k}_3)^{2\alpha_4} (\vec{p}_{123})^{2\alpha_5} (\vec{p} - \vec{k}_1)^{2\alpha_6} (\vec{k}_{32})^{2\alpha_7} (\vec{k}_{12})^{2\alpha_8}}, \quad (\text{A.41c})$$


with  $\vec{k}_{ij} = \vec{k}_i - \vec{k}_j$  and  $\vec{p}_{123} = \vec{p} - \vec{k}_1 + \vec{k}_2 - \vec{k}_3$ . Similarly to the one- and two-loop cases, the external momentum ( $p$ ) dependence is easily extracted from dimensional analysis which allows us to write the diagrams in the following form

$$J_X(d, \vec{p}, \alpha_1, \dots, \alpha_8) = \frac{(p^2)^{3d/2 - \sum_{i=1}^8 \alpha_i}}{(4\pi)^{3d/2}} G_X(D, \alpha_1, \dots, \alpha_8), \quad X \in \{\text{L3}, \text{B3}, \text{N3}\}, \quad (\text{A.42})$$

where  $G_X(D, \alpha_1, \dots, \alpha_8)$  is the (dimensionless) coefficient function of the diagram with topology  $X$ . In this manuscript, at three loops, we consider only theories where all indices  $\alpha_i$  ( $i = 1, \dots, 8$ ) are integers, in which case the IBP reduction technique is very powerful. In the following, we choose the ladder (L3) topology to be the default one. This implies that if a diagram is sufficiently trivial to be issued from several topologies, we shall choose the ladder (L3) one. Using IBP-reduction techniques discussed earlier, all possible three-loop diagrams can be expressed on three different basis corresponding to the three topologies

- The Ladder (L3) master integral basis:

$$J_{\text{L3}}(d, \vec{p}, 0, 0, 1, 0, 0, 1, 1, 1) = \int \frac{[d^d k_1][d^d k_2][d^d k_3]}{k_1^{2\alpha_1} k_2^{2\alpha_2} k_3^{2\alpha_3} (\vec{p} - \vec{k}_3)^{2\alpha_4} (\vec{p} - \vec{k}_2)^{2\alpha_5} (\vec{p} - \vec{k}_1)^{2\alpha_6} (\vec{k}_{12})^{2\alpha_7} (\vec{k}_{23})^{2\alpha_8}} = \frac{(p^2)^{3d/2-4}}{(4\pi)^{3d/2}} G(d, 1, 1) G(d, 1, 2-d/2) G(d, 1, 3-d), \quad (\text{A.43a})$$


<sup>2</sup>It somehow looks like a two-step ladder.

<sup>3</sup>In reference to the similar looking Mercedes-Benz logo.

<sup>4</sup>This diagram is called Non-planar because of the necessity to overlap two lines while drawing it.

$$J_{L3}(d, \vec{p}, 0, 1, 0, 1, 0, 1, 1, 1) = \text{Diagram} = \frac{(p^2)^{3d/2-5}}{(4\pi)^{3d/2}} G^2(d, 1, 1) G(d, 1, 4-d), \quad (\text{A.43b})$$

$$J_{L3}(d, \vec{p}, 0, 1, 1, 1, 0, 1, 1, 0) = \text{Diagram} = \frac{(p^2)^{3d/2-5}}{(4\pi)^{3d/2}} G^2(d, 1, 1) G(d, 1, 2-d/2), \quad (\text{A.43c})$$

$$J_{L3}(d, \vec{p}, 1, 0, 1, 1, 0, 1, 1, 1) = \text{Diagram} = \frac{(p^2)^{3d/2-6}}{(4\pi)^{3d/2}} G(d, 1, 1) G(d, 1, 1, 1, 1, 2-d/2), \quad (\text{A.43d})$$

$$J_{L3}(d, \vec{p}, 1, 1, 1, 1, 1, 1, 0, 0) = \text{Diagram} = \frac{(p^2)^{3d/2-6}}{(4\pi)^{3d/2}} G^3(d, 1, 1). \quad (\text{A.43e})$$

- The Benz (B3) master integral basis:

$$J_{B3}(d, \vec{p}, 0, 0, 1, 0, 1, 1, 1, 0) = \text{Diagram} = \frac{(p^2)^{3d/2-4}}{(4\pi)^{3d/2}} G(d, 1, 1) G(d, 1, 2-d/2) G(d, 1, 3-d), \quad (\text{A.44a})$$

$$J_{B3}(d, \vec{p}, 0, 1, 0, 1, 1, 1, 1, 0) = \text{Diagram} = \frac{(p^2)^{3d/2-5}}{(4\pi)^{3d/2}} G^2(d, 1, 1) G(d, 1, 4-d), \quad (\text{A.44b})$$

$$J_{B3}(d, \vec{p}, 0, 1, 1, 1, 1, 1, 0, 0) = \text{Diagram} = \frac{(p^2)^{3d/2-5}}{(4\pi)^{3d/2}} G^2(d, 1, 1) G(d, 1, 2-d/2), \quad (\text{A.44c})$$

$$J_{B3}(d, \vec{p}, 1, 0, 1, 1, 1, 1, 1, 0) = \text{Diagram} = \frac{(p^2)^{3d/2-6}}{(4\pi)^{3d/2}} G(d, 1, 1) G(d, 1, 1, 1, 1, 2-d/2). \quad (\text{A.44d})$$

- The Non-planar (N3) master integral basis:

$$J_{N3}(d, \vec{p}, 0, 0, 1, 0, 0, 1, 1, 1) = \text{Diagram} = \frac{(p^2)^{3d/2-4}}{(4\pi)^{3d/2}} G(d, 1, 1) G(d, 1, 2-d/2) G(d, 1, 3-d), \quad (\text{A.45a})$$

$$J_{N3}(d, \vec{p}, 0, 1, 0, 1, 0, 1, 1, 1) = \text{Diagram} = \frac{(p^2)^{3d/2-5}}{(4\pi)^{3d/2}} G^2(d, 1, 1) G(d, 1, 4-d), \quad (\text{A.45b})$$

$$J_{N3}(d, \vec{p}, 0, 1, 1, 1, 0, 1, 0, 1) = \text{Diagram} = \frac{(p^2)^{3d/2-5}}{(4\pi)^{3d/2}} G^2(d, 1, 1) G(d, 1, 2-d/2), \quad (\text{A.45c})$$

$$J_{N3}(d, \vec{p}, 1, 0, 1, 1, 0, 1, 1, 1) = \text{Diagram} = \frac{(p^2)^{3d/2-6}}{(4\pi)^{3d/2}} G(d, 1, 1) G(d, 1, 1, 1, 1, 2-d/2), \quad (\text{A.45d})$$

$$J_{N3}(d, \vec{p}, 1, 1, 1, 1, 1, 1, 1, 1) = \text{Diagram} = \frac{(p^2)^{3d/2-8}}{(4\pi)^{3d/2}} G_{N3}(d, 1, 1, 1, 1, 1, 1, 1, 1). \quad (\text{A.45e})$$

We remark that all these master integrals can be expressed only via the trivial one-loop integral  $G(d, \alpha, \beta)$  and two new non-trivial integrals;  $G(d, 1, 1, 1, 1, 2-d/2)$  and  $G_{N3}(d, 1, 1, 1, 1, 1, 1, 1, 1)$ , that we have to compute.



Let us first focus on  $G_{N3}(d,1,1,1,1,1,1,1)$ . The latter is not reducible in terms of simpler integrals. To this regard, it is the only three-loop integral that we have to compute explicitly. The result of this integral in  $d=4-2\varepsilon$  can be found, *e.g.*, in the work [347] and reads

$$G_{N3}(4-2\varepsilon,1,1,1,1,1,1,1) = e^{-3\varepsilon\gamma_E} \left[ 20\zeta_5 + O(\varepsilon) \right], \quad (\text{A.46})$$

where  $\zeta_5 \approx 1.037$  is the Riemann  $\zeta$  function evaluated at integer value 5. It turns out that this integral, thanks to its finiteness, won't be required to compute any of the three-loop RG-functions in this manuscript. Nevertheless, this result will be required to access some three-loop renormalized self-energies.

Let us now focus on the second non-trivial integral to compute,  $G(d,1,1,1,1,2-d/2)$  which  $G(d,1,1,1,1,\varepsilon)$  in  $d=4-2\varepsilon$ , a two-loop diamond integral with a non-integer index on the central line. A more general integral,  $G(d,1,1,1,1,\alpha)$ , has been evaluated exactly in [332] and reads

$$G(d,1,1,1,1,\alpha) = -2\Gamma(\lambda)\Gamma(\lambda-\alpha)\Gamma(1-2\lambda+\alpha) \times \left[ \frac{\Gamma(\lambda)}{\Gamma(2\lambda)\Gamma(3\lambda-\alpha-1)} \sum_{n=0}^{\infty} \frac{\Gamma(n+2\lambda)\Gamma(n+1)}{n!\Gamma(n+1+\alpha)} \frac{1}{n+1-\lambda+\alpha} + \frac{\pi \cot \pi(2\lambda-\alpha)}{\Gamma(2\lambda)} \right], \quad (\text{A.47})$$

where  $\lambda = (d-2)/2 = (1-2\varepsilon)/2$ . Note that (A.47) may be written with a generalized hypergeometric function  ${}_3F_2$  of argument 1, since

$${}_3F_2 \left( \begin{matrix} 1 & \alpha-\lambda+1 & 2\lambda \\ \alpha+1 & \alpha-\lambda+2 \end{matrix} \middle| 1 \right) = \frac{(\alpha-\lambda+1)\Gamma(\alpha+1)}{\Gamma(2\lambda)} \sum_{n=0}^{\infty} \frac{\Gamma(n+2\lambda)\Gamma(n+1)}{n!\Gamma(n+\alpha+1)} \frac{1}{n+1-\lambda+\alpha}. \quad (\text{A.48})$$

There is also an equivalent representation with a  ${}_3F_2$  of argument  $-1$  in the earlier work [331], see [211] for a review. We can then set  $\alpha=\varepsilon$  in (A.48) and expand it in series. This step is non-trivial, since expanding generalized hypergeometric functions in series is in general very hard. For our case, it can be achieved in an automated way using the MATHEMATICA package HYPEXP [348,349] and we obtain

$$G(4-2\varepsilon,1,1,1,1,1,\varepsilon) = e^{-2\varepsilon\gamma_E} \left[ \frac{1}{3\varepsilon^2} + \frac{5}{3\varepsilon} + \frac{17-\zeta_2}{3} + \frac{\varepsilon}{9} (123-15\zeta_2+28\zeta_3) + \frac{\varepsilon^2}{36} (348-204\zeta_2+560\zeta_3+189\zeta_4) - \frac{\varepsilon^3}{180} (27060+2460\zeta_2-13840\zeta_3+560\zeta_2\zeta_3-4725\zeta_4-21936\zeta_5) + O(\varepsilon^4) \right]. \quad (\text{A.49})$$

The non-trivial master integrals series expansions (A.46) and (A.49) have also been checked numerically using sector decomposition Monte-Carlo technique with the MATHEMATICA package FIESTA [350–352].

## A.5 Arbitrary and half-integer indices

### A.5.1 One loop

As a complementary note on the one-loop IBP reduction technique, let us underline that the procedure is also working when arbitrary indices are present. The master integral(s) will simply be different, and can be chosen arbitrarily. Let us illustrate, *e.g.*, with an integral of the form  $J(d,\vec{p},\alpha,\beta+z)$  where  $z$  is an arbitrary coefficient, *e.g.*,  $z \in \mathbb{C}$ . This integral can then be reduced, *e.g.*, onto the master integral  $J(d,\vec{p},1,z)$  with similar technique. It is easily implemented simply by shifting  $\beta \rightarrow \beta+z$  in the IBP identity (A.26a). For example, taking the integral  $J(d,1,3+z)$ , it reads

$$J(d,\vec{p},1,3+z) = \dots = \frac{(2-d+z)(3-d+z)(4-d+z)}{p^6 z(1+z)(2+z)} J(d,\vec{p},1,z). \quad (\text{A.50})$$

More generally, for an integral  $J(d, \vec{p}, 1, n+z)$  with  $n \in \mathbb{N}$  and  $z \in \mathbb{C}$ , it is easy to show that

$$J(d, \vec{p}, 1, n+z) = \frac{\prod_{i=2}^{n+1} (i-d+z)}{p^{2n} \prod_{i=0}^{n-1} (i+z)} J(d, \vec{p}, 1, z). \quad (\text{A.51})$$

Reductions of integrals of the type  $J(d, \vec{p}, \alpha, n+z)$  are much more non-trivial. Using a modified version of the MATHEMATICA package LITERED [345, 346], we showed that only one master integral is needed in this case, *e.g.*,  $J(d, \vec{p}, 1, z)$ .

These kinds of IBP reduction techniques for integrals with an arbitrary index  $z$  are very useful, at least in two cases. First,  $z$  might be the dimensional regulator itself,  $\varepsilon$ . Indeed, as we saw in, *e.g.*, (A.43) reducing higher-loop integrals may create factors of  $G(d, \alpha, \beta + \varepsilon)$  that one might want to reduce to  $G(d, 1, \varepsilon)$ . Second, in the second part of this thesis, we deal with three-dimensional theories where the gauge propagator may have half integer indices, *i.e.*,  $\sim 1/\sqrt{p^2}$ . In this case, the factor  $z$  is taken to be  $1/2$  so that we can perform reductions like

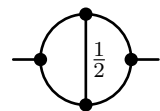
$$J(d, \vec{p}, 1, 3/2) = J(d, \vec{p}, 1, 1+1/2) = \frac{5-2d}{p^2} J(d, \vec{p}, 1, 1/2), \quad (\text{A.52})$$

where  $J(d, \vec{p}, 1, 1/2) = \frac{(p^2)^{d/2-3/2}}{(4\pi)^{d/2}} G(d, 1, 1/2)$ , that can be computed easily from (A.11) and reads

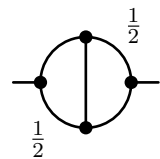
$$G(3-2\varepsilon, 1, 1/2) = 4^{-\varepsilon} \pi^{-1/2} e^{-\varepsilon\gamma_E} \left( \frac{2}{\varepsilon} + 8 + (32-7\zeta_2)\varepsilon + \left( 128-28\zeta_2 - \frac{98\zeta_3}{3} \right) + \mathcal{O}(\varepsilon^3) \right). \quad (\text{A.53})$$

### A.5.2 Two loops

Focusing on half integer indices, using similar IBP reduction techniques (and a modified version of the MATHEMATICA package LITERED [345, 346] to automatize the procedures) allow us to reduce any two-loop integral onto masters that can be expressed with the trivial one-loop function  $G(d, \alpha, \beta)$  together with two non-trivial two-loop masters



$$= \frac{(p^2)^{d-9/2}}{(4\pi)^d} G(d, 1, 1, 1, 1, 1/2), \quad (\text{A.54a})$$



$$= \frac{(p^2)^{d-4}}{(4\pi)^d} G(d, 1, 1/2, 1, 1/2, 1). \quad (\text{A.54b})$$

The first one is easily computed from the general case  $G(d, 1, 1, 1, 1, \alpha)$ , see (A.47) with  $\alpha = 1/2$ , yielding in  $d = 3 - 2\varepsilon$

$$G(3-2\varepsilon, 1, 1, 1, 1, 1/2) = 3\pi 4^{-\varepsilon} e^{-2\varepsilon\gamma_E} \left( 2\zeta_2 + 21\zeta_3\varepsilon + \mathcal{O}(\varepsilon^2) \right). \quad (\text{A.55})$$

The second integral is highly non-trivial and can, in principle, be computed from the results of Appendix B in [147] (based on the Gegenbauer polynomial technique [332]), where the general integral  $G(d, 1, \alpha, 1, \beta, 1)$  has been derived exactly as a combination of two generalized hyper-geometric functions  ${}_3F_2$  of argument 1, reading

$$G(d, 1, \alpha, 1, \beta, 1) = \frac{\Gamma(\lambda)\Gamma(-\alpha+\lambda+1)\Gamma(-\beta+\lambda+1)}{\alpha(\alpha-2\lambda)(\alpha-\lambda)\Gamma(\alpha)(\beta-\lambda)\Gamma(\beta+1)\Gamma(2\lambda)\Gamma(2\lambda-\alpha)\Gamma(\alpha+\beta-\lambda+1)\Gamma(-\alpha-\beta+3\lambda)} \left[ \alpha\Gamma(2\lambda)\Gamma(2\lambda-\alpha)\Gamma(\alpha+\beta-2\lambda+1)\Gamma(\alpha+\beta-\lambda+1) {}_3F_2(1, 2\lambda, 2\lambda-\alpha; \beta+1, -\alpha+2\lambda+1; 1) \right]$$

$$\begin{aligned}
& -(\alpha - 2\lambda)\Gamma(\beta + 1)\sin(\pi(\beta - 2\lambda))\csc(\pi(\alpha + \beta - 3\lambda - 1))\left( \right. \\
& \Gamma(\lambda)\Gamma(2\lambda)\Gamma(\alpha - \lambda + 1)\Gamma(\beta - \lambda + 1) {}_3F_2(\alpha, \alpha - \lambda + 1, 2\lambda; \alpha + 1, \alpha + \beta - \lambda + 1; 1) \\
& \left. + \pi\alpha\Gamma(\alpha)\sin(\pi(-\alpha + \lambda + 1))\Gamma(2\lambda - \alpha)\csc^2(\pi(\beta - 2\lambda))\Gamma(\alpha + \beta - \lambda + 1) \right), \tag{A.56}
\end{aligned}$$

where  $\lambda = (d - 2)/2$ . However, even for our special case of interest, *i.e.*,  $d = 3 - 2\varepsilon$  and  $\alpha = \beta = 1/2$ , this result is extremely hard to expand in series of  $\varepsilon$  due to the presence of half integer indices, implying branch-cuts. The MATHEMATICA package HYPEXP [348, 349] is not able to expand it in series. Upon studying the result with very high numerical precision and, cross-checking our results with the numerical (Monte-Carlo) sector decomposition MATHEMATICA package FIESTA [350–352] and the study [105] (that uses PSLQ techniques [353]), we were able to (re-)derive the needed result, reading

$$G(3 - 2\varepsilon, 1, 1/2, 1, 1/2, 1) = \frac{8}{3\pi} \left( \pi^2 C + 24\text{Cl}_4(\pi/2) + \mathcal{O}(\varepsilon) \right), \tag{A.57}$$

where  $\text{Cl}_z(\theta)$  is the Clausen function, defined for even  $z$  index as

$$\text{Cl}_z(\theta) = \sum_{n=1}^{\infty} \frac{\sin(n\theta)}{n^z}, \tag{A.58}$$

such that

$$\text{Cl}_2(\pi/2) = C = 0.9160, \quad \text{Cl}_4(\pi/2) = 0.9889, \tag{A.59}$$

where  $C$  is the Catalan number. From our computation, the result (A.57) is correct numerically at least up to 100 digits precision, we therefore consider it exact.

# Bibliography

- [1] S. Metayer, D. Mouhanna, and S. Teber, “Three-loop order approach to flat polymerized membranes,” *Phys. Rev. E* 105 no. 1, (2022) L012603, [arXiv:2109.03796].
- [2] S. Metayer, D. Mouhanna, and S. Teber, “Flat polymerized membranes at three-loop order,” *J. Phys. Conf. Ser.* 2438 no. 1, (2023) 012141, [arXiv:2210.04309]. Conference proceedings (ACAT 2021).
- [3] S. Metayer and D. Mouhanna, “Flat phase of quenched disordered membranes at three-loop order,” *Phys. Rev. E* 106 no. 6, (2022) 064114, [arXiv:2206.01633].
- [4] S. Metayer and S. Teber, “Two-loop mass anomalous dimension in reduced quantum electrodynamics and application to dynamical fermion mass generation,” *JHEP* 09 (2021) 107, [arXiv:2107.07807].
- [5] S. Metayer and S. Teber, “Critical properties of three-dimensional many-flavor QEDs,” *Symmetry* 15 no. 9, (2023).
- [6] S. Metayer and S. Teber, “Electron mass anomalous dimension at  $O(1/N_f^2)$  in three-dimensional  $\mathcal{N}=1$  supersymmetric QED,” *Phys. Lett. B* 838 (2023) 137729, [arXiv:2212.09609].
- [7] A. James, S. Metayer, and S. Teber, “ $\mathcal{N}=1$  supersymmetric three-dimensional QED in the large- $N_f$  limit and applications to super-graphene,” [arXiv:2102.02722].
- [8] R. Hook, “Lectures de potentia restitutiva, or, of spring explaining the power of springing bodies.” 1678. [name.umdl.umich.edu/A44322.0001.001].
- [9] L. Landau and E. Lifshitz’s, *Theory of elasticity*, vol. 7. Physics Today, 1959.
- [10] P.-G. D. Gennes, *Scaling concepts in polymer physics*. Cornell university press, 1979. [PDF].
- [11] M. J. Bowick and A. Travesset, “The Statistical mechanics of membranes,” *Phys. Rept.* 344 (2001) 255–308, [arXiv:cond-mat/0002038].
- [12] P. Le Doussal and L. Radzihovsky, “Anomalous elasticity, fluctuations and disorder in elastic membranes,” *Annals of Physics* 392 (May, 2018) 340–410, [arXiv:1708.05723].
- [13] K. J. Wiese, “Polymerized membranes, a review,” [arXiv:cond-mat/0001345]. [PDF].
- [14] O. Coquand, *Fluctuations dans la phase plate des membranes cristallines*. PhD thesis, Sorbonne Université, 2018. In French, theses.fr/2018SORUS096, [PDF].
- [15] A. Elgsaeter, B. T. Stokke, A. Mikkelsen, and D. Branton, “The molecular basis of erythrocyte shape,” *Science* 234 no. 4781, (1986) 1217–1223.
- [16] C. F. Schmidt, K. Svoboda, N. Lei, I. B. Petsche, L. E. Berman, C. R. Safinya, and G. S. Grest, “Existence of a flat phase in red cell membrane skeletons,” *Science* 259 no. 5097, (1993) 952–955.
- [17] M. Katsnelson, *Graphene: Carbon in Two Dimensions*. Cambridge University Press, 2012.
- [18] B. Amorim, A. Cortijo, *et al.*, “Novel effects of strains in graphene and other two dimensional materials,” *Physics Reports* 617 (Mar, 2016) 1–54, [arXiv:1503.00747].
- [19] T. Hwa, E. Kokufuta, and T. Tanaka, “Conformation of graphite oxide membranes in solution,” *Phys. Rev. A* 44 (Aug, 1991) R2235–R2238.
- [20] X. Wen, C. W. Garland, T. Hwa, M. Kardar, E. Kokufuta, Y. Li, M. Orkisz, and T. Tanaka, “Crumpled and collapsed conformation in graphite oxide membranes,” *Nature* 355 no. 6359, (Jan., 1992) 426–428.
- [21] M. S. Spector, E. Naranjo, S. Chiruvolu, and J. A. Zasadzinski, “Conformations of a tethered membrane: Crumpling in graphitic oxide?” *Phys. Rev. Lett.* 73 (Nov, 1994) 2867–2870.
- [22] R. Podgornik, “Statistical thermodynamics of surfaces, interfaces, and membranes,” *Journal of Statistical Physics* 78 no. 3, (Feb, 1995) 1175–1177.
- [23] J. F. Wheeler, “Random surfaces: from polymer membranes to strings,” *Journal of Physics A: Mathematical and General* 27 no. 10, (May, 1994) 3323.
- [24] F. David, “Random surfaces and the statistics of membranes,” *Physics Reports* 184 no. 2, (1989) 221–227.
- [25] M. Falcioni, M. J. Bowick, E. Gutter, and G. Thorleifsson, “The Poisson ratio of crystalline surfaces,” *EPL (Europhysics Letters)* 38 no. 1, (Apr., 1997) 7–12, [arXiv:cond-mat/9610007].
- [26] K. S. Novoselov, A. K. Geim, S. V. Morozov, D. Jiang, Y. Zhang, S. V. Dubonos, I. V. Grigorieva, and A. A. Firsov, “Electric field effect in atomically thin carbon films,” *Science* 306 no. 5696, (Oct., 2004) 666–669, [arXiv:cond-mat/0410550].
- [27] K. S. Novoselov, A. K. Geim, S. V. Morozov, D. Jiang, M. I. Katsnelson, I. V. Grigorieva, S. V. Dubonos, and A. A. Firsov, “Two-dimensional gas of massless Dirac fermions in graphene,” *Nature* 438 (2005) 197, [arXiv:cond-mat/0509330].
- [28] Nelson, D.R. and Peliti, L., “Fluctuations in membranes with crystalline and hexatic order,” *J. Phys. France* 48 no. 7, (1987) 1085–1092. [PDF].
- [29] J. A. Aronovitz and T. C. Lubensky, “Fluctuations of solid membranes,” *Phys. Rev. Lett.* 60 (Jun, 1988) 2634–2637.

- [30] O. Coquand, “Spontaneous symmetry breaking and the flat phase of crystalline membranes,” *Phys. Rev. B* 100 no. 12, (2019) 125406, [arXiv:1906.04455].
- [31] E. Gutter, F. David, S. Leibler, and L. Peliti, “Crumpling and buckling transitions in polymerized membranes,” *Phys. Rev. Lett.* 61 (Dec, 1988) 2949–2952.
- [32] J. Aronovitz, L. Golubovic, and T. C. Lubensky, “Fluctuations and lower critical dimensions of crystalline membranes,” *J. Phys. France* 50 no. 6, (1989) 609–631. [PDF].
- [33] Gutter, E., David, F., Leibler, S., and Peliti, L., “Thermodynamical behavior of polymerized membranes,” *J. Phys. France* 50 no. 14, (1989) 1787–1819.
- [34] F. David and E. Gutter, “Crumpling Transition in Elastic Membranes: Renormalization Group Treatment,” *EPL* 5 (1988) 709.
- [35] I. V. Gornyi, V. Y. Kachorovskii, and A. D. Mirlin, “Rippling and crumpling in disordered free-standing graphene,” *Phys. Rev. B* 92 (Oct, 2015) 155428, [arXiv:1505.04483].
- [36] D. Saykin, I. Gornyi, V. Kachorovskii, and I. Burmistrov, “Absolute poisson’s ratio and the bending rigidity exponent of a crystalline two-dimensional membrane,” *Annals of Physics* 414 (Mar, 2020) 168108, [arXiv:2002.04554].
- [37] D. Gazit, “The Structure of Physical Crystalline Membranes within the Self-Consistent Screening Approximation,” *Phys. Rev. E* 80 (2009) 041117, [arXiv:0907.3718].
- [38] K. V. Zakharchenko, R. Roldán, A. Fasolino, and M. I. Katsnelson, “Self-consistent screening approximation for flexible membranes: Application to graphene,” *Phys. Rev. B* 82 (Sep, 2010) 125435, [arXiv:1006.1534].
- [39] R. Roldán, A. Fasolino, K. V. Zakharchenko, and M. I. Katsnelson, “Suppression of anharmonicities in crystalline membranes by external strain,” *Phys. Rev. B* 83 (May, 2011) 174104, [arXiv:1101.6026].
- [40] P. Le Doussal and L. Radzihovsky, “Self-consistent theory of polymerized membranes,” *Phys. Rev. Lett.* 69 (Aug, 1992) 1209–1212, [arXiv:cond-mat/9208023].
- [41] J.-P. Kownacki and D. Mouhanna, “Crumpling transition and flat phase of polymerized phantom membranes,” *Phys. Rev. E* 79 (Apr, 2009) 040101, [arXiv:0811.0884].
- [42] F. L. Braghin and N. Hasselmann, “Thermal fluctuations of free-standing graphene,” *Phys. Rev. B* 82 (Jul, 2010) 035407, [arXiv:1003.5116].
- [43] N. Hasselmann and F. L. Braghin, “Nonlocal effective-average-action approach to crystalline phantom membranes,” *Phys. Rev. E* 83 (Mar, 2011) 031137, [arXiv:1012.0313].
- [44] K. Essafi, J.-P. Kownacki, and D. Mouhanna, “Crumpled-to-tubule transition in anisotropic polymerized membranes: Beyond the  $\epsilon$  expansion,” *Phys. Rev. Lett.* 106 (Mar, 2011) 128102.
- [45] K. Essafi, J. P. Kownacki, and D. Mouhanna, “First order phase transitions in polymerized phantom membranes,” *Phys. Rev. E* 89 no. 4, (2014) 042101, [arXiv:1402.0426].
- [46] O. Coquand and D. Mouhanna, “Flat phase of quantum polymerized membranes,” *Phys. Rev. E* 94 no. 3, (2016) 032125, [arXiv:1607.03335].
- [47] O. Coquand, D. Mouhanna, and S. Teber, “Flat phase of polymerized membranes at two-loop order,” *Phys. Rev. E* 101 no. 6, (2020) 062104, [arXiv:2003.13973].
- [48] Z. Zhang, H. T. Davis, and D. M. Kroll, “Scaling behavior of self-avoiding tethered vesicles,” *Phys. Rev. E* 48 (Aug, 1993) R651–R654.
- [49] M. J. Bowick, S. M. Catterall, M. Falcioni, G. Thorleifsson, and K. N. Anagnostopoulos, “The Flat phase of crystalline membranes,” *J. Phys. I(France)* 6 (1996) 1321–1345, [arXiv:cond-mat/9603157].
- [50] A. Tröster, “High-precision fourier monte carlo simulation of crystalline membranes,” *Phys. Rev. B* 87 (Mar, 2013) 104112, [arXiv:1303.3726].
- [51] J. H. Los, M. I. Katsnelson, O. V. Yazyev, K. V. Zakharchenko, and A. Fasolino, “Scaling properties of flexible membranes from atomistic simulations: Application to graphene,” *Phys. Rev. B* 80 (Sep, 2009) 121405, [arXiv:0903.3847].
- [52] C. Gourier, J. Daillant, *et al.*, “Bending energy of amphiphilic films at the nanometer scale,” *Phys. Rev. Lett.* 78 (Apr, 1997) 3157–3160.
- [53] J. A. Jackson, N. Romeo, A. Mietke, K. J. Burns, J. F. Tutz, A. C. Martin, J. Dunkel, and J. I. Alsous, “Dynamics, scaling behavior, and control of nuclear wrinkling,” *arXiv e-prints* (Oct., 2022) arXiv:2210.11581, [arXiv:2210.11581].
- [54] G. López-Polín, C. Gómez-Navarro, V. Parente, F. Guinea, M. Katsnelson, F. Pérez-Murano, and J. Gómez-Herrero, “Increasing the elastic modulus of graphene by controlled defect creation,” *Nature Physics* 11 no. 1, (Jan, 2015) 26–31.
- [55] A. Mauri and M. I. Katsnelson, “Scaling behavior of crystalline membranes: An  $\epsilon$ -expansion approach,” *Nuclear Physics B* 956 (2020) 115040.
- [56] O. Coquand and D. Mouhanna, “Wrinkling transition in quenched disordered membranes at two loops,” *Phys. Rev. E* 103 (2021) 031001, [arXiv:2011.01550].
- [57] A. Pikelner, “Four-loop critical properties of polymerized membranes,” *EPL* 138 no. 1, (2022) 17002, [arXiv:2112.07340].
- [58] A. Mauri and M. I. Katsnelson, “Scale without conformal invariance in membrane theory,” *Nuclear Physics B* 969 (2021) 115482, [arXiv:2104.06859].
- [59] P. Nogueira, “Automatic feynman graph generation,” *Journal of Computational Physics* 105 no. 2, (1993) 279–289.
- [60] P. Nogueira, “Feynman graph generation and propagator mixing, I,” *Comput. Phys. Commun.* 269 (2021) 108103.



- [61] A. Grozin, “Lectures on QED and QCD,” *arXiv e-prints* (Aug., 2005) hep-ph/0508242, [[arXiv:hep-ph/0508242](#)].
- [62] V. A. Smirnov and K. G. Chetyrkin, “Dimensional regularization and infrared divergences,” *Theoretical and Mathematical Physics* 56 no. 2, (Aug., 1983) 770–776.
- [63] A. N. Vasiliev, Y. M. Pismak, and Y. R. Khonkonen, “ $1/n$  Expansion: Calculation of the exponents  $\eta$  and  $\nu$  in the order  $1/n^2$  for arbitrary number of dimensions,” *Theoretical and Mathematical Physics* 47 no. 3, (June, 1981) 465–475.
- [64] F. Tkachov, “A theorem on analytical calculability of 4-loop renormalization group functions,” *Physics Letters B* 100 no. 1, (1981) 65–68.
- [65] K. G. Chetyrkin and F. V. Tkachov, “Integration by parts: The algorithm to calculate  $\beta$ -functions in 4 loops,” *Nuclear Physics B* 192 no. 1, (Nov., 1981) 159–204.
- [66] J. P. Boyd, “The devil’s invention: Asymptotic, superasymptotic and hyperasymptotic series,” *Acta Applicandae Mathematica* 56 no. 1, (Mar, 1999) 1–98.
- [67] C. Wetterich, “Exact evolution equation for the effective potential,” *Physics Letters B* 301 no. 1, (1993) 90–94, [[arXiv:1710.05815](#)].
- [68] C. Bagnuls and C. Bervillier, “Exact renormalization group equations: an introductory review,” *Physics Reports* 348 no. 1, (2001) 91–157. Renormalization group theory in the new millennium. II.
- [69] J. Berges, N. Tetradis, and C. Wetterich, “Non-perturbative renormalization flow in quantum field theory and statistical physics,” *Physics Reports* 363 no. 4, (2002) 223–386, [[arXiv:hep-ph/0005122](#)]. Renormalization group theory in the new millennium. IV.
- [70] B. Delamotte, D. Mouhanna, and M. Tissier, “Nonperturbative renormalization-group approach to frustrated magnets,” *Phys. Rev. B* 69 (Apr, 2004) 134413, [[arXiv:cond-mat/0309101](#)].
- [71] J. M. Pawłowski, “Aspects of the functional renormalisation group,” *Annals of Physics* 322 no. 12, (2007) 2831–2915, [[hep-th/0512261](#)].
- [72] O. J. Rosten, “Fundamentals of the exact renormalization group,” *Physics Reports* 511 no. 4, (2012) 177–272, [[arXiv:1003.1366](#)].
- [73] L. Canet, B. Delamotte, D. Mouhanna, and J. Vidal, “Nonperturbative renormalization group approach to the ising model: A derivative expansion at order  $\partial^4$ ,” *Phys. Rev. B* 68 (Aug, 2003) 064421.
- [74] G. De Polsi, I. Balog, M. Tissier, and N. Wschebor, “Precision calculation of critical exponents in the  $o(n)$  universality classes with the nonperturbative renormalization group,” *Phys. Rev. E* 101 (Apr, 2020) 042113, [[arXiv:2001.07525](#)].
- [75] I. Balog, H. Chaté, B. Delamotte, M. Marohnić, and N. Wschebor, “Convergence of nonperturbative approximations to the renormalization group,” *Phys. Rev. Lett.* 123 (Dec, 2019) 240604, [[arXiv:1907.01829](#)].
- [76] T. Papenbrock and C. Wetterich, “Two-loop results from improved one loop computations,” *Zeitschrift für Physik C Particles and Fields* 65 no. 3, (Sep, 1995) 519–535.
- [77] T. R. Morris and J. F. Tighe, “Convergence of derivative expansions of the renormalization group,” *Journal of High Energy Physics* 1999 no. 08, (Sep, 1999) 007.
- [78] A. J. Bray, “Self-consistent screening calculation of the critical exponent  $\eta$ ,” *Phys. Rev. Lett.* 32 (Jun, 1974) 1413–1416.
- [79] P. L. Doussal, “Tethered membranes with long-range self-avoidance: large-dimension limit,” *Journal of Physics A: Mathematical and General* 25 no. 8, (Apr, 1992) L469.
- [80] F. F. Abraham and D. R. Nelson, “Diffraction from polymerized membranes,” *Science* 249 no. 4967, (1990) 393–397.
- [81] S. Komura and A. Baumgärtner, “Tethered vesicles at constant pressure: Monte carlo study and scaling analysis,” *Phys. Rev. A* 44 (Sep, 1991) 3511–3518.
- [82] S. Leibler and A. C. Maggs, “Entropic interactions between polymerized membranes,” *Phys. Rev. Lett.* 63 (Jul, 1989) 406–409.
- [83] Gutter, E., Leibler, S., Maggs, A.C., and David, F., “Stretching and buckling of polymerized membranes: a monte carlo study,” *J. Phys. France* 51 no. 11, (1990) 1055–1060.
- [84] Z. Zhang, H. T. Davis, and D. M. Kroll, “Molecular dynamics simulations of tethered membranes with periodic boundary conditions,” *Phys. Rev. E* 53 (Feb, 1996) 1422–1429.
- [85] I. B. Petsche and G. S. Grest, “Molecular dynamics simulations of the structure of closed tethered membranes,” *Journal de Physique I* 3 no. 8, (Aug., 1993) 1741–1754.
- [86] B. K. Von Helmut Föll, “Agglomerates of interstitial atoms (swirl defects) in silicon - their importance for basic research and technology,”. Yearbook of the Academy of Sciences in Göttingen 1976, [[LINK](#)].
- [87] A. H. Castro Neto, F. Guinea, N. M. R. Peres, K. S. Novoselov, and A. K. Geim, “The electronic properties of graphene,” *Rev. Mod. Phys.* 81 (2009) 109–162, [[arXiv:0709.1163](#)].
- [88] M. I. Katsnelson, “Graphene: carbon in two dimensions,” *arXiv e-prints* (Dec., 2006) cond-mat/0612534, [[arXiv:cond-mat/0612534](#)].
- [89] D. Akinwande, C. J. Brennan, *et al.*, “A review on mechanics and mechanical properties of 2d materials—graphene and beyond,” *Extreme Mechanics Letters* 13 (2017) 42–77.
- [90] L. Liu, M. Qing, Y. Wang, and S. Chen, “Defects in graphene: Generation, healing, and their effects on the properties of graphene: A review,” *Journal of Materials Science & Technology* 31 no. 6, (2015) 599–606. A Special Issue on 1D Nanomaterials.
- [91] G. Yang, L. Li, W. B. Lee, and M. C. Ng, “Structure of graphene and its disorders: a review,” *Science and Technology of Advanced Materials* 19 no. 1, (2018) 613–648. PMID: 30181789.

- [92] E. Sackmann, P. Egg, C. Fahn, H. Bader, H. Ringsdorf, and M. Schollmeier, "Compound membranes of linearly polymerized and cross-linked macrolipids with phospholipids: Preparation, microstructure and applications," *Berichte der Bunsengesellschaft für physikalische Chemie* 89 no. 11, (1985) 1198–1208.
- [93] M. Mutz, D. Bensimon, and M. J. Brienne, "Wrinkling transition in partially polymerized vesicles," *Phys. Rev. Lett.* 67 (Aug, 1991) 923–926.
- [94] S. Chaieb, V. K. Natrajan, and A. A. El-rahman, "Glassy conformations in wrinkled membranes," *Phys. Rev. Lett.* 96 (Feb, 2006) 078101.
- [95] S. Chaieb, Šárka Málková, and J. Lal, "Why the wrinkling transition in partially polymerized membranes is not universal? fractal-multifractal hierarchy," *Journal of Theoretical Biology* 251 no. 1, (2008) 60–67.
- [96] S. Chaieb, "Elasto-plasticity in wrinkled polymerized lipid membranes," *Scientific Reports* 4 no. 1, (Jan, 2014) 3699.
- [97] S. Chaieb, "Correction: Corrigendum: Elasto-plasticity in wrinkled polymerized lipid membranes," *Scientific Reports* 4 no. 1, (Dec, 2014) 7347.
- [98] D. R. Nelson and L. Radzihovsky, "Polymerized membranes with quenched random internal disorder," *Europhysics Letters* 16 no. 1, (Sep, 1991) 79.
- [99] L. Radzihovsky and D. R. Nelson, "Statistical mechanics of randomly polymerized membranes," *Phys. Rev. A* 44 (Sep, 1991) 3525–3542.
- [100] Leo Radzihovsky and Pierre Le Doussal, "Crumpled glass phase of randomly polymerized membranes in the large  $d$  limit," *J. Phys. I France* 2 no. 5, (1992) 599–613.
- [101] D. C. Morse, T. C. Lubensky, and G. S. Grest, "Quenched disorder in tethered membranes," *Phys. Rev. A* 45 (Feb, 1992) R2151–R2154.
- [102] D. C. Morse and T. C. Lubensky, "Curvature disorder in tethered membranes: A new flat phase at  $t=0$ ," *Phys. Rev. A* 46 (Aug, 1992) 1751–1768.
- [103] O. Coquand, K. Essafi, J.-P. Kownacki, and D. Mouhanna, "Glassy phase in quenched disordered crystalline membranes," *Phys. Rev. E* 97 (Mar, 2018) 030102.
- [104] O. Coquand, K. Essafi, J.-P. Kownacki, and D. Mouhanna, "Universal behaviors in the wrinkling transition of disordered membranes," *Phys. Rev. E* 101 (Apr, 2020) 042602, [arXiv:1909.13268].
- [105] A. F. Pikelner, V. P. Gusynin, A. V. Kotikov, and S. Teber, "Four-loop singularities of the massless fermion propagator in quenched three-dimensional QED," *Phys. Rev. D* 102 no. 10, (2020) 105012, [arXiv:2008.09400].
- [106] D. R. Saykin, V. Y. Kachorovskii, and I. S. Burmistrov, "Phase diagram of a flexible two-dimensional material," *Phys. Rev. Res.* 2 (Oct, 2020) 043099.
- [107] M. Mezard, G. Parisi, and M. Virasoro, *Spin Glass Theory and Beyond*. WORLD SCIENTIFIC, 1986.
- [108] P. A. M. Dirac, "The Quantum Theory of the Emission and Absorption of Radiation," *Proceedings of the Royal Society of London Series A* 114 no. 767, (Mar., 1927) 243–265.
- [109] R. P. Feynman, *QED: The Strange Theory of Light and Matter*. Princeton University Press, rev - revised ed., 1985. [LINK].
- [110] M. E. Peskin and D. V. Schroeder, *An Introduction to Quantum Field Theory*. Westview Press, 1995. Reading, USA: Addison-Wesley (1995) 842 p.
- [111] J. Schwinger, "On quantum-electrodynamics and the magnetic moment of the electron," *Phys. Rev.* 73 (Feb, 1948) 416–417.
- [112] B. C. Odom, D. Hanneke, B. D'Urso, and G. Gabrielse, "New Measurement of the Electron Magnetic Moment Using a One-Electron Quantum Cyclotron," *Phys. Rev. Lett.* 97 (2006) 030801.
- [113] D. Hanneke, S. F. Hoogerheide, and G. Gabrielse, "Cavity Control of a Single-Electron Quantum Cyclotron: Measuring the Electron Magnetic Moment," *Phys. Rev. A* 83 (2011) 052122, [arXiv:1009.4831].
- [114] L. Morel, Z. Yao, P. Cladé, and S. Guellati-Khélifa, "Determination of the fine-structure constant with an accuracy of 81 parts per trillion," *Nature* 588 no. 7836, (Dec, 2020) 61–65.
- [115] T. Aoyama, M. Hayakawa, T. Kinoshita, and M. Nio, "Tenth-order qed contribution to the electron  $g-2$  and an improved value of the fine structure constant," *Phys. Rev. Lett.* 109 (Sep, 2012) 111807.
- [116] P. D. Group, P. A. Zyla, *et al.*, "Review of Particle Physics," *Progress of Theoretical and Experimental Physics* 2020 no. 8, (08, 2020) . 083C01.
- [117] J. A. Gracey, "Large  $N_f$  quantum field theory," *Int. J. Mod. Phys. A* 33 no. 35, (2019) 1830032, [arXiv:1812.05368].
- [118] E. V. Gorbar, V. P. Gusynin, and V. A. Miransky, "Dynamical chiral symmetry breaking on a brane in reduced QED," *Phys. Rev. D* 64 (2001) 105028, [arXiv:hep-ph/0105059].
- [119] D. B. Kaplan, J.-W. Lee, D. T. Son, and M. A. Stephanov, "Conformality Lost," *Phys. Rev. D* 80 (2009) 125005, [arXiv:0905.4752].
- [120] E. C. Marino, "Quantum electrodynamics of particles on a plane and the Chern-Simons theory," *Nucl. Phys. B* 408 (1993) 551–564, [arXiv:hep-th/9301034].
- [121] D. T. Son, "Is the Composite Fermion a Dirac Particle?," *Phys. Rev. X* 5 no. 3, (2015) 031027, [arXiv:1502.03446].
- [122] E. V. Gorbar, V. P. Gusynin, V. A. Miransky, and I. A. Shovkovy, "Magnetic field driven metal insulator phase transition in planar systems," *Phys. Rev. B* 66 (2002) 045108, [arXiv:cond-mat/0202422].
- [123] G. E. Volovik, *The Universe in a Helium Droplet*. Oxford University Press, 02, 2009.

- [124] V. P. Gusynin, S. G. Sharapov, and J. P. Carbotte, “AC conductivity of graphene: from tight-binding model to 2+1-dimensional quantum electrodynamics,” *Int. J. Mod. Phys. B* **21** (2007) 4611–4658, [[arXiv:0706.3016](#)].
- [125] V. N. Kotov, B. Uchoa, V. M. Pereira, A. H. C. Neto, and F. Guinea, “Electron-Electron Interactions in Graphene: Current Status and Perspectives,” *Rev. Mod. Phys.* **84** (2012) 1067, [[arXiv:1012.3484](#)].
- [126] S. Teber, *Field theoretic study of electron-electron interaction effects in Dirac liquids*. Habilitation, Sorbonne Université, 2017. [[arXiv:1810.08428](#)].
- [127] P. R. Wallace, “The band theory of graphite,” *Phys. Rev.* **71** (May, 1947) 622–634.
- [128] G. W. Semenoff, “Condensed Matter Simulation of a Three-dimensional Anomaly,” *Phys. Rev. Lett.* **53** (1984) 2449.
- [129] J. Gonzalez, F. Guinea, and M. A. H. Vozmediano, “NonFermi liquid behavior of electrons in the half filled honeycomb lattice (A Renormalization group approach),” *Nucl. Phys. B* **424** (1994) 595–618, [[arXiv:hep-th/9311105](#)].
- [130] R. Mattuck, *A Guide to Feynman Diagrams in the Many-Body Problem: Second Edition*. Dover Books on Physics. Dover Publications, 2012. [[LINK](#)].
- [131] T. Appelquist, D. Nash, and L. C. R. Wijewardhana, “Critical Behavior in (2+1)-Dimensional QED,” *Phys. Rev. Lett.* **60** (1988) 2575.
- [132] M. S. Nevius, M. Conrad, F. Wang, A. Celis, M. N. Nair, A. Taleb-Ibrahimi, A. Tejada, and E. H. Conrad, “Semiconducting Graphene from Highly Ordered Substrate Interactions,” *Phys. Rev. Lett.* **115** no. 13, (Sept., 2015) 136802, [[arXiv:1505.00435](#)].
- [133] M. J. Allen, V. C. Tung, and R. B. Kaner, “Honeycomb carbon: A review of graphene,” *Chemical Reviews* **110** no. 1, (Jan, 2010) 132–145.
- [134] A. Kotikov and S. Teber, “Critical behaviour of reduced QED<sub>4,3</sub> and dynamical fermion gap generation in graphene,” *Phys. Rev. D* **94** no. 11, (2016) 114010, [[arXiv:1610.00934](#)]. [Erratum: *Phys.Rev.D* **99**, 119902 (2019)].
- [135] A. Kovner and B. Rosenstein, “Kosterlitz-thouless mechanism of two-dimensional superconductivity,” *Phys. Rev. B* **42** (Sep, 1990) 4748–4751.
- [136] N. Dorey and N. E. Mavromatos, “QED in three-dimension and two-dimensional superconductivity without parity violation,” *Nucl. Phys. B* **386** (1992) 614–680.
- [137] M. Franz and Z. Tesanovic, “Algebraic Fermi Liquid from Phase Fluctuations: ‘Topological’ Fermions, Vortex ‘Berryons,’ and QED-3 Theory of Cuprate Superconductors,” *Phys. Rev. Lett.* **87** (2001) 257003, [[arXiv:cond-mat/0012445](#)].
- [138] I. F. Herbut, “QED(3) theory of underdoped high temperature superconductors,” *Phys. Rev. B* **66** (2002) 094504, [[arXiv:cond-mat/0202491](#)].
- [139] K. Farakos and N. E. Mavromatos, “Gauge theory approach to planar doped antiferromagnetics and external magnetic fields,” *Int. J. Mod. Phys. B* **12** (1998) 809, [[arXiv:cond-mat/9710288](#)].
- [140] M. Polini, F. Guinea, M. Lewenstein, H. C. Manoharan, and V. Pellegrini, “Artificial honeycomb lattices for electrons, atoms and photons,” *Nature Nanotechnology* **8** no. 9, (Sept., 2013) 625–633, [[arXiv:1304.0750](#)].
- [141] M. Z. Hasan and C. L. Kane, “Colloquium: Topological insulators,” *Reviews of Modern Physics* **82** no. 4, (Oct., 2010) 3045–3067, [[arXiv:1002.3895](#)].
- [142] E. C. Marino, L. O. Nascimento, V. S. Alves, and C. M. Smith, “Interaction induced quantum valley hall effect in graphene,” *Phys. Rev. X* **5** (Mar, 2015) 011040, [[arXiv:1309.5879](#)].
- [143] W. Pan, W. Kang, K. W. Baldwin, K. W. West, L. N. Pfeiffer, and D. C. Tsui, “Berry phase and anomalous transport of the composite fermions at the half-filled Landau level,” *Nature Physics* **13** no. 12, (Dec., 2017) 1168–1172, [[arXiv:1702.07307](#)].
- [144] S. Teber, “Electromagnetic current correlations in reduced quantum electrodynamics,” *Phys. Rev. D* **86** (2012) 025005, [[arXiv:1204.5664](#)].
- [145] A. V. Kotikov and S. Teber, “Note on an application of the method of uniqueness to reduced quantum electrodynamics,” *Phys. Rev. D* **87** no. 8, (2013) 087701, [[arXiv:1302.3939](#)].
- [146] I. F. Herbut and V. Mastropietro, “Universal conductivity of graphene in the ultrarelativistic regime,” *Phys. Rev. B* **87** no. 20, (2013) 205445, [[arXiv:1304.1988](#)].
- [147] A. V. Kotikov and S. Teber, “Two-loop fermion self-energy in reduced quantum electrodynamics and application to the ultrarelativistic limit of graphene,” *Phys. Rev. D* **89** no. 6, (2014) 065038, [[arXiv:1312.2430](#)].
- [148] D. Valenzuela, S. Hernández-Ortiz, M. Loewe, and A. Raya, “Graphene transparency in weak magnetic fields,” *J. Phys. A* **48** no. 6, (2015) 065402, [[arXiv:1410.5501](#)].
- [149] S. Hernández-Ortiz, D. Valenzuela, A. Raya, and S. Sánchez-Madrigal, “Light absorption in distorted graphene,” *International Journal of Modern Physics B* **30** no. 14, (Apr., 2016) 1650084, [[arXiv:1509.06717](#)].
- [150] S. Teber and A. V. Kotikov, “Field theoretic renormalization study of reduced quantum electrodynamics and applications to the ultrarelativistic limit of Dirac liquids,” *Phys. Rev. D* **97** no. 7, (2018) 074004, [[arXiv:1801.10385](#)].
- [151] V. Sérgio Alves, R. O. C. Junior, E. C. Marino, and L. O. Nascimento, “Dynamical Mass Generation in Pseudo Quantum Electrodynamics with Four-Fermion Interactions,” *arXiv e-prints* (Apr., 2017) [arXiv:1704.00381](#), [[arXiv:1704.00381](#)].



- [152] S. Teber and A. V. Kotikov, “Review of Electron-Electron Interaction Effects in Planar Dirac Liquids,” *Theor. Math. Phys.* **200** no. 2, (2019) 1222–1236.
- [153] E. C. Marino, L. O. Nascimento, V. S. Alves, and C. M. Smith, “Unitarity of theories containing fractional powers of the d’Alembertian operator,” *Phys. Rev. D* **90** no. 10, (2014) 105003, [arXiv:1408.1637].
- [154] A. Ahmad, J. J. Cobos-Martínez, Y. Concha-Sánchez, and A. Raya, “Landau-Khalatnikov-Fradkin transformations in Reduced Quantum Electrodynamics,” *Phys. Rev. D* **93** no. 9, (2016) 094035, [arXiv:1604.03886].
- [155] A. James, A. V. Kotikov, and S. Teber, “Landau-Khalatnikov-Fradkin transformation of the fermion propagator in massless reduced QED,” *Phys. Rev. D* **101** no. 4, (2020) 045011, [arXiv:1912.05982].
- [156] W.-H. Hsiao and D. T. Son, “Duality and universal transport in mixed-dimension electrodynamics,” *Phys. Rev. B* **96** no. 7, (2017) 075127, [arXiv:1705.01102].
- [157] C. P. Herzog and K.-W. Huang, “Boundary Conformal Field Theory and a Boundary Central Charge,” *JHEP* **10** (2017) 189, [arXiv:1707.06224].
- [158] V. Bashmakov, M. Bertolini, and H. Raj, “On non-supersymmetric conformal manifolds: field theory and holography,” *JHEP* **11** (2017) 167, [arXiv:1709.01749].
- [159] A. Karch and Y. Sato, “Conformal Manifolds with Boundaries or Defects,” *JHEP* **07** (2018) 156, [arXiv:1805.10427].
- [160] D. Dudal, A. J. Mizher, and P. Pais, “Exact quantum scale invariance of three-dimensional reduced QED theories,” *Phys. Rev. D* **99** no. 4, (2019) 045017, [arXiv:1808.04709].
- [161] L. Di Pietro, D. Gaiotto, E. Lauria, and J. Wu, “3d Abelian Gauge Theories at the Boundary,” *JHEP* **05** (2019) 091, [arXiv:1902.09567].
- [162] S. Giombi and H. Khanchandani, “ $O(N)$  models with boundary interactions and their long range generalizations,” *JHEP* **08** no. 08, (2020) 010, [arXiv:1912.08169].
- [163] C. P. Herzog, K.-W. Huang, I. Shamir, and J. Virrueta, “Superconformal Models for Graphene and Boundary Central Charges,” *JHEP* **09** (2018) 161, [arXiv:1807.01700].
- [164] R. Kumar Gupta, C. P. Herzog, and I. Jeon, “Duality and Transport for Supersymmetric Graphene from the Hemisphere Partition Function,” *JHEP* **05** (2020) 023, [arXiv:1912.09225].
- [165] E. Dagotto, J. B. Kogut, and A. Kocic, “A Computer Simulation of Chiral Symmetry Breaking in (2+1)-Dimensional QED with  $N$  Flavors,” *Phys. Rev. Lett.* **62** (1989) 1083.
- [166] E. Dagotto, A. Kocic, and J. B. Kogut, “Chiral Symmetry Breaking in Three-dimensional QED With  $N(f)$  Flavors,” *Nucl. Phys. B* **334** (1990) 279–301.
- [167] S. J. Hands, J. B. Kogut, L. Scorzato, and C. G. Strouthos, “Non-compact QED(3) with  $N(f) = 1$  and  $N(f) = 4$ ,” *Phys. Rev. B* **70** (2004) 104501, [arXiv:hep-lat/0404013].
- [168] C. Strouthos and J. B. Kogut, “The Phases of Non-Compact QED(3),” *PoS LATTICE2007* (2007) 278, [arXiv:0804.0300].
- [169] N. Karthik and R. Narayanan, “No evidence for bilinear condensate in parity-invariant three-dimensional QED with massless fermions,” *Phys. Rev. D* **93** no. 4, (2016) 045020, [arXiv:1512.02993].
- [170] N. Karthik and R. Narayanan, “Scale-invariance of parity-invariant three-dimensional QED,” *Phys. Rev. D* **94** no. 6, (2016) 065026, [arXiv:1606.04109].
- [171] C. D. Roberts and A. G. Williams, “Dyson-Schwinger equations and their application to hadronic physics,” *Prog. Part. Nucl. Phys.* **33** (1994) 477–575, [arXiv:hep-ph/9403224].
- [172] J. C. R. Bloch, *Numerical investigation of fermion mass generation in QED*. Doctoral thesis, University of Durham, 1995. [arXiv:hep-ph/0208074].
- [173] M. Reenders, *Dynamical symmetry breaking in the gauged Nambu-Jona-Lasinio model*. Doctoral thesis, University of Groningen, 1999. [arXiv:hep-th/9906034].
- [174] A. Kızılersü, T. Sizer, M. R. Pennington, A. G. Williams, and R. Williams, “Dynamical mass generation in unquenched QED using the Dyson-Schwinger equations,” *Phys. Rev. D* **91** no. 6, (2015) 065015, [arXiv:1409.5979].
- [175] T. Appelquist and R. D. Pisarski, “High-Temperature Yang-Mills Theories and Three-Dimensional Quantum Chromodynamics,” *Phys. Rev. D* **23** (1981) 2305.
- [176] T. Appelquist and U. W. Heinz, “Three-dimensional  $O(N)$  theories at large distances,” *Phys. Rev. D* **24** (1981) 2169.
- [177] R. D. Pisarski, “Chiral Symmetry Breaking in Three-Dimensional Electrodynamics,” *Phys. Rev. D* **29** (1984) 2423.
- [178] J. S. Ball and T.-W. Chiu, “Analytic Properties of the Vertex Function in Gauge Theories. I.,” *Phys. Rev. D* **22** (1980) 2542.
- [179] D. C. Curtis and M. R. Pennington, “Truncating the Schwinger-Dyson equations: How multiplicative renormalizability and the Ward identity restrict the three point vertex in QED,” *Phys. Rev. D* **42** (1990) 4165–4169.
- [180] A. Kizilersu and M. R. Pennington, “Building the Full Fermion-Photon Vertex of QED by Imposing Multiplicative Renormalizability of the Schwinger-Dyson Equations for the Fermion and Photon Propagators,” *Phys. Rev. D* **79** (2009) 125020, [arXiv:0904.3483].
- [181] D. Nash, “Higher Order Corrections in (2+1)-Dimensional QED,” *Phys. Rev. Lett.* **62** (1989) 3024.

- [182] A. V. Kotikov, “Critical behavior of 3D electrodynamics,” *JETP Lett.* 58 (1993) 731–735.
- [183] A. V. Kotikov, “On the Critical Behavior of (2+1)-Dimensional QED,” *Phys. Atom. Nucl.* 75 (2012) 890–892, [[arXiv:1104.3888](#)].
- [184] V. P. Gusynin and P. K. Pyatkovskiy, “Critical number of fermions in three-dimensional QED,” *Phys. Rev.* D94 no. 12, (2016) 125009, [[arXiv:1607.08582](#)].
- [185] A. V. Kotikov, V. I. Shilin, and S. Teber, “Critical behavior of (2+1)-dimensional QED:  $1/N_f$  corrections in the Landau gauge,” *Phys. Rev.* D94 no. 5, (2016) 056009, [[arXiv:1605.01911](#)]. [Erratum: *Phys. Rev.* D99, no. 11, 119901 (2019)].
- [186] A. Kotikov and S. Teber, “Critical behavior of (2+1)-dimensional QED:  $1/N_f$  corrections in an arbitrary nonlocal gauge,” *Phys. Rev. D* 94 no. 11, (2016) 114011, [[arXiv:1902.03790](#)]. (Addendum: *Phys. Rev. D* 99, 059902 (2019)).
- [187] A. V. Kotikov and S. Teber, “Critical Behavior of (2+1)-Dimensional QED:  $1/N$  Expansion,” *Particles* 3 no. 2, (2020) 345–354.
- [188] L. Di Pietro, Z. Komargodski, I. Shamir, and E. Stamou, “Quantum Electrodynamics in  $d=3$  from the  $\epsilon$  Expansion,” *Phys. Rev. Lett.* 116 no. 13, (2016) 131601, [[arXiv:1508.06278](#)].
- [189] S. Giombi, I. R. Klebanov, and G. Tarnopolsky, “Conformal QED<sub>d</sub>, F-Theorem and the  $\epsilon$  Expansion,” *J. Phys. A* 49 no. 13, (2016) 135403, [[arXiv:1508.06354](#)].
- [190] S. M. Chester and S. S. Pufu, “Anomalous dimensions of scalar operators in QED<sub>3</sub>,” *JHEP* 08 (2016) 069, [[arXiv:1603.05582](#)].
- [191] L. Janssen, “Spontaneous breaking of Lorentz symmetry in  $(2+\epsilon)$ -dimensional QED,” *Phys. Rev. D* 94 no. 9, (2016) 094013, [[arXiv:1604.06354](#)].
- [192] I. F. Herbut, “Chiral symmetry breaking in three-dimensional quantum electrodynamics as fixed point annihilation,” *Phys. Rev. D* 94 no. 2, (2016) 025036, [[arXiv:1605.09482](#)].
- [193] S. Gukov, “RG Flows and Bifurcations,” *Nucl. Phys. B* 919 (2017) 583–638, [[arXiv:1608.06638](#)].
- [194] L. Di Pietro and E. Stamou, “Operator mixing in the  $\epsilon$ -expansion: Scheme and evanescent-operator independence,” *Phys. Rev. D* 97 no. 6, (2018) 065007, [[arXiv:1708.03739](#)].
- [195] L. Di Pietro and E. Stamou, “Scaling dimensions in QED<sub>3</sub> from the  $\epsilon$ -expansion,” *JHEP* 12 (2017) 054, [[arXiv:1708.03740](#)].
- [196] S. Benvenuti and H. Khachatryan, “QED’s in 2+1 dimensions: complex fixed points and dualities,” [[arXiv:1812.01544](#)].
- [197] S. Benvenuti and H. Khachatryan, “Easy-plane QED<sub>3</sub>’s in the large  $N_f$  limit,” *JHEP* 05 (2019) 214, [[arXiv:1902.05767](#)].
- [198] H. Khachatryan, *Exploring the space of many-flavor QED’s in  $2 < d < 6$* . Doctoral thesis, SISSA, 2019. [[PDF](#)].
- [199] W. A. Bardeen, C. N. Leung, and S. T. Love, “The Dilaton and Chiral Symmetry Breaking,” *Phys. Rev. Lett.* 56 (1986) 1230.
- [200] C. N. Leung, S. Love, and W. A. Bardeen, “Spontaneous Symmetry Breaking in Scale Invariant Quantum Electrodynamics,” *Nucl. Phys. B* 273 (1986) 649–662.
- [201] V. A. Miransky and K. Yamawaki, “On Gauge Theories with Additional Four Fermion Interaction,” *Mod. Phys. Lett. A* 4 (1989) 129–135.
- [202] C. N. Leung, S. T. Love, and W. A. Bardeen, “Aspects of Dynamical Symmetry Breaking in Gauge Field Theories,” *Nucl. Phys. B* 323 (1989) 493–512.
- [203] K.-i. Kondo, M. Tanabashi, and K. Yamawaki, “Renormalization in the gauged Nambu-Jona-Lasinio model,” *Prog. Theor. Phys.* 89 (1993) 1249–1302, [[arXiv:hep-ph/9212208](#)].
- [204] K. D. Lane, “Asymptotic Freedom and Goldstone Realization of Chiral Symmetry,” *Phys. Rev. D* 10 (1974) 2605.
- [205] H. D. Politzer, “Effective Quark Masses in the Chiral Limit,” *Nucl. Phys. B* 117 (1976) 397–406.
- [206] V. A. Miransky, “On dynamical chiral symmetry breaking,” *Phys. Lett. B* 165 (1985) 401–404.
- [207] A. G. Cohen and H. Georgi, “Walking Beyond the Rainbow,” *Nucl. Phys. B* 314 (1989) 7–24.
- [208] V. A. Miransky, *Dynamical symmetry breaking in quantum field theories*. World Scientific, 1994.
- [209] S. G. Samko, A. A. Kilbas, O. I. Marichev, *et al.*, *Fractional integrals and derivatives*, vol. 1. Gordon and Breach science publishers, Yverdon Yverdon-les-Bains, Switzerland, 1993.
- [210] A. Vladimirov, “Method for Computing Renormalization Group Functions in Dimensional Renormalization Scheme,” *Theor. Math. Phys.* 43 (1980) 417.
- [211] A. V. Kotikov and S. Teber, “Multi-loop techniques for massless Feynman diagram calculations,” *Phys. Part. Nucl.* 50 no. 1, (2019) 1–41, [[arXiv:1805.05109](#)].
- [212] V. Gusynin, A. Hams, and M. Reenders, “Nonperturbative infrared dynamics of three-dimensional QED with four fermion interaction,” *Phys. Rev. D* 63 (2001) 045025, [[arXiv:hep-ph/0005241](#)].
- [213] J. Gracey, “Computation of critical exponent  $\eta$  at  $O(1/N(f)^{**2})$  in quantum electrodynamics in arbitrary dimensions,” *Nucl. Phys. B* 414 (1994) 614–648, [[arXiv:hep-th/9312055](#)].
- [214] K. Johnson, M. Baker, and R. Willey, “Selfenergy of the electron,” *Phys. Rev.* 136 (1964) B1111–B1119.
- [215] M. Baker and K. Johnson, “Asymptotic form of the electron propagator and the selfmass of the electron,” *Phys. Rev. D* 3 (1971) 2516–2526.
- [216] R. Tarrach, “The Pole Mass in Perturbative QCD,” *Nucl. Phys. B* 183 (1981) 384–396.
- [217] O. Nachtmann and W. Wetzel, “The Beta Function for Effective Quark Masses to Two Loops in QCD,” *Nucl. Phys. B* 187 (1981) 333–342.

- [218] O. V. Tarasov, “Anomalous dimensions of quark masses in the three-loop approximation,” *Phys. Part. Nucl. Lett.* **17** no. 2, (2020) 109–115, [[arXiv:1910.12231](#)].
- [219] T. Luthe, A. Maier, P. Marquard, and Y. Schröder, “Five-loop quark mass and field anomalous dimensions for a general gauge group,” *JHEP* **01** (2017) 081, [[arXiv:1612.05512](#)].
- [220] P. A. Baikov, K. G. Chetyrkin, and J. H. Kühn, “Five-loop fermion anomalous dimension for a general gauge group from four-loop massless propagators,” *JHEP* **04** (2017) 119, [[arXiv:1702.01458](#)].
- [221] N. M. R. Peres, “Colloquium: The Transport properties of graphene: An Introduction,” *Rev. Mod. Phys.* **82** (2010) 2673–2700, [[arXiv:1007.2849](#)].
- [222] R. R. Nair, P. Blake, A. N. Grigorenko, K. S. Novoselov, T. J. Booth, T. Stauber, N. M. R. Peres, and A. K. Geim, “Universal Dynamic Conductivity and Quantized Visible Opacity of Suspended Graphene,” *arXiv e-prints* (Mar., 2008) [[arXiv:0803.3718](#), [arXiv:0803.3718](#)].
- [223] K. F. Mak, M. Y. Sfeir, Y. Wu, C. H. Lui, J. A. Misewich, and T. F. Heinz, “Measurement of the Optical Conductivity of Graphene,” *Phys. Rev. Lett.* **101** no. 19, (Nov., 2008) 196405, [[arXiv:0810.1269](#)].
- [224] R. R. Nair, P. Blake, A. N. Grigorenko, K. S. Novoselov, T. J. Booth, T. Stauber, N. M. R. Peres, and A. K. Geim, “Fine Structure Constant Defines Visual Transparency of Graphene,” *Science* **320** no. 5881, (June, 2008) 1308.
- [225] E. G. Mishchenko, “Minimal conductivity in graphene: Interaction corrections and ultraviolet anomaly,” *EPL (Europhysics Letters)* **83** no. 1, (Jun, 2008) 17005.
- [226] J. A. Gracey, “Electron mass anomalous dimension at  $O(1/(N_f(2)))$  in quantum electrodynamics,” *Phys. Lett.* **B317** (1993) 415–420, [[arXiv:hep-th/9309092](#)].
- [227] D. Dudal, A. J. Mizher, and P. Pais, “Remarks on the Chern-Simons photon term in the QED description of graphene,” *Phys. Rev. D* **98** no. 6, (2018) 065008, [[arXiv:1801.08853](#)].
- [228] M. Mulligan and F. J. Burnell, “Topological Insulators Avoid the Parity Anomaly,” *Phys. Rev. B* **88** (2013) 085104, [[arXiv:1301.4230](#)].
- [229] A. Lopez and E. Fradkin, “Fractional quantum hall effect and chern-simons gauge theories,” *Phys. Rev. B* **44** (Sep, 1991) 5246–5262.
- [230] S. L. Adler, “Axial-vector vertex in spinor electrodynamics,” *Phys. Rev.* **177** (Jan, 1969) 2426–2438.
- [231] J. S. Bell and R. Jackiw, “A PCAC puzzle:  $\pi^0 \rightarrow \gamma\gamma$  in the  $\sigma$  model,” *Nuovo Cim. A* **60** (1969) 47–61.
- [232] A. N. Redlich, “Parity Violation and Gauge Noninvariance of the Effective Gauge Field Action in Three-Dimensions,” *Phys. Rev. D* **29** (1984) 2366–2374.
- [233] A. J. Niemi and G. W. Semenoff, “Axial Anomaly Induced Fermion Fractionization and Effective Gauge Theory Actions in Odd Dimensional Space-Times,” *Phys. Rev. Lett.* **51** (1983) 2077.
- [234] P. Rembiesa, “Gauge independent bifurcation to the chiral symmetry breaking solution of the Dyson-Schwinger equation in continuum QED,” *Phys. Rev. D* **41** (1990) 2009–2014.
- [235] D. Atkinson, J. C. R. Bloch, V. P. Gusynin, M. R. Pennington, and M. Reenders, “Strong QED with weak gauge dependence: Critical coupling and anomalous dimension,” *Phys. Lett. B* **329** (1994) 117–122.
- [236] R. Fukuda and T. Kugo, “Schwinger-Dyson Equation for Massless Vector Theory and Absence of Fermion Pole,” *Nucl. Phys. B* **117** (1976) 250–264.
- [237] P. I. Fomin, V. P. Gusynin, V. A. Miransky, and Y. A. Sitenko, “Dynamical Symmetry Breaking and Particle Mass Generation in Gauge Field Theories,” *Riv. Nuovo Cim.* **6N5** (1983) 1–90.
- [238] V. A. Miransky, “Dynamics of Spontaneous Chiral Symmetry Breaking and Continuum Limit in Quantum Electrodynamics,” *Nuovo Cim. A* **90** (1985) 149–170.
- [239] A. W. Schreiber, T. Sizer, and A. G. Williams, “Dimensionally regularized study of nonperturbative quenched QED,” *Phys. Rev. D* **58** (1998) 125014, [[arXiv:hep-ph/9804385](#)].
- [240] V. P. Gusynin, A. W. Schreiber, T. Sizer, and A. G. Williams, “Chiral symmetry breaking in dimensionally regularized nonperturbative quenched QED,” *Phys. Rev. D* **60** (1999) 065007, [[arXiv:hep-th/9811184](#)].
- [241] T. Luthe, A. Maier, P. Marquard, and Y. Schroder, “Complete renormalization of QCD at five loops,” *JHEP* **03** (2017) 020, [[arXiv:1701.07068](#)].
- [242] K. G. Chetyrkin, G. Falcioni, F. Herzog, and J. A. M. Vermaseren, “Five-loop renormalisation of QCD in covariant gauges,” *JHEP* **10** (2017) 179, [[arXiv:1709.08541](#)]. [Addendum: *JHEP* **12**, 006 (2017)].
- [243] D. C. Curtis and M. R. Pennington, “Nonperturbative study of the fermion propagator in quenched qed in covariant gauges using a renormalizable truncation of the schwinger-dyson equation,” *Phys. Rev. D* **48** (Nov, 1993) 4933–4939.
- [244] A. Bashir, R. Bermudez, L. Chang, and C. D. Roberts, “Dynamical chiral symmetry breaking and the fermion–gauge–boson vertex,” *Phys. Rev. C* **85** (2012) 045205, [[arXiv:1112.4847](#)].
- [245] D. V. Khveshchenko, “Massive Dirac fermions in single-layer graphene,” *Journal of Physics Condensed Matter* **21** no. 7, (Feb., 2009) 075303, [[arXiv:0807.0676](#)].
- [246] G.-Z. Liu, W. Li, and G. Cheng, “Interaction and excitonic insulating transition in graphene,” *Phys. Rev. B* **79** no. 20, (May, 2009) 205429, [[arXiv:0811.4471](#)].
- [247] L. D. Landau, A. Abrikosov, and L. Halatnikov, “On the Quantum theory of fields,” *Nuovo Cim. Suppl.* **3** (1956) 80–104.

- [248] V. P. Gusynin, “Vacuum Polarization and Dynamical Chiral Symmetry Breaking in Quantum Electrodynamics,” *Mod. Phys. Lett. A* 5 (1990) 133.
- [249] C. Popovici, C. S. Fischer, and L. von Smekal, “Fermi velocity renormalization and dynamical gap generation in graphene,” *Phys. Rev. B* 88 no. 20, (2013) 205429, [arXiv:1308.6199].
- [250] A. A. Katanin, “Effect of vertex corrections on the possibility of chiral symmetry breaking induced by long-range Coulomb repulsion in graphene,” *Phys. Rev. B* 93 no. 3, (2016) 035132, [arXiv:1508.07224].
- [251] J.-R. Wang and G.-Z. Liu, “Absence of dynamical gap generation in suspended graphene,” *New Journal of Physics* 14 no. 4, (Apr., 2012) 043036, [arXiv:1202.1014].
- [252] J. González, “Phase diagram of the quantum electrodynamics of two-dimensional and three-dimensional Dirac semimetals,” *Phys. Rev. B* 92 no. 12, (Sept., 2015) 125115, [arXiv:1502.07640].
- [253] M. E. Carrington, C. S. Fischer, L. von Smekal, and M. H. Thoma, “Role of frequency dependence in dynamical gap generation in graphene,” *Phys. Rev. B* 97 no. 11, (2018) 115411, [arXiv:1711.01962].
- [254] J. E. Drut and T. A. Lahde, “Is graphene in vacuum an insulator?,” *Phys. Rev. Lett.* 102 (2009) 026802, [arXiv:0807.0834].
- [255] J.-R. Wang and G.-Z. Liu, “Dynamic gap generation in graphene under the long-range coulomb interaction,” *Journal of Physics: Condensed Matter* 23 no. 34, (Aug, 2011) 345601.
- [256] J. Gonzalez, “Electron self-energy effects on chiral symmetry breaking in graphene,” *arXiv e-prints* (Feb., 2012) arXiv:1202.0443, [arXiv:1202.0443].
- [257] O. V. Gamayun, E. V. Gorbar, and V. P. Gusynin, “Gap generation and semimetal-insulator phase transition in graphene,” *Phys. Rev. B* 81 (2010) 075429, [arXiv:0911.4878].
- [258] P. V. Buividovich and M. I. Polikarpov, “Monte-Carlo study of the electron transport properties of monolayer graphene within the tight-binding model,” *Phys. Rev. B* 86 (2012) 245117, [arXiv:1206.0619].
- [259] O. Vafek and M. J. Case, “Renormalization group approach to two-dimensional Coulomb interacting Dirac fermions with random gauge potential,” *Phys. Rev. B* 77 no. 3, (Jan., 2008) 033410, [arXiv:0710.2907].
- [260] K.-i. Kondo and H. Nakatani, “Phase Structure of Strong Coupling Unquenched QED. I. Analytical Study,” *Nucl. Phys. B* 351 (1991) 236–258.
- [261] K. Kondo and H. Nakatani, “Strong Coupling Unquenched QED. II — Numerical Study —,” *Progress of Theoretical Physics* 88 no. 4, (Oct., 1992) 737–749.
- [262] J. Oliensis and P. W. Johnson, “Possible second-order phase transition in strongly coupled unquenched planar four-dimensional qed,” *Phys. Rev. D* 42 (Jul, 1990) 656–664.
- [263] P. Rakow, “Renormalisation group flow in qed - an investigation of the schwinger-dyson equations,” *Nuclear Physics B* 356 no. 1, (1991) 27–45.
- [264] D. Atkinson, H. J. D. Groot, and P. W. Johnson, “Phase Transitions in Strong Coupling QED<sub>4</sub>[N],” *International Journal of Modern Physics A* 7 no. 30, (Jan., 1992) 7629–7646.
- [265] K.-I. Kondo, H. Mino, and H. Nakatani, “Self-Consistent Solution of the Simultaneous Schwinger-Dyson Equation in Strong Coupling QED,” *Modern Physics Letters A* 7 no. 17, (Jan., 1992) 1509–1518.
- [266] M. Ukita, M. Komachiya, and R. Fukuda, “Gauge invariant study of the strong coupling phase of massless quantum electrodynamics,” *Int. J. Mod. Phys. A* 5 (1990) 1789–1800.
- [267] K.-I. Kondo, T. Iizuka, E. Tanaka, and T. Ebihara, “Flavor dependence and higher orders of gauge independent solutions in strong coupling gauge theory,” *Phys. Lett. B* 325 (1994) 423–429, [arXiv:hep-th/9401012].
- [268] F. Akram, A. Bashir, L. X. Gutiérrez-Guerrero, B. Masud, J. Rodríguez-Quintero, C. Calcaneo-Roldan, and M. E. Tejada-Yeomans, “Vacuum Polarization and Dynamical Chiral Symmetry Breaking: Phase Diagram of QED with Four-Fermion Contact Interaction,” *Phys. Rev. D* 87 no. 1, (2013) 013011, [arXiv:1209.1292].
- [269] T. W. Appelquist, M. J. Bowick, D. Karabali, and L. Wijewardhana, “Spontaneous Chiral Symmetry Breaking in Three-Dimensional QED,” *Phys. Rev. D* 33 (1986) 3704.
- [270] R. Jackiw and S. Templeton, “How Superrenormalizable Interactions Cure their Infrared Divergences,” *Phys. Rev. D* 23 (1981) 2291.
- [271] S. Templeton, “Summation of Coupling Constant Logarithms in QED in Three-dimensions,” *Phys. Rev. D* 24 (1981) 3134.
- [272] E. I. Guendelman and Z. M. Radulovic, “Infrared Divergences in Three-dimensional Gauge Theories,” *Phys. Rev. D* 30 (1984) 1338.
- [273] E. I. Guendelman and Z. M. Radulovic, “Loop Expansion in Massless QED in three-dimensions,” *Phys. Rev. D* 27 (1983) 357–365.
- [274] I. D. King and G. Thompson, “Non-Perturbative Analysis of Leading Logarithms in Three-Dimensional QED,” *Phys. Rev. D* 31 (1985) 2148–2150.
- [275] N. Karthik and R. Narayanan, “Flavor and topological current correlators in parity-invariant three-dimensional QED,” *Phys. Rev. D* 96 no. 5, (2017) 054509, [arXiv:1705.11143].
- [276] V. P. Gusynin, A. V. Kotikov, and S. Teber, “Landau-Khalatnikov-Fradkin transformation in three-dimensional quenched QED,” *Phys. Rev. D* 102 no. 2, (2020) 025013, [arXiv:2006.09315].
- [277] D. Atkinson, P. W. Johnson, and P. Maris, “Dynamical Mass Generation in QED in Three-dimensions: Improved Vertex Function,” *Phys. Rev. D* 42 (1990) 602–609.



- [278] M. R. Pennington and D. Walsh, “Masses from nothing: A Nonperturbative study of QED in three-dimensions,” *Phys. Lett.* B253 (1991) 246–251.
- [279] V. P. Gusynin, A. H. Hams, and M. Reenders, “(2+1)-dimensional QED with dynamically massive fermions in the vacuum polarization,” *Phys. Rev.* D53 (1996) 2227–2235, [[arXiv:hep-ph/9509380](#)].
- [280] P. Maris, “The Influence of the full vertex and vacuum polarization on the fermion propagator in QED in three-dimensions,” *Phys. Rev.* D54 (1996) 4049–4058, [[arXiv:hep-ph/9606214](#)].
- [281] V. P. Gusynin and M. Reenders, “Infrared cutoff dependence of the critical flavor number in QED(3),” *Phys. Rev.* D68 (2003) 025017, [[arXiv:hep-ph/0304302](#)].
- [282] C. S. Fischer, R. Alkofer, T. Dahm, and P. Maris, “Dynamical chiral symmetry breaking in unquenched QED(3),” *Phys. Rev.* D70 (2004) 073007, [[arXiv:hep-ph/0407104](#)].
- [283] N. Karthik and R. Narayanan, “Numerical determination of monopole scaling dimension in parity-invariant three-dimensional noncompact QED,” *Phys. Rev.* D100 no. 5, (2019) 054514, [[arXiv:1908.05500](#)].
- [284] S. R. Coleman and J. Mandula, “All Possible Symmetries of the S Matrix,” *Phys. Rev.* 159 (1967) 1251–1256.
- [285] T. E. Clark and S. T. Love, “Supersymmetric Quantum Electrodynamics and Dynamical Chiral Symmetry Breaking,” *Nucl. Phys. B* 310 (1988) 371–386.
- [286] M. Koopmans and J. J. Steringa, “Dynamical Mass Generation in Supersymmetric QED in Three-dimensions,” *Phys. Lett.* B226 (1989) 309–312.
- [287] M. Walker and C. Burden, “Chiral symmetry in supersymmetric three-dimensional quantum electrodynamics,” *Phys. Rev. D* 59 (1999) 125013, [[arXiv:hep-th/9901070](#)].
- [288] A. Campbell-Smith and N. Mavromatos, “On dynamical mass generation in three dimensional supersymmetric U(1) gauge field theory,” *Phys. Rev. D* 60 (1999) 105011, [[arXiv:hep-th/9904173](#)].
- [289] A. Campbell-Smith, N. Mavromatos, and J. Papavassiliou, “Gauge coupling instability and dynamical mass generation in N=1 supersymmetric QED(3),” *Phys. Rev. D* 60 (1999) 085002, [[arXiv:hep-th/9905132](#)].
- [290] M. Gremm and E. Katz, “Mirror symmetry for N=1 QED in three-dimensions,” *JHEP* 02 (2000) 008, [[arXiv:hep-th/9906020](#)].
- [291] S. Gukov and D. Tong, “D-brane probes of special holonomy manifolds, and dynamics of N = 1 three-dimensional gauge theories,” *JHEP* 04 (2002) 050, [[arXiv:hep-th/0202126](#)].
- [292] V. Bashmakov, J. Gomis, Z. Komargodski, and A. Sharon, “Phases of  $\mathcal{N} = 1$  theories in 2 + 1 dimensions,” *JHEP* 07 (2018) 123, [[arXiv:1802.10130](#)].
- [293] F. Benini and S. Benvenuti, “ $\mathcal{N} = 1$  dualities in 2+1 dimensions,” *JHEP* 11 (2018) 197, [[arXiv:1803.01784](#)].
- [294] D. Gaiotto, Z. Komargodski, and J. Wu, “Curious Aspects of Three-Dimensional  $\mathcal{N} = 1$  SCFTs,” *JHEP* 08 (2018) 004, [[arXiv:1804.02018](#)].
- [295] F. Benini and S. Benvenuti, “ $\mathcal{N} = 1$  QED in 2+1 dimensions: Dualities and enhanced symmetries,” [[arXiv:1804.05707](#)].
- [296] S.-S. Lee, “Emergence of supersymmetry at a critical point of a lattice model,” *Phys. Rev. B* 76 (2007) 075103, [[arXiv:cond-mat/0611658](#)].
- [297] B. Roy, V. Juričić, and I. F. Herbut, “Quantum superconducting criticality in graphene and topological insulators,” *Phys. Rev. B* 87 no. 4, (Jan., 2013) 041401, [[arXiv:1210.3576](#)].
- [298] T. Grover, D. N. Sheng, and A. Vishwanath, “Emergent Space-Time Supersymmetry at the Boundary of a Topological Phase,” *Science* 344 no. 6181, (2014) 280–283, [[arXiv:1301.7449](#)].
- [299] P. Ponte and S.-S. Lee, “Emergence of supersymmetry on the surface of three dimensional topological insulators,” *New J. Phys.* 16 no. 1, (2014) 013044, [[arXiv:1206.2340](#)].
- [300] S.-K. Jian, Y.-F. Jiang, and H. Yao, “Emergent Spacetime Supersymmetry in 3D Weyl Semimetals and 2D Dirac Semimetals,” *Phys. Rev. Lett.* 114 no. 23, (2015) 237001, [[arXiv:1407.4497](#)].
- [301] W. Witczak-Krempa and J. Maciejko, “Optical conductivity of topological surface states with emergent supersymmetry,” *Phys. Rev. Lett.* 116 no. 10, (2016) 100402, [[arXiv:1510.06397](#)]. [Addendum: *Phys.Rev.Lett.* 117, 149903 (2016)].
- [302] S.-K. Jian, C.-H. Lin, J. Maciejko, and H. Yao, “Emergence of supersymmetric quantum electrodynamics,” *Phys. Rev. Lett.* 118 no. 16, (2017) 166802, [[arXiv:1609.02146](#)].
- [303] S. Han, J. Lee, and E.-G. Moon, “Lattice vibration as a knob for novel quantum criticality: Emergence of supersymmetry from spin-lattice coupling,” [[arXiv:1911.01435](#)].
- [304] P.-L. Zhao and G.-Z. Liu, “Absence of emergent supersymmetry at superconducting quantum critical points in Dirac and Weyl semimetals,” *Materials* 4 (2019) 37, [[arXiv:1706.02231](#)].
- [305] E. M. C. Abreu, M. A. De Andrade, L. P. G. De Assis, J. A. Helayel-Neto, A. L. M. A. Nogueira, and R. C. Paschoal, “A supersymmetric model for graphene,” *JHEP* 05 (2011) 001, [[arXiv:1002.2660](#)].
- [306] E. M. C. Abreu, M. A. De Andrade, L. P. G. De Assis, J. A. Helayel-Neto, A. L. M. A. Nogueira, and R. C. Paschoal, “Vortex Solutions and a Novel Role for R-parity in an N=2-Supersymmetric Model for Graphene,” [[arXiv:1308.2028](#)].
- [307] S. Hikami, “Renormalization Group Functions of CP\*\*1N Nonlinear Sigma Model and N Component Scalar QED Model,” *Prog. Theor. Phys.* 62 (1979) 226.

- [308] A. N. Vasiliev and M. Y. Nalimov, “The CP<sup>\*\*</sup>(n-1) model: calculation of anomalous dimensions and the mixing matrices in the order 1/N,” *Theor. Math. Phys.* **56** (1983) 643–653.
- [309] B. Ihrig, N. Zerf, P. Marquard, I. F. Herbut, and M. M. Scherer, “Abelian Higgs model at four loops, fixed-point collision and deconfined criticality,” *Phys. Rev. B* **100** no. 13, (2019) 134507, [[arXiv:1907.08140](#)].
- [310] H. Khachatryan, “Higher Derivative Gauge theory in  $d=6$  and the  $\mathbb{CP}^{(N_f-1)}$  NLSM,” *JHEP* **12** (2019) 144, [[arXiv:1907.11448](#)].
- [311] W. Siegel, “Supersymmetric Dimensional Regularization via Dimensional Reduction,” *Phys. Lett. B* **84** (1979) 193–196.
- [312] W. Siegel, “Inconsistency of Supersymmetric Dimensional Regularization,” *Phys. Lett. B* **94** (1980) 37–40.
- [313] D. Capper, D. Jones, and P. van Nieuwenhuizen, “Regularization by Dimensional Reduction of Supersymmetric and Nonsupersymmetric Gauge Theories,” *Nucl. Phys. B* **167** (1980) 479–499.
- [314] I. Jack and D. Jones, *Regularization of supersymmetric theories*, vol. 21, pp. 494–513. Kane, Gordon L., 2010. [[arXiv:hep-ph/9707278](#)].
- [315] W. Hollik, E. Kraus, and D. Stockinger, “Renormalization and symmetry conditions in supersymmetric QED,” *Eur. Phys. J. C* **11** (1999) 365–381, [[arXiv:hep-ph/9907393](#)].
- [316] C. Rupp, R. Scharf, and K. Sibold, “Susy Ward identity and its use in SQED,” *Nucl. Phys. B Proc. Suppl.* **89** (2000) 272–276.
- [317] C. Vafa and E. Witten, “Parity Conservation in QCD,” *Phys. Rev. Lett.* **53** (1984) 535.
- [318] T. Appelquist, M. J. Bowick, D. Karabali, and L. Wijewardhana, “Spontaneous Breaking of Parity in (2+1)-dimensional QED,” *Phys. Rev. D* **33** (1986) 3774.
- [319] J. Wess and B. Zumino, “Consequences of anomalous Ward identities,” *Phys. Lett. B* **37** (1971) 95–97.
- [320] I. Jack, D. Jones, and K. Roberts, “Equivalence of dimensional reduction and dimensional regularization,” *Z. Phys. C* **63** (1994) 151–160, [[arXiv:hep-ph/9401349](#)].
- [321] T. Jones, “Dimensional reduction (and all that),” *PoS LL2012* (2012) 011.
- [322] L. Mihaila, “Precision Calculations in Supersymmetric Theories,” *Adv. High Energy Phys.* **2013** (2013) 607807, [[arXiv:1310.6178](#)].
- [323] C. Gnendiger, A. Signer, D. Stöckinger, A. Broggio, A. Cherchiglia, *et al.*, “To  $d$ , or not to  $d$ : recent developments and comparisons of regularization schemes,” *Eur. Phys. J. C* **77** no. 7, (2017) 471, [[arXiv:1705.01827](#)].
- [324] R. V. Harlander, L. Mihaila, and M. Steinhauser, “The SUSY-QCD beta function to three loops,” *Eur. Phys. J. C* **63** (2009) 383–390, [[arXiv:0905.4807](#)].
- [325] A. Denner, H. Eck, O. Hahn, and J. Kublbeck, “Compact Feynman rules for Majorana fermions,” *Phys. Lett. B* **291** (1992) 278–280.
- [326] A. Denner, H. Eck, O. Hahn, and J. Kublbeck, “Feynman rules for fermion number violating interactions,” *Nucl. Phys. B* **387** (1992) 467–481.
- [327] J. Wess and B. Zumino, “Supergauge Invariant Extension of Quantum Electrodynamics,” *Nucl. Phys. B* **78** (1974) 1.
- [328] B. Zumino, “Gauge properties of propagators in quantum electrodynamics,” *J. Math. Phys.* **1** (1960) 1–7.
- [329] M. Walker, “A Completely invariant SUSY transform of supersymmetric QED,” *J. Phys. G* **30** (2004) 1219–1224, [[arXiv:hep-th/0310098](#)].
- [330] W. H. Furry, “A Symmetry Theorem in the Positron Theory,” *Phys. Rev.* **51** (1937) 125–129.
- [331] D. I. Kazakov, “Multiloop Calculations: Method of Uniqueness and Functional Equations,” *Teor. Mat. Fiz.* **62** (1984) 127–135.
- [332] A. V. Kotikov, “The Gegenbauer Polynomial technique: the evaluation of a class of Feynman diagrams,” *Physics Letters B* **375** no. 1, (Feb., 1996) 240–248, [[arXiv:hep-ph/9512270](#)].
- [333] E. Dagotto, A. Kocic, and J. B. Kogut, “Collapse of the wave function, anomalous dimensions and continuum limits in model scalar field theories,” *Phys. Lett. B* **237** (1990) 268–273.
- [334] Y. Shamir, “Chiral symmetry breaking in supersymmetric QCD,” *Phys. Rev. Lett.* **66** (1991) 3101–3104.
- [335] Y. Shamir, “Supersymmetric QCD chiral symmetry breaking in the ladder approximation,” *Nucl. Phys. B* **352** (1991) 469–488.
- [336] T. Appelquist, A. Nyffeler, and S. B. Selipsky, “Analyzing chiral symmetry breaking in supersymmetric gauge theories,” *Phys. Lett. B* **425** (1998) 300–308, [[arXiv:hep-th/9709177](#)].
- [337] D. Curtis, M. Pennington, and D. Walsh, “Dynamical mass generation in qed3 and the 1/n expansion,” *Physics Letters B* **295** no. 3, (1992) 313–319.
- [338] R. D. Pisarski, “Fermion mass in three dimensions and the renormalization group,” *Phys. Rev. D* **44** (Sep, 1991) 1866–1872.
- [339] V. Azcoiti and X.-Q. Luo, “(2+1)-dimensional compact qed with dynamical fermions,” *Nuclear Physics B - Proceedings Supplements* **30** (1993) 741–744.
- [340] V. Azcoiti, V. Laliena, and X.-Q. Luo, “Investigation of spontaneous symmetry breaking from a nonstandard approach,” *Nucl. Phys. B Proc. Suppl.* **47** (1996) 565–568, [[arXiv:hep-lat/9605022](#)].
- [341] J. Braun, H. Gies, L. Janssen, and D. Roscher, “Phase structure of many-flavor QED<sub>3</sub>,” *Phys. Rev. D* **90** no. 3, (2014) 036002, [[arXiv:1404.1362](#)].

- [342] K.-i. Kubota and H. Terao, “Dynamical symmetry breaking in QED(3) from the Wilson RG point of view,” *Prog. Theor. Phys.* 105 (2001) 809–825, [[arXiv:hep-ph/0101073](#)].
- [343] S. Giombi, G. Tarnopolsky, and I. R. Klebanov, “On  $C_J$  and  $C_T$  in Conformal QED,” *JHEP* 08 (2016) 156, [[arXiv:1602.01076](#)].
- [344] T. Appelquist, A. G. Cohen, and M. Schmaltz, “A New constraint on strongly coupled gauge theories,” *Phys. Rev. D* 60 (1999) 045003, [[arXiv:hep-th/9901109](#)].
- [345] R. N. Lee, “Presenting LiteRed: a tool for the Loop InTEgrals REDuction,” [[arXiv:1212.2685](#)].
- [346] R. N. Lee, “LiteRed 1.4: a powerful tool for reduction of multiloop integrals,” *J. Phys. Conf. Ser.* 523 (2014) 012059, [[arXiv:1310.1145](#)].
- [347] P. A. Baikov and K. G. Chetyrkin, “Four loop massless propagators: An algebraic evaluation of all master integrals,” *Nuclear Physics B* 837 no. 3, (Oct., 2010) 186–220, [[arXiv:1004.1153](#)].
- [348] T. Huber and D. Maître, “HypExp, a Mathematica package for expanding hypergeometric functions around integer-valued parameters,” *Computer Physics Communications* 175 no. 2, (July, 2006) 122–144, [[arXiv:hep-ph/0507094](#)].
- [349] T. Huber and D. Maître, “HypExp 2, Expanding hypergeometric functions about half-integer parameters,” *Computer Physics Communications* 178 no. 10, (May, 2008) 755–776, [[arXiv:0708.2443](#)].
- [350] A. V. Smirnov and M. N. Tentyukov, “Feynman Integral Evaluation by a Sector decomposition Approach (FIESTA),” *Computer Physics Communications* 180 no. 5, (May, 2009) 735–746, [[arXiv:0807.4129](#)].
- [351] A. V. Smirnov and M. Tentyukov, “FIESTA 2: Parallelizeable multiloop numerical calculations,” *Computer Physics Communications* 182 no. 3, (Mar., 2011) 790–803, [[arXiv:0912.0158](#)].
- [352] A. V. Smirnov, “FIESTA 3: Cluster-parallelizable multiloop numerical calculations in physical regions,” *Computer Physics Communications* 185 no. 7, (July, 2014) 2090–2100, [[arXiv:1312.3186](#)].
- [353] H. R. P. Ferguson, D. H. Bailey, and S. Arno, “Analysis of PSLQ, an integer relation finding algorithm,” *Math. Comput.* 68 (1999) 351–369.





---

**Sujet : Étude de l'effet des interactions élastiques et électroniques dans les théories de champs en basse dimension**

---

**Résumé :** Cette thèse explore l'impact des interactions dans diverses théories de basse dimension en utilisant des techniques analytiques perturbatives et non perturbatives de la théorie des champs. Notre focalisation principale concerne les systèmes planaires de la matière condensée et leurs transitions de phase, thermiques ou quantiques, dues aux interactions. Ces dernières sont caractérisées par des dimensions anormales, ou exposants critiques, observables physiques universelles calculables grâce aux techniques des diagrammes de Feynman multi-boucles. Une première partie se penche sur l'étude des fluctuations élastiques dans diverses théories statistiques des champs associées à la phase plane des membranes polymérisées, présentes dans de nombreux domaines de la physique. Nous explorons leurs propriétés mécaniques critiques, notamment la rigidité anormale induite par les corrélations à longue portée, à un ordre élevé en boucles. Nous examinons également une variante désordonnée en utilisant la technique des répliques, révélant une nouvelle transition de plissement vers une phase vitreuse. Une deuxième partie se penche sur plusieurs théories de jauge abéliennes en basse dimension, particulièrement utiles pour décrire des systèmes quantiques fermioniques planaires fortement corrélés, tels que le graphène à basse énergie. Nous étudions également une extension supersymétrique minimale en relation avec un potentiel supergraphène. Pour ces modèles, nous calculons les exposants critiques à l'aide d'un développement en boucles ou large  $N_f$ , et nous examinons la possibilité d'une transition de phase métal-isolant due à la génération dynamique d'une masse pour l'électron.

**Mots clés :** Groupe de renormalization; Calcul multiboucles; Transitions de phases; Effets non-perturbatifs; Membranes; Désordre; Théorie de jauge; Supersymétrie.

---

**Subject : Study of elastic and electronic interaction effects in low-dimensional field theories**

---

**Abstract:** This thesis delves into the impact of interactions in various low-dimensional theories using both perturbative and non-perturbative analytical field theory methods. We primarily focus on planar condensed matter systems and their, thermal or quantum, interaction-driven phase transitions. The latter are characterized by anomalous dimensions, or critical exponents, which are universal physical quantities computed using multiloop Feynman diagram techniques. A first part explores elastic fluctuations in different statistical field theories associated with the flat phase of polymerized membranes, commonly found in physics. We investigate their critical mechanical properties, especially the anomalous stiffness resulting from long-range correlations, computed at a high loop order. We also consider a variant involving disorder, revealing a new wrinkling transition to a glassy phase. A second part investigates several abelian gauge field theories in low dimensions, particularly useful for describing strongly correlated planar fermionic quantum systems like low-energy graphene. We also examine a minimally supersymmetric extension related to potential supergraphene materials. For these models, we compute critical exponents through loop or large  $N_f$  expansions and explore the possibility of a metallic-to-insulating phase transition through the generation of a dynamical mass for electrons.

**Keywords :** Renormalization group; Multi-loop calculations; Phase transitions; Non-perturbative effects; Membranes; Disorder; Gauge theory; Supersymmetry.